HORIZONS IN BUILT ENVIRONMENT

EDITED BY: Izuru Takewaki, Ian F. C. Smith, Joan Ramon Casas, Forrest J. Masters, Gregory A. Kopp, Vagelis Plevris and George Tsiatas

PUBLISHED IN: Frontiers in Built Environment

frontiers Research Topics

frontiers

ISSN 1664-8714
ISBN 978-2-88976-165-4
DOI 10.3389/978-2-88976-165-4

About Frontiers

Frontiers is more than just an open-access publisher of scholarly articles: it is a pioneering approach to the world of academia, radically improving the way scholarly research is managed. The grand vision of Frontiers is a world where all people have an equal opportunity to seek, share and generate knowledge. Frontiers provides immediate and permanent online open access to all its publications, but this alone is not enough to realize our grand goals.

Frontiers Journal Series

The Frontiers Journal Series is a multi-tier and interdisciplinary set of open-access, online journals, promising a paradigm shift from the current review, selection and dissemination processes in academic publishing. All Frontiers journals are driven by researchers for researchers; therefore, they constitute a service to the scholarly community. At the same time, the Frontiers Journal Series operates on a revolutionary invention, the tiered publishing system, initially addressing specific communities of scholars, and gradually climbing up to broader public understanding, thus serving the interests of the lay society, too.

Dedication to Quality

Each Frontiers article is a landmark of the highest quality, thanks to genuinely collaborative interactions between authors and review editors, who include some of the world's best academicians. Research must be certified by peers before entering a stream of knowledge that may eventually reach the public - and shape society; therefore, Frontiers only applies the most rigorous and unbiased reviews.
Frontiers revolutionizes research publishing by freely delivering the most outstanding research, evaluated with no bias from both the academic and social point of view. By applying the most advanced information technologies, Frontiers is catapulting scholarly publishing into a new generation.

What are Frontiers Research Topics?

Frontiers Research Topics are very popular trademarks of the Frontiers Journals Series: they are collections of at least ten articles, all centered on a particular subject. With their unique mix of varied contributions from Original Research to Review Articles, Frontiers Research Topics unify the most influential researchers, the latest key findings and historical advances in a hot research area! Find out more on how to host your own Frontiers Research Topic or contribute to one as an author by contacting the Frontiers Editorial Office: frontiersin.org/about/contact

HORIZONS IN BUILT ENVIRONMENT

Topic Editors:
Izuru Takewaki, Kyoto University, Japan
Ian F. C. Smith, Swiss Federal Institute of Technology Lausanne, Switzerland
Joan Ramon Casas, Universitat Politecnica de Catalunya, Spain
Forrest J. Masters, University of Florida, United States
Gregory A. Kopp, Western University (Canada), Canada
Vagelis Plevris, Qatar University, Qatar
George Tsiatas, University of Patras, Greece

Citation: Takewaki, I., Smith, I. F. C., Casas, J. R., Masters, F. J., Kopp, G. A., Plevris, V., Tsiatas, G., eds. (2022). Horizons in Built Environment. Lausanne: Frontiers Media SA. doi: 10.3389/978-2-88976-165-4

Table of Contents

frontiers in Built Environment

REVIEW
published: 17 January 2022
doi: 10.3389/fbuil.2021.805014

Comprehensive Review on the Dynamic and Seismic Behavior of Flat-Bottom Cylindrical Silos Filled With Granular Material

Sulyman Mansour[1], Luca Pieraccini[2], Michele Palermo[2], Dora Foti[1], Giada Gasparini[2], Tomaso Trombetti[2] and Stefano Silvestri[2]*

[1]Department DICAR, Polytechnic University of Bari, Bari, Italy, [2]Department DICAM, University of Bologna, Bologna, Italy

The seismic design of industrial flat-bottom ground-supported silos filled with granular material still presents several challenges to be addressed. They are related to the main aspects which differentiate silo structures containing granular material from other civil structural typologies: 1) the relatively low silo structure mass as compared to the ensiled content mass; 2) the granular nature of the ensiled material. Indeed, the internal actions in the structural members are governed by the complex dynamic interactions along the interfaces between granular content and silo wall or base, or even the internal interaction between particles. More in detail, even though the scientific interest in such complex interactions dates back to the middle of the 19th century, several issues are still unclear such as the dependency of the fundamental dynamic properties (period of vibration and damping ratio) on the characteristics of the dynamic excitation (intensity, frequency content, duration) or the amount of ensiled material mass activated during a seismic excitation and provoking extra pressures on the wall (effective mass). Therefore, most of current seismic code provisions for silos are grounded on rather approximate and simplified assumptions leading to often over-conservative evaluations. The present paper intends to provide a comprehensive summary of the mainly acknowledged experimental and theoretical advances in the dynamic and seismic behavior of silos, supporting the potential researcher in the field to understand the real differences between the code assumptions and recommendations and the actual conditions, as well as illustrating the open issues to be still further investigated.

Keywords: silo, flat-bottom, granular material, earthquake, effective mass, frequency, damping ratio

OPEN ACCESS

Edited by:
Izuru Takewaki,
Kyoto University, Japan

Reviewed by:
Yutaka Nakamura,
Shimane University, Japan
Ersin Aydin,
Niğde Ömer Halisdemir University, Turkey

****Correspondence:***
Sulyman Mansour
sulyman.mansour@poliba.it

Specialty section:
This article was submitted to Earthquake Engineering, a section of the journal Frontiers in Built Environment

Received: *29 October 2021*
Accepted: *13 December 2021*
Published: *17 January 2022*

Citation:
Mansour S, Pieraccini L, Palermo M, Foti D, Gasparini G, Trombetti T and Silvestri S (2022) Comprehensive Review on the Dynamic and Seismic Behavior of Flat-Bottom Cylindrical Silos Filled With Granular Material. Front. Built Environ. 7:805014. doi: 10.3389/fbuil.2021.805014

INTRODUCTION

Storage containers of bulk material are known as bins (or grain bins), silos or even bunkers. Although there is no globally accepted definition for each of the previous terms, "bins" or "bunkers" are commonly used to refer to squat containers with a shallow filling condition of a variety of material like coal, ore, gravel and crushed stones, while slender containers of food supplies (e.g., wheat, corn . . .) and cement are usually called "silos" (Li, 1994). The European design provisions EN 1991-4: 2006, EN 1998-4:2006 and EN 1993-4:2007 (European Committee for Standardization, 2006a; European Committee for Standardization, 2006b; European Committee for Standardization, 2007) adopt the term "silo" as an inclusive term for all structures for the storage of granular solid, whilst the

term "bin" is common in the north American countries (ANSI-ASAE S433.1: 2019). Flat-bottom ground-supported silos, typically made of steel or reinforced concrete (r.c.), are storage structures that are directly placed on a r.c. plate foundation. Typically, cast in-situ r.c. silos present circular hollow section with uniform thickness; while steel silos are made up either of isotropic flat wall or orthotropic corrugated cold-formed wall with variable thicknesses, usually supported with bolted C- or open hat-shaped vertical stiffeners.

The type of granular material (wheat, corn, rice, sugar, soya beans, maize, barley, . . .) has to be clearly specified in the design phase, since its mechanical properties (which can substantially change from a product to another one, as per the Table E.1 of Annex E of EN 1991-4:2006) strongly affect both the static and the dynamic behavior of the filled silo system and the choice of the more appropriate wall section (e.g., flat-walled section is commonly used for powder content, whist corrugated-walled section is preferred for bulk solids).

Steel silos are thin-walled structures which are very sensitive to human made mistakes and construction errors, as well as to damages occurred during shipment and transportation. Moreover, special care should be paid during the first filling procedure, considering even the adjacent silos (i.e., the whole silo battery), since specific filling programs on different steps should be envisaged to guarantee the stability of the whole silo battery without causing any differential settlements leading eventually to structural defects that might also affect the dynamic response of silos during seismic events.

Several earthquakes, that occurred in the last decades, had catastrophic consequences on storage facilities and mainly silos. Description of damages and main causes of collapses can be found in the in-situ post-earthquake surveys reports (Dogangun et al., 2009; Fierro et al., 2011; Uckan et al., 2015). In December 1988, Northern Armenia was hit by a M6.8 earthquake with devastating consequences on several industrial facilities including silos mainly due to construction imperfections accompanied by inadequate inspections (Arze, 1992, Arze, 1993; Griffin et al., 1995). Another interesting case was noticed after the M6.3 L'Aquila (Central Italy) earthquake, where the failure was reported of three adjacent tall steel silos in a chemical facility near L'Aquila city due to the collision with a close r.c. structure (Grimaz, 2014). During the M8.8 2010 Chile earthquake, extensive damages and collapses stroke many silos in an industrial facility in the city of Concepción, where two rows of silos collapsed due to the failure of the base connections (Villalobos and Mendoza. 2011). In addition, several silo failures occurred across the region, where some fully filled silos up to 5,000 tons capacity showed different failure modes, including global overturning and buckling mechanisms due to the lack of stiffening elements (Grossi et al., 2010). In May 2012, Emilia-Romagna region (Northern Italy) was hit by two M5.8 earthquakes and several metal silos collapsed in various ways, including plastic hinge development near the silo base (Augenti et al., 2013; Gioncu and Mazzolani, 2014). In general, most of the reported failures were associated with brittle behavior in the absence of structural redundancy and alternative resisting mechanisms, which represents an inherent common deficiency due to the structural configuration of silos. Finally, the majority of the reported silo failures (85%) are related to incorrect adopted design concepts, or executive construction problems (Arze, 1992). **Figure 1** schematically represents the most common failure mechanisms during earthquake events.

It is thus clear that the proper evaluation of the forces transmitted by the stored material to the silo structure, during both filling and discharging phases or in the event of an earthquake ground-motion, is of fundamental importance. This task is particularly complex since the granular nature of the ensiled content triggers off a highly non-linear behaviour strongly affecting the highly vulnerable thin cylindrical wall (especially, in empty conditions or asymmetric discharging conditions). Specific additional loading cases accounting for the potential eccentric pipe flow phenomenon (e.g., when side discharging is required), and empty conditions loading combinations (at least one for wind and one for seismic loads) must be considered since it might lead to buckling problems or deformations with a strong impact on the filled silo system behavior during the seismic event. In this respect, specific design recommendations for silo structures can be found in several international building codes, including the Eurocode provisions (EN 1991-4: 2006; EN 1993-4: 2006; EN 1998-4: 2006), U.S. building codes FEMA P-750 (ASCE-7, 2005; UBC, 1994; American Concrete Institute, 1997), and the Japanese building code (Architectural Institute of Japan (AIJ), 2010). Nevertheless, most of the mentioned design provisions are based on rather approximate and over-conservative assumptions which reflect the current state of knowledge regarding the dynamic behavior and complex interaction of the granular solid with the silo structure.

In light of this (*Seismic Design of Silos: Main Issues and Current Provisions*), this work intends to present a comprehensive overview of the available research works on the dynamic behavior of filled silo systems. The experimental works aimed at characterizing the dynamic properties of the granular materials and the dynamic response of small- and full-scaled silos are summarized (*Dynamic Experimental Tests on Granular Media, Empty and Filled Silo Systems*), as well as the main theoretical studies and numerical investigations to develop predictive models (*Theoretical Studies and Numerical Modelling on the Dynamic Behavior of Filled Silo Systems*). The final objective is to identify the main challenges for future research (*Future Research Challenges*).

SEISMIC DESIGN OF SILOS: MAIN ISSUES AND CURRENT PROVISIONS

The structural response of storage units filled with granular solid, in static but particularly in dynamic conditions, is strongly affected by the not fully understood interaction between the structural elements and the stored content particles. This aspect is especially important for steel silos characterized by a very low self-weight with respect to the stored material. In this respect, the essential matters far from being fully understood might be outlined in two points:

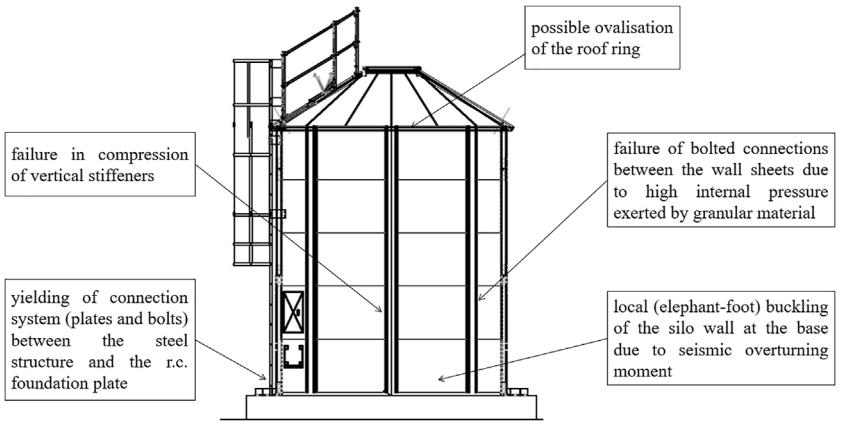

FIGURE 1 | Common failure mechanisms of flat-bottom filled silo systems during earthquake events.

- the *effective mass*, or the portion of the overall particulate material interacting with the silo structure wall under seismic conditions and provoking additional dynamic overpressures onto the shell wall of the silo;
- the *fundamental period* (or, equivalently, the *fundamental frequency*) corresponding to the first mode of vibration of the filled silo system, due to uncertainties concerning both the above-mentioned effective mass and the lateral stiffness provided by the ensiled material.

Both aspects are of central importance for the evaluation of the earthquake actions since, in practice, the seismic design of silos is generally conducted by means of equivalent static analysis. In detail, the static horizontal forces are usually given in terms of dynamic overpressures (additional horizontal pressures with respect to the static ones) generated by the stored material onto the wall of the silo and are related to the effective mass. The ensiled content, pushing on the silo wall, tends to lean against the wall due to the particle-wall friction, exerting non-negligible actions, as reported by numerous theoretical studies and experimental research works since the end of the 19th century (Janssen, 1895; Naito, 1988; Nielsen, 1998; Vanel and Clément, 1999; Ovarlez et al., 2003; Rotter, 2008; Qadir et al., 2010; Silvestri et al., 2012; Pieraccini et al., 2015; Qadir et al., 2016; Silvestri et al., 2016; Silvestri et al., 2021). A brief review of the current provisions in standards is presented hereafter with specific reference to the two above-mentioned issues.

UBC (Uniform Building Code, 1994) provisions recommend to design ground-supported silos using the procedures for rigid structures (defined by a fundamental period of vibration smaller than 0.06 s), considering a seismic force resulting from an effective mass composed by the total mass of the silo structure and the whole content material.

ACI 313-97 (American Concrete Institute, 1997) provisions suggest that the effective mass should be estimated at 80% of the actual mass of the stored material in order to calculate the lateral seismic inertia forces. Lateral force reduction is permitted due to energy loss caused by intergranular motion and internal frictional conditions in the ensiled solid, as found by both Chandrasekaran and Jain (1968) and Harris and Von Nad (1985), which the standard expressly refers to. Moreover, the provisions highlight the necessity of rational method to evaluate the period of vibration.

EN 1998-4 (European Committee for Standardization, 2006b) provisions provide general principles and practical application rules for the earthquake design of elevated and ground-supported silos. They refer to: 1) the evaluation of the extra horizontal pressures during a seismic event onto the wall height; 2) seismic analysis methods; 3) numerical modelling of silos for seismic analysis. Silo structures are supposed to operate in the elastic field; thus, the elastic analysis of the silo shell wall is to be considered. In the absence of more accurate evaluations, global seismic response should be evaluated modelling the particulate material as an effective mass with related rotational inertia located at the center of mass based on the assumption that particulate contents move in unison with the wall. Barring a more accurate evaluation, 80% of the stored material can be assumed as activated effective mass. If the dynamic response and the mechanical properties of the particulate material are not explicitly represented and accurately considered in the analysis (by adopting adequate modelling techniques to reproduce its dynamic response and mechanical properties), the effect on the silo wall of the solid particulate's response to the horizontal component of the seismic input may be summarized in additional horizontal pressures onto the wall (leading to normal radial and tangential circumferential components). The provisions recommend structural damping ratio of 5% and contents damping ratio of 10% (in the absence of specific information). The provisions of EN 1998-4: 2006 are mainly based on: 1) the theoretical formulation by Trahair et al. (1983) proposing the dynamic overpressure exerted by the stored material under seismic excitation onto the wall and 2) the numerical study findings of Rotter and Hull (1989).

FEMA P-750 (NEHRP, 2009) provisions classify silos as "*non-building structures not similar to buildings*". They provide guidelines on the evaluation of: 1) the global horizontal seismic action on the silo, and 2) the distribution of overpressures acting on the silo wall. Only the impulsive type of global lateral seismic forces is considered due to the

TABLE 1 | Summary of the provisions in current standards.

Code	m_{eff} [%]	Δp	T	Methods of analysis
UBC (1994)	100	Not given	≤0.06 s	ELF
ACI 313-97 (1997)	80	Not given	To be predicted using a rational method	ELF
EN 1998-4 (2006)	≥80	Given	—	ELF MRS NLS NLTH
FEMA P-750 (2009)	≥50	Reference to Trahair et al. (1983)	≤0.06 s	ELF
ASCE 7-10 (2010)	—	Not given	≤0.06 s	ELF
Architectural Institute of Japan (AIJ) (2010)	≥80	Not given	0.60 s (if unknown)	ELF MRS

ELF, Equivalent Lateral Force; MRS, Modal Response Spectrum; NLS, Non-Linear Static; NLTH, Non-Linear Time History.

fundamental period of vibration of the silo itself, which is considered to be noticeably short, corresponding to the highest acceleration value from the design spectral response (in the plateau area of the spectrum). Global lateral seismic forces should be determined on the basis of an effective mass equal to the total volume weight of the filled material reduced by two multiplication factors: effective mass and density factors, where the product of those two factors should not be less than 0.5, in addition to the self-weight of the silo. Concerning the forces distribution on the silo wall and foundation, the standard suggests using the formula proposed by Trahair et al. (1983) according to the filling aspect ratio, that results in significant reductions in the effective mass for the squat silo case.

ASCE 7-10 (2010) provisions provide guidelines regarding the evaluation of: 1) the global lateral actions applied on a silo and 2) the distribution of these forces on the shell wall and foundation. The horizontal forces applied on silos are to be evaluated using a short period structure acceleration value. The effective mass is introduced as the fraction of the total stored material interacting with the silo shell during the seismic event and should be used for the evaluation of the total inertial shear force as well as the overturning moment at the base level of the silo. It is also reported that the effective mass is affected by: 1) the physical and mechanical properties of stored solids; 2) the silo filling aspect ratio; 3) the intensity of the earthquake ground motion. The shear force portion transferred to the base by the inter-granular behavior (friction) of the stored material should be considered when evaluating the value of the effective mass. However, the standard does not provide any formulae to estimate the effective mass.

Architectural Institute of Japan (AIJ) (2010) provisions mainly refer to the *impulsive mass* (i.e., the effective mass) that interacts with the silo wall at the structure's base. Owing to loss of energy triggered by the friction between the silo wall and particles as well as by the internal friction within the granular material itself, the impulsive mass is smaller than the total ensiled mass. Nevertheless, it should be considered not lower than 80% of the whole mass. Design seismic loads evaluation for the ground-supported storage silos can be performed by two methods: 1) the "modified seismic coefficient method" and 2) the classical modal analysis. The former uses the "Equivalent Lateral Force" method, assuming a value of 0.60 s for the first period of the filled silo system (if unknown), to evaluate horizontal design acceleration. The latter models the filled silo system as a cantilever beam with different point masses (lumped masses model) to evaluate the actions exerted on the structure. The standard does not provide a specific value of the damping ratio on which the parameters necessary for the two aforementioned methods are based on (S_{aj}: design acceleration response spectrum corresponding to the first natural period, D_h: coefficient determined by the radiation damping of the silo basement and depending on the area of the silo foundation).

Table 1 compares the afore-mentioned provisions highlighting the main shortcomings. In detail, for each code, **Table 1** shows: 1) the effective mass (m_{eff}) expressed as a percentage of the total mass; 2) the presence of specific formulae to estimate the horizontal overpressures (Δp) exerted on the silo wall; 3) suggested values for the fundamental period of vibration (T); 4) the proposed seismic analysis methods.

As concluding remarks on the code provisions, it is generally acknowledged that the building seismic standards are not directly applicable to agricultural/industrial facilities and storage units (Arze, 1992), such as silos. Indeed, the absence of a widely accepted theoretical framework on the dynamic response of filled silo systems highlights significant shortcomings in the existing provisions for seismic design (Brown and Nielsen, 1998; Holler and Meskouris 2006; Carson and Craig 2015). Consequently, significant scientific progress is required for a wider understanding of the topic, as acknowledged by some of the most pre-eminent researchers (Dowrick, 1988; Ayuga et al., 2001; Ayuga et al., 2005; Holler and Meskouris, 2006; Rotter, 2008) and experienced professionals (Carson and Craig, 2015) in the field.

Figure 2 conceptually summarises the differences between the state-of-art of the scientific knowledge for the filled silos systems and the frame structures. The graphical representation takes inspiration from the set theory; the idea is that the size of the oval is somehow proportional to the extent of the knowledge or the accuracy of the code provisions. The knowledge is still limited for silos and consequently the code provisions are far to be accurate and comprehensive, in contrast to the case of frame structures.

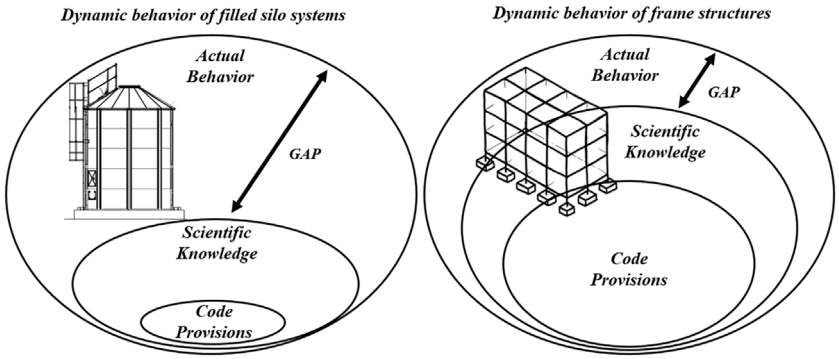

FIGURE 2 | Code provisions vs. scientific knowledge vs. actual behavior: filled silo systems vs. frame structures.

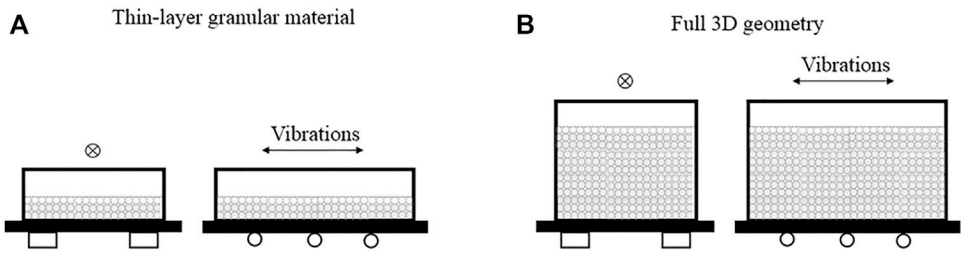

FIGURE 3 | General setup for the shaking bed test of granular material: **(A)** thin-layer; **(B)** full 3D geometry.

DYNAMIC EXPERIMENTAL TESTS ON GRANULAR MEDIA, EMPTY AND FILLED SILO SYSTEMS

This section provides a summary of the essential results from experimental investigations on the dynamic and seismic response of granular material and of cylindrical flat-bottom ground-supported silos.

Experimental Dynamic Tests on the Granular Solid

Granular material state [jammed, glassy or fluid (Raihane et al., 2009)] is highly affected by the seismic input nature and the physical/mechanical properties of the particles. Several experimental studies were developed trying to investigate the transition limits between such states in both qualitative and quantitative ways. These tests were usually conducted by imposing a harmonic motion (characterized by a certain frequency content f with a maximum acceleration amplitude a, commonly indicated in units of gravity acceleration g) at the base of a rectangular box containing granular material (**Figure 3**).

Ristow et al. (1997) tried to understand the dynamic behavior of granular solid, by studying the response of a thin 20-mm layer of Ballottini glass (with a small average diameter 0.5–0.6 mm) using a horizontal shaking apparatus (**Figure 3A**). Particles do not move at low frequencies; they begin to move as the frequency increases. Then, the granular solid showed a complete transition into a fluidized phase beyond a critical value of the frequency.

Metcalfe et al. (2002) performed an experimental study on the transition limits of the granular material under the effect of horizontal shaking (sand, glass beads). Analysis of the system evolution involved keeping the frequency constant while gradually increasing the acceleration a. A critical value of a (0.40–0.60 g) results in a loose behavior characterized by dilatation response and strong sloshing of the solid at the surface level as particles exceed friction, including a small number of "sliders" (free particles) at the surface level that move for any a value. For frequencies between 2 and 8 Hz, fluid state appears at a critical acceleration value a_{cu}. a_{cu} seemingly depends on the material's physical properties and increases for rougher particles.

Raihane et al. (2009) studied the impact of the vibrations induced by a harmonic sinusoidal input on a 3-dimensional sand granular medium (as in **Figure 3B**). The container base was subjected to widely variable frequency content range (from 20 up to 300 Hz) sinusoidal vibrations with an acceleration amplitude between 0.10 and 8.00 g. Particles movement during vibrations was monitored using ultra-fast acquisition video recording. At a given acceleration value (around 0.40 g, similar to that found in other studies), the state of granular media changes from

uniformly rigid to multi state layered over the depth, with fluidized particles at the top surface.

Dynamic Tests on Cylindrical Flat-Bottom Ground-Supported Silos

Various experimental tests were performed starting from the second half of the last century to study the dynamic behavior of ground-supported cylindrical silos and comprehend the complex interaction of shell wall and particulate material under seismic excitation. Shaking table tests were used in almost all the investigations. Different types of dynamic inputs have been commonly used: 1) white noise "random input" signals (referred to as WN), 2) impulsive loads (IL), 3) stationary "sinusoidal" harmonic signals (HS), and 4) earthquake recorded signals (EQK). Scientific literature also reports on some free vibration tests (FV).

Chandrasekaran and Jain (1968) performed the first vibrating motion tests on cylindrical containers filled with granular material. Two silos of steel and perspex were equipped with vibration transducers and strain gauges. The silos were tested in empty and different filling conditions, where the corresponding aspect ratio in the maximum filling condition h_c/d_c (h_c: filling height, d_c: silo diameter) was close to 10. Silo specimens were filled with different materials, like sand, cement and wheat. The silos were excited by means of the sudden releasing of the silo after forcing an initial displacement, allowing for free vibrations (FV) to be developed. Later, the effective mass was evaluated using a theoretical formula proposed by Chandrasekaran and Saini (1969). The effective mass values, evaluated for 25 different configurations, were found to be significantly lower than the unity (barely exceeding 50%).

Lee (1981) conducted an experimental shaking table campaign on a scaled lucite cylindrical silo (h = 1,500 mm as "silo height", d_c = 300 mm) specimen filled with sand at different filling heights (h_c). The specimen was equipped with 6 accelerometers over the wall height and several longitudinal and circumferential strain gauges. The test included free vibration tests (FV) and sinusoidal inputs (HS) to investigate: the profile of the horizontal accelerations (related to dynamic amplification) over the wall height, the equivalent damping ratio, the fundamental period of vibration, as well as the stresses experienced by the wall. It was found that the fundamental frequency of vibration decreases as the filling height increases, while the damping ratio varies with input frequency till reaching a maximum value at the resonance frequency.

Yokota et al. (1983) performed a series of shaking table tests on a scaled acrylic resin cylindrical silo ($h = d_c$ = 1,500 mm) filled with coal and instrumented with different accelerometers either on the wall or within the filled material, in addition to strain gauges and earth pressure sensors. Different configurations were considered including empty and fully filled conditions, and with/without lid/roof too. The testing program encompassed free vibration (FV) tests on the empty silo and random white noise vibration (WN) tests on the filled silo systems. The main objective of the campaign was to identify the natural frequencies, the modal shapes, the damping ratios of the silo, and the differences in the measured values of horizontal accelerations between the wall and the ensiled material. In fully filled conditions, the damping ratio was four times larger than the one obtained in the empty silo case, while the dynamic amplification factor at the top level was around 3.0 under HS excitation.

Shimamoto et al. (1984) studied the response of a silo filled with coal system through shaking table tests on four scaled PVC and steel silos (h = 1,600 mm, d_c = 1,500 mm). The specimens were instrumented with accelerometers on the wall (along the input direction) and in the middle of the filled material. The testing program was performed considering stationary sinusoidal waves (HS) and real seismic records (EQK). Under HS excitation, rigid body motion occurs for input with a much lower frequency than the fundamental one of the filled silo system and acceleration amplitude $a \leq 0.20$ g. Noticeable differences were observed in the vertical profiles (over the silo height) of the horizontal acceleration of the filled material near the wall and along the central line when the input frequency content was close to the first or the second natural silo frequencies. By introducing the real seismic records (EQK), the maximum response of the acceleration amplitude value measured from all controlled points (either on the wall or inside the filled material) was registered at the same time instant at which the maximum peak table acceleration happened; the highest dynamic amplifications noticed at the silo wall upper part were around 1–4; dynamic amplifications inside the granular material increased from the base to the solid surface, reaching an amplification factor of around 2–5.

Harris and von Nad (1985) performed shaking tests on two very slender steel silos (h = 3,050 mm, d_c = 457 and h = 1,520 mm, d_c = 203 mm) filled with sand and wheat. The silo base was welded to an elastic support frame, and a hydraulic actuator was used to apply horizontal harmonic excitation (HS). Displacement measurements at the base and at the top of the silo were registered. The tests were performed with the purpose of determining the effective mass, as the unknown quantity of the dynamic equilibrium equations with known displacements (coinciding with the recorded ones) assuming flexible bending silo response and considering the rotational and translational flexibility of the support frame. The obtained results from their approach supported the 80% effective mass rule as suggested by some standards in that period.

Sasaki and Yoshimura (1984) conducted shaking table tests on a scaled uniform mortar cylindrical silo filled with brown rice. They used a stave-silo (h = 2030 mm, d_c = 1,020 mm) constructed with blocks of mortar and confined by steel hoops, and they filled it with various materials. Empty and filled conditions of the silo model were tested. Both harmonic (HS) and seismic (EQK) tests were performed. In general, it was noticed that 1) the stored materials produced distinct changes in the vibration characteristics of the silo system, where the resonant frequency gets lowered by filling the silo; 2) the interaction between the silo wall and granular solid during a seismic event can be different due to the variation of the filled material; and 3) the maximum registered horizontal dynamic overpressure distribution was

quasi uniform over the entire height, except for an unexpected peak which was observed near the base.

Sasaki and Yoshimura (1988) performed tests on two scaled silos (h = 1985mm, d_c = 820 mm): a stave silo model obtained with mortar blocks and circumferential steel hoops, in addition to another silo model realized as a continuous uniform mortar model, in order to study the structural discontinuity effect on the actual earthquake response of the silo model. The silo specimens were filled with rice and equipped with different instrumentation: strain gauges, accelerometers, lateral pressure sensors. The tests were performed by using both sinusoidal inputs (HS) and real recorded earthquakes (EQK) (Tokachu-oki 1968 and Nemurohanto-oki 1973) in empty and full conditions. Under harmonic excitation, the presence of the ensiled material reduced the fundamental resonance frequency of the stave silo model where the effect of the joints of staves produced the degradation of stiffness. Moreover, a gradual decrease of acceleration response (amplification) factor was noticed with the increase of the peak table acceleration.

Naito (1988) reported on shaking table tests (Kawazoe et al., 1983 in Japanese) performed on a scaled steel coal silo ($h = d_c$ = 1,500 mm). The silo was equipped with accelerometers positioned over the height along the center vertical line inside the stored material, while the silo wall was instrumented by strain gauges. The base plate and silo wall rested on two different load cells to measure the global shear force at the wall base level and at the table level. Sinusoidal inputs (HS) were used to provoke and investigate resonance response of the granular material. It was found that the resonance frequency and response magnification at resonance frequency decrease with increasing excitation. Moreover, the response decreases at frequencies above the first resonance and with increasing frequency, which becomes less steep with the increment of frequency.

Holler and Meskouris (2006) reported some results of shaking table tests (performed at Saclay in France) on a scaled steel silo (h = 1,100 mm, d_c = 1,000 mm) filled with sand. The silo wall was equipped with three pressure sensors and one accelerometer placed on the table. The experimental results were used to calibrate a representative Finite Element (FE) model in order to verify load assumptions stipulated in current European standards.

Tatko and Kobielak (2008) excited a scaled flat-bottom slender silo (h = 1,200 mm, d_c = 400 mm) filled with sand with horizontal impulsive loads (IL). The silo was supported by a spring system to simulate different soil stiffness, since the main objective was to analyze the dynamic interaction between the silo structure and the soil. The specimen was instrumented by horizontal pressure sensors placed at different heights of the silo wall. Dynamic inputs were generated using a ballistic pendulum in the form of a single pulse applied horizontally to the bottom plate. Fundamental frequencies, horizontal time-pressure variation and radial overpressure vertical profiles were measured. The dynamic overpressures over the silo height are influenced by subsoil stiffness. Moreover, the distribution of the maximum dynamic pressures over wall height is nonlinear, while the overpressure value changes depending on the direction. Nonetheless, the relationship between the average lateral dynamic pressure exerted by the ensiled solid and the maximum acceleration amplitude of subsoil is nonlinear.

Silvestri et al. (2016) conducted shaking table tests on two scaled polycarbonate silos (h = 1,500 mm, d_c = 1200 mm) filled with Ballottini glass beads and equipped with an upper stiffening ring. Three different configurations were tested to account for two wall friction conditions and two aspect ratios (0.5 and 1.0). The silos were instrumented with accelerometers (on the wall along the input direction at various heights, and over three vertical lines inside the granular solid), strain gauges over the wall height and around the circumference to evaluate the internal actions in the wall and a Linear Variable Displacement Transducer to measure the lateral displacements of the upper stiffening ring. The silos were subjected to: 1) white noise (WN) excitation; 2) harmonic excitation (HS), and 3) recorded earthquakes (EQK). Natural frequencies were evaluated from WN tests. The main purpose of the tests was to experimentally verify the analytical model proposed by Silvestri et al. (2012) for the estimation of the peak global forces at the silo base (shear force and overturning moment). The findings showed that the particle-wall friction influences the wall base overturning moment and the effective mass for the squat silo is considerably lower than 80%.

Recently, Silvestri et al. (2021) performed a large experimental campaign of shaking table tests on a full-scale flat-bottom steel manufactured silo (h = 5,500 mm, d_c = 3,640 mm) characterized by a horizontally corrugated wall profile, open C hat-shaped vertical stiffeners and a paneled conically shaped roof. The filling material was soft wheat achieving an aspect ratio of around 0.9, corresponding to a squat silo case according to EN 1991-4:2006 classification. The filled silo system was tested under two base conditions: fixed and seismically isolated (**Figure 4**). The testing program included white noise signals (WN), low-frequency (0.5 and 1 Hz) sinusoidal signals (HS), and three earthquake records (EQK): an artificial earthquake record, a real "far-from-resonance frequency content" input, and a second real "close-to-resonance frequency content" input. The main findings are summarized hereafter: *"The damping ratio increases with increasing acceleration (enhanced frictional dissipative mechanisms associated to relative sliding of granular particles) … [omissis] … The resonance frequency … [omissis] … slightly decreases with increasing acceleration (increasing of damping ratio and larger effective mass) and it slightly increases with increasing compaction (higher stiffness provided by the granular material). No significant dynamic amplification was observed for the whole filled silo system (both the silo wall and the ensiled granular material) for low-frequency sinusoidal inputs. For the most demanding earthquake input (in terms of close-to resonance frequency content), the dynamic amplification factor increased along the silo wall height up to values around 1.4 at the top surface of the solid content [omissis] … The measured dynamic overpressures seemed to increase slightly more than linearly with depth from the top to the bottom."*

General Observations

The previous section introduced the main available experimental studies (see **Table 2** for a detailed comparison of their main findings) on the dynamic behavior of filled silo systems in the literature. It can be noticed that the majority of the experimental campaign was conducted during the 1980s. After then, the rate of interest became less mainly due to the technical difficulties and

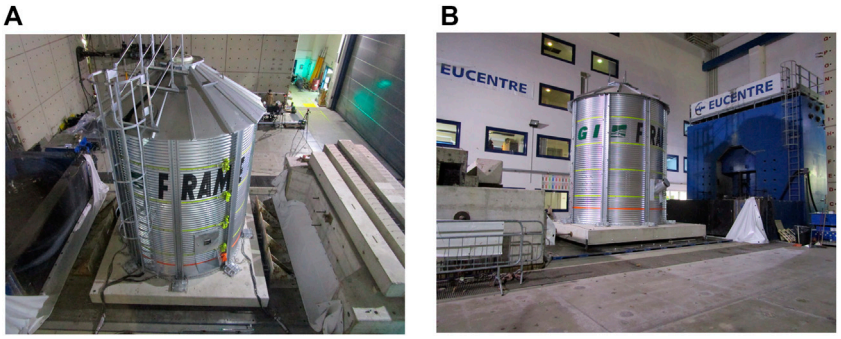

FIGURE 4 | The tested flat-bottom steel silo of the SERA-SILOS project (Silvestri et al., 2021): **(A)** fully restrained and **(B)** seismically isolated.

the expensive costs, even if the academic focus on this field could not give definite answers leaving various open issues. Nevertheless, the main remarks from the above summarized experimental works are:

1- The nature of the dynamic base excitation, the frequency content and the peak acceleration values have a strong impact on the dynamic response of the filled silo system. This is caused by the non-steady state of the stored granular material depending on the input properties (e.g., a granular material characterized by high intergranular friction properties and high particle-wall friction coefficient typically leads to a relatively high damping ratio and a high activated portion of the stored material as an effective mass) that leads to a non-linear response of the filled silo system.
2- The effective mass was evaluated using different methods, which might affect the reliability of the results (analysis of the variation of the frequency between empty and filled silos, or interpretation of the dynamic overpressure measurements, or global assessment evaluation of the overturning bending moment at the silo base). Moreover, it resulted to be influenced by the input properties. For instance, a high effective mass was always obtained as a result of the application of an input with a frequency content close the resonance of the filled silo system.
3- The acceleration measurements recorded by the accelerometers placed along the centerline of the stored material showed higher amplification factors than those recorded from the monitored points over the silo wall height.
4- In most cases, the small size of the adopted scaled silo models was not suitable to account for the role of the vertical stiffeners. In addition, the effect of the silo roof on the silo system response was included only in few works.

THEORETICAL STUDIES AND NUMERICAL MODELLING ON THE DYNAMIC BEHAVIOR OF FILLED SILO SYSTEMS

This section provides a summary of the theoretical studies and numerical modelling techniques presented in the scientific literature for the estimation of the dynamic behavior of ground supported cylindrical silos.

Analytical Models

Yang (1976) and Haroun (1980) studied the dynamic behavior of a liquid-filled cylindrical shell. Although focusing on liquid storage containers, the works provided a novel analytical method for evaluating the fundamental period of cylindrical storage tanks. The tank wall was modelled as a uniform linear-elastic cantilever beam, considering both shear and flexural deformations when determining the vibration properties of the liquid-filled shell system. The entire liquid mass was considered rigidly attached to the tank wall to determine the fundamental period of vibration.

Lee (1981) proposed an analytical model to estimate the effective mass of ground-supported cylindrical silos subjected to harmonic base excitation. More specifically, the effective mass is obtained from the variation of the fundamental frequency of vibration in empty and full conditions. The analytical framework includes the following hypotheses: 1) the stored material does not provide any additional stiffness to the equivalent system; 2) the participating mass of the equivalent system in the motion consists of the wall mass plus the activated portion of stored material under seismic excitation; 3) the filled silo system behaves like a uniform flexible cantilever beam in terms of the distribution of mass, inertia and material. The analytical framework is based on the works by Chandrasekaran and Saini (1969) and Chandrasekaran and Jain (1968).

Trahair et al. (1983) proposed the first analytical simple formulae to estimate the distribution of the dynamic overpressures (additional with respect to the static pressures) depending on the filling height of the content; two categories of ground-supported structures were identified (squat and slender) depending on the aspect ratio. The analytical model was first proposed for the rectangular silo and then extended to the case of the circular one. A uniform static horizontal body force corresponding to a time-constant acceleration was considered. For the slender silo, the model assumes a total mass participation, reflected in a uniform overpressure profile along the height of the silo wall. For the squat silo, the activated mass is lower than the total one depending on the filling height. The formulation does

TABLE 2 | Summary of the main experimental results of dynamic tests on filled silo systems found in the scientific literature.

References	Specimen silo properties						Input			Main results		
	Scaling factor	Wall material	Filling height h_c (mm)	Silo diameter d_c (mm)	Aspect ratio h_c/d_c (-)	Ensiled material	Type	Acceleration a (g)	HS frequency f (Hz)	Effective mass m_{eff} (-)	Fund. frequency f_1 (Hz)	Damping ratio ξ (%)
Chandrasekaran and Jain (1968)	—	Perspex	—	—	5.3–10.6	Sand, cement, wheat,	FV	—	—	0.22–0.48	—	—
	—	Steel	—	—	4.9–9.8	aggregate	FV	—	—	0.27–0.54	—	—
Lee (1981)	3:5	Lucite	1,500	300	empty	—	HS/FV	0.5	15	0	26	3
					1.3	Sand				0.04	23	6
					2.5					0.18	14	9
					3.8					0.46	8	5
					5.0					0.68	6	3
Yokota et al. (1983)	—	Acrylic resin	1,500	1,500	empty	—	FV				76	4
					1.0	Coal	WN	0.05	—	—	19	10
Shimamoto et al. (1984)	3:80	PVC resin	1,600	1,500	1.0	Coal	HS/EQK	0.1–0.3	5–45	—	14–21	—
	3:80	Steel	1,600	1,500	1.0		HS/EQK	0.1–0.3	5–45	—	23	—
Harris and Von Nad (1985)	—	Steel	3,050	457	6.7	Sand, wheat	HS	—	1–9	0.60–0.90	—	—
	—		1,520	203	7.5		HS	—	1–9	0.58–0.85	—	—
Sasaki and Yoshimura (1988)	1:8	Stave/shell	1985	820	empty	—	HS/EQK	0.3–1.0	5–50	—	31–46	—
					1.9	Rice	HS/EQK	0.1–1.0	5–50	—	19–30	—
Naito (1988) Kawazoe et al. (1983)	—	Steel	1,500	1,500	1.0	Coal	HS	0.02–0.2	—	—	15–20	—
Tatko and Kobielak (2008)	—	Steel	1,200	400	3.0	Coarse sand	IL	0.06–0.23	—	—	—	—
Silvestri et al. (2016)	—	Polycarbonate (smooth)	1,200	1,200	empty	—	WN	0.1	—	—	30–35	1–4
					1.0	Ballottini glass	WN/HS/EQK	0.05–0.55	1–2	0.32	14	6–21
		Polycarbonate (roughened)	600 and 1,200		0.5–1.0	Ballottini glass	WN/HS	0.05–1.20	1–2	0.43	16	10
Silvestri et al. (2021)	1:1	Steel (corrugated wall)	3,300	3,640	0.9	Soft wheat	WN/HS/EQK	0.05–0.6	0.5–8	—	10–12	5–25

not account for the shear stresses developed along the particle-wall interface (Rotter and Hull 1989).

Younan and Veletsos (1998) and Veletsos and Younan (1998) investigated the response of cylindrical containers characterized by both rigid and flexible vertical walls, and filled with homogeneous, linear, viscoelastic media under dynamic excitation, with the following fundamental assumptions: 1) the container with the filled material is modelled by a cantilever shear-beam (identified with a natural frequency); 2) the entire mass of the viscoelastic material dynamically interacts with the cylinder shell; 3) the sliding of the contained material with respect to the base is not allowed. The dynamic response of the filled container system was described in terms of vertical and radial modes. The fundamental circular frequency of the system depends on the stored material physical and mechanical properties, wall roughness, frictional interfaces conditions and slenderness ratio of the silo. The natural frequencies of the equivalent model are not affected by the wall mechanical properties. *"For liquid-containing flexible tanks, the effective mass is effectively equal to or only somewhat smaller than that for the corresponding rigid tanks, whereas the amplification factor AF may be substantially larger than the unit value appropriate for rigid tanks. By contrast, for solid-containing flexible tanks, not only is the effective mass significantly smaller than for the corresponding rigid tanks, but the AF, . . . [omissis] . . ., is of the same order of magnitude as, or substantially higher than, for the corresponding rigid tanks"*. Due to these opposite effects regarding effective mass and amplification factor, *"the critical responses of the solid-containing systems may be higher than, equal to, or lower than those induced in tanks of the same dimensions by liquids of the same density"*.

Silvestri et al. (2012) extended the Janssen (1895) and Koenen (1896) static model to derive analytical formulae for the additional dynamic overpressures provoked by the stored material on the wall of flat-bottom silos. The first analytical theory, later refined by Pieraccini et al. (2015), was developed for "*an idealized system of a cylindrical silo filled with an incompressible compacted material under idealized dynamic conditions such as a time-constant acceleration input*". The proposed theoretical model considers the particle-wall friction coefficient, as well as the potential sliding of the contained material with respect to the base. The model subdivides the filled material into a central portion transfering its inertial forces directly to the ground by means of base friction, and an effective mass interacting with the silo wall. For shallow filled silo systems (commonly classified as "squat"), the model predicts a noticeably smaller activated portion of the material than the entire mass.

Durmuş and Livaoglu (2015) presented analytical formulae to estimate the fundamental period of vibration of a filled silo system. The formulae are derived assuming an equivalent Single-Degree-Of-Freedom (SDOF) model as an inverted pendulum fixed at the bottom with a top lumped mass, corresponding to a cantilever beam with flexural response. The stored material is treated as an elastic homogeneous medium. The overall mass of the model accounts for the self-weight of the silo and 2/3 of the entire solid weight (reduced according to the ACI 371R-98). The equivalent lateral stiffness of the model is provided by the silo wall section (flexural stiffness) and the interacting portion of the confined granular particles.

Numerical Simulations

Yokota et al. (1983) built a linear Finite Element (FE) representative model of the silo specimen in empty and filled-with-coal conditions, to interpret the experimental results of the tests described in *Dynamic Tests on Cylindrical Flat-Bottom Ground-Supported Silos*. The empty container was modeled as a shell structure with cylindrical shape using 26 linear elements, while the filled one consisted of 253 triangular-shaped axisymmetric elements. The stored material was modeled as a multi-layered element with different elastic moduli (Young's modulus decreases going from the bottom to the top surface) to consider the effects of the corresponding confining pressure and strain level at each elevation as resulted from dynamic triaxial tests. On one hand, the first natural frequency obtained from the analytical results of the empty silo case moderately exceeded the experimental value, whilst the analytical and experimental frequency values resulted closer for the higher modes. On the other hand, the filled model gave close frequency values for the first two modes of vibration, whilst the gap was larger for the higher modes.

Shimamoto et al. (1984) developed a FE model of the tested silos using shell elements with a conical shape. The stored coal was modelled using non-linear asymmetric solid elements. Cyclic triaxial tests were performed on coal samples for the experimental assessment of the mechanical properties (shear modulus) of the coal material. The dependency of the coal's dynamic properties on the experimental strain was considered through the application of the equivalent linear analysis method, which was originally developed by Schanable et al. (1972). Numerically simulated and experimental results were compared for two peak acceleration values (a = 0.03 and 0.10 g). The developed model was able to well capture the resonance frequency in both cases, and also to reproduce the dynamic amplification effects for the lower acceleration value, but not for the higher acceleration value, due to particles sliding phenomena that occurred after exceeding an acceleration limit.

Naito (1988) studied numerically the non-linear behavior of filled silo systems under dynamic conditions. Solid axisymmetric elements were used to build the FE model for both the cylindrical wall and the silo content. The mechanical properties of the stored material (coal) were selected on the basis of elastic wave velocity diagnosing method for different confining pressure conditions. The proposed numerical model was verified by comparing the obtained results with shaking table results.

Rotter and Hull (1989) simulated the seismic response of a cylindrical silo filled with granular material in shallow filling condition corresponding to a "squat" aspect ratio. The FE model considered an axisymmetric body assuming the elastic response of both the cylindrical silo wall and the particulate material under dynamic excitations. The dynamic input consisted of a uniform lateral acceleration without accounting for any amplification over the height. The simulation assumed no vertical slipping phenomena between the silo wall and adjacent particles and

replicated their synchronized movement. The roof was ignored because it provided negligible effects in containing the wall upper part displacements. The base of the silo wall was fixed, and the particle-wall interface was ideally rough. The membrane stresses in the wall were examined by performing a parametric study accounting for the variation in different geometrical aspects and material properties. The findings indicated that stresses increase with increasing filling condition from "squat" to "slender" (with a stable value in case of slender silos) and with increasing radius-to-wall thickness ratio.

Sasaki and Yoshimura (1992) reproduced numerically the dynamic testing conditions of a 1:8 scaled model ($h_c/d_c \approx 2.0$) of a stave-silo reported in previous research works (Sasaki and Yoshimura, 1984; Sasaki et al., 1986; Sasaki and Yoshimura, 1988), i.e., a rice-filled silo characterized by structural discontinuities. The silo wall was modelled using a so-called "stave silo element", using the shell element theory to account for the stiffness provided from the shell. The participation of the granular material in the seismic interaction was assured by using a "fictitious mass density" giving an effective mass of 0.70 to fit the resonance curves from the experimental tests.

Holler and Meskouris (2006) developed a numerical model to study the dynamic behavior of filled silo systems based on the assemblage of the filled material, the wall of the silo, the wall-particle friction interface, the silo foundation, as well as the surrounding soil to consider Soil-Structure-Interaction effects. Elastic shell elements were adopted to model the silo wall. The filled material nonlinearity was considered by assigning a hypoplastic behavior to the representative solid elements. The frictional interface of the material particles with the wall was modelled by means of contact elements preserving the essential geometrical compatibility between the structure and content. The model was calibrated on the basis of reported results of shaking table test, so that it was able to capture the dynamic overpressure profile exerted by the stored material. The modelling approach was applied to the cases of steel slender and squat silos and allowed the comparison of the obtained radial and circumferential dynamic overpressures with the theoretical predictions suggested by prEN 1998-4 (CEN 2003b). The numerical findings highlighted that, for the squat case, the inertia force corresponding to a considerable fraction of the total filled material is transmitted directly to the ground by means of the particle-base friction, resulting in the theoretical overestimation of the dynamic overpressure by the European standard for this slenderness category.

Lately and due to the lack of the experimental comparable results for full-scale models, the research trend was drifted towards the numerical investigation of the filled silo system behavior. Different shell and solid elements were implemented to simulate the container and the content behavior in linear and non-linear conditions, and different techniques were applied to model the friction interface between the main granular solid and silo flat wall (Nateghi and Yakhchalian, 2011; Nateghi and Yakhchalian, 2012; Jagtap et al., 2015; Livaoğlu and Durmus, 2015; Guo et al., 2016; Livaoğlu and Durmuş, 2016; Katsanos et al., 2018). The differences of the modelling techniques and assumptions have strong impact on the outcomes of these works.

General Observations

The theoretical studies, either accompanied or not by experimental validation, aim usually at investigating the suitability of the Single Degree Of Freedom model to approximate the dynamic behavior of the filled/empty silo system. Furthermore, a clear effort was devoted to the effect of the filling aspect ratio on the seismic behavior (Trahair et al., 1983; Silvestri et al., 2012; Pieraccini et al., 2015); in this respect, the reduction of the effective mass was identified for squat silos. In addition, various numerical modelling attempts were performed to reproduce the real silos conditions which showed some promising results despite the strong assumptions on the granular solid behavior and the various interfaces conditions. The main shortcomings of these works can be associated with neglecting the effect of the intergranular friction through modelling the granular solid as a solid layer, beside neglecting the effect of the possible sliding of the particles over the base when exceeding a certain input magnitude limit (acceleration) corresponding to the friction coefficient of the stored particles with base material. Moreover, the adopted numerical models considered always simple silos with a flat wall section in order to reduce the computation cost, which leaves many uncertainties by not accounting for the effect of the vertical stiffeners and the connection details (e.g., base plate connections, roof details, sheet overlapping areas and the bolted connection between the sheets and the stiffeners) on the system response or even the variant corrugated wall sections as well.

Table 3 shows a summary of the essential characteristics of the previously introduced numerical research works.

FUTURE RESEARCH CHALLENGES

The dynamic response of filled silo systems is different from the one of any other type of structures due to the complicated nature of the components and the potential interaction conditions varying in accordance with filling aspect ratios, and physical and mechanical properties of the stored material. Therefore, a careful planning for future research is indeed necessary, especially for the experimental studies which are fundamental to verify analytical and numerical models. Many unexpected problems may arise either related to the testing conditions or to the functionality of the instrumentations (the technical difficulties may increase with the use of corrugated walls, vertical stiffeners and paneled roof). Advancements in the analytical models are still necessary to fill the gap concerning reliable formulae for the estimation of the fundamental frequency and the effective mass. Finally, numerical results are very sensitive to the modelling techniques and input parameters, where it is very hard to develop a representative model capable of giving trustworthy results. Thus, potential developments in the future should consider different aspects as detailed below, either experimentally or theoretically.

In the experimental field:

1- The *frictional properties* of the ensiled granular material may change from static conditions (silo at rest) to dynamic conditions (seismic excitation, filling and discharging).

TABLE 3 | Summary of the main characteristics in the cited numerical studies found in scientific literature.

References	Modelling techniques				Analyzing method	Motivation	Experimental validation (Yes/No)
	silo wall	Ensiled material	Particle-wall interface	SSI			
Yokota et al. (1983)	LE shell	LE solid	—	—	M	natural frequencies	Y
Shimamoto et al. (1984)	LE shell	NLE solid	—	—	ELS	resonance curves	Y
Naito (1988)	LE shell	NLE solid	—	—	ELS	resonance curves	Y
Rotter and Hull (1989)	LE shell	LE solid	—	—	PS	wall stresses	N
Sasaki and Yoshimura (1992)	LE shell	-	—	—	TH	resonance curves	Y
Hardin et al. (1996)	LE shell	NLE solid	—	—	ELS	seismic response	N
Holler and Meskouris (2006)	LE shell	HP solid	contact element	yes	TH	wall pressures	Y
	LE shell	LE solid	—	yes	M	natural frequencies	N
	LE shell	-	—	—	ELS	wall stresses	N

LE, Linear Elastic; NLE, Non-Linear Elastic; HP, Hypo-Plastic; M, Modal; ELS, Equivalent Linear Static; PS, Pseudo-Static; TH, Time-History.

Different friction coefficients may lead to considerably different overpressures.

2- The effects of the *wall corrugation* on the particle-wall effective friction coefficient and on the global dynamic and seismic response of the filled silo system have to be still fully understood. Furthermore, the loads transferred by means of the vertical stiffeners to the ground should be assessed. That would allow to expand the current knowledge on the effects of the flat and corrugated wall sections, in terms of captured vertical forces, from the static to the seismic conditions.
3- The actual after-filling conditions on the dynamic response should be better considered, mainly in terms of the obtained *eccentricity of the top pile*, since the current standards account for it in static conditions only after exceeding a certain limit.
4- The difference in terms of *dynamic amplification* captured in the granular material between the centerline of the whole granular volume and the near-wall position should be understood. It is thus suggested monitoring those locations carefully by using 3-axial accelerometers and pressure cells, in order to understand the relationships between the measured accelerations and the provoked dynamic overpressures.
5- A critical point is also represented by the full understanding of the dependence of the overpressure distribution and effective mass on the different *filling heights* and thus on different *aspect ratios*.
6- The effect of the *base roughness* should be considered, to understand the possible movement of the granular mass as solid mass under high magnitude seismic input conditions.
7- The effect of the *vertical component* of the seismic input should be also accounted for in future studies.

In the theoretical field:

1- An *overall theoretical framework* is still missing which accounts for the effects of frictional properties of the granular material, the aspect ratios, the input acceleration level, etc.
2- The local distribution of the *dynamic overpressure* components along the section circumference and over the silo height should be further assessed, allowing for more robust design formula since the majority of the analytical studies assume uniform distribution of overpressures and the majority of the standards do not approach this problem.
3- A reliable formula for the prediction of the *fundamental frequency* of the filled silo system is needed, in which the *effective mass* would play a fundamental role as well as the effect of the additional stiffness provided by the granular material. Although this issue was already faced in some previous works, major differences were noticed in terms of the considered behavior of the equivalent SDOF model assumed for the filled silo system.

In conclusion, research advances in the field are urgently needed. Otherwise, in the lack of a full understanding, the solution would be represented by a design-oriented approach which must consider larger safety factors, as suggested by Carson (2001).

CONCLUSION

This paper reviews the main steps of the historical developments of research work in the field of the dynamic and seismic behavior of flat-bottom filled silo systems. A comprehensive summary of the essential experimental, theoretical and numerical studies since the 1960s has been reported, highlighting the main findings along with the open issues still to be investigated.

The challenging side of such a topic is deeply related to the nonlinear behavior of the granular material due to the non-stable friction conditions varying with the input type and pressure level, as well as the complicated interaction with the silo structure considering different possible interfaces (flat or corrugated wall section).

Despite the considerable number of the performed experimental works in the last decades, it is not surprising that the main outputs helped only underlining the main aspects of the system behavior, treating some topics like the dynamic overpressure qualitatively and leaving the quantitative assessment as an unresolved matter. However, the experimental findings related to the fundamental frequency and the corresponding equivalent damping ratio are of a great importance. Furthermore, many theoretical studies were developed in parallel with the experimental ones looking for a more mature understanding of the problem.

Finally, it must be highlighted that the performed research studies are not capable of providing definite answers yet. That is reflected through the absence of a universally accepted theoretical framework to predict the seismic response of the filled silo system, hence the lack of design formulae in almost all the standards. Thus, additional research is necessary to address the unresolved issues by proposing efficient analytical models, mainly related to the estimation of the fundamental frequency and the effective mass of the filled silo system.

AUTHOR CONTRIBUTIONS

All authors listed have made a substantial, direct, and intellectual contribution to the work and approved it for publication. Collection of Data: LP and SM. Writing–Original Draft: LP, MP, and SM. Visualization: LP, MP, and SM. Writing–Reviewing and Editing: SM, SS, and GG. Resources: DF and SS. Supervision: TT and SS.

REFERENCES

American Concrete Institute (ACI) (1997). *Standard Practice for Design and Construction of concrete Silos and Stacking Tubes for Storing Granular Materials and Commentary*. Farmington Hills, MI: American Concrete Institute. ACI 313-97/313-R97.

ANSI/ASAE S433.1 (2019). Loads Exerted by Free-Flowing Grain on Bins. Available at: https://www.scribd.com/document/365669904/ANSI-ASAE-EP433-Loads-Exerted-by-Free-Flowing-Grain-on-Bins.

Architectural Institute of Japan (AIJ) (2010). *Design Recommendation for Storage Tanks and Their Supports with Emphasis on Seismic Design*. Tokyo, Japan: AIJ.

Arze, E. (1992). "Seismic Deisgn Practices of Industries," in *Earthquake Engineering, Proceedings of the Tenth World Conference*. Editor A. Bernal (Rotterdam: Balkema), 5019–5023.

Arze, E. (1993). Seismic Design of Industrial Facilities. *Tectonophysics* 218, 23–41. doi:10.1016/0040-1951(93)90257-K

ASCE-7 (2005). *Chapter 15. Seismic Design Requirements for Nonbuilding Structures*. Reston, VA: ASCE Library. doi:10.1061/9780784408094

Augenti, N., Nanni, A., and Parisi, F. (2013). Construction Failures and Innovative Retrofitting. *Buildings* 3 (1), 100–121. doi:10.3390/buildings3010100

Ayuga, F., Aguado, P., Gallego, E., and Ramírez, Á. (2005). New Steps towards the Knowledge of Silos Behaviour. *Int. Agrophysics* 19 (1), 7–17.

Ayuga, F., Guaita, M., and Aguado, P. (2001). SE-structures and Environment. *J. Agric. Eng. Res.* 78 (3), 299–308. doi:10.1006/jaer.2000.0640

Brown, C. J., and Nielsen, J. (1998). *Silos: Fundamentals of Theory, Behavior and Design*. Florida, United States: CRC Press.

Carson, J., and Craig, D. (2015). Silo Design Codes: Their Limits and Inconsistencies. *Proced. Eng.* 102, 647–656. doi:10.1016/j.proeng.2015.01.157

Carson, J. W. (2001). Silo Failures: Case Histories and Lessons Learned. *Handb. Powder Technol.* 10, 153–166. doi:10.1016/S0167-3785(01)80017-8

Chandrasekaran, A. R., and Jain, P. C. (1968). Effective Live Load of Storage Materials under Dynamic Conditions. *Indian Concrete J.* 42 (9), 364–365.

Chandrasekaran, A. R., and Saini, S. S. (1969). Live Load Effect on Dynamic Response of Structures. *J. Struct. Div.* 95 (4), 649–660. doi:10.1061/JSDEAG.0002243

Dogangun, A., Karaca, Z., Durmus, A., and Sezen, H. (2009). Cause of Damage and Failures in Silo Structures. *J. Perform. Constr. Facil.* 23 (2), 65–71. doi:10.1061/(asce)0887-3828(2009)23:2(65)

Dowrick, D. J. (1988). Edgecumbe Earthquake. *Bnzsee* 21 (3), 198–203. doi:10.5459/bnzsee.21.3.198-203

Durmuş, A., and Livaoglu, R. (2015). A Simplified 3 D.O.F. Model of A FEM Model for Seismic Analysis of a Silo Containing Elastic Material Accounting for Soil-Structure Interaction. *Soil Dyn. Earthquake Eng.* 77, 1–14. doi:10.1016/j.soildyn.2015.04.015

European Committee for Standardization (2006a). *EN 1991-4 Eurocode 1. Actions on Structures, Part 4 -Silos, Tanks and Pipelines*. Brussels: CEN.

European Committee for Standardization (2007). *EN 1993-4 Eurocode 3. Design of Steel Structures - Part 4-1: Silos*. Brussels: CEN.

European Committee for Standardization (2006b). *EN 1998-4 Eurocode 8. Design of Structures for Earthquake Resistance, Part 4 -Silos, Tanks and Pipelines*. Brussels: CEN.

Fierro, E., Miranda, E., and Perry, C. "Behavior of Nonstructural Components in Recent Earthquakes," in Proceedings of the Architectural Engineering Conference (AEI), Oakland, California, United States, March-April 2011, 235–243. doi:10.1061/41168(399)44

Gioncu, V., and Mazzolani, F. M. (2014). *Seismic Design of Steel Structures*. Florida, United States: CRC Press. ISBN 9781138075375.

Griffin, M. J., Bragagnolo, L. J., and Yanev, P. I. (1995). The December 7,1988 Armenia Earthquake Effects on Selected Power, Industrial and Commercial Facilities. Available at: https://inis.iaea.org/collection/NCLCollectionStore/_Public/30/052/30052386.pdf.

Grimaz, S. (2014). Can Earthquakes Trigger Serious Industrial Accidents in Italy? Some Considerations Following the Experiences of 2009 L'Aquila (Italy) and 2012 Emilia (Italy) Earthquakes. *Boll. di Geofis. Teor. Ed. Appl.* 55 (1), 227–237. doi:10.4430/bgta0116

Grossi, P., Williams, C., Cabrera, C., Tabucchi, T., Sarabandi, P., Rodríguez, A., et al. (2010). *The 2010 Maule, Chile Earthquake: Lessons and Future Challenges*. Newark, California, United States: Risk Managed. Solutions. Inc., 1–46.

Guo, K., Zhou, C., Meng, L., and Zhang, X. (2016). Seismic Vulnerability Assessment of Reinforced concrete Silo Considering Granular Material-Structure Interaction. *Struct. Des. Tall Spec. Build* 25 (18), 1011–1030. doi:10.1002/tal.1295

Hardin, B. O., Bucklin, R. A., and Ross, I. J. (1996). Shear-Beam Analysis for Seismic Response of Metal Wheat Bins. *Transact. ASAE* 39 (2), 677–687. doi:10.13031/2013.27552

Haroun, M. (1980). "Dynamic Analysis of Liquid Storage Tanks - EERL,". Report, 80-04 (Pasadena, CA: California Institute of Technology). doi:10.7907/1JZR-HK48

Harris, E. C., and von Nad, J. D. (1985). Experimental Determination of Effective Weight of Stored Material for Use in Seismic Design of Silos. *ACI J. Proc.* 82 (6), 828–833.

Holler, S., and Meskouris, K. (2006). Granular Material Silos under Dynamic Excitation: Numerical Simulation and Experimental Validation. *J. Struct. Eng.* 132 (10), 1573–1579. doi:10.1061/(asce)0733-9445(2006)132:10(1573)

Jagtap, P., Chakraborty, T., and Matsagar, V. (2015). Nonlinear Dynamic Behavior of Granular Materials in Base Excited Silos. *Mech. Adv. Mater. Structures* 22 (4), 313–323. doi:10.1080/15376494.2014.947821

Janssen, H. A. (1895). Versucheübergetreidedruck in Silozellen. *Z. Ver. Dtsch. Ing.* 39 (35), 1045–1049.

Katsanos, E. I., Tuska, M., and Latini, C. "Ida-based Definition of Damage States for Rc Silo Subjected to Seismic Excitations," in Proceedings of the 16th European Conference on Earthquake Engineering, Thessaloniki, Greece, June 2018, 1–12.

Kawazoe, H., et al. (1983). Shaking Table Tests and Simulation of a Coal Silo. *Ann. Rep. Kajima Instit. Construct. Technol.* 31, 127–134.

Koenen, M. (1896). Berechnung des Seiten-und Bodendrucks in Silozellen. *Centralblatt der Bauverwaltung* 16, 446–449.

Lee, S. J. (1981). "Experimental Study of Cylindrical Silos Subject to Seismic Excitation,". PhD thesis (Ohio: The Ohio State University).

Li, H. (1994). "Analysis of Steel Silo Structures on Discrete Supports,". PhD thesis (Edinburgh: The University of Edinburgh). Available at: http://hdl.handle.net/1842/289.

Livaoglu, R., and Durmuş, A. (2016). A Simplified Approximation for Seismic Analysis of Silo-Bulk Material System. *Bull. Earthquake Eng.* 14 (3), 863–887. doi:10.1007/s10518-015-9851-x

Livaoğlu, R., and Durmuş, A. (2015). Investigation of wall Flexibility Effects on Seismic Behavior of Cylindrical Silos. *Struct. Eng. Mech.* 53 (1), 000. doi:10.12989/sem.2015.53.1.159

Metcalfe, G., Tennakoon, S. G. K., Kondic, L., Schaeffer, D. G., and Behringer, R. P. (2002). Granular Friction, Coulomb Failure, and the Fluid-Solid Transition for Horizontally Shaken Granular Materials. *Phys. Rev. E* 65 (3), 1–15. doi:10.1103/PhysRevE.65.031302

Naito, Y. "Equivalent Linear Technique in the Finite Element Method Applied to Deformation with Volume Change and to an Axisymmetric Body under an

Unaxisymmetric Load," in Proceedings of the 9th World Conference on Earthquake Engineering, Tokyo-Kyoto, Japan, August 1988, 133–138.3

Nateghi, F., and Yakhchalian, M. (2011). Seismic Behavior of Reinforced concrete Silos Considering Granular Material-Structure Interaction. *Proced. Eng.* 14, 3050–3058. doi:10.1016/j.proeng.2011.07.384

Nateghi, F., and Yakhchalian, M. (2012). Seismic Behavior of Silos with Different Height to Diameter Ratios Considering Granular Material-Structure Interaction. *Ije* 25, 25–35. doi:10.5829/idosi.ije.2012.25.01b.04

NEHRP (2009). *Recommended Seismic Provisions for New Buildings and Other Structures*. Washington D.C: FEMA P750.

Nielsen, J. (1998). Pressures from Flowing Granular Solids in Silos. *Philos. Trans. R. Soc. Lond. Ser. A: Math. Phys. Eng. Sci.* 356, 2667–2684. doi:10.1098/rsta.1998.0292

Ovarlez, G., Fond, C., and Clément, E. (2003). Overshoot Effect in the Janssen Granular Column: A Crucial Test for Granular Mechanics. *Phys. Rev. E* 67 (6), 060302/1–060302/4. doi:10.1103/PhysRevE.67.060302

Pieraccini, L., Silvestri, S., and Trombetti, T. (2015). Refinements to the Silvestri's Theory for the Evaluation of the Seismic Actions in Flat-Bottom Silos Containing Grain-like Material. *Bull. Earthquake Eng.* 13 (11), 3493–3525. doi:10.1007/s10518-015-9786-2

Qadir, A., Guo, H., Liang, X., Shi, Q., and Sun, G. (2010). Effect of the Ratios of Diameter of Silo to Bead on the Pressure Screening in Granular Columns. *Eur. Phys. J. E* 31 (3), 311–314. doi:10.1140/epje/i2010-10581-7

Qadir, A., Ispalove, N., Ali, A., Chand, R., Shah, M. A., Khan, A., et al. (2016). Experimental and Numerical Determination of Apparent Mass Variation of Granular media Confined in Silo Geometry. *Acta Phys. Pol. A.* 129 (3), 378–382. doi:10.12693/APhysPolA.129.378

Raihane, A., Bonnefoy, O., Gelet, J.-L., Chaix, J.-M., and Thomas, G. (2009). Experimental Study of a 3D Dry Granular Medium Submitted to Horizontal Shaking. *Powder Technol.* 190 (1), 252–257. doi:10.1016/j.powtec.2008.04.068

Ristow, G. H., Straßburger, G., and Rehberg, I. (1997). Phase Diagram and Scaling of Granular Materials under Horizontal Vibrations. *Phys. Rev. Lett.* 79 (5), 833–836. doi:10.1103/PhysRevLett.79.833

Rotter, J. M., and Hull, T. S. (1989). Wall Loads in Squat Steel Silos during Earthquakes. *Eng. Structures* 11 (3), 139–147. doi:10.1016/0141-0296(89)90002-3

Rotter, J. (2008). "Structures, Stability, Silos and Granular Solids," in *Structures, Stability, Silos and Granular Solids: A Personal Adventure Structures and Granular Solids: From Scientific Principles to Engineering Applications*. Editors J. F. Chen and J. G. Teng (Florida, United States: CRC PRESS-TAYLOR and FRANCIS GROUP), 1–17. doi:10.1201/9780203884447.ch1

Sasaki, Y., and Yoshimura, J. (1984). "Dynamic Behavior of concrete Stave Silos," in *Proceedings of the 8th World Conference on Earthquake Engineering* (Hoboken, New Jersey, United States: Prentice-Hall).

Sasaki, Y., and Yoshimura, J. (1992). "Dynamic Discrete Modeling and Computer Simulation of Seismic Response of concrete Stave Silos with Structural Discontinuity," in *Earthquake Engineering, Proceedings of the Tenth World Conference* (Rotterdam: Balkema), 5065–6070.

Sasaki, Y., and Yoshimura, J. "Seismic Response of Concrete Stave Silos with Structural Discontinuity," in Proceedings of the Ninth World Conference on Earthquake Engineering, Tokyo-Kyoto, Japan, August 1988.

Sasaki, Y., Yoshimura, J., and Dohkoshi, J. (1986). Experimental Studies of the Earthquake Response Characteristics of Concrete Stave Silos. *Nogyo Shisetsu* 17 (2), 24–33. doi:10.11449/sasj1971.17.2_24

Schanable, P. B., Lysmer, J., and Seed, H. B. (1972). "SHAKE: A Computer Program for Earthquake Response Analysis of Horizontally Layered Sites,". Report No. EERC, 72-12 (Berkeley: Earthquake Engineering Research Center, University of California).

Shimamoto, A., Kodama, M., and Yamamura, M. (1984). "Vibration Tests for Scale Model of Cylindrical Coal Storing Silo," in *Proceedings of the 8th World Conference on Earthquake Engineering* (Hoboken, New Jersey, United States: Prentice-Hall), 5, 287–294.

Silvestri, S., Gasparini, G., Trombetti, T., and Foti, D. (2012). On the Evaluation of the Horizontal Forces Produced by Grain-like Material inside Silos during Earthquakes. *Bull. Earthquake Eng.* 10 (5), 1535–1560. doi:10.1007/s10518-012-9370-y

Silvestri, S., Ivorra, S., Chiacchio, L. D., Trombetti, T., Foti, D., Gasparini, G., et al. (2016). Shaking-table Tests of Flat-Bottom Circular Silos Containing Grain-like Material. *Earthquake Engng Struct. Dyn.* 45 (1), 69–89. doi:10.1002/eqe.2617

Silvestri, S., Mansour, S., Marra, M., Distl, J., Furinghetti, M., Lanese, I., et al. (20212022). Shaking Table Tests of a Full-scale Flat-bottom Manufactured Steel Silo Filled with Wheat: Main Results on the Fixed-base Configuration. *Earthquake Engng Struct. Dyn.* 51, 169–190. doi:10.1002/eqe.3561

Tatko, R., and Kobielak, S. (2008). Horizontal Bulk Material Pressure in Silo Subjected to Impulsive Load. *Shock and Vibration* 15 (5), 543–550. doi:10.1155/2008/289317

Trahair, N. S., Abel, A., Ansourian, P., Irvine, H. M., and Rotter, J. M. (1983). *Structural Design of Steel Bins for Bulk Solids*. Sydney, Australia: Australian Institute of Steel Construction, 30. ISBN 0909945357.

UBC "Uniform Building Code. Structural Engineering Design Provisions," in Proceedings of the International Conference of Building Officials, Whittier, May 1994, 492.

Uckan, E., Akbas, B., Shen, J., Wen, R., Turandar, K., and Erdik, M. (2015). Seismic Performance of Elevated Steel Silos during Van Earthquake, October 23, 2011. *Nat. Hazards* 75 (1), 265–287. doi:10.1007/s11069-014-1319-9

Vanel, L., and Clément, E. (1999). Pressure Screening and Fluctuations at the Bottom of a Granular Column. *Eur. Phys. J. B* 11 (3), 525–533. doi:10.1007/s100510050965

Veletsos, A. S., and Younan, A. H. (1998). Dynamics of Solid-Containing Tanks. II: Flexible Tanks. *J. Struct. Eng.* 124 (1), 62–70. doi:10.1061/(asce)0733-9445(1998)124:1(62)

Villalobos, F., and Mendoza, M. "Damages Observed in the 2010 Concepción Earthquake Related to Soil Phenomena," in Proceedings of the 5th International Conference on Earthquake Geotechnical Engineering, Santiago, Chile, January 2011.

Yang, J. Y. (1976). "Dynamic Behavior of Fluid-Tank Systems," Ph.D.Thesis. Houston, TX: Rice University.

Yokota, H., Sugita, M., and Mita, I. (1983). "Vibration Tests and Analyses of Coal-Silo Model," in *Proc., 2nd Int. Conf. On the Design of Silos for Strength and Flow* (Stratford-upon-Avon: Powder Advisory Centre), 107–116.

Younan, A. H., and Veletsos, A. S. (1998). Dynamics of Solid-Containing Tanks. I: Rigid Tanks. *J. Struct. Eng.* 124 (1), 52–61. doi:10.1061/(asce)0733-9445(1998)124:1(52)

Conflict of Interest: The authors declare that the research was conducted in the absence of any commercial or financial relationships that could be construed as a potential conflict of interest.

frontiers in Built Environment

REVIEW
published: 01 February 2022
doi: 10.3389/fbuil.2021.815153

Graph Rewriting Techniques in Engineering Design

Lothar Kolbeck, Simon Vilgertshofer, Jimmy Abualdenien and André Borrmann†*

Chair of Computational Modeling and Simulation, TUM School of Engineering and Design, Technical University of Munich, Munich, Germany

Capturing human knowledge underlying the design and engineering of products has been among the main goals of computational engineering since its very beginning. Over the last decades, various approaches have been proposed to tackle this objective. Among the most promising approaches is the application of graph theory for representing product structures by defining nodes representing entities and edges representing relations among them. The concrete meaning of these structures ranges from geometry representations over hierarchical product breakdowns to functional descriptions and flows of information or resources. On top of these graph structures, graph rewriting techniques provide another powerful layer of technology. By enabling the formal definition of rules for transforming graph structures, they allow on the one hand side to formally capture the engineering development process. On the other hand, the assembly of rewriting rules into graph grammars allows for an exhaustive search of the solution space of the engineering problem at hand. In combination with search strategies, an automated optimization of the design under given constraints and objectives can be realized. The paper provides an overview of the current state-of-the-art in graph rewriting and its applications in engineering design, with a focus on the built environment. It concludes with a discussion of the progress achieved and the missing research gaps.

Keywords: graph grammars, spatial grammars, graph theory, design synthesis, graph rewriting

OPEN ACCESS

Edited by:
Vagelis Plevris,
Qatar University, Qatar

Reviewed by:
Jiansong Zhang,
Purdue University, United States
Linzi Fan,
Sanjiang University, China

****Correspondence:***
Lothar Kolbeck
lothar.kolbeck@tum.de

†ORCID ID:
André Borrmann
orcid.org/0000-0003-2088-7254

Specialty section:
This article was submitted to Computational Methods in Structural Engineering, a section of the journal Frontiers in Built Environment

Received: *15 November 2021*
Accepted: *28 December 2021*
Published: *01 February 2022*

Citation:
Kolbeck L, Vilgertshofer S, Abualdenien J and Borrmann A (2022) Graph Rewriting Techniques in Engineering Design. Front. Built Environ. 7:815153. doi: 10.3389/fbuil.2021.815153

1 INTRODUCTION

With the advance of modern information technology, computers take over work that was considered to be reserved for humans. Initially, repetitive and error-prone tasks in data processing were significantly accelerated, while computation today complements human intelligence in domains requiring creativity. To this end, graphs have proven their capabilities and flexibility to provide the necessary representations for numerous real-world problems. As a data structure, graphs provide a rich foundation to represent engineering product models with entities of arbitrarily abstract and concrete meaning. In the same context, the manipulation of graphs was investigated for decades and proven to be powerful for complex problems in various domains. Most prominently, the method of graph rewriting is well established to capture manipulation patterns in the form of rules.

Solving a design problem by graph rewriting methods requires twofold: a graph representation of particular world entities and rewriting rules that operate on this model to manipulate its nodes, edges, and their attributes. The rules formalize domain knowledge by declaring design processes as graphlets consisting each of a conditional and a rewriting pattern. Once formalized, mature software frameworks ensure an efficient application of the rules to evolve the design representation. Graph rewriting allows an engineer to define a design not directly as an end result, but in terms of a

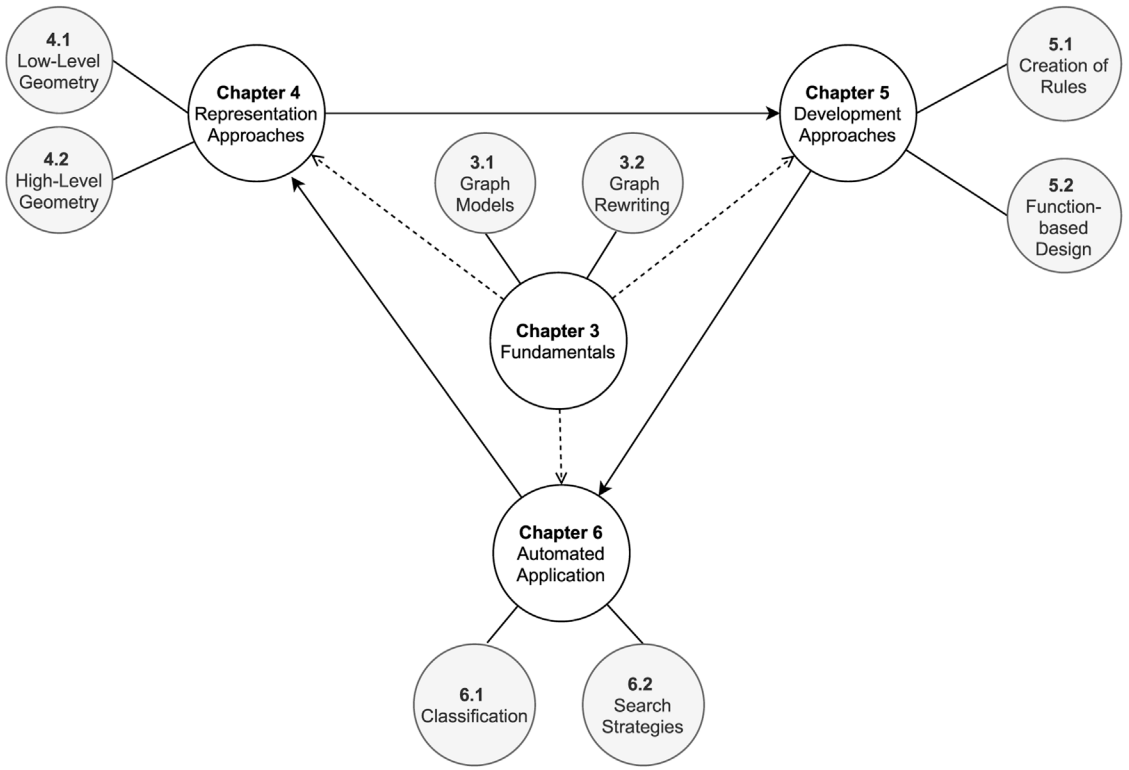

FIGURE 1 | Visualized outline of the review, following the cycle inherent to rewriting methods: The representation of a problem, the formulation of rules, and the application of rules.

procedural construction history. Arranging the rules in a flow they may be applied in, an engineering product can be gradually synthesized. In order to generate an illustrative variety of a prior unknown design, the engineer may vary the rules selected, the matches chosen, and variable parameters along that flow. The exploration of such a solution space may suggest creative, new ideas and then may be further restricted. This is achieved by either specifying the generation process or by directed stochastic search.

Originally, all rewriting methods emerged from linguistics (Chomsky, 1959), with fundamental branches dealing with shapes (Stiny, 1980), biological modeling (Lindenmayer, 1968), and later graphs (Nagl, 1979). Thanks to this background, a large part of the terminology used is related to linguistics. A *grammar* is formed when a set of rewriting rules, a *rewriting system*, is complemented by a start symbol, sometimes called *axiom*, a set of non-terminal symbols, and a set of terminal symbols. The terminal and non-terminal symbols are often referred to as *vocabulary* of the grammar. A defined grammar may be applied to exhaustively generate all possible different combinations of rule applications and parameters, constituting the *language*, the constituted solution space. The linguistic theory of *formal grammars* is rich and provides mathematical notations, terminology, and taxonomy available to many specific applications. Yet, the abstractness and extensiveness of the field also motivated researchers to enter specialized debates. In engineering design, expert systems were an early attempt to give a framework to the use of rewriting rules for design tasks. The research greatly decreased in the 1990s and is widely inactive today, due to various reasons, ranging from the difficulty of expert system maintenance and extensibility (Puppe, 1990).

Instead, several other frameworks emerged around the millennium. Cagan et al. (2005) achieved to encompass several schools of thought and several strategies for automated design synthesis along a simple, generic framework. The four key steps are the *representation* of the problem, the *generation* of solutions, their *evaluation*, and finally the *guidance* of the subsequent cycle of search. This framework is agreed to cover wide ranges of automation efforts under the collective term *computational design synthesis* (CDS). As one important stream, Chakrabarti et al. (2011) distinguished grammar-based synthesis. In parallel to the harmonization attempts of CDS, Rudolph (2002) motivated the so-called *graph-based design languages* as a powerful graph- and graph rewriting based methodology. Certainly complying with the broad definition of CDS, the field of graph-based design languages can be seen as a specification of the method. However, it is based on a stricter mathematical treatment of design objects and the formal design process (Riestenpatt and Rudolph, 2019).

In this review paper, we aim to break down this broad and extensive research field to the essential technological and conceptual questions. At a first glance, graph rewriting methods and the covering frameworks may appear very abstract. Yet, treating distinctly the

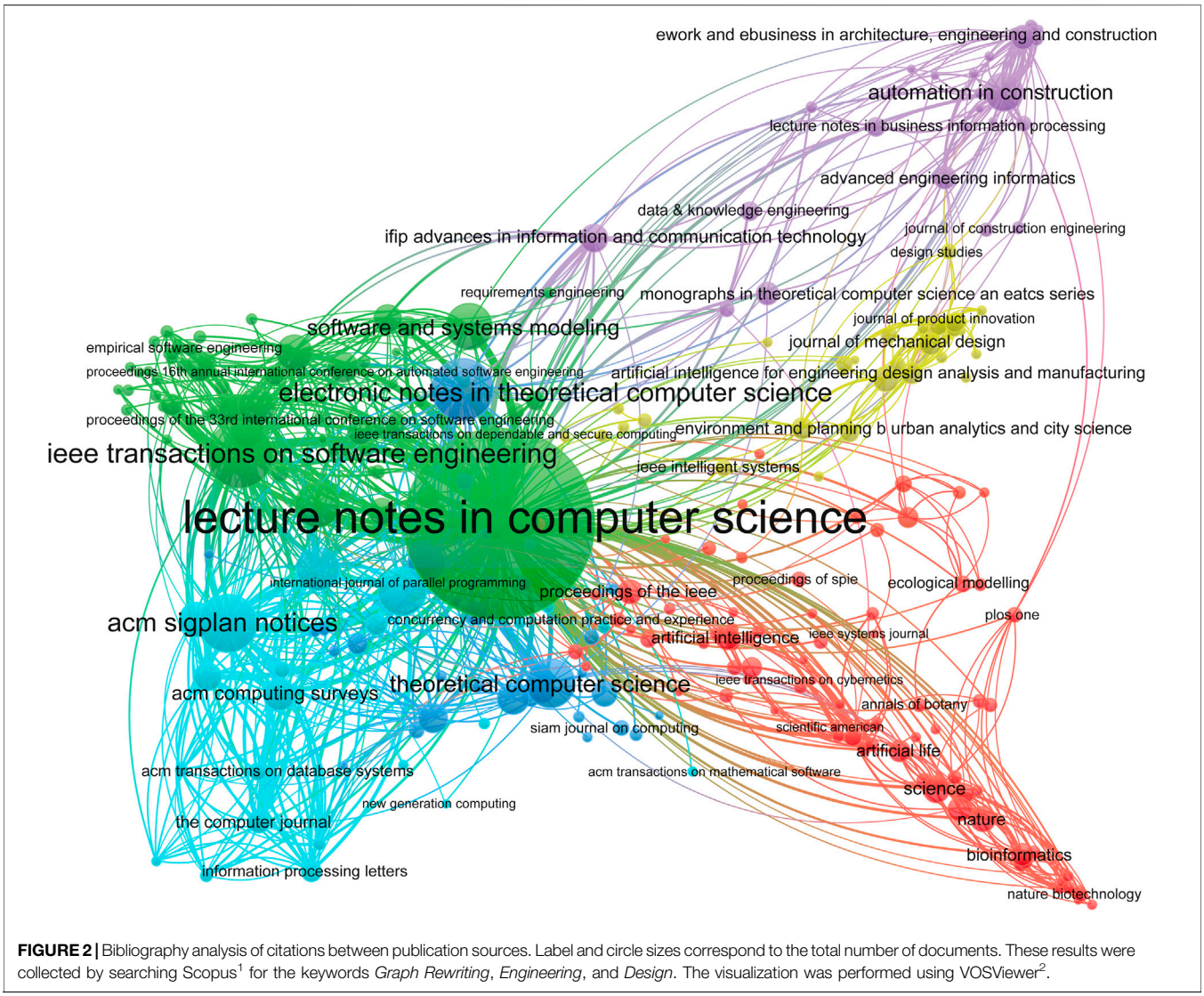

FIGURE 2 | Bibliography analysis of citations between publication sources. Label and circle sizes correspond to the total number of documents. These results were collected by searching Scopus[1] for the keywords *Graph Rewriting*, *Engineering*, and *Design*. The visualization was performed using VOSViewer[2].

essential steps of representation, rule definition, and the later application of rules, we aim to make comprehensible associated concepts. Following the outline shown in **Figure 1**, we hope to communicate the relevancy, potentials, and challenges to a broader audience. The review starts with a bibliography analysis where we attempted to quantify the scientific interest to graph rewriting methods, with special attention to the building sector. To make current developments comprehensible to readers with little prior knowledge, we introduce the fundamentals of graph theory and graph rewriting in chapter 3. Chapter 4 draws attention to the various approaches for forming a graph representation of an engineering model with semantic and geometric meaning[1]. Supports to the development and organization of rewriting rules are introduced in chapter 5. Finally, chapter 6 focuses on issues of automatically applying rewriting rules for design generation while chapter 7 concludes the review by summarizing potentials and shortcomings for further research[2].

2 BIBLIOGRAPHY ANALYSIS

The terms *Graph Rewriting* and *Graph Transformation* appear in the literature along with the keywords *Engineering* and *Design* since the 1970s. Although combining multiple keywords reduces the search scope, there are numerous engineering and design domains that have investigated graph rewriting for their challenges. **Figure 2** depicts the citation network between journals when searching for those keywords combined. The journals of computer science and software engineering (appearing at the center) are the most dominant journals for this field, where graph rewriting was used as a technique for

[1]https://www.scopus.com/

[2]vosviewer.com

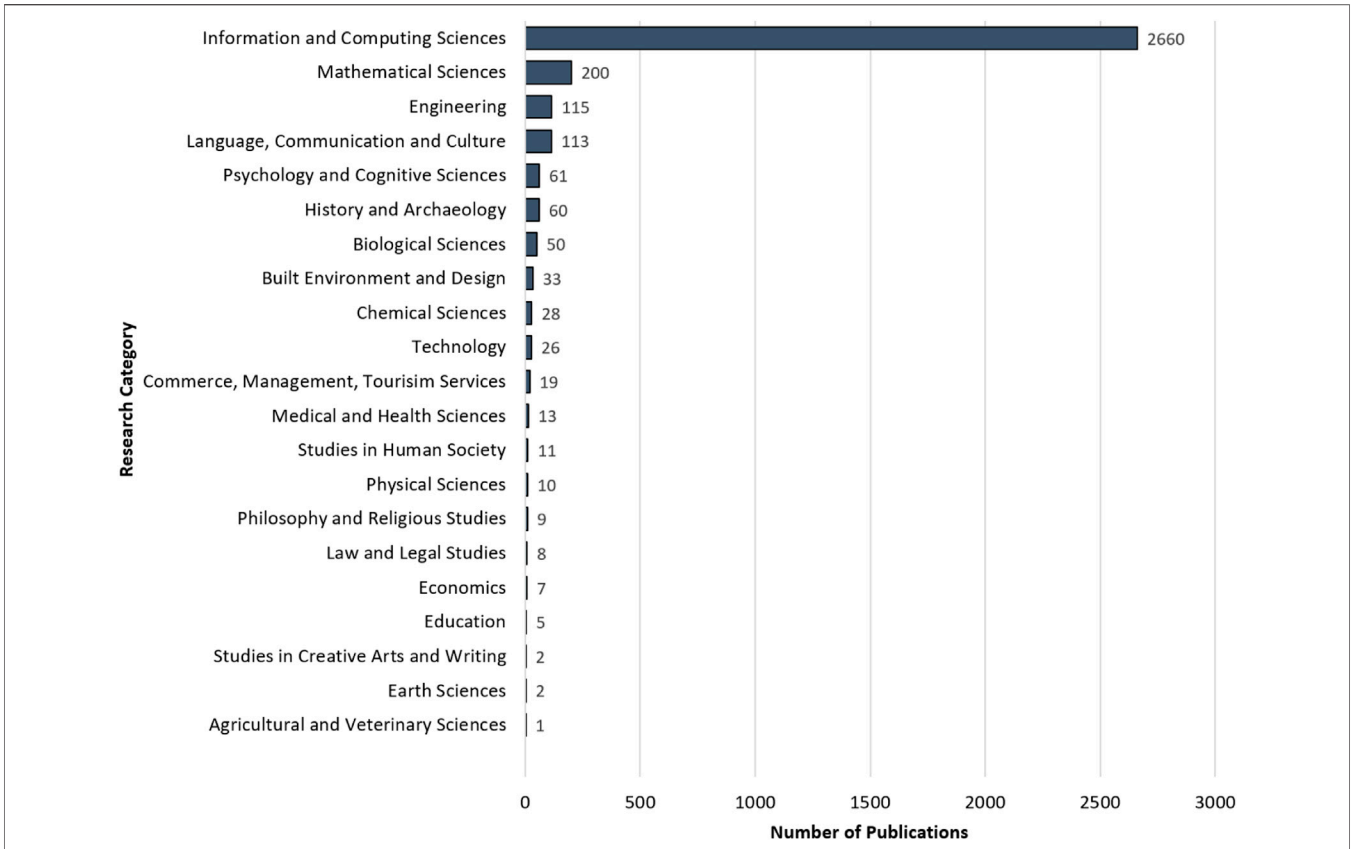

FIGURE 3 | An ordered grouped list of publications according to their research categories. These results were collected by searching Scopus[3] for the keywords *Graph Rewriting*, *Engineering*, and *Design*.

manipulating data structures, source codes, and more. Zooming out of the center, other application domains appear, such as biotechnology, business and engineering.

To get more insights into the involved research domains, **Figure 3** shows a grouped list of search domains and their corresponding publication counts. The field of *Information and Computing Sciences* provides a high percentage of the publications, as graph rewriting was introduced and developed by this domain. The rest of the domains typically adapt and apply the techniques developed in computer science to their particular challenges. Among others, engineering is ranked third, with 115 publications, whereas built environment and design is ranked eighth.

From this broad overview in engineering and design, a more detailed literature analysis was conducted with a special focus on publications that additionally include *Building Information Modeling* as a keyword. The first papers that appeared in the literature that included both *Graph Rewriting* and *Building Information Modeling* are from 2010 (Tratt, 2010). Afterward, there is a trend in increasing the number of relevant publications per year, as shown in **Figure 4**, where 23 relevant papers were published in 2018 alone and 58 in total until the year 2020.

The conducted bibliography analysis provides the necessary ground for the reviewed publications in the following sections. In this regard, the fundamentals of graph representations, graph rewriting, and the used software frameworks are described[3].

3 FUNDAMENTALS

3.1 Graph Representations

3.1.1 Theoretical Specifications

All graphs $G = (V, E)$ have in common that they consist of a set of nodes or vertices V and edges E, with each edge being represented by an ordered or unordered list of nodes. This generic definition encompasses a variety of specifications. In engineering design, it is commonly implied a typed and attributed graph, sometimes referred to as *property graph* (Robinson et al., 2015). Types, sometimes referred to as *labels* or *tags*, can serve to specify different categories of objects within a system. In an architectural context, this might serve to distinguish different room types (Langenhan et al., 2013), different building elements (Abualdenien and Borrmann, 2021), or load-bearing elements and their joints (Vestartas, 2021). Attributes in turn can serve to store relevant data about

[3]https://www.scopus.com/

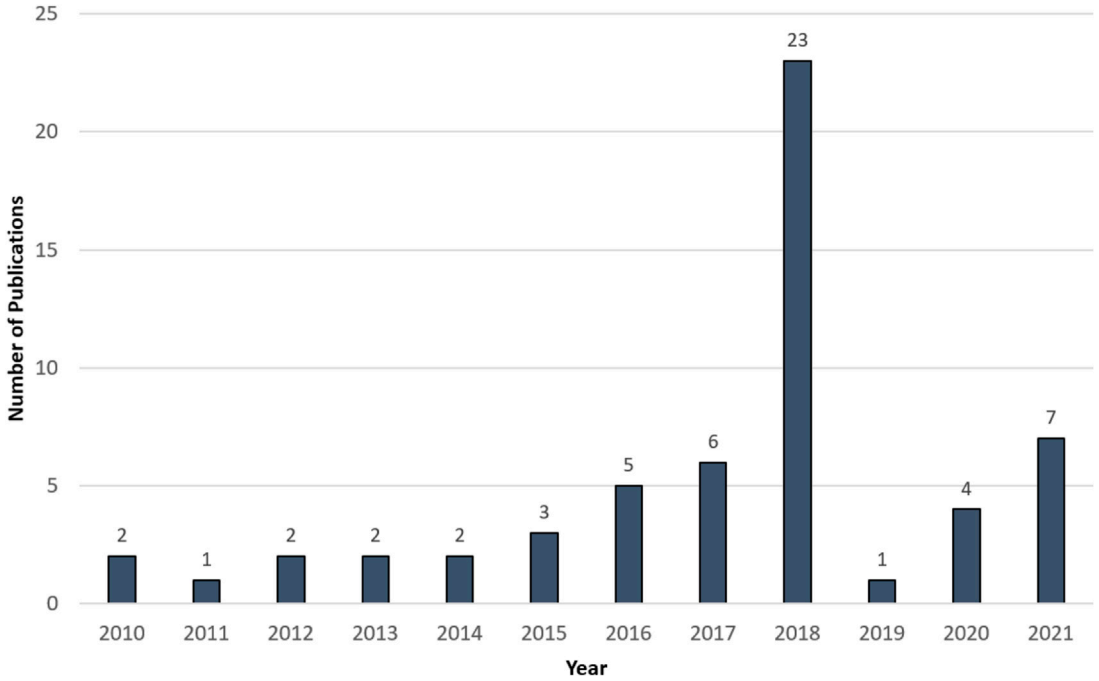

FIGURE 4 | An ordered grouped list of publications according to their publication year. These results were collected by searching Scopus[4] for the keywords *Graph Rewriting* and *Building Information Modeling*.

the objects in the form of key-value pairs. This data might be as simple as an identifier, a reference to external data sources, or as complex as a parametrization of geometric descriptions, see **Section 4.2**. Thus, graph structures are an expressive means to represent engineering systems as a network of objects with rich semantic and geometric meanings. However, most engineers find it difficult to formulate and solve their problems employing graph theory, except for of well-known applications like path planning. A look at two key motivations for the use of the data structure explains the difficulty.

One key advantage of graph theory is its ability to formally and flexibly represent relationships between entities. Large networks of objects can be created and queried for certain patterns of relationship to analyze or manipulate the represented system. However, the scale of these networks easily gets overwhelming. Therefore, there are specialized graph types that facilitate structuring complex domains and thus are better suited for certain applications[4]. As one example, *trees*, are special graphs that may serve to simplify analysis and manipulation of problems with an inherently hierarchical structure. Such a hierarchy can be applied to model the spatial structure of buildings, for example, where a site may comprise multiple buildings, each building may comprise multiple stories and each story comprises a number of spaces or rooms (Wonka et al., 2003; Grabska et al., 2012). To give a second example, *port graphs*, sometimes labeled composition graphs (Strug et al., 2022), are special graph types that distinguish two types of nodes: Object nodes and connector nodes. The connector nodes, the ports, restrict how the object nodes are allowed to be coupled to each other. This may be extremely useful for tasks that formalize assembly processes, as in the context of chemical reactions, bond graphs (Helms and Shea, 2012), or the design of segmented structures (Rossi and Tessmann, 2017a; Kolbeck et al., 2021). Many more specifications originate from the need to efficiently depict and manage complex networks, even leading to complex combinations like hierarchical hypergraphs (Drewes et al., 2002) and others currently experimented within engineering (Strug et al., 2022). Encountering all those specifications may easily overdemand a learning person, whereas all specifications branch off from the simple and comprehensible notation given above.

A second key advantage is the flexibility of graphs to adapt to arbitrary levels of scale and abstraction. For example, nodes and edges can represent geometric vertices and edges, but may also stand for complex objects such as walls or a building story. To illustrate the range of semantics a graph model can have in a design context, we discuss diverse applications in the building sector in the next section. Thereby, we highlight the characteristics of graph models used for the transformation of design by a comparison to the ones used for analysis tasks.

3.1.2 Applications in Architecture and Civil Engineering

An old stream of research aims to depict engineering systems as a graph to perform efficient analysis of the data structure. The well-

[4]https://www.scopus.com/

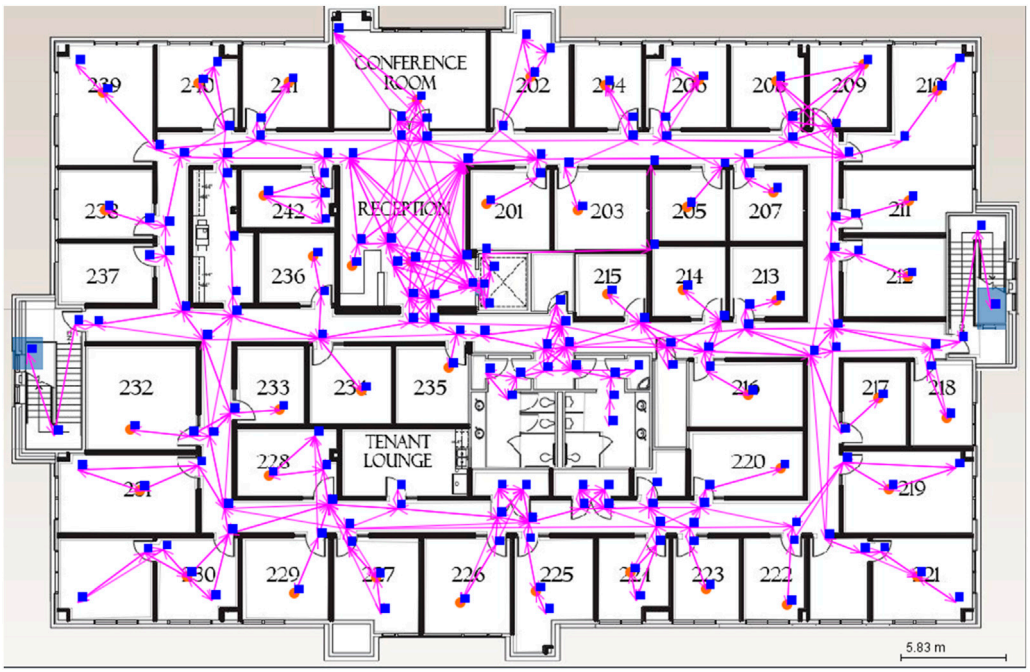

FIGURE 5 | Generation of a navigation graph from building geometry (Kneidl et al., 2012).

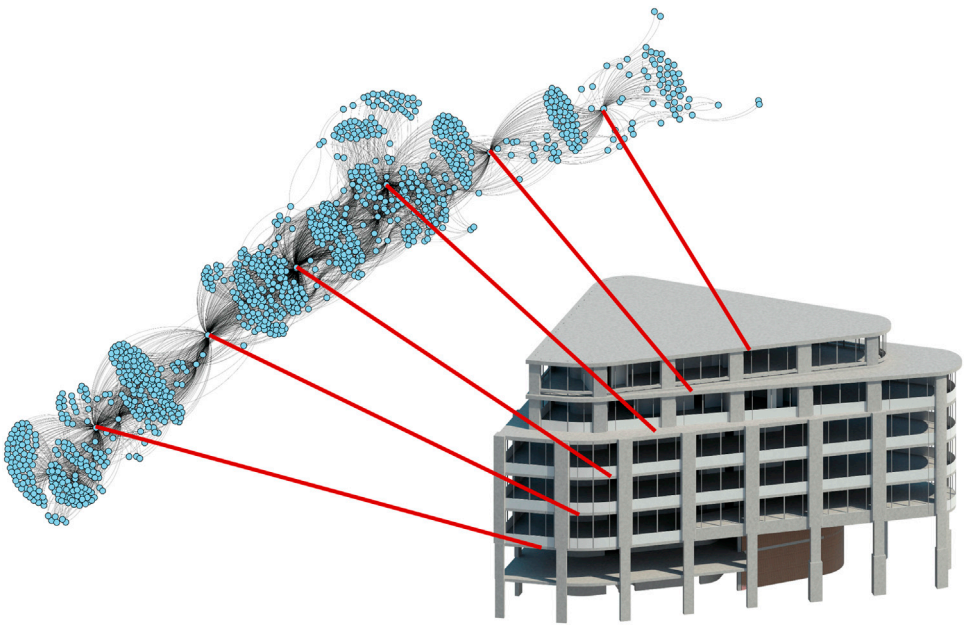

FIGURE 6 | A precedence relationship graph represents the order of erection of individual building components and their mutual dependencies (Braun et al., 2015).

known Dijkstra algorithm or the A* algorithm for path planning is familiar to most engineers. For a building, this can be adopted by translating architectural rooms and their mutual accessibility into a navigation graph, see **Figure 5**. A similar graph model of a building may be used to suggest architects preferable room layouts when dividing a floor into spaces (Langenhan et al., 2013). Equally, structural aspects of construction can be represented. Vestartas (2021) used a graph model to describe the different joints of crooked wooden beams. Braun et al. (2015) recorded the precedence relationships of construction

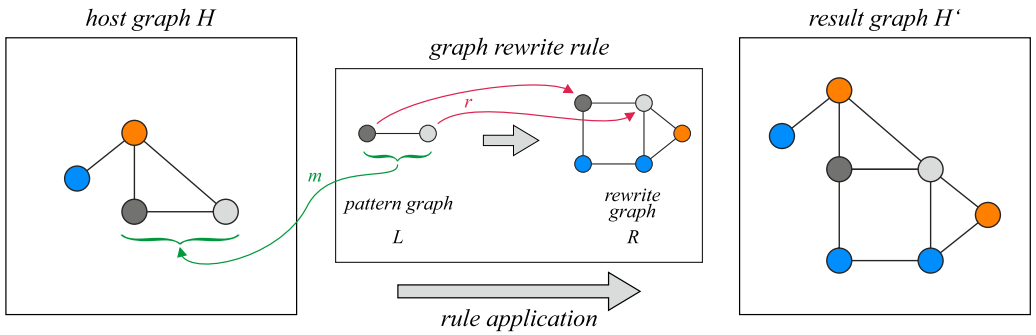

FIGURE 7 | A graph rewriting rule, graphically described in the middle, is applied to the host graph on the left side. The result graph is depicted on the right side. Here, the preservation morphism *r* is defined by the mapping of the grey nodes.

execution in a graph, where every node represents a column, wall, or floor and edges represent precedence relationships. The resulting graph model, depicted in **Figure 6**, was generated through a spatio-temporal analysis of the building construction process.

From a formal point of view, graph models for the dynamic manipulation of a design are identical to the ones for the analysis of a static design. However, a crucial difference is that design activities require a much greater amount of topological and geometrical adaptivity. Property graphs commonly enable topological extensibility while dynamic geometric transformations pose a less common challenge. In concrete terms, it is comparably easy to construct the system entities and their relationships for a coffee machine (Tonhäuser and Rudolph, 2017) or a bridge (Slusarczyk and Strug, 2017). Still, a valid topological and semantic configuration does not guarantee to make the components form a valid and harmonic assembly, without collisions and gaps at emerging interfaces. In comparison, a graph structure that merely analyzes a static design must capture the exact geometry only once. Without the need to dynamically change it, the geometry may even be stored and referenced employing external databases, for example in a point cloud format (Braun et al., 2015; Vestartas, 2021).

The characteristics of graph structures for dynamic manipulation of design is subject to further discussion in chapter 4. Since a representation for design is strongly linked to the manipulation mechanisms applied to evolve it, the next sections attempt to give a fundamental understanding of graph rewriting methods before.

3.2 Graph Rewriting

3.2.1 Theoretical Specifications

Graph rewriting, also referred to as graph transformation, describes the process of manipulating a graph structure by adding, removing, and altering nodes and edges, steered by declaratively defined rules. Each rule consists of a *left-hand side* (LHS or pattern graph) and a *right-hand side* (RHS or rewrite graph). Providing a *host graph* and a set of rules, the matches of the LHS in this host graph can be identified and be replaced by the RHS to generate the result graph as depicted in **Figure 7**. A *preservation morphism r* can be defined in order to specify that parts of the LHS are matched to the RHS to ensure that they are preserved.

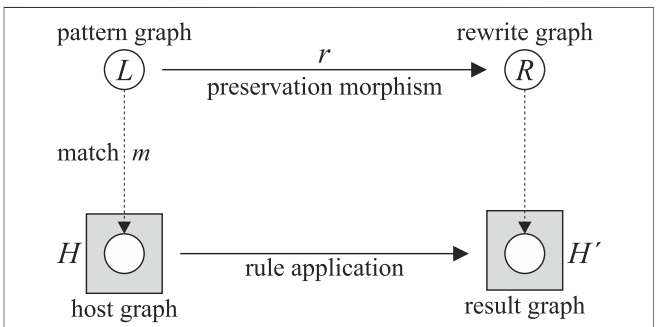

FIGURE 8 | Basic principle of graph rewriting using the Single Pushout Approach according to Geiß (2008) and Jakumeit et al. (2010).

Several characteristics can increase the expressiveness of a rewriting rule. Rules may be more concise by including attributes and multiple labels per node. For example, a graph representation of a building may enable a matching for objects labeled both "wall" and "load-bearing," with an attribute "height" at a certain value. Further, a rule may be context-sensitive, meaning that it specifies conditions that exclude possible matches depending on the surrounding of the pattern. These application conditions may concern the left or the right side of the rule (Habel et al., 1996). Rules can be defined to be more flexible for a wider range of applications by defining them parametrically, computing variables instead of fixed values. In order to span a wide solution space in a generative application of rules, variable rule parameters may be stochastically chosen.

Rules, potentially defined with all described characteristics, need to be applied to a host graph (H). To this end, it is necessary to detect correctly typed and attributed matches for the LHS (or pattern graph), as well as their rewriting to produce a valid result graph (H') containing the RHS (or rewrite graph) inserted. Efforts have been undertaken to significantly improve the computational complexity of match detection algorithms (Geiß et al., 2006; Batz et al., 2008). As well, a variety of rewriting methods has been researched for decades. In distinction to the algorithmic

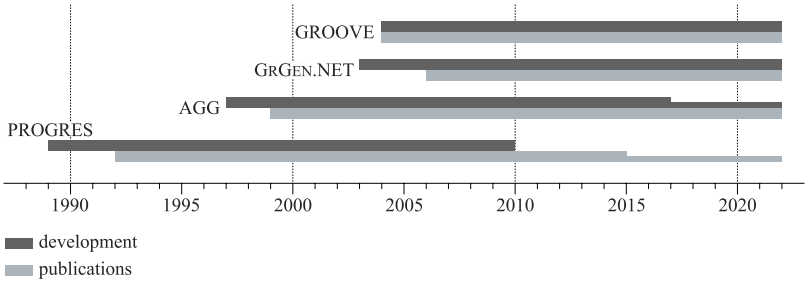

FIGURE 9 | Not all of the presented frameworks are still continued and maintained. This figure gives an overview of the times of development and reference and use in research projects. Smaller bars indicate that only small updates were published or references only list the tool without using it.

approaches, the prevailing algebraic approaches consider graph rewriting as a mapping problem between two algebras of nodes and edges. The main algebraic methods are the single pushout approach (SPO), shown in **Figure 8**, and the double pushout approach (DPO). The fundamental difference between both lies in the greater expressiveness of the SPO, which conducts the rewriting in a single step. On the other hand, the DPO introduces an intermediary *gluing graph* that allows a more restrictive avoidance of problematic situations, as for dangling edges in the result graph (Corradini et al., 1997). For further reading on the fundamentals of algebraic graph transformation approaches, we refer to Rozenberg (1997) and Ehrig (2006), while an application-oriented introduction to graph rewriting can be found in Heckel (2006).

3.2.2 Software Frameworks for Graph Rewriting

The modeling of graph representations and their transformations can be conducted with diverse software frameworks. The term *framework* describes an assembly of specialized tools. This includes at least an *interpreter* that processes human-readable descriptions of graph metamodels as well as graph rewriting rules and gives feedback in case of errors. A *compiler* then translates this into source code or libraries for further use. Most frameworks also have some sort of graphical user interface to display graphs and visualize rule execution. In this section, we give a short overview of the major frameworks that are available (see **Figure 9**). This list is not meant to be complete as there exist many further frameworks, although many of them are not maintained anymore. Extensive but rather outdated lists are provided in Nagl et al. (2003) and Rensink and Taentzer (2007). More recent comparisons were documented by Aouat et al. (2012), Bak (2015) and Kahani et al. (2019). Tools addressing graph transformation are also regularly presented amongst others in the annual *Transformation ToolContest*[5] that aims to evaluate and compare the expressiveness, usability, and performance of transformation tools for structured data.

A widely used graph transformation framework is the Graph Rewrite Generator GRGEN.NET for the .NET environment (Jakumeit et al., 2010; Jakumeit et al., 2021). GRGEN.NET offers declarative languages for graph modeling, pattern matching, and rewriting. GrGen allows users to define an object-oriented graph metamodel, a blueprint of the desired design representation, describing node and edge types including attributes and inheritance. The metamodel may also include connection assertions that define the allowed connections of nodes and edges in a graph. The frameworks offers many possibilities when defining rewriting rules including negative application conditions which may be applied with logical and iterative control of their application. Rewriting is generally based on the SPO approach, but also the DPO approach may be used. As GRGEN.NET creates .NET libraries for the graph metamodel and transformation rules defined in its own language, it can be easily used in custom projects. A major benefit is that the software including its documentation is regularly updated and well maintained. A quantification of the computational efficiency of GrGen can be found in (Geiß et al., 2006), including a relative comparison to the following two frameworks.

The Attributed Graph Grammar **AGG** is a rule-based visual language supporting an algebraic approach to graph transformation implemented in Java (Ermel et al., 1999; Runge et al., 2011). AGG allows the definition of attributed type graphs with inheritance. The defined graphs may be attributed by Java objects and types. A main feature is that the framework provides graphical editors for graphs and rules and a text editor for Java expressions including visual interpretation and validation. AGG is primarily based on the SPO approach but offers the possibility to enable rewriting based on the DPO approach. The main functionality of the framework is provided by a graph transformation engine that is independent of the graphical environment. Therefore, the transformation functionalities may also be used by other software. The last major update for AGG has been released in 2017, whereas a patch has been published in early 2021, so it can be considered to be maintained.

Another sophisticated and well established framework is **PROGRES** (PROgrammed Graph REwriting Systems) which is being developed at RWTH Aachen since 1989 (Schürr et al., 1995). It is based on directed, attributed and typed graphs, which can represent extensive and complicated issues in a clear and structured manner. PROGRES consists on the one hand of a specification language and on the other hand of a complex, integrated environment. The framework allows the specification of a graph schema with inheritance and edge cardinalities that can be used for type-checking of productions. Besides the graph schema, graph transformations can be specified graphically and textually. The PROGRES

[5]https://www.transformation-tool-contest.eu/aims_and_scope.html.

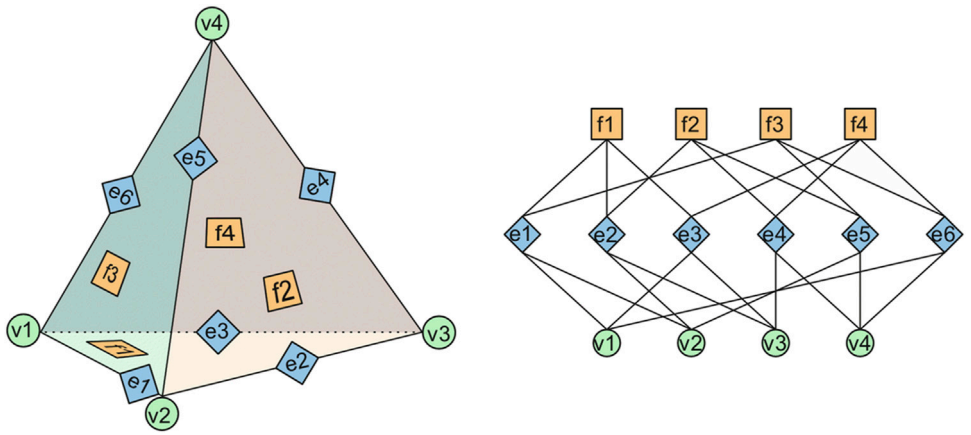

FIGURE 10 | A pyramid represented by a vertex-edge-face graph, illustrated geometrically (left) and topologically (right).

environment consists of three integrated frameworks. Graph schema and transformations can be defined in a syntax-controlled editor that highlights violations. The interpreter with a corresponding graph browser assists the user in debugging and the compiler automatically translates the specification into C or Java source code. However, PROGRES is not regularly maintained and has been last updated in 2005. While it is regularly referenced in recent articles giving an overview of graph rewriting frameworks, the last publication that describes its use in a project dates back to 2015.

The **GROOVE** tool set (Graph-based Object-Oriented VErification) is being developed since 2004 and is still regularly updated (Rensink, 2003; Ghamarian et al., 2012). With GROOVE simple graphs can be used for modeling the design-time, compile-time, and run-time structure of object-oriented systems. Therefore, it provides graph transformations as a basis for model transformation and operational semantics. GROOVE is a general-purpose graph transformation framework that uses simple labeled graphs and transformation rules based on the SPO approach. The framework is Java-based and provides an intuitive interface that allows graphical editing of rules and graphs.

Among this rich body of available alternatives, an engineer can deliberate the choice of a framework for specialized applications in design. This deliberation is a problem-specific evaluation of necessary and desirable characteristics in modeling, development, and execution. Building upon this fundamental understanding of both graph theory and the implications of rewriting, we address approaches to represent engineering products in the next chapter.

4 REPRESENTATION APPROACHES

Graph structures for design synthesis approaches require an efficient approach to both the representation and manipulation of the geometry of relevant design objects. In the aspect of identifying the crucial objects and linking them elegantly to a geometric representation, we see the key problem to the successful use of graph rewriting methods in design synthesis. Thereby, a first stream follows the idea of a very fine-grained representation and control of geometry, giving the graph an intuitive geometric meaning. The second stream attempts to further abstract objects, making it easier to define and describe transformations on a semantically higher level of abstraction. Both are discussed in the following sections.

4.1 Low-Level Representation of Geometry

An engineer familiar with computational geometry would likely associate the terms "graph" and "geometry" with well-known classical data structures. As such, the *vertex-edge-face* graph, illustrated in **Figure 10**, may be mentioned, used in boundary representation approaches. Two key advantages of such graph models with a strong linkage of topology and geometry may be highlighted:

They give a very fine-grained control of the geometry of objects, down to every single geodetic point. For an engineering model with objects in such a representation, efficient and detailed spatial-topological queries and consistency checks exist (Borrmann and Rank, 2009; Jabi et al., 2018). Another advantage to the low-level integration of topology and geometry is the geometric intuitiveness of a graph model. This is both beneficial to the development of rules, and the analysis of structures, e.g., when evaluating them by defining cost functions. Many applications illustrate these benefits. An early and widely known example is the optimal truss generation problem (Shea, 1997; Kaveh and Koohestani, 2008; Hooshmand and Campbell, 2016). Thereby, nodes commonly represent joins, while edges represent the beams of the truss. Describing and manipulating more complex structures is equally possible, as shown by the origami figures of Chen et al. (2019) or the walls and floors described in the architectural solid grammars by Heisserman (1994).

Despite not being specific to engineering, the implementation of shape grammars utilizing graph models must be mentioned in this context, too. For these implementations, graphs were recognized to have beneficial characteristics as a model of

geometry. On the one hand, graphs were proven capable of implementing shape grammars that support the recognition of *emergent* shapes (Knight, 2003), i.e., to cope with ambiguous recognition problems as in the Sierpinski-triangle. More relevant to engineering applications is the question of topological-associative shape recognition (Grasl and Economou, 2013; Wortmann, 2013). Instead of depending on similarity transformations to geometrically match LHS patterns (Krishnamurti and Earl, 1992), graphs enable efficient queries for *topological* patterns of geometric entities. This enables the formulation of much more flexible and expressive rewriting rules. A rule defined for a quadrilateral may apply to any quadrilateral in a shape of a design.

This leads to two significant downsides of graph models in such a high resolution of geometry. First, what does a human intend when he defines a rewriting pattern that consists of a closed loop of four vertices and lines? Can the matching algorithm assume that orthogonal and parallel lines play a role or not? Did the human intend a void quadrilateral or may the pattern intersect itself or be intersected by other elements? Krishnamurti and Earl (1992) discuss why it is a very difficult task to capture the exact designer's intent. Recently, these questions were revisited by Stouffs (2019). Second, is it really necessary and desirable to have such high flexibility and control of geometry? It must be weighed up that this comes with the toll of defining rules that may easily become very complex.

These two problems have been known for a very long time and two main responses exist to remedy them. On the one hand, the introduction of an additional layer of abstraction, i.e., a user interface, could help humans to more intuitively express their intentions of a rule. Such an abstraction layer may be either graphical or textual (Dy and Stouffs, 2018), as further discussed in **Section 5.1**. Another remedy is to move from a geometrical to a more object-oriented view of design artifacts. If an architect wanted to formulate rules for the design of a house in natural language, likely very little would be explicitly stated about the relations between points, lines, and faces. Instead, the architect would reference columns, walls, and slabs (Mitchell, 1991). Many of those symbolic objects may be sufficiently described by a fixed or parametrized geometry. A column may be described by a point, a diameter, and a height. Instead of a large graph pattern with nodes representing points, lines and faces, a node with three key-value pairs may be precise enough for the scope of many practical problems.

This is the basic idea of a group of grammars for design that follow an object-oriented idea of design: instead of reasoning geometrically, *set grammars* discretize a design problem to a set of comprehensible entities. Those entities are processed in the grammar by rules that allow the set-theoretic operations of union, intersection, and difference among them. In the context of design problems, such entities are commonly tangible objects like stories, walls, or windows (Wonka et al., 2003), with complex geometry such as a parametrized solid (Alber and Rudolph, 2003). This enables the formulation of rules on a more natural level of abstraction and simplifies geometrical challenges as e.g. the shape recognition problem (Krishnamurti and Earl, 1992).

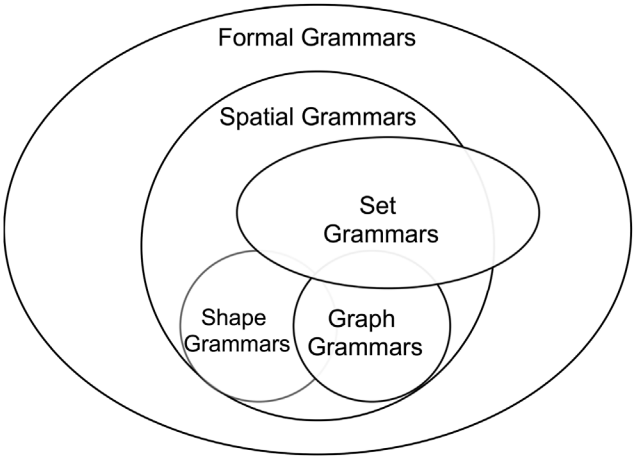

FIGURE 11 | Taxonomy of formal grammars utilized for engineering design problems.

However, the relations between shape grammars and set grammars often are unclear due to fuzzy terminology in the field (Lienhard, 2017). Many terms circulate and may be confusing as they treat very similar concepts. An early attempt to give a taxonomy to the various terms encountered is found in Krishnamurti and Stouffs (1993): all grammars with strong geometric implications may be subsumed under the term *spatial grammar*, including *L-systems* (Lindenmayer, 1968) as well as classical *shape grammars* (Stiny, 1980). Set grammars may be defined for a variety of objects, like strings, shapes, or graphs. Graphs recently were also used to implement shape grammars (Grasl and Economou, 2013; Wortmann, 2013). Our understanding of the different terms we summarized in **Figure 11**. The next section will focus on the intersection of graph grammars and set grammars.

4.2 High-Level Representations of Geometry

4.2.1 Set Grammar Approaches

In the former section, we discussed that many practical engineering problems allow the system to be represented as a composition of objects that can be sufficiently described by high-level geometric primitives. Thereby, one may roughly differentiate two types of object descriptions.

The first type associates an object to an individual from a set of strictly uniform geometries. This may be a column of a fixed diameter and height (Mitchell, 1991) or standardized, serially prefabricated parts. The expressiveness may be increased by discretizing the vocabulary as groups of the same object type, e.g., by introducing five columns with slightly different heights and diameters. Then, eventually, a wide enough solution space is opened up, while ensuring a geometrically elegant and comprehensible way of processing and interpreting the graph.

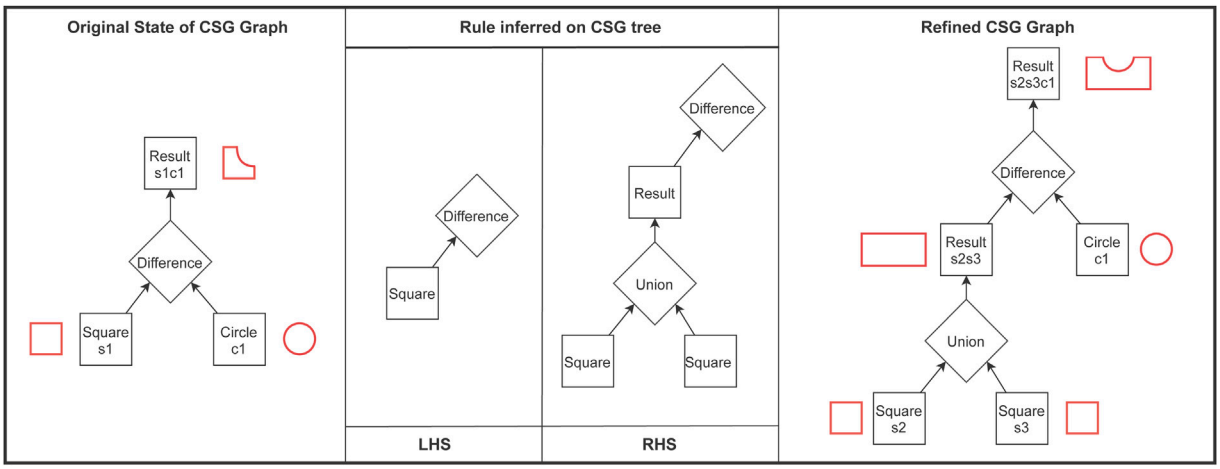

FIGURE 12 | Refinement of a CSG tree based on a graph rewriting rule.

Further, a sufficient degree of discreteness is certainly helpful to simplify the reasoning with rules (Peyshakov and Regli, 2003).

The second type relies on geometric descriptions with a parametrization defined by continuous or discrete variables. As a first example, Alber and Rudolph (2003) described the assembly of electricity pylons from a few, adaptive segments. As a second example, Vogel (2016) developed a method to construct exhaust filter systems by various, adaptive pieces of tubes and joints. One example from the building sector is the *split grammar* of Wonka et al. (2003), where buildings are efficiently generated by allowing every RHS pattern to be only a subset of a LHS object. In concrete terms, this results in a hierarchical "sculpturing" of buildings from a mass model over stories over walls to windows, following a strictly hierarchical order of the vocabulary. The split grammars were brought into a graph model by Lipp et al. (2008), with graph rewriting rules definable and applicable according to a concept by Patow (2012). To give a second example from the building sector, Abualdenien and Borrmann (2021) adopted the object parametrizations of commercial BIM software to capture design patterns in the context of high-rise buildings. Even though not using a graph data structure, Hoisl and Shea (2011, 2013) implemented the spatial grammar interpreter *Spapper* with a wide range of parametrized solid objects, ranging from tori to ellipsoids.

They mention, however, that the expressiveness of the interpreter could be further improved by including powerful procedures like sweeps or extrusions. This is an inherent restriction of the set grammar idea that defines vocabulary according to the objects present in the final design configuration (Hou and Stouffs, 2018). An alternative is to explicitly introduce *operations* that apply a certain transformation to the input objects. This idea, commonly known by techniques like constructive solid geometry (CSG), motivated another stream of graph structures for design discussed in the next section.

4.2.2 Explicit Description of Operations

The use of graph models for the geometric design of engineering products is, unconsciously, familiar to many engineers. In many undergraduate courses, the CSG approach is commonly taught. Intuitively, the technique allows applying Boolean operators (union, difference, intersection) on high-level geometric primitives. A procedural construction history based on CSG operations may be formally depicted as a directed, bipartite and hierarchical graph pointing toward one final geometry. The graph is bipartite because nodes can either represent objects or operations. Essentially, the visual programming interfaces of computer-aided drawing (CAD) software like Grasshopper Rhinoceros (Mc Neel and Associates, 2021) can also be represented as a directed graph, with nodes being either input objects or operations, performing imperative logic on the input objects. Because these procedural parametric models abide by the formal definitions of graph theory, they can also be refined by graph rewriting patterns. This basic idea of refining a procedural definition with a rule-based paradigm is illustrated in **Figure 12**. Therein, a simple CSG operation is manipulated, computing the difference between a square and a circle. The RHS pattern of the rule replaces the square with a rectangle. The rectangle is generated by a union operation that merges two new leaf nodes that each represent a square.

Procedural parametric modeling approaches draw their expressiveness from explicitly introducing operations as a part of the grammar vocabulary. The difference to other design grammar approaches is subtle but important. The greater part of grammars for design declare rules as a static *configuration* pattern before and after a rewriting step. When applying the rule, an interpreter derives from the difference between the sides the necessary procedures to take, i.e., manipulations, additions, and removals of objects. However, some operations may be much more intuitive to be stated in an *imperative* manner. To give an example from the building sector, Vilgertshofer and Borrmann (2017) distinguished "Sketch Nodes" and "Procedural Nodes" for

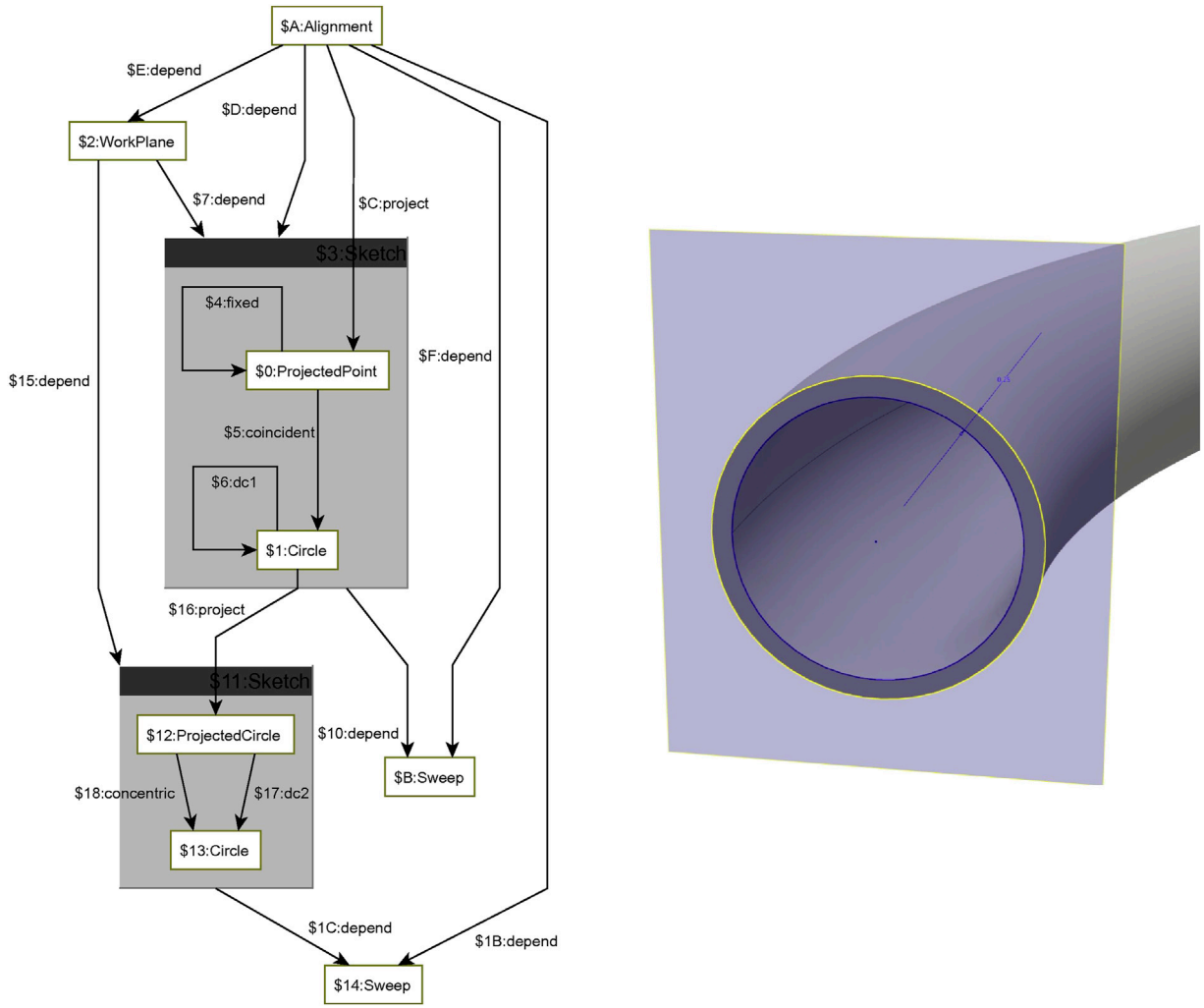

FIGURE 13 | A stage in the graph-driven design development process presented in Vilgertshofer and Borrmann (2017). Left-hand side: Graph structure consisting of entities and procedural operations, created by graph transformation. Right-hand: Interpretation of the graph by a parametric CAD system.

refining tunnel geometry, see **Figure 13**. The former described the composition of sketches, e.g. describing a tunnel profile. On the other hand, the procedural nodes enabled the transformation of geometry, e.g., by extrusion of a tunnel profile. These development steps are illustrated in **Figure 14**.

The introduction of explicit operations enables the straightforward integration of powerful features accessible by programming interfaces of CAD software. Silva et al. (2013) gave another example of a graph model that explicitly includes operations, in this case related to urban model generation. Thinking of a graph model as a network of objects or operations can make graph models in design much more expressive.

Finally, a noteworthy trend in the field of grammars and computational geometry is the investigation of mixed programming paradigms. Of course, it is more elegant to define a design problem within one of the various paradigms of procedural modeling. Yet, for considerations of efficiency, the combination of paradigms is worth further investigation. Many of the design grammars published partially needed to use imperative programming techniques (Hohmann et al., 2010). Leblanc et al. (2011) presented a modeling language based on CSG techniques, with imperative as well as rewriting characteristics. A second example, given by Hohmann et al. (2010), employs rewriting rules to refine commands of the stack-based, generative modeling language GML (Havemann, 2005). Certainly, these approaches are difficult to classify at a first glance. However, they may be a promising way to the pragmatic and widespread use of rewriting rules, specialized to the situations in which they are beneficial.

In the context of grammar-based design, any representation is just an important means for a purpose. This purpose is the development of a design from an initial state towards a goal state. This is performed by defining rules, which may be applied to incrementally evolve the design representation. Unarguably, the finding of appropriate and expressive rules is a demanding step. Therefore, we dedicate the next chapter to research treating the process of grammar development.

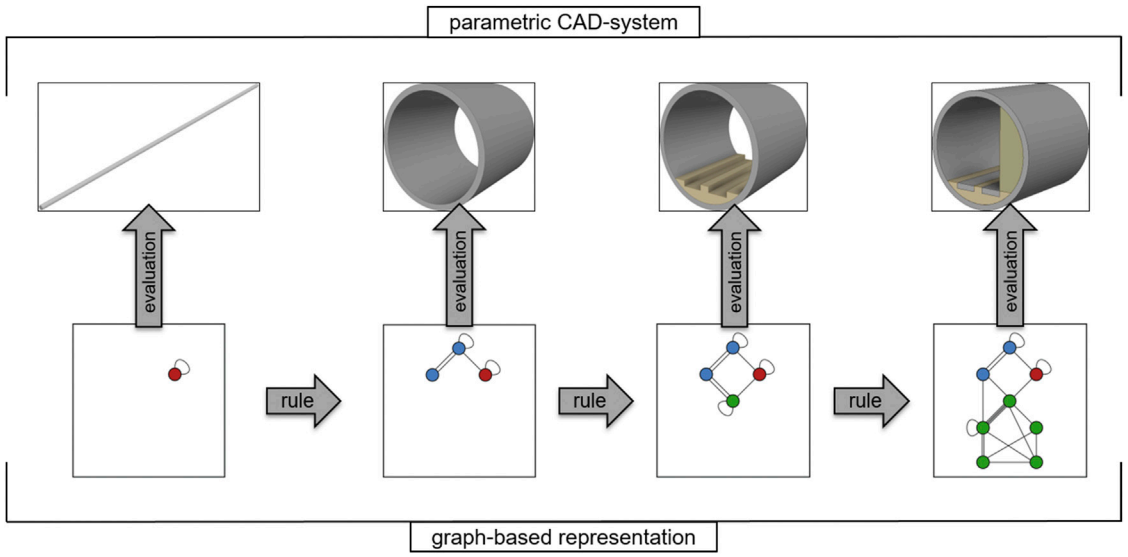

FIGURE 14 | Gradual Refinement of tunnel geometry by means of graph rewriting and according to a level of development concept (Vilgertshofer and Borrmann, 2017).

5 DEVELOPMENT OF GRAPH REWRITING APPROACHES

The variety of grammars published is commonly described as original pieces of handcraft. The representation chosen is demonstrated to have captured the essence of the problem and the rules to allow steering an efficient evolution of the system. Still, scientifically valid questions are "polemically" (Economou and Grasl, 2018) left out: why did the engineer choose these and not other rules? Did the developers follow certain guidelines to make the approach transparent and extensible? Is the approach transferable to other problems? Developing answers to such questions might be difficult, but is indispensable to make rewriting methods better understood and widespread. In this review, we distinguish two fields of research that attempt to make the development of grammars more transparent and streamlined: first, the facilitated creation of grammars and second, the idea of using rewriting methods within a standardized system modeling language, synthesizing a design solution from an abstract network of functions.

5.1 Facilitated Development of Rewriting Rules

In the practice of grammar development, a significant problem to be remedied is that domain experts are rarely familiar with the computational aspects of rewriting. A simple solution might be to let developers and domain experts collaborate, which was the strategy in expert systems research. Unfortunately, this strategy needed to be omitted, acknowledging that experts have limited time, motivation and that arising communication barriers may cause frustration (Puppe, 1990).

As a first alternative, one may attempt to not let domain experts define the grammar, but to generate the rules based on design artifacts they produced in the past. The problem of automatically "learning" or creating a grammar from a given dataset is referred to as *inverse procedural modeling* and is commonly assessed to be very complex (Puppe, 1990; Lienhard, 2017). Nevertheless, a modest amount of research has been classified by Lienhard (2017). One set of works attempts to adapt relatively generic template grammars to a given dataset, mostly in the context of facade parsing (Nishida et al., 2016). This approach likely has a limited potential to generally automate the development of grammars as any template grammar needs to be developed a priori and relatively specialized on the problems to be covered. Instead, the second class of research deals with the induction of set grammar vocabulary and rules with the help of statistical models. These approaches were considered to require very structured and annotated data structures, as in a hierarchical tree structure (Leblanc et al., 2011). Otherwise, it was thought to be impossible to identify the nodes representing the vocabulary of the grammar (Talton et al., 2012). However, recent efforts indicate that it might be possible to induce grammars for more unstructured datasets, including hierarchical and non-hierarchial, one- and more dimensional representations (Whiting et al., 2018). Despite these efforts, this research field is certainly still at a very fundamental level and inverse grammar modeling is not yet applicable to a wider range of engineering design problems.

A second alternative is to look for solutions that empower a wide range of domain experts to develop grammars. Besides guidelines to teach non-specialists good practices in the definition and organization of rewriting patterns (McCormack et al., 2008; Oster and McCormack, 2011), attention is drawn to provide less technical interfaces. As first example of this trend, Abualdenien and Borrmann (2021) recently proposed a method

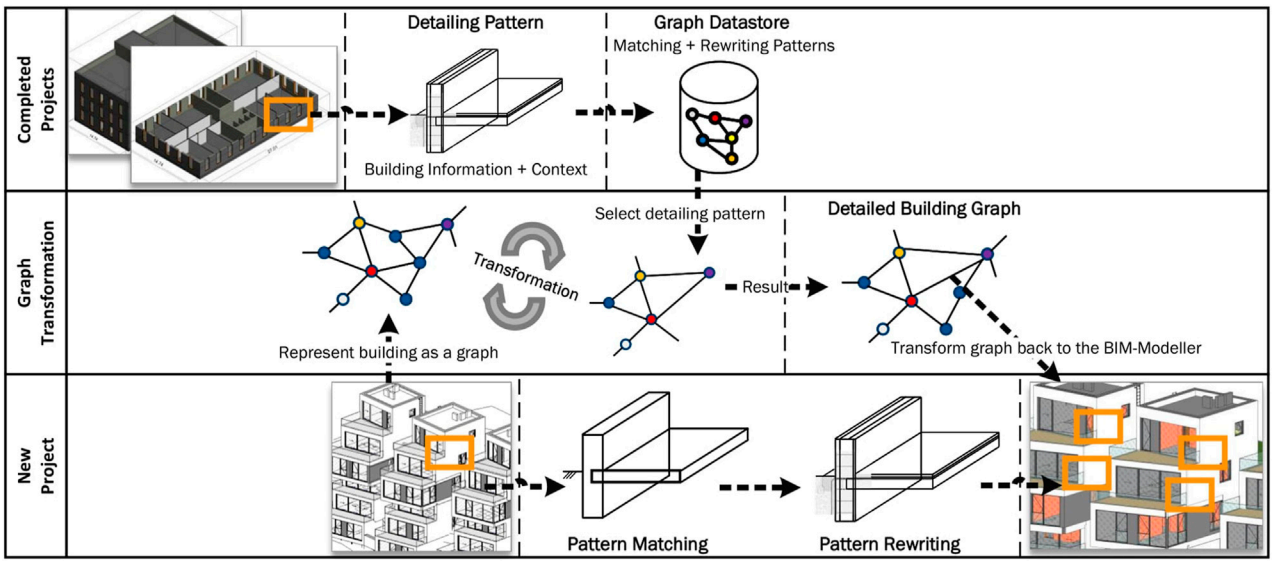

FIGURE 15 | Worfklow proposing a user-oriented interface to formalize architectural design patterns without knowledge of underlying representation and algorithms (Abualdenien and Borrmann, 2021).

to graphically capture architectural detailing patterns through the interfaces of common BIM software. The translation of these patterns to rewriting rules and the later application of rules is possible without knowledge of the underlying computational processes. A conceptual sketch of the workflow is shown in **Figure 15**.

Comparable in intention, Rossi (2021) developed a largely graphical interface to define vocabulary, rules, and a geometrically constrained search procedure for the assembly of segmented structures (Rossi and Tessmann, 2017b). Patow (2012) made the split grammars of Wonka et al. (2003) accessible in an interactive graph visualization and allowed users to refine a procedure by rewriting patterns. Equally, the interfaces of spatial grammar interpreters incrementally require less technical knowledge to define geometrically and semantically complex grammars. Hoisl and Shea (2011), Dy and Stouffs (2018) and Grasl (2021) developed largely graphical interfaces to their spatial grammar interpreters, requiring little knowledge of the underlying computational processes. These interfaces can be advantageous when learning a specific implementation of a rewriting formalism or for the rapid prototyping of design grammars departing from their geometrical frontend.

The interfaces discussed make it easier to define smaller sets of rules. From a certain amount of rules captured, a stricter organization or modularization of the rule sets is important. A promising approach to this end offers the research field of function-based design synthesis.

5.2 Function-Based Design Synthesis

Graphs have the ability to represent a system in any degree of abstraction. This property is exploited in model-based systems engineering (Haberfellner et al., 2019; Hick et al., 2021), also referred to as function-based design synthesis (Cagan et al., 2005; Chakrabarti et al., 2011). The fundamental idea is to begin the design with a set of requirements a system needs to fulfill and to convert respectively map them to a network of functions, the functions to subfunctions, and finally, the subfunctions to components, sometimes *structures*. Only the latter are assigned concrete geometry. Each of those layers can be represented as a network of objects, i.e. in a graph-based representation. The most common modeling conventions have been adopted by standard modeling languages like SysML (2021).

Graph rewriting can be employed within the scope of function-based design synthesis in two ways: first, for model-to-model transformations between the different abstraction layers. If a subfunction can be met by different components, different rules can be created to depict these possible transformations. By exploring the possible options, different concepts of an engineering system can be generated. This has been illustrated for mechanical engineering products by Bryant et al. (2006) or for the conceptual design of bridges by Slusarczyk and Strug (2017). A second use of graph rewriting techniques is of course on the structural level of abstraction, where rules can be embedded to determine the (optimal) configuration of function-derived elements. Tonhäuser and Rudolph (2017) show the entire process revisiting the well-known coffee maker example.

The abstraction involved in function-based design synthesis is a burden and a potential at the same time. Engineers naturally tend to details and visualizations, but thereby run the risk to get stuck in fixed ideas of design (Haberfellner et al., 2019). The abstraction of products by requirements and functions is a demanding and time-consuming process but may enable a better focus on the product essentials and trigger creativity. Further, it can simplify the definition and organization of rewriting rules (Helms and Shea, 2012). To understand the difference, the classification of engineering problems by Puppe (1990) can be referred to: deriving the structural components of a

design from a model-based representation of functionality results in a combination of an *assignment* and a *configuration* problem. For further search and optimization tasks, this is easier to solve than the *planning* task most design grammars aim to solve. Nevertheless, it is also possible to use a set of rules to evolve a design through an optimized sequence of actions, traversing various incomplete, intermediary states. Techniques to guide such a generation process are discussed in the next chapter.

6 GENERATIVE USE OF REWRITING RULES

6.1 Classification of Approaches

A graph rewriting system represents a set of process steps, without specifying their logic of application. Thus, besides the rules, the process of applying them to one or a range of specific problems must be designed. This difference is essential, whereas often the misconception is encountered that a given grammar can simply "crank out" (Krishnamurti and Stouffs, 1993) design solutions. Likely, this misconception comes from the fact that many early grammars for design, e.g., the palladian grammar (Stiny and Mitchell, 1978), included a lot of domain knowledge. These rules were restricted to be applied in a relatively specific order and to relatively specific problems. Further, another set of grammars must be taken into consideration. These grammars have very generic rules, applicable to a variety of problems. Most grammars that aim to solve the truss optimization problem (Shea, 1997) belong to this type. These grammars heavily rely on a sound description of their *dynamic* application to a variable environment. To highlight the difference between these two types of grammars, Ruiz-Montiel et al. (2013) introduced the terms *expert grammars* and *naive grammars*. This classification is comprehensible, even though there can be observed some hybrid approaches combining naive and expert rules (Puentes et al., 2020).

The distinction of reasoning approaches according to the problem-specificity of rules is certainly comprehensible but is not the only one. Hou and Stouffs (2018) prefer to categorize grammars according to the generation logic involved, distinguishing an *object-oriented* and a *goal-oriented* type. The former studies the configuration of the desired design outcome and restricts the vocabulary to the subsystems which are finally present, e.g., the building elements of a built house (Mitchell, 1991). This principle, found in the set grammars discussed in **Section 4.2**, facilitates the definition of rules and the exploration of design alternatives. The goal-oriented type, instead, defines rules by reflecting the most concise design process, commonly leading to more abstract non-terminal vocabulary and intermediary design states. To prioritize among the many options of action that may lead to the desired goal state, either a global search with an evaluation of the entire design or a local reasoning mechanism is applied. This categorization into object-oriented and goal-oriented approaches is equally comprehensible and applicable to most works discussed in this review.

The presented criteria enable to reflect a given grammar by it's specificity to one application environment and by the characteristics of the vocabulary. However, there is no commonly agreed taxonomy that can subsume a wide range of grammar-based reasoning techniques or could even practically support engineers in the design of their rule application strategy. Of course, not every grammar needs to be utilized with a sophisticated process control. Especially for expert grammars and object-oriented grammars, engineers often can constrain the search to a few variable parameters and few necessary choices. If this is possible, the exploration of the solution space may be achieved manually, by combinatorial methods as the enumerative generation or black-box methods as *generate and test* optimization algorithms. These three methods are commonly understood and agreed (Cagan et al., 2005; Grasl and Economou, 2013; Ruiz-Montiel et al., 2013). Still, some research should be mentioned that attempts to get more fine-grained control of the generation process. Thereby, a body of research can be subsumed into the paradigm of agent-based modeling, e.g., Heckel (2006), Ruiz-Montiel et al. (2013), McComb et al. (2017), and Puentes et al. (2020), another one to the use of logical descriptions (Duarte, 2005; Stouffs, 2015; Hou and Stouffs, 2019). The cited literature is referred to for further reading, while the following sections are limited to the well-established approaches.

6.2 Search Strategies

6.2.1 Enumerative Generation

If the engineer is able to define a sequence of rule applications that likely lead to valid designs, it is possible to simply enumerate all possible outcomes. Thereby, a search tree may be used to depict the options of generation. This tree commonly has as root the initial design state, and as edges the applicable rewriting rules. The linked children nodes are derived designs (Campbell et al., 2009). Filtered for repetitive and invalid leaf nodes, the search tree can serve for an enumerative generation of designs. This is a relatively old idea (Stiny and Mitchell, 1978), but still popular, due to the good impression it gives about the strictness, respectively expressiveness of a given grammar. To remedy the computational load and complexity of filtering the entire solution space, some remedies exist. Lienhard (2017) proposed clustering methods for building designs that make the solution space more comprehensible to a user. Campbell et al. (2009) and Kumar et al. (2014) propose to only generate a small set of possible solutions from a search tree. Depending on the quality of the produced designs, the later generations are optimized by updating the probabilities of decisions that led to good designs.

This is essentially the idea of a set of optimization algorithms that can be summarized as *generate and test* approaches. Generate-and test approaches do not use search trees but optimize only the input parameters of a generation process based on the cost of the outcome. No formal model of the generation process is required, wherefore one may think of it as a black-box process. Iteratively, the configuration shall be improved until only one or a set of few good designs remain. The two main algorithmic ideas used are simulated annealing and genetic programming (Ruiz-Montiel et al., 2013).

6.2.2 Optimization Algorithms

Simulated annealing optimizes a single design configuration based on the analogy of the cooling of metal. A steadily

decreasing "temperature" curve quantifies the willingness to accept deteriorations of cost by a rule application. An in-depth explanation of the algorithmic ideas is given by Cagan and Mitchell (1993), some recent applications include the optimization of piping systems of exhaust filters (Vogel, 2016) or rollerblade wheels (Zimmermann et al., 2018). For simulated annealing and a similar optimization algorithm, Königseder (2015) introduced methods to better understand the internals of grammars in a search process, e.g., the sensitivity and frequency of rules used. Remedying the restriction of simulated annealing to a single design solution, McComb et al. (2017) or Zimmermann et al. (2018) discuss the organization of multiple optimizations in parallel.

Genetic programming relies on a biological "survival of the fittest" principle. In every cycle, a set of designs is created where only the best ones are selected to go into the next phase or cycle. During every generation process, rules can be applied to conduct mutations of individuals. Further, the cross-over exchange of parameters is a desirable mechanism to create diversity within a population. The latter is desirable but very difficult as grammar-generated designs often do not share a common configuration of objects (van Diepen and Shea, 2019; Grzesiak-Kopeć et al., 2021). For hierarchical and well-structured representations, the works of Alber and Rudolph (2003), Talton et al. (2012), and Lienhard (2017) propose a possible solution: instead of processing the individual designs generated, it might be more promising to consider the rules the subject of a genetic optimization. Different variants are generated by different grammars in the first step. In further cycles, the grammars authoring the most successful individuals may be merged, by splitting and merging their vocabulary. This approach requires a deeper understanding of reasoning with grammars, but may contribute to make genetic optimization more powerful.

This concludes the overview of approaches to the reasoning for grammar-based design. In the last chapter, both potentials and shortcomings for further applications in the building sector are summarized.

7 CONCLUSION

7.1 Potentials

Graph models provide a powerful and flexible representation for many engineering products. For engineering design, the use of graph rewriting methods can enable the automation of complex design sequences. To this end, a variety of representation approaches can be distinguished, which can be classified according to the geometric meaning of the graph entities chosen. Low-level geometry representations give a high control and intuitiveness regarding geometric aspects, even though they require the introduction of higher-level textual or graphical interfaces. Set grammar approaches allow defining the design and design steps in a semantically more intuitive, object-oriented way. The extension of employed graph structures to entities of imperative logic or the combination of different programming paradigms may leverage the practical applicability of grammars in a broader context.

The development of graph rewriting systems for applications in engineering design receives increasingly more support. On the one hand, domain experts and learners with little knowledge about the underlying technology are encouraged by less technical and more graphical interfaces. In order to generate and optimize designs based on graph rewriting systems, established approaches can be relied on to perform an efficient search of vast solution spaces.

7.2 Shortcomings

To date, only a few industrial applications of graph rewriting methods have been known in engineering design. This may be owed to several challenges we discussed. One aspect is that the representation of a design problem by a graph model requires abstracting the system in a suitable manner. A variety of different approaches exists, with advantages and disadvantages. A key factor thereby is to represent and manipulate the geometry of engineering products properly. Approaches with a low-level representation of geometry often have the shortcoming of not enabling the definition of rules at a level of abstraction natural to engineers. Approaches with a high-level representation of geometry pose the challenge to efficiently store, transform, and interpret geometry. Despite a rich body of applied works, there is little theoretical discussion about the demanding task of defining a graph representation for a synthesis problem. Ideally, guidelines should be available to support engineers in the conceptual and technical design.

Given a meaningful representation, the efficient design of small sets of rules is a comparably resolved challenge. Still, the technical organization of grammars with larger rule sets to enable an efficient but variable generation of designs is a challenge. To this end, the use of function-based synthesis approaches seems promising, but yet has very few applications in the building sector. Further, the design of search methodologies in combination with a grammar is challenging. A large set of reasoning approaches have been described, differing by the way domain knowledge is formalized, the type of vocabulary, or the locality of evaluation criteria. However, a better uniform characterization and supportive guidelines could support engineers to better understand and design the functionalities of grammars for a generative design process.

AUTHOR CONTRIBUTIONS

LK: Main author, corresponding author SV: Writing sections, proofreading and contributing by prior research JA: Writing sections, proofreading and contributing by prior research AB: Writing sections, proofreading and contributing by prior research.

FUNDING

The authors gratefully acknowledge the financial support of the Deutsche Forschungsgemeinschaft (DFG) in the frame of the programs SPP 2187 "Adaptive modularized constructions made in a flux" (Project Number 423969184) and Transregio 277 "Additive Manufacturing in Construction—The Challenge of Large Scale" (Project Number 414265976).

REFERENCES

Abualdenien, J., and Borrmann, A. (2021). "PBG: A Parametric Building Graph Capturing and Transferring Detailing Patterns of Building Models," in Proc. of the CIB W78 Conference 2021 (Luxembourg: International Council for Research and Innovation in Building and Construction).

Alber, R., and Rudolph, S. (2003). 43 - a Generic Approach for Engineering Design Grammars: Aaai Technical Report Ss-03-02

Aouat, A., Bendella, F., and Deba, E. a. (2012). "Tools of Model Transformation by Graph Transformation," in 2012 IEEE International Conference on Computer Science and Automation Engineering (IEEE), 425–428. doi:10.1109/icsess.2012.6269495

Bak, C. (2015). *GP 2: Efficient Implementation of a Graph Programming Language* (York, United Kingdom: University of York). Ph.D. thesis.

Borrmann, A., and Rank, E. (2009). Topological Analysis of 3D Building Models Using a Spatial Query Language. *Adv. Eng. Inform.* 23, 370–385. doi:10.1016/j.aei.2009.06.001

Braun, A., Tuttas, S., Borrmann, A., and Stilla, U. (2015). "Automated Progress Monitoring Based on Photogrammetric point Clouds and Precedence Relationship Graphs," in The 32nd International Symposium on Automation and Robotics in Construction and Mining (ISARC 2015) (Oulu, Finnland: The International Association for Automation and Robotics in Construction (IAARC)). doi:10.22260/isarc2015/0034

Bryant, C. R., McAdams, D. A., Stone, R. B., Kurtoglu, T., and Campbell, M. I. (2006). "A Validation Study of an Automated Concept Generator Design Tool," in Volume 4a: 18th International Conference on Design Theory and Methodology (Philadelphia, United States: ASME), 283–294. doi:10.1115/DETC2006-99489

Cagan, J., Campbell, M. I., Finger, S., and Tomiyama, T. (2005). A Framework for Computational Design Synthesis: Model and Applications. *J. Comput. Inf. Sci. Eng.* 5, 171–181. doi:10.1115/1.2013289

Cagan, J., and Mitchell, W. J. (1993). Optimally Directed Shape Generation by Shape Annealing. *Environ. Plann. B* 20, 5–12. doi:10.1068/b200005

Campbell, M. I., Rai, R., and Kurtoglu, T. (2009). "A Stochastic Graph Grammar Algorithm for Interactive Search," in Volume 8: 14th Design for Manufacturing and the Life Cycle Conference; 6th Symposium on International Design and Design Education; 21st International Conference on Design Theory and Methodology, Parts A and B (Las Vegas, United States: ASME), 829–840. doi:10.1115/DETC2009-86804

Chakrabarti, A., Shea, K., Stone, R., Cagan, J., Campbell, M., Hernandez, N. V., et al. (2011). Computer-based Design Synthesis Research: An Overview. *ASME J. Comput. Inf. Sci. Eng.* 11 (2), 021003. doi:10.1115/1.3593409

Chen, Y., Sareh, P., Yan, J., Fallah, A. S., and Feng, J. (2019). An Integrated Geometric-Graph-Theoretic Approach to Representing Origami Structures and Their Corresponding Truss Frameworks. *J. Mech. Des.* 141 (9), 091402. doi:10.1115/1.4042791

Chomsky, N. (1959). On Certain Formal Properties of Grammars. *Inf. Control.* 2, 137–167. doi:10.1016/s0019-9958(59)90362-6

Corradini, A., Montanari, U., Rossi, F., Ehrig, H., Heckel, R., and Löwe, M. (1997). "Algebraic Approaches to Graph Transformation - Part I: Basic Concepts and Double Pushout Approach," in *Handbook of Graph Grammars and Computing by Graph Transformation*. Editor G. Rozenberg (Pisa, Italy: World Scientific), 163–245. doi:10.1142/9789812384720_0003

Drewes, F., Hoffmann, B., and Plump, D. (2002). Hierarchical Graph Transformation. *J. Comput. Syst. Sci.* 64, 249–283. doi:10.1006/jcss.2001.1790

Duarte, J. P. (2005). A Discursive Grammar for Customizing Mass Housing: the Case of Siza's Houses at Malagueira. *Automation in Construction* 14, 265–275. doi:10.1016/j.autcon.2004.07.013

Dy, B., and Stouffs, R. (2018). Combining Geometries and Descriptions: A Shape Grammar Plug-In for Grasshopper. *eCAADe* 36 (2), 498–598.

Economou, A., and Grasl, T. (2018). "Paperless Grammars," in *Computational Studies on Cultural Variation and Heredity*. Editor J.-H. Lee (Singapore: Springer), 139–160. KAIST Research Series. doi:10.1007/978-981-10-8189-7_12

Ehrig, H. (2006). *Fundamentals of Algebraic Graph Transformation*. Berlin/Heidelberg: Springer-Verlag. doi:10.1007/3-540-31188-2

Ermel, C., Rudolf, M., and Taentzer, G. (1999). "The AGG Approach: Language and Environment," in *Handbook of Graph Grammars and Computing by Graph Transformation: Volume 2: Applications, Languages and Tools* (Singapore: World Scientific), 551–603. doi:10.1142/9789812815149_0014

Geiß, R., Batz, G. V., Grund, D., Hack, S., and Szalkowski, A. (2006). "GrGen: A Fast SPO-Based Graph Rewriting Tool," in *Graph Transformations*. Editors D. Hutchison, T. Kanade, J. Kittler, J. M. Kleinberg, F. Mattern, J. C. Mitchell, et al. (Berlin, Heidelberg: Springer), 383–397. vol. 4178 of Lecture Notes in Computer Science. doi:10.1007/11841883_27

Geiß, R. (2008). *Graphersetzung mit Anwendungen im Übersetzerbau* (Karlsruhe, Germany: Karlsruhe Institute of Technology). Ph.D. thesis.

Ghamarian, A. H., de Mol, M., Rensink, A., Zambon, E., and Zimakova, M. (2012). Modelling and Analysis Using GROOVE. *Int. J. Softw. Tools Technol. Transfer* 14, 15–40. doi:10.1007/s10009-011-0186-x

Grabska, E., Łachwa, A., and Ślusarczyk, G. (2012). New Visual Languages Supporting Design of Multi-Storey Buildings. *Adv. Eng. Inform.* 26, 681–690. doi:10.1016/j.aei.2012.03.009

Grasl, T., and Economou, A. (2013). From Topologies to Shapes: Parametric Shape Grammars Implemented by Graphs. *Environ. Plann. B* 40, 905–922. doi:10.1068/b38156

Grasl, T. (2021). Grape Web Editor. Vienna, Austria: SWAP Architekten Zt GmbH. Available at: http://grape.swap-zt.com/App.

Grzesiak-Kopeć, K., Strug, B., and Ślusarczyk, G. (2021). Evolutionary Methods in House Floor Plan Design. *Appl. Sci.* 11, 8229. doi:10.3390/app11178229

Habel, A., Heckel, R., and Taentzer, G. (1996). Graph Grammars with Negative Application Conditions. *Fundamenta Informaticae* 26, 287–313. doi:10.3233/fi-1996-263404

Haberfellner, R., de Weck, O. L., Fricke, E., and Vössner, S. (2019). *Systems Engineering: Fundamentals and Applications*. Cham, Switzerland: Birkhäuser.

Havemann, S. (2005). *Generative Mesh Modeling* (Braunschweig: Technical University of Braunschweig). Ph.D. thesis. doi:10.24355/DBBS.084-200603150100-7

Heckel, R. (2006). Graph Transformation in a Nutshell. *Electron. Notes Theor. Comput. Sci.* 148, 187–198. doi:10.1016/j.entcs.2005.12.018

Heisserman, J. (1994). Generative Geometric Design. *IEEE Comput. Grap. Appl.* 14, 37–45. doi:10.1109/38.267469

Helms, B., and Shea, K. (2012). Computational Synthesis of Product Architectures Based on Object-Oriented Graph Grammars. *J. Mech. Des.* 134. doi:10.1115/1.4005592

H. Hick, K. Küpper, and H. Sorger (Editors) (2021). *Systems Engineering for Automotive Powertrain Development*. 1st ed (Cham: Springer International Publishing). Springer eBook Collection. doi:10.1007/978-3-319-99629-5

Hohmann, B., Havemann, S., Krispel, U., and Fellner, D. (2010). A GML Shape Grammar for Semantically Enriched 3d Building Models. *Comput. Graphics* 34, 322–334. doi:10.1016/j.cag.2010.05.007

Hoisl, F., and Shea, K. (2011). An Interactive, Visual Approach to Developing and Applying Parametric Three-Dimensional Spatial Grammars. *AIEDAM* 25, 333–356. doi:10.1017/s0890060411000205

Hoisl, F., and Shea, K. (2013). Three-dimensional Labels: A Unified Approach to Labels for a General Spatial Grammar Interpreter. *AIEDAM* 27, 359–375. doi:10.1017/S0890060413000188

Hooshmand, A., and Campbell, M. I. (2016). Truss Layout Design and Optimization Using a Generative Synthesis Approach. *Comput. Structures* 163, 1–28. doi:10.1016/j.compstruc.2015.09.010

Hou, D., and Stouffs, R. (2019). An Algorithmic Design Grammar Embedded with Heuristics. *Automation in Construction* 102, 308–331. doi:10.1016/j.autcon.2019.01.024

Hou, D., and Stouffs, R. (2018). An Algorithmic Design Grammar for Problem Solving. *Automation in Construction* 94, 417–437. doi:10.1016/j.autcon.2018.07.013

Jabi, W., Aish, R., Lannon, S., and Wardhana, N. (2018). "Topologic: A Toolkit for Spatial and Topological Modeling," in *Computing for a Better Tomorrow* (Poland: Lodz University of Technology).

Jakumeit, E., Blomer, J., and Geiß, R. (2021). GrGen Documentation. Karlsruhe, Germany: Institut für Programmstrukturen und Datenorganisation, Universität Karlsruhe. Available at: http://www.info.uni-karlsruhe.de/software/grgen/GrGenNET-Manual.pdf.

Jakumeit, E., Buchwald, S., and Kroll, M. (2010). Grgen.net. *Int. J. Softw. Tools Technol. Transfer* 12, 263–271. doi:10.1007/s10009-010-0148-8

Kahani, N., Bagherzadeh, M., Cordy, J. R., Dingel, J., and Varró, D. (2019). Survey and Classification of Model Transformation Tools. *Softw. Syst. Model.* 18, 2361–2397. doi:10.1007/s10270-018-0665-6

Kaveh, A., and Koohestani, K. (2008). Graph Products for Configuration Processing of Space Structures. *Comput. Structures* 86, 1219–1231. doi:10.1016/j.compstruc.2007.11.005

Kneidl, A., Borrmann, A., and Hartmann, D. (2012). Generation and Use of Sparse Navigation Graphs for Microscopic Pedestrian Simulation Models. *Adv. Eng. Inform.* 26, 669–680. EG-ICE 2011 + SI: Modern Concurrent Engineering. doi:10.1016/j.aei.2012.03.006

Knight, T. (2003). Computing with Emergence. *Environ. Plann. B Plann. Des.* 30, 125–155. doi:10.1068/b12914

Kolbeck, L., Auer, D., Fischer, O., Vilgertshofer, S., and Borrmann, A. (2021). "Modulare Brückenbauwerke aus carbonfaserbewehrtem Ultrahochleistungsbeton," in *Beton- und Stahlbetonbau Sonderheft "Schneller Bauen"* (Berlin, Germany: Ernst & Sohn), 116.

Königseder, C. (2015). *A Methodology for Supporting Design Grammar Development and Application in Computational Design Synthesis* (ETH Zurich). Ph.D. thesis. doi:10.3929/ethz-a-010567138

Krishnamurti, R., and Earl, C. F. (1992). Shape Recognition in Three Dimensions. *Environ. Plann. B* 19, 585–603. doi:10.1068/b190585

Krishnamurti, R., and Stouffs, R. (1993). "Spatial Grammars: Motivation, Comparison and New Results," in Proceedings of the 5th International Conference on Computer-Aided Architectural Design Futures (Pittsburgh, USA: Springer), 57–74.

Kumar, M., Campbell, M. I., Königseder, C., and Shea, K. (2014). "Rule Based Stochastic Tree Search," in *Design Computing and Cognition '12*. Editor J. S. Gero (Dordrecht: Springer Netherlands), 571–587. doi:10.1007/978-94-017-9112-0_31

Langenhan, C., Weber, M., Liwicki, M., Petzold, F., and Dengel, A. (2013). Graph-based Retrieval of Building Information Models for Supporting the Early Design Stages. *Adv. Eng. Inform.* 27, 413–426. doi:10.1016/j.aei.2013.04.005

Leblanc, T., Leblanc, J., and Poulin, P. (2011). "Component-based Modeling of Complete Buildings," in *Proceedings of Graphics Interface 2011* (Toronto, Ontario, Canada: Canadian Human-Computer Communications Society), 39, 87–100. GI 2011. doi:10.1177/009182961103900111

Lienhard, S. (2017). *Visualization, Adaptation, and Transformation of Procedural Grammars*. Ph.D. thesis. Lausanne: EPFL Lausanne. doi:10.5075/EPFL-THESIS-7627

Lindenmayer, A. (1968). Mathematical Models for Cellular Interactions in Development I. Filaments with One-Sided Inputs. *J. Theor. Biol.* 18, 280–299. doi:10.1016/0022-5193(68)90079-9

Lipp, M., Wonka, P., and Wimmer, M. (2008). Interactive Visual Editing of Grammars for Procedural Architecture. *ACM Trans. Graph.* 27, 1–10. doi:10.1145/1360612.1360701

Mc Neel and Associates (2021). Grasshopper Rhino. Seattle, United States: Mc Neel & Associates.

McComb, C., Cagan, J., and Kotovsky, K. (2017). Capturing Human Sequence-Learning Abilities in Configuration Design Tasks through Markov Chains. *J. Mech. Des.* 139 (9), 091101. doi:10.1115/1.4037185

McCormack, J., Cagan, J., and Antaki, J. (2008). "Aligning Shape Rule Creation with Modular Design: Minimizing the Cost of Using Shape Grammars," in Volume 4: 20th International Conference on Design Theory and Methodology; Second International Conference on Micro- and Nanosystems (ASMEDC), 107–118. doi:10.1115/DETC2008-49366

Mitchell, W. J. (1991). "Functional Grammars: An Introduction," in *Reality and Virtual Reality* (Newark, NJ: Association for Computer Aided Design in Architecture School of Architecture New Jersey Institute of Technology).

Nagl, M. (1979). *Graph-Grammatiken: Theorie Anwendungen Implementierung*. Wiesbaden: Vieweg. Studienbücher Informatik. doi:10.1007/978-3-663-01443-0

Nagl, M., Schürr, A., and Münch, M. (Editors) (2003). Applications of Graph Transformations with Industrial Relevance: International Workshop, AGTIVE'99, Kerkrade, The Netherlands, September 1-3, 1999 (Berlin: Springer-Verlag). Proceedings.

Nishida, G., Garcia-Dorado, I., Aliaga, D. G., Benes, B., and Bousseau, A. (2016). Interactive Sketching of Urban Procedural Models. *ACM Trans. Graph.* 35, 1–11. doi:10.1145/2897824.2925951

Oster, A., and McCormack, J. (2011). A Methodology for Creating Shape Rules during Product Design. *J. Mech. Des.* 133 (6), 061007. doi:10.1115/1.4004195

Patow, G. (2012). User-friendly Graph Editing for Procedural Modeling of Buildings. *IEEE Comput. Grap. Appl.* 32, 66–75. doi:10.1109/MCG.2010.104

Peysakhov, M., and Regli, W. C. (2003). Using Assembly Representations to Enable Evolutionary Design of Lego Structures. *AIEDAM* 17, 155–168. doi:10.1017/S0890060403172046

Puentes, L., Cagan, J., and McComb, C. (2020). Heuristic-guided Solution Search through a Two-Tiered Design Grammar. *J. Comput. Inf. Sci. Eng.* 20 (1), 011008. doi:10.1115/1.4044694

Puppe, F. (1990). *Problemlösungsmethoden in Expertensystemen*. Berlin, Heidelberg: Springer Berlin Heidelberg. Springer eBook Collection Computer Science and Engineering. doi:10.1007/978-3-642-76133-1

Rensink, A., and Taentzer, G. (2007). "Agtive 2007 Graph Transformation Tool Contest," in *International Symposium on Applications of Graph Transformations with Industrial Relevance* (Berlin: Springer-Verlag), 487–492.

Rensink, A. (2003). "The Groove Simulator: A Tool for State Space Generation," in *International Workshop on Applications of Graph Transformations with Industrial Relevance* (Berlin: Springer-Verlag), 479–485.

Riestenpatt, M., and Rudolph, S. (2019). "A Scientific Discourse on Creativity and Innovation in the Formal Context of Graph-Based Design Languages," in *Heron Island Conference on Computational and Cognitive Models of Creative Design*. Association for Computer Aided Design in Architecture. Herons Islands, Australia: Design Research Society (DRS).

Robinson, I., Webber, J., and Eifrem, E. (2015). *Graph Databases: New Opportunities for Connected Data*. second edition edn. Beijing and Boston and Farnham: O'Reilly.

Rossi, A., and Tessmann, O. (2017a). "Aggregated Structures: Approximating Topology Optimized Material Distribution with Discrete Building Blocks," in Proceedings of the IASS Annual Symposium 2017 Interfaces: Architecture, Engineering, Science, Hamburg, Germany. International Association of Shell & Spatial Structures.

Rossi, A., and Tessmann, O. (2017b). "Designing with Digital Materials: A Computational Framework for Discrete Assembly Design," in *Protocols, Flows and Glitches*. Editors P. Janssen, P. Loh, A. Raonic, and M. A. Schnabel (Hong Kong: CAADRIA).

Rossi, A. (2021). Wasp: Grasshopper Plugin for Discrete Assemblies.

Rozenberg, G. (1997). *Handbook of Graph Grammars and Computing by Graph Transformation*, Vol. 1. Singapore: World Scientific.

Rudolph, S. (2002). *Übertragung von Ähnlichkeitsbegriffen*. Stuttgart: Habilitation, Universität Stuttgart.

Ruiz-Montiel, M., Boned, J., Gavilanes, J., Jiménez, E., Mandow, L., and Pérez-de-la-Cruz, J.-L. (2013). Design with Shape Grammars and Reinforcement Learning. *Adv. Eng. Inform.* 27, 230–245. doi:10.1016/j.aei.2012.12.004

Runge, O., Ermel, C., and Taentzer, G. (2011). "AGG 2.0–new Features for Specifying and Analyzing Algebraic Graph Transformations," in *International Symposium on Applications of Graph Transformations with Industrial Relevance* (Berlin: Springer-Verlag), 81–88.

Schürr, A., Winter, A. J., and Zündorf, A. (1995). "Graph Grammar Engineering with PROGRES,". *Software Engineering - ESEC '95*. Editor W. Schäfer (Berlin: Springer-Verlag).

Shea, K. (1997). *Essays of Discrete Structures: Purposeful Design of Grammatical Structures by Directed Stochastic Search* (Pittsburgh: Carnegie Mellon University). Dissertation.

Silva, P. B., Müller, P., Bidarra, R., and Coelho, A. (2013). "Node-based Shape Grammar Representation and Editing," in Proceedings of the Workshop on Procedural Content Generation in Games PCG'13 (New York, United States: Association for Computing Machinery), 1–8.

Slusarczyk, E. G., and Strug, B. (2017). "A Graph-Based Generative Method for Supporting Bridge Design," in *24th EG-ICE International Workshop on Intelligent Computing in Engineering (EG-ICE 2017)*. Editors C. Koch, W. Tizani, and J. Ninić (Red Hook, NY: Curran Associates Inc).

Stiny, G. (1980). Introduction to Shape and Shape Grammars. *Environ. Plann. B* 7, 343–351. doi:10.1068/b070343

Stiny, G., and Mitchell, W. J. (1978). Counting Palladian Plans. *Environ. Plann. B Plann. Des.* 5, 189–198. doi:10.1068/b050189

Stouffs, R. (2015). "Description Grammars: An Overview," in *Emerging Experience in Past, Present and Future of Digital Architecture*. Editors Y. Ikeda, C. M. Herr,

S. Holzer, M. Kaijima, and M. Kim (Hong Kong: Association for Computer-Aided Architectural Design Research in Asia (CAADRIA)), 137–146.

Stouffs, R. (2019). "Predicates and Directives for a Parametric-Associative Matching Mechanism for Shapes and Shape Grammars," in *Blucher Design Proceedings* (São Paulo: Editora Blucher), 403–414. doi:10.5151/proceedings-ecaadesigradi2019_658

Strug, B., Ślusarczyk, G., Paszyńska, A., and Palacz, W. (2022). "A Survey of Different Graph Structures Used in Modeling Design, Engineering and Computer Science Problems," in *Graph-Based Modeling in Science, Technology and Art*. Editors S. Zawiślak and J. Rysiński (Cham: Springer International Publishing), 243–275. vol. 107 of Mechanisms and Machine Science. doi:10.1007/978-3-030-76787-7_12

Sysml (2021). SysML Open Source Project - what Is SysML? Who Created SysML. Available at: SysML.org.

Talton, J., Yang, L., Kumar, R., Lim, M., Goodman, N., and Měch, R. (2012). "Learning Design Patterns with Bayesian Grammar Induction," in *Proceedings of the 25th Annual ACM Symposium on User Interface Software and Technology - UIST '12*. Editors R. Miller, H. Benko, and C. Latulipe (New York, New York, USA: ACM Press), 63. doi:10.1145/2380116.2380127

Tonhäuser, C., and Rudolph, S. (2017). "Individual Coffee Maker Design Using Graph-Based Design Languages," in *Design Computing and Cognition '16*. Editor J. S. Gero (Cham: Springer International Publishing), 513–533. doi:10.1007/978-3-319-44989-0_28

Tratt, L. (2010). "Theory and Practice of Model Transformations," in Third International Conference, ICMT 2010, Malaga, Spain, June 28-July 2. 2010. Proceedings. doi:10.1007/978-3-642-13688-7

van Diepen, M., and Shea, K. (2019). A Spatial Grammar Method for the Computational Design Synthesis of Virtual Soft Locomotion Robots. *J. Mech. Des.* 141 (10), 101402. doi:10.1115/1.4043314

Veit Batz, G., Kroll, M., and Geiß, R. (2008). "A First Experimental Evaluation of Search Plan Driven Graph Pattern Matching," in *Applications of Graph Transformations with Industrial Relevance*. Editors A. Schürr, M. Nagl, and A. Zündorf (Berlin, Heidelberg: Springer), 471–486. doi:10.1007/978-3-540-89020-1_32

Vestartas, P. (2021). *Design-to-Fabrication Workflow for Raw-Sawn-Timber Using Joinery Solver* (LausanneSwitzerland: EPFL). Ph.D. thesis. doi:10.5075/EPFL-THESIS-8928

Vilgertshofer, S., and Borrmann, A. (2017). Using Graph Rewriting Methods for the Semi-automatic Generation of Parametric Infrastructure Models. *Adv. Eng. Inform.* 33, 502–515. doi:10.1016/j.aei.2017.07.003

Vogel, S. (2016). *Über Ordnungsmechanismen im wissensbasierten Entwurf von SCR-Systemen* (Stuttgart: Universität Stuttgart). Dissertation. doi:10.18419/opus-8829

Whiting, M. E., Cagan, J., and LeDuc, P. (2018). Efficient Probabilistic Grammar Induction for Design. *AIEDAM* 32, 177–188. doi:10.1017/S0890060417000464

Wonka, P., Wimmer, M., Sillion, F., and Ribarsky, W. (2003). "Instant Architecture," in *ACM SIGGRAPH 2003 Papers on - SIGGRAPH '03*. Editor A. P. Rockwood (New York, USA: ACM Press), 669. doi:10.1145/1201775.882324

Wortmann, T. (2013). *Representing Shapes as Graphs : A Feasible Approach for the Computer Implementation of Parametric Visual Calculating* (USA: Massachusetts Institute of Technology). Diploma thesis.

Zimmermann, L., Chen, T., and Shea, K. (2018). A 3d, Performance-Driven Generative Design Framework: Automating the Link from a 3d Spatial Grammar Interpreter to Structural Finite Element Analysis and Stochastic Optimization. *AIEDAM* 32, 189–199. doi:10.1017/S0890060417000324

Conflict of Interest: The authors declare that the research was conducted in the absence of any commercial or financial relationships that could be construed as a potential conflict of interest.

Publisher's Note: All claims expressed in this article are solely those of the authors and do not necessarily represent those of their affiliated organizations, or those of the publisher, the editors and the reviewers. Any product that may be evaluated in this article, or claim that may be made by its manufacturer, is not guaranteed or endorsed by the publisher.

frontiers in Built Environment

REVIEW
published: 09 February 2022
doi: 10.3389/fbuil.2022.815717

Machine Learning in Structural Design: An Opinionated Review

Christian Málaga-Chuquitaype *

Department of Civil and Environmental Engineering, Imperial College London, London, United Kingdom

The prominence gained by Artificial Intelligence (AI) over all aspects of human activity today cannot be overstated. This technology is no newcomer to structural engineering, with logic-based AI systems used to carry out design explorations as early as the 1980s. Nevertheless, the advent of low-cost data collection and processing capabilities have granted new impetus and a degree of ubiquity to AI-based engineering solutions. This review paper ends by posing the question of how long will the human engineer be needed in structural design. However, the paper does not aim to answer this question, not least because all such predictions have a history of going wrong. Instead, the paper assumes throughout as valid the claim that the need for human engineers in conventional design practice has its days numbered. In order to build the case towards the final question, the paper starts with a general description of the currently available AI frameworks and their Machine Learning (ML) sub-classes. The paper then proceeds to review a selected number of studies on the application of AI in structural engineering design. A discussion of specific challenges and future needs is presented with emphasis on the much exalted roles of "engineering intuition" and "creativity". Finally, the conclusion section of the paper compiles the findings and outlines the challenges and future research directions.

Keywords: artificial intelligence, machine learning, structural design, structural engineering, design space

OPEN ACCESS

Edited by:
Izuru Takewaki,
Kyoto University, Japan

Reviewed by:
Xinzheng Lu,
Tsinghua University, China
Kazuki Hayashi,
Kyoto University, Japan

***Correspondence:**
Christian Málaga-Chuquitaype
c.malaga@imperial.ac.uk

Specialty section:
This article was submitted to Earthquake Engineering, a section of the journal Frontiers in Built Environment

Received: *15 November 2021*
Accepted: *13 January 2022*
Published: *09 February 2022*

Citation:
Málaga-Chuquitaype C (2022) Machine Learning in Structural Design: An Opinionated Review. Front. Built Environ. 8:815717. doi: 10.3389/fbuil.2022.815717

1 INTRODUCTION

We call structural design the process by which the number, distribution, shape and size of structural elements, and their connectivity is determined so that a given design objective is achieved while meeting a number of constraints of serviceability and resistance. The objective can be the minimization of material consumption but in practice, it is more likely to be related to cost minimization and to involve trade-offs between manufacturing, logistical and sometimes sustainability considerations. At the beginning of the structural design process, human engineers are usually provided with the overall geometry—through Building Information Models (Jung and Joo, 2011), for example—and their task is to come up with specifications of the distribution of structural elements including their materials and sections. This process is carried out using a diverse collection of computational tools, from information modelling to structural analysis; sampling from catalogues involving hundreds of structural sections and with constant reference to thousands of pages of codes of practice. Consequently, as it stands today, structural design entails a significant and oftentimes tedious solution-searching process involving various complex and non-fully overlapping multi-dimensional domains, multiple constraints and large uncertainties, whereby arriving to a global optima would be a prohibitively time-consuming endeavour. Therefore, more often than not, the engineer's search will be brief and they will settle for the first sub-optimal design that satisfies all

the hard constraints. Unsurprisingly, a range of tools have been proposed to carry out the optimization of some of the better-posed problems involving a relatively low number of structural elements, e.g., (Jewett and Carstensen, 2019; Amir and Shakour, 2018; Tsavdaridis et al., 2015); and more recently these tools have started to incorporate additional and more realistic complexities like dynamic actions (Giraldo-Londoño and Paulino, 2021), manufacturing processes (Zegard and Paulino, 2016; Carstensen, 2020), etc. However, the emphasis of this paper is not on the generation of targeted topology-optimized solutions for which excellent review articles can be found elsewhere, e.g., (Thomas et al., 2021). Instead, this opinionated review concentrates on the exploration of large and complex integrated design spaces with the aid of artificial intelligence (AI) and, more specifically, the increasing role that Machine Learning (ML) algorithms are playing in this search.

Artificial Intelligence (AI) is the branch of science that is concerned with the re-creation of human cognitive functions by artificial means. Although this is most commonly attempted via digital computers, other media, notably biological systems (Qian et al., 2011; Sarkar et al., 2021), have been and continue to be used with this purpose. This paper, however, focuses on the role of intelligent algorithms for digital computers; or more precisely, algorithms whose distinctive feature is their ability to learn. In this context, Machine Learning (ML) is a branch of AI whose central advantage is its potential to automatically detect patterns in data under uncertainty (Murphy, 2012). This uncertainty arises inevitably from the limited size of the datasets employed but it also reflects errors in data collection (including measurement) as well as hard epistemic paucities.

One of the first approaches to replicate human cognition was to organize "knowledge" as a collection of mutually related facts. Once a database of facts was built, so the belief went, inference rules could be used to query it, revealing the interconnections and allowing questions, including those related to engineering design, to be answered. The use of this type of AI in structural design was discussed as early as 1978 by Fenves and Norabhoompipat (1978) and application examples appeared in the early 1980s. For example, Bennett et al. (1978) developed a program consisting of 170 production rules and 140 consultation parameters to assist the engineer in the application of Finite Element Analysis (FEA) to the design of building structures. Also, Maher and Fenves (1985) constructed an expert system for the preliminary design of high-rise framed buildings. They used weighing factors to compare different gravity and lateral resisting structural systems highlighting the "best" design according to the criterion of a linear evaluation function. Other researchers like Ishizuka et al. (1981) used rule-based systems to infer seismic damage on the basis of a database of earthquake accelerograms and visual inspection reports. However, it soon became apparent that hard rules can not replicate the human inferential process and that their contribution to design would be limited, not least because the world for which engineers design is brimming with uncertainty but also because exceptions to the rule are all too common. Logic-based AI was abandoned.

With the passage of time, probabilistic reasoning made its way into ML and message passing architectures, which model

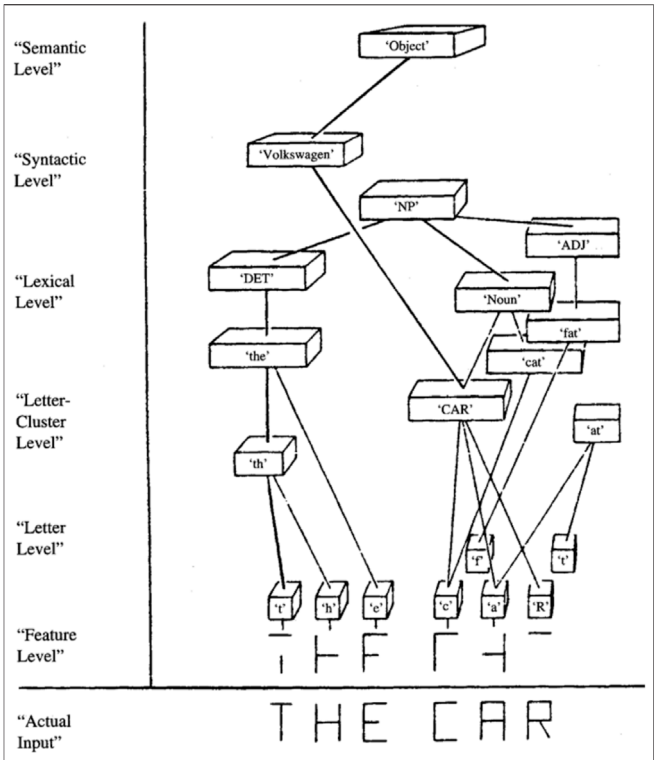

FIGURE 1 | (Rumelhart, 1994) Message Center near the end of processing when the semantics of the imput have been well defined.

intelligence on the basis of human neural information passing (Rumelhart et al., 1986), started to take the computational demands on storage and processing down to manageable levels. By the end of the 1980s, Bayesian Networks (BN) had become a practical scheme for ML (Pearl, 1988). BN have proven useful in evaluating the reliability of structures and infrastructure systems with multiple components and multiple failure sequences (Mahadevan et al., 2001). And Naive Bayes classifiers have been used to construct damage fragilities, e.g. (Kiani et al., 2019), predict the strength of structural components, e.g. (Mangalathu and Jeon, 2018), or estimate structural failure modes, e.g. (Mangalathu et al., 2020).

Meanwhile, Artificial Neural Networks, or Neural Networks (NN) for short, started to be used in all branches of engineering design. One of the first studies to apply back-propagation NN—an approach initially devised by Rumelhart et al. (1986)—to structural engineering was conducted by Vanluchene and Sun (1990). In their pioneering study, Vanluchene and Sun (1990) applied NN to the pattern recognition of a loaded beam, to the design of a simply supported reinforced concrete beam and to the structural analysis of a plate. NNs are abstractions of the functioning of the human brain that aim to replicate its ability to acquire knowledge through learning and storing in the form of interconnecting synaptic weights. In true fashion of the process originally hypothesised by Rumelhart et al. (**Figure 1**) the network takes a set of features as inputs and applies complex

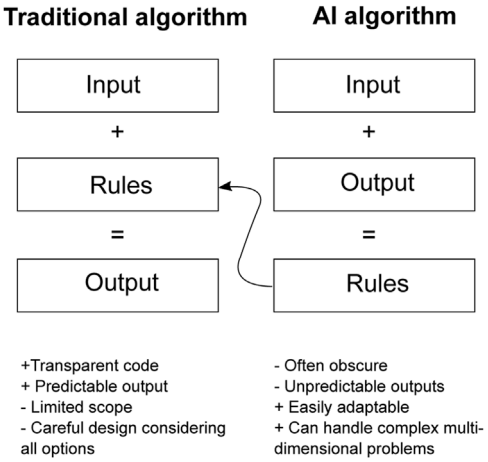

FIGURE 2 | Traditional vs. AI algorithms.

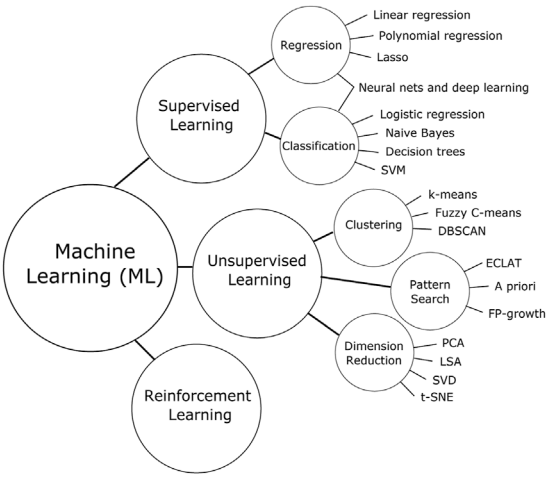

FIGURE 3 | Categories of ML algorithms.

feature fusion operations through a series of layers of neurons. The final layer outputs the end response either as a prediction or as a form of classification.

NN models (and their deep learning variants) have become extremely popular nowadays driven by the media coverage of their superb feature recognition capabilities and the notorious increase in computational power together with the wide accessibility of tools and libraries. Accordingly, NN have been used in seismic response prediction, e.g., Morfidis and Kostinakis (2017); Lagaros and Fragiadakis (2007), system identification, e.g., Sivandi-Pour et al. (2020), damage localization, e.g., Bani-Hani et al. (1999); Gharehbaghi et al. (2021) and in structural control, e.g., (Khalatbarisoltani et al., 2019; Suresh et al., 2010), among other structural engineering tasks. The literature on NN (and indeed ML) applications to structural engineering is vast. Sun et al. (2021) provide a comprehensive review of ML methods used to predict and asses structural performance and to identify structural conditions. Some of these can be used in support of structural design but do not directly deal with structural design *per se*, defined in the form presented earlier in this paper. In fact, issues related to ML and structural design, as defined above, are not particularly well covered in the literature despite the proven potential brought about by leveraging AI technologies and ML algorithms to improve the exploration of design alternatives beyond current human cognitive levels.

It follows from the previous discussion that existing design optimization methods concentrate on individual structural subassemblies and do not serve to automate the design of entire structures. By contrast, this paper will explore the use of ML algorithms to automate structural designs *stricto sensu*. To this end, this paper proceeds to review a selected number of studies on the application of ML in structural engineering design. A discussion of specific challenges and future needs is presented with emphasis on the much exalted roles of 'engineering intuition' and 'creativity'. Finally, the conclusion section of the paper compiles the findings and outlines the challenges and future research directions. But first, the paper will provide a general introduction to AI and ML methods.

2 BACKGROUND ON AI AND ML

As mentioned above, central to AI and ML algorithms is the ability to learn, potentially achieving the super-human ability of recognising patters in high-dimensional datasets that have remained impenetrable to the human mind. **Figure 2** compares the way traditional and AI software operate. In a traditional piece of software, the coder writes a "comprehensive" set of rules that the program must follow. Therefore, it is the sole responsibility of the programmer to consider all possible scenarios and to hard-code into the algorithm all the appropriate responses to these scenarios. It should be possible, in principle, to arrive to the precise output by following the path through the code given a specific input. By contrast, in AI algorithms the rules are created by the algorithm itself and the coder only provides the scaffold (or architecture) and feeds data into it. The AI algorithm will analyse the data and fill this scaffold with its own through training. Once those rules are established, they can then be used in the traditional way to predict other outputs given an input. The fact that the coder is exempt from considering and including all potential scenarios makes AI particularly useful when dealing with large datasets or complex processes.

The differences in construction and operation between traditional and AI software express themselves in a number of ways. Traditional code is naturally transparent and generally easy to predict while ML can be obscure and may produce unexpected results or include biases that are not always easy to detect. On the other hand, traditional algorithms will be limited to what the coder has predicted at first, while AI software is in principle easy to adapt without significant changes in the code. Traditional software demands the coder to capture carefully and accurately all the potential scenarios, while AI can handle complex problems

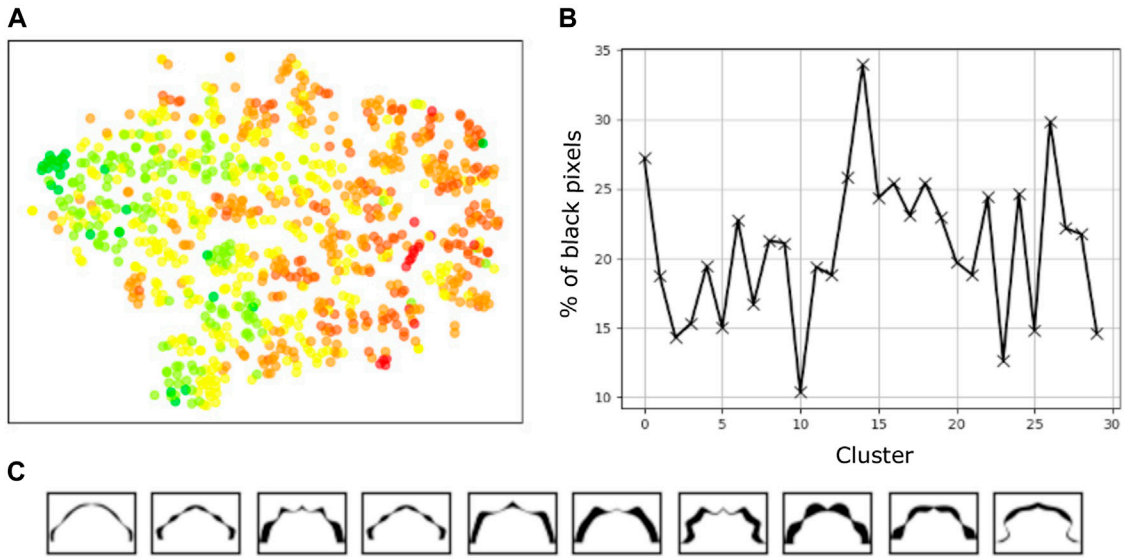

FIGURE 4 | Latent space representation of the data points coloured depending on the occupancy of the arches (a measure of the material usage) for the seismic design scenario. The latent space **(A)** is presented together with the plot of the mean occupancy of each cluster **(B)** and sample shapes from the best selected cluster **(C)**. Adapted from Palmeri et al. (2021) based on the CAE model of Maqdah et al. (2021).

more efficiently than humans, especially when they involve multiple dimensions or large datasets.

Broadly speaking, ML algorithms can be categorized in three main groups: supervised, unsupervised and reinforcement learning, depicted in **Figure 3**. Supervised learning is probably the closest to human learning. A series of "examples" is used by the ML algorithm to build "knowledge" about a given task in a similar way to how humans build and use "past experience" (Dietterich, 1996) like when small children are guided in their association of words to meanings. To this end, supervised models are given a set of features as input and labels as output. Then, the models attempt to find a set of rules to match a given set of features to the correct label guided by some measure of success. The process employs statistical methods for the learning operations and manual adjustments are usually not required. However, supervised ML relies on large amounts of correctly labelled input data, in quantities that can be significantly larger than those required by humans (Kühl et al., 2020).

On the other hand, unsupervised learning can be applied to different data types. In this approach, labels are not required, just features. The model is given those features and its algorithm then groups them according to some unknown property. In general, unsupervised models try to do one of three things: either cluster the data provided, find an anomaly in it, or reduce the number of dimensions in which to express the dataset. Grouping works by clustering data points that share some features without knowing what labels or indeed what categories are present. In anomaly detection or pattern recognition, a defining set of features is found and the model classifies the data point as either part of the set or as an anomaly. This is very helpful in failure identification or structural characterization. Reinforcement learning builds on these ideas and sometimes uses the algorithms developed for supervised and unsupervised learning. It is used in situations where it is difficult to get perfectly correct labels. In such cases, the algorithm is provided with an input and a reward function that gives an indication of how well or bad the algorithm is doing. The algorithm then learns how to maximise the reward.

In general, the creation of a typical AI algorithm involves four main stages. It starts with the data preparation. This is a crucial stage that can take longer than the others. It involves the acquisition of data, its analysis and pre-processing. The quality and quantity of data are determinant for a good output of the model. The second stage is the design of the model, which is followed by the third stage of training and evaluation. It is not uncommon that at the end of this process, the coder realises that changes are required in the data or the model architecture, and the design should be re-adjusted. Once the model is considered well designed and trained it is ready to enter its final stage of deployment.

3 AI AND THE DESIGN OF SPATIAL STRUCTURES

Although shells, vaults and other spatial structures are already among the most efficient structural forms and have a notoriously complex structural response, they have been fertile ground for many structural design optimization explorations. This may be because shells can be discretised as meshes with known support locations which, despite requiring hundreds of variables, are usually single-layered and lend themselves more easily to parametrization than the reticulated multi-storey frames with a multitude of potential element locations, sizes and connection types used in buildings. However, even if a highly parametrized design space is used, its sheer size still makes it trackless to the human mind. Therefore, the basic capability of machine learning

to discover and rebuild complicated underlying connections between input and output variables from a relatively big dataset (Liu et al., 2020) can be of great use while designing spatial structures.

Mirra and Pugnale (2021) examined AI-generated design spaces built using Variational Autoencoder (VAE) models, and compared their outputs with those coming from a human-generated explicit definition of design variables. Two relatively simple but realistic cases were explored by Mirra and Pugnale involving triangular and square footprints. A dataset of 800 depth maps obtained from 3D models were used to train the VAE. Three objectives were set for the optimization, including: 1) the maximisation of the structural performance, quantified in terms of deformations obtained from Finite Element Analysis (FEA), 2) the maximisation of the height of the shell openings, and 3) the minimisation of the difference between the final and target footprints. They found that the AI-generated outputs had a greater diversity and responded better to the performance criteria in comparison with the solutions obtained from human-defined generative designs. Besides, AI solutions included structural configurations that would not have been possible to find within the human-defined design space. This hints to one of the main advantages of using AI in design: the possibility of exploring design options beyond those traditionally developed by human intelligence (Mueller, 2014).

The exploration of diverse design options brought about by AI was also exploited by Maqdah et al. (2021) and Palmeri et al. (2021) while studying the provision of structurally-efficient regolith-based arch forms for extraterrestrial construction. They built unsupervised machine learning models (Convolutional Autoencoders, CAE) capable of detecting patterns and differentiating between arch geometries and their stress and deformation contours (**Figure 4**). These models were then used to search for optimal sectional geometries considering the effects of extreme thermal changes and seismic action under low-gravity conditions. Various datasets, each one with over 500 thermal and static FEA analysis and a 60–40% training-validation split were constructed for this purpose. Although the optimal configurations found resembled those obtained by more traditional approaches (McLean et al., 2021), the possibility of including a diversity of design actions (gravity, thermal, and seismic) and a substantial number of dimensions that are then reduced to a smaller latent space where a holistic search process can be used was featured as a clear contribution of AI. Moreover, Maqdah et al. (2021) and Palmeri et al. (2021) were able to elucidate some of the dependencies of the latent space (reduced) dimensions on geometric and structural parameters which can be helpful in making informed (partially explainable) searches. Alongside the CAE, regression models were used to allow the visualisation of the changes in the arch shape and stress fields when moving towards a certain direction in the design space.

The works of Zheng et al. (2020) and Fuhrimann et al. (2018) have explored the use of ML in leveraging the fundamental relationship between force and form in shells. Zheng et al. (2020) trained a NN model to predict the relations between subdivision rules and structural and constructional performance metrics on the basis of graphic statics results. This surrogate use of ML models to enable a rapid exploration of design spaces constitutes one of many important attempts to improve the machine-human collaboration. Unfortunately, the parameters employed; notably for constructibility (i.e., number of faces with areas greater than a given threshold), may seem too simple proxies to capture the complexities of the manufacturing and construction challenges. On the other hand, Fuhrimann et al. (2018) also explored the potential of combining form-finding with ML in the form of Combinatorial Equilibrium Modelling and Self Organizing Maps. Central to these works is the need to grasp a complex space of solutions in order to both increase its diversity and to make it manageable to the designer.

The previously mentioned works have highlighted the basic capability of ML to discover and rebuild complicated underlying connections between input and output variables and to find relationships between structural shape and performance. Once those relationships are established, the corresponding optimization of the structural configuration is simplified (Liu et al., 2020). However, to set an optimization process where the design parameters are chosen automatically by the machine (algorithm) without human intervention remains difficult. This is because these parameters must exist in a low-dimensional space that can be optimized while not sacrificing their representational capacity. An issue that was also observed while optimizing the design of materials (Xue et al., 2020).

An alternative approach was followed by Danhaive and Mueller (2021) who tackled the design of a long span roof structure. For this purpose, they used variational auto encoders (VAE) to train low-dimensional (2D) models that are intuitive to explore by the human engineer. By conditioning the models on different performance indicators, the models can adapt their mappings. A new performance-driven sampling algorithm was proposed to generate databases that are biased towards design regions with high performing structures. The structural performance indicators employed in the case study are only mass dependent and are normalized so they are evenly distributed on the unit segment. A total of 36 design variables, mainly topological, were used in the design and dimensioning of the truss elements using the cross-section optimizer available in Karamba (Preisinger and Heimrath, 2014). The salient feature of this approach is that it gives the human designer a greater control over performance trade-offs standing in the middle between optimization methods, on the one side, and undirected search algorithms, on the other.

The support provided by ML algorithms to the design of spatial structures are not conscripted to structural calculations but can include the quantification of traditionally less quantifiable metrics such as aesthetics. For example, Zheng (2019) developed a NN that could be used to quantitatively evaluate the personal taste of an architect. By using force diagrams of polyhedral geometries with unique and distinguishable forms and a clear data structure and asking the human architect to score the inputs, a NN was trained to learn their design preferences. The results, which may seem unsurprising at first sight, put in evidence the capability of ML to express what may be considered as inexplicit. In doing so, Zheng demonstrated not only that solutions with

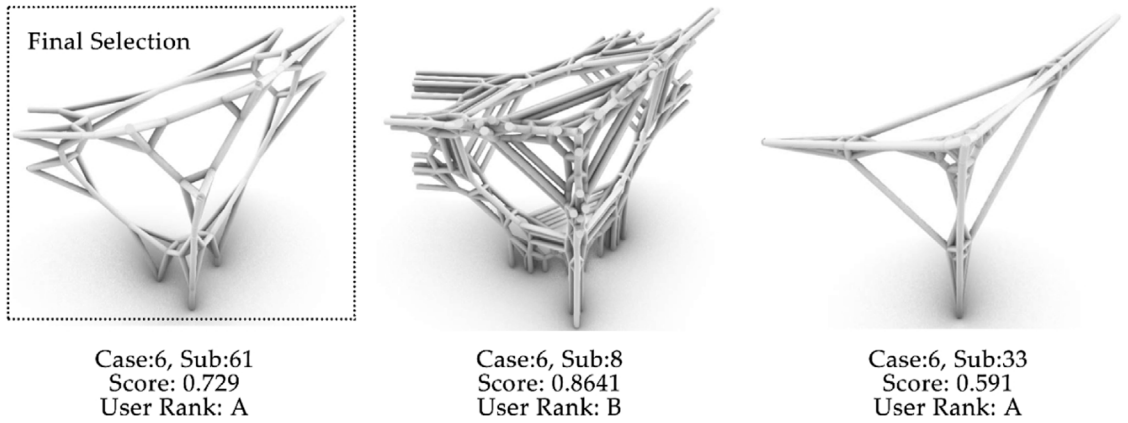

FIGURE 5 | Selection of form-found structures considering user taste by Zheng (2019).

higher scores can be generated with a higher probability of satisfying any personal design taste, but what is more important, that ML can learn relationships that may be difficult to articulate in human parlance. It should be noted that, given the natural difficulties human designers face when asked to score many forms consistently to the same standard. In these cases, the scores were mapped into a grading scale, from A to D, which considers the number of times the forms have been selected. This explains the final selection presented in **Figure 5** where a structure with an initial score of 0.729 is chosen on top of another with a score of 0.864. This is a compromised solution, but one that massively narrows down the variety of forms from which the designer has to choose. Thus, the door is open to integrate both mechanistic and quantifiable metrics with other kinds of design considerations and to apply this to a diversity of design tasks.

4 AI APPLIED TO THE DESIGN OF BUILDING STRUCTURES

The rationalization of the design process of building structures, within a structural optimization framework, has usually been separated into three components (Havelia, 2016): 1) topology, which involves decisions on the number and connectivity of members, usually done without optimizing the connection itself; 2) shape, which involves decisions related to the location of elements and the layout of joints; and 3) sizing, which involves defining member cross sections. More often than not, these components are treated separately in the scientific literature, however, they are strongly interrelated and decisions involving one will greatly affect the others. Usually, the layout space is reduced by architectural considerations, but it will still encompass a large number of potential locations that are difficult to explore without any pre-determining guiding principle. Besides, early estimates of the building cost are usually based on weight, however, the majority of the total cost can sometimes be attributed to fabrication and erection which are not always directly proportional to weight (Kang and Miranda, 2005) In addition, material costs depend not only on tonnage, but also on the type and size of cross sections utilized and erection costs are also highly contingent on geography and local market conditions Klanšek and Kravanja (2006). These facts will automatically render impractical most topology optimization studies carried out to date.

Some studies have incorporated, albeit in a simplified manner, the design complexities outlined above. For example, Torii et al. (2016) developed an optimization algorithm that penalizes the number of members and joints in the structure in proportion to the number of connected elements. Unfortunately, this was only applied to trusses and no consideration was given to the fact that the connection type is determinant in their cost. Hassett and Putkey (2002) collected a comprehensive list of cost drivers and their values for the most common moment-resisting and pinned connections in the AISC catalogue. And Zhu et al. (2014) considered constructibility issues in the optimization of frames and demonstrated that some structures with a less efficient load path can improve constructibility and lead to overall lower costs. Zolfagharian and Irizarry (2017) used Principal Component Analysis, a clustering ML technique, to group constructibility factors into six major categories. To this end, they assembled a dataset, via industry interviews, on 79 different constructibility factors with given scores. As the design space increases exponentially with the number of structural elements, the number of structural typologies analysed, their connectivity and the constructibility considerations, most currently available optimization methods are rendered impractical for full-scale real implementation. Other proposals, like that of Havelia (2016) have used methods based on topology and sizing optimization within a multi-disciplinary architecture suitable for 2D steel framed buildings. Again, Havelia's study showed that a heavier structure can be more economical than its lighter counterpart when connection and fabrication costs are taken into account. One drawback of this study is that serviceability constraints like maximum deflection or vibrations are not considered and therefore its applicability to real designs is hampered. On the other hand, high profile applications of structural optimization like the Chicago 800

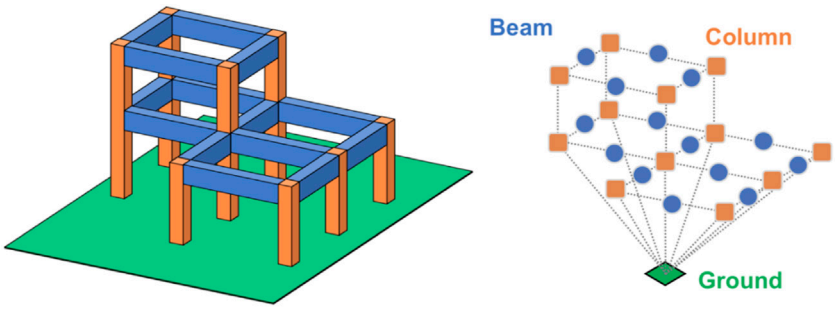

FIGURE 6 | An example building structure and its structural graph representation suitable for analysis by GNN, from Chang and Cheng (2020).

West Fulton Market or Shezhen's Financial Center do not aim to optimize the whole building economy or constructibility but are concerned with only a small proportion of its load carrying elements.

One of the first studies that departs from the above mentioned trend is that of Ranalli (2021) who proposed a new AI-based optimization module for the design of a flooring system with varying degrees of composite action. User-defined variables employed include the depth of the slab, the height of the steel deck, the properties of concrete, a range of possible cambers, the option to use shoring during construction, the degree of composite action, and the range of wide flange sections. The optimization framework iterates through each beam and girder, automatically determines its static scheme, computes the governing moment and deflection demands under the applied loads, and efficiently iterates through the set of available design options to find the most economical and feasible solution. Serviceability limits are considered and material and labour rates are assigned to arrive to an optimal solution through a scenario exploration. However, the gravity resisting columns are not considered, nor are issues related to their continuity and the rotational restraint (or flexibility) they provide to the floor. Nevertheless, the main strengths of Ranalli's AI-driven optimization framework are its computational scalability and its readiness of applicability to new steel frame designs with minimal pre-processing efforts.

Another interesting work was performed by Chang and Cheng (2020) who re-formulate building frames as graphs (**Figure 6**)and use Graph NN (or GNN) trained on simulation results that can learn to suggest optimal beam and column cross-sections. This is one of the first attempts to use GNN in the realm of design optimization aided by differentiable approximators. The optimization objective employed by Chang and Cheng (2020) is simplistic, involving only mass minimization, but a variety of constraints is considered together with serviceability limits to produce optimal designs. The results are reported to be consistent with typical engineering designs and also comparable to outputs from Genetic Algorithm optimizations. The main limitations of this work are related to the absence of slab continuity effects and the treatment of the building skeleton as an input. However, the possibility of implementing a graph representation and generation algorithm in the initial phases of design to provide an end-do-end solution generating tool is worth exploring further.

Similarly, Ampanavos et al. (2021) developed a ML system for the automatic generation of building layouts aimed at helping architects present structurally feasible solutions during the early stages of the project. A peculiarity of the system is that it does not aim to estimate the full structure to start with, but uses an iterative approach where the neural network gradually extends the solution as necessary. In this way, the NN has better changes of identifying patterns on a small building area at each step. However, this approach is also prone to error accumulation for large structures, although this error is dependent on the size of the training dataset. Besides, the column positioning can be noisy. However, future combinations of this approach with element sizing tools and more sound structural considerations are likely to produce a scalable and helpful methodology.

In his thesis, Ranalli (2021), mentioned above, also considered the problem of sizing lateral load resisting systems against strong loads typical of earthquakes. The author treated this problem in two iterative phases, the first of which searches for the most economical solution that meets strength, constructibility and ductility criteria. The second phase checks for lateral drift compliance and design load combinations. An energy based analysis is performed in case particular floors need to be adapted to comply with the drift limits. The strength of this study is that is able to combine commonly used analysis tools and relatively justified cost functions to provide a whole-encompassing approach to building design. It is also worth noting that a high variance of cost across different design scenarios was observed highlighting the important role of even small changes in the variables on the overall building cost.

The above mentioned studies are mainly devoted to steel framed solutions, where the domain is discrete since only a certain number of steel sections are available. This may simplify and reduce the design space and facilitate the consideration of constructibility functions. By contrast, designing concrete structures may introduce additional complications since a relatively broader design space is to be considered with added variations in member detailing. These issues were approached by Pizarro and Massone (2021) who aimed at supporting the design of reinforced concrete buildings by keeping track of previously accepted design solutions, in

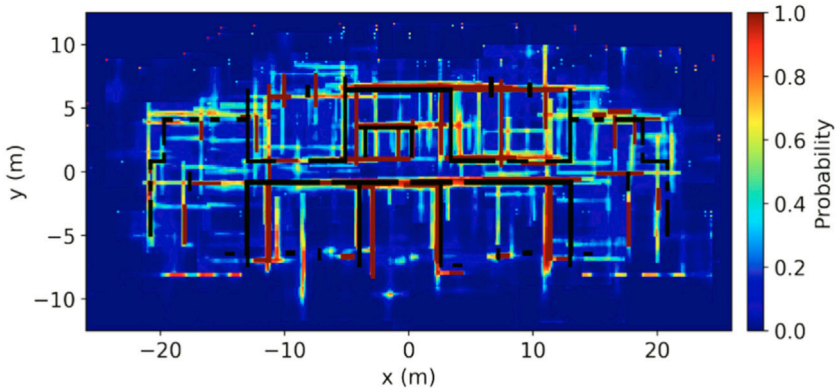

FIGURE 7 | Predicted plan obtained by Pizarro et al. (2021).

contrast with other topology optimization methods based on more heuristic approaches like those proposed by Zhang and Mueller (2017), which do not have this feature.

Pizarro and Massone (2021) proposed a predictive model for the length and thickness of reinforced concrete building walls based on Deep NN trained with 165 Chilean residential projects. The walls were described in both geometrical and topological domains and three variations of the data, achieved by modifying the building plan angle and its scale, were considered. Highly accurate predictions of wall thickness and length were obtained and the authors recommend the method to provide the engineer with a preliminary but reliable wall plan. Although not holistic in its scope, this work stresses the potential of ML-based tools to enhance the engineer-architect interaction via the machine. Besides, although important in number, the database of 165 building designs employed puts in evidence the small-data nature of most structural engineering problems. In addition, the regressive model proposed by Pizarro and Massone (2021) does not incorporate contextual information and can lead to poor estimations of wall translation.

In a companion paper, Pizarro et al. (2021) improve upon their previous work and present Convolutional NN models that take the architectural data as input and can output the final engineering floor plan. To this end, two regressive models are used to predict the thickness, length, and translations of the wall. A second prediction of plan is obtained by using a model that generates a likely image of each wall. Both independently predicted plans are combined to lead to the final engineering design as shown in **Figure 7**. This methodology was proven to be a feasible option to accelerate decisions regarding the building layout and can be adapted to incorporate estimations of building drift demands or force distributions.

Along the same vein as the above-mentioned studies, the work of Liao et al. (2021) uses generative adversarial networks (GAN), that have been previously used to generate building floor plans (Chaillou, 2020), to perform structural designs of shear wall residential buildings. To this end, the authors use a semantic process to extract essential architectural and structural features from technical drawings of around 250 pairs of architectural-structural human designs. The outputs of the GAN model are evaluated in two case studies where their safety and economy are compared against designs carried out by competent human engineers. It is concluded that GAN-generated designs can improve significantly the speed at which new designs are generated without compromising the quality of building structures. Similarly, Lou et al. (2021) optimized the shear wall layout of high-rise buildings through a tabu search algorithm. Support vector machines (SVM) were used to construct surrogate models and speed-up the analysis time. Their objective was to minimize the structural weight with constraints on the period ratio and story drift. Through a series of case studies, the authors showed that the proposed approach works well. In this case, however, a meta-heuristic algorithm was used for the optimization part and the ML model was employed only to reduce the computational cost due to repetitive structural analyses.

5 THE GRAILS OF CREATIVITY AND INTUITION

Modelling human intelligence on the perceived way we process and understand information has lead to remarkable tools that can augment the engineers' design skills, allowing them to operate over large datasets and make ever more accurate predictions of response and performance. However, understanding and reasoning are not the only, or even the most frequent, ways engineers use to solve problems (Graziano and Leone, 2019). Intuition, understood as "a form of recognition" (Simon, 1995), or the ability to understand something almost instinctively without concious reasoning, plays an important role in engineering decisions. In fact, engineers, who may prefer to call it judgement, use intuition even when developing computer models such as when framing the design question the model is set to answer or deciding what to include and what to leave out of that question. Appeals to recognize the importance of intuition in engineering design have grown almost in parallel with the proliferation of computational tools in engineering (Young, 2018).

Recent pioneering research has started to look at ways to integrate intuition into AI and ML with encouraging results in areas as diverse as chemical engineering (Duros et al., 2019), automated planning (Kim et al., 2017), and mathematics (Davies et al., 2021). In all these cases, the authors propose schemes for the incorporation of a human experimenter as part of the solution-generation process. For example, Davies et al. (2021) approach is akin to a "test bed for intuition" where ML algorithms guide the experimenter by: 1) verifying the existence of a hypothesized mathematical pattern using supervised ML; and 2) if the pattern exists, by helping in understanding it using Attribution Techniques. Likewise, Duros et al. (2019) propose the integration of human and machine in the selection of potential chemical experiments within a single decision-making loop. In all these cases, by making human and machine work together, a significantly higher performance is achieved than either of them could achieve individually.

In the structural engineering field, a relatively similar approach has been attempted by Danhaive and Mueller (2021). In their work, briefly described in the previous section, Danhaive and Mueller allow the design engineer access to a family of 2D latent spaces that can be adapted by changing the user-defined performance condition. This feature encourages designers to investigate different trade-offs between performance and other design features and opens the door for a more integrated machine-designer collaboration that does not aim to replace intuition with deterministic and quantitative rules but instead to incorporate it within the design process. However, to make the latent space intuitive and apt for human exploration, Danhaive and Mueller have to limit it to two dimensions. This highlights a defining feature of human intuition: that it emerges from the natural inability of the human mind to process scenarios with multiple variables (Halford et al., 2005). It is when faced with high uncertainties and multiple unknowns that the engineer resorts to intuition to be able to define a direction of exploration without getting boggled by the details. One would expect that the growing ability of AI to identify complex patterns in high-dimensional spaces will supersede the advantages of rules of thumb and educated guesses in determining high level features of the design process. Until then, the integration of human and machine intelligence offers a promising alternative. In addition, intuition's deciding role during the initial design stages fades down as the design is gradually informed by mechanics and structural analyses. Nevertheless, intuition remains as one of the last strongholds of traditional structural engineering practice as it adapts and responds to the challenges of digitalization. The other being creativity.

Creativity is usually defined as the generation of novel and useful ideas (Jung et al., 2013). This immediately invokes the existence of a judge, a person to whom the idea, or in our case the design, would appear novel or useful. It is perhaps this subjective strength of the term the reason for its recent prominence in the discussions around the training of the next generation of structural engineers (Ibell, 2015) where it is usually pitted against the more quantifiable (and declining) numerical skills. However, this subjectivity is not amorphous or ethereal since creativity does not emerge in the vacuum but is rather tied to socially contextualized phenomena (Kaufman and Sternberg, 2010). As such it will appear that creativity can be taught and learnt, if by humans also by machines. In this regard, the examples presented in previous sections have highlighted the possibility of incorporating measures of taste in ML tools and algorithms have been shown to enhance the diversity of the solutions found. In this context, it has been argued that novelty constitutes a critical issue to address with computational approaches, e.g., (Amabile, 2020). This is due to the fact that training of ML models usually relies on minimizing a loss expectation function and therefore the model is encouraged to perform well in the most common elements of already established knowledge.

A number of approaches could be taken to improve the "creativity" of ML algorithms (Boden, 1998), namely: 1) by producing novel designs from the combination of familiar solutions, 2) by discovering new paths in conceptual spaces, and 3) by disrupting the design space with solutions that were not previously considered. Consequently, it would seem that there are yet many routes to encourage artificial creativity. These aspects are in fact being developed within (and are probably more suited to) reinforcement learning approaches. Similarly, efforts to incorporate heuristic thinking into AI have been trialled in other branches of design (Nanda and Koder, 2010) and it may be beneficial to explore those in structural engineering also. At the end of the day, heuristics (intuition) is already routinely used by engineers to reduce the search space of potentially feasible designs, e.g., (Maqdah et al., 2021; Palmeri et al., 2021; Danhaive and Mueller, 2021). A perceived hurdle, however, comes form the fact that much of the progress of ML and AI has come from the formalization of mathematical and logical approaches aiming at well defined problems with clear goals. To answer this, may be the distinction between: 1) algorithms that search the entire decision space, and 2) those that perform bounded searches to provide satisfactory solutions (Simon, 2019) can be helpful here. Ultimately, much to the regret of the new breed of curriculum transformation proposers, computer programs constitute a body of empirical phenomena to which the student of design can address himself and which he can seek to understand. There is no question, since these programs exist, of the design process hiding behind the cloak of "judgment" or "experience" (Simon, 2019). To which we may add:" or creativity".

None of the above mentioned explorations to embed artificial intuition or to enhance artificial creativity in machine intelligence has yet been fully explored in structural engineering design. This constitutes an area of great research potential. Since much of the ML research has been based on mimicking the theories of human cognition it is entirely possible that the restrictions of human creativity and intuition are in turn limiting machine intelligence. This calls for a re-evaluation of the human-machine creative partnership. New investigations that take at face value the human-machine duo, like it has been done in other creative industries (Nika and Bresson, 2021), are

likely to benefit the realm of structural design with fresh and surprising views. So it seems that in the short term we may be seeing more design cooperation between human and machine where the role of ML, however, is not circumscribed to repetitive tasks but can assist in the creative work itself.

6 CONCLUSION

It has been suggested (Gero, 1994) that there are three views that can be taken about artificial intelligence in design: 1) AI as a framework in which to explore ideas about design; 2) AI as provider of a schema to model human design; and 3) AI as a means to allow the development of tools for human designers. This review paper has concerned itself with a strong version of the third view, by highlighting the path not only towards the development and proliferation of ML tools but also towards the automation of entire parts of the design process. In fact, a multitude of ML tools have been proposed aimed at different individual tasks along the design chain (like predicting the strength or condition of a given element, or the optimization of a section or connection). Design, however, is more complex than any of these individual tasks and ML methods aimed at it are more scarce.

It has been shown that ML tools have now started to appear that allow engineers to access complex multi-dimensional spaces beyond the ability of human intelligence alone. It was argued that the defining characteristic of ML to identify complex patterns and use those to predict or propose new engineering design solutions will form the basis for the automatization of increasingly large portions of the design endeavour. Importantly, these ML-enabled explorations can include not only hard mechanistic constraints but also metrics of taste and intuition. Indeed, although currently still producing timid results, the learning capacity of ML algorithms can be used to incorporate aesthetic and creative criteria that is sometimes difficult to articulate but which nevertheless the machine can learn. In addition, this learning can feed not only from engineering precedents at large but from the "best" precedents we currently have.

Another advantage of ML algorithms applied to design is found in the increased diversity of outputs produced. ML algorithms have been shown to increase the design diversity by recombining the features that characterise individual designs producing solutions beyond those which would have been imagined by human engineers. This recombination is usually neglected in engineering designs due to the large demands of data and time associated with it. However, with the use of data augmentation tools and computer simulation, it is expected that this hurdle will be solved sooner rather than later.

Nonetheless, the data requirements of ML algorithms will continue to be a limiting factor, particularly in the structural engineering field. If the ML-enabled design automation is to be attained, larger datasets of real-world designs should be made freely available. Most of the ML algorithms reviewed herein have used training datasets in the order of the hundreds. This is "small data" science and requires specific data augmentation techniques that the focus on "big data" is currently concealing. Data acquisition and curation is indeed the single most important step in the development of ML models. Robust, complete and reliable data sources should be produced and shared. Echoing current public demands in the sustainability and industrial ecology quarters of the design enterprise (in terms of environmental impact, LCA, etc.) (D'Amico et al., 2019) the field of structural ML design also needs all its stakeholders to contribute their design databases. Only then, truly optimal and "out of the box" ML-enabled design solutions can be realistically proposed paving the way towards more resilient, economical and sustainable new structures.

All in all, we should continue to guard against the well known dangers lurking around ML implementation. To this end, issues of interpretability and overfitting should continue to be raised and efforts made to increase model explainability (by conducting and reporting sensitivity tests and marginal effects studies for example), increase data sources, improve noise filtering processes and carefully select the ML models (to reduce overfitting) should carry on. Finally, it has been said that ML tremendous success so far has been achieved by showing that some cognitive processes thought to be complex and difficult are, in fact, not so. This, taken together with the acceptance that routine design is broadly defined as that activity that occurs when all the necessary knowledge is available (Gero, 1994); should prepare us well to be less surprised when the next generation of ML tools hits the structural design enterprise with the automation of large portions of the design process. Hence the question of how long until, not if, the human engineer is superseded in structural design.

AUTHOR CONTRIBUTIONS

CM-C contributed to conception and design of the study, it organisation, wrote the paper, read and revised it.

REFERENCES

Amabile, T. M. (2020). Creativity, Artificial Intelligence, and a World of Surprises. *Acad. Management Discoveries* 6, 351–354. doi:10.5465/amd.2019.0075

Amir, O., and Shakour, E. (2018). Simultaneous Shape and Topology Optimization of Prestressed concrete Beams. *Struct. Multidisc Optim* 57, 1831–1843. doi:10.1007/s00158-017-1855-5

Ampanavos, S., Nourbakhsh, M., and Cheng, C.-Y. (2021). *Structural Design Recommendations in the Early Design Phase Using Machine Learning*. arXiv preprint arXiv:2107.08567.

Bani-Hani, K., Ghaboussi, J., and Schneider, S. P. (1999). Experimental Study of Identification and Control of Structures Using Neural Network. Part 1: Identification. *Earthquake Engng. Struct. Dyn.* 28, 995–1018. doi:10.1002/(sici)1096-9845(199909)28:9<995:aid-eqe851>3.0.co;2-8

Bennett, J., Creary, L., Englemore, R., and Melosh, R. (1978). "SACON: A Knowledge-Based Consultant for Structural Analysis," in *Tech. Rep.* (Stanford, CA: Stanford Univ Calif Dept of Computer Science).

Boden, M. A. (1998). Creativity and Artificial Intelligence. *Artif. intelligence* 103, 347–356. doi:10.1016/s0004-3702(98)00055-1

Carstensen, J. V. (2020). Topology Optimization with Nozzle Size Restrictions for Material Extrusion-type Additive Manufacturing. *Struct. Multidisc Optim* 62, 2481–2497. doi:10.1007/s00158-020-02620-5

Chaillou, S. (2020). "Archigan: Artificial Intelligence X Architecture," in *Architectural Intelligence* (Singapore: Springer), 117–127. doi:10.1007/978-981-15-6568-7_8

Chang, K.-H., and Cheng, C.-Y. (2020). "Learning to Simulate and Design for Structural Engineering," in *International Conference on Machine Learning* (PMLR), 1426–1436.

D'Amico, B., Myers, R. J., Sykes, J., Voss, E., Cousins-Jenvey, B., Fawcett, W., et al. (2019). Machine Learning for Sustainable Structures: a Call for Data. *Structures* 19, 1–4. doi:10.1016/j.istruc.2018.11.013

Danhaive, R., and Mueller, C. T. (2021). Design Subspace Learning: Structural Design Space Exploration Using Performance-Conditioned Generative Modeling. *Automation in Construction* 127, 103664. doi:10.1016/j.autcon.2021.103664

Davies, A., Veličković, P., Buesing, L., Blackwell, S., Zheng, D., Tomašev, N., et al. (2021). Advancing Mathematics by Guiding Human Intuition with Ai. *Nature* 600, 70–74. doi:10.1038/s41586-021-04086-x

Dietterich, T. (1996). *Special Issue on Reinforcement Learning*. Dordrecht, Netherlands: Kluwer Academic Publ.

Duros, V., Grizou, J., Sharma, A., Mehr, S. H. M., Bubliauskas, A., Frei, P., et al. (2019). Intuition-enabled Machine Learning Beats the Competition when Joint Human-Robot Teams Perform Inorganic Chemical Experiments. *J. Chem. Inf. Model.* 59, 2664–2671. doi:10.1021/acs.jcim.9b00304

Fenves, S. J., and Norabhoompipat, T. (1978). Potentials for Artificial Intelligence Applications in Structural Engineering Design and Detailing. *Artif. intelligence pattern recognition Comput. aided Des.*, 105–119.

Fuhrimann, L., Moosavi, V., Ohlbrock, P. O., and D'acunto, P. (2018). Data-driven Design: Exploring New Structural Forms Using Machine Learning and Graphic Statics. *Proc. IASS Annu. Symposia (International Assoc. Shell Spat. Structures (Iass))* 2018, 1–8.

Gero, J. S. (1994). "Computational Models of Creative Design Processes," in *Artificial Intelligence and Creativity* (Dordrecht: Springer), 269–281. doi:10.1007/978-94-017-0793-0_19

Gharehbaghi, V., Kalbkhani, H., Noroozinejad, E., Yang, T., Nguyene, A., Mirjalili, S., et al. (2021). A Novel Approach for Deterioration and Damage Identification in Building Structures Based on stockwell-transform and Deep Convolutional Neural Netwokr. *J. Struct. Integrity Maintenance*. doi:10.1080/24705314.2021.2018840

Giraldo-Londoño, O., and Paulino, G. H. (2021). Polydyna: a Matlab Implementation for Topology Optimization of Structures Subjected to Dynamic Loads. *Struct. Multidisciplinary Optimization* 64, 957–990. doi:10.1007/s00158-021-02859-6

Graziano, M., and Leone, G. (2019). *Artificial Intuition*. Turin, Italy: Politecnico de Torino.

Halford, G. S., Baker, R., McCredden, J. E., and Bain, J. D. (2005). How many Variables Can Humans Process? *Psychol. Sci.* 16, 70–76. doi:10.1111/j.0956-7976.2005.00782.x

Hassett, P. M., and Putkey, J. J. (2002). *Steel Tips*. Moraga, CA: Structural Steel Educational Council.

Havelia, P. (2016). A Ground Structure Method to Optimize Topology and Sizing of Steel Frame Structures to Minimize Material, Fabrication and Erection Cost. Ph.D. thesis. Stanford, CA: Stanford University.

Ibell, T. (2015). *President's Address (IStructE)*. London, United Kingdom.

Ishizuka, M., Fu, K., and Yao, J. T. (1981). Speril 1-computer Based Structural Damage Assessment System. *NASA Sti/recon Tech. Rep. N* 82, 31580.

Jewett, J. L., and Carstensen, J. V. (2019). Topology-optimized Design, Construction and Experimental Evaluation of concrete Beams. *Automation in Construction* 102, 59–67. doi:10.1016/j.autcon.2019.02.001

Jung, R. E., Mead, B. S., Carrasco, J., and Flores, R. A. (2013). The Structure of Creative Cognition in the Human Brain. *Front. Hum. Neurosci.* 7, 330. doi:10.3389/fnhum.2013.00330

Jung, Y., and Joo, M. (2011). Building Information Modelling (Bim) Framework for Practical Implementation. *Automation in construction* 20, 126–133. doi:10.1016/j.autcon.2010.09.010

Kang, S., and Miranda, E. (2005). *Toward Fully Automated Robotic Crane for Construction Erection*. Stanford, CA: Stanford University.

Kaufman, J. C., and Sternberg, R. J. (2010). *The Cambridge Handbook of Creativity*. Cambridge: Cambridge University Press.

Khalatbarisoltani, A., Soleymani, M., and Khodadadi, M. (2019). Online Control of an Active Seismic System via Reinforcement Learning. *Struct. Control. Health Monit.* 26, e2298. doi:10.1002/stc.2298

Kiani, J., Camp, C., and Pezeshk, S. (2019). On the Application of Machine Learning Techniques to Derive Seismic Fragility Curves. *Comput. Structures* 218, 108–122. doi:10.1016/j.compstruc.2019.03.004

Kim, J., Banks, C. J., and Shah, J. A. (2017). "Collaborative Planning with Encoding of Users' High-Level Strategies," in *Thirty-First AAAI Conference on Artificial Intelligence*. San Francisco: AAAI.

Klanšek, U., and Kravanja, S. (2006). Cost Estimation, Optimization and Competitiveness of Different Composite Floor Systems—Part 1: Self-Manufacturing Cost Estimation of Composite and Steel Structures. *J. Constructional Steel Res.* 62, 434–448.

Kühl, N., Goutier, M., Baier, L., Wolff, C., and Martin, D. (2020). *Human vs. Supervised Machine Learning: Who Learns Patterns Faster?* arXiv preprint arXiv:2012.03661.

Lagaros, N. D., and Fragiadakis, M. (2007). Fragility Assessment of Steel Frames Using Neural Networks. *Earthquake Spectra* 23, 735–752. doi:10.1193/1.2798241

Liao, W., Lu, X., Huang, Y., Zheng, Z., and Lin, Y. (2021). Automated Structural Design of Shear wall Residential Buildings Using Generative Adversarial Networks. *Automation in Construction* 132, 103931. doi:10.1016/j.autcon.2021.103931

Liu, F., Jiang, X., Wang, X., and Wang, L. (2020). Machine Learning-Based Design and Optimization of Curved Beams for Multistable Structures and Metamaterials. *Extreme Mech. Lett.* 41, 101002. doi:10.1016/j.eml.2020.101002

Lou, H., Gao, B., Jin, F., Wan, Y., and Wang, Y. (2021). Shear wall Layout Optimization Strategy for High-Rise Buildings Based on Conceptual Design and Data-Driven Tabu Search. *Comput. Structures* 250, 106546. doi:10.1016/j.compstruc.2021.106546

Mahadevan, S., Zhang, R., and Smith, N. (2001). Bayesian Networks for System Reliability Reassessment. *Struct. Saf.* 23, 231–251. doi:10.1016/s0167-4730(01)00017-0

Maher, M. L., and Fenves, S. (1985). *Hi-rise—an Expert System for the Preliminary Structural Design of High Rise Buildings*. Amsterdam: North-Holland.

Mangalathu, S., Jang, H., Hwang, S.-H., and Jeon, J.-S. (2020). Data-driven Machine-Learning-Based Seismic Failure Mode Identification of Reinforced concrete Shear walls. *Eng. Structures* 208, 110331. doi:10.1016/j.engstruct.2020.110331

Mangalathu, S., and Jeon, J.-S. (2018). Classification of Failure Mode and Prediction of Shear Strength for Reinforced concrete Beam-Column Joints Using Machine Learning Techniques. *Eng. Structures* 160, 85–94. doi:10.1016/j.engstruct.2018.01.008

Maqdah, J., Málaga-Chuquitaype, C., Kampas, G., and Memarzadeh, M. (2021). "AI-based Structural Design of Extra-terrestrial Outposts," in *Tech. rep., "Tehcnical Report 21/02", Emerging Structural Technologies* (London, United Kingdom: Imperial College London).

McLean, T., Málaga-Chuquitaype, C., Kalapodis, N., and Kampas, G. (2021). Openarch: An Open-Source Package for Determining the Minimum-Thickness of Arches under Seismic Loads. *Software* 15, 100731. doi:10.1016/j.softx.2021.100731

Mirra, G., and Pugnale, A. (2021). Comparison between Human-Defined and Ai-Generated Design Spaces for the Optimisation of Shell Structures. *Structures* 34, 2950–2961. doi:10.1016/j.istruc.2021.09.058

Morfidis, K., and Kostinakis, K. (2017). Seismic Parameters' Combinations for the Optimum Prediction of the Damage State of R/C Buildings Using Neural Networks. *Adv. Eng. Softw.* 106, 1–16. doi:10.1016/j.advengsoft.2017.01.001

Mueller, C. T. (2014). Computational Exploration of the Structural Design Space. Ph.D. thesis. Cambridge, MA: Massachusetts Institute of Technology.

Murphy, K. P. (2012). *Machine Learning: A Probabilistic Perspective*. Cambridge, MA: MIT press.

Nanda, V., and Koder, R. L. (2010). Designing Artificial Enzymes by Intuition and Computation. *Nat. Chem* 2, 15–24. doi:10.1038/nchem.473

Nika, J., and Bresson, J. (2021). "Composing Structured Music Generation Processes with Creative Agents," in *2nd Joint Conference on AI Music Creativity* (AIMC 2021), 12.

Palmeri, M., Málaga-Chuquitaype, C., Kampas, G., and Memarzadeh, M. (2021). "AI-based Optimization of Off-Earth Habitat Structures," in *Tech. rep., "Tehcnical Report 21/03", Emerging Structural Technologies* (London, United Kingdom: Imperial College London).

Pearl, J. (1988). *Probabilistic Reasoning in Intelligent Systems: Networks of Plausible Inference (Morgan Kaufmann)*. San Francisco, CA: Morgan Kaufmann.

Pizarro, P. N., Massone, L. M., Rojas, F. R., and Ruiz, R. O. (2021). Use of Convolutional Networks in the Conceptual Structural Design of Shear wall Buildings Layout. *Eng. Structures* 239, 112311. doi:10.1016/j.engstruct.2021.112311

Pizarro, P. N., and Massone, L. M. (2021). Structural Design of Reinforced concrete Buildings Based on Deep Neural Networks. *Eng. Structures* 241, 112377. doi:10.1016/j.engstruct.2021.112377

Preisinger, C., and Heimrath, M. (2014). Karamba-A Toolkit for Parametric Structural Design. *Struct. Eng. Int.* 24, 217–221. doi:10.2749/101686614x13830790993483

Qian, L., Winfree, E., and Bruck, J. (2011). Neural Network Computation with Dna Strand Displacement Cascades. *Nature* 475, 368–372. doi:10.1038/nature10262

Ranalli, F. (2021). An Artificial Intelligence Framework for Multi-Disciplinary Design Optimization of Steel Buidlings. Ph.D. thesis. Stanford University.

Rumelhart, D. E., Hinton, G. E., and Williams, R. J. (1986). Learning Representations by Back-Propagating Errors. *nature* 323, 533–536. doi:10.1038/323533a0

Rumelhart, D. E. (1994). "Toward an Interactive Model of reading," in *Theoretical Models and Processes of reading*. Editors R. B. Ruddell, M. R. Ruddell, and H. Singer (Newark, DE: International Reading Association), 864–894.

Sarkar, K., Bonnerjee, D., Srivastava, R., and Bagh, S. (2021). A single layer artificial neural network type architecture with molecular engineered bacteria for reversible and irreversible computing. *Chem. Sci.* 12 (48), 15821–15832.

Simon, H. A. (1995). "Explaining the Ineffable: Al on the Topics of Intuition, Insight and Inspiration," in *Fourteenth International Joint Conference on Artificial Intelligence* (San Francisco: Morgan Kaufmann Citeseer), 939–948.

Simon, H. A. (2019). *The Sciences of the Artificial*. Cambridge, MA: MIT press.

Sivandi-Pour, A., Farsangi, E. N., and Takewaki, I. (2020). Estimation of Vibration Frequency of Structural Floors Using Combined Artificial Intelligence and Finite Element Simulation. *J. Eng. Res.* 8. doi:10.36909/jer.v8i3.8149

Sun, H., Burton, H. V., and Huang, H. (2021). Machine Learning Applications for Building Structural Design and Performance Assessment: State-Of-The-Art Review. *J. Building Eng.* 33, 101816. doi:10.1016/j.jobe.2020.101816

Suresh, S., Narasimhan, S., Nagarajaiah, S., and Sundararajan, N. (2010). Fault-tolerant Adaptive Control of Nonlinear Base-Isolated Buildings Using Emran. *Eng. Structures* 32, 2477–2487. doi:10.1016/j.engstruct.2010.04.024

Thomas, S., Li, Q., and Steven, G. (2021). Finite Periodic Topology Optimization with Oriented Unit-Cells. *Struct. Multidisc Optim* 64, 1765–1779. doi:10.1007/s00158-021-03045-4

Torii, A. J., Lopez, R. H., and F. Miguel, L. F. (2016). Design Complexity Control in Truss Optimization. *Struct. Multidisc Optim* 54, 289–299. doi:10.1007/s00158-016-1403-8

Tsavdaridis, K. D., Kingman, J. J., and Toropov, V. V. (2015). Application of Structural Topology Optimisation to Perforated Steel Beams. *Comput. Structures* 158, 108–123. doi:10.1016/j.compstruc.2015.05.004

Vanluchene, R. D., and Sun, R. (1990). Neural Networks in Structural Engineering. *Computer-Aided Civil Infrastructure Eng.* 5, 207–215. doi:10.1111/j.1467-8667.1990.tb00377.x

Xue, T., Wallin, T. J., Menguc, Y., Adriaenssens, S., and Chiaramonte, M. (2020). Machine Learning Generative Models for Automatic Design of Multi-Material 3d Printed Composite Solids. *Extreme Mech. Lett.* 41, 100992. doi:10.1016/j.eml.2020.100992

Young, M. T. (2018). Heuristics and Human Judgment: what We Can Learn about Scientific Discovery from the Study of Engineering Design. *Topoi* 1–9, 987–995. doi:10.1007/s11245-018-9550-8

Zegard, T., and Paulino, G. H. (2016). Bridging Topology Optimization and Additive Manufacturing. *Struct. Multidisc Optim* 53, 175–192. doi:10.1007/s00158-015-1274-4

Zhang, Y., and Mueller, C. (2017). Shear wall Layout Optimization for Conceptual Design of Tall Buildings. *Eng. Structures* 140, 225–240. doi:10.1016/j.engstruct.2017.02.059

Zheng, H. (2019). "Form Finding and Evaluating through Machine Learning: the Prediction of Personal Design Preference in Polyhedral Structures," in *The International Conference on Computational Design and Robotic Fabrication* (Singapore: Springer), 169–178. doi:10.1007/978-981-13-8153-9_15

Zheng, H., Moosavi, V., and Akbarzadeh, M. (2020). Machine Learning Assisted Evaluations in Structural Design and Construction. *Automation in Construction* 119, 103346. doi:10.1016/j.autcon.2020.103346

Zhu, M., Yang, Y., Gaynor, A. T., and Guest, J. K. (2014). Considering Constructability in Structural Topology Optimization. *Structures Congress* 2014, 2754–2764. doi:10.1061/9780784413357.241

Zolfagharian, S., and Irizarry, J. (2017). Constructability Assessment Model for Commercial Building Designs in the united states. *J. Constr. Eng. Manage.* 143, 04017031. doi:10.1061/(asce)co.1943-7862.0001323

Conflict of Interest: The author declares that the research was conducted in the absence of any commercial or financial relationships that could be construed as a potential conflict of interest.

frontiers in Built Environment

ORIGINAL RESEARCH
published: 21 February 2022
doi: 10.3389/fbuil.2022.855112

Predicting the Response of Laminated Composite Beams: A Comparison of Machine Learning Algorithms

George C. Tsiatas[1]*, *Sotiris Kotsiantis*[1] and *Aristotelis E. Charalampakis*[2]

[1]Department of Mathematics, University of Patras, Patras, Greece, [2]Department of Civil Engineering, University of West Attica, Athens, Greece

A comparative study of machine learning regression algorithms for predicting the deflection of laminated composite beams is presented herein. The problem of the scarcity of experimental data is solved by ample numerically prepared data, which are necessary for the training, validation, and testing of the algorithms. To this end, the pertinent geometric and material properties of the beam are discretized appropriately, and a refined higher-order beam theory is employed for the accurate evaluation of the deflection in each case. The results indicate that the Extra-Trees algorithm performs best, demonstrating excellent predictive capabilities.

Keywords: machine learning, regression models, composite beams, orthotropic material model, higher-order beam theories

OPEN ACCESS

Edited by:
Makoto Ohsaki,
Kyoto University, Japan

Reviewed by:
Ömer Civalek,
Akdeniz University, Turkey
Ahmad N. Tarawneh,
Hashemite University, Jordan

***Correspondence:**
George C. Tsiatas
gtsiatas@upatras.gr

Specialty section:
This article was submitted to Computational Methods in Structural Engineering, a section of the journal Frontiers in Built Environment

Received: *14 January 2022*
Accepted: *31 January 2022*
Published: *21 February 2022*

Citation:
Tsiatas GC, Kotsiantis S and Charalampakis AE (2022) Predicting the Response of Laminated Composite Beams: A Comparison of Machine Learning Algorithms. Front. Built Environ. 8:855112. doi: 10.3389/fbuil.2022.855112

INTRODUCTION

Beams as structural components are crucial in many structural systems. The prediction of their deflection is essential since excessive values can lead to the structural system losing its operational serviceability (Serviceability Limit State—SLS). On the other hand, composite materials are increasingly used in structural engineering due to their enhanced stiffness combined with reduced weight. Several shear deformation theories have been developed so far to evaluate the response of thin, moderately thick, or deep beams. They fall into three main categories: the Euler-Bernoulli beam theory (or Classical Beam Theory—CBT), the Timoshenko beam theory (or First Order Beam Theory—FOBT) and the Higher-Order Beam Theories (HOBTs). CBT is applicable for thin beams with no shear effect. In the FOBT, a constant state of transverse shear strain is assumed that does not satisfy the zero shear stress condition at the top and bottom edges of the beam and thus requires a shear correction factor to compensate for this error (see, e.g., Wang et al., 2000; Eisenberger, 2003; Civalek and Kiracioglu, 2010; Lin and Zhang, 2011; Endo, 2016). In general, the HOBTs adopt a specific function (parabolic, trigonometric, exponential, or hyperbolic) to more accurately represent the shear stress distribution along the beam's thickness and do not require the shear correction factor (see e.g., Reddy, 1984; Heyliger and Reddy, 1988; Khdeir and Reddy, 1997; Murthy et al., 2005; Vo and Thai, 2012; Pawar et al., 2015; Nguyen et al., 2017; Srinivasan et al., 2019). The literature contains a plethora of publications on the subject, and the interested reader is referred to the excellent review paper of Liew et al. (2019). In this investigation, a refined higher-order beam theory is utilized for the analysis of laminated composite beams based on Reddy-Bickford's third-order beam theory (Wang et al., 2000) which was derived independently by Bickford (1982) and Reddy (1984).

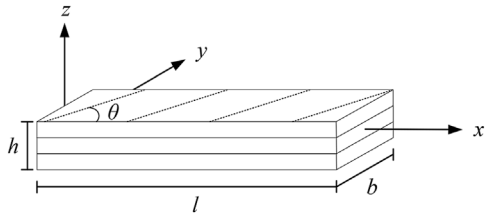

FIGURE 1 | Geometry of a cross-ply laminated composite beam.

Utilizing higher-order beam theories for more accurate analyses entails a significant increase in complexity as compared to low-order theories, as the latter are mathematically simpler and more widely used. The main motivation of this work is to bridge this gap and provide a simple computational tool to allow for the fast design of beams while keeping the best of both worlds, i.e., the more accurate results of a refined high-order theory and the ease of application of the low-order theories. In order to achieve that, the geometric and material variables are discretized within fairly wide, yet reasonable ranges. After applying the high-order analyses, the results are collected, tabulated, and used as input for multiple machine learning algorithms, i.e., regression models. These models provide a fast and easy-to-use computational tool that can be used for preliminary design and optimization. Regression analysis also yields important insights regarding the performance of each model, the effect of boundary conditions, and the relative importance of each input variable for the problem at hand.

The rest of the paper is organized as follows. A theoretical formulation of the problem is carried out and explained in detail next, followed by a summary of the regression methods utilized in this work. The numerical results are presented next, along with their discussion. Finally, the conclusions drawn based on the findings of this work are presented.

THEORETICAL FORMULATION

Consider an elastic symmetric cross-ply laminated rectangular beam ($b \times h$) of length l, with x being the axial coordinate and z being the coordinate along the thickness of the beam. The fibers of each ply are aligned at an angle θ with respect to the x axis (see **Figure 1**).

The beam is subjected to a transverse distributed loading p_z, respectively. Based on the higher-order theory for laminated composite plates introduced by Reddy (1984), the displacement field of an arbitrary point on the beam cross-section is given by

$$u_1(x,z) = z\left[\psi(x) - \frac{4}{3}\frac{z^2}{h^2}\left(\psi(x) + \frac{\partial w(x)}{\partial x}\right)\right] \tag{1}$$

$$u_2(x,z) = 0 \tag{2}$$

$$u_3(x,z) = w(x) \tag{3}$$

where $w(x)$ is the transverse displacement of the midplane ($z = 0$); $\psi(x)$ is the rotation of a normal to the midplane, and x, z are the axial and thickness coordinates of the beam.

Splitting the transverse displacement $w(x)$ into a bending $w_b(x)$ and a shear $w_s(x)$ component, i.e., Vo and Thai (2012).

$$w(x) = w_b(x) + w_s(x) \tag{4}$$

and introducing the transformation

$$\frac{\partial w_s(x)}{\partial x} = \psi(x) + \frac{\partial w(x)}{\partial x} \text{ or } \psi(x) = -\left[\frac{\partial w(x)}{\partial x} - \frac{\partial w_s(x)}{\partial x}\right] = -\frac{\partial w_b(x)}{\partial x} \tag{5}$$

Equations 1–3 can be rewritten in the following form

$$u_1(x,z) = -z\frac{\partial w_b(x)}{\partial x} - f(z)\frac{\partial w_s(x)}{\partial x} \tag{6}$$

$$u_2(x,z) = 0 \tag{7}$$

$$u_3(x,z) = w_b(x) + w_s(x) \tag{8}$$

where $f(z) = \frac{4}{3}\frac{z^3}{h^2}$. The displacement field given above yields the following nonzero components of the strain tensor

$$\varepsilon_x = -z\frac{\partial^2 w_b}{\partial x^2} - f(z)\frac{\partial^2 w_s}{\partial x^2} \tag{9}$$

$$\gamma_{xz} = \left[1 - \frac{df(z)}{dz}\right]\frac{\partial w_s}{\partial x} = g(z)\frac{\partial w_s}{\partial x} \tag{10}$$

where $g(z) = (1 - \frac{4z^2}{h^2})$, and for reasons of brevity $w_b = w_b(x)$ and $w_s = w_s(x)$.

Substituting **Eqs 9**, **10** into the stress-strain relations for the kth lamina in the lamina coordinate we obtain (Khdeir and Reddy, 1997)

$$\sigma_x^{(k)} = \bar{Q}_{11}^{(k)}\varepsilon_x \tag{11}$$

$$\tau_{xz}^{(k)} = \bar{Q}_{55}^{(k)}\gamma_{xz} \tag{12}$$

with $\bar{Q}_{11}^{(k)}$, $\bar{Q}_{55}^{(k)}$ being the well-known transformed elastic stiffnesses

$$\bar{Q}_{11}^{(k)} = Q_{11}^{(k)}\cos^4\theta_k + 2\left(Q_{12}^{(k)} + 2Q_{66}^{(k)}\right)\sin^2\theta_k\cos^2\theta_k + Q_{22}^{(k)}\sin^4\theta_k \tag{13}$$

$$\bar{Q}_{55}^{(k)} = Q_{44}^{(k)}\sin^2\theta_k + Q_{55}^{(k)}\cos^2\theta_k \tag{14}$$

and $Q_{11}^{(k)}$, $Q_{12}^{(k)}$, $Q_{22}^{(k)}$, $Q_{44}^{(k)}$, and $Q_{55}^{(k)}$ are

$$Q_{11}^{(k)} = \frac{E_1^{(k)}}{1 - \nu_{12}^{(k)}\nu_{21}^{(k)}},\ Q_{12}^{(k)} = \frac{E_2^{(k)}\nu_{12}^{(k)}}{1 - \nu_{12}^{(k)}\nu_{21}^{(k)}},\ Q_{22}^{(k)} = \frac{E_2^{(k)}}{1 - \nu_{12}^{(k)}\nu_{21}^{(k)}} \tag{15}$$

$$Q_{44}^{(k)} = G_{23}^{(k)},\ Q_{55}^{(k)} = G_{13}^{(k)},\ Q_{66}^{(k)} = G_{12}^{(k)} \tag{16}$$

while θ_k is the angle between the principal material axis and the coordinate x axis.

Applying the Principle of Virtual Work

$$\int_0^l \int_A \left[\sigma_x^{(k)}\delta\varepsilon_x + \tau_{xz}^{(k)}\delta\gamma_{xz}\right]dA\,dx - \int_0^l \left[p_z\delta(w_b + w_s)\right]dx = 0 \tag{17}$$

TABLE 1 | Boundary conditions examined for the prediction of the maximum deflection $\max \bar{w}$.

Boundary conditions	x = 0	x = l
Clamped-Clamped (CC)	$w_b = 0,\ w_s = 0$	$w_b = 0,\ w_s = 0$
	$\frac{\partial w_b}{\partial x} = 0,\ \frac{\partial w_b}{\partial s} = 0$	$\frac{\partial w_b}{\partial x} = 0,\ \frac{\partial w_b}{\partial s} = 0$
Simply Supported (SS)	$w_b = 0,\ w_s = 0$	$w_b = 0,\ w_s = 0$
	$M_b = 0,\ M_s = 0$	$M_b = 0,\ M_s = 0$
Clamped-Roller (CR)	$w_b = 0,\ w_s = 0$	$w_b = 0,\ w_s = 0$
	$\frac{\partial w_b}{\partial x} = 0,\ \frac{\partial w_b}{\partial s} = 0$	$M_b = 0,\ M_s = 0$
Clamped-Free (CF)	$w_b = 0,\ w_s = 0$	$M_b = 0,\ M_s = 0$
	$\frac{\partial w_b}{\partial x} = 0,\ \frac{\partial w_b}{\partial s} = 0$	$Q_b = 0,\ Q_s = 0$

and substituting **Eqs 9**, **10** yields

$$\int_0^l \int_A \left\{ \sigma_x^{(k)} \left[-z\frac{\partial^2 \delta w_b}{\partial x^2} - f(z)\frac{\partial^2 \delta w_s}{\partial x^2} \right] + \tau_{xz}^{(k)} g(z)\frac{\partial \delta w_s}{\partial x} \right\} dA dx - \int_0^l [p_z(\delta w_b + \delta w_s)] dx = 0 \tag{18}$$

Introducing now the following stress resultants

$$M_b = \int_A z\sigma_x^{(k)} dA,\ M_s = \int_A f(z)\sigma_x^{(k)} dA,\ Q = \int_A g(z)\tau_{xz}^{(k)} dA \tag{19}$$

Eq. 18 become

$$\int_0^l \left(-M_b\frac{\partial^2 \delta w_b}{\partial x^2} - M_s\frac{\partial^2 \delta w_s}{\partial x^2} + Q\frac{\partial \delta w_s}{\partial x} \right) dx - \int_0^l [p_z(\delta w_b + \delta w_s)] dx = 0 \tag{20}$$

Integrating the appropriate terms in the above equation and collecting the coefficients of δw_b, and δw_s we obtain the following governing equations

$$\frac{\partial^2 M_b}{\partial x^2} = -p_z \tag{21}$$

$$\frac{\partial^2 M_s}{\partial x^2} + \frac{\partial Q}{\partial x} = -p_z \tag{22}$$

together with the following associated boundary conditions of the form: specify

$$w_b \text{ or } Q_b \equiv \frac{\partial M_b}{\partial x} \tag{23}$$

$$w_s \text{ or } Q_s \equiv \frac{\partial M_s}{\partial x} + Q \tag{24}$$

$$\frac{\partial w_b}{\partial x} \text{ or } M_b \tag{25}$$

$$\frac{\partial w_s}{\partial x} \text{ or } M_s \tag{26}$$

Substituting **Eqs 11**, **12** into **Eq. 19** and using **Eqs 9**, **10** yields the stress resultants in terms of the displacements as

$$M_b = -D_{11}\frac{\partial^2 w_b}{\partial x^2} - F_{11}\frac{\partial^2 w_s}{\partial x^2} \tag{27}$$

$$M_s = -F_{11}\frac{\partial^2 w_b}{\partial x^2} - H_{11}\frac{\partial^2 w_s}{\partial x^2},\ Q = A_{55}\frac{\partial w_s}{\partial x} \tag{28}$$

where

$$D_{11} = b\int_{-h/2}^{h/2} \bar{Q}_{11}^{(k)} z^2 dz,\ F_{11} = b\int_{-h/2}^{h/2} \bar{Q}_{11}^{(k)} z f(z) dz,$$

$$H_{11} = b\int_{-h/2}^{h/2} \bar{Q}_{11}^{(k)} f^2(z) dz \tag{29}$$

$$A_{55} = b\int_{-h/2}^{h/2} \bar{Q}_{55}^{(k)} g^2(z) dz \tag{30}$$

Finally, after the substitution of the stress resultants, **Eqs 27**, **28** into **Eqs 21**, **22**, we arrive at the equilibrium equations in terms of the displacements

$$-D_{11}\frac{\partial^4 w_b}{\partial x^4} - F_{11}\frac{\partial^4 w_s}{\partial x^4} = -p_z \tag{31}$$

$$-F_{11}\frac{\partial^4 w_b}{\partial x^4} - H_{11}\frac{\partial^4 w_s}{\partial x^4} + A_{55}\frac{\partial^2 w_s}{\partial x^2} = -p_z \tag{32}$$

which together with the pertinent boundary conditions (**23**)–(**26**) constitute the boundary value problem solved using the Analog Equation Method (AEM), a robust numerical method based on an integral equation technique (Katsikadelis and Tsiatas, 2003; Tsiatas et al., 2018).

REGRESSION MODELS

In this work, several linear and nonlinear regression models are comparatively examined. Linear regression is a linear model that assumes a linear relationship between the input variables and the output variable, and the predicted value can be calculated from a linear combination of the input variables (Narula and Wellington, 1982). The distance from each data point to the predicted values is calculated and sum all these squared errors together. This quantity is minimized by the ordinary least squares method to estimate the optimal values for the coefficients of each independent variable.

There are extensions of the linear model called regularization methods. These methods seek to both minimize the sum of the squared error of the model on the training set but also to reduce the complexity of the model. Two popular regularization methods for linear regression are the Lasso Regression (Zou et al., 2007) where Ordinary Least Squares is modified to also minimize the absolute sum of the coefficients (L1 regularization), and the Ridge Regression (Hoerl et al., 1985) where Ordinary Least Squares is modified to also minimize the squared absolute sum of the coefficients (L2 regularization). A Bayesian view of ridge regression is obtained by noting that the minimizer can be considered as the posterior mean of a model (Tipping, 2001). The elastic net (Friedman et al.,

TABLE 2 | Evaluation metrics for the clamped-clamped beam.

Model	MAE	MSE	RMSE	R^2	RMSLE	MAPE
Extra Trees Regressor	0.0251	0.0074	0.0834	0.9994	0.0132	0.0148
Random Forest Regressor	0.0381	0.0135	0.1148	0.9988	0.0157	0.0187
Decision Tree Regressor	0.0556	0.0301	0.1705	0.9975	0.0242	0.0271
Light Gradient Boosting Machine	0.0598	0.0203	0.1407	0.9983	0.0257	0.1170
Gradient Boosting Regressor	0.2771	0.3469	0.5881	0.9706	0.1271	0.8407
K Neighbors Regressor	0.3146	1.3540	1.1630	0.8856	0.1017	0.0909
AdaBoost Regressor	1.0111	2.0725	1.4199	0.8252	0.3944	3.6655
Huber Regressor	1.0685	7.6780	2.7694	0.3521	0.3831	4.0658
Elastic Net	1.3421	7.9422	2.8167	0.3297	0.4896	3.1981
Lasso Regression	1.4131	8.3905	2.8951	0.2919	0.5120	3.6771
Bayesian Ridge	1.4203	6.2225	2.4931	0.4749	0.5315	8.7274
Ridge Regression	1.4205	6.2225	2.4931	0.4749	0.5316	8.7319
Linear Regression	1.4206	6.2225	2.4931	0.4749	0.5317	8.7329
Least Angle Regression	1.4206	6.2225	2.4931	0.4749	0.5317	8.7329
Orthogonal Matching Pursuit	1.5371	8.2780	2.8759	0.3011	0.5044	4.2803
Passive Aggressive Regressor	1.9945	11.1782	3.3257	0.0605	0.7021	10.8439
Lasso Least Angle Regression	1.9986	11.8425	3.4402	0.0001	0.7724	11.0424

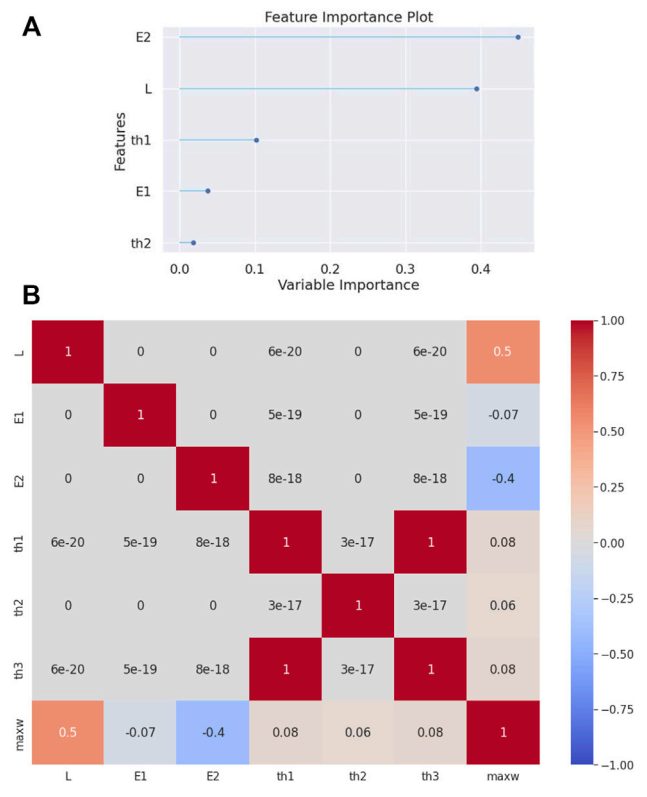

FIGURE 2 | (A) Feature importance plot and **(B)** correlation matrix heatmap for the clamped-clamped beam.

2010) is a regularized regression method that linearly combines the L1 and L2 penalties of the lasso and ridge methods. Huber's criterion is a hybrid of squared error for relatively small errors and absolute error for relatively large ones. Lambert-Lacroix and Zwald (2011) proposed Huber regressor to combine Huber's criterion with concomitant scale and Lasso.

An L1 penalty minimizes the size of all coefficients and allows any coefficient to go to the value of zero, acting as a type of feature selection method since removes input features from the model. Least Angle Regression (Efron et al., 2004) is a forward stepwise version of feature selection for regression that can be adapted for the Lasso not to require a hyperparameter that controls the weighting of the penalty in the loss function since the weighting is discovered automatically by Least Angle Regression method *via* cross-validation. LassoLars is a lasso model implemented using the Least Angle Regression algorithm, where unlike the implementation based on coordinate descent, this yields the exact solution, which is piecewise linear as a function of the norm of its coefficients.

Orthogonal matching pursuit (Pati et al., 1993) tries to find the solution for the L0-norm minimization problem, while Least Angle Regression solves the L1-norm minimization problem. Although these methods solve different minimization problems, they both depend on a greedy framework. They start from an all-zero solution, and then iteratively construct a sparse solution based on the correlation between features of the training set and the output variable. They converge to the final solution when the norm approaches zero.

K Neighbors Regressor (KNN) algorithm uses feature similarity to predict the values of new instances (Altman, 1992). The distance between the new instance and each training instance is calculated, the closest k instances are selected based on the preferred distance and finally, the prediction for the new instance is the average value of the dependent variable of these k instances.

Unlike linear regression, Classification and Regression Tree (CART) does not create a prediction equation, but data are partitioned into subsets at each node according to homogeneous values of the dependent variable and a decision tree is built to be used for making predictions about new instances (Breiman et al., 1984). We can enlarge the tree until always gives the correct value in the training set. However, this tree would overfit the data and not generalize well to new data. The correct policy is to use some combination of a minimum number of instances in a tree node and maximum depth of tree to avoid overfitting.

TABLE 3 | Evaluation metrics for the simply supported beam.

Model	MAE	MSE	RMSE	R^2	RMSLE	MAPE
Extra Trees Regressor	0.0749	0.0767	0.2718	0.9994	0.0157	0.0135
Random Forest Regressor	0.1127	0.1591	0.3935	0.9987	0.0187	0.0180
Decision Tree Regressor	0.1465	0.2294	0.4735	0.9981	0.0265	0.0258
Light Gradient Boosting Machine	0.2106	0.3258	0.5617	0.9973	0.0479	0.1556
K Neighbors Regressor	0.8682	12.9351	3.5942	0.8948	0.1158	0.0934
Gradient Boosting Regressor	1.1417	6.0163	2.4496	0.9510	0.2931	1.8173
AdaBoost Regressor	3.0602	22.0956	4.6723	0.8184	0.5993	4.5067
Huber Regressor	3.5208	82.9872	9.1049	0.3260	0.6283	7.3794
Elastic Net	4.1196	77.5224	8.7998	0.3705	0.7620	5.9456
Lasso Regression	4.2209	71.8424	8.4713	0.4166	0.7876	10.1221
Bayesian Ridge	4.6000	68.3098	8.2607	0.4452	0.9092	16.0915
Ridge Regression	4.6008	68.3098	8.2607	0.4452	0.9094	16.1014
Linear Regression	4.6010	68.3098	8.2607	0.4452	0.9094	16.1033
Least Angle Regression	4.6010	68.3098	8.2607	0.4452	0.9094	16.1033
Passive Aggressive Regressor	4.6651	90.8374	9.5039	0.2608	0.8824	10.9468
Orthogonal Matching Pursuit	4.8283	83.9710	9.1597	0.3178	0.8392	9.1774
Lasso Least Angle Regression	6.4298	123.0726	11.0899	0.0002	1.2440	19.9475

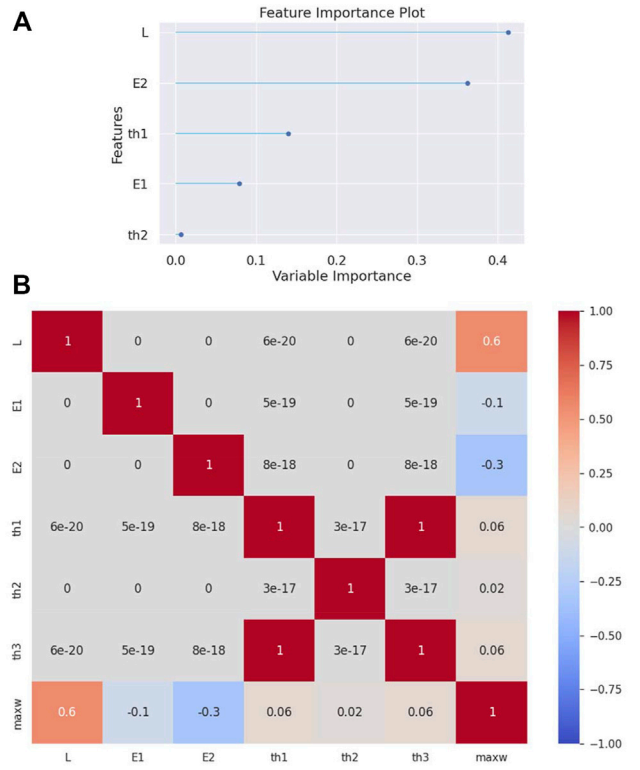

FIGURE 3 | (A) Feature importance plot and **(B)** correlation matrix heatmap for the simply supported beam.

The basic idea of Boosting is to combine several weak learners into a stronger one. AdaBoost (Freund and Schapire, 1997) fits a regression tree on the training set and then retrains a new regression tree on the same dataset but the weights of each instance are adjusted according to the error of the previous tree predictions. In this way, subsequent regressors focus more on difficult instances.

Random Forests algorithm (Breiman, 2001) builds several trees with the CART algorithm using for each tree a bootstrap replica of the training set with a modification. At each test node, the optimal split is derived by searching a random subset of size K of candidate features without replacement from the full feature set.

Like Random Forests, Gradient Boosting (Friedman, 2001) is an ensemble of trees, however, there are two main differences. Firstly, the Random forests algorithm builds each tree independently while Gradient Boosting builds one tree at a time since it works in a forward stage-wise manner, introducing a weak learner to improve the shortcomings of existing weak learners. Secondly, Random Forests combine results at the end (by averaging the result of each tree) while Gradient Boosting combines results during the process.

LightGBM (Ke et al., 2017) extends the gradient boosting algorithm by adding automatic feature selection and focusing on instances with larger gradients to speed up training and sometimes even improve predictive performance.

The Extra-Trees algorithm (Geurts et al., 2006) creates an ensemble of unpruned regression trees according to the well-known top-down procedure of the regression trees. The main differences concerning other tree-based ensemble methods are that the Extra-Trees algorithm splits nodes by choosing fully at random cut-points and that uses the whole learning set (instead of a bootstrap replica) to grow the trees.

Passive-Aggressive regressor (Crammer et al., 2006) is generally used for large-scale learning since it is an online learning algorithm. In online learning, the input data come sequentially, and the learning model is updated step-by-step, as opposed to batch learning, where the entire dataset is used at once.

NUMERICAL RESULTS AND DISCUSSION

The scope of the current study is to exploit predictive models for the maximum deflection max w of a symmetric cross-ply ($\theta_1^\circ/\theta_2^\circ/\theta_3^\circ$) rectangular beam for various span-to-depth ratios and

TABLE 4 | Evaluation metrics for the clamped-roller beam.

Model	MAE	MSE	RMSE	R^2	RMSLE	MAPE
Extra Trees Regressor	0.0397	0.0210	0.1403	0.9993	0.0142	0.0142
Random Forest Regressor	0.0601	0.0376	0.1918	0.9987	0.0172	0.0186
Decision Tree Regressor	0.0852	0.0721	0.2638	0.9976	0.0254	0.0268
Light Gradient Boosting Machine	0.0993	0.0666	0.2549	0.9978	0.0332	0.1292
K Neighbors Regressor	0.4656	3.2736	1.8083	0.8909	0.1071	0.0919
Gradient Boosting Regressor	0.5088	1.1518	1.0700	0.9615	0.1890	1.2013
Huber Regressor	1.7188	19.7571	4.4425	0.3424	0.4678	5.1283
AdaBoost Regressor	1.9549	6.6004	2.5493	0.7802	0.5716	4.7368
Lasso Regression	2.0176	18.5644	4.3062	0.3821	0.5470	4.0458
Elastic Net	2.0676	19.4144	4.4038	0.3538	0.5769	3.7886
Bayesian Ridge	2.2615	16.1679	4.0188	0.4618	0.6690	11.0123
Ridge Regression	2.2619	16.1679	4.0188	0.4618	0.6691	11.0184
Linear Regression	2.2620	16.1679	4.0188	0.4618	0.6691	11.0197
Least Angle Regression	2.2620	16.1679	4.0188	0.4618	0.6691	11.0197
Passive Aggressive Regressor	2.3236	22.4124	4.7312	0.2528	0.6799	8.8763
Orthogonal Matching Pursuit	2.4143	20.6503	4.5424	0.3123	0.6195	5.8559
Lasso Least Angle Regression	3.1842	30.0259	5.4778	0.0001	0.9493	13.8389

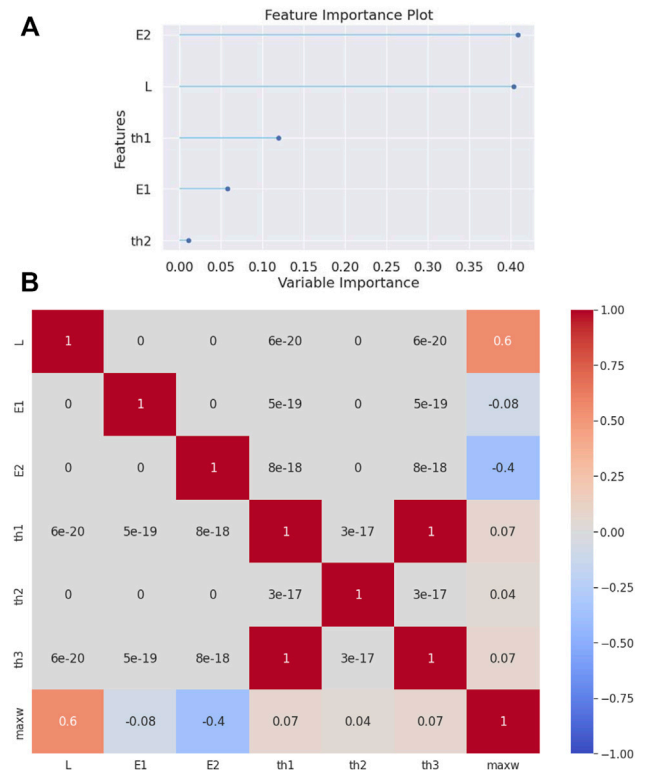

FIGURE 4 | (A) Feature importance plot and **(B)** correlation matrix heatmap for the clamped-roller beam.

boundary conditions subjected to a uniformly distributed load p_z. All laminates are of equal thickness and made of the same orthotropic material. The main parameters that influence the response of the composite beams are the moduli of elasticity E_1, E_2, the span-to-depth $L = l/h$ and the ply angles $\theta_1^\circ/\ \theta_2^\circ/\ \theta_3^\circ$. The range of values of the parameters together with the material properties are given as: $E_1, E_2 = \{1, 2, 3, ...15\}, G_{12} = G_{13} = 0.5E_2$, $G_{23} = 0.2E_2$, $\nu_{12} = 0.25$, $L = l/h = \{1, 2, 3, 4, 5\}$, $\theta_1, \theta_2 = \{0, \pi/8, \pi/4,\ 3\pi/4, \pi/2\}$, and $\theta_1 = \theta_3$ (due to symmetry). For the given range of the parameters, **Eqs 31**, **32** are solved numerically producing a comprehensive database for each one of the examined boundary conditions presented in **Table 1**. This dataset contains $15 \times 15 \times 5 \times 5 \times 5 = 28125$ values of $\max w$ which are used in the regression analysis.

A plethora of regression algorithms, presented in the previous section, were employed for building corresponding predictive models of the $\max w$ using pyCaret (Ali, 2020), which is an open-source software machine learning library. A 5-fold cross-validation resampling procedure was used for evaluating the performance of the predictive models. The dataset was randomly divided into five folds of equal size and each fold was used for evaluating the performance of the model trained on the rest folds, whereas the final measure was the average value of the computed evaluation metrics on each test fold. Evaluation metrics are a measure of how well a model performs. The most popularly used evaluation metrics for regression problems are the mean absolute error (MAE), the mean absolute percentage error (MAPE), the mean square error (MSE), the root mean square error (RMSE), the root mean squared log error (RMSLE) and the coefficient of determination. The lower the value of these metrics the better the model. The perfect value of metrics is 0, indicating that the prediction model is perfect. To quantify the accuracy of the examined algorithms, the following evaluation metrics are used herein:

Mean absolute error (MAE)

$$\mathrm{MAE} = \frac{1}{n}\sum_{i=1}^{n}\left|y'_i - y_i\right| \tag{33}$$

Mean absolute percentage error (MAPE)

$$\mathrm{MAPE} = \frac{1}{n}\sum_{i=1}^{n}\left(\left|y'_i - y_i\right|\right)/\left|y'_i\right| \tag{34}$$

TABLE 5 | Evaluation metrics for the clamped-free beam.

Model	MAE	MSE	RMSE	R^2	RMSLE	MAPE
Extra Trees Regressor	0.5528	4.8885	2.1609	0.9995	0.0207	0.0122
Random Forest Regressor	0.8671	11.6799	3.3623	0.9987	0.0230	0.0165
Decision Tree Regressor	1.0436	17.3124	4.0909	0.9982	0.0314	0.0228
Light Gradient Boosting Machine	1.8359	25.0335	4.9130	0.9973	0.1280	0.2147
K Neighbors Regressor	7.1088	960.7922	30.9752	0.8967	0.1458	0.0958
Gradient Boosting Regressor	10.4671	513.5992	22.6138	0.9448	0.7340	3.1057
AdaBoost Regressor	27.1617	1772.9870	41.8579	0.8069	1.1216	6.1978
Huber Regressor	30.9933	6409.2110	80.0145	0.3120	1.2242	11.7426
Passive Aggressive Regressor	32.4646	6467.0355	80.3816	0.3054	1.3298	14.5124
Elastic Net	36.0246	5755.0187	75.8199	0.3823	1.4109	11.3018
Lasso Regression	39.6877	5288.4303	72.6848	0.4323	1.6179	24.8280
Bayesian Ridge	40.2698	5283.6727	72.6527	0.4328	1.6414	26.0519
Ridge Regression	40.2777	5283.6730	72.6527	0.4328	1.6417	26.0694
Linear Regression	40.2791	5283.6732	72.6527	0.4328	1.6418	26.0725
Least Angle Regression	40.2791	5283.6734	72.6527	0.4328	1.6418	26.0725
Orthogonal Matching Pursuit	41.8498	6342.4469	79.6055	0.3189	1.5624	15.6819
Lasso Least Angle Regression	55.7829	9312.0379	96.4636	0.0002	2.0693	32.0586

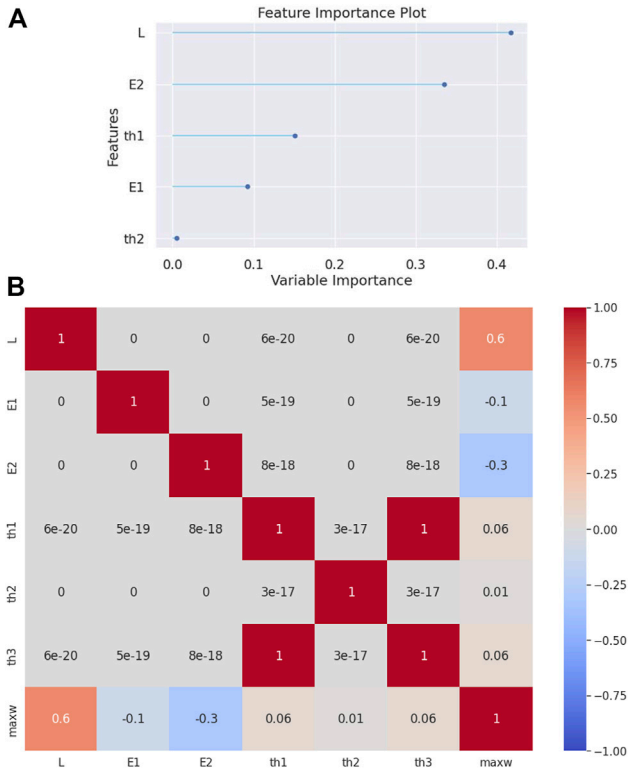

FIGURE 5 | (A) Feature importance plot and **(B)** correlation matrix heatmap for the clamped-free beam.

Mean square error (MSE)

$$\mathrm{MSE} = \frac{1}{n}\sum_{i=1}^{n}\left(y_i' - y_i\right)^2 \tag{35}$$

Root mean square error (RMSE)

$$\mathrm{RMSE} = \sqrt{\frac{1}{n}\sum_{i=1}^{n}\left(y_i' - y_i\right)^2} \tag{36}$$

Root mean squared log error (RMSLE)

$$\mathrm{RMSLE} = \sqrt{\frac{1}{n}\sum_{i=1}^{n}\left(\log\left(y_i' + 1\right) - \log\left(y_i + 1\right)\right)^2} \tag{37}$$

Coefficient of determination (R^2)

$$R^2 = \frac{SS_{reg}}{SS_{tot}} = \frac{\sum_j\left(y_i' - \bar{y}\right)^2}{\sum_i\left(y_i - \bar{y}\right)^2}, \tag{38}$$

where y'_i refers to predicted values, and y_i refers to true values. SS_{reg} is the regression sum of squares (i.e., explained sum of squares), and SS_{tot} is the total sum of squares, which is proportional to the variance of the data. The coefficient of determination (R^2) is the square of the correlation between the actual and predicted variable and ranges from 0 to 1. A zero value indicates that the model cannot explain any of the predicted variables. A value of 1 indicates that the regression model explains perfectly the predicted variable.

Apart from the evaluation metrics of the machine learning algorithms, two other useful tools are presented for the predictive analysis of the max w. First, the *feature importance* is a technique for assigning scores to input features that indicate the relative importance of each feature for the prediction. The scores can highlight which features are most relevant to the target and the opposite, i.e., which features are the least relevant. Most importance scores are calculated using the most accurate predictive model that has been fit on our data (Louppe et al., 2013). Second, the *correlation matrix heatmap* illustrates the correlation dependence between the variables of the database. That is, each square of the matrix represents the correlation between the attributes paired on the two axes. A value of +1 (or −1) indicates a perfect correlation between two variables, with +1 indicating a positive correlation and −1 a negative (inverse)

TABLE 6 | Friedman ranking.

Model	Rank (w.r.t. MAE)	Model	Rank (w.r.t. MAPE)	Model	Rank (w.r.t. R^2)
Extra-Trees Regressor	1	Extra-Trees Regressor	1	Extra-Trees Regressor	1
Random Forest Regressor	2	Random Forest Regressor	2	Random Forest Regressor	2
Decision Tree Regressor	3	Decision Tree Regressor	3	Light Gradient Boosting Machine	3.5
Light Gradient Boosting Machine	4	K Neighbors Regressor	4	Decision Tree Regressor	3.5
K Neighbors Regressor	5.25	Light Gradient Boosting Machine	5	Gradient Boosting Regressor	5
Gradient Boosting Regressor	5.75	Gradient Boosting Regressor	6	K Neighbors Regressor	6
AdaBoost Regressor	7.25	Elastic Net	7.5	AdaBoost Regressor	7
Huber Regressor	7.75	AdaBoost Regressor	7.75	Ridge Regression	9.5
Elastic Net	9.5	Huber Regressor	9.5	Linear Regression	9.5
Lasso Regression	10	Lasso Regression	10	Bayesian Ridge	9.5
Bayesian Ridge	11.25	Orthogonal Matching Pursuit	10.75	Least Angle Regression	9.5
Ridge Regression	12.25	Passive Aggressive Regressor	12.5	Lasso Regression	12.75
Passive Aggressive Regressor	13.75	Bayesian Ridge	12.75	Elastic Net	13
Linear Regression	13.75	Ridge Regression	13.75	Huber Regressor	13.75
Least Angle Regression	13.75	Linear Regression	15.25	Orthogonal Matching Pursuit	14.5
Orthogonal Matching Pursuit	15.75	Least Angle Regression	15.25	Passive Aggressive Regressor	16
Lasso Least Angle Regression	17	Lasso Least Angle Regression	17	Lasso Least Angle Regression	17

correlation; a value in the range from 0.6 to 1 (or from −0.6 to −1) indicates a strong correlation; a value between 0.4 and 0.6 (or between −0.4 and −0.6) indicates a moderate correlation; a value in the range from 0 to 0.4 (or from 0 to −0.4) indicates a weak correlation.

Clamped-Clamped Beam

First, a clamped-clamped beam is analyzed. The evaluation metrics of the employed regression algorithms are tabulated in **Table 2**. The Extra-Trees Regressor algorithm is the most effective algorithm reaching a R^2 value of 0.9994, followed by the Random Forest Regressor and the Decision Tree Regressor. By examination of the evaluation metrics, it is obvious that there are significant differences in the effectiveness between algorithms. Nevertheless, the algorithms that perform best do so consistently for all problems, as will be demonstrated.

From the feature importance plot (see **Figure 2A**), it is observed that the most important parameters for predicting the target attribute $\max w$ is the modulus of elasticity E_2 and the span-to-depth ratio $L(=l/h)$. Next comes the ply angle $\text{th1}(=\theta_1^\circ)$ which is more important than E_1, and $\text{th2}(=\theta_2^\circ)$. Moreover, the correlation matrix heatmap has been evaluated for this problem; in this figure, the blue color indicates a negative correlation between the two parameters, while the red one indicates a positive correlation. Moreover, the intensity of the color implies how strongly these attributes are correlated, meaning that the deeper color corresponds to a stronger correlation. The correlation matrix heatmap of **Figure 2B** reveals that the maximum deflection is positively correlated with the parameters L, θ_1°, θ_2° and negatively correlated with E_1 and E_2. This means that increase of the span-to-depth ratio or increase of the angles of the plies leads to an increase of the maximum deflection. Conversely, an increase of either elastic moduli leads to a decrease in the maximum deflection. Nevertheless, E_2 is more strongly correlated with $\max w$ than E_1. Finally, the ply angle θ_1° seems to be more important than the angle θ_2° in making the beam stiffer, yet the difference is small.

Simply Supported Beam

In this second example, a simply supported beam is analyzed. The Extra-Trees Regressor algorithm outperforms the other regression algorithms once again (see **Table 3**). The feature importance plot (see **Figure 3A**) shows an importance sequence different from that of the previous example. That is, the span-to-depth ratio $L(=l/h)$ is more important than the modulus of elasticity E_2, while the ply angle $\text{th1}(=\theta_1^\circ)$ is more important than E_1 and $\text{th2}(=\theta_2^\circ)$. Furthermore, the correlation matrix heatmap shown in **Figure 3B** reveals that, again, the maximum deflection is positively correlated with the parameters L, θ_1°, θ_2° and negatively correlated with E_1 and E_2. As previously, the correlation of E_2 is significantly stronger than that of E_1. The ply angles exhibit weak positive correlations with the maximum deflection, with $\text{th1}(=\theta_1^\circ)$ being the prevailing one.

Clamped-Roller Beam

In this example, a clamped-roller beam is analyzed. In **Table 4** it is shown that the Extra-Trees Regressor algorithm is again the most effective, as compared to the other regression algorithms. The feature importance plot (see **Figure 4A**) shows once more a similar to the clamped-clamped beam importance sequence. That is, the most important parameter is the modulus of elasticity E_2, followed closely by the span-to-depth ratio $L(=l/h)$. The ply angle $\text{th1}(=\theta_1^\circ)$ is more important than E_1, and $\text{th2}(=\theta_2^\circ)$. Furthermore, the correlation matrix heatmap shown in **Figure 4B** reveals that, again, the maximum deflection is positively correlated with the parameters L, θ_1°, θ_2° and negatively correlated with E_1 and E_2. The elastic modulus E_2 exhibits a stronger correlation with the maximum deflection than E_1. As in the case of the clamped-clamped beam, the ply angle θ_1° is more important than the angle θ_2°.

Clamped-free Beam

In the case of a clamped-free beam (cantilever), while the evaluation metrics designates once more the Extra-Trees Regressor algorithm superiority (see **Table 5**), the feature

importance plot (see **Figure 5A**) presents a similar to the simply supported beam importance sequence. That is, the most important parameter is the span-to-depth ratio $L(=l/h)$ followed the modulus of elasticity E_2. The ply angle th1 $(=\theta_1^\circ)$ is more important than E_1, and th2 $(=\theta_2^\circ)$.

The correlation matrix heatmap (see **Figure 5B**) again shows that the max w is positively correlated with the parameters L, θ_1°, θ_2° and negatively correlated with E_1 and E_2. In this case, the ply angle θ_1° is significantly more strongly correlated with the maximum deflection than the angle θ_2°.

Friedman Ranking

Finally, to better assess the results obtained from each algorithm, the Friedman test methodology proposed by Demšar (2006) was employed for the comparison of several algorithms over multiple datasets (**Table 6**). As was expected, the Extra-Trees Regressor algorithm is the most accurate in our case. A simple computational tool, written in JAVA programming language using Weka API (Hall et al., 2009) along with the relevant data, is provided to the interested reader as **Supplementary Data** to this article.

CONCLUSION

In this paper, several machine learning regression models were employed for the prediction of the deflection of symmetric laminated composite beams subjected to a uniformly distributed load. Training, validation, and testing of the models require large amounts of data that cannot be provided by the scarce experiments. Instead, ample amounts of data are generated numerically using a refined higher-order beam theory for various span-to-depth ratios and boundary conditions, by appropriate discretization of all pertinent geometric and material properties.

The main conclusion that can be drawn from this investigation are as follows:

- Regarding the regression models, the Extra-Trees algorithm is, without doubt, the best performer for all cases of boundary conditions, followed by the Random Forest Regressor, the Decision Tree Regressor, the Light Gradient Boosting Machine, and the K Neighbors Regressor.
- The prediction errors of the best-performing models are adequately small for engineering purposes. This allows for the rapid design of the composite beams without resolving to a mathematical implementation of higher-order beam theories. Moreover, these models can be integrated into modern metaheuristic optimization algorithms which use only payoff data (i.e., no derivative data) to allow for the fast and reliable optimization of such beams.
- Regarding the relative importance of the design variables for the evaluation of the deflection, the span-to-depth ratio and the modulus of elasticity E_2 are unambiguously the most important features. The next level of importance includes the angle ply θ_1 and the modulus of elasticity E_1. Surprisingly, the angle θ_2 is the least important variable.
- The span-to-depth ratio L has the strongest positive correlation to the target attribute max w for all cases of boundary conditions, as evidenced by the correlation matrices. In all cases, the maximum deflection is positively correlated with the parameters L, θ_1, θ_2 and negatively correlated with E_1 and E_2.
- An easy-to-use computational tool has been implemented which is provided as **Supplementary Material** to the present article.

DATA AVAILABILITY STATEMENT

The original contributions presented in the study are included in the article/**Supplementary Material**, further inquiries can be directed to the corresponding author.

AUTHOR CONTRIBUTIONS

GT had the research idea, drafted the article, and contributed to the theoretical formulation of the beam theory. SK and AC contributed to the conception and design of the work, and the theoretical analysis of the regression techniques. The manuscript was written through the contribution of all authors. All authors discussed the results, reviewed, and approved the final version of the manuscript.

SUPPLEMENTARY MATERIAL

The Supplementary Material for this article can be found online at: https://www.frontiersin.org/articles/10.3389/fbuil.2022.855112/full#supplementary-material

REFERENCES

Ali, M. (2020). *PyCaret: An Open-Source, Low-Code Machine Learning Library in Python*. Available at: https://www.pycaret.org

Altman, N. S. (1992). An Introduction to Kernel and Nearest-Neighbor Nonparametric Regression. *The Am. Statistician* 46, 175–185. doi:10.1080/00031305.1992.10475879

Bickford, W. B. (1982). A Consistent Higher Order Beam Theory. *Dev. Theor. Appl. Mech.* 11, 137–150.

Breiman, L., Friedman, J. H., Olshen, R. A., and Stone, C. J. (1984). *Classification and Regression Trees*. New York, NY: Routledge. doi:10.1201/9781315139470

Breiman, L. (2001). Random Forests. *Mach. Learn.* 45, 5–32. doi:10.1023/A:1010933404324

Civalek, Ö., and Kiracioglu, O. (2010). Free Vibration Analysis of Timoshenko Beams by DSC Method. *Int. J. Numer. Meth. Biomed. Engng.* 26, 1890–1898. doi:10.1002/CNM.1279

Crammer, K., Dekel, O., Keshet, J., Shai, S.-S., and Singer, Y. (2006). Online Passive-Aggressive Algorithms. *J. Mach. Learn. Res.* 7, 551–585.

Demšar, J. (2006). Statistical Comparisons of Classifiers over Multiple Data Sets. *J. Mach. Learn. Res.* 7, 1–30.

Efron, B., Hastie, T., Johnstone, I., Tibshirani, R., Ishwaran, H., Knight, K., et al. (2004). Least Angle Regression. *Ann. Statist.* 32, 407–499. doi:10.1214/009053604000000067

Eisenberger, M. (2003). An Exact High Order Beam Element. *Comput. Structures* 81, 147–152. doi:10.1016/S0045-7949(02)00438-8

Endo, M. (2016). An Alternative First-Order Shear Deformation Concept and its Application to Beam, Plate and Cylindrical Shell Models. *Compos. Structures* 146, 50–61. doi:10.1016/J.COMPSTRUCT.2016.03.002

Freund, Y., and Schapire, R. E. (1997). A Decision-Theoretic Generalization of On-Line Learning and an Application to Boosting. *J. Comput. Syst. Sci.* 55, 119–139. doi:10.1006/JCSS.1997.1504

Friedman, J., Hastie, T., and Tibshirani, R. (2010). Regularization Paths for Generalized Linear Models via Coordinate Descent. *J. Stat. Soft.* 33, 1. doi:10.18637/jss.v033.i01

Friedman, J. H. (2001). Greedy Function Approximation: A Gradient Boosting Machine. *Ann. Stat.* 29, 1189–1232. doi:10.1214/aos/1013203451

Geurts, P., Ernst, D., and Wehenkel, L. (20062006). Extremely Randomized Trees. *Mach. Learn.* 63, 3–42. doi:10.1007/S10994-006-6226-1

Hall, M., Frank, E., Holmes, G., Pfahringer, B., Reutemann, P., and Witten, I. H. (2009). The WEKA Data Mining Software. *SIGKDD Explor. Newsl.* 11, 10–18. doi:10.1145/1656274.1656278

Heyliger, P. R., and Reddy, J. N. (1988). A Higher Order Beam Finite Element for Bending and Vibration Problems. *J. Sound Vibration* 126, 309–326. doi:10.1016/0022-460X(88)90244-1

Hoerl, A. E., Kennard, R. W., and Hoerl, R. W. (1985). Practical Use of Ridge Regression: A Challenge Met. *Appl. Stat.* 34, 114–120. doi:10.2307/2347363

Katsikadelis, J. T., and Tsiatas, G. C. (20032003). Large Deflection Analysis of Beams with Variable Stiffness. *Acta Mechanica* 164, 1–13. doi:10.1007/S00707-003-0015-8

Ke, G., Meng, Q., Finley, T., Wang, T., Chen, W., Ma, W., et al. (2017). LightGBM: A Highly Efficient Gradient Boosting Decision Tree. Adv. Neural Inf. Process. Syst. 30. Available at: https://github.com/Microsoft/LightGBM (Accessed December 14, 2021).

Khdeir, A. A., and Reddy, J. N. (1997). An Exact Solution for the Bending of Thin and Thick Cross-Ply Laminated Beams. *Compos. Structures* 37, 195–203. doi:10.1016/S0263-8223(97)80012-8

Lambert-Lacroix, S., and Zwald, L. (2011). Robust Regression through the Huber's Criterion and Adaptive Lasso Penalty. *Electron. J. Statist* 5, 1015–1053. doi:10.1214/11-EJS635

Liew, K. M., Pan, Z. Z., and Zhang, L. W. (2019). An Overview of Layerwise Theories for Composite Laminates and Structures: Development, Numerical Implementation and Application. *Compos. Structures* 216, 240–259. doi:10.1016/J.COMPSTRUCT.2019.02.074

Lin, X., and Zhang, Y. X. (2011). A Novel One-Dimensional Two-Node Shear-Flexible Layered Composite Beam Element. *Finite Elem. Anal. Des.* 47, 676–682. doi:10.1016/J.FINEL.2011.01.010

Louppe, G., Wehenkel, L., Sutera, A., and Geurts, P. (2013). Understanding Variable Importances in Forests of Randomized Trees. *Adv. Neural Inf. Process. Syst.* 26, 431–439.

Murthy, M. V. V. S., Roy Mahapatra, D., Badarinarayana, K., and Gopalakrishnan, S. (2005). A Refined Higher Order Finite Element for Asymmetric Composite Beams. *Compos. Structures* 67, 27–35. doi:10.1016/J.COMPSTRUCT.2004.01.005

Narula, S. C., and Wellington, J. F. (1982). The Minimum Sum of Absolute Errors Regression: A State of the Art Survey. *Int. Stat. Rev./Revue Internationale de Statistique* 50, 317. doi:10.2307/1402501

Nguyen, T.-K., Nguyen, N.-D., Vo, T. P., and Thai, H.-T. (2017). Trigonometric-Series Solution for Analysis of Laminated Composite Beams. *Compos. Structures* 160, 142–151. doi:10.1016/J.COMPSTRUCT.2016.10.033

Pati, Y. C., Rezaiifar, R., and Krishnaprasad, P. S. (1993). "Orthogonal Matching Pursuit: Recursive Function Approximation with Applications to Wavelet Decomposition," in Conf. Rec. Asilomar Conf. Signals, Syst. Comput., Pacific Grove, CA, November 1–3, 1993 1, 40–44. doi:10.1109/ACSSC.1993.342465

Pawar, E. G., Banerjee, S., and Desai, Y. M. (2015). Stress Analysis of Laminated Composite and Sandwich Beams Using a Novel Shear and Normal Deformation Theory. *Lat. Am. J. Sol. Struct.* 12, 1340–1361. doi:10.1590/1679-78251470

Reddy, J. N. (1984). A Simple Higher-Order Theory for Laminated Composite Plates. *J. Appl. Mech.* 51, 745–752. doi:10.1115/1.3167719

Srinivasan, R., Dattaguru, B., and Singh, G. (2019). Exact Solutions for Laminated Composite Beams Using a Unified State Space Formulation. *Int. J. Comput. Methods Eng. Sci. Mech.* 20, 319–334. doi:10.1080/15502287.2019.1644394

Tipping, M. E. (2001). Sparse Bayesian Learning and the Relevance Vector Machine. *J. Mach. Learn. Res.* 1, 211–244.

Tsiatas, G. C., Siokas, A. G., and Sapountzakis, E. J. (2018). A Layered Boundary Element Nonlinear Analysis of Beams. *Front. Built Environ.* 4, 52. doi:10.3389/FBUIL.2018.00052/BIBTEX

Vo, T. P., and Thai, H.-T. (2012). Static Behavior of Composite Beams Using Various Refined Shear Deformation Theories. *Compos. Structures* 94, 2513–2522. doi:10.1016/J.COMPSTRUCT.2012.02.010

Wang, C. M., Reddy, J. N., and Lee, K. H. (2000). *Shear Deformable Beams and Plates : Relationships with Classical Solutions*. Elsevier.

Zou, H., Hastie, T., and Tibshirani, R. (2007). On the "Degrees of freedom" of the Lasso. *Ann. Stat.* 35, 2173–2192. doi:10.1214/009053607000000127

Conflict of Interest: The authors declare that the research was conducted in the absence of any commercial or financial relationships that could be construed as a potential conflict of interest.

Publisher's Note: All claims expressed in this article are solely those of the authors and do not necessarily represent those of their affiliated organizations, or those of the publisher, the editors and the reviewers. Any product that may be evaluated in this article, or claim that may be made by its manufacturer, is not guaranteed or endorsed by the publisher.

frontiers in Built Environment

REVIEW
published: 10 March 2022
doi: 10.3389/fbuil.2022.830207

Performance-Based Wind Engineering: Background and State of the Art

Seymour M. J. Spence and Srinivasan Arunachalam*

Department of Civil and Environmental Engineering, University of Michigan, Ann Arbor, MI, United States

This paper surveys the rapidly growing field of performance-based wind engineering (PBWE) of engineered systems, with focus on not only how PBWE has evolved since its early incarnations inspired by performance-based seismic engineering, but also the unique challenges of PBWE and the research that continues to emerge to tackle them. The limitations of traditional prescriptive wind design approaches are discussed with the aim of illustrating how such approaches are inadequate for providing acceptable building performance during extreme wind events, thus motivating why performance-based strategies for wind engineering are gaining traction and are poised to complement, if not replace, current approaches to wind design. In this respect, the current state of knowledge on the factors that affect building performance via extreme structural response, damage to the envelope system, and nonstructural components, is reviewed and challenges are identified. Lastly, the potential benefit of integrating optimization methods is identified while acknowledging the computational difficulty associated with such approaches.

Keywords: performance-based wind engineering, hurricanes, building envelopes, probabilistic damage and loss modeling, extreme winds, performance-based design optimization

OPEN ACCESS

Edited by:
Gregory A Kopp,
Western University, Canada

Reviewed by:
Luca Caracoglia,
Northeastern University, United States
Kurtis Robert Gurley,
University of Florida, United States

****Correspondence:***
Seymour M. J. Spence
smjs@umich.edu

Specialty section:
This article was submitted to Wind Engineering and Science, a section of the journal Frontiers in Built Environment

Received: *06 December 2021*
Accepted: *09 February 2022*
Published: *10 March 2022*

Citation:
Spence SMJ and Arunachalam S (2022) Performance-Based Wind Engineering: Background and State of the Art. Front. Built Environ. 8:830207. doi: 10.3389/fbuil.2022.830207

1 INTRODUCTION

With the burgeoning growth of high-rise building construction around the globe and an increased awareness for the creation of sustainable urban habitats, solutions for performance-oriented efficient and economical building systems are in great need. To address this, extensive research has been carried out over the past four decades in the area of performance-based engineering (PBE). While initial focus was on developing methods for achieving buildings systems with greater earthquake resistance (e.g., Moehle and Deierlein (2004)), the concepts of PBE have extended to other hazards, including wind, fire and tsunamis (e.g., Ciampoli et al. (2011); Wang et al. (2012); Attary et al. (2017). Furthermore, the successful development of performance-based seismic engineering (PBSE) and its adoption in codes and practice over the past two decades has provided strong evidence for, not only the application of similar approaches for other natural and man-made hazards, but also risk-consistent multi-hazard design approaches (Gardoni and LaFave (2016); Suksuwan and Spence (2018); Kwag et al. (2021). To successfully transfer this knowledge to wind engineering, the fundamental differences between seismic and wind effects for both structural and non-structural components, especially the envelope system, must be embraced while respecting the unique characteristics of wind loading and concurrent hazards (e.g., rainfall and debris impact).

Wind-excited structures have been historically designed to respond elastically under strength-level loads. In transitioning to a PBE setting, there is growing interest in allowing controlled inelastic

deformation in specifically designed members under extreme winds (ASCE/SEI, 2019). The advantages of such a design approach are two fold, first it provides a means to engineer more economic systems through enabling the exploration of the full resistance of materials and components, secondly, it provides a means to design innovative systems for resisting both wind and seismic actions when they are comparable. These advantages come at the price of requiring careful assessment of the response of both the deformation-controlled components as well as the system as a whole. This implies the need for development of design guidelines that are informed by research on the hysteretic response and damage accumulation until collapse of structures designed with controlled inelasticity, as well as the consequences of such a design philosophy on the performance metrics and reliabilities of such systems. In the same vein, performance assessment frameworks for the building envelope (i.e. cladding system) and nonstructural components/systems need to be capable of quantifying potential damage arising from dynamic wind pressures, structural response, wind-driven rain, and wind-borne debris. Fundamental to such an assessment is the proper capture of the dependence between structural response and the net pressure demands of the envelope system as this will dictate the capacity of the cladding system to resist the hazards (Ouyang and Spence, 2019).

This paper is written and organized to serve as a review of the origins of PBWE. Through reflecting on the beginnings of PBSE, the major considerations enabling the leap from the current state-of-practice to a PBWE setting are discussed. The unique challenges and the latest developments in this transition are outlined. The potential benefits and challenges to integrating PBWE with optimization are also discussed.

2 PERFORMANCE-BASED ENGINEERING

Performance-based engineering may be defined as the practice of thinking and working in terms of ends rather than means (Gibson, 1982; Ellingwood, 1998). Considering a building system as an example, performance-based design (PBD) centers on what the building system is required to do rather than explicitly prescribing how it is to be constructed. While there is a strong interest in moving towards such an approach when it comes to designing buildings to resist natural hazards, most building codes are still prescriptive in nature (Meacham, 2010). In a typical building design process, design professionals select, proportion, and detail components to satisfy prescriptive criteria contained within a building code. Many of these criteria were developed with the intent to provide some level of performance; however, the intended performance levels are often fuzzy, and the actual ability of the resulting designs to provide the intended reliability is seldom evaluated or understood (Federal Emergency Management Agency (FEMA), 2012a; Ellingwood, 2001). An area of structural engineering that has been particularly active in attempting to apply the principles of PBD is that concerning the design of buildings to resist earthquakes.

3 PERFORMANCE-BASED SEISMIC ENGINEERING

3.1 First Generation of Performance-Based Seismic Engineering

Traditional prescriptive provisions for seismic design were developed commencing from the late 1920s (Applied Technology Council (ATC), 1995a) and can be viewed as implicitly performance-oriented in that they were developed with the intent of achieving specific performance, that is avoidance of collapse and assurance of life safety. However, damage assessments made on buildings following minor, moderate and intense ground shaking over the past 80+ years have shown that these implicit performance targets cannot be reliably realized following such an approach (Whittaker et al., 2003). The significant economic losses, as well as the loss of function of critical facilities, during the 1989 Loma Prieta and 1994 Northridge earthquakes may be seen as the events that spurred the initial development of modern performance-based seismic design with the aim of developing resilient, loss-resistant communities (Whittaker et al., 2003; Ghobarah, 2001). Indeed, in the early to mid 1990s, FEMA funded the Applied Technology Council (ATC) and the Building Seismic Safety Council (BSSC) with the aim of developing procedures for the implementation of performance-based seismic design (PBSD). This led to the publication of the NEHRP Guidelines and Commentary for Seismic Rehabilitation of Buildings (Federal Emergency Management Agency (FEMA), 1997). The concepts and procedures proposed in this work are generally considered to constitute the foundation of the first generation of PBSD methods. In particular, several important earthquake-related concepts that may now be considered not only as a baseline for understanding the underlying philosophy of PBSD, but also the starting point for applying the principles of PBD to resist other natural and man-made hazards, were conceptualized (Whittaker et al., 2003; Moehle and Deierlein, 2004). Other important pioneering PBSD efforts that significantly contributed to this end include the SEAOC's Vision 2000 (Structural Engineers Association of California (SEAOC), 1995), ATC-32 (Applied Technology Council (ATC), 1996a) and ATC-40 (Applied Technology Council (ATC), 1996b) reports as well as the FEMA 356 (Federal Emergency Management Agency (FEMA), 2000a) report. The key concept introduced by the aforementioned works was the idea of performance objective, consisting of a design event of specified intensity (earthquake hazard), which the building is to be designed to resist, and a permissible level of damage (performance level) given that the design event occurs. In particular, standard performance levels with performance-oriented descriptions (Fully Operational, Functional - referred to as Immediate Occupancy in Applied Technology Council (ATC) (1995b) - Life Safety, and Near Collapse - referred to as Collapse Prevention in Applied Technology Council (ATC) (1995b)) - were introduced for quantifying both structural and non-structural damage in terms of typical response parameters (inter-story drifts, inelastic member deformations, member

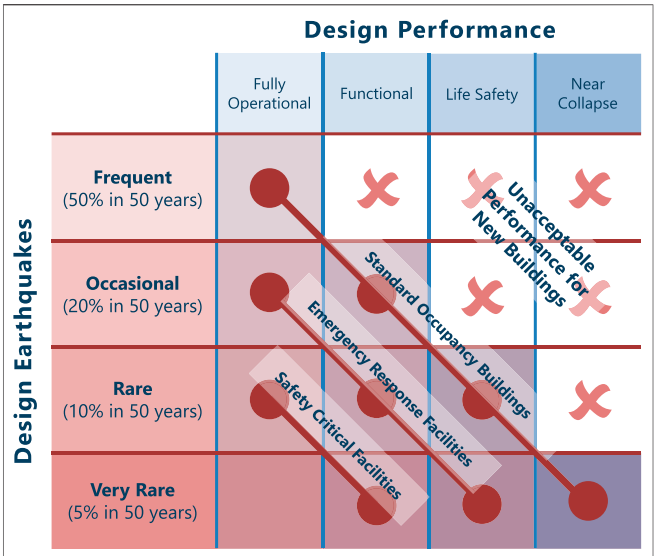

FIGURE 1 | Standard performance objectives, SEAOC's Vision 2000 (Structural Engineers Association of California (SEAOC), 1995).

forces etc.) therefore defining a number of standard performance objectives as illustrated in **Figure 1** for three different occupancy categories. For this first generation of PBSD procedures, a building was said to satisfy its global objectives if structural analyses indicated that the member forces or deformations imposed on each element did not exceed predefined limits (Porter, 2003).

3.2 Current State of Research for Performance-Based Seismic Engineering

While the first generation of PBSD methodologies represented an important milestone in the practical application of PBD principles to earthquake resilient design, several shortcomings were identified (Porter, 2003; Whittaker et al., 2003; Moehle and Deierlein, 2004). Among these were: 1) the performance of the system is identified on the basis of damage sustained at a component-level; 2) the inherent uncertainty that affects all aspects of the structural response prediction was not explicitly modeled (Ellingwood, 2008); and 3) the standard discrete performance levels did not directly address some primary stakeholders' concerns, such as probable repair costs and time of occupancy loss in the building, due to earthquake induced damage. To address these and other limitations, FEMA published an action plan (Federal Emergency Management Agency (FEMA), 2000b; Federal Emergency Management Agency (FEMA), 2006) for the development of the next generation of PBSD procedures. This resulted in the publication by FEMA of the P-58 volumes (Federal Emergency Management Agency (FEMA), 2012a; 2012b; 2012c). These volumes outline a general methodology for the seismic performance assessment of individual buildings that explicitly accounts for the inevitable uncertainty in the ability to accurately predict response while communicating performance through system-level measures that are easily understood by decision-makers and/or stakeholders, i.e. probable consequences, in terms of human losses (deaths and serious injuries), direct economic losses (building repair or replacement costs), and indirect losses. The recent completion of phase 2 of the FEMA P-58 project, in which, among other products, the performance of a suite of archetype code conforming buildings were evaluated in terms of the P-58 performance metrics (Federal Emergency Management Agency (FEMA), 2018), promise to continue the evolution of seismic standards and codes towards the principles of PBE. The technical backbone of the procedure is based on the well-known analytical framework developed by the researchers at the Pacific Earthquake Engineering Research Center (PEER) during the period between 1997 and 2010 (Cornell and Krawinkler, 2000; Moehle and Deierlein, 2004; Yang et al., 2009; Günay and Mosalam, 2013). Unlike the first generation of PBD methodologies, in order to provide results that can be used by a multitude of decision models, performance can be assessed for a particular earthquake scenario or intensity, or considering all earthquakes that could occur, and the likelihood of each, over a specified period of time. While the framework was developed for PBSD, it is relatively general and can be considered as a convenient analytical language with which to implement the principles of PBD for obtaining resilient and risk-consistent structures to mitigate the effects of other natural hazards.

4 WIND ENGINEERING

4.1 Current Practice

The current state-of-the-practice in wind engineering involves the selection of hazard intensities, derived from an appropriate code or standard, with which to carry out performance assessments and therefore design the structural elements of a building or facility. Taking for example the ASCE 7-16 (ASCE 7-16 (2016)), the hazard intensity is given by the maximum 3-s gust wind speed with prescribed mean recurrence interval (MRI). Which MRI to consider is generally governed by the level of resilience that the designer/stakeholder wishes to give the structure, e.g., in the ASCE 7-16 a risk category I, II, III, or IV is selected. Based on the wind speed with prescribed MRI, wind loads are derived that account for aspects such as wind exposure, topography, wind directionality as well as the external geometry of the building under consideration. The loads so obtained are in general to be used for strength level design, i.e., the ultimate limit state that has the purpose of ensuring life safety. Serviceability design is generally left to the purview of the engineer and stakeholder. Once the loads are defined for a given building/facility, an appropriate material code (e.g., ACI 318-11 (2012) for reinforced concrete buildings and AISC 360-16 (2016) for structural steel buildings) is generally adopted for designing the structural elements. These provide detailed prescriptive requirements that the design engineer should comply with in order to ensure life safety. While the procedure outlined above is relatively effective in ensuring the adequacy of the main wind force resisting system (MWFRS), some observations can be made: 1) the process is prescriptive, therefore the actual performance of

the system is not known, it is only implicitly assumed to be achieved through following the prescriptions (Griffis et al., 2013; Ghosn et al., 2016b,a); 2) the process is largely deterministic, even though it is known that modeling assumptions greatly affect the results of the procedure (Griffis et al., 2013; Ghosn et al., 2016b,a); 3) the damage sustained by non-structural elements due to excessive drift of the MWFRS is not explicitly contemplated even though it often plays an important economic role in defining the overall building performance (Griffis, 1993; Aswegan et al., 2015; Ghosn et al., 2016b,a); 4) only prescriptive measures, instructions to use impact resistant glazing or storm shutters in wind prone regions etc., are considered for mitigating the risk of debris impact to the building envelope, i.e., no explicit assessment of the risk associated with this important loss mechanism (ASTM, 2007a,b; Vickery, 1970; Wyatt and May 1971; Tsujita et al., 1998; Ohkuma et al., 1998; Chen and Davenport, 2000; Tamura et al., 2001; Hong, 2004; Gani and Légeron, 2011; Vamvatsikos and Cornell, 2002; Maier, 1979; König and Maier, 1981; König, 1987; Maier and Munro, 1982; Maier and Lloyd-Smith, 1986) is contemplated; and 5) losses associated with water ingress due to wind-driven rain, and therefore damage to interior non-structural elements such as partitions, fixed furniture, ceilings, doors etc., are not considered even though they can account for a significant portion of the total losses associated with extreme wind events (Maier et al., 2000).

4.2 Limitations of Current Practice

The limitations outlined above of current wind engineering practice can only be rectified through the definition of a full PBD philosophy similar to that outlined in **Section 3** concerning the earthquake resistant design of structures. However, the direct transfer of these concepts to the field of wind engineering is not possible due to: 1) the unique excitation mechanism associated with complex phenomena such as turbulence, detached flow and vortex shedding, that are the driving forces behind pressure induced damage to the building envelope; 2) the difference in the ultimate performance of wind excited structures compared to earthquake excited structures (e.g., wind excited structural components generally experience less damage than non-structural components); 3) the considerably longer duration of wind excitation that makes progressive and interdependent damage mechanisms the norm; and 4) the important role played by performance objectives, such as envelope penetration due to debris or water ingress, that are not contemplated in earthquake resistant design. Notwithstanding these differences, the framework proposed by FEMA in Federal Emergency Management Agency (FEMA) (2012a,b,c) represents a useful and established language with which the principles of PBD can be applied to other natural hazards, including severe windstorms. Additionally, it is important to recognize that while performance objectives, such as fully operational and immediate occupancy, originate in PBSE (as discussed in **Section 3.1**), they represent statements of desired building functionality at specified load intensities. Therefore, in defining target performance objectives for wind excited structures, the qualitative goals of the aforementioned performance objectives can be retained. Having said this, it should be recognized that additional performance objectives, such as those associated with evacuation prior to severe hurricanes, may be required in developing frameworks for the effective implementation of PBWE.

5 PERFORMANCE-BASED WIND ENGINEERING: THE FRONTIER

5.1 Beginnings

The devastation and significant economic losses caused by hurricanes Andrew [$27.3 billion (1992 USD)], Iniki [$3.1 billion (1992 USD)] and Opal [$4.7 billion (1995 USD)] during the 1990s, together with the growing acceptance of PBSE, can be seen as events that spurred initial interest in applying the principles of PBE in the assessment and design of wind excited structures (Ellingwood et al., 2004). One of the first frameworks to be proposed for PBWE focused on the performance assessment of residential wood structures (Rosowsky and Ellingwood, 2002). Important contributions of this work included the conceptualization of a suite of performance objectives (from serviceability to ultimate load levels) for wind excited residential buildings, the identification of the need for system-level analysis (as opposed to traditional component-level analysis) if greater confidence in performance predictions were to be achieved, as well as the need to consider uncertainty. Subsequent to this work, the possibility of modeling the performance of wind excited engineered structures within a PBWE setting began to take root (Paulotto et al., 2004; Bashor and Kareem, 2007; Augusti and Ciampoli, 2008; Ciampoli et al., 2011). The initial focus of these works was primarily on establishing the applicability of the PEER framework (Cornell and Krawinkler, 2000; Yang et al., 2009; Günay and Mosalam, 2013), or similar (i.e. reliability integral), to the performance assessment of wind excited tall buildings and long span bridges. Since these initial research efforts, PBWE has seen an explosion of interest with numerous frameworks being proposed for both residential buildings (Rosowsky and Ellingwood, 2002; Barbato et al., 2013; Baheru et al., 2015; Peng et al., 2016; Unnikrishnan and Barbato, 2017) as well as engineered systems (Ciampoli et al., 2011; Griffis et al., 2013; Spence and Kareem, 2014; Bernardini et al., 2015; Judd and Charney, 2015; Chuang and Spence, 2017; Cui and Caracoglia, 2018; Judd, 2018; Chuang and Spence, 2019; Ierimonti et al., 2019; Micheli et al., 2019; Mohammadi et al., 2019; Cui and Caracoglia, 2020; Ouyang and Spence, 2020).

5.2 Current Status

Over the past decade, significant progress has been made towards the development of general PBWE frameworks for the probabilistic assessment and optimal design of engineered systems subject to severe winds. Major breakthroughs have been achieved in modeling structural and non-structural damage and loss due to both synoptic and hurricane winds through probabilistic system-level metrics associated with repair costs, downtime, life cycle costs, as well as occupant comfort (Ciampoli et al., 2011; Petrini and Ciampoli, 2012;

Griffis et al., 2013; Spence and Kareem, 2014; Bernardini et al., 2015; Judd and Charney, 2015; Chuang and Spence, 2017; Cui and Caracoglia, 2018; Judd, 2018; Ierimonti et al., 2019; Mohammadi et al., 2019; Chuang and Spence, 2019; Micheli et al., 2019; Cui and Caracoglia, 2020; Ouyang and Spence, 2020). Progress has also been made to extend PBWE for non-synoptic wind events characterized by intricate vortical flows, such as those found in tornadoes and thunderstorm downbursts (Le and Caracoglia, 2018, 2020; Masoomi and van de Lindt, 2016). Notwithstanding these efforts, there is still a lack of consensus on the most appropriate wind field models for capturing the complexities of tornado and thunderstorm downburst flows within a PBWE setting, as well as a need for more general models for simulating the non-stationary and non-straight fluctuating load component while retaining computational efficiency. Interestingly, the closer relationship of non-synoptic winds (as compared to synoptic) to seismic loading may indicate the possibility of translating some of the approaches used in seismic engineering for dissipating energy through material nonlinearity to PBWE. The adoption of such an approach, however, would require careful validation, since non-synoptic winds are not necessarily zero-mean. As will be discussed in more detail in **Section 6**, approaches have also been proposed for the single-/multi-objective design optimization within the space of the aforementioned probabilistic system-level metrics (Spence and Kareem, 2014; Spence, 2018; Suksuwan and Spence, 2019b,a; Venanzi et al., 2020; Petrini et al., 2020). While many of these frameworks were initially inspired by the fragility/consequence function-based damage/loss modeling approaches introduced by the PEER framework (and subsequently refined in the P-58 methodologies), they have since evolved to include additional metrics, e.g., life cycle costs, as well as wind specific performance criteria associated with, for example, occupant comfort (Bernardini et al., 2015). Importantly, during this evolution, they have generally preserved the fundamental idea underpinning the PEER framework of explicit evaluation of probabilistic system-level metrics that can be understood by a wide range of technical and non-technical decision makers.

Two important limitations of many of the aforementioned frameworks include: 1) the neglect of damage to the envelope system due to direct action of local net wind pressures; and 2) the assumption that the MWFRS can be modeled as elastic (structural damage is only implicitly modeled through fragility functions evaluated from demands estimated from elastic models of the MWFRS).

With respect to the first point, recent extensions of the Florida Public Hurricane Loss Model (FPHLM) to mid-rise residential buildings (e.g. Pita et al. (2016)) have considered these aspects. Nevertheless, the intent of the FPHLM is the performance assessment of portfolios containing hundreds of buildings. The detail with which each building is modeled is not therefore at the level of PBWE where the focus is on the performance assessment of individual buildings. With an explicit focus on individual buildings and PBWE, a fragility-based progressive damage model was recently introduced in Ouyang and Spence (2019). Within the framework, each component of the envelope system is modeled as susceptible to multiple coupled damage states characterized through suites of fragility functions. Demands are modeled through dynamic drift and net pressure characterized through non-Gaussian stochastic models calibrated to specific wind tunnel tests. To model the wind driven rain on the envelope due to the rain event that inevitably accompanies severe windstorms, Eulerian multiphase models based on computational fluid dynamics were adopted. The approach was subsequently embedded with a conditional stochastic simulation scheme, therefore defining a PBWE framework capable of estimating system-level loss and consequences related to decision variables such as repair costs and ingressed water due to envelope damage (Ouyang and Spence, 2020). This approach has recently been extended to consider nonlinearity in the MWFRS (Ouyang and Spence, 2021b) as well as more complex representations of the wind hazard, i.e., the non-stationary/-straight/Gaussian wind pressures that are characteristic of hurricanes before idealization (Ouyang and Spence, 2021a).

With respect to the second point, the neglect of potential nonlinearity in the MWFRS can be traced back to the following difficulties: 1) the long duration (in the order of hours) of typical dynamic wind loads, therefore creating a significant computational barrier to propagating uncertainty through nonlinear models of the MWFRS in determining the probabilistic performance metrics; and 2) the complexity of modeling the nonlinear response of the MWFRS where the presence of a substantial mean wind load component (for certain wind directions) creates theoretical difficulties in applying state-of-the-art nonlinear modeling approaches that have been calibrated to zero mean seismic loads. The long duration and substantial mean wind load for certain directions also make the exploitation of nonlinear material behavior for energy dissipation less straightforward than in seismic engineering, since potential issues can arise due to low-cycle fatigue failure and lack of complete internal force reversal in the structural elements. Notwithstanding these challenges, the neglect of potential damage to the MWFRS is fundamentally contrary to the concept of PBE that is based on the explicit modeling of performance of the system over a full range of hazard intensities. This has inspired interest in developing methods that can explicitly treat damage through nonlinear modeling of the MWFRS. In addition to studies that have looked at understanding specific aspects of inelasticity from a fundamental standpoint, e.g. (Hong, 2004; Gani and Légeron, 2011; Feng and Chen, 2017, 2018; Bezabeh et al., 2021a,b), two approaches have essentially been investigated within the setting of PBWE. The first is based on application of the theory of plasticity through defining the state of dynamic shakedown as a collapse prevention performance objective (Tabbuso et al., 2016; Chuang and Spence, 2017, 2019; Chuang and Spence, 2020; Chuang and Spence, 2022), while the second is based on directly applying nonlinear modeling approaches developed in seismic engineering for the nonlinear analysis of the MWFRS (Judd and Charney, 2015; Mohammadi et al., 2019; Nikellis et al., 2019; Ouyang and Spence, 2021b; Ghaffary and Moustafa, 2021; Huang and Chen, 2022). The intent of the first approach is to rapidly provide a means for identifying a region in which inelasticity can occur safely, i.e. without potential failure due to low-cycle fatigue

(acrosswind failure), ratcheting (alongwind failure), instantaneous plastic collapse, or excessive plastic deformation. The computational efficacy of the approach enables evaluation of reliability through direct stochastic simulation (Chuang and Spence, 2022). While the second approach provides greater modeling flexibility, a major challenge lies in the huge computational effort necessary to propagate uncertainty through the nonlinear finite element models (due to the long duration of wind events as compared to earthquakes) and therefore estimate general system-level damage/loss metrics that are consistent with current PBWE frameworks.

The need to bring low-rise buildings under the umbrella of PBWE is strongly recognized as they represent the majority of the building stock in the United States. Better damage assessment through frameworks that are based on the principles of PBWE would support improved residential building practices, and limit economic losses and social disruption (Ellingwood et al., 2008). Interestingly, as mentioned in **Section 5.1**, one of the earliest works in conceptualizing PBWE concerned the performance assessment of residential wood structures (Rosowsky and Ellingwood, 2002). Although research in the area of PBWE of low-rise buildings has lagged that of engineered buildings, some notable recent research efforts include the development of initial PBWE frameworks for non-engineered buildings with multi-hazard considerations (Unnikrishnan and Barbato, 2017, 2016), introduction of scales for classifying post-disaster structural functionality within the setting of PBWE (Nevill and Lombardo, 2020), wind-induced damage assessment of low-rise building envelopes with potential openings (Ji et al., 2020), and the experimental investigation of the propagation of wind-driven rain into the building interior of low-rise buildings (Raji et al., 2020).

5.3 Translation to Codes and Standards

The important research developments outlined in **Section 5.2**, coupled with the significant interest from industry to implement PBWE in practice, has culminated in the recent publication by the American Society of Civil Engineers (ASCE) of the Prestandard on PBWD (ASCE/SEI, 2019). Major innovations of this document are the introduction of limit states that explicitly allow (for the first time) nonlinearity in the MWFRS, the explicit integration of acceptance criteria related to the performance of the envelope system, and the definition of performance objectives over a full range of hazard intensities.

The performance objectives span occupant comfort through serviceability to ultimate strength where additional capacity arising from controlled inelasticity is permitted. To demonstrate building functionality across the range of objectives, linear elastic analysis is permitted for evaluating occupant comfort and operational performance targets since the system itself is required to remain elastic, whereas advanced analysis procedures can be employed to evaluate the continuous occupancy performance objective. To this end, three methods have been proposed, with two of them requiring nonlinear response history analysis at collapse or reliability-based dynamic shakedown to evaluate the intended performance of the deformation-controlled elements. The Prestandard has also explicitly included performance objectives and acceptance criteria for the evaluation of the building envelope and non-structural components.

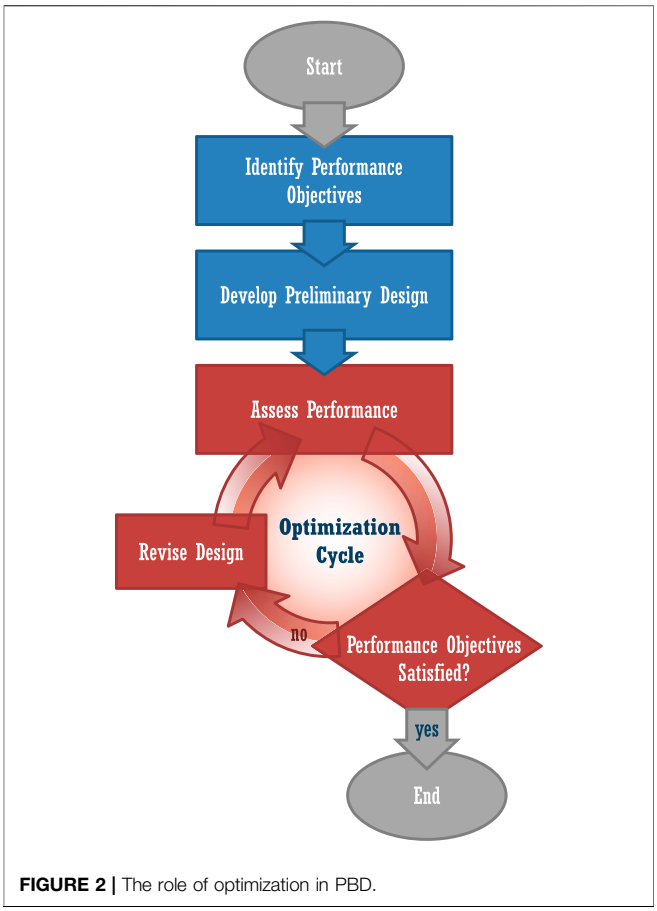

FIGURE 2 | The role of optimization in PBD.

As a relevant example of adoption in building design/construction practices of performance-based engineering, PBSE took around 25–30 years to advance from conception to widespread acceptance in practice. As highlighted in **Section 2**, first-generation of PBSE began in the early 1990s with second-generation PBSE starting in the early 2000s and achieving a certain maturity by the mid-2010s with widespread acceptance and adoption by industry thereafter. Similarly, since the beginning of focused research on PBWE in the late 2000s, significant progress has been made over the past decade. The release of the Prestandard on PBWD is a major milestone and, if current research and standards development efforts continue, a similar trend as seen for PBSE can be expected, leading to the widespread implementation in practice of PBWE in the next 10–15 years.

6 THE ROLE OF OPTIMIZATION IN PERFORMANCE-BASED WIND ENGINEERING

6.1 General Comments

As has been outlined in the previous sections, the practical implementation of modern PBD requires the rigorous use of

reliability/probabilistic models for the performance evaluation of the system. Compared to traditional deterministic design, this approach therefore entails the use of more complex and computationally cumbersome models. This makes the traditional trial-and-error approach to finding designs that satisfy the multiple performance objectives both time-consuming and non-intuitive. This is further compounded if systems that are economically optimum in meeting the performance goals are also desired. To overcome these difficulties, PBD procedures must be coupled with optimization algorithms, as shown in **Figure 2**, that are capable of rigorously handling the reliability/probabilistic performance assessment models of current PBWE frameworks. A class of optimization methodologies that respond to this need is constituted by the reliability-based design optimization (RBDO) algorithms (Schuëller and Jensen, 2008; Valdebenito and Schuëller, 2010). Indeed, in RBDO the aim is the resolution of problems that are characterized by generally deterministic cost/objective functions subject to a number of probabilistic constraints (e.g., Valdebenito and Schuëller (2010)). The recent boom in computational power has spawn intense research in this area as it has opened the door to the possibility of solving problems that were previously deemed intractable. Notwithstanding these research efforts, there is still need for the development of specific RBDO algorithms that efficiently yield optimum solutions to practical probabilistic PBD problems that are often posed in terms of multiple performance constraints, high-dimensional random variable vectors as well as discrete high-dimensional design variable vectors. As outlined in Federal Emergency Management Agency (FEMA) (2006), each of these characteristics makes the RBDO problem non-trivial due to the implicit nature, in terms of the design variable vector, of the probabilistic constraints and the inherently nested nature of the reliability analysis within the optimization loop (Aoues and Chateauneuf, 2010; Valdebenito and Schuëller, 2010).

6.2 Challenges, Existing Solutions and Opportunities

The main difficulty in solving the optimization loop outlined in **Figure 2** is presented by the probabilistic nature of the performance assessment that essentially requires the resolution of a reliability integral similar to that of the classic PEER framework (Ouyang and Spence, 2020; 2021b). Indeed, the treatment of this type of integral within an optimization problem is characterized by the following difficulties: 1) it is implicit in the design variable vector therefore hindering sensitivity analyses; and 2) its evaluation requires probabilistic analyses which will in general be computationally cumbersome. These difficulties are further compounded if the design variable vector is of high dimensions (hundreds of components), as is the case for many practical applications, and if the number of constraints to be considered is also elevated. Further complication is added if the uncertain vector has more than a handful of components as this will practically eliminate the possibility of using approximate reliability analysis (first or second order reliability methods) due to the increasing difficulty this produces in finding the design point (Schuëller et al., 2003). In addition, the various methods that have been developed over the years for optimizing stochastic systems modeled through large and complex finite element models (e.g., metamodeling approaches (Zhu et al., 2011; Chen et al., 2015; Moustapha et al., 2016), subset simulation optimization (SSO) (Taflanidis and Beck, 2009; Jia and Taflanidis, 2013; Jia et al., 2015), and sequential optimization methods (Du and Chen, 2004; Zou and Mahadevan, 2006; Jensen et al., 2008; Valdebenito and Schuëller, 2011; Jensen et al., 2012)), are not generally applicable to systems with more than a dozen or so free design parameters. The main reason for this can be traced back to how the focus of the aforementioned approaches is mainly on treating problems with complex and generally nonlinear response behaviors. In the case of the large-scale structures often found in practice, this can represent a significant limitation as these systems are generally designed in terms of hundreds of free parameters. A philosophical approach that can in theory efficiently treat problems with high-dimensional design spaces is that based on decoupling the probabilistic analysis from the optimization loop through approximations that are constructed from information pertaining to a limited number of probabilistic analyses (Spence and Gioffrè, 2012; Royset et al., 2001; Du and Chen, 2004; Zou and Mahadevan, 2006; Ching and Hsieh, 2007; Jensen et al., 2008; Valdebenito and Schuëller, 2011). This approach has been explored within the context of PBWE with the introduction of schemes for both single and multi-objective optimization while considering performance metrics ranging from accelerations at the performance objective of occupant comfort (Spence, 2018), through drifts and component responses at the performance objectives of serviceability and continuous occupancy (Spence and Kareem, 2014), to explicit evaluation of system-level loss metrics (Suksuwan and Spence, 2019b,a; Subgranon and Spence, 2021). This approach has also been extended to topology optimization formulated explicitly in the space of PBWE metrics (Kareem et al., 2013; Bobby et al., 2014; Bobby et al., 2016). The difficulty associated with optimizing in high-dimensional spaces of design variables can be avoided by choosing small subsets of parameters that are most influential to the performance metrics. For example, recent works have looked at optimally choosing the parameters of auxiliary damping devices for minimizing a variety of performance metrics (Petrini et al., 2020; Venanzi et al., 2020).

7 SUMMARY AND CONCLUSION

This paper reviewed the origins and current state-of-the-art of PBWE that is poised to inform the next generation of load and design codes for wind. A historical account is presented and pioneering works are briefly summarized with key emphasis on the differences between PBSE and PBWE. The current state of practice is reviewed, and its limitations are highlighted. The broad areas of active research within PBWE are identified as the inelastic modeling/design of wind excited structures and the

modeling of the envelope performance that includes consideration of the risk from wind driven rain and debris impact. The role of optimization was discussed within the context of optimally satisfying the performance objectives associated with occupant comfort, serviceability and ultimate capacity. Additional areas of future research include the experimental validation of the state-of-the-art numerical frameworks associated with, but not limited to, wind load modeling and nonlinear structural analysis, with particular attention on assessing the validity of models/tools borrowed from seismic engineering. In a similar vein, the applicability of the R-factor (force reduction factor), ductile detailing concepts and innovative damping devices in PBWE, and more in general, in mixed hazard environments, requires investigation. Additional research developments that would be of relevance concern the assimilation in the models of field data on cladding performance during hurricane events. This would enable the establishment of better semi-empirical fragility functions as well as damage states and consequence functions for describing building envelope performance. More research on PBWE of low-rise structures as well as PBWE for non-synoptic winds is also needed. In conclusion, the significant advances in PBWE of the past decade are changing the way buildings are assessed and designed against wind. Although there is still much to be done, the continued development of PBWE promises to enhance the resilience of future communities to extreme wind events while increasing sustainability through enabling greater design innovation.

DATA AVAILABILITY STATEMENT

The original contributions presented in the study are included in the article/Supplementary Material, further inquiries can be directed to the corresponding author.

AUTHOR CONTRIBUTIONS

All authors listed have made a substantial, direct, and intellectual contribution to the work and approved it for publication.

FUNDING

The research effort was supported in part by the United States National Science Foundation (NSF) under Grants No. CMMI-1462084, CMMI-1562388, CMMI-1750339, and CMMI-2118488.

REFERENCES

ACI 318-11 (2012). *Building Code Requirements for Structural concrete and Commentary*. Michigan, USA: American Concrete Institute.

AISC 360-16 (2016). *Specification for Structural Steel Buildings*. Chicago, IL: American Institute of Steel Construction.

Aoues, Y., and Chateauneuf, A. (2010). Benchmark Study of Numerical Methods for Reliability-Based Design Optimization. *Struct. Multidisc Optim* 41, 277–294. doi:10.1007/s00158-009-0412-2

Applied Technology Council (ATC) (1995a). *A Critical Review of Current Approaches to Earthquake-Resistant Design*. Redwood City, CA: Tech. rep., Report no. ATC-34.

Applied Technology Council (ATC) (1995b). *Guidelines and Commentary for Seismic Rehabilitation of Buildings*. Redwood City, CA: Tech. rep., Report no. ATC-33.

Applied Technology Council (ATC) (1996a). *Seismic Design Criteria for California Bridges: Provisional Recommendations*. Redwood City, CA: Tech. rep., Report no. ATC-32.

Applied Technology Council (ATC) (1996b). *Seismic Evaluation and Retrofit of concrete Buildings*. Redwood City, CA: Tech. rep., Report no. ATC-40.

ASCE 7-16 (2016). *Minimum Design Loads and Associated Criteria for Buildings and Other Structures*. Reston, VA: American Society of Civil Engineers.

ASCE/SEI (2019). *Prestandard for Performance-Based Wind Design (Prepared by Structural Engieering Institute (SEI)*. American Society of Civil Engineers.

ASTM (2007a). "Standard Guide for Seismic Risk Assessment of Buildings," in *ASTM E2026-07* (West Conshohocken, PA: ASTM International).

ASTM (2007b). "Standard Practice for Probable Maximum Loss (Pml) Evaluations for Earthquake Due-Diligence Assessments," in *ASTM E2557-07* (West Conshohocken, PA: ASTM International).

Aswegan, K., Charney, F. A., and Jarrett, J. (2015). Recommended Procedures for Damage Based Serviceability Design of Steel Buildings under Wind Loads. *AISC Eng. J.* 52, 1–25.

Attary, N., Unnikrishnan, V. U., van de Lindt, J. W., Cox, D. T., and Barbosa, A. R. (2017). Performance-based Tsunami Engineering Methodology for Risk Assessment of Structures. *Eng. Structures* 141, 676–686. doi:10.1016/j.engstruct.2017.03.071

Augusti, G., and Ciampoli, M. (2008). Performance-based Design in Risk Assessment and Reduction. *Probabilistic Eng. Mech.* 23, 496–508. doi:10.1016/j.probengmech.2008.01.007

Baheru, T., Chowdhury, A. G., and Pinelli, J.-P. (2015). Estimation of Wind-Driven Rain Intrusion through Building Envelope Defects and Breaches during Tropical Cyclones. *Nat. Hazards Rev.* 16, 04014023. doi:10.1061/(asce)nh.1527-6996.0000158

Barbato, M., Petrini, F., Unnikrishnan, V. U., and Ciampoli, M. (2013). Performance-based hurricane Engineering (PBHE) Framework. *Struct. Saf.* 45, 24–35. doi:10.1016/j.strusafe.2013.07.002

Bashor, R., and Kareem, A. (2007). "Probabilistic Performance Evaluation of Buildings: an Occupant comfort Perspective." in Proceedings of the 12th International Conference on Wind Engineering (12-ICWE). 1335–1342.

Bernardini, E., Spence, S. M. J., Kwon, D.-K., and Kareem, A. (2015). Performance-based Design of High-Rise Buildings for Occupant comfort. *J. Struct. Eng.* 141, 04014244. doi:10.1061/(asce)st.1943-541x.0001223

Bezabeh, M. A., Bitsuamlak, G. T., and Tesfamariam, S. (2021a). Nonlinear Dynamic Response of Single-Degree-Of-freedom Systems Subjected to Along-Wind Loads. I: Parametric Study. *J. Struct. Eng.* 147, 04021177. doi:10.1061/(asce)st.1943-541x.0003125

Bezabeh, M. A., Bitsuamlak, G. T., and Tesfamariam, S. (2021b). Nonlinear Dynamic Response of Single-Degree-Of-freedom Systems Subjected to Along-Wind Loads. II: Implications for Structural Reliability. *J. Struct. Eng.* 147, 04021178. doi:10.1061/(asce)st.1943-541x.0003124

Bobby, S., Spence, S. M. J., Bernardini, E., and Kareem, A. (2014). Performance-based Topology Optimization for Wind-Excited Tall Buildings: A Framework. *Eng. Structures* 74, 242–255. doi:10.1016/j.engstruct.2014.05.043

Bobby, S., Spence, S. M. J., and Kareem, A. (2016). Data-driven Performance-Based Topology Optimization of Uncertain Wind-Excited Tall Buildings. *Struct. Multidisc Optim* 54, 1379–1402. doi:10.1007/s00158-016-1474-6

Chen, D., and Davenport, A. G. (2000). Vulnerability of Tall Buildings in Typhoons. *Adv. Struct. Dyn.* 2, 1455–1462.

Chen, Z., Peng, S., Li, X., Qiu, H., Xiong, H., Gao, L., et al. (2015). An Important Boundary Sampling Method for Reliability-Based Design Optimization Using Kriging Model. *Struct. Multidisc Optim* 52, 55–70. doi:10.1007/s00158-014-1173-0

Ching, J., and Hsieh, Y.-H. (2007). Approximate Reliability-Based Optimization Using a Three-step Approach Based on Subset Simulation. *J. Eng. Mech.* 133, 481–493. doi:10.1061/(asce)0733-9399(2007)133:4(481)

Chuang, W.-C., and Spence, S. M. J. (2017). A Performance-Based Design Framework for the Integrated Collapse and Non-collapse Assessment of Wind Excited Buildings. *Eng. Structures* 150, 746–758. doi:10.1016/j.engstruct.2017.07.030

Chuang, W.-C., and Spence, S. M. J. (2019). An Efficient Framework for the Inelastic Performance Assessment of Structural Systems Subject to Stochastic Wind Loads. *Eng. Structures* 179, 92–105. doi:10.1016/j.engstruct.2018.10.039

Chuang, W.-C., and Spence, S. M. J. (2020). Probabilistic Performance Assessment of Inelastic Wind Excited Structures within the Setting of Distributed Plasticity. *Struct. Saf.* 84, 101923. doi:10.1016/j.strusafe.2020.101923

Chuang, W. C., and Spence, S. M. J. (2022). A Framework for the Efficient Reliability Assessment of Inelastic Wind Excited Structures at Dynamic Shakedown. *J. Wind Eng. Ind. Aerodynamics*. In Press. doi:10.1016/j.jweia.2021.104834

Ciampoli, M., Petrini, F., and Augusti, G. (2011). Performance-based Wind Engineering: towards a General Procedure. *Struct. Saf.* 33, 367–378. doi:10.1016/j.strusafe.2011.07.001

Cornell, C. A., and Krawinkler, H. (2000). Progress and Challenges in Seismic Performance Assessment. *PEER Cent. News* 3, 1–4.

Cui, W., and Caracoglia, L. (2018). A Unified Framework for Performance-Based Wind Engineering of Tall Buildings in hurricane-prone Regions Based on Lifetime Intervention-Cost Estimation. *Struct. Saf.* 73, 75–86. doi:10.1016/j.strusafe.2018.02.003

Cui, W., and Caracoglia, L. (2020). Performance-based Wind Engineering of Tall Buildings Examining Life-Cycle Downtime and Multisource Wind Damage. *J. Struct. Eng.* 146, 04019179. doi:10.1061/(asce)st.1943-541x.0002479

Du, X., and Chen, W. (2004). Sequential Optimization and Reliability Assessment Method for Efficient Probabilistic Design. *J. Mech. Des.* 126, 225–233. doi:10.1115/1.1649968

Ellingwood, B. R. (2001). Acceptable Risk Bases for Design of Structures. *Prog. Struct. Engng Mater.* 3, 170–179. doi:10.1002/pse.78

Ellingwood, B. R. (1998). "Reliability-based Performance Concept for Building Construction," in Proceedings of Structural Engineering World Wide. T178-4, CD-ROM.

Ellingwood, B. R., Rosowsky, D. V., Li, Y., and Kim, J. H. (2004). Fragility Assessment of Light-Frame wood Construction Subjected to Wind and Earthquake Hazards. *J. Struct. Eng.* 130, 1921–1930. doi:10.1061/(asce)0733-9445(2004)130:12(1921)

Ellingwood, B. R., Rosowsky, D. V., and Pang, W. (2008). Performance of Light-Frame wood Residential Construction Subjected to Earthquakes in Regions of Moderate Seismicity. *J. Struct. Eng.* 134, 1353–1363. doi:10.1061/(asce)0733-9445(2008)134:8(1353)

Ellingwood, B. R. (2008). Structural Reliability and Performance-Based Engineering. *Structures and Buildings* 161, 199–207. doi:10.1680/stbu.2008.161.4.199

Federal Emergency Management Agency (FEMA) (2000b). *Action Plan for Performance Based Seismic Design*. Washington, DC: Tech. rep., Report no. FEMA-349.

Federal Emergency Management Agency (FEMA) (1997). *NEHRP Guidelines for the Seismic Rehabilitation of Buildings*. Washington, DC: Tech. rep., Report no. FEMA-273.

Federal Emergency Management Agency (FEMA) (2006). *Next-generation Performance-Based Seismic Design Guidelines - Program Plan for New and Existing Buildings*. Washington, DC: Tech. rep., Report no. FEMA-445.

Federal Emergency Management Agency (FEMA) (2000a). *Prestandard and Commentary for Seismic Rehabilitation of Buildings*. Washington, DC: Tech. rep., Report no. FEMA-356.

Federal Emergency Management Agency (FEMA) (2012a). *Seismic Performance Assessment of Buildings, Volume 1 - Methodology (FEMA Publication P-58-1)*. Washington, D.C.: Tech. rep.

Federal Emergency Management Agency (FEMA) (2012b). *Seismic Performance Assessment of Buildings, Volume 2 - Implementation (FEMA Publication P-58-2)*. Washington, D.C.: Tech. rep.

Federal Emergency Management Agency (FEMA) (2012c). *Seismic Performance Assessment of Buildings, Volume 3 - Supporting Electronic Materials and Background Documentation (FEMA Publication P-58-3)*. Washington, D.C.: Tech. rep.

Federal Emergency Management Agency (FEMA) (2018). *Seismic Performance Assessment of Buildings, Volume 5 - Expected Seismic Performance of Code-Conforming Buildings (FEMA Publication P-58-5)*. Washington, D.C.: Tech. rep.

Feng, C., and Chen, X. (2017). Crosswind Response of Tall Buildings with Nonlinear Aerodynamic Damping and Hysteretic Restoring Force Character. *J. Wind Eng. Ind. Aerodynamics* 167, 62–74. doi:10.1016/j.jweia.2017.04.012

Feng, C., and Chen, X. (2018). Inelastic Responses of Wind-Excited Tall Buildings: Improved Estimation and Understanding by Statistical Linearization Approaches. *Eng. structures* 159, 141–154. doi:10.1016/j.engstruct.2017.12.041

Gani, F., and Légeron, F. (2011). Relationship between Specified Ductility and Strength Demand Reduction for Single Degree-Of-freedom Systems under Extreme Wind Events. *J. Wind Eng. Ind. Aerodynamics* 109, 31–45.

Gardoni, P., and LaFave, J. M. (2016). "Multi-hazard Approaches to Civil Infrastructure Engineering: Mitigating Risks and Promoting Resilence," in *Multi-hazard Approaches to Civil Infrastructure Engineering* (Berlin, Germany: Springer), 3–12. doi:10.1007/978-3-319-29713-2_1

Ghaffary, A., and Moustafa, M. A. (2021). Performance-based Assessment and Structural Response of 20-story SAC Building under Wind Hazards through Collapse. *J. Struct. Eng.* 147, 04020346. doi:10.1061/(asce)st.1943-541x.0002911

Ghobarah, A. (2001). Performance-based Design in Earthquake Engineering: State of Development. *Eng. structures* 23, 878–884. doi:10.1016/s0141-0296(01)00036-0

Ghosn, M., Dueñas-Osorio, L., Frangopol, D. M., McAllister, T., Bocchini, P., Manuel, L., et al. (2016a). Performance Indicators for Structural Systems and Infrastructure Networks. *J. Struct. Eng.* 142, F4016003. doi:10.1061/(asce)st.1943-541x.0001542

Ghosn, M., Frangopol, D. M., McAllister, T. P., Shah, M., Diniz, S. M. C., Ellingwood, B. R., et al. (2016b). Reliability-based Performance Indicators for Structural Members. *J. Struct. Eng.* 142, F4016002. doi:10.1061/(asce)st.1943-541x.0001546

Gibson, E. J. (1982). *Working with the Performance Approach in Building*. Rotterdam, Netherlands: Tech. rep., CIB.

Griffis, L. G., Patel, V., Muthukumar, S., and Baldava, S. (2013). "A Framework for Performance-Based Wind Engineering," in Proceedings of the 2012 ATC & SEI Conference on Advances in Hurricane Engineering, Miami, FL. doi:10.1061/9780784412626.105

Griffis, L. G. (1993). Serviceability Limit States under Wind Loads. *Eng. J.* 30, 1–16.

Günay, S., and Mosalam, K. M. (2013). Peer Performance-Based Earthquake Engineering Methodology, Revisited. *J. Earthquake Eng.* 17, 829–858.

Hong, H. P. (2004). Accumulation of Wind Induced Damage on Bilinear Sdof Systems. *Wind and Structures* 7, 145–158. doi:10.12989/was.2004.7.3.145

Huang, J., and Chen, X. (2022). Inelastic Performance of High-Rise Buildings to Simultaneous Actions of Alongwind and Crosswind Loads. *J. Struct. Eng.* 148, 04021258. doi:10.1061/(asce)st.1943-541x.0003236

Ierimonti, L., Venanzi, I., Caracoglia, L., and Materazzi, A. L. (2019). Cost-based Design of Nonstructural Elements for Tall Buildings under Extreme Wind Environments. *J. Aerosp. Eng.* 32, 04019020. doi:10.1061/(asce)as.1943-5525.0001008

Jensen, H. A., Kusanovic, D. S., Valdebenito, M. A., and Schuëller, G. I. (2012). Reliability-based Design Optimization of Uncertain Stochastic Systems: Gradient-Based Scheme. *J. Eng. Mech.* 138, 60–70. doi:10.1061/(asce)em.1943-7889.0000304

Jensen, H. A., Valdebenito, M. A., and Schuëller, G. I. (2008). An Efficient Reliability-Based Optimization Scheme for Uncertain Linear Systems Subject to General Gaussian Excitation. *Comput. Methods Appl. Mech. Eng.* 198, 72–87. doi:10.1016/j.cma.2008.01.003

Ji, X., Huang, G., Wu, F., and Lu, Z.-H. (2020). Wind-induced hazard Assessment for Low-Rise Building Envelope Considering Potential Openings. *J. Struct. Eng.* 146, 04020039. doi:10.1061/(asce)st.1943-541x.0002553

Jia, G., Taflanidis, A. A., and Beck, J. L. (2015). Non-parametric Stochastic Subset Optimization for Design Problems with Reliability Constraints. *Struct. Multidisc Optim* 52, 1185–1204. doi:10.1007/s00158-015-1300-6

Jia, G., and Taflanidis, A. A. (2013). Non-parametric Stochastic Subset Optimization for Optimal-Reliability Design Problems. *Comput. Structures* 126, 86–99. doi:10.1016/j.compstruc.2012.12.009

Judd, J. P., and Charney, F. A. (2015). Inelastic Behavior and Collapse Risk for Buildings Subjected to Wind Loads. *Structures Congress* 2015, 2483–2496. doi:10.1061/9780784479117.215

Judd, J. P. (2018). Windstorm Resilience of a 10-story Steel Frame Office Building. *Asce-asme J. Risk Uncertainty Eng. Syst. Part. A: Civ. Eng.* 4, 04018020. doi:10.1061/ajrua6.0000971

Kareem, A., Spence, S. M. J., Bernardini, E., Bobby, S., and Wei, D. (2013). Wind Engineering: Using Computational Fluid Dynamics to Optimize Tall Building Design. *CTBUH J.* 2013, 38–43.

König, A., and Maier, G. (1981). Shakedown Analysis of Elastoplastic Structures: a Review of Recent Developments. *Nucl. Eng. Des.* 66, 81–95.

König, A. (1987). Shakedown of Elastic-Plastic Structures. *Fundam. Stud. Eng.* 7.

Kwag, S., Gupta, A., Baugh, J., and Kim, H.-S. (2021). Significance of Multi-hazard Risk in Design of Buildings under Earthquake and Wind Loads. *Eng. Structures* 243, 112623. doi:10.1016/j.engstruct.2021.112623

Le, V., and Caracoglia, L. (2020). A Neural Network Surrogate Model for the Performance Assessment of a Vertical Structure Subjected to Non-stationary, Tornadic Wind Loads. *Comput. Structures* 231, 106208. doi:10.1016/j.compstruc.2020.106208

Le, V., and Caracoglia, L. (2018). Computationally Efficient Stochastic Approach for the Fragility Analysis of Vertical Structures Subjected to Thunderstorm Downburst Winds. *Eng. structures* 165, 152–169. doi:10.1016/j.engstruct.2018.03.007

Maier, G., Carvelli, V., and Cocchetti, G. (2000). On Direct Methods for Shakedown and Limit Analysis. *Eur. J. Mech. - A/Solids* 19, 79–100.

Maier, G., and Lloyd-Smith, D. (1986). "Mathematical Programming Applications to Engineering Plastic Analysis: Upyear to November 1985," in *Applied Mechanics Upyear 1986*. Editors C. R. Steele and G. S. Springer (New York: ASME), 377–383.

Maier, G., and Munro, J. (1982). Mathematical Programming Methods in Engineering Plastic Analysis. *Appl. Mech. Rev. - ASME* 35, 1631–1643.

Maier, G. (1979). "Shakedown Analysis," in *Engineering Plasticity by Mathematical Programming*. Editors M. Z. Cohn and G. Maier (Oxford, UK: Pergamon Press), 107–134. chap. 6.

Masoomi, H., and van de Lindt, J. W. (2016). Tornado Fragility and Risk Assessment of an Archetype Masonry School Building. *Eng. Structures* 128, 26–43. doi:10.1016/j.engstruct.2016.09.030

Meacham, B. J. (2010). Risk-informed Performance-based Approach to Building Regulation. *J. Risk Res.* 13, 877–893. doi:10.1080/13669871003703260

Micheli, L., Alipour, A., Laflamme, S., and Sarkar, P. (2019). Performance-based Design with Life-Cycle Cost Assessment for Damping Systems Integrated in Wind Excited Tall Buildings. *Eng. Structures* 195, 438–451. doi:10.1016/j.engstruct.2019.04.009

Moehle, J., and Deierlein, G. G. (2004). "A Framework Methodology for Performance-Based Earthquake Engineering," in Proceedings of the 13th World Conference on Earthquake Engineering.

Mohammadi, A., Azizinamini, A., Griffis, L., and Irwin, P. (2019). Performance Assessment of an Existing 47-story High-Rise Building under Extreme Wind Loads. *J. Struct. Eng.* 145, 04018232. doi:10.1061/(asce)st.1943-541x.0002239

Moustapha, M., Sudret, B., Bourinet, J.-M., and Guillaume, B. (2016). Quantile-based Optimization under Uncertainties Using Adaptive Kriging Surrogate Models. *Struct. Multidisc Optim* 54, 1403–1421. doi:10.1007/s00158-016-1504-4

Nevill, J. B., and Lombardo, F. T. (2020). Structural Functionality Scale for Light-Framed wood Buildings with Indicators for Windstorm Damage. *J. Struct. Eng.* 146, 04020033. doi:10.1061/(asce)st.1943-541x.0002551

Nikellis, A., Sett, K., and Whittaker, A. S. (2019). Multihazard Design and Cost-Benefit Analysis of Buildings with Special Moment-Resisting Steel Frames. *J. Struct. Eng.* 145, 04019031. doi:10.1061/(asce)st.1943-541x.0002298

Ohkuma, T., Kurita, T., and Ninomiya, M. (1998). "Response Estimation Based on Energy Balance for Elasto-Plastic Vibration of Tall Building in Across-Wind Direction," in ICOSSAR 97: Proceedings of the 7th International Conference on Structural Safety and Reliability, Kyoto, Japan, 1379–1386.

Ouyang, Z., and Spence, S. M. J. (2019). A Performance-Based Damage Estimation Framework for the Building Envelope of Wind-Excited Engineered Structures. *J. Wind Eng. Ind. Aerodynamics* 186, 139–154. doi:10.1016/j.jweia.2019.01.001

Ouyang, Z., and Spence, S. M. J. (2021a). A Performance-Based Wind Engineering Framework for Engineered Building Systems Subject to Hurricanes. *Front. Built Environ.* 7, 133. doi:10.3389/fbuil.2021.720764

Ouyang, Z., and Spence, S. M. J. (2020). A Performance-Based Wind Engineering Framework for Envelope Systems of Engineered Buildings Subject to Directional Wind and Rain Hazards. *J. Struct. Eng.* 146, 04020049. doi:10.1061/(asce)st.1943-541x.0002568

Ouyang, Z., and Spence, S. M. J. (2021b). Performance-based Wind-Induced Structural and Envelope Damage Assessment of Engineered Buildings through Nonlinear Dynamic Analysis. *J. Wind Eng. Ind. Aerodynamics* 208, 104452. doi:10.1016/j.jweia.2020.104452

Paulotto, C., Ciampoli, M., and Augusti, G. (2004). "Some Proposals for a First Step towards a Performance Based Wind Engineering," in Forum in Engineering Decision Making (IFED), Stoos, Switzerland.

Peng, X., Roueche, D. B., Prevatt, D. O., and Gurley, K. R. (2016). "An Engineering-Based Approach to Predict Tornado-Induced Damage," in *Multi-hazard Approaches to Civil Infrastructure Engineering* (Berlin, Germany: Springer), 311–335. doi:10.1007/978-3-319-29713-2_15

Petrini, F., and Ciampoli, M. (2012). Performance-based Wind Design of Tall Buildings. *Struct. Infrastructure Eng.* 8, 954–966.

Petrini, F., Giaralis, A., and Wang, Z. (2020). Optimal Tuned Mass-Damper-Inerter (TMDI) Design in Wind-Excited Tall Buildings for Occupants' comfort Serviceability Performance and Energy Harvesting. *Eng. Structures* 204, 109904. doi:10.1016/j.engstruct.2019.109904

Pita, G. L., Pinelli, J.-P., Gurley, K., Weekes, J., Cocke, S., and Hamid, S. (2016). Hurricane Vulnerability Model for Mid/high-Rise Residential Buildings. *Wind and Structures* 23, 449–464. doi:10.12989/was.2016.23.5.449

Porter, K. A. (2003). "An Overview of Peer's Performance-Based Earthquake Engineering Methodology," in Proceedings of the 9th International Conference on Applications of Statistics and Probability in Civil Engineering (ICASP9), San Francisco, CA, 973–980. Vol. 2.

Raji, F., Zisis, I., and Pinelli, J. P. (2020). Experimental Investigation of Wind-Driven Rain Propagation in a Building interior. *J. Struct. Eng.* 146, 04020114. doi:10.1061/(asce)st.1943-541x.0002670

Rosowsky, D. V., and Ellingwood, B. R. (2002). Performance-based Engineering of wood Frame Housing: Fragility Analysis Methodology. *J. Struct. Eng.* 128, 32–38. doi:10.1061/(asce)0733-9445(2002)128:1(32)

Royset, J. O., Der Kiureghian, A., and Polak, E. (2001). Reliability-based Optimal Structural Design by the Decoupling Approach. *Reliability Eng. Syst. Saf.* 73, 213–221. doi:10.1016/s0951-8320(01)00048-5

Schuëller, G. I., and Jensen, H. A. (2008). Computational Methods in Optimization Considering Uncertainties - an Overview. *Comput. Methods Appl. Mech. Eng.* 198, 2–13.

Schuëller, G. I., Pradlwarter, H. J., and Koutsourelakis, P. S. (2003). "A Comparative Study of Reliability Estimation Procedures for High Dimensions," in Proceedings of the 16th ASCE Engineering Mechanics Conference, Seattle, WA.

Spence, S. M. J., and Gioffrè, M. (2012). Large Scale Reliability-Based Design Optimization of Wind Excited Tall Buildings. *Probabilistic Eng. Mech.* 28, 206–215. doi:10.1016/j.probengmech.2011.08.001

Spence, S. M. J., and Kareem, A. (2014). Performance-based Design and Optimization of Uncertain Wind-Excited Dynamic Building Systems. *Eng. Structures* 78, 133–144. doi:10.1016/j.engstruct.2014.07.026

Spence, S. M. J. (2018). Optimization of Uncertain and Dynamic High-Rise Structures for Occupant comfort: An Adaptive Kriging Approach. *Struct. Saf.* 75, 57–66. doi:10.1016/j.strusafe.2018.05.008

Structural Engineers Association of California (SEAOC) (1995). *Vision 2000 - A Framework for Performance Based Design*. Sacramento, CA: Tech. rep., vol. I, II, III.

Subgranon, A., and Spence, S. M. J. (2021). Performance-based Bi-objective Optimization of Structural Systems Subject to Stochastic Wind Excitation. *Mech. Syst. Signal Process.* 160, 107893. doi:10.1016/j.ymssp.2021.107893

Suksuwan, A., and Spence, S. M. J. (2019a). Performance-based Bi-objective Design Optimization of Wind-Excited Building Systems. *J. Wind Eng. Ind. Aerodynamics* 190, 40–52. doi:10.1016/j.jweia.2019.03.028

Suksuwan, A., and Spence, S. M. J. (2019b). Performance-based Design Optimization of Uncertain Wind Excited Systems under System-Level Loss Constraints. *Struct. Saf.* 80, 13–31. doi:10.1016/j.strusafe.2019.03.004

Suksuwan, A., and Spence, S. M. J. (2018). Performance-based Multi-hazard Topology Optimization of Wind and Seismically Excited Structural Systems. *Eng. Structures* 172, 573–588. doi:10.1016/j.engstruct.2018.06.039

Tabbuso, P., Spence, S. M. J., Palizzolo, L., Pirrotta, A., and Kareem, A. (2016). An Efficient Framework for the Elasto-Plastic Reliability Assessment of Uncertain Wind Excited Systems. *Struct. Saf.* 58, 69–78. doi:10.1016/j.strusafe.2015.09.001

Taflanidis, A. A., and Beck, J. L. (2009). Stochastic Subset Optimization for Reliability Optimization and Sensitivity Analysis in System Design. *Comput. Structures* 87, 318–331. doi:10.1016/j.compstruc.2008.12.015

Tamura, Y., Yasui, H., and Marukawa, H. (2001). Non-elastic Responses of Tall Steel Buildings Subjected to Across-Wind Forces. *Wind and Structures* 4, 147–162. doi:10.12989/was.2001.4.2.147

Tsujita, O., Hayabe, Y., and Ohkuma, T. (1998). "A Study on Wind-Induced Response for Inelastic Structure," in ICOSSAR 97: Proceedings of the 7th International Conference on Structural Safety and Reliability, Kyoto, Japan, 1359–1366.

Unnikrishnan, V. U., and Barbato, M. (2017). Multihazard Interaction Effects on the Performance of Low-Rise wood-frame Housing in hurricane-prone Regions. *J. Struct. Eng.* 143, 04017076. doi:10.1061/(asce)st.1943-541x.0001797

Unnikrishnan, V. U., and Barbato, M. (2016). Performance-based Comparison of Different Storm Mitigation Techniques for Residential Buildings. *J. Struct. Eng.* 142, 04016011. doi:10.1061/(asce)st.1943-541x.0001469

Valdebenito, M. A., and Schuëller, G. I. (2010). A Survey on Approaches for Reliability-Based Optimization. *Struct. Multidisc Optim* 42, 645–663. doi:10.1007/s00158-010-0518-6

Valdebenito, M. A., and Schuëller, G. I. (2011). Efficient Strategies for Reliability-Based Optimization Involving Non-linear, Dynamical Structures. *Comput. Structures* 89, 1797–1811. doi:10.1016/j.compstruc.2010.10.014

Vamvatsikos, D., and Cornell, C. A. (2002). Incremental Dynamic Analysis. *Earthquake Engng. Struct. Dyn.* 31, 491–514. doi:10.1002/eqe.141

Venanzi, I., Ierimonti, L., and Caracoglia, L. (2020). Life-cycle-cost Optimization for the Wind Load Design of Tall Buildings Equipped with Tmds. *Wind & Structures* 30, 379–392.

Vickery, B. J. (1970). Wind Action on Simple Yielding Structures. *J. Engrg. Mech. Div.* 96, 107–120. doi:10.1061/jmcea3.0001221

Wang, Y., Burgess, I., Wald, F., and Gillie, M. (2012). *Performance-based Fire Engineering of Structures*. Boca Raton, Florida, USA: CRC Press.

Whittaker, A., Hamburger, R., and Mahoney, M. (2003). "Performance-based Engineering of Buildings for Extreme Events," in *Proceedings of the AISC-SINY Symposium on Resisting Blast and Progressive Collapse* (New York, NY: American Institute of Steel Construction), 55–66.

Wyatt, T. A., and May, H. I. (1971). "The Ultimate Load Behavior of Structures under Wind Loading," in Proceedings of the 3rd International Conference on Wind Effects on Buildings and Structures, Tokyo, Japan, 501–510.

Yang, T. Y., Moehle, J., Stojadinovic, B., and Der Kiureghian, A. (2009). Seismic Performance Evaluation of Facilities: Methodology and Implementation. *J. Struct. Eng.* 135, 1146–1154. doi:10.1061/(asce)0733-9445(2009)135:10(1146)

Zhu, P., Zhang, Y., and Chen, G. (2011). Metamodeling Development for Reliability-Based Design Optimization of Automotive Body Structure. *Comput. Industry* 62, 729–741. doi:10.1016/j.compind.2011.05.008

Zou, T., and Mahadevan, S. (2006). A Direct Decoupling Approach for Efficient Reliability-Based Design Optimization. *Struct. Multidisc Optim* 31, 190–200. doi:10.1007/s00158-005-0572-7

Conflict of Interest: The authors declare that the research was conducted in the absence of any commercial or financial relationships that could be construed as a potential conflict of interest.

Publisher's Note: All claims expressed in this article are solely those of the authors and do not necessarily represent those of their affiliated organizations, or those of the publisher, the editors, and the reviewers. Any product that may be evaluated in this article, or claim that may be made by its manufacturer, is not guaranteed or endorsed by the publisher.

frontiers in Built Environment

REVIEW
published: 16 March 2022
doi: 10.3389/fbuil.2022.811460

Applications of Machine Learning to Wind Engineering

Teng Wu[1]* *and Reda Snaiki*[2]

[1]Department of Civil, Structural and Environmental Engineering, University at Buffalo, Buffalo, NY, United States, [2]Department of Construction Engineering, École de Technologie Supérieure, University of Quebec, Montreal, QC, Canada

Advances of the analytical, numerical, experimental and field-measurement approaches in wind engineering offers unprecedented volume of data that, together with rapidly evolving learning algorithms and high-performance computational hardware, provide an opportunity for the community to embrace and harness full potential of machine learning (ML). This contribution examines the state of research and practice of ML for its applications to wind engineering. In addition to ML applications to wind climate, terrain/topography, aerodynamics/aeroelasticity and structural dynamics (following traditional Alan G. Davenport Wind Loading Chain), the review also extends to cover wind damage assessment and wind-related hazard mitigation and response (considering emerging performance-based and resilience-based wind design methodologies). This state-of-the-art review suggests to what extend ML has been utilized in each of these topic areas within wind engineering and provides a comprehensive summary to improve understanding how learning algorithms work and when these schemes succeed or fail. Moreover, critical challenges and prospects of ML applications in wind engineering are identified to facilitate future research efforts.

Keywords: machine learning, wind engineering, wind climate, terrain and topography, aerodynamics and aeroelasticity, structural dynamics, wind damage assessment, hazard mitigation and response

OPEN ACCESS

Edited by:
Forrest J. Masters, University of Florida, United States

Reviewed by:
Girma Bitsuamlak, Western University, Canada
Pedro L. Fernández-Cabán, Clarkson University, United States
Muhammad Hajj, Stevens Institute of Technology, United States

***Correspondence:**
Teng Wu
tengwu@buffalo.edu

Specialty section:
This article was submitted to Wind Engineering and Science, a section of the journal Frontiers in Built Environment

Received: *08 November 2021*
Accepted: *27 January 2022*
Published: *16 March 2022*

Citation:
Wu T and Snaiki R (2022) Applications of Machine Learning to Wind Engineering. Front. Built Environ. 8:811460. doi: 10.3389/fbuil.2022.811460

1 INTRODUCTION

Wind engineering is an interdisciplinary field to provide rational treatment of interaction between the atmospheric boundary-layer winds and human activities (Cermak 1975). There is a long and significant history for machine learning (ML) applications in several subfields involved in wind engineering, such as fluid mechanics (Brunton et al., 2020), meteorology (Chen et al., 2020) and mechanics of structures (Salehi and Burgueño 2018). The application of statistical learning to turbulence modeling in early 1940s (Kolmogorov 1941) and perceptron learning to structural design in late 1980s (Adeli and Yeh 1989) are representative examples. On the other hand, it seems similar passions have not been shared by researchers in the wind engineering community. Actually, ML-based wind engineering is still in its infancy stage and the full-capacity of ML has not been leveraged yet. However, the exceptional performance of ML to extract hidden informative features from data shows great promise for addressing unresolved complexities and issues originated from first principles investigations in the field of wind engineering. In addition, recent advances in performance-/resilience-based wind engineering have placed new demands on wind characterization, aerodynamics modeling and structural analysis that need powerful simulation tools such as ML to overcome the emerging challenges by simultaneously achieving high computational efficiency and accuracy. It is reasonable to expect the revitalization of ML within the wind engineering field that is fueled by 1) rapidly evolving learning algorithms and

high-performance computational hardware, 2) unprecedented volume of data generated with improved wind engineering techniques and methodologies, and 3) urgent needs for more accurate and efficient learning and modeling of complex phenomena in wind-related problems.

As a key subfield of artificial intelligence (AI) [that together with natural intelligence plays a role of the computational part of the ability to achieve goals in the world (McCarthy 2007)], ML develops learning algorithms that use inputs from a sample generator and observations from a system to generate an approximation of its outputs (Cherkassky and Mulier 2007). The evolution of learning algorithms started when McCulloch and Pitts (1943) invented the first mathematical model of a neural network. In 1952, Arthur Samuel from IBM introduced the first self-learning computer program to play the game of checkers (Wiederhold et al., 1990). Then, Rosenblatt (1957) designed the first neural network for computers (the perceptron) that set the foundation of deep neural networks (DNNs). Kelley (1960) presented the method of gradients (or method of steepest descent) in his analytical development of flight performance optimization, which was used to develop the basics of a continuous backpropagation model for training feedforward neural networks (Rumelhart et al., 1986). On the other hand, Hopfield (1982) created a feedback neural network that was considered as the first recurrent neural network (RNN). LeCun et al. (1989) combined convolutional neural network (CNN) and backpropagation algorithm to recognize handwritten digits. Watkins (1989) introduced the concept of Q-learning based on Markov process to significantly enhance the practicability and feasibility of reinforcement learning. Later, Cortes and Vapnik (1995) designed a support-vector network considered as a new learning machine for two-group classification problems with high generalization ability. Hochreiter and Schmidhuber (1997) introduced a long short-term memory cell to address the long-term dependency issue in RNN. To overcome the learning difficulty in DNNs, Hinton et al. (2006) derived a fast, greedy algorithm that can learn deep, directed belief networks one layer at a time and hence facilitate the rapid development of deep learning. Recently, Goodfellow et al. (2014) proposed a generative adversarial network consisting of two models (i.e., generative and discriminative models) that compete with each other in a zero-sum game. The sophisticated ML algorithm needs the help of advanced computational hardware [e.g., graphics processing unit (GPU) and tensor processing unit (TPU)] to unlock its full potential (Berggren et al., 2020). For example, the great success of AlexNet (a deep CNN on GPU) is essentially attributed to its ability to leverage GPU for training (Krizhevsky et al., 2012).

Equipped with both sophisticated algorithms and advanced computational hardware, the learning machine (LM) is driven by data. Both the quantity (data rich and comprehensive) and quality of the training/testing data are important to ensure good performance of ML applications. Wind engineering by nature is a data-rich field (e.g., high spatial and temporal resolution), and it is rapidly becoming a data-comprehensive domain due to recent advances of analytical, numerical, experimental and field-measurement methods (Kareem and Wu 2013; Hangan et al., 2017). The data of spatiotemporally varying wind flows are extended from synoptic events measured by airport wind observation system with traditional anemometers to non-synoptic events measured by several field campaigns with advanced doppler radars and Lidars (Light Detection and Ranging) [e.g., Verification of the Origins of Rotation in Tornadoes Experiment (VORTEX) and Radar Observations of Tornadoes and Thunderstorms Experiment (ROTATE) campaigns for tornado events and Severe Convective OUtflow in Thunderstorms (SCOUT) and Wind Ports and Sea (WPS) campaigns for thunderstorm downburst events]. Massive wind data over complex terrain/topography are collected by continuous-wave short-range WindScanner systems (e.g., Berg et al., 2013). The low Reynolds-number, straight-line-wind, stationary aerodynamics data generated in conventional boundary-layer wind tunnels are extended to 1) high-Reynolds-number aerodynamics data resulting from recently built large-scale facilities [e.g., windstorm simulation facility at Insurance Institute for Business and Home Safety (IBHS), Wall of Wind (WOW) at Florida International University and Wind Engineering Energy and Environment (WindEEE) at Western University], 2) vortex-flow aerodynamics data produced by tornado simulators (e.g., tornado-like vortex simulator at Iowa State University and VorTECH at Texas Tech University), and 3) transient aerodynamics data generated in emerging actively controlled wind tunnels (e.g., individually-controlled multi-fan wind tunnels at Tongji University, University at Buffalo and University of Florida). Also, significant nonlinear and inelastic structural dynamics data under strong winds are being created in laboratories due to advances in performance-based wind design methodology (Abdullah et al., 2020). In addition to the experimental and field-measurement approaches the comprehensive data are further enriched by high-fidelity large-scale simulation tools that are advanced by theoretical developments in wind engineering field (Blocken 2014; Kareem 2020), such as computational fluid dynamics/computational structural dynamics (CFS/CSI)-based hybrid modeling of transient structural response (Hao and Wu 2018) and statistics-based synthesis of nonstationary wind field (Wang and Wu 2021). The Computational Modeling and Simulation Center (SimCenter) of the Natural Hazards Engineering Research Infrastructure (NHERI) program provides an effective way to integrate various simulation tools (Deierlein and Zsarnóczay 2021). Furthermore, novel real-time aerodynamics hybrid simulation techniques are emerging to effectively generate nonlinear and full-scale data in wind engineering by seamlessly stitching the numerical modeling in computer and physical testing in wind tunnel (Wu et al., 2019; Wu and Song 2019). Data quality is essential to facilitate curation and reuse of the diverse and large datasets generated in the field of wind engineering. There are numerous methods and criteria specified by various wind engineering research groups/centers to ensure the high data quality, and the NHERI DesignSafe cyberinfrastructure platform recently suggested the best practices for detailed data quality assessment in terms of metadata quality, data content quality, data completeness and representation and data publications review (Rathje et al., 2017).

The improved understanding concerning the complex nature of wind fields (e.g., nonstationary and non-Gaussian features), the

associated structural aerodynamics/aeroelasticity (e.g., transient and nonlinear features) and the resulting load effects (e.g., nonlinear and inelastic structural response), as well as the necessary shift from a prescriptive design approach to performance-based design methodology and further to resilience-based design philosophy (i.e., improving the rapidity, robustness, resourcefulness and redundancy), poses new challenges in wind engineering field. Hence, there is an urgent need of more accurate and efficient learning and modeling tools for effective solutions. The conventional stationary and linear analysis framework for wind-structure interactions established by Robert H. Scanlan (1914–2001) and Alan G. Davenport (1932–2009) has been very successful due to its simplicity and applicability, however, its shortcomings have begun to surface since the underlying complexities associated with many wind engineering problems clearly show a departure from implicit assumptions of stationarity, Gaussianity and linear features. A number of semi-empirical nonlinear reduced-order models have been developed in this context and improvement in their efficiency and robustness is a topic of cutting-edge research in the wind engineering community (Wu 2013). Unfortunately, these reduced-order models do not always have a satisfactory representation of the full nonlinear equations which govern the complex phenomena in wind-related problems. An alternate way is to utilize the CFD techniques, however, their computational effort is too high considering the three-dimensional nature of winds and associated bluff-body aerodynamics. While CFD plays a significant role in generating high-fidelity data of complex wind-structure interactions, its high computational cost makes it not easy to be used either in an informational mode to enhance wind hazard-related planning and development activities (e.g., risk mitigation that needs to quickly run thousands of scenarios at minimal computational expense) or in an operational mode to support emergency management and response associated with a wind hazard (e.g., decision making that needs real-time prediction capability under an uncertain environment). To address the emerging challenges, data-driven machine learning offers a promising approach that is capable of processing big data in wind engineering field as well as modeling associated complex phenomena with high computational efficiency and simulation accuracy.

With the rapid development of ML applications in wind engineering due to the confluence of advanced learning algorithms, high-performance computational hardware and big data, it is believed that a systematic review on this subject is important to suggest to what extend ML has been utilized in each of the topic areas within wind engineering and provide a comprehensive summary to improve understanding how learning algorithms work and when these schemes succeed or fail. Specifically, a total of 65 ML algorithms (**Appendix A**) are identified for their applications in the five topic areas of wind climate, terrain/topography, aerodynamics/aeroelasticity, structural dynamics and damage assessment, and mitigation and response. This review first presents technical background of typical ML approaches in terms of supervised learning, unsupervised learning, semi-supervised learning and reinforcement learning (RL), followed by the state of research and practice of ML applications to each topic area within wind engineering field, and concluded with critical research gaps and future prospects. While ML can augment the analytical approaches [e.g., data-driven discovery of closure models (Raissi et al., 2019)], numerical schemes [e.g., data-driven turbulence modeling (Duraisamy et al., 2019)], experimental tests [e.g., data-driven active control of transient wind simulation (Li et al., 2021a)] and field measurements [e.g., data-driven sparse sensor placement (Manohar et al., 2018)] in wind engineering, the review only focuses on its role to complement existing methodologies and hence potentially extend/transform current lines of wind engineering research and practice.

2 BACKGROUND OF MACHINE LEARNING

Machine learning (ML) is a subclass of artificial intelligence (AI) that extracts the underlying pattern within a set of data (e.g., Murphy 2012; Goodfellow et al., 2016; Mohri et al., 2018). To acquire the hidden pattern and knowledge of a problem, the learning process involves in general five important steps, namely data collection, data preparation, training, evaluation and parameters tuning. Once the learning machine is trained based on the available data (usually retrieved from analytical solutions, numerical simulations, experimental tests or full-scale measurements), it can predict future or unseen events. Based on the data fed into the learning machine, ML algorithms can be classified into four categories, namely supervised learning, unsupervised learning, semi-supervised learning and reinforcement learning (**Figure 1**).

To train the algorithm, the supervised learning fully depends on labeled data, the unsupervised learning relies purely on unlabeled data and the semi-supervised learning combines limited labeled data with a large amount of unlabeled data. For reinforcement learning (RL), there is essentially no predefined data. Although RL is occasionally treated as semi-supervised learning considering the agent learns from its own experiences in terms of infrequent and partial rewards, it is classified here into separate category to highlight there is no explicit, external supervisory information provided to the learning agent. It is noted the kriging and polynomial chaos expansions as two widely-used, data-driven statistical interpolation approaches are not reviewed in this study.

2.1 Supervised Learning

Supervised learning models are a set of algorithms that learn the mapping, from given labeled training data, between known inputs and outputs. The trainable parameters of these models are determined based on the minimization of the loss function. Supervised learning models usually require a large amount of reliable and unbiased data for training which might not be always available. These algorithms can be employed for two important tasks, namely regression and classification.

2.1.1 Regression

Regression is a type of supervised learning in which the output is a numeric variable. Among many regression models, feed-forward

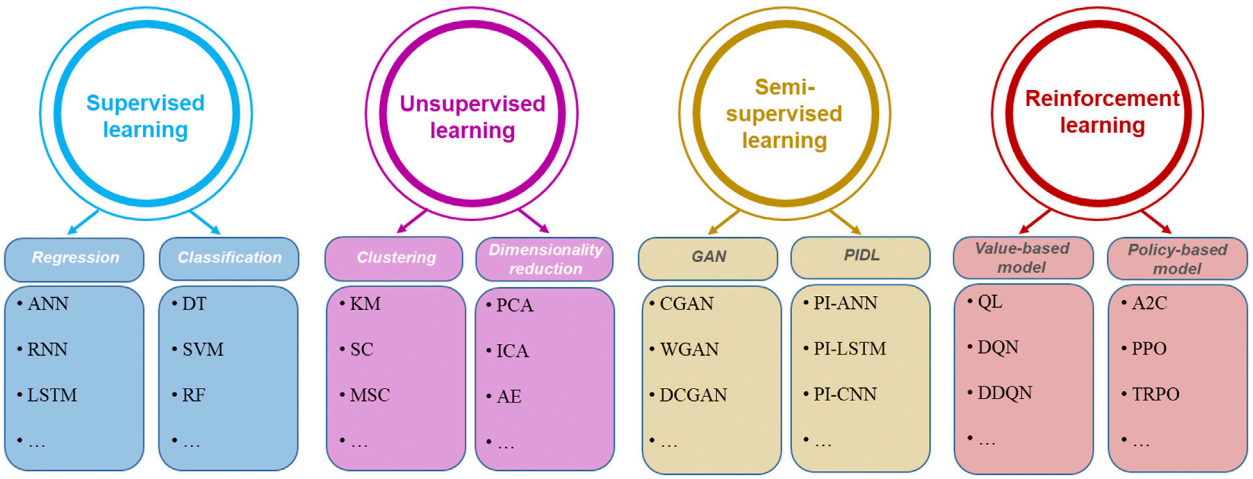

FIGURE 1 | Machine learning categories.

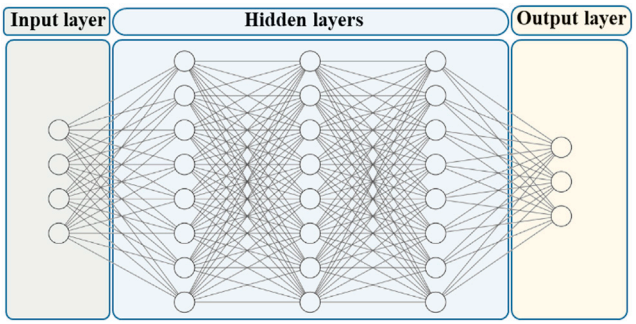

FIGURE 2 | Architecture of a typical FFNN.

neural networks (FFNN) are widely utilized in wind engineering field [**Figure 2**]. They are statistical models inspired by biological learning (McCulloch and Pitts 1943) and characterized by adaptive weights between neurons which are tuned using a learning algorithm from observed training data. For simplicity, the FFNN is also denoted as artificial neural network (ANN) in this study.

Deep neural networks (DNN) are also a type of FFNN characterized by a deep architecture equipped with multiple layers, and hence allows for better generalization and accuracy (Deng and Yu 2014; Pouyanfar et al., 2018). The convolutional neural networks (CNN) is another important FFNN with sparse convolutional matrices that are usually employed for pattern recognition and image classification (Krizhevsky et al., 2012; Goodfellow et al., 2016). Recurrent neural networks (RNN) are a class of feedback neural networks that allow previous outputs to be used as inputs while having hidden states and are suited to model time-dependent regression problems (e.g., Medsker and Jain 1999; Mandic and Chambers 2001). Long short-term memory (LSTM) are an advanced version of RNN to alleviate the gradient vanishing and exploding issue by only keeping necessary past information in future model states (Bengio et al., 1994).

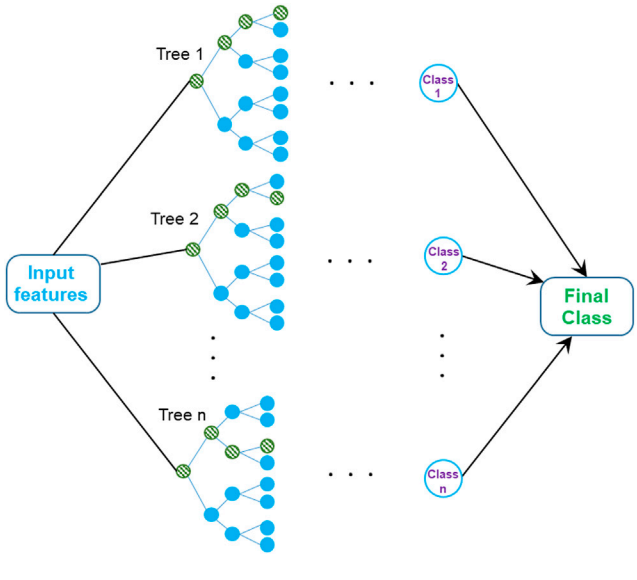

FIGURE 3 | Architecture of a typical random forest classifier.

2.1.2 Classification

Classification is another type of supervised learning in which the output is a categorical variable or a class. Support vector machines (SVM) (Scholkopf and Smola 2018) and random forest (RF) (Breiman 2001) are two classical examples of classification algorithms. SVM classifier identifies a hyperplane in a high-dimensional space in which a simple linear classification can be performed. RF classifier, on the other hand, fits a number of decision tree classifiers on various sub-samples of the dataset, then averages the results to improve outcome accuracy [**Figure 3**].

2.2 Unsupervised Learning

Unsupervised learning models draw inferences from datasets to describe hidden structures from unlabeled data based on

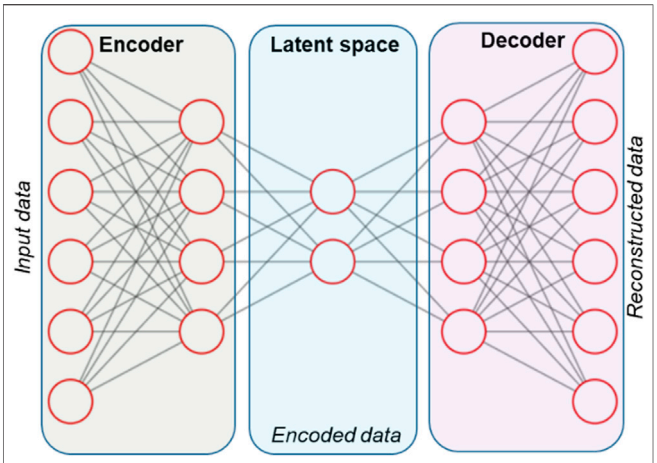

FIGURE 4 | Architecture of a typical autoencoder model.

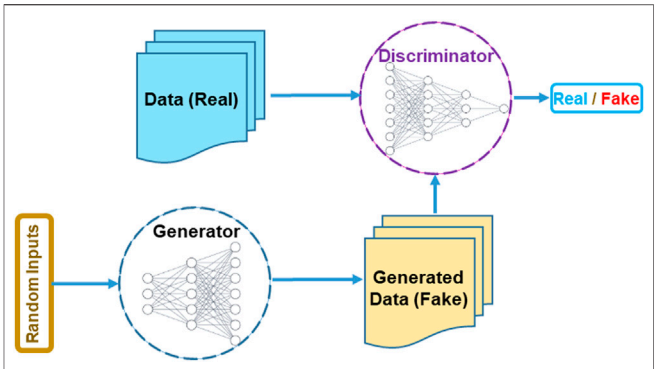

FIGURE 5 | Architecture of a typical GAN model.

inherent characteristics (Russell and Norvig 2016). These models usually group instances of input data using a defined similarity index (global criterion). Clustering and dimensionality reduction are two standard examples of unsupervised learning applications.

2.2.1 Clustering

Clustering is an unsupervised learning task used for pattern recognition that automatically discovers natural groups or clusters in data. A cluster refers to a collection of data points aggregated together with similar features (Maulik and Bandyopadhyay 2002). The k-means clustering is one of the simplest unsupervised ML models. It is a centroid-based algorithm that partitions the data into k clusters. Mean-shift clustering is another unsupervised model with a sliding-window-based algorithm to identify dense areas of data points. Other clustering algorithms such as the density-based spatial clustering of applications with noise, the expectation–maximization clustering using gaussian mixture models and the agglomerative hierarchical clustering are also popularly used for statistical data analysis.

2.2.2 Dimensionality Reduction

Dimensionality reduction aims to find the most important features within the dataset by identifying lower-dimensional representations for high-dimensional data. It minimizes the storage space, reduces the computation time and avoids overfitting. The ML-based dimensionality reduction can be divided into linear and nonlinear algorithms. The principal component analysis (PCA) is a commonly used linear technique that can be regarded as a two-layer neural network with a linear activation function. It essentially provides new uncorrelated variables, also denoted as principal components, which maximize the variance. The nonlinear autoencoder is a specific type of FFNN that compresses the initial input space into a reduced dimensional space using the encoder and then decompresses the obtained latent space back to the original input space using the decoder. Accordingly, deep autoencoders have a "bottleneck" architecture designed for extraction of representative features [**Figure 4**]. The autoencoder algorithm has been attracting attention in fluid mechanics community for efficient development of reduced-order models.

2.3 Semi-Supervised Learning

Semi-supervised learning models operate based on limited labeled data with a large amount of unlabeled data. Hence, they can be regarded as combination results of supervised learning and unsupervised learning algorithms. The generative adversarial network (GAN) is a well-known semi-supervised learning algorithm for estimating generative models via an adversarial process. One important feature of semi-supervised learning algorithms is their labelled-data efficiency. To this end, it may be reasonable to consider the physics-informed deep learning (PIDL) as a semi-supervised model that leverages physics-based equations in the augmented loss function to significantly reduce the data demand during training process.

2.3.1 Generative Adversarial Network

The GAN model consists of two competing neural networks, namely the generator and the discriminator (Goodfellow et al., 2014). It generates new data based on a probability distribution that approximately represents the training data (true or labelled data). Specifically, the generator produces fake samples to imitate the distribution of a real dataset, then the discriminator tries to distinguish (through a classification process) between the real samples and fake ones (from the generator). The GAN model is trained such that the new generated samples accurately represent the underlying mechanisms of the studied system. The architecture of a typical GAN model is illustrated in **Figure 5**.

2.3.2 Physics-Informed Deep Learning

The concept of PIDL models was originally proposed several decades ago (Psichogios and Ungar 1992; Dissanayake and Phan-Thien 1994) in which prior knowledge (in terms of the physics-based governing equations) is integrated within the neural networks to reduce the high-volume of required training data. Typically, a small amount of labelled data along with a large number of unlabeled data that satisfy the underlying physics of the system of interest (also denoted as collocations points) are used to train these models. Hence, self-supervision plays a significant role in PIDL models. Recently, Raissi et al. (2017a,

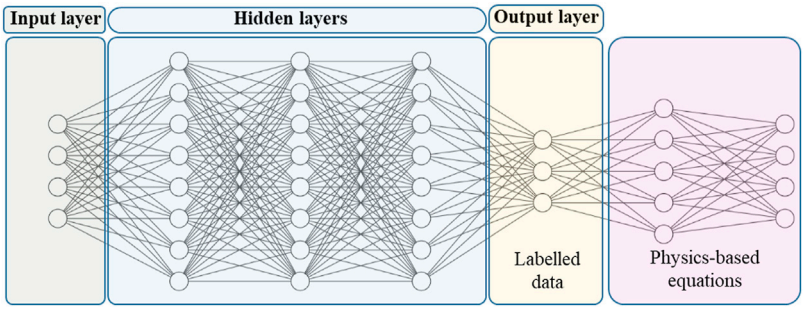

FIGURE 6 | Architecture of a typical PIDL model.

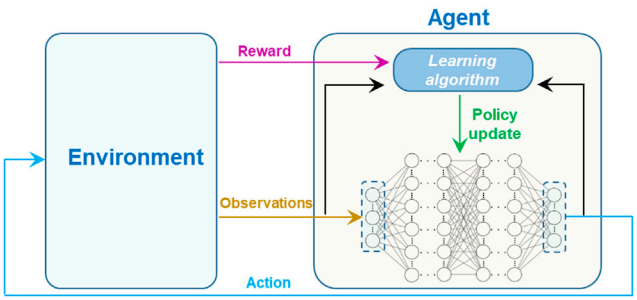

FIGURE 7 | Architecture of a typical RL.

b) advanced the PIDL models by leveraging the automatic differentiation technique to solve partial differential equations. The architecture of a typical PIDL model is presented in **Figure 6**.

2.4 Reinforcement Learning

RL algorithm is usually formulated based on Markov decision process (Sutton and Barto, 2018). The core part of RL is its agent that interacts with its environment. Accordingly, the agent learns a policy that maps the states to the actions by maximizing the expected cumulative reward using an automated trial-and-error process (e.g., Mnih et al., 2015; Silver et al., 2017). Typical reinforcement learning models include value-based models (e.g., Q-learning or deep Q-learning) (Watkins and Dayan 1992), policy-based models (e.g., deep deterministic policy gradient) (Lillicrap et al., 2015) and hybrid models (e.g., actor-critic) (Williams 1992). Recently, the deep RL (with DNN-based policy) has been gaining attention in wind engineering community as an efficient way for dynamic control and shape optimization (Li et al., 2021a; 2021b). The architecture of a typical deep RL is depicted in **Figure 7**.

3 APPLICATIONS OF MACHINE LEARNING TO WIND ENGINEERING

This section provides a comprehensive review of the state of research and practice of ML for its applications to wind engineering. In addition to ML applications to wind climate, terrain/topography, aerodynamics/aeroelasticity and structural dynamics (following traditional Alan G. Davenport Wind Loading Chain), the review also extends to cover wind damage assessment and wind-related hazard mitigation and response (considering emerging performance-based and resilience-based wind design methodologies). Considering the overwhelming number of existing research publications, this review is by no means exhaustive. Rather, it attempts to provide a state-of-the-art perspective on ML applications to wind engineering-related fields.

3.1 Wind Climate

The review of ML applications to wind climate is organized by classifying it into classical boundary-layer winds, tropical cyclones and non-synoptic events. By leveraging the increasingly available datasets (e.g., satellite data), ML has become a supporting tool or even a reliable competitor of classical approaches for wind climate modeling (e.g., CFD). Most reviewed articles employed ML algorithms as a regression (e.g., long-term prediction of surface wind speed) or a classification (e.g., downburst occurrence prediction) tool. The selected metrics to evaluate the performance of ML algorithms included the root mean square (RMS), coefficient of correlation, mean squared error (MSE), mean absolute error (MAE), mean absolute percentage error (MAPE), coefficient of determination (R2), among others.

3.1.1 Classical Boundary-Layer Winds

Air movement in the planetary boundary layer plays a fundamental role in current wind design of structures and infrastructure. Although a detailed universal description of flow characteristics in the boundary-layer region has not been possible, the classical boundary-layer winds in gales from large depressions or in monsoons can be well represented by a number of empirical or semi-empirical models [e.g., power-law profile for distribution of mean wind speed (Davenport 1960) and power spectrum for turbulent fluctuations (Panofsky and McCormick 1960)]. The major research efforts have been focused on the accurate estimate of design wind speed in a statistical analysis framework (Simiu and Scanlan 1978). Specifically, long-term wind data from meteorological observations are analyzed based on extreme value theory to obtain the design wind speed at each location. However, the accurate forecast of

classical boundary-layer winds is very challenging since it involves a large range of various temporal and spatial scales (e.g., from fractions of a meter to several thousand kilometers for spatial scale and from fractions of seconds to several years for time scales). Usually, the temporal and spatial resolutions from the state-of-the-art weather forecast models [e.g., global forecast system from National Oceanic and Atmospheric Administration (NOAA)] are not sufficient for wind engineering purpose. On the other hand, the unprecedented volumes of data from field measurements (e.g., weather station and satellite) provide a solid foundation to advance ML applications for classical boundary-layer winds.

Table 1 presents the reviewed applications of ML for classical boundary-layer winds, where the ML model, training scheme, input data, output data, data source and performance metric are summarized for each application. The training/testing data were essentially retrieved from field measurements. From **Table 1**, it can be concluded that most applications used ML as a regression model for prediction of mean wind speed (averaging time ranged from minutes to months), while the short-term prediction of turbulent fluctuations that are very important to structural dynamics is very limited. In many applications, the selection of ML models is simply based on gut feeling or past experience. Although several researchers conducted comparison studies to select good ML models for their specific applications, it might be very challenging to generalize the obtained results to other applications due to a lack of a systematic comparison framework.

3.1.2 Tropical Cyclones

Tropical cyclones (TCs), also commonly known as hurricanes in North Atlantic, typhoons in western North Pacific and cyclones in Australia, are low-pressure storms that form over a warm ocean surface (Holton and Hakim 2013). With an average of 90 events reported annually (Zhao et al., 2012), TCs and their cascading hazards (e.g., wind, rain, storm surge and wave) pose a serious threat to public safety, livelihoods and local economies in many coastal regions around the globe. Hence, significant efforts have been made in modeling and predicting TCs and relatively well-established mesoscale numerical weather prediction frameworks [e.g., Weather Research and Forecasting (WRF) model] are available for high-fidelity simulations. However, the high-fidelity computationally expensive models might not be always appropriate for planning activities in an uncertain environment where Monte Carlo simulations are needed or emergency managements where real-time or near-real-time predictions are required. The high demand for a rapid and reliable technique used to assist decision-makers and planers results in many ML models for efficient simulations of key stages in the life cycle of a TC. These ML applications to TCs are fueled by increasingly available remotely-sensed and high-fidelity numerical data. The review in this section is organized following the four important components of full track of a TC, namely genesis, translation, intensity and wind field.

3.1.2.1 Tropical Cyclone Genesis

TC genesis requires several necessary environmental conditions (e.g., existence of low-pressure area and sea surface temperature of at least 26°C), however, the exact mechanisms of TC formation are still not well understood (Gray 1968, 1979; Emanuel 2003; Holton and Hakim 2013). To predict the TC genesis, both numerical and statistical models were developed. The numerical models (e.g., global forecast system) are essentially based on the physical principles and their performance heavily depends on improved understanding of TC genesis mechanism. The statistical models (e.g., Michael 2017; Chen and Duan 2018; Cui and Caracoglia 2019) linearly relate the TC genesis to a few selected environmental factors, and hence show poor interpolation and limited predictability. The lack of a deep understanding of underlying mechanisms stimulated data-driven techniques for TC genesis simulations. As a result, increasing ML applications are available to accurately predict TC genesis. **Table 2i** presents the reviewed applications of ML for TC genesis, where the ML model, training scheme, input data, output data, data source and performance metric are summarized for each application. The training/testing data were essentially retrieved from satellite measurements along with reanalysis results. It is expected the improved spatial resolution of currently available datasets will further enhance simulation results of ML models. From **Table 2i**, it can be concluded that most applications used ML as a classification model for either short-term or long-term forecasting of TC genesis. Although more dynamic and thermodynamic environmental factors can be retrieved using advanced remote sensing technologies in recent years, the identification of the most appropriate set of inputs to ML models (predictors) is still very challenging.

3.1.2.2 Tropical Cyclone Translation

Numerical forecast models have been successfully applied in forecasting normal TC trajectories, but they are computationally expensive. Although several statistical models were also developed based on a large amount of historical TC path records (e.g., Vickery et al., 2000,2009; Emanuel et al., 2006; Hall and Jewson 2007; Chen and Duan 2018; Snaiki and Wu 2020a; Snaiki and Wu 2020b), their linear nature makes them incapable of capturing the inherent nonlinearities in such a complex dynamic system (Zhang and Nishijima 2012). Both numerical and statistical models or their combinations (statistical-dynamics models) show poor performance in forecasting sudden speed change, recurvature and stagnation in TC movement (Chen et al., 2020). To satisfy both simulation accuracy and efficiency, increasing ML applications emerged for TC path prediction. **Table 2ii** presents the reviewed applications of ML for TC translation, where the ML model, training scheme, input data, output data, data source and performance metric are summarized for each application. The training/testing data were essentially retrieved from meteorological databases (e.g., satellite data) and reanalysis results. Typically, the TC track information is available only at each 6-h interval. From **Table 2ii**, it can be concluded that most applications used ML as a regression model for TC path prediction. Since the forecast of TC track can be regarded as a

TABLE 1 | Summary of ML applications for classical boundary-layer winds.

Application	ML model	Training scheme	Input data	Output data	Data source	Performance metric	Remarks
Forecasting mean hourly wind speed time series Sfetsos (2000)	LNN-ANN-NLN-RBF-ANFIS-ERNN	Gradient descent, Levenberg Marquardt	Past mean hourly data (six past measurements)	Next mean hourly wind speed	Field measurements at the Odigitria of the Greek island of Crete on March 1996 (total of 744 h)	RMS	NLN with logic rule outperformed all other models
Forecasting daily, weekly and monthly mean wind speeds More and Deo (2003)	ANN-JRNN	Back-propagation, cascade correlation	Past daily-, weekly- and monthly averaged mean wind speed	Next daily, weekly and monthly averaged mean wind speeds	Field measurements from 1989 to 2000 in two locations in Mumbai, India	Coefficient of correlation	Best performance by RNN trained with the cascade correlation
Prediction of the next daily mean wind speed Mohandes et al. (2004)	ANN-SVM	Levenberg-Marquardt	mean daily wind speed of previous days (ranging between 1 and 11)	Next daily mean wind speed	12 years of mean daily wind speed in Medina city, Saudi Arabia	MSE	SVM model outperformed the ANN model
Long-term wind speed and power forecasting Barbounis et al. (2006)	IIRANN, DRNN, LAFMN	Global recursive prediction error	3-days forecast of wind speed and direction provided by meteorological models at four nearby sites	Hourly mean wind speed and power for up to 72-h	Atmospheric modeling system SKIRON and wind turbines data from April 1st, 2000 until 31 December 2000 in Rokas' wind park on the Greek island of Crete	MAE-RMS	Similar performance results for the three models
Short-term mean wind speed forecasting Potter and Negnevitsky (2006)	ANFIS	least-squares estimator and the gradient descent	4 to 6 past mean wind speeds and direction with a 2.5 min time step	Next mean wind speed and direction at 2.5 min	21-month time series of 2.5 min mean wind from Hydro Tasmania at Tasmania, Australia	Mean absolute percentage error	ANFIS model outperformed a locally developed persistence model
Prediction of the next hourly mean wind speed Li and Shi (2010)	ANN, RBF, ALEN	Levenberg–Marquardt	Past hourly mean wind speed observations (up to 8 observations)	Next hourly mean wind speed	Anemometers data for 1 year (2002) in two sites in North Dakota	Mean absolute error and RMSE	ANN outperformed other models
Prediction of the hourly mean wind speed and direction Lahouar and Slama (2014)	SVM (radial basis kernel)	-	Past hourly mean wind speed and direction in the site (up to 10 past samples)	Next hourly mean wind speed and direction for a lead time up to 10 h	Sidi Daoud wind farm in Tunisia from 2010 to 2011	RMSE and MAE	Satisfactory results
Short-term wind direction forecasting Tagliaferri et al. (2015)	ANN, SVM (RBF kernel)	Gradient descent	Wind direction at past minutes	Next 1–2 min wind direction	34 days data from the 34th America's Cup in 2013, San Francisco	Mean absolute error and mean effectiveness index	SVM model outperformed the ANN model
Prediction of the monthly averaged mean wind speed Kumar and Malik (2016)	ANN, GRNN	Missing	10 variables (e.g., latitude, longitude, earth temperature, atmospheric pressure)	Monthly averaged mean wind speed	Data retrieved from NASA corresponding to various cities in India	MSE and RMSE	GRNN outperformed the ANN model
Predict of short-term	Hybrid model (wavelet packet	-	Past values of the wind speeds	Mean wind speed for up to 1 day	Data from several sites in the Sichuan	MAE and RMSE	WPD-DBSCAN-ENN

(Continued on following page)

TABLE 1 | (*Continued*) Summary of ML applications for classical boundary-layer winds.

Application	ML model	Training scheme	Input data	Output data	Data source	Performance metric	Remarks
mean wind speed Yu et al. (2018)	decomposition [WPD] + density-based spatial clustering of applications with noise [DBSCAN] + ENN), WPD-ENN, ENN		determined based on the gradient boosted regression trees	with a 10-min time step	Province, China over 16 days with an average wind speed of 10 min		outperformed all other models
Time-series prediction of mean wind speed Khosravi et al. (2018a)	ANN, SVR, FIS, ANFIS, GMDH	Bayesian Regularization, Scaled Conjugate Gradient, BFGS Quasi-Newton, Levenberg Marquardt and Resilient backpropagation	Past values of wind speed (number not mentioned)	Mean wind speed for approximately 361-time steps ahead with several time intervals (e.g., 5-min and 30-min)	Osorio wind farm in the south of Brazil	RMSE, MSE	SVR, GMDH and ANFIS models preformed the best. The prediction accuracy of ANFIS was increased when coupled with particle swarm optimization (PSO) and genetic algorithm (GA). The Levenberg Marquardt performed the best
Prediction of the mean wind speed, direction and power Khosravi et al. (2018b)	ANN, SVR (with radial basis function), ANFIS	Levenberg Marquardt, Conjugate Gradient and Bayesian Regularization	Pressure, local time, temperature and relative humidity	Mean wind speed, direction and power (in 5-min, 10-min, 30-min and 1-h intervals) for up to 24 h	Wind farm in Bushehr, Iran	RMSE	Levenberg Marquardt and Bayesian Regularization algorithms gave the best performance for ANN. SVR was the best to simulate the wind speed. Low prediction results were obtained by the 3 models for the wind direction
Short-term prediction of wind speed and direction Chitsazan et al. (2019)	ESN, ANFIS, NESN-P with polynomial functions and NESN-MP with multivariable polynomials	-	Past values of wind speed and direction at time interval of 10 min (the exact number was not specified)	Mean wind speed and direction at 10 min intervals for up to 1 day and 6 days, respectively	Several Nevada weather information stations in Reno, Nevada	RMSE	The best prediction results given by the NESN-MP
Probabilistic prediction of the wind gusts Wang et al. (2020)	Ensemble of 3 machines models (RF, LSTM and GPR), RF, LSTM and GBRT	Adaptive momentum estimation	Past values of wind speed (the number was determined based on the partial autocorrelation function)	Wind gusts for up to 72 h	Sutong Cable-Stayed Bridge in Jiangsu province of China (sampling frequency of 1 Hz with a total of a total of 720 h)	RMSE, MAE and the mean absolute percent error (MAPE)	The ensemble model achieves the highest accuracy
Prediction of mean wind speed Sharma et al. (2020)	MFQL, SVR, KNN	-	7 intrinsic mode functions obtained from past wind speed values using empirical model decomposition technique	1-min ahead mean wind speed	National Institute of Wind Energy and Wind Resource Assessment data portal (in ten Indian cities)	Mean Absolute Percentage Error (MAPE)	MFQL outperformed the other models
		-					

(Continued on following page)

TABLE 1 | (*Continued*) Summary of ML applications for classical boundary-layer winds.

Application	ML model	Training scheme	Input data	Output data	Data source	Performance metric	Remarks
Prediction of mean wind speed Zhongda Tian et al. (2020)	LSSVM optimized with four algorithms Backtracking search, genetic algorithm, particle swarm, and improved feature selection		Past values of mean (hourly) wind speed (50 values)	1-h mean wind speed (next 1-48 h)	The training data were sampled every 1-h from a wind farm in Jinzhou, China	RMSE, MAE, mean absolute percentile error (MAPE), R-square and reliability	LSSVM optimized with the backtracking search optimization algorithm outperformed all other models

time series prediction problem, the feedback neural networks such as RNNs and LSTMs are preferred and lead to good performance. However, their performance within each 6-h interval is unknown due to the sampling limitation in the training data.

3.1.2.3 Tropical Cyclone Intensity

The TC intensity (over ocean or land) can be measured in terms of central pressure or maximum sustained wind speed. It is impacted by several complicated physical phenomena (e.g., atmosphere-ocean interaction and vertical wind shear), and hence remains one of the most challenging issues in TC forecasting especially for rapid intensification prediction. To avoid the high computational cost of numerical forecast models, both statistics-based (e.g., Vickey et al., 2000; DeMaria et al., 2005; Hall and Jewson 2007; Vickey et al., 2009) and physics-based (e.g., Snaiki and Wu 2020a) tools were developed for fast prediction of TC intensity. However, neither statistical nor physical models guarantee prediction accuracy of TC intensity due essentially to the over-simplification of such a complicated dynamic system. To improve simulation accuracy while keeping a high efficiency, increasing ML applications are available for TC intensity prediction. **Table 2iii** presents the reviewed applications of ML for TC intensity, where the ML model, training scheme, input data, output data, data source and performance metric are summarized for each application. The training/testing data were essentially retrieved from meteorological databased (e.g., satellite data) and reanalysis results. From **Table 2iii**, it can be concluded that most applications used ML as a regression (or a classification) model for estimation of intensity time series (or levels). Although encouraging simulation results indicate a good performance of ML models in predicting TC intensity for their specific applications, the selection of the most appropriate set of inputs (including the number of predictors and previous time steps) is still very challenging. In addition, it is not easy to conduct a systematic comparison among reviewed ML models since the used performance metrics differ substantially from one application to another.

3.1.2.4 Tropical Cyclone Wind Field

TC wind hazard is of great significance since it (directly) induces significant damage to life and property and (indirectly) triggers other TC-induced hazards (e.g., storm surge and waves). Substantial research efforts have been made for development of numerical models (e.g., WRF) or analytical models (e.g., Snaiki and Wu 2017a; Snaiki and Wu 2017b; Snaiki and Wu 2018; Snaiki and Wu 2020c; Fang et al., 2018; He et al., 2019) to simulate the boundary-layer wind field. However, none of these models can simultaneously achieve simulation accuracy and efficiency. To address this issue, increasing ML applications emerged for TC boundary-layer wind field simulation. **Table 2iv** presents the reviewed applications of ML for TC wind field, where the ML model, training scheme, input data, output data, data source and performance metric are summarized for each application. The training/testing data were essentially retrieved from meteorological databases (e.g., satellite data) and high-fidelity simulations. It is expected the improved spatial resolution of currently available datasets will further enhance simulation results of ML models. From **Table 2iv**, it can be concluded that most applications use ML as a regression model for prediction of surface wind speed. Since these ML models were often trained and fine-tuned to predict the TC wind field at a specific region, it might be very challenging to generalize the obtained results to other locations. It is noted that only wind field at a certain altitude is available in most ML applications due essentially to training data sparsity issue in vertical dimension. The widely-used logarithmic or power-law profiles are typically employed to obtain the TC boundary-layer winds. Accordingly, the supergradient winds that may have significant implications to the wind design of tall buildings is not captured (Snaiki and Wu 2020c).

3.1.3 Non-synoptic Winds

Unlike synoptic winds that are associated with large-scale meteorological systems characterized by horizontal scales of thousands of kilometers and time scales of days, the non-synoptic wind systems are local phenomena (e.g., a horizontal scale of several hundreds of meters) and short lived (e.g., a time scale of a few minutes) (Chowdhury and Wu 2021). Furthermore, the transient nature of non-synoptic winds makes them exhibit time-varying mean wind speeds and nonstationary/non-Gaussian fluctuations. Accordingly, the detection, measurement, and modeling of non-synoptic wind systems lag behind those of synoptic winds. However, numerous studies have demonstrated the importance of the non-synoptic wind events on the structural design (e.g., Holmes 1999; Letchford et al., 2002; Hao and Wu 2017). For example, the design wind speeds with relatively high return periods are usually dominated by the thunderstorm downbursts (Twisdale and Vickery 1992; Solari

et al., 2015) and the ASCE 7–22 includes the first-ever criteria for tornado-resistant design (ASCE, 2021). Recently, there is a rapid development of field-measurement networks (e.g., THUNDERR project at University of Genova) and laboratory facilities (e.g., WindEEE at Western University) for improved understanding of non-synoptic wind systems. These advances offer an unprecedented volume of data, and hence provide an opportunity to facilitate ML applications to non-synoptic winds. Although the non-synoptic wind systems can be originated from various mechanisms (e.g., convective storm, gravity wave or negative buoyancy) (Bluestein 2021), the review only focuses on those associated with convective storms. Specifically, ML applications to thunderstorms (subsynoptic-scale weather system) are first presented, followed by detailed reviews of its applications to two important types of non-synoptic wind events associated with thunderstorms, namely downbursts and tornadoes.

3.1.3.1 Thunderstorms

A thunderstorm is short-lived atmospheric weather system accompanied by lightning and thunder, gusty winds, heavy rain, and sometimes hail (Solari 2020). The life cycle of a thunderstorm usually consists of cumulus stage, mature stage and dissipative stage, and it typically lasts around 30 min. Both mesoscale and microscale numerical models have been developed for simulation of thunderstorms (Hawbecker 2021). Mesoscale modeling covers a large-scale computational domain (and hence fully considers physics involved), however, it is limited to a low spatiotemporal resolution. Microscale modeling utilizes a high spatiotemporal resolution (and hence obtains important small-scale features in the simulation of winds), however, it is limited to a relatively small-scale computational domain resulting in insufficiently reliable boundary conditions. To avoid shortcomings of currently available numerical models, ML models may provide a promising approach for efficient and accurate simulation of key stages in the life cycle of a thunderstorm. **Table 3i** presents the reviewed applications of ML thunderstorms, where the ML model, training scheme, input data, output data, data source and performance metric are summarized for each application. The training/testing data were essentially retrieved from meteorological databases and reanalysis results. From **Table 3i**, it can be concluded that most applications used ML as either a classification or a regression model for prediction of thunderstorm occurrence. Obviously, there is still room for more comprehensive applications of ML in terms of modeling and forecasting each aspect of the thunderstorm from formation to dissipation. In addition, most ML applications to thunderstorm were limited to simple models with standard algorithms (e.g., ANN with backpropagation).

3.1.3.2 Downbursts

Downbursts are one of the most spectacular and dangerous events resulting from thunderstorms (Solari 2020). Their radial outflows and ring vortices after touchdown produce strong wind gusts very close to the ground and therefore lead to substantial structural damages (e.g., Yang et al., 2018). Downbursts are typically simulated numerically using CFD (e.g., Mason et al., 2009; Aboshosha et al., 2015; Haines and Taylor 2018; Hao and Wu 2018; Oreskovic et al., 2018; Oreskovic and Savory 2018; Iida and Uematsu 2019) or experimentally using wind tunnels (e.g., Jesson et al., 2015; Jubayer et al., 2016; Hoshino et al., 2018; Aboutabikh et al., 2019; Asano et al., 2019; Junayed et al., 2019; Romanic et al., 2019). Both numerical and experimental approaches to obtain wind fields associated with downbursts are very time consuming (either computational expensive or labor intensive). This shortcoming motivated increasing use of ML tools for efficient and accurate simulations of downbursts. **Table 3ii** presents the reviewed applications of ML for downbursts, where the ML model, training scheme, input data, output data, data source and performance metric are summarized for each application. The training/testing data were essentially retrieved from field measurement. From **Table 3ii**, it can be concluded that most applications used ML as a classification model for prediction of the occurrence of downburst or probability of damaging wind. There are a very limited number of ML applications for modeling and forecasting the downburst wind field, hence more research efforts are needed in this aspect. It is noted that the reviewed ML applications usually involved a high number of predictors. The employment of relatively high number of input variables may be necessary due to the complexity of downburst prediction. However, it makes the ML models not easy to use since these input variables might not be always available.

3.1.3.3 Tornadoes

Tornadoes are characterized by a rotating column of air descending from supercell thunderstorms lasting from several minutes to few hours. They are the most intense of all non-synoptic wind events, and hence result in significant damage and collapse of structures (Hao and Wu 2016, 2020). Several analytical and empirical models have been developed to simulate the vertical and radial wind profiles of tornado-like vortices (e.g., Wen and Chu 1973; Baker and Sterling 2017). These models are clearly over-simplified. The tornado wind fields are also modeled using CFD simulations (e.g., Kuai et al., 2008; Ishihara et al., 2011; Liu and Ishihara 2015; Eguchi et al., 2018; Gairola and Bitsuamlak 2019; Kawaguchi et al., 2019; Huo et al., 2020; Liu et al., 2021) or laboratory tests (e.g., Sarkar et al., 2006; Refan and Hangan 2016; Razavi and Sarkar 2018; Tang et al., 2018; Ashton et al., 2019; Gillmeier et al., 2019; Hou and Sarkar 2020; Razavi and Sarkar 2021). However, CFD simulations of tornadoes are computational expensive while the laboratory tests are labor intensive. These shortcomings motivated increasing use of ML tools for efficient and accurate modeling of tornadoes. **Table 3iii** presents the reviewed applications of ML for tornadoes, where the ML model, training scheme, input data, output data, data source and performance metric are summarized for each application. The training/testing data were essentially retrieved from meteorological datasets (e.g., Radio-based data). From **Table 3iii**, it can be concluded that most applications use ML as a classification or a regression model for prediction of tornado occurrence. Obviously, there is still room for more comprehensive applications of ML in terms of simulation of the full track of a tornado (including its intensity and associated

TABLE 2 | Summary of ML applications for tropical cyclones.

	Application	ML model	Training scheme	Input data	Output data	Data source	Performance metric	Remarks
i) Genesis	Prediction of the number of TCs in the northwest of Australia Richman and Leslie (2012)	SVR with radial basis function coupled with sequential minimal optimization algorithm, MLR	-	Nine predictors (e.g., El Niño Southern Oscillation)	Number of TCs in the northwest of Australia	Australian Government, Bureau of Meteorology website	RMSE, MAE, R^2	SVR outperformed the MLR model – The prediction accuracy was further improved by coupling the SVR model with Quasi-Biennial Oscillation
	Prediction of TC genesis in the South Pacific Ocean and Australian region Wijnands et al. (2014)	SVM with polynomial kernel, LDA	-	El Niño—Southern Oscillation indices, Multivariate ENSO Index, El Niño Modoki Index, Dipole Mode Index and the Southern Oscillation Index	TC genesis (number of TCs) in the South Pacific Ocean and Australian region	Bureau of Meteorology's National Climate Center - Australia	MAE	SVM outperformed LDA model. Overall prediction performance for both models is low
	Prediction of TCs genesis in the western North Pacific region Zhang et al. (2015)	DT (C4.5 algorithm)	-	Sea surface temperature, rainfall intensity, divergence averaged between 1000- and 500-hPa levels, maximum 800-hPa relative vorticity and the 300-hPa air temperature anomaly	TCs genesis in the western North Pacific region	Navy Operational Global Atmospheric Prediction System and the Tropical Rainfall Measuring Mission (TRMM) Microwave Imager (TMI) from 2004 to 2013	Prediction accuracy = (correctly classified samples/number of samples in the whole dataset)	Satisfactory results were obtained based on the C4.5 algorithm
	Variable selection and prediction of TC genesis Wijnands et al. (2016)	LR and Peter-Clark algorithm	-	Selected variables: relative vorticity (925 hPa), potential vorticity (600 hPa) and vertical wind shear (200–700 hPa)	TCs genesis in region between 30°N and 30°S	IBTrACS, tropical cloud cluster (TCC) and ERA-Interim (1979–2014)	*p*-value and area under the receiver operating characteristic (ROC) curve	Top ranked variables include the relative vorticity (925 hPa), potential vorticity (600 hPa) and vertical wind shear (200–700 hPa)
	Development a TC genesis detection model over the western North Pacific Park et al. (2016)	DT (C5.0 algorithm)	-	8 WindSat-derived indices tested and 2 were selected as the most dominant predictors: circulation symmetry and intensity	TC genesis	WindSat satellite data (wind and rainfall) were used to extract the training/testing data from 2005 to 2009 over the western North Pacific	Prediction accuracy = (correctly classified samples/number of samples in the whole dataset)	Good simulation results were obtained
	Prediction of the number of seasonal TCs in the North Atlantic region Richman et al. (2017)	SVR (with 2 kernels: polynomial and radial basis function)	-	SST and El Niño 3.4 were the best attributes	Number of seasonal TCs in the North Atlantic region	Hurricane database in the North Atlantic basin and Hadley Centre Sea Ice and Sea Surface Temperature dataset	RMSE	The SVR model gave enhanced prediction compared to an operational statistical model that was developed by Colorado State University. The polynomial kernel gave a slightly improved simulation results compared to the RBF kernel
	Prediction of TC formation from mesoscale convective system Zhang et al. (2019)	LR, NB, DT, KNN, ANN, QDA, SVM (with a radial basis function kernel), AdaBoostRF.	-	Several thermodynamic and dynamic predictors were employed in this study (e.g., genesis potential index, 850-hPa vorticity and vertical wind shear)	Genesis prediction at different lead times (e.g., 6 h)	Mesoscale convective system (MCS) dataset, IBTrACS, and ERA-Interim (1985–2008)	F1-score accuracy	AdaBoost algorithm was the best classifier. Both the genesis potential index and the low-level vorticity were the most dominant predictors for the tropical cyclone genesis
	Detection of TC genesis over the western North Pacific Kim M et al. (2019)	DT, RF, SVM (with three different kernels: linear, polynomial, and radial basis functions), LDA	-	8 dynamic and hydrological predictors (e.g., rain rate, circular variance of wind speed)	Genesis detection for a lead time up to 30 h	WindSat satellite measurements from 2005 to 2009 over the western North Pacific basin	F1-score accuracy and PSS score	Best performance from the SVM model with a radial basis function kernel
ii) Translation	Prediction of cyclone track over	ANN	Pseudo invert learning	12 h of past track observations (in terms	24 h of cyclone track over the	Joint Typhoon Warning Center	MAE	Acceptable accuracy

(Continued on following page)

TABLE 2 | (*Continued*) Summary of ML applications for tropical cyclones.

	Application	ML model	Training scheme	Input data	Output data	Data source	Performance metric	Remarks
	the Indian Ocean Ali et al. (2007)			of latitude and longitude)	Indian Ocean at 6 h intervals	(JTWC) from 1971 to 2002		
	Prediction of TCs track of over the western North Pacific basin Wang et al. (2011)	ANN	Levenberg Marquardt	2 previous 6-h positions and the current one (in terms of latitude and longitude)	24 h of cyclone track over the western North Pacific basin at 6 hourly intervals	20 years of historical tack data from the JTWC	Correlation coefficient	Good simulation results
	Trajectory Prediction of Atlantic Hurricanes Moradi Kordmahalleh et al. (2016)	RNN	Genetic algorithm	Past hurricane track locations which are selected by the RNN model (6-hourly hurricane center's latitude and longitude)	hurricane track for up to 12 h in advance	National Oceanic and Atmospheric Administration (NOAA) from 1900 to 2013	MAE	Acceptable accuracy
	Cyclone track prediction over the South Indian ocean Zhang et al. (2018)	MNN, RNN, LSTM, GRU	Backpropagation	Past hurricane trajectories -automatically selected by the algorithm-	1-step of 6-h ahead TC trajectory (in terms of latitude and longitude)	JTWC between 1985 and 2013 in the South Indian ocean	RMSE	MNN-based model outperformed the three recurrent neural networks
	Prediction of hurricane trajectories over the Atlantic basin Alemany et al. (2019)	Grid-based RNN, sparse RNN	Backpropagation	Past hurricane locations (6-hourly distributed)	Hurricane tracks over the Atlantic basin up to 120 h	NOAA database	MSE, RMSE	The grid-based algorithm outperformed the sparse RNN
	Prediction of a typhoon track in the Korean Peninsula Rüttgers et al. (2019)	GAN	Backpropagation	Satellite images	Typhoon tracks in the Korean Peninsula at 6 h lead time	Korean Meteorological Administration and the ERA-interim databases with a total of 76 typhoons that hit the Korean peninsula from 1993 till 2017	Average absolute error	Acceptable accuracy
	Prediction of the spatial-temporal hurricane trajectory Kim S et al. (2019)	ConvLSTM	AdaGrad	Last 5 consecutive hurricane density-maps	Spatial-temporal hurricane trajectory (up to 15-h) with a 3-h time steps	Community Atmospheric Model v5 from 1995 to 2015	RMSE	The error increased with the increasing leading time
	Tropical cyclone track forecasting Giffard-Roisin et al. (2020)	CNN	Adam	Atmospheric fields (image-like data) corresponding to the current and past data (with a 6-h time step) including the latitude, longitude and geospatial height fields at three pressure levels: 700, 500, and 225 hPa (e.g., wind speed components)	TC trajectory (in terms of latitude and longitude) for up to 24-h leading time	TCs data in both hemispheres from NOAA, IBTrACS and ERA-Interim since 1979 (more than 3,000 storms with 6-h time steps)	RMSE, MAE	The proposed model outperformed the statistical CLP5 model
iii) Intensity	Prediction of typhoon intensity changes in the western North Pacific basin Baik and Paek (2000)	ANN, MLR	Backpropagation	11 predictors (e.g., initial storm intensity, initial storm latitude, vertical wind shear and 850-mb horizontal moisture flux)	Typhoon intensity changes in the western North Pacific basin from 12-h and up to 72-h (1 output)	National Centers for Environmental Prediction/National Center for Atmospheric Research (NCEP/NCAR) reanalysis from 1983 to 1996	Average error	The ANN-based model outperformed THE MLR model
	Prediction of the cyclone intensity over the Arabian Sea and Bay of Bengal Chaudhuri et al. (2013)	ANN, RBF, MLR, OLR	Backpropagation	5 predictors: sea surface temperature, central pressure, pressure drop, maximum sustained surface wind speed and total ozone column	Cyclone intensity over the Arabian Sea and Bay of Bengal for approximately 72 h lead time (1 output)	Indian Meteorological Department from 2005 to 2010	RMSE, MAE	ANN model provided the best prediction results
	Prediction of the cyclone intensity levels Chen et al. (2018)	ANN, MLR, SVM	Backpropagation	Multispectral Imagery	Cyclone intensity level (class labels)	Tropical cyclone Nalgae data from 04/08/2017 till 06/08/2017 retrieved from No. 4 meteorological satellite (FY-4) of China	Kappa coefficient and overall accuracy (%)	The three models provided comparable classification results
	Prediction of time series of typhoon	RNN	Backpropagation	3 previous time steps along with the current	Time series prediction of	Western North Pacific typhoon database	Average forecast error	Performance comparable to the

(Continued on following page)

TABLE 2 | (*Continued*) Summary of ML applications for tropical cyclones.

	Application	ML model	Training scheme	Input data	Output data	Data source	Performance metric	Remarks
	intensity Pan et al. (2019)			time of typhoon location and intensity	intensity up to 48 h with a 6 h time step	from the Chinese Meteorological Administration and the Shanghai Typhoon Institute from 1949 till 2016		Japanese Meteorological Agency-Global Spectral model
	Cyclone intensify forecasting over the Western Pacific, Eastern Pacific and North Atlantic basins Chen et al. (2019)	Hybrid CNN-LSTM model (2D-CNN, 3D-CNN and LSTM)	Gradient descent and Adam	3-D atmospheric variables (wind components, temperature, relative humidity and geopotential height) and 2-D sea surface variables (sea surface temperature)	Intensity (24-h lead time) with a 6 h time step	International Best Track Archive for Climate Stewardship (IBTrACS) and ERA-Interim reanalysis	MAE	Good simulation results comparable to other operational forecast models (e.g., Hurricane Weather and Research Forecasting Model)
	TC intensity prediction over the Pacific Northwest and Atlantic Ocean Wei Tian et al. (2020)	CNN	Adam	Satellite images of TCs in real time	TC intensity in near real time	Satellite outputs from 2003 till 2016 from the Meteorological Satellite Research Cooperation Institute and JWTC	RMSE	Good simulation results
	Hurricane intensity prediction Maskey et al. (2020)	CNN	Adam	Satellite images of TCs in real time	TC intensity in near real time	U.S. Naval research laboratory and the NOAA Geostationary Operational Environmental Satellite from 2000 through 2019	RMSE	Acceptable simulation results
iv) Wind field hazard	Estimation of surface wind field based on satellite data Stiles et al. (2014)	ANN (a total of 3 were used)	Levenberg-Marquardt	ANN 1: SeaWinds scatterometer measurements ANN 2: Outputs of ANN 1 ANN 3: 6 predictors (outputs of the first two ANNs, QuikSCAT radiometer rain rate and rain impact quantity, maximum likelihood estimation direction interval wind speed and cross-track distance)	ANN 1: wind speed from 0 to 20 m/s ANN 2: corrected wind speed over 20 m/s (retrieved from H*Wind) ANN 3: final optimized wind speed with a 12.5 km resolution	QuikSCAT mission and H*Wind between 1999 and 2009 for all basins (globally)	MAE	Good simulation results for the surface wind speed were obtained
	Forecasting surface wind speeds during tropical cyclones Wei (2015)	SVM with 4 kernels: linear, polynomial, radial basis function and Pearson VII	-	13 features are considered (e.g., central pressure, latitude, longitude, sea surface pressure) based on stepwise regression method	Surface wind speed (1-h average) for up to 6 h over two offshore islands near Taiwan	Central Weather Bureau of Taiwan from 2000 till 2012 (84 typhoon events)	RMSE	-Pearson VII SVR model is the most accurate technique among all other tested kernel-based SVM models -Resolution not discussed
	Estimation of TCs inner-core surface wind structure based on infrared satellite images Zhang et al. (2017)	LSSVM, RBFNN, linear regression	-	TC age, center latitude and maximum surface wind speed	Critical wind radii of 34- and 50-kt winds in real time	National Satellite Meteorological Centre of China and the Shanghai Typhoon Institute from 2005 to 2008	MAE	LSSVM outperformed all other models
	Simulation of TC boundary-layer winds Snaiki and Wu (2019)	KEDL	L-BFGS-B	Storm parameters (e.g., spatial coordinates, storm size and intensity)	Hurricane boundary-layer winds	H*Wind snapshots	RMSE	Good simulation results were obtained
	Surface wind simulation in near real time Wei (2019)	DNN	Back-propagation algorithm	16 inputs for Taipei and 14 for Keelung corresponding to the typhoon characteristics (e.g., central pressure) and surface meteorological data (e.g., relative humidity)	Hourly surface wind field with 1-degree by 1-degree resolution in 2 locations in Taiwan (Taipei and Keelung)	Central Weather Bureau of Taiwan and Weather Research and Forecasting (47 typhoons from 2000 till 2017)	RMSE	Good consistency between the simulated and WRF results

TABLE 3 | Summary of ML applications for non-synoptic winds.

	Application	ML model	Training scheme	Input data	Output data	Data source	Performance metric	Remarks
i) Thunderstorm	Prediction of severe thunderstorms McCann (1992)	ANN	Backpropagation	Lifted index and surface moisture convergence	Value between 0 and 1 representing the likelihood of the thunderstorm occurrence for a 3-7 h lead time	Centralized Storm Information System of the National Severe Storms Forecast Center (NSSFC) from April to August 1990 over the eastern two-thirds of the United States	critical success index	Acceptable results
	Prediction of the surface peak gust wind speed during thunderstorm events Chaudhuri and Middey (2011)	ANFIS, ANN, RBFNN, MLR	Gradient descent and the least squares estimate	Lift index, Convective Inhibition Energy, Convective Available Potential Energy and bulk Richardson number	Surface peak gust wind speed in Kolkata, India with a lead time up to 12 h	Radiosonde and rawinsonde from the Department of Atmospheric Sciences, University of Wyoming for the location of Kolkata, India from 1997 till 2009	RMSE, MAE	ANFIS model outperformed the other machine learning models
	Prediction of thunderstorms occurrences Litta et al. (2012)	ANN	Levenberg Marquardt, Momentum, Conjugate Gradient, Delta Bar Delta, Quick Propagation and Step	Wind speed, humidity and mean sea level pressure	Hourly temperature during thunderstorm, proxy for thunderstorm occurrence, over the northeastern region of India	Indian meteorological department from 2007 to 2009 (hourly data)	RMSE, MAE, correlation coefficient	Best results with Levenberg–Marquardt learning algorithm
	Prediction of severe thunderstorms occurrences Chakrabarty et al. (2013)	ANN, KNN	Gradient descent	2 predictors at 5 geopotential heights: dry adiabatic lapse rate and moisture difference (a total of 10 inputs)	Likelihood of occurrence of severe thunderstorms with a lead time between 10 and 14 h over the northeastern region of India	Indian Meteorological Department from 1969 to 2008	Correlation coefficient	KNN model was the best classifier
	Prediction of thunderstorm occurrence Yasen et al. (2017)	ANN, Bayes Network, C4.5 decision Tree, KNN	Artificial Bee Colony (ABC), gradient descent	31 thermodynamic and dynamic predictors	Thunderstorm occurrence	METeorological Aerodrome Reports and Surface Synoptic observation from December 2015 to November 2016 at lake Charles airport in Louisiana	Accuracy, AUC, and F-measure	ANN model optimized with ABC algorithm outperformed the other classifiers in detecting thunderstorms
	Prediction of thunderstorm occurrence Ukkonen et al. (2017)	ANN	Scaled conjugate gradient	15 inputs (e.g., most unstable lifted index and relative humidity near 700 hPa) identified based on skill scores	Thunderstorm occurrence in the next 6-h period	ERA-Interim database from 2002 to 2015 over Finland	Heidke skill score	Acceptable results
	Forecasting thunderstorms occurrence Kamangir et al. (2020)	SD-AE	Stochastic gradient descent	38 features (e.g., total predictable water and convective precipitation)	Thunderstorm occurrence through cloud-to-ground lightning parameter for a maximum lead time of 15 h and within 400 km^2 of a selected site in South Texas	North American Mesoscale Forecast System and the National Lightning Data Network from the 2004–2012	Peirce skill score	The SD-AE model outperformed an ANN model developed by Collins and Tissot (2015, 2016) for the same region and with similar lead time
	Forecasting the occurrence of thunderstorms events (Chen and Lombardo 2020)	CNN	Backpropagation	91-min time series of wind speed and direction	Event type (thunderstorm or non-thunderstorm event)	Automated Surface Observing System (ASOS) (1-min averaged data) from 2000 to 2018 with a total of 76,480 time series of 91 min of wind speed and direction	F1 score and average success rate	Reliable classifier for thunderstorms occurrences

(Continued on following page)

TABLE 3 | (*Continued*) Summary of ML applications for non-synoptic winds.

	Application	ML model	Training scheme	Input data	Output data	Data source	Performance metric	Remarks
ii) Downburst	Prediction of damaging wind from tornadic and straight-line events (including downbursts) (Marzban and Stumpf 1998)	ANN	Conjugate gradient	23 radar-derived predictors characterizing the circulations (e.g., depth of circulation, maximum rotational velocity and low altitude shear)	Probability of damaging wind (with a damaging wind excessing 25 m/s) with a lead time of 20-min	National Severe Storms Laboratory (NSSL) Mesocyclone Detection Algorithm (MDA)	Fraction Correct and Heidke's Skill Score	Acceptable results
	Classification of damaging downburst winds (Smith et al. (2004)	LDA	-	26 reflectivity and radial velocity-based attributes (e.g., cell volume, max reflectivity and height of the max reflectivity)	Severity of downburst winds (severe or non-severe events) with a maximum lead time of 15 min	WSR-88D radars (in several locations within the U.S.) from the National Climatic Data Center's Storm. It contains 91 events that produced severe downbursts and 1247 events that did not produce severe downbursts	median Heidke skill	Acceptable results for the prediction of severe downburst events
	Prediction of the probability of occurrence of damaging straight-line winds (including downbursts) from storm cells Lagerquist et al. (2017)	LR, LR with an elastic network, ANN, RF, GBTE	Gradient descent	431 predictors. They can be divided into 4 main categories, namely radar statistics, storm shape parameters, storm motion and sounding indices	Probability of occurrence of damaging winds with a lead time up to 90 min	Near-surface wind observations (from the Meteorological Assimilation Data Ingest System, the Oklahoma Mesonet, and the National Weather Service), radar scans (from the Multiyear Reanalysis of Remotely Sensed Storms) and soundings (from the Rapid Update Cycle and the North American Regional Reanalysis) [from 2001 to 2011]	AUC	- The simulation results indicated that storm motion and sounding indices are the dominant predictors - Both random forest and gradient-boosted tree ensembles gave the best simulation results
	Downburst wind speed forecasting Li and Li (2018)	LSSVM (coupled with variational mode decomposition and particle swarm) – with several kernels (linear, polynomial, Mexican Hat, radial basis function, and Morlet wavelet)	-	Time series of downburst wind (up to 1600 s)	Time series of downburst wind from 1600 s through 1800 s	Time series of downburst wind from two measurements data consisting of 450 sample points with a sampling frequency of 0.25 Hz for a total of 1800 s (the data source was not mentioned)	MAE, RMSE, 2-norms relative error and Pearson correlation coefficient	The combined Morlet wavelet and radial basis kernel functions (RBF) gave the best simulation results
	Identification of the downburst occurrence Medina et al. (2019)	RF	-	8 dual-polarization radar signatures (e.g., maximum vertically integrated liquid and temperature colder than 0°C)	Downburst related events or null events around the Cape Canaveral Air Force Station and Kennedy Space Center	Weather observation towers around the Cape Canaveral Air Force Station and Kennedy Space Center from 2015 to 2016	Mean Decrease Accuracy (MDA) and Mean Decrease Gini (MDG)	Although the model provided good simulation results, strong events were better classified compared to weaker ones
iii) Tornado	Prediction of the tornado's occurrences Marzban and Stumpf (1996); Marzban et al. (1997); Marzban (2000)	ANN	Conjugate Gradient	23 input variables (e.g., maximum shear, low- and mid-altitude convergence)	occurrence/non-occurrence of tornados for a given mesoscale circulation in the next 20 min	National Severe Storms Laboratory's (NSSL) Mesocyclone Detection Algorithm (MDA) with a total of 3258 circulation events	Critical Success Index	The ANN model outperformed other statistical models such as the discriminant analysis bur still the performance is low
	Detection of the tornado's occurrences Lakshmanan et al. (2005)	ANN	Resilient backpropagation	13 features (e.g., rotational velocity)	Tornado occurrence from given circulations in the next 20 min	National Severe Storms Laboratory based on the Mesocyclone Detection Algorithm (MDA) and the near-storm environment (NSE) with 110 storm days	Heidke Skill Score	Simulation results acceptable

(Continued on following page)

TABLE 3 | (*Continued*) Summary of ML applications for non-synoptic winds.

Application	ML model	Training scheme	Input data	Output data	Data source	Performance metric	Remarks
Prediction of the tornado occurrence Santosa (2007)	SVM, LDA, BNN	Backpropagation	34 input features (e.g., meso core depth and meso low-level shear)	Tornado occurrence in the next 20 min	Weather Surveillance Radar 1998 Doppler	Heidke Skill Score	- linear programming support vector machine was used for feature selection - BNN model gave the best performance in detecting tornados from given circulations
Prediction of the tornado occurrence Adrianto et al. (2009)	SVM with 3 kernels (linear, polynomial and RBF), ANN, LDA	Backpropagation	53 input features (e.g., azimuthal shear low level average, gradient direction maximum and reflectivity aloft average)	Tornado occurrence in the next 30 min	Radar measurements from the National Climatic Data center with a total of 33 storm days sampled at 30 min	Heidke Skill Score	-The best classifier was the SVM model with the RBF kernel -SVM model outperformed the other algorithms
Prediction of the tornado occurrence Trafalis et al. (2014)	SVM (radial basis function kernel), LR, RF, rotation forest	-	22 attributes (e.g., wind shear and humidity)	Tornado occurrence from mesocyclones events (no leading time indicated)	MDA and NSE databases with 111 storm days	Heidke Skill Score	-Feature selection was performed using the SVM-Recursive Feature Elimination algorithm with a radial basis function kernel - SVM with threshold adjustment outperformed all other classifiers
Prediction of the probability of occurrence of a tornado Lagerquist et al. (2018), (2020)	CNN	Adam	Storm-centered radar image and a proximity sounding	Probability of occurrence of a tornado in the next-hour	Multiyear Reanalysis of Remotely Sensed Storms (MRRSS) in the [period from 2000 to 2011] and Gridded NEXRAD WSR-88D Radar (GNWR) [period from 2011 to 2018]	Area under the receiver-operating-characteristic curve (AUC) score	Excellent simulation results
Predicting property damage from tornadoes Diaz and Joseph (2019)	ANN (2)	AdaGrad	Storm, land cover, socioeconomic and demographic features	ANN1: occurrence or non-occurrence of damage due to a tornado event ANN2: level of damage when it occurs	NOAA's tornado database, the National Land Cover database and the American Community Survey	AUC, MSE, R^2	-Only the initial tornado coordinates are accounted for rather than the tornado path -Acceptable results
Prediction of the occurrence of tornadic events Coffer et al. (2020)	RF, CNN	Stochastic gradient descent	222 input features at various geopotential heights were initially selected (e.g., temperature, pressure) –Exact final parameters not mentioned-	Tornadic and non-tornadic events	Rapid Update Cycle sounding data from the National Climatic Data Center from 2003 to 2017	Overall accuracy score (in %)	-The input feature selection was carried out using RF which indicated that the pressure terms are not as important as the other environmental parameters (e.g., v-wind component) - RF outperformed CNN

TABLE 4 | Summary of ML applications for terrain and topography.

Application	ML model	Training scheme	Input data	Output data	Data source	Performance metric	Remarks
Modeling the effects of topography on the wind profile Bitsuamlak (2004); Bitsuamlak et al. (2002), (2006), (2007)	ANN	Cascade correlation	6 inputs including simple geometric properties (i.e., "Windward slope of the hill", "Distance between hills", "Height from the crest of the hill" and "Longitudinal location"), roughness element and hill count	Fractional speed-up ratio	CFD simulations corresponding to different topographic configurations: single and multiple hills and escarpments	R^2 coefficient	-Comparison with experimental data from wind tunnel -Good performance
Wind field simulation considering terrain effects Martínez-Vázquez and Rodríguez-Cuevas (2007)	ANN combined with conditional simulation technique	Backpropagation	Terrain roughness, mean wind profile and spectral density	Wind velocity time series (3 min of time series with a time step of 0.1 s) at different points	The time series of wind speed were generated using the procedure of Simiu and Scanlan (1978) at two heights (i.e., 10 and 200 m) with 11 local velocities (from 0.5 to 100 m/s) and surface roughness between 0.001 and 0.050 m	MSE	-The conditional simulation technique significantly decreased the number of required layers in the ANN -Good simulation results
Estimation of the effect of wind direction on wind speed prediction in complex terrain Lopez et al. (2008)	ANN	Bayesian regularization	4 inputs: 10-min mean wind speed from 3 stations nearby and wind direction from another nearby station	Annual average wind speed at a given site with complex terrain configuration	Meteo-Galicia during 2003 at the Galicia region in the northwest Spain corresponding to 5 stations and representing various terrain conditions (e.g., inland and offshore conditions) and elevations	RMS	-Wind direction is important to be considered to improve the simulation results for a site with complex terrain
Prediction of typhoon wind speed and profile over complex terrain Huang and Xu (2013)	ANN	Backpropagation	Upstream wind speed and direction at height z	Wind speed and direction at height z on a bridge site	Reynolds-averaged Navier-Stokes simulations which provides the wind profiles at the bridge site given an inlet upstream wind field (which does not account for topographic effects)	MAE	Good simulation results for both wind speed and direction
Prediction of the wind flow over complex topographies Mayo et al. (2018)	DNN	Proximal adagrad	3 cartesian coordinates (x,y,z) of the selected point and the incoming uniform mean wind speed	Mean wind speed over a given site with complex topography	4 CFD simulations of the wind field in a given coastal dune system with complex terrain	MAE	Acceptable simulation results
Selection of the experimental hardware within a wind tunnel Abdi et al. (2009)	ANN (2)	cascade correlation	ANN1: height from floor, the bottom-spire width, the surface roughness and the top spire width	ANN1: mean longitudinal wind velocity and turbulence intensity	RWDI USA LLC wind tunnel in Miramar, Florida	No error scores were provided	- Visual inspection of the predicted wind profile and turbulence intensity of the first neural network

(Continued on following page)

TABLE 4 | (*Continued*) Summary of ML applications for terrain and topography.

Application	ML model	Training scheme	Input data	Output data	Data source	Performance metric	Remarks
							indicated good simulation results - Results from ANN2 were not satisfactory
			ANN2: target mean longitudinal wind speed, target turbulence intensity and height from floor	ANN2: difference between top and bottom spire width and the surface roughness			
Prediction of wind properties in urban environments based on wind tunnel tests Varshney and Poddar (2012)	ANN (2)	Lavenberg–Marquardt	ANN1: number of roughness elements, number of barriers, height from floor and slot width ANN2: number of roughness elements, number of barriers and slot width	ANN1: mean wind speed, turbulence intensity and length scale factor ANN2: instantaneous velocity	Boundary-layer wind tunnel tests of the National Wind Tunnel Facility in Kanpur, India (18 configurations)	No error scores were provided	- Visual inspection of the predicted results indicated satisfactory simulations
Designing laboratory wind simulations Križan et al. (2015)	ANN (2)	RPROP Riedmiller and Braun (1993)	ANN1: basis barrier height, barrier castellation height, surface roughness elements' spacing density, surface roughness elements' height and height of measurement points	ANN1: mean wind speed, turbulent intensities (in the three directions), length scales (in the three directions) and turbulent Reynolds stress	Boundary-layer wind tunnel at the Technische Universität München with a total of 23 configurations of hardware setups	R^2	-ANN1: except the turbulent length scale in the *x*-direction (not that accurate) all other results were good
			ANN2: basis barrier height, surface roughness elements' spacing density, surface roughness elements' height, frequency and height of measurement points	ANN2: power spectral densities of the velocity fluctuations in the three directions			- ANN2: good simulation results were obtained

wind field). Just like ML applications to downbursts, a high number of input variables (predictors) were utilized for the reviewed ML models. The identification of the most appropriate set of predictors is still very challenging, and a trail-and error approach was typically employed. In addition, it is not easy to conduct a systematic comparison among reviewed ML models since the used performance metrics differ substantially from one application to another.

3.2 Terrain and Topography

Wind characteristics including mean wind speeds and turbulent fluctuations are much affected by the surrounding terrain and topography. As a consequence, careful consideration of local terrain roughness and topographic features as well as surrounding obstacles is vital to the accurate determination of wind pressures on structures and pedestrian level winds. Wind codes and standards consider the terrain effects corresponding to limited (and simplified) terrain geometries (e.g., escarpment and single hill) through correction factors. To examine the effects of complex terrain condition on wind fields, wind tunnel tests are usually employed with a very small geometric scale (e.g., 1:500). Alternatively, numerical schemes such as the mass-conservation or momentum-conservation model can be used to capture the terrain effects on oncoming wind fields. Although the topographic effects can be well simulated based on momentum-conservation models (e.g., using Reynolds-averaged Navier-Stokes equations), the needed computational time makes it impractical for use as a real-time decision support tool. The mass-conservation model computes wind fields over complex terrain in seconds to a few minutes (Forthofer et al., 2014a; 2014b), but the accuracy of simulation may be poor because nonlinear momentum effects are not considered (Jackson and Hunt 1975). Considering the complex terrain-wind data from high-fidelity CFD simulations, wind tunnel tests and field measurements are increasingly available, ML tools can be utilized (as computationally efficient reduced-

order models that possess high simulation accuracy of complex nonlinear systems) to provide rapid estimation of wind flows over various terrain conditions. However, ML development for terrain and topographic considerations is still at an early stage with a limited number of studies reported in the literature. **Table 4** presents the reviewed applications of ML for terrain and topography, where the ML model, training scheme, input data, output data, data source and performance metric are summarized for each application. The training/testing data were essentially retrieved from either CFD simulations or wind tunnel tests. From **Table 4**, it can be concluded that most applications used ML as a regression model for prediction of wind fields over various terrain conditions and topographic configurations. There are a few studies that applied ML techniques to assist in efficient search for a correct layout of passive flow altering devices (e.g., spires and roughness elements) in the boundary-layer wind tunnel. It is noted that the current ML applications to consider topographic effects on wind fields are usually limited to terrain configurations that can be characterized by several parameters, hence, the employed ML models and training schemes are simple and standard (e.g., ANN with backpropagation). However, several advanced ML models such as autoencoder (e.g., Fukami et al., 2019) and GAN (Kim and Lee 2020) have been utilized to assist in the generation of turbulent inflow (as a realistic inlet boundary condition of CFD simulations).

3.3 Aerodynamics and Aeroelasticity

The bluff-body aerodynamics and aeroelasticity play a critical role in the safe and cost-effective design of wind-sensitive structures, and their considerations rely heavily on boundary-layer wind tunnels. In addition to the Reynolds number effects (due to very small model scales), wind tunnel tests are very time consuming and labor intensive. To this end, CFD techniques have been rapidly developed for simulations of structural aerodynamics (gust-induced effects) and aeroelasticity (motion-induced effects). The purpose is to make CFD simulations serve as a complementary or even alternative approach to wind tunnel tests. Despite significant advances of hardware and algorithms, the reliable CFD simulations of wind-structure interactions are still computationally very expensive due to three-dimensional nature of wakes and intensive flow separations from structures. Hence, a number of reduced-order models have been developed to efficiently model structural aerodynamics and aeroelasticity (Wu and Kareem 2013). Unfortunately, these reduced-order models do not always have a satisfactory representation of the full nonlinear equations that govern the wind-structure interactions. Specifically, modern bridge decks and super tall buildings with unusually geometries all exhibit nonlinear unsteady aerodynamics and aeroelasticity that limit the applicability of the state-of-the-art reduced-order modeling methodologies. On the other hand, the Kolmogorov Neural Network existence theorem offers mathematical foundation for applying multilayer neural networks to approximate arbitrary nonlinear systems with any precision (Huang and Lippmann 1988; Hornik, 1991). With high-fidelity data and advanced algorithms, ML models can simultaneously achieve great simulation efficiency and accuracy. It is noted that there are numerous ML applications to aerodynamics and aeroelasticity of both bluff bodies (e.g., circular cylinder) and streamlined bodies (e.g., airfoil) in fluid mechanics community (e.g., Kutz 2017; Brunton et al., 2020), however, they are not discussed here. The review in this section only covers wind-sensitive structures in civil engineering. The ML applications for bridge aerodynamics and aeroelasticity are first reviewed in **Table 5i** and then followed by buildings and other structures in **Table 5ii**, where the ML model, training scheme, input data, output data, data source and performance metric are summarized for each application. The training/testing data were essentially retrieved from either CFD simulations or wind tunnel tests. From **Table 5**, it can be concluded that most applications used ML as a regression model for prediction of steady-state force coefficients, flutter derivatives and vortex-induced vibrations (VIV) of various bridges and for modeling of wind pressure coefficients of various buildings (as well as estimation of the interference factors for adjacent buildings). The different aerodynamic representations in bridges (mainly using global quantities such as force coefficients) and buildings (mainly using local quantities such as pressure coefficients) are partially due to available data types from wind tunnel tests. Although satisfactory ML simulation results have been obtained (in terms of interpolations), most reviewed applications do not necessarily have good performance in terms of extrapolations outside the training datasets. It is noted that the currently available ML models of aerodynamics and aeroelasticity are developed for the main purpose of being used as preliminary design tools to avoid the high-cost wind tunnel tests in the early design stage. There is a lack of systematic comparison among various ML models, hence, their selection for specific applications is rather rudimentary.

3.4 Structural Dynamics and Damage Assessment

Due to the computational complexity of numerical techniques (e.g., finite element method) for solving wind-induced nonlinear structural response, reduced-order models (e.g., ANN) have been developed to alleviate the computational cost of the high-fidelity models. The ML models have been used for structural dynamics and damage assessment for several decades mainly in the field of earthquake engineering (e.g., Wu et al., 1992; Masri et al., 1993; Jiang and Adeli 2005; Pei et al., 2005; Gholizadeh et al., 2009; Facchini et al., 2014; Derkevorkian et al., 2015; Liang 2019; Wu and Jahanshahi 2019; Yu et al., 2020). However, similar applications have not emerged in wind engineering community until recently due essentially to the linear consideration of the wind-induced structural response [ASCE 7-16 (ASCE, 2017)]. Recent advances of performance-based wind design methodology have placed increasing importance on effective simulations of nonlinear, inelastic structural dynamics response under strong winds. The numerical estimation of wind-induced nonlinear structural response using a high-fidelity finite element model is computationally very expensive due to its small time-step size and long simulation duration. Accordingly, several ML applications to wind-induced structural dynamics have been

TABLE 5 | Summary of ML applications for aerodynamics and aeroelasticity.

	Application	ML model	Training scheme	Input data	Output data	Data source	Performance metric	Remarks
i) Bridges	Estimation of aeroelastic parameters of bridge decks Jung et al. (2004)	ANN	Resilient backpropagation Riedmiller and Braun (1993)	100 inputs:90 inputs representing the section geometry and 10 inputs for the nondimensional velocity	Flutter derivatives (6) of a rectangular section	Wind tunnel test (total of 17 experiments)	MSE	Acceptable performance
	Prediction of flutter derivatives of a rectangular section model Chen et al. (2008)	ANN (total of 8)	Gradient descent	Width-to-depth ratio and a set of reduced frequency	8 flutter derivatives (each given by 1 ANN separately) of rectangular section model	Experimental data from wind tunnel tests	No error metrics	From the graphical results, the simulation results were in good agreement with the experimental ones
	Prediction of flutter derivatives of a cable stayed bridge Lute et al. (2009)	SVM (RBF kernel)	-	Non-dimensional velocity and width to depth ratio of bridge deck	8 flutter derivatives of a cable stayed bridge	Wind tunnel tests were retrieved form Matsumoto et al. (1996)	MSE	Good simulation results
	Estimation of flutter derivatives of a rectangular section Chung et al. (2012)	ANN (total of 8)	Backpropagation	Width-to-depth ratio, reduced frequency and reduced velocities	8 flutter derivatives (each given by 1 ANN separately) of rectangular section model	CFD simulations and forced-vibration test in a wind tunnel	No error metrics	Good performance
	Modeling vortex-induced vibration of a long-span suspension bridge Li et al. (2018)	DT, SVR (with Gaussian radial basis kernel)	-	DT: incoming wind speed and direction at three locations on the bridge deck SVR: same inputs as DT model at the current step along with the response of the previous step	DT: VIV modes (a total of 6) SVR: VIV amplitudes	Field measurements of a full-scale suspension bridge over a period of 6-years (2010–2015) located in the eastern ocean of China	RMSE, accuracy (%), squared correlation coefficient	Good simulation results
	Prediction of nonlinear unsteady bridge aerodynamics Li et al. (2020)	LSTM	Back-pass algorithm	Bridge deck motions	Motion-induced aerodynamic forces	CFD simulations (total of 14,880 input-output data corresponding to a 2-D bridge deck cross-section)	No error metrics	Excellent agreement (through visual inspection) between the LSTM model and CFD was obtained
	Prediction of aeroelastic response of bridge decks Abbas et al. (2020)	ANN	Levenberg-Marquardt	18 inputs corresponding to the response for heave and pitch (in terms of displacement, velocity and acceleration) at previous time steps with three lag terms	Normalized lift force and torsional moment coefficients at current time step	2 dimensional CFD simulations for the two bridge cross-sections	MSE	Good simulation results were obtained
	Prediction of the flutter velocity of suspension bridges Rizzo and Caracoglia (2020)	ANN (different topologies)	Levenberg-Marquardt	1st ANN category: deck chord, deck weight or the ratio between the 1st torsional and the 1st vertical circular frequencies of the bridge, structural damping, air density and the flutter derivatives 2nd ANN category: deck chord, the ratio between the first torsional and the first vertical circular frequencies of the bridge, and the flutter derivatives	Critical flutter velocity of suspension bridge with closed box deck sections	Wind tunnel experiments along with finite element-based simulation corresponding to various geometrical and mechanical parameters of the bridge deck cross-section	R^2	While the performance of the ANN models varied according to the topology, their performance was good

(Continued on following page)

TABLE 5 | (*Continued*) Summary of ML applications for aerodynamics and aeroelasticity.

	Application	ML model	Training scheme	Input data	Output data	Data source	Performance metric	Remarks
ii) Building & other structures	Prediction of wind load distribution for air-supported structures Turkkan and Srivastava (1995)	ANN	Gradient descent	Hemispherical membrane: internal pressure ratio and two spatial orientations Cylindrical membrane: Similar inputs as the first case + membrane aspect ratio	Steady-state wind pressure coefficient for air-supported structures (e.g., cylindrical and hemispherical membranes)	Wind tunnel tests	R^2	Acceptable results
	Modelling wind-induced interference effects on high-rise buildings Khanduri et al. (1997)	ANN	Generalized delta rule	Spacing between two adjacent buildings in the along- and across-wind directions	Mean and dynamic along- and across-wind directions interference factors	Wind-tunnel tests from two references Saunders and Melbourne (1980); Taniike and Inaoka (1988)	No error metrics	-
	Modelling wind-induced interference effects on high-rise buildings English and Fricke (1999)	ANN	Backpropagation	Building aspect ratio, normalized separation distance and power law index	Interference index	Wind tunnel tests from several sources e.g., Zambrano and Peterka (1978); Blessmann and Riera (1985)	No error metrics	-
	Interpolation of wind-induced pressure time series on a scaled model Chen et al. (2002)	ANN	Levenberg–Marquardt	4 adjacent experimental pressure taps at the next time step (t+1) and values of the pressure taps at current & two previous time steps in the target tap (central one)	Wind pressure coefficient at the next time step	Wind tunnel tests of a 1:50 scale model	R^2	Good simulation results
	Prediction of pressure coefficients on roofs of low buildings Chen et al. (2003)	ANN (2 models)	Levenberg–Marquardt	Roof height, wind direction and two normalized roof coordinates (for the two models)	ANN1: mean pressure coefficients on a gable roof of low-rise building ANN2: root-mean-square pressure coefficients on a gable roof of low-rise building	Wind tunnels experimental data	MSE	Good simulation results
	Prediction of building interference effects Zhang and Zhang (2004)	ANN, RBFNN (with Gaussian kernel)	Backpropagation	Ground roughness, relative orientation of two buildings	Inference factor	Experimental data from literature e.g., Bailey and Kwok (1985)	MSE	RBF outperformed the ANN model
	Prediction of wind loads on a large flat roof Fu et al., (2006), (2007)	FNN (2 models)	Backpropagation	FNN1: wind direction and the positions of the available pressure taps FNN2: wind direction and the frequency for the few selected tap locations	FNN1: Mean pressure coefficients on a large flat roof FNN2: Power spectral density (at given input frequencies) at few locations in the roof corners and leading edge	Boundary-layer wind tunnels tests	MSE	- Acceptable results for the 1st FNN model - No error metrics were reported for the 2nd FNN model
	Wind load evaluation for the design of roof cladding of spherical domes Uematsu and Tsuruishi (2008)	ANN (4 models)	Quickprop algorithm Fahlman (1988)	'2 geometric parameters of the dome', '2 coordinates parameters x and y', 'turbulence intensity of the incoming wind at the mean roof height'	Statistics of wind pressure coefficient on the roof of a spherical dome: mean, standard deviation, skewness and kurtosis	Experimental wind tunnel tests	Predefined error index (normalized by the standard deviation of the target data)	- Acceptable results
	Estimation of the wind force coefficients on a rectangular building Wang et al. (2013),	ANN, RBFNN, GRNN	Backpropagation	Aspect & side ratio and ground roughness	Along-wind mean coefficient of base shear of a rectangular building	Wind tunnel tests	RMSE	RBFNN outperformed all other models

(Continued on following page)

TABLE 5 | (*Continued*) Summary of ML applications for aerodynamics and aeroelasticity.

Application	ML model	Training scheme	Input data	Output data	Data source	Performance metric	Remarks
Wang and Cheng (2015), (2017)							
Wind load prediction of large-span dry coal sheds Sun et al. (2017)	GRNN	-	rise-span ratio, depth-span ratio, wind angle, and local coordinates	Statistics of the pressure coefficients: mean, RMS. Skewness, kurtosis of pressure coefficients, three auto-correlation coefficients and coherence exponent	Wind tunnel tests	R^2	While the mean pressure coefficient was predicted accurately, the kurtosis of the pressure coefficient was poorly predicted
Prediction of wind loads on high-rise building Huang et al. (2017)	ANN (2 models)	Levenberg–Marquardt	ANN1: coordinates (x, y, z) of the pressure taps	ANN1: mean or root-mean-square pressure coefficients on a high-rise building	Wind tunnel tests	RMSE	- No error metric was reported for the 1st ANN model
			ANN2: coordinates (x, y, z) of the pressure taps and time	ANN2: time series of wind-induced pressures on a high-rise building			- Good simulation results for the 2nd ANN model based on RMSE.
Prediction of wind pressure coefficients on building surfaces Bre et al. (2018)	ANN (3 models for flat-, gable, and hip-roofed low-rise buildings)	Levenberg–Marquardt	Wind direction and building characteristics (1 parameter for the flat-roofed building, and 2 parameters for the gable roofed and hip-roofed buildings)	Mean pressure coefficients over few locations on the roofs and walls (5 outputs for the flat-roofed, 6 for the gable-roofed and 8 for the hip-roofed)	Tokyo Polytechnique University experimental database	MSE, R^2	Good simulation accuracies
Prediction of roof pressures on a low-rise structure Fernández-Cabán et al. (2018)	ANN	Levenberg–Marquardt	Turbulence intensity (at eave height) and 2 normalized roof coordinates	Mean, root-mean-square, and peak pressure coefficients on the roof (at 152 roof taps) of 3 scaled low-rise buildings (1: 50, 1:30, and 1:20)	Wind tunnel tests	RMSE, MAE, R^2	The accuracy of simulation results depends on the pressure taps location
Modeling for unsteady flows around bluff bodies of various shapes Hasegawa et al. (2019), (2020)	CNN-AE + LSTM	Adam	Temporal variation of the flow field around different 2-D cross-sections shapes: 2 velocity components and pressure	Temporal variation (next time step) of the flow field around different 2-D cross-sections shapes: 2 velocity components and pressure	Direct numerical simulation (DNS): 100 different bluff-bodies shapes (in 2-D space) with 500 instantaneous time-series flow fields each	MSE	-The use of CNN-AE allows the mapping between the high-dimensional space and a low-dimensional latent space which facilitates the training of the LSTM model - Excellent performance
Prediction of wind pressures on a tall building under interference effects Hu et al. (2020)	DT, RF, XGBoost, GAN	-	GAN: wind direction and location of the interfering building DT, RF, XGBoost: wind direction, the coordinates of the pressure tap and the location of the interfering building	GAN: mean and fluctuating pressure coefficients over all faces of the building DT, RF, XGBoost: mean and fluctuating pressure coefficient at one point on the building surface	Aerodynamic database of Tokyo Polytechnic University	R^2	The GANs-based model outperformed the other three machine learning algorithms and provided accurate mean and fluctuating pressure coefficients on the principle building
Prediction of low-rise gable roof building pressures Jianqiao Tian et al. (2020)	DNN	Levenberg–Marquardt	Prediction's location (x, y, z) and the incoming wind direction	Mean and peak wind pressure coefficients on the surface of a scale model corresponding to a low-rise, gable roof building	Wind tunnel tests	R^2	Excellent performance results
Predicting wind pressures around circular cylinders Hu and Kwok (2020)	RF, DT, GBRT	Gradient descent	Turbulence intensity, incoming wind, Reynolds number and circumferential angle of the cylinder	Mean and fluctuating wind pressures around a circular cylinder for high Reynolds numbers	From published papers e.g., Cheng et al. (2016), Gao et al. (2017)	R^2	GBRT outperformed all other models

TABLE 6 | Summary of ML applications for structural dynamics and damage assessment.

	Application	ML model	Training scheme	Input data	Output data	Data source	Performance metric	Remarks
i) Structural dynamics	Modeling hysteretic nonlinear behavior of bridge aerodynamics Wu and Kareem (2011)	ANN	Gradient descent	12 inputs: mean wind velocity in the current and next time steps, fluctuating components in the longitudinal and vertical direction in the current and next time steps, and the vertical and torsional displacement with their first and second derivatives in the current time step	Vertical (torsional) acceleration of the bridge deck section in the next time step	Tongji-1 wind tunnel at State Key Lab in Tongji University	No error metrics	- Cellular automata-based system was employed to optimize the ANN configuration - The visual inspection of the results indicated the good agreement between the simulated and measured - ANN model showed good promise in simulating the hysteretic nonlinear behavior of the bridge deck which interacts with the incoming fluctuating wind
	Analysis of tall building for across wind response Vyavahare et al. (2012)	ANN	Backpropagation	Building shape (height, breadth and depth), the terrain category and incoming wind speed	Shear force and bending moments of tall buildings	Data generated from numerical examples	No error metrics	From visual inspection, it can be concluded that a good agreement between the simulated and numerical results has been obtained
	Identification of the dynamic properties high-rise buildings subjected to wind Oh et al. (2017)	ERBFN	Genetic algorithm	Wind speed and direction	Column stress of a tall building subjected to wind loads	Wind tunnel tests	RMSE, maximum error between the measured and estimated values	Good simulation results were obtained
	Identification of the dynamic properties high-rise buildings subjected to wind Nikose and Sonparote (2019a); (2019b), (2020)	ANN	Backpropagation	Building geometry (height, breadth and depth), incoming wind velocity and terrain category	Dynamic response in the along-wind and across-wind in terms of base shear and base bending moment	Dataset were generated based on the Indian Wind Code (IWC) for various building configurations	RMSE	Good simulation results were obtained
	Wind-induced response estimation for tall buildings Oh et al. (2019)	CNN	Backpropagation	Top-level (top floor of a tall building) wind induced displacement in both time and frequency domain and measured wind speed in the	Maximum and minimum strains of the building columns	Wind tunnel tests	RMSE	Good simulation results were obtained

(Continued on following page)

TABLE 6 | (*Continued*) Summary of ML applications for structural dynamics and damage assessment.

	Application	ML model	Training scheme	Input data	Output data	Data source	Performance metric	Remarks
				frequency domain				
	Wind-induced nonlinear structural dynamic analysis Wang and Wu (2020)	KE-LSTM	AdaMax	Wavelet coefficients of the normalized wind excitation (external wind force)	Normalized structural displacement at different nodes	Numerically for the case of SDOF and MDOF	MAE	- The governing equation of motion was embedded within the loss function - Excellent simulation results
	Prediction of structural response of wind-excited tall buildings Micheli et al. (2020)	AWN	Backpropagation	Wind load and high-performance control systems (HPCS) characteristics	Maximum absolute acceleration of the structure	Dataset generated numerically corresponding to a 39-stoery steel-frame system building subjected to wind load and equipped with several equipment (e.g., damping devices, sensors and global controller)	RMSE	- AWN parameters were updated sequentially each time data arrives (online training) - Good simulation results
ii) Damage assessment	Constructing and validating geographically refined HAZUS-MH4 hurricane wind risk models Subramanian et al. (2013)	Ensemble models composed of 50 bagged DT	-	10 predictors were identified (e.g., number of floors, terrain roughness, wind speed and direction)	Classification: Structures that were correctly or not well predicted by HAZUS-MH4 (in terms of hurricane induced wind damage) in 1-km square blocks	The data contains the damage states and corresponds to approximately 700,000 residences in the Harris County following hurricane Ike (2008)	Accuracy (%) and customized error metric	- The results of this study suggest that HAZUS-MH4 fragility curves for certain home types, need to be refined to improve the prediction results
	Probabilistic damage estimation for asphalt shingle roofing Huang et al. (2015)	ANN	Backpropagation	8 predictors: wind speed, angle of attack, shingle resistance, building length, building width, building height, roof slope and surface roughness	Mean damage ratio of an asphalt shingle roof	Boundary-layer wind tunnel tests from the University of Western Ontario	Accuracy (%)	Good performance
	Estimatin of the fatigue damage of coastal bridges under coupled loads Zhu and Zhang (2018)	SVR (with Gaussian kernel)	-	Gross vehicle weight; 10-min wind speed; significant wave height; and peak wave period	Daily equivalent fatigue damage accumulation	Traffic data from a cable-stayed bridge located in southern China coastal regions & the wind/wave data from Meteorological Observatory near the bridge location from 1980 to 2012	RMSE, MAE, MAPE	Good simulation results were obtained
	Performance assessment of a vertical structure subjected to non-stationary, tornadic wind	ANN	Levenberg-Marquadt	Maximum mean tangential velocity of the tornado and its radial length scale	Fragility values associated with each intensity measures combination	Numerically generated in which the Monte Carlo simulation was employed	Absolute differences	Various architectures were tested and the best ANN model has one

(Continued on following page)

TABLE 6 | (*Continued*) Summary of ML applications for structural dynamics and damage assessment.

Application	ML model	Training scheme	Input data	Output data	Data source	Performance metric	Remarks
loads Le and Caracoglia (2020)							hidden layer with 4 neurons
Object detection in aerial imagery for disaster response and recovery after the occurrence of hurricanes Pi et al. (2020)	Series of CNN trained using transfer learning	Backpropagation	Digital images and videos	Bounding boxes of the ground objects of interest (i.e., flooded area, building roofs damage, debris, vegetation and cars) and their corresponding class labels (e.g., damaged or undamaged)	-The models were pretrained on the common objects in context/visual object classes (COCO/VOC) databases Everingham et al. (2010); Lin et al. (2017) - Then they were retrained on new aerial video dataset Volan 2018 (corresponding to hurricanes that occurred in 2017–2018) obtained using web mining algorithms	Mean average precision	Acceptable results

developed in recent years for simultaneously achieving high simulation accuracy and efficiency. The performance-based (and further resilience-ba sed) wind design philosophies also require accurate damage assessment of structures and infrastructure under extreme storms. The structural damages under winds depend on numerous factors including wind features (e.g., wind speed/direction and topography) and built environment characteristics (e.g., building opening and roof slope), hence its assessment and quantification are extremely challenging. On the other hand, increasingly available field-measurement data characterizing structural damages under strong wind events [e.g., resulting from post-disaster reconnaissance activities such NHERI Natural Hazards Reconnaissance (RAPID) Facility and NSF Structural Extreme Events Reconnaissance (StEER) Network] provide a great opportunity to learn from data by using various ML models. The ML applications for structural dynamics are first reviewed in **Table 6i** and then followed by damage assessment in **Table 6ii**, where the ML model, training scheme, input data, output data, data source and performance metric are summarized for each application. The training/testing data were essentially retrieved from numerical simulations, wind tunnel tests and field measurements. From **Table 6**, it can be concluded that most applications used ML as a regression model for modeling structural dynamics and as a regression or a classification model for structural damage assessment. While many applications employed simple ML models and standard training schemes (e.g., ANN with backpropagation), some advanced schemes such as knowledge-enhanced LSTM have been successfully applied to predict time series of wind-induced nonlinear structural response. It is noted that the selection of the most appropriate set of inputs to ML models for damage assessment (predictors or features) is still very challenging.

3.5 Mitigation and Response

Both long-term and short-term strategies are needed to enhance resilience of individual structures or communities to withstand wind-related hazards. One important long-term consideration is to mitigate structural response/vibration subjected to winds through structural optimization and/or control. For structural optimization under winds, the shape optimization is probably the most effective approach to reduce aerodynamic loading. For wind-induced vibration control, both aerodynamic and mechanical measures are well recognized in wind engineering community. Although the structural performance evaluation under winds is typically a very complicated task, the corresponding simulations during optimization or (active) control process is required to be efficient and accurate because they need to be conducted either repeatedly for numerous scenarios or in a (near) real-time sense. As noted earlier, the ML models are very promising to simultaneously achieve the high simulation efficiency and accuracy goal. In addition, the RL models that have gained increasing popularity in recent years can be used as very effective optimization or control algorithms compared to conventional approaches (Silver et al., 2017). In the consideration of short-term actions, efficient management strategies are critically important. Although the ML models used in the disaster (including wind-related hazard) management framework (i.e., covering preparedness, response and recovery) have recently been systematically reviewed (e.g., Sun et al., 2020), its applications to social media-informed response are still discussed here since the unprecedentedly

TABLE 7 | Summary of ML applications for mitigation and response.

	Application	ML model	Training scheme	Input data	Output data	Data source	Performance metric	Remarks
i) Structural optimization & control under winds	Vibration control of wind-induced response of tall buildings with active tuned mass damper Bani-Hani (2007)	ANN (2 models)	Backpropagation	ANN1&2: 20 inputs-absolute wind-induced acceleration of 3 selected floors at the current and previous 4-time steps, and the active tuned mass damper control forces at the current and previous 4-time steps	ANN1: 4-time steps ahead the absolute acceleration of three floors (i.e., 50th, 60th and 70th) ANN2: future control force at the next time step of the active tuned mass damper	Numerically generated using a SIMULINK model with a total of 50 s of data and a sampling time of 0.001s for a tall building with 76-stoery (data generated with and without random white noise control force of up to 5 Hz frequency)	RMS and defined dimensionless performance indexes	The coupled ANN models were able to reduce substantially the peak displacement and the absolute acceleration response of the building storeys
	Aerodynamic shape optimization of tall buildings Elshaer et al. (2016), (2017)	ANN with a genetic algorithm	-	Geometric variables of the cross section and the wind angle of attacks	Objective function = the mean drag coefficient or the standard deviation of the lift coefficient	LES simulations of a two-dimensional flow corresponding to different geometric properties of the cross section	R^2	- Good simulation results - Significant optimization of the mean drag coefficient and standard deviation of the lift coefficient
	Aerodynamic shape optimization of tall buildings Li et al. (2021a)	KE-DRL	Gradient descent	State: external shape of the structure	Action: design adjustment of the cross section to maximize the aerodynamic mitigation (by minimizing the drag of a high-rise building)	RANS and LES simulation of a 2-D cross section example	-	- Both specific direct-domain and cross-domain knowledge are leveraged through transfer-learning and meta-learning - The deep deterministic policy gradient algorithm (DDPG) was used for the RL algorithm - RL-based shape optimizer outperformed the basic gradient descent, particle swarm optimization (PSO) and typical RL without knowledge
	Bluff body active flow control in experiments and simulations Fan et al. (2020)	DRL	Adam	States: drag and lift coefficients	Action: ratio of the rotation rate for each rotating cylinder and the maximum rotation rate to minimize the drag in both simulations and experiments	Entropy-viscosity-based large eddy simulation (LES) (for the numerical simulation) and an experimental setup	-	-The Twin Delayed Deep Deterministic policy gradient algorithm was selected as the RL-algorithm to update the agent - The RL-agent was capable to efficiently learn a control strategy, for both experiment and simulation, that will allow the reattachment of flow behind the cylinder and reduce the drag coefficient
ii) Disaster response informed by social media	Information classification from disaster-related messages in twitter Imran et al. (2013)	NB (2 classifiers)	-	NB1: tweets	NB1: classification of tweets as personal, direct informative, indirect informative direct-indirect informative and other following the tornado event in Joplin, Missouri (2011)	206,764 tweets collected during the Joplin tornado of 2011 in Joplin, Missouri	F1 score	Acceptable performance

(Continued on following page)

TABLE 7 | (*Continued*) Summary of ML applications for mitigation and response.

Application	ML model	Training scheme	Input data	Output data	Data source	Performance metric	Remarks
			NB2: informative tweets	NB2: classification of informative tweets as caution, donation, advice, or information source			
Classification of tweets to inform disaster response Ashktorab et al. (2014)	SLDA, LR, KNN, NB, DT	-	Tweets	Classification of tweets to identify those that reported human casualties or structural damage (requiring intervention)	17 million tweets collected during 12 different natural disasters in the U.S since 2006 (e.g., tornado and hurricane)	AUC	The LR was the best classifier
Information classification from disaster-related messages in twitter Imran et al. (2016)	RF, SVM, NB	-	Tweets	9 classes (e.g., injured or dead people, infrastructure and utilities damage, displaced people and evacuations, caution and advice)	52 million tweets for events related to 19 natural hazards and crisis (e.g., typhoon, floods and earthquake) occurring between 2013 and 2015 in different parts of the world was used	Area under ROC curve	- Good results were obtained for all classes (for the three classifiers) except for the "*missing trapped or found people*" - poor classification-
Information classification from disaster-related events O'Neal et al. (2018)	SVM, KNN, GNB, MNB, BNB, DT, SGD	-	Images	Image classes in terms of human roles: rescuees or rescuers	The images were collected from August 17th to 3 September 2017 based on private social media platforms (e.g., twitter) during Hurricane Harvey (2017)	Average precision	SVM-based model gave the best prediction accuracy
Real-time disaster communication Robertson et al. (2019)	VGG-16 CNN, ANN	Adam	Tweeter-based images	VGG-16 CNN: informative features (pre-storm, landfall and the period after landfall) ANN: urgency level (highly urgent, moderately urgent, somewhat urgent, not urgent, and unrelated to the hurricane event)	A total of 17,483 images were extracted from Twitter between 17th August and 17 September 2017 from Hurricane Harvey (2017)	Accuracy	Acceptable simulation results
Information classification from disaster-related events Manna and Nakai (2019)	ANN, SVM, NB, LR	-	Tweets	2 classes: crisis-related tweets and non-crisis-related tweets	6 crisis related datasets were used (e.g., hurricane Harvey 2017 and the 2011 Joplin Tornado) with approximately 10,000 tweets for each event	Accuracy	ANN classifier outperformed all other classifiers
Real-time information classification from hurricane-related events Yu et al., (2019)	CNN, SVM, LR	RMSprop	Tweets	5 classes: Information Sources, Caution and Advice, Infrastructure and Resources, Casualties and Damage, and Donation and Aid	3 manually labeled datasets were used corresponding to hurricane Sandy (2012), Irma (2017) and Harvey (2017), respectively with approximatively 2000–3000 tweets per each event	Accuracy	CNN outperformed other classifiers
Identification of social media-based requests for urgent help during hurricanes Devaraj et al., (2020)	DT, SVM, ANN, LR, NB, AdaBoost, RR	-	Tweets	Tweets from people requiring or not urgent rescue by first responders	2,072,715 tweets related to Hurricane Harvey (2017) event	F1-score	CNN, SVM and ANN achieve the best simulation results

abundant data from various powerful communication tools (e.g., Twitter) greatly facilitate the rapid ML model developments in this field. **Table 7i,ii** respectively present the reviewed applications of ML for mitigation and response, where the ML model, training scheme, input data, output data, data source and performance metric are summarized for each application. The training/testing data were essentially retrieved from CFD simulations and experimental tests for structural mitigation or

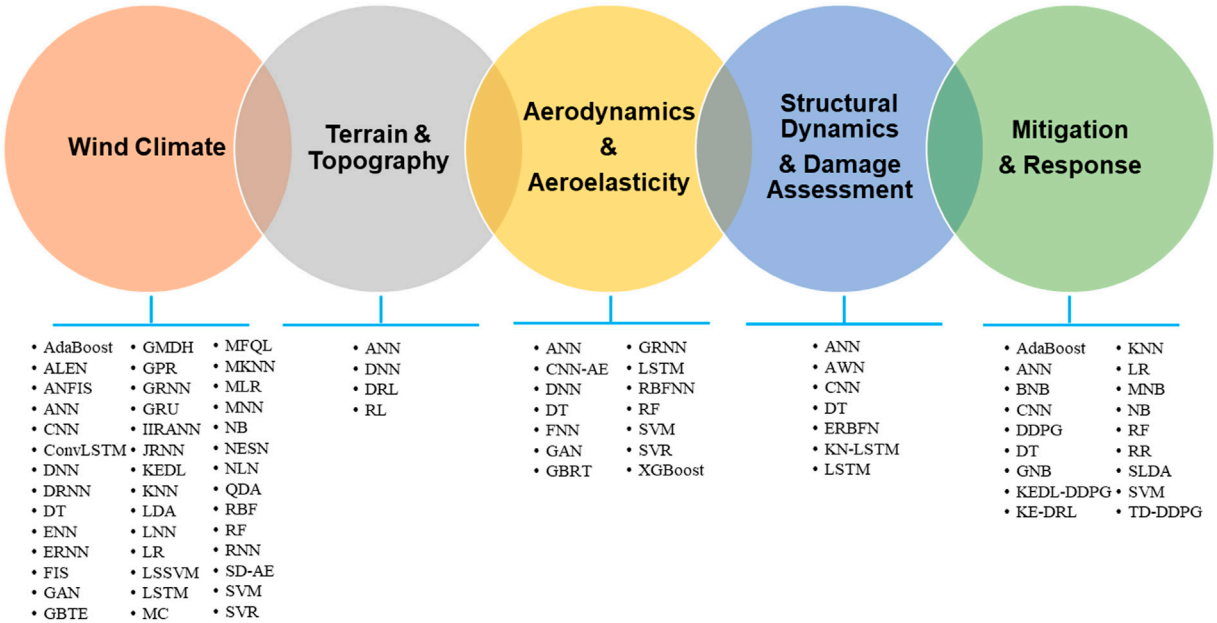

FIGURE 8 | Overview of reviewed ML applications in wind engineering (following Alan G. Davenport Wind Loading Chain).

from social media platforms for disaster response. From **Table 7i**, it can be concluded that the structural performance evaluations in mitigation applications usually used ML as a regression model while RL was typically utilized as an effective optimization or control algorithm. It is noted that relatively few ML applications for structural optimization and control under winds have been generated compared to those in earthquake engineering community (e.g., Ghaboussi and Joghataie 1995; Adam and Smith 2008; Jiang and Adeli 2008; Yakut and Alli 2011; Subasri et al., 2014; Khodabandehlou et al., 2018; Khalatbarisoltani et al., 2019; Hayashi and Ohsaki 2020). From **Table 7ii**, it can be concluded that most social media-informed response applications used ML as a classification model for disaster rescue and relief information dissemination. Although these ML applications present promising results in terms of effectively supporting timely decision-making, there is a concern of using information from social media platforms due to a lack of data quality control.

3.6 Summary

The ML applications in each topical area of wind engineering are summarized in **Figure 8**. As shown in the figure, ML models are unevenly distributed among these areas. The wind climate area has the most ML applications followed by the aerodynamics and aeroelasticity area, and they are respectively contributed by wind engineering-related fields of meteorology and fluid mechanics. On the other hand, the wind engineering-exclusive field of terrain and topography has the least applications of ML. Although ML models have been instrumental in modern structural design for winds, their developments are in a very preliminary stage and there is still a long way to go before they can complement or even replace existing approaches of wind tunnel tests and CFD simulations. In general, the supervised learning dominates the ML applications in wind engineering with the podium position attributed to simple models with standard algorithms (e.g., ANN with backpropagation). Actually, the selection of various ML models is rather rudimentary since there is a lack of systematic comparison among them (e.g., in terms of model complexity and performance). It is noted that the great potential of semi-supervised learning and unsupervised learning (as well as RL) with little or no labelled data is not leveraged yet. Accordingly, the current ML developments in wind engineering heavily rely on available labelled data. For example, the ML applications to non-synoptic winds are much less than those of synoptic winds due essentially to the difficulty in obtaining the data of local and short-lived storms. On the other hand, the recent emergence of numerous ML applications to social media-informed disaster response is due mainly to the unprecedentedly abundant data from various powerful communication tools. For the reviewed ML applications, the training/testing data are retrieved from several major sources (e.g., field measurements, wind tunnel tests, numerical simulations and social media platforms). In the determination of ML model inputs and outputs, a good understanding of underlying physics of each application is critical to effectively select an appropriate set of predictors (ML inputs) while the output types heavily depend on the needs of traditional analysis procedure in each application (e.g., local wind pressures for building design and global wind forces for bridge design).

4 CHALLENGES AND PROSPECTS

The rapidly increasing ML applications to wind engineering have generated a large volume of datasets associated with a large set of

domain-specific algorithms. It is strongly believed that the platforms encouraging open sharing of these datasets and algorithms would greatly benefit the ML research progress in wind engineering. The openly available wind engineering datasets will greatly reduce efforts for their creation/collection and pre-processing, and open-source ML algorithms will save significant time for their re-implementation. The reduced need of time and effort to use the state-of-the-art or latest developed ML tools under such a culture of openness would spur interests among researchers in wind engineering, and hence result in more related ML applications. Moreover, the developed cyberinfrastructure to store and share data usually has a systematic curation procedure to ensure the high quality of its standardized benchmark datasets. Also, the open-source software allows the hidden bugs/tricks of ML algorithms to be easily uncovered and accordingly makes them more robust. In addition to availability, the reproducibility and testability of wind engineering data and domain-specific algorithms due to a culture of openness would also facilitate the adoption of the obtained transparent and trustworthy ML tools in real-world problems. Although the wind engineering community has started to embrace the prevalent openness of ML community (e.g., NHERI DesignSafe platform), the culture of openness is still in its early stage. It is expected that more incentives based on the existing reward system (e.g., a digital object identifier for each dataset or algorithm published by the platform) are needed to motivate the ML wind engineering community towards open science. Given a potential open-science environment with openly available datasets and open-source algorithms (supported by open-access scientific publications), some remaining challenges and future prospects are discussed in terms of data in wind engineering and algorithms in ML. It is noted that both challenge and prospect lists are not exhaustive.

4.1 Challenges and Research Gaps

The reviewed various ML models for a wide range of topics in wind engineering suggests that their cross field has recently attracted much interest. However, there are still numerous challenges to advance ML applications to wind engineering from conception and research into practice. These remaining challenges of data in wind engineering and algorithms in ML are discussed in this sub-section.

4.1.1 Wind Engineering Data Challenges

Wind engineering data could be rich in some dimensions but may be poor in others. For example, a large volume of flow data or pressure data could be obtained by one wind tunnel test (using advanced measurement systems with high resolution in space and high sampling rate in time), however, all these data would be located at a point in the Reynolds number dimension. For structural response under winds, most of the data are located in the linear elastic domain, while very limited nonlinear inelastic data needed to advance implementation of performance-based wind design are available. Another example is that the anemometric monitoring network typically generates abundant data in time dimension but sparse data in space. More importantly, it is usually very challenging or expensive to create extra points in currently data-scarce dimensions. Wind engineering data could be short in time span of their collection. For example, the climate changing impacts are not easy to be considered based on the currently available wind data since their record period is much shorter than the time scale of climate changing. Also, few structural performance data under winds are long enough to take the life-span deterioration behaviors into account. Essentially, the learning machine based on current wind-structure interaction data cannot be used for accurately predicting future long-term behaviors of the same wind-structure system. Wind engineering data could be highly heterogeneous for collaborative or large-scale ML applications. Many complex tasks (e.g., life-cycle performance evaluation of structures under winds) and/or real-world problems (e.g., hurricane resilience assessment of coastal communities) in wind engineering need collaborative efforts and/or large-scale implementations. The datasets generated from these activities may result from various CFD simulation tools or field measurement devices, and they are typically interpreted by different entities before sent to a central processing platform. Accordingly, significant processing efforts (e.g., data cleaning, data aggregation, dimension reduction and data standardization) are needed for these heterogeneous datasets with high variability of data types and formats (e.g., mixtures of structured, semi-structured and unstructured data). In addition, advanced powerful learning machines are necessary to generate new knowledge from large, heterogeneous sets of wind engineering data.

4.1.2 Machine Learning Algorithm Challenges

ML algorithms commonly-used in wind engineering are standard ones designed for solving problems in other fields (e.g., handwriting recognition or computer vision). While these classical algorithms (e.g., ANN with backpropagation) achieved great success for simple wind engineering applications, they are not necessarily concise and efficient. More importantly, the immediate applications of these popular algorithms to modern wind engineering (involving nonstationary and non-Gaussian wind flow, transient and nonlinear aerodynamics, nonlinear and inelastic structural dynamics, or time-variant wind-structure system under a changing climate) may be very challenging. On the other hand, the newly developed ML algorithms (e.g., advanced LSTM and GAN) need to be carefully scrutinized for their applicability to these complex problems. ML algorithms commonly-used in wind engineering are supervised ones that need a significant amount of labelled data. Although the cost of obtaining/collecting the data from various sources (e.g., numerical simulations, wind tunnel tests, or field measurements) is greatly reduced and accordingly unprecedented volume of data are increasingly available, these datasets may be limited to unlabeled due to a lack of sufficient human resources (with expert knowledge) for data labeling. ML algorithms commonly-used in wind engineering are purely data-driven ones that are usually consider as black boxes. Furthermore, currently available ML models usually present a conflict between their advances (and hence performance) and explainability. One important feature of human intelligence is the ability to explain the rationale behind its decisions to others, hence, the explainability of

learning machines is often an essential prerequisite for establishing a trust relationship between human intelligence and artificial intelligence. The highly non-transparent nature of ML algorithms may be acceptable for some applications in wind engineering (e.g., a CNN mapping the oncoming winds to pressure fields on or velocity fields around various bridge decks), however, it may be a clear drawback for many high-stake applications (e.g., evacuation planning or transportation infrastructure management under a landfalling hurricane) since any error in prediction may have catastrophic consequences. It is noted that the high-stake applications also place a high demand for quantification of uncertainties involved in ML algorithm selection, training and performance evaluation (along with data collection), whereas the formalization of uncertainty quantification for purely data-driven approaches is very challenging and not well established yet. ML algorithms commonly-used in wind engineering are typically selected based on past experience (or simply by "gut feeling") and the associated model hyperparameters (e.g., layer and neuron numbers, activation function and learning rate) are usually obtained by extensive trial and error. While the selected ML algorithms present good performance for the particular applications of interest, they are not necessarily an optimal choice. A systematic approach to identify the most appropriate ML model and associated best hyperparameters essentially needs a global optimization within a high dimensional space, and is currently very challenging for wind engineering applications.

4.2 Prospects and Future Directions

The remaining challenges, while not trivial, provide new research opportunities for the development of more effective ML tools. The identified prospects of data in wind engineering and algorithms in ML are discussed in this sub-section.

4.2.1 Wind Engineering Data Prospects

To generate/collect wind engineering data that are scarce in certain dimensions, advanced full-scale/laboratory/numerical tools and technologies need to be utilized or developed. In addition to large-scale facilities (e.g., WindEEE), various high-fidelity and efficient modern CFD techniques (e.g., hybrid large eddy simulation/Reynolds-averaged Navier-Stokes schemes) should be exploited to generate data of high-Reynolds number scenarios. The rational loading protocols for extreme wind performance cyclic testing of deformation-controlled MWFRS (Main Wind Force Resisting System) members need to be designed to generate the wind-induced nonlinear inelastic structural response data. Also, data reconstructions using linear/nonlinear dimensionality reduction techniques (e.g., singular value decomposition/autoencoder) should be employed to enhance spatial resolution of full-scale measurements. To generate/collect wind engineering data that cover sufficiently-long time span of structural behaviors, more reliable long-term structural health monitoring systems should be established in addition to high-fidelity modeling of aging and deterioration of wind-sensitive structures. For the consideration of wind engineering data under a changing climate, synthesized wind fields (resulting from tropical cyclones, extratropical cyclones or local non-synoptic storms) need to be generated by global climate models coupled with accurate and efficient downscaling exercises under projected climate conditions [e.g., various RCP (Representative Concentration Pathway) scenarios]. To effectively learn from heterogeneous data that need to be first unified, they can be efficiently processed by advanced big data analytics. For example, unsupervised or semi-supervised clustering techniques could be used for data cleaning, data fusion techniques of Kalman filters could be used for data aggregation, and linear principal component analysis or nonlinear self-organizing map could be used for dimensional reduction.

4.2.2 ML Algorithm Prospects

To facilitate ML applications to complex wind engineering problems, the state-of-the-art or latest algorithms emerging in ML community could be leveraged. For example, the GAN could be used for effectively generating nonstationary and non-Gaussian wind flow through its two competing sub-networks, the CNN could be employed for efficiently mapping oncoming winds to pressure fields (characterizing transient and nonlinear aerodynamics) on structures with an arbitrary shape because it is particularly good at handling input-output data with a known grid-like topology, the LSTM could be utilized for accurately simulating nonlinear and inelastic structural dynamics since its forget gates ensure a reliable consideration of long-term dependencies (where the structural response at the current time depends on not only the current wind load but also the load history), and the lifelong learning networks should be explored for adaptively modeling time-variant wind-structure system assuming their underlying parameters can be continuously modified to accommodate new data inputs. The direct or immediate applications of the advanced ML algorithms to complex wind engineering problems may not necessarily result in parsimonious models that may need specialized customization for each application. To reduce the demand for labelled data in ML applications to wind engineering, both unsupervised learning and semi-supervised learning (including physics-informed machine learning) are promising alternatives to popularly used supervised learning. In addition, advanced ML algorithms have been emerging (e.g., reservoir computing) for processing information generated by complicated dynamical systems using very small training datasets. To open the ML black box, model explainability and interpretability in wind engineering applications needs to be enhanced. Various general techniques have been developed to improve understanding of the ML model predictions, such as sensitivity analysis and layer-wise relevance propagation. On the other hand, the definitions of explainability and interpretability are typically domain dependent, hence, the domain knowledge in wind engineering should be leveraged for enhanced explainability/interpretability of each ML application. It is expected that the explainability/interpretability analysis (along with uncertain quantification) will likely become a fundamental building block for bounding the overall confidence in ML applications in wind engineering (parallel to verification and validation in CFD simulations). To enable an

automatic search of ML model hyperparameters in wind engineering applications, increasingly available optimization schemes with improved efficiency and accuracy (e.g., grid search, random search, Bayesian optimization and population-based training) can be utilized to find the best configuration for each task. On the other hand, it is believed that a practical guide to selection of ML models in wind engineering applications will greatly facilitate their appropriate use. The best practices for model selection in each application are essentially consistent with the principle of Ockham's razo by first testing simple linear ML models (due to their easy to implement and high model explainability), and then followed by more complex nonlinear models (without data overfitting). Among ML models with similar complexity, a predetermined performance metric is typically used for further model selection. Since iteration is generally needed in a purely performance-driven ML model selection, the domain knowledge is suggested to be utilized for a more effective search process.

4.3 Knowledge-Enhanced Machine Learning

As discussed in preceding sections, domain knowledge could be leveraged for improved selection of ML model and its inputs and outputs in wind engineering applications. Hence, a good understanding of fundamental physics and other types of domain knowledge underlying each subfield of wind engineering would enable more effective use of ML tools. It is noted that the fundamental physics in terms of governing equations is a special type of domain knowledge, and recent studies have demonstrated that the required labelled datasets could be significantly reduced by incorporating the underlying physics into training process (and hence enhancing the regularization mechanism) (e.g., Raissi et al., 2017a; 2017b). Other equation-based domain knowledge such as empirical/semi-empirical formulas were also employed as part of the loss function in deep learning to provide machine-readable prior knowledge that facilitates the effective regularization of the neural networks for simulations of tropical cyclone winds (Snaiki and Wu 2019) and nonlinear structural dynamics (Wang and Wu 2020). In addition, the equation-free domain knowledge has been integrated into a deep RL-based aerodynamic shape optimizer (via the transfer-learning and meta-learning techniques) to remarkably enhance the training efficiency for wind engineering applications (Li et al., 2021a). These emerging successful applications indicate that this novel scheme of knowledge-enhanced machine learning (KEML) could significantly enhance ML applications to wind engineering. To fully embrace the promising potential of KEML, systematic research efforts are needed to efficiently identify knowledge representations (invariances, physics equations, empirical formulas, probabilistic relations, logic rules, simulation results, field observations, human feedback, and others) in various subfields of wind engineering and then to effectively integrate them into each module of machine learning pipeline (data preparation, model selection, model training, and others). While domain knowledge could be employed to enhance purely data-driven ML tools, it is expected that learning machines could be utilized for harnessing data to discover new knowledge in wind engineering (e.g., governing laws characterizing transport of turbulence quantities or optimization of wind-structure system).

5 CONCLUDING REMARKS

A total of 65 machine learning (ML) algorithms were reviewed in terms of their applications to each topical area of wind engineering, namely wind climate, terrain/topography, aerodynamics/aeroelasticity, structural dynamics, wind damage assessment and wind-related hazard mitigation and response. The most ML applications were found in wind climate area, while the terrain/topography area had the least applications of ML. Although the ML-based wind engineering is fueled by the unprecedented volume of analytical, numerical, experimental and field-measurement data together with rapidly evolving learning algorithms and high-performance computational hardware, it is still at an early stage of development. Most of wind engineering applications employed supervised learning with standard ML models designed for solving problems in other fields, and the promising unsupervised and semi-supervised learning tools were rarely used to reduce the high demand of labelled data. For the selection of ML models and associated hyperparameters in wind engineering applications, it was typically based on expertise and extensive trial and error. In this review, the culture of openness, explainability/interpretability and uncertainty quantification were identified as important research gaps that need to be addressed in ML-based wind engineering community. Furthermore, the knowledge-enhanced machine learning was considered as a very promising scheme to enhance ML applications to wind engineering.

AUTHOR CONTRIBUTIONS

All authors contributed to the study conception and design, data collection, analysis and interpretation of results, drafted manuscript preparation, reviewed the results, and approved the final version of the manuscript.

REFERENCES

Abbas, T., Kavrakov, I., Morgenthal, G., and Lahmer, T. (2020). Prediction of Aeroelastic Response of Bridge Decks Using Artificial Neural Networks. *Comput. Structures* 231, 106198. doi:10.1016/j.compstruc.2020.106198

Abdi, D., Levine, S., and Bitsuamlak, G. "Application of an Artificial Neural Network Model for Boundary Layer Wind Tunnel Profile Development," in Proceedingsof the 11th Americas Conference on Wind Engineering, San Juan, Puerto Rico, June 2009.

Abdullah, S. A., Aswegan, K., Jaberansari, S., Klemencic, R., and Wallace, J. W. (2020). Performance of Reinforced Concrete Coupling Beams Subjected to

Simulated Wind Loading. *ACI Struct. J.* 117 (3), 283–295. doi:10.14359/51724555

Aboshosha, H., Bitsuamlak, G., and El Damatty, A. (2015). Turbulence Characterization of Downbursts Using LES. *J. Wind Eng. Ind. Aerodynamics* 136, 44–61. doi:10.1016/j.jweia.2014.10.020

Aboutabikh, M., Ghazal, T., Chen, J., Elgamal, S., and Aboshosha, H. (2019). Designing a Blade-System to Generate Downburst Outflows at Boundary Layer Wind Tunnel. *J. Wind Eng. Ind. Aerodynamics* 186, 169–191. doi:10.1016/j.jweia.2019.01.005

Adam, B., and Smith, I. F. (2008). Reinforcement Learning for Structural Control. *J. Comput. Civ. Eng.* 22 (2), 133–139. doi:10.1061/(asce)0887-3801(2008)22:2(133)

Adeli, H., and Yeh, C. (1989). Perceptron Learning in Engineering Design. *Computer-Aided Civil Infrastructure Eng.* 4 (4), 247–256.

Adrianto, I., Trafalis, T. B., and Lakshmanan, V. (2009). Support Vector Machines for Spatiotemporal Tornado Prediction. *Int. J. Gen. Syst.* 38, 759–776. doi:10.1080/03081070601068629

Alemany, S., Beltran, J., Perez, A., and Ganzfried, S. (2019). Predicting Hurricane Trajectories Using a Recurrent Neural Network. *Aaai* 33 (01), 468–475. doi:10.1609/aaai.v33i01.3301468

Ali, M. M., Kishtawal, C. M., and Jain, S. (2007). Predicting Cyclone Tracks in the north Indian Ocean: An Artificial Neural Network Approach. *Geophys. Res. Lett.* 34 (4), L04603. doi:10.1029/2006gl028353

American Society of Civil Engineers (2017). *Minimum Design Loads and Associated Criteria for Buildings and Other Structures*. Reston, VA: Structural Engineering Institute of American Society of Civil Engineers.

American Society of Civil Engineers (2021). *Minimum Design Loads for Buildings and Other Structures*. Reston, VA: Structural Engineering Institute of American Society of Civil Engineers.

Asano, K., Iida, Y., and Uematsu, Y. (2019). Laboratory Study of Wind Loads on a Low-Rise Building in a Downburst Using a Moving Pulsed Jet Simulator and Their Comparison with Other Types of Simulators. *J. Wind Eng. Ind. Aerodynamics* 184, 313–320. doi:10.1016/j.jweia.2018.11.034

Ashktorab, Z., Brown, C., Nandi, M., and Culotta, A. "Tweedr: Mining Twitter to Inform Disaster Response," in Proceedings of the 11th International ISCRAM Conference, Pennsylvania, USA, May 2014, 269–272.

Ashton, R., Refan, M., Iungo, G. V., and Hangan, H. (2019). Wandering Corrections from PIV Measurements of Tornado-like Vortices. *J. Wind Eng. Ind. Aerodynamics* 189, 163–172. doi:10.1016/j.jweia.2019.02.010

Baik, J.-J., and Paek, J.-S. (2000). A Neural Network Model for Predicting Typhoon Intensity. *J. Meteorol. Soc. Jpn.* 78 (6), 857–869. doi:10.2151/jmsj1965.78.6_857

Bailey, P. A., and Kwok, K. C. S. (1985). Interference Excitation of Twin Tall Buildings. *J. Wind Eng. Ind. Aerodynamics* 21 (3), 323–338. doi:10.1016/0167-6105(85)90043-1

Baker, C. J., and Sterling, M. (2017). Modelling Wind fields and Debris Flight in Tornadoes. *J. Wind Eng. Ind. Aerodynamics* 168, 312–321. doi:10.1016/j.jweia.2017.06.017

Bani-Hani, K. A. (2007). Vibration Control of Wind-induced Response of Tall Buildings with an Active Tuned Mass Damper Using Neural Networks. *Struct. Control. Health Monit.* 14 (1), 83–108. doi:10.1002/stc.85

Barbounis, T. G., Theocharis, J. B., Alexiadis, M. C., and Dokopoulos, P. S. (2006). Long-term Wind Speed and Power Forecasting Using Local Recurrent Neural Network Models. *IEEE Trans. Energ. Convers.* 21 (1), 273–284. doi:10.1109/tec.2005.847954

Bengio, Y., Simard, P., and Frasconi, P. (1994). Learning Long-Term Dependencies with Gradient Descent Is Difficult. *IEEE Trans. Neural Netw.* 5 (2), 157–166. doi:10.1109/72.279181

Berg, J., Mann, J., and Patton, E. G. (2013). Lidar-observed Stress Vectors and Veer in the Atmospheric Boundary Layer. *J. Atmos. oceanic Technol.* 30 (9), 1961–1969. doi:10.1175/jtech-d-12-00266.1

Berggren, K., Xia, Q., Likharev, K. K., Strukov, D. B., Jiang, H., Mikolajick, T., et al. (2020). Roadmap on Emerging Hardware and Technology for Machine Learning. *Nanotechnology* 32 (1), 012002. doi:10.1088/1361-6528/aba70f

Bitsuamlak, G., Stathopoulos, T., and Bedard, C. (2006). Effects of Upstream Two-Dimensional hills on Design Wind Loads: a Computational Approach. *Wind and Structures* 9 (1), 37–58. doi:10.12989/was.2006.9.1.037

Bitsuamlak, G. T., Bédard, C., and Stathopoulos, T. (2007). Modeling the Effect of Topography on Wind Flow Using a Combined Numerical-Neural Network Approach. *J. Comput. Civ. Eng.* 21 (6), 384–392. doi:10.1061/(asce)0887-3801(2007)21:6(384)

Bitsuamlak, G. T. (2004). "Evaluating the Effect of Topographic Elements on Wind Flow: a Combined Numerical Simulation-Neutral Network Approach," (Montreal, Quebec, Canada: Concordia University). Doctoral dissertation.

Bitsuamlak, G. T., Stathopoulos, T., and Bédard, C. "Neural Network Predictions of Wind Flow over Complex Terrain," in 4th Structural Specialty Conf. of the Canadian Society for Civil Engineering, Whistler, BC Canada, May 2002.

Blessmann, J., and Riera, J. D. (1985). Wind Excitation of Neighbouring Tall Buildings. *J. wind Eng. Ind. aerodynamics* 18 (1), 91–103. doi:10.1016/0167-6105(85)90076-5

Blocken, B. (2014). 50 Years of Computational Wind Engineering: Past, Present and Future. *J. Wind Eng. Ind. Aerodynamics* 129, 69–102. doi:10.1016/j.jweia.2014.03.008

Bluestein, H. B. (2021). "The Types of Non-synoptic Wind Systems," in *The Oxford Handbook of Non-synoptic Wind Storms*. Editors H. Hangan and A. Kareem (Oxford, United Kingdom: Oxford University Press). doi:10.1093/oxfordhb/9780190670252.013.1

Bre, F., Gimenez, J. M., and Fachinotti, V. D. (2018). Prediction of Wind Pressure Coefficients on Building Surfaces Using Artificial Neural Networks. *Energy and Buildings* 158, 1429–1441. doi:10.1016/j.enbuild.2017.11.045

Breiman, L. (2001). Random Forests. *Mach Learn.* 45, 5–32. doi:10.1023/a:1010933404324

Brunton, S. L., Noack, B. R., and Koumoutsakos, P. (2020). Machine Learning for Fluid Mechanics. *Annu. Rev. Fluid Mech.* 52, 477–508. doi:10.1146/annurev-fluid-010719-060214

Cermak, J. E. (1975). Applications of Fluid Mechanics to Wind Engineering—A Freeman Scholar Lecture. *J. Fluids Eng.* 97 (1), 9–38. doi:10.1115/1.3447225

Chakrabarty, H., Murthy, C. A., and Gupta, A. D. (2013). Application of Pattern Recognition Techniques to Predict Severe Thunderstorms. *Ijcte* 5 (6), 850–855. doi:10.7763/ijcte.2013.v5.810

Chaudhuri, S., Dutta, D., Goswami, S., and Middey, A. (2013). Intensity Forecast of Tropical Cyclones over North Indian Ocean Using Multilayer Perceptron Model: Skill and Performance Verification. *Nat. Hazards* 65 (1), 97–113. doi:10.1007/s11069-012-0346-7

Chaudhuri, S., and Middey, A. (2011). Adaptive Neuro-Fuzzy Inference System to Forecast Peak Gust Speed during Thunderstorms. *Meteorology Atmos. Phys.* 114 (3-4), 139. doi:10.1007/s00703-011-0158-4

Chen, C. H., Wu, J. C., and Chen, J. H. (2008). Prediction of Flutter Derivatives by Artificial Neural Networks. *J. wind Eng. Ind. aerodynamics* 96 (10-11), 1925–1937. doi:10.1016/j.jweia.2008.02.044

Chen, G., and Lombardo, F. T. (2020). An Automated Classification Method of Thunderstorm and Non-thunderstorm Wind Data Based on a Convolutional Neural Network. *J. Wind Eng. Ind. Aerodynamics* 207, 104407. doi:10.1016/j.jweia.2020.104407

Chen, R., Wang, X., Zhang, W., Zhu, X., Li, A., and Yang, C. (2019). A Hybrid CNN-LSTM Model for Typhoon Formation Forecasting. *Geoinformatica* 23 (3), 375–396. doi:10.1007/s10707-019-00355-0

Chen, R., Zhang, W., and Wang, X. (2020). Machine Learning in Tropical Cyclone Forecast Modeling: A Review. *Atmosphere* 11 (7), 676. doi:10.3390/atmos11070676

Chen, Y., and Duan, Z. (2018). A Statistical Dynamics Track Model of Tropical Cyclones for Assessing Typhoon Wind hazard in the Coast of Southeast China. *J. Wind Eng. Ind. Aerodynamics* 172, 325–340. doi:10.1016/j.jweia.2017.11.014

Chen, Y., Kopp, G. A., and Surry, D. (2002). Interpolation of Wind-Induced Pressure Time Series with an Artificial Neural Network. *J. Wind Eng. Ind. Aerodynamics* 90 (6), 589–615. doi:10.1016/s0167-6105(02)00155-1

Chen, Y., Kopp, G. A., and Surry, D. (2003). Prediction of Pressure Coefficients on Roofs of Low Buildings Using Artificial Neural Networks. *J. wind Eng. Ind. aerodynamics* 91 (3), 423–441. doi:10.1016/s0167-6105(02)00381-1

Chen, Z., Yu, X., Chen, G., and Zhou, J. "Cyclone Intensity Estimation Using Multispectral Imagery from the FY-4 Satellite," in Proceedings of the 2018 International Conference on Audio, Language and Image Processing (ICALIP), Shanghai, China, July 2018 (Piscataway, New Jersey, United States: IEEE), 46–51.

Cheng, X. X., Zhao, L., and Ge, Y.-J. (2016). Field Measurements on Flow Past a Circular cylinder in Transcritical Reynolds Number Regime. *Acta Phys. Sin.* 65 (21), 214701. doi:10.7498/aps.65.214701

Cherkassky, V., and Mulier, F. M. (2007). *Learning from Data: Concepts, Theory, and Methods*. Hoboken, New Jersey, United States: John Wiley & Sons.

Chitsazan, M. A., Sami Fadali, M., and Trzynadlowski, A. M. (2019). Wind Speed and Wind Direction Forecasting Using echo State Network with Nonlinear Functions. *Renew. Energ.* 131, 879–889. doi:10.1016/j.renene.2018.07.060

Chowdhury, J., and Wu, T. (2021). "Aerodynamic Loading Due to Non-synoptic Wind Systems," in *The Oxford Handbook of Non-synoptic Wind Storms*. Editors H. Hangan and A. Kareem (Oxford, United Kingdom: Oxford University Press), 337.

Chung, J., Lee, S. W., Chang, S., and Kim, Y. S. "Estimation of Flutter Derivatives of Various Sections Using Numerical Simulation and Neural Network," in The 2012 World Congress on Advances in Civil, Environmental, and Materials Research (ACEM' 12), Seoul, Korea, August 26-30, 2012.

Coffer, B., Kubacki, M., Wen, Y., Zhang, T., Barajas, C. A., and Gobbert, M. K. (2020). "Using Machine Learning Techniques for Supercell Tornado Prediction with Environmental Sounding Data," in *Tech. Rep. HPCF–2020–18, UMBC High Performance Computing Facility* (Baltimore County: University of Maryland).

Collins, W. G., and Tissot, P. (2016). *Thunderstorm Predictions Using Artificial Neural networksArtificial Neural Networks-Models and Applications*. London: IntechOpen.

Collins, W., and Tissot, P. (2015). An Artificial Neural Network Model to Predict Thunderstorms within 400 Km2 South Texas Domains. *Met. Apps* 22 (3), 650–665. doi:10.1002/met.1499

Cortes, C., and Vapnik, V. (1995). Support-vector Networks. *Mach Learn.* 20 (3), 273–297. doi:10.1007/bf00994018

Cui, W., and Caracoglia, L. (2019). A New Stochastic Formulation for Synthetic hurricane Simulation over the north Atlantic Ocean. *Eng. Structures* 199, 109597. doi:10.1016/j.engstruct.2019.109597

Davenport, A. G. (1960). Rationale for Determining Design Wind Velocities. *J. Struct. Div.* 86 (5), 39–68. doi:10.1061/jsdeag.0000521

Deierlein, G. G., and Zsarnóczay, A. (2021). *State of the Art in Computational Simulation for Natural Hazards Engineering*. Second Edition. Plano, Texas: Center Comput. Modeling Simulation. SimCenter.

DeMaria, M., Mainelli, M., Shay, L. K., Knaff, J. A., and Kaplan, J. (2005). Further Improvements to the Statistical hurricane Intensity Prediction Scheme (SHIPS). *Weather Forecast.* 20 (4), 531–543. doi:10.1175/waf862.1

Deng, L., and Yu, D. (2014). Deep Learning: Methods and Applications. *Foundations Trends. Signal. Processing* 7 (3–4), 197–387. doi:10.1561/2000000039

Derkevorkian, A., Hernandez-Garcia, M., Yun, H.-B., Masri, S. F., and Li, P. (2015). Nonlinear Data-Driven Computational Models for Response Prediction and Change Detection. *Struct. Control. Health Monit.* 22 (2), 273–288. doi:10.1002/stc.1673

Devaraj, A., Murthy, D., and Dontula, A. (2020). Machine-learning Methods for Identifying Social media-based Requests for Urgent Help during Hurricanes. *Int. J. Disaster Risk Reduction* 51, 101757. doi:10.1016/j.ijdrr.2020.101757

Diaz, J., and Joseph, M. B. (2019). Predicting Property Damage from Tornadoes with Zero-Inflated Neural Networks. *Weather Clim. Extremes* 25, 100216. doi:10.1016/j.wace.2019.100216

Dissanayake, M. W. M. G., and Phan-Thien, N. (1994). Neural-network-based Approximations for Solving Partial Differential Equations. *Commun. Numer. Meth. Engng.* 10 (3), 195–201. doi:10.1002/cnm.1640100303

Duraisamy, K., Iaccarino, G., and Xiao, H. (2019). Turbulence Modeling in the Age of Data. *Annu. Rev. Fluid Mech.* 51, 357–377. doi:10.1146/annurev-fluid-010518-040547

Eguchi, Y., Hattori, Y., Nakao, K., James, D., and Zuo, D. (2018). Numerical Pressure Retrieval from Velocity Measurement of a Turbulent Tornado-like Vortex. *J. Wind Eng. Ind. Aerodynamics* 174, 61–68. doi:10.1016/j.jweia.2017.12.021

Elshaer, A., Bitsuamlak, G., and El Damatty, A. (2017). Enhancing Wind Performance of Tall Buildings Using Corner Aerodynamic Optimization. *Eng. Structures* 136, 133–148. doi:10.1016/j.engstruct.2017.01.019

Elshaer, A., Bitsuamlak, G., and El Damatty, A. "June. Aerodynamic Shape Optimization of Tall Buildings Using Twisting and Corner Modifications," in Proceedings of the 8th International Colloquium on Bluff Body Aerodynamics and Applications, June 2016Northeastern University. Boston, Massachusetts.

Emanuel, K., Ravela, S., Vivant, E., and Risi, C. (2006). A Statistical Deterministic Approach to hurricane Risk Assessment. *Bull. Amer. Meteorol. Soc.* 87 (3), 299–314. doi:10.1175/bams-87-3-299

Emanuel, K. (2003). Tropical Cyclones. *Annu. Rev. Earth Planet. Sci.* 31 (1), 75–104. doi:10.1146/annurev.earth.31.100901.141259

English, E. C., and Fricke, F. R. (1999). The Interference index and its Prediction Using a Neural Network Analysis of Wind-Tunnel Data. *J. Wind Eng. Ind. Aerodynamics* 83 (1-3), 567–575. doi:10.1016/s0167-6105(99)00102-6

Everingham, M., Van Gool, L., Williams, C. K. I., Winn, J., and Zisserman, A. (2010). The Pascal Visual Object Classes (Voc) challenge. *Int. J. Comput. Vis.* 88 (2), 303–338. doi:10.1007/s11263-009-0275-4

Facchini, L., Betti, M., and Biagini, P. (2014). Neural Network Based Modal Identification of Structural Systems through Output-Only Measurement. *Comput. Structures* 138, 183–194. doi:10.1016/j.compstruc.2014.01.013

Fahlman, S. E. (1988). "Faster-learning Variations of Back-Propagation: An Empirical Study," in *Proc. 1988 Connectionist Models Summer School*. Editors D. Touretzky, G. Hinton, and T. Sejnowski (San Mateo, CA: Morgan Kaufmann), 38–51.

Fang, G., Zhao, L., Cao, S., Ge, Y., and Pang, W. (2018). A Novel Analytical Model for Wind Field Simulation Under Typhoon Boundary Layer Considering Multi-Field Correlation and Height-Dependency. *J. Wind. Eng. Ind. Aerodyn.* 175, 77–89.

Fan, D., Yang, L., Wang, Z., Triantafyllou, M. S., and Karniadakis, G. E. (2020). Reinforcement Learning for bluff Body Active Flow Control in Experiments and Simulations. *Proc. Natl. Acad. Sci. USA* 117 (42), 26091–26098. doi:10.1073/pnas.2004939117

Fernández-Cabán, P. L., Masters, F. J., and Phillips, B. M. (2018). Predicting Roof Pressures on a Low-Rise Structure from Freestream Turbulence Using Artificial Neural Networks. *Front. Built Environ.* 4, 68. doi:10.3389/fbuil.2018.00068

Forthofer, J. M., Butler, B. W., McHugh, C. W., Finney, M. A., Bradshaw, L. S., Stratton, R. D., et al. (2014b). A Comparison of Three Approaches for Simulating fine-scale Surface Winds in Support of Wildland Fire Management. Part II. An Exploratory Study of the Effect of Simulated Winds on Fire Growth Simulations. *Int. J. Wildland Fire* 23 (7), 982–994. doi:10.1071/wf12090

Forthofer, J. M., Butler, B. W., and Wagenbrenner, N. S. (2014a). A Comparison of Three Approaches for Simulating fine-scale Surface Winds in Support of Wildland Fire Management. Part I. Model Formulation and Comparison against Measurements. *Int. J. Wildland Fire* 23 (7), 969–981. doi:10.1071/wf12089

Fu, J. Y., Li, Q. S., and Xie, Z. N. (2006). Prediction of Wind Loads on a Large Flat Roof Using Fuzzy Neural Networks. *Eng. Structures* 28 (1), 153–161. doi:10.1016/j.engstruct.2005.08.006

Fu, J. Y., Liang, S. G., and Li, Q. S. (2007). Prediction of Wind-Induced Pressures on a Large Gymnasium Roof Using Artificial Neural Networks. *Comput. structures* 85 (3-4), 179–192. doi:10.1016/j.compstruc.2006.08.070

Fukami, K., Nabae, Y., Kawai, K., and Fukagata, K. (2019). Synthetic Turbulent Inflow Generator Using Machine Learning. *Phys. Rev. Fluids* 4 (6), 064603. doi:10.1103/physrevfluids.4.064603

Gairola, A., and Bitsuamlak, G. (2019). Numerical Tornado Modeling for Common Interpretation of Experimental Simulators. *J. Wind Eng. Ind. Aerodynamics* 186, 32–48. doi:10.1016/j.jweia.2018.12.013

Gao, D.-L., Chen, W.-L., Li, H., and Hu, H. (2017). Flow Around a Circular cylinder with Slit. *Exp. Therm. Fluid Sci.* 82, 287–301. doi:10.1016/j.expthermflusci.2016.11.025

Ghaboussi, J., and Joghataie, A. (1995). Active Control of Structures Using Neural Networks. *J. Eng. Mech.* 121 (4), 555–567. doi:10.1061/(asce)0733-9399(1995)121:4(555)

Gholizadeh, S., Salajegheh, J., and Salajegheh, E. (2009). An Intelligent Neural System for Predicting Structural Response Subject to Earthquakes. *Adv. Eng. Softw.* 40 (8), 630–639. doi:10.1016/j.advengsoft.2008.11.008

Giffard-Roisin, S., Yang, M., Charpiat, G., Kumler Bonfanti, C., Kégl, B., and Monteleoni, C. (2020). Tropical Cyclone Track Forecasting Using Fused Deep Learning from Aligned Reanalysis Data. *Front. Big Data* 3, 1–13. doi:10.3389/fdata.2020.00001

Gillmeier, S., Sterling, M., and Hemida, H. (2019). Simulating Tornado-like Flows: the Effect of the Simulator's Geometry. *Meccanica* 54 (15), 2385–2398. doi:10.1007/s11012-019-01082-4

Goodfellow, I., Bengio, Y., and Courville, A. (2016). *Deep Learning*, 1. Cambridge: MIT press, 2.

Goodfellow, I., Pouget-Abadie, J., Mirza, M., Xu, B., Warde-Farley, D., Ozair, S., et al. (2014). "Generative Adversarial Nets," in *Advances in Neural Information Processing Systems*. Editors M. I. Jordan, Y. LeCun, and S. A. Solla (Cambridge, Massachusetts, United States: MIT Press), 2672–2680.

Gray, W. M. (1968). Global View of the Origin of Tropical Disturbances and Storms. *Mon. Wea. Rev.* 96 (10), 669–700. doi:10.1175/1520-0493(1968)096<0669:gvotoo>2.0.co;2

Gray, W. M. (1979). "Hurricanes: Their Formation, Structure and Likely Role in the Tropical Circulation. Meteorology over the Tropical Oceans," in *Meteorology over the Tropical Oceans*. Editor D. B. Shaw (James Glaisher House, Grenville, Bracknell: Royal Meteorological Society), 155–218.

Haines, M., and Taylor, I. (2018). Numerical Investigation of the Flow Field Around Low Rise Buildings Due to a Downburst Event Using Large Eddy Simulation. *J. Wind Eng. Ind. Aerodynamics* 172, 12–30. doi:10.1016/j.jweia.2017.10.028

Hall, T. M., and Jewson, S. (2007). Statistical Modelling of North Atlantic Tropical Cyclone Tracks. *Tellus A: Dynamic Meteorology and Oceanography* 59 (4), 486–498. doi:10.1111/j.1600-0870.2007.00240.x

Hangan, H., Refan, M., Jubayer, C., Romanic, D., Parvu, D., LoTufo, J., et al. (2017). Novel Techniques in Wind Engineering. *J. Wind Eng. Ind. Aerodynamics* 171, 12–33. doi:10.1016/j.jweia.2017.09.010

Hao, J., and Wu, T. (2018). Downburst-induced Transient Response of a Long-Span Bridge: A CFD-CSD-Based Hybrid Approach. *J. Wind Eng. Ind. Aerodynamics* 179, 273–286. doi:10.1016/j.jweia.2018.06.006

Hao, J., and Wu, T. (2017). Nonsynoptic Wind-Induced Transient Effects on Linear Bridge Aerodynamics. *J. Eng. Mech.* 143 (9), 04017092. doi:10.1061/(asce)em.1943-7889.0001313

Hao, J., and Wu, T. (2020). Numerical Analysis of a Long-Span Bridge Response to Tornado-like Winds. *Wind and Structures* 31 (5), 459–472.

Hao, J., and Wu, T. "Tornado-induced Effects on Aerostatic and Aeroelastic Behaviors of Long-Span Bridge," in Proceeding of the 2016 World Congress on Advances in Civil Environmental & Materials Research, Jeju, Korea, September 2016.

Hasegawa, K., Fukami, K., Murata, T., and Fukagata, K. "Data-driven Reduced Order Modeling of Flows Around Two-Dimensional bluff Bodies of Various Shapes," in Fluids Engineering Division Summer Meeting, American Society of Mechanical Engineers, San Francisco, CA, July 28–August 1, 2019, V002T02A075.

Hasegawa, K., Fukami, K., Murata, T., and Fukagata, K. (2020). Machine-learning-based Reduced-Order Modeling for Unsteady Flows Around bluff Bodies of Various Shapes. *Theor. Comput. Fluid Dyn.* 34, 367–383. doi:10.1007/s00162-020-00528-w

Hawbecker, P. (2021). "Mesoscale, Microscale, and Numerical Models," in *The Oxford Handbook of Non-synoptic Wind Storms*. Editors H. Hangan and A. Kareem (Oxford, United Kingdom: Oxford University Press), 239.

Hayashi, K., and Ohsaki, M. (2020). Reinforcement Learning for Optimum Design of a Plane Frame under Static Loads. *Eng. Comput.* 37, 1999–2011. doi:10.1007/s00366-019-00926-7

He, Y. C., Li, Y. Z., Chan, P. W., Fu, J. Y., Wu, J. R., and Li, Q. S. (2019). A Height-Resolving Model of Tropical Cyclone Pressure Field. *J. Wind. Eng. Ind. Aerodyn.* 186, 84–93.

Hinton, G. E., Osindero, S., and Teh, Y.-W. (2006). A Fast Learning Algorithm for Deep Belief Nets. *Neural Comput.* 18 (7), 1527–1554. doi:10.1162/neco.2006.18.7.1527

Hochreiter, S., and Schmidhuber, J. (1997). Long Short-Term Memory. *Neural Comput.* 9 (8), 1735–1780. doi:10.1162/neco.1997.9.8.1735

Holmes, J. D. (1999). "Modeling of Extreme Thunderstorm Winds for Wind Loading of Structures and Risk Assessment," in *Wind Engineering into the 21st Century, Proceedings of the Tenth International Conference on Wind Engineering, Copenhagen, Denmark, 21-24 June 1999*. Editor A. Larsen (Boca Raton, Florida, United States: CRC Press), 1409–1415.

Holton, J. R., and Hakim, G. J. (2013). *An Introduction to Dynamic Meteorology*. Fifth edition. Amsterdam: Academic Press.

Hopfield, J. J. (1982). Neural Networks and Physical Systems with Emergent Collective Computational Abilities. *Proc. Natl. Acad. Sci.* 79 (8), 2554–2558. doi:10.1073/pnas.79.8.2554

Hornik, K. (1991). Approximation Capabilities of Multilayer Feedforward Networks. *Neural networks* 4 (2), 251–257. doi:10.1016/0893-6080(91)90009-t

Hoshino, N., Iida, Y., and Uematsu, Y. (2018). Effects of Non-stationarity of Downburst on the Wind Loading of Buildings. *J. Wind Eng.* 43 (1), 1–13. doi:10.5359/jwe.43.1

Hou, F., and Sarkar, P. P. (2020). Aeroelastic Model Tests to Study Tall Building Vibration in Boundary-Layer and Tornado Winds. *Eng. Structures* 207, 110259. doi:10.1016/j.engstruct.2020.110259

Hu, G., and Kwok, K. C. S. (2020). Predicting Wind Pressures Around Circular Cylinders Using Machine Learning Techniques. *J. Wind Eng. Ind. Aerodynamics* 198, 104099. doi:10.1016/j.jweia.2020.104099

Hu, G., Liu, L., Tao, D., Song, J., Tse, K. T., and Kwok, K. C. S. (2020). Deep Learning-Based Investigation of Wind Pressures on Tall Building under Interference Effects. *J. Wind Eng. Ind. Aerodynamics* 201, 104138. doi:10.1016/j.jweia.2020.104138

Huang, D., Shiqing, H., Xuhui, H., and Xue, Z. (2017). Prediction of Wind Loads on High-Rise Building Using a BP Neural Network Combined with POD. *J. Wind Eng. Ind. Aerodynamics* 170, 1–17. doi:10.1016/j.jweia.2017.07.021

Huang, G., He, H., Mehta, K. C., and Liu, X. (2015). Data-based Probabilistic Damage Estimation for Asphalt Shingle Roofing. *J. Struct. Eng.* 141 (12), 04015065. doi:10.1061/(asce)st.1943-541x.0001300

Huang, W. F., and Xu, Y. L. (2013). Prediction of Typhoon Design Wind Speed and Profile over Complex Terrain. *Struct. Eng. Mech.* 45 (1), 1–18. doi:10.12989/sem.2013.45.1.001

Huang, W. Y., and Lippmann, R. P. (1988). "Neural Net and Traditional Classifiers," in *Neural Information Processing Systems*. Editor D. Z. Anderson (Berlin/Heidelberg, Germany: Springer Science & Business Media), 387–396.

Huo, S., Hemida, H., and Sterling, M. (2020). Numerical Study of Debris Flight in a Tornado-like Vortex. *J. Fluids Structures* 99, 103134. doi:10.1016/j.jfluidstructs.2020.103134

Iida, Y., and Uematsu, Y. (2019). Numerical Study of Wind Loads on Buildings Induced by Downbursts. *J. Wind Eng. Ind. Aerodynamics* 191, 103–116. doi:10.1016/j.jweia.2019.05.018

Imran, M., Elbassuoni, S., Castillo, C., Diaz, F., and Meier, P. "Extracting Information Nuggets from Disaster-Related Messages in Social media," in Proceedings of the 10th International Conference on Information Systems for Crisis Response and Management, Information Systems for Crisis Response and Management, Baden-Baden, Germany, May 2013, 791–801.

Imran, M., Mitra, P., and Castillo, C. "Twitter as a Lifeline: Human-Annotated Twitter Corpora for NLP of Crisis-Related Messages," in Proceedings of the Tenth International Conference on Language Resources and Evaluation (LREC 2016), European Language Resources Association (ELRA), Portorož, Slovenia, May 2016.

Ishihara, T., Oh, S., and Tokuyama, Y. (2011). Numerical Study on Flow fields of Tornado-like Vortices Using the LES Turbulence Model. *J. Wind Eng. Ind. Aerodynamics* 99 (4), 239–248. doi:10.1016/j.jweia.2011.01.014

Jackson, P. S., and Hunt, J. C. R. (1975). Turbulent Wind Flow over a Low hill. *Q.J R. Met. Soc.* 101 (430), 929–955. doi:10.1002/qj.49710143015

Jesson, M., Sterling, M., Letchford, C., and Haines, M. (2015). Aerodynamic Forces on Generic Buildings Subject to Transient, Downburst-type Winds. *J. wind Eng. Ind. aerodynamics* 137, 58–68. doi:10.1016/j.jweia.2014.12.003

Jiang, X., and Adeli, H. (2008). Dynamic Fuzzy Wavelet Neuroemulator for Non-linear Control of Irregular Building Structures. *Int. J. Numer. Meth. Engng* 74 (7), 1045–1066. doi:10.1002/nme.2195

Jiang, X., and Adeli, H. (2005). Dynamic Wavelet Neural Network for Nonlinear Identification of Highrise Buildings. *Comp-aided Civil Eng.* 20 (5), 316–330. doi:10.1111/j.1467-8667.2005.00399.x

Jubayer, C., Elatar, A., and Hangan, H., "Pressure Distributions on a Low-Rise Building in a Laboratory Simulated Downburst." in Proceedings of the 8th

International Colloquium on Bluff Body Aerodynamics and Applications, Boston, Massachusetts, USA. June 2016

Junayed, C., Jubayer, C., Parvu, D., Romanic, D., and Hangan, H. (2019). Flow Field Dynamics of Large-Scale Experimentally Produced Downburst Flows. *J. Wind Eng. Ind. Aerodynamics* 188, 61–79. doi:10.1016/j.jweia.2019.02.008

Jung, S., Ghaboussi, J., and Kwon, S.-D. (2004). Estimation of Aeroelastic Parameters of Bridge Decks Using Neural Networks. *J. Eng. Mech.* 130 (11), 1356–1364. doi:10.1061/(asce)0733-9399(2004)130:11(1356)

Kamangir, H., Collins, W., Tissot, P., and King, S. A. (2020). Deep-learning Model Used to Predict Thunderstorms within 400 Km2 of South Texas Domains. *Meteorol. Appl.* 27 (2), e1905. doi:10.1002/met.1905

Kareem, A. (2020). Emerging Frontiers in Wind Engineering: Computing, Stochastics, Machine Learning and beyond. *J. Wind Eng. Ind. Aerodynamics* 206, 104320. doi:10.1016/j.jweia.2020.104320

Kareem, A., and Wu, T. (2013). Wind-induced Effects on bluff Bodies in Turbulent Flows: Nonstationary, Non-gaussian and Nonlinear Features. *J. Wind Eng. Ind. Aerodynamics* 122, 21–37. doi:10.1016/j.jweia.2013.06.002

Kawaguchi, M., Tamura, T., and Kawai, H. (2019). Analysis of Tornado and Near-Ground Turbulence Using a Hybrid Meteorological Model/engineering LES Method. *Int. J. Heat Fluid Flow* 80, 108464. doi:10.1016/j.ijheatfluidflow.2019.108464

Kelley, H. J. (1960). Gradient Theory of Optimal Flight Paths. *Ars J.* 30 (10), 947–954. doi:10.2514/8.5282

Khalatbarisoltani, A., Soleymani, M., and Khodadadi, M. (2019). Online Control of an Active Seismic System via Reinforcement Learning. *Struct. Control. Health Monit.* 26 (3), e2298. doi:10.1002/stc.2298

Khanduri, A. C., Bédard, C., and Stathopoulos, T. (1997). Modelling Wind-Induced Interference Effects Using Backpropagation Neural Networks. *J. wind Eng. Ind. aerodynamics* 72, 71–79. doi:10.1016/s0167-6105(97)00259-6

Khodabandehlou, H., Pekcan, G., Fadali, M. S., and Salem, M. M. A. (2018). Active Neural Predictive Control of Seismically Isolated Structures. *Struct. Control. Health Monit.* 25 (1), e2061. doi:10.1002/stc.2061

Khosravi, A., Koury, R. N. N., Machado, L., and Pabon, J. J. G. (2018b). Prediction of Wind Speed and Wind Direction Using Artificial Neural Network, Support Vector Regression and Adaptive Neuro-Fuzzy Inference System. *Sustainable Energ. Tech. Assessments* 25, 146–160. doi:10.1016/j.seta.2018.01.001

Khosravi, A., Machado, L., and Nunes, R. O. (2018a). Time-series Prediction of Wind Speed Using Machine Learning Algorithms: A Case Study Osorio Wind Farm, Brazil. *Appl. Energ.* 224, 550–566. doi:10.1016/j.apenergy.2018.05.043

Kim, J., and Lee, C. (2020). Deep Unsupervised Learning of Turbulence for Inflow Generation at Various Reynolds Numbers. *J. Comput. Phys.* 406, 109216. doi:10.1016/j.jcp.2019.109216

Kim, M., Park, M.-S., Im, J., Park, S., and Lee, M.-I. (2019). Machine Learning Approaches for Detecting Tropical Cyclone Formation Using Satellite Data. *Remote Sensing* 11 (10), 1195. doi:10.3390/rs11101195

Kim, S., Kim, H., Lee, J., Yoon, S., Kahou, S. E., Kashinath, K., et al. "Deep-hurricane-tracker: Tracking and Forecasting Extreme Climate Events," in Proceedings of the 2019 IEEE Winter Conference on Applications of Computer Vision (WACV), Waikoloa, HI, USA, January 2019 (Piscataway, New Jersey, United States: IEEE), 1761–1769.

Kolmogorov, A. N. (1941). The Local Structure of Turbulence in Incompressible Viscous Fluid for Very Large Reynolds Numbers. *Cr Acad. Sci. URSS* 30, 301–305.

Križan, J., Gašparac, G., Kozmar, H., Antonić, O., and Grisogono, B. (2015). Designing Laboratory Wind Simulations Using Artificial Neural Networks. *Theor. Appl. climatology* 120 (3-4), 723–736. doi:10.1007/s00704-014-1201-4

Krizhevsky, A., Sutskever, I., and Hinton, G. E. (2012). Imagenet Classification with Deep Convolutional Neural Networks. *Adv. Neural Inf. Process. Syst.* 60, 84–90. doi:10.1145/3065386

Kuai, L., Haan, F. L. J., Jr., Gallus, W. A. J., Jr., and Sarkar, P. P. (2008). CFD Simulations of the Flow Field of a Laboratory-Simulated Tornado for Parameter Sensitivity Studies and Comparison with Field Measurements. *Wind and Structures* 11 (2), 75–96. doi:10.12989/was.2008.11.2.075

Kumar, G., and Malik, H. (2016). Generalized Regression Neural Network Based Wind Speed Prediction Model for Western Region of India. *Proced. Comput. Sci.* 93, 26–32. doi:10.1016/j.procs.2016.07.177

Kutz, J. N. (2017). Deep Learning in Fluid Dynamics. *J. Fluid Mech.* 814, 1–4. doi:10.1017/jfm.2016.803

Lagerquist, R. A., Homeyer, C. R., McGovern, A., Potvin, C. K., Sandmael, T., and Smith, T. M. "Deep Learning for Real-Time Storm-Based Tornado Prediction," in Proceedings of the 29th Conference on Severe Local Storms, Stowe, VT, October 2018 (Boston, Massachusetts, United States: AMS).

Lagerquist, R., McGovern, A., Homeyer, C. R., Gagne, D. J., and Smith, T. (2020). Deep Learning on Three-Dimensional Multiscale Data for Next-Hour Tornado Prediction. *Monthly Weather Rev.* 148, 2837–2861. doi:10.1175/mwr-d-19-0372.1

Lagerquist, R., McGovern, A., and Smith, T. (2017). Machine Learning for Real-Time Prediction of Damaging Straight-Line Convective Wind. *Weather Forecast.* 32 (6), 2175–2193. doi:10.1175/waf-d-17-0038.1

Lahouar, A., and Slama, J. B. H. "Wind Speed and Direction Prediction for Wind Farms Using Support Vector Regression." in Proceedings of the 2014 5th International Renewable Energy Congress (IREC). Hammamet, Tunisia. March 2014 (Piscataway, New Jersey, United States: IEEE), 1–6.

Lakshmanan, V., Stumpf, G., and Witt, A. "A Neural Network for Detecting and Diagnosing Tornadic Circulations Using the Mesocyclone Detection and Near Storm Environment Algorithms," in Proceedings of the AI Applications with a Nowcasting Flavor (Joint between the Fourth Conference on Artificial Intelligence and the 21st International Conference on Interactive Information and Processing Systems (IIPS) for Meteorology, Oceanography, and Hydrology), San Diego, CA, USA, January 2005 (Boston, Massachusetts, United States: AMS).

Le, V., and Caracoglia, L. (2020). A Neural Network Surrogate Model for the Performance Assessment of a Vertical Structure Subjected to Non-stationary, Tornadic Wind Loads. *Comput. Structures* 231, 106208. doi:10.1016/j.compstruc.2020.106208

LeCun, Y., Boser, B., Denker, J. S., Henderson, D., Howard, R. E., Hubbard, W., et al. (1989). Backpropagation Applied to Handwritten Zip Code Recognition. *Neural Comput.* 1 (4), 541–551. doi:10.1162/neco.1989.1.4.541

Letchford, C. W., Mans, C., and Chay, M. T. (2002). Thunderstorms—their Importance in Wind Engineering (A Case for the Next Generation Wind Tunnel). *J. Wind Eng. Ind. Aerodynamics* 90 (12-15), 1415–1433. doi:10.1016/s0167-6105(02)00262-3

Li, G., and Shi, J. (2010). On Comparing Three Artificial Neural Networks for Wind Speed Forecasting. *Appl. Energ.* 87 (7), 2313–2320. doi:10.1016/j.apenergy.2009.12.013

Li, S., Laima, S., and Li, H. (2018). Data-driven Modeling of Vortex-Induced Vibration of a Long-Span Suspension Bridge Using Decision Tree Learning and Support Vector Regression. *J. Wind Eng. Ind. Aerodynamics* 172, 196–211. doi:10.1016/j.jweia.2017.10.022

Li, S., Snaiki, R., and Wu, T. (2021a). A Knowledge-enhanced Deep Reinforcement Learning-based Shape Optimizer for Aerodynamic Mitigation of Wind-sensitive Structures. *Computer-Aided Civil Infrastructure Eng.* 36 (6), 733–746. doi:10.1111/mice.12655

Li, S., Snaiki, R., and Wu, T. (2021b). Active Simulation of Transient Wind Field in a Multiple-Fan Wind Tunnel via Deep Reinforcement Learning. *J. Eng. Mech.* 147 (9), 04021056. doi:10.1061/(asce)em.1943-7889.0001967

Li, T., Wu, T., and Liu, Z. (2020). Nonlinear Unsteady Bridge Aerodynamics: Reduced-Order Modeling Based on Deep LSTM Networks. *J. Wind Eng. Ind. Aerodynamics* 198, 104116. doi:10.1016/j.jweia.2020.104116

Li, Z., and Li, C. (2018). "Selection of Kernel Function for Least Squares Support Vector Machines in Downburst Wind Speed Forecasting," in Proceedings of the 2018 11th International Symposium on Computational Intelligence and Design (ISCID), Hangzhou, China (Piscataway, New Jersey, United States: IEEE), 337–341. doi:10.1109/iscid.2018.10178

Liang, X. (2019). Image-based post-disaster Inspection of Reinforced concrete Bridge Systems Using Deep Learning with Bayesian Optimization. *Computer-Aided Civil Infrastructure Eng.* 34 (5), 415–430. doi:10.1111/mice.12425

Lillicrap, T. P., Hunt, J. J., Pritzel, A., Heess, N., Erez, T., Tassa, Y., et al. (2015). Continuous Control with Deep Reinforcement Learning. *arXiv*. arXiv: 1509.02971.

Lin, T. Y., Goyal, P., Girshick, R., He, K., and Dollár, P. "Focal Loss for Dense Object Detection," in Proceedings of the IEEE international conference on computer vision, Venice, Italy, October 2017, 2980–2988. doi:10.1109/iccv.2017.324

Litta, A. J., Idicula, S. M., and Francis, C. N. (2012). Artificial Neural Network Model for the Prediction of Thunderstorms over kolkata. *Int. J. Comput. Appl.* 50 (11), 50–55. doi:10.5120/7819-1135

Liu, Z., Cao, Y., Cao, J., Wang, Y., and Cao, S. (2021). Numerical Study of Tornado-Borne Debris on a Low-Rise Building through Large Eddy Simulation. *J. Fluids Structures* 106, 103379. doi:10.1016/j.jfluidstructs.2021.103379

Liu, Z., and Ishihara, T. (2015). Numerical Study of Turbulent Flow fields and the Similarity of Tornado Vortices Using Large-Eddy Simulations. *J. Wind Eng. Ind. Aerodynamics* 145, 42–60. doi:10.1016/j.jweia.2015.05.008

López, P., Velo, R., and Maseda, F. (2008). Effect of Direction on Wind Speed Estimation in Complex Terrain Using Neural Networks. *Renew. Energ.* 33 (10), 2266–2272. doi:10.1016/j.renene.2007.12.020

Lute, V., Upadhyay, A., and Singh, K. K. (2009). Support Vector Machine Based Aerodynamic Analysis of cable Stayed Bridges. *Adv. Eng. Softw.* 40 (9), 830–835. doi:10.1016/j.advengsoft.2009.01.008

Mandic, D., and Chambers, J. (2001). *Recurrent Neural Networks for Prediction: Learning Algorithms, Architectures and Stability*. Hoboken, New Jersey, United States: John Wiley & Sons.

Manna, S., and Nakai, H. "Effectiveness of Word Embeddings on Classifiers: A Case Study with Tweets," in Proceedings of the 2019 IEEE 13th International Conference on Semantic Computing (ICSC), Newport Beach, CA, USA, January 2019 (Piscataway, New Jersey, United States: IEEE), 158–161.

Manohar, K., Brunton, B. W., Kutz, J. N., and Brunton, S. L. (2018). Data-driven Sparse Sensor Placement for Reconstruction: Demonstrating the Benefits of Exploiting Known Patterns. *IEEE Control. Syst. Mag.* 38 (3), 63–86. doi:10.1109/MCS.2018.2810460

Martínez-Vázquez, P., and Rodríguez-Cuevas, N. (2007). Wind Field Reproduction Using Neural Networks and Conditional Simulation. *Eng. structures* 29 (7), 1442–1449. doi:10.1016/j.engstruct.2006.08.024

Marzban, C. (2000). A Neural Network for Tornado Diagnosis: Managing Local Minima. *Neural Comput. Appl.* 9, 133–141. doi:10.1007/s005210070024

Marzban, C., Paik, H., and Stumpf, G. J. (1997). Neural Networks vs. Gaussian Discriminant Analysis. *AI Appl.* 11 (1), 49–58.

Marzban, C., and Stumpf, G. J. (1998). A Neural Network for Damaging Wind Prediction. *Wea. Forecast.* 13, 151–163. doi:10.1175/1520-0434(1998)013<0151:annfdw>2.0.co;2

Marzban, C., and Stumpf, G. J. (1996). A Neural Network for Tornado Prediction Based on Doppler Radar-Derived Attributes. *J. Appl. Meteorol.* 35, 617–626. doi:10.1175/1520-0450(1996)035<0617:annftp>2.0.co;2

Maskey, M., Ramachandran, R., Ramasubramanian, M., Gurung, I., Freitag, B., Kaulfus, A., et al. (2020). Deepti: Deep-Learning-Based Tropical Cyclone Intensity Estimation System. *IEEE J. Sel. Top. Appl. Earth Observations Remote Sensing* 13, 4271–4281. doi:10.1109/jstars.2020.3011907

Mason, M. S., Wood, G. S., and Fletcher, D. F. (2009). Numerical Simulation of Downburst Winds. *J. Wind Eng. Ind. Aerodynamics* 97 (11-12), 523–539. doi:10.1016/j.jweia.2009.07.010

Masri, S. F., Chassiakos, A. G., and Caughey, T. K. (1993). Identification of Nonlinear Dynamic Systems Using Neural Networks. *J. Appl. Mech.* 60 (1), 123–133. doi:10.1115/1.2900734

Matsumoto, M., Kobayashi, Y., and Shirato, H. (1996). The Influence of Aerodynamic Derivatives on Flutter. *J. Wind Eng. Ind. Aerodynamics* 60, 227–239. doi:10.1016/0167-6105(96)00036-0

Maulik, U., and Bandyopadhyay, S. (2002). Performance Evaluation of Some Clustering Algorithms and Validity Indices. *IEEE Trans. Pattern Anal. Machine Intell.* 24 (12), 1650–1654. doi:10.1109/tpami.2002.1114856

Mayo, M., Wakes, S., and Anderson, C. "Neural Networks for Predicting the Output of Wind Flow Simulations over Complex Topographies," in Proceedings of the 2018 IEEE International Conference on Big Knowledge (ICBK), Singapore, November 2018 (Piscataway, New Jersey, United States: IEEE), 184–191.

McCann, D. W. (1992). A Neural Network Short-Term Forecast of Significant Thunderstorms. *Wea. Forecast.* 7 (3), 525–534. doi:10.1175/1520-0434(1992)007<0525:annstf>2.0.co;2

McCarthy, J. (2007). From Here to Human-Level AI. *Artif. Intelligence* 171 (18), 1174–1182. doi:10.1016/j.artint.2007.10.009

McCulloch, W. S., and Pitts, W. (1943). A Logical Calculus of the Ideas Immanent in Nervous Activity. *Bull. Math. Biophys.* 5 (4), 115–133. doi:10.1007/bf02478259

Medina, B., Carey, L., Amiot, C., Mecikalski, R., Roeder, W., McNamara, T., et al. (2019). A Random forest Method to Forecast Downbursts Based on Dual-Polarization Radar Signatures. *Remote Sensing* 11 (7), 826. doi:10.3390/rs11070826

Medsker, L., and Jain, L. C. (1999). *Recurrent Neural Networks: Design and Applications*. Boca Raton, Florida, United States: CRC Press.

Michael, B. (20172017). *Tropical Cyclone Genesis Forecasting and Pre-genesis Forecasts Report*. Miami, FL, USA: National Hurricane Center.

Micheli, L., Hong, J., Laflamme, S., and Alipour, A. (2020). Surrogate Models for High Performance Control Systems in Wind-Excited Tall Buildings. *Appl. Soft Comput.* 90, 106133. doi:10.1016/j.asoc.2020.106133

Mnih, V., Kavukcuoglu, K., Silver, D., Rusu, A. A., Veness, J., Bellemare, M. G., et al. (2015). Human-level Control through Deep Reinforcement Learning. *nature* 518 (7540), 529–533. doi:10.1038/nature14236

Mohandes, M. A., Halawani, T. O., Rehman, S., and Hussain, A. A. (2004). Support Vector Machines for Wind Speed Prediction. *Renew. Energ.* 29 (6), 939–947. doi:10.1016/j.renene.2003.11.009

Mohri, M., Rostamizadeh, A., and Talwalkar, A. (2018). *Foundations of Machine Learning*. Cambridge, Massachusetts, United States: MIT press.

Moradi Kordmahalleh, M., Gorji Sefidmazgi, M., and Homaifar, A. (2016). "A Sparse Recurrent Neural Network for Trajectory Prediction of atlantic Hurricanes," in *Proceedings of the Genetic and Evolutionary Computation Conference 2016*. Editor F. Neumann (New York, United States: Association for Computing Machinery), 957–964.

More, A., and Deo, M. C. (2003). Forecasting Wind with Neural Networks. *Mar. structures* 16 (1), 35–49. doi:10.1016/s0951-8339(02)00053-9

Murphy, K. P. (2012). *Machine Learning: A Probabilistic Perspective*. Cambridge, Massachusetts, United States: MIT press.

Nikose, T. J., and Sonparote, R. S. (2020). Computing Dynamic Across-Wind Response of Tall Buildings Using Artificial Neural Network. *J. Supercomput* 76 (5), 3788–3813. doi:10.1007/s11227-018-2708-8

Nikose, T. J., and Sonparote, R. S. (2019a). Dynamic along Wind Response of Tall Buildings Using Artificial Neural Network. *Cluster Comput.* 22 (2), 3231–3246. doi:10.1007/s10586-018-2027-0

Nikose, T. J., and Sonparote, R. S. (2019b). Dynamic Wind Response of Tall Buildings Using Artificial Neural Network. *The Struct. Des. Tall Spec. Buildings* 28 (13), e1657. doi:10.1002/tal.1657

Oh, B. K., Glisic, B., Kim, Y., and Park, H. S. (2019). Convolutional Neural Network-Based Wind Induced Response Estimation Model for Tall Buildings. *Comput. Aided Civ. Infrastruct. Eng.* 34, 843–858. doi:10.1111/mice.12476

Oh, B. K., Kim, K. J., Kim, Y., Park, H. S., and Adeli, H. (2017). Evolutionary Learning Based Sustainable Strain Sensing Model for Structural Health Monitoring of High-Rise Buildings. *Appl. Soft Comput.* 58, 576–585. doi:10.1016/j.asoc.2017.05.029

O'Neal, A., Rodgers, B., Segler, J., Murthy, D., Lakuduva, N., Johnson, M., et al. "Training an Emergency-Response Image Classifier on Signal Data," in Proceedings of the 2018 17th IEEE International Conference on Machine Learning and Applications (ICMLA), Orlando, FL, USA, December 2018 (Piscataway, New Jersey, United States: IEEE), 751–756.

Oreskovic, C., Orf, L. G., and Savory, E. (2018). A Parametric Study of Downbursts Using a Full-Scale Cooling Source Model. *J. Wind Eng. Ind. Aerodynamics* 180, 168–181. doi:10.1016/j.jweia.2018.07.020

Oreskovic, C., and Savory, E. (2018). Evolution and Scaling of a Simulated Downburst-Producing Thunderstorm Outflow. *Wind and Structures* 26 (3), 147–161. doi:10.12989/was.2018.26.3.147

Pan, B., Xu, X., and Shi, Z. (2019). Tropical Cyclone Intensity Prediction Based on Recurrent Neural Networks. *Electron. Lett.* 55 (7), 413–415. doi:10.1049/el.2018.8178

Panofsky, H. A., and McCormick, R. A. (1960). The Spectrum of Vertical Velocity Near the Surface. *Q.J R. Met. Soc.* 86 (370), 495–503. doi:10.1002/qj.49708637006

Park, M.-S., Kim, M., Lee, M.-I., Im, J., and Park, S. (2016). Detection of Tropical Cyclone Genesis via Quantitative Satellite Ocean Surface Wind Pattern and Intensity Analyses Using Decision Trees. *Remote sensing Environ.* 183, 205–214. doi:10.1016/j.rse.2016.06.006

Pei, J. S., Wright, J. P., and Smyth, A. W. (2005). Mapping Polynomial Fitting into Feedforward Neural Networks for Modeling Nonlinear Dynamic Systems and beyond. *Comput. Methods Appl. Mech. Eng.* 194 (42-44), 4481–4505. doi:10.1016/j.cma.2004.12.010

Pi, Y., Nath, N. D., and Behzadan, A. H. (2020). Convolutional Neural Networks for Object Detection in Aerial Imagery for Disaster Response and Recovery. *Adv. Eng. Inform.* 43, 101009. doi:10.1016/j.aei.2019.101009

Potter, C. W., and Negnevitsky, M. (2006). Very Short-Term Wind Forecasting for Tasmanian Power Generation. *IEEE Trans. Power Syst.* 21 (2), 965–972. doi:10.1109/tpwrs.2006.873421

Pouyanfar, S., Sadiq, S., Yan, Y., Tian, H., Tao, Y., Reyes, M. P., et al. (2018). A Survey on Deep Learning: Algorithms, Techniques, and Applications. *ACM Comput. Surv. (Csur)* 51 (5), 1–36. doi:10.1145/3234150

Psichogios, D. C., and Ungar, L. H. (1992). A Hybrid Neural Network-First Principles Approach to Process Modeling. *Aiche J.* 38 (10), 1499–1511. doi:10.1002/aic.690381003

Raissi, M., Perdikaris, P., and Karniadakis, G. E. (2017a). Physics Informed Deep Learning (Part I): Data-Driven Solutions of Nonlinear Partial Differential Equations. *arXiv preprint*. arXiv:1711.10561.

Raissi, M., Perdikaris, P., and Karniadakis, G. E. (2017b). Physics Informed Deep Learning (Part II): Data-Driven Discovery of Nonlinear Partial Differential Equations. *arXiv* 1711, 10566.

Raissi, M., Perdikaris, P., and Karniadakis, G. E. (2019). Physics-informed Neural Networks: A Deep Learning Framework for Solving Forward and Inverse Problems Involving Nonlinear Partial Differential Equations. *J. Comput. Phys.* 378, 686–707. doi:10.1016/j.jcp.2018.10.045

Rathje, E. M., Dawson, C., Padgett, J. E., Pinelli, J.-P., Stanzione, D., Adair, A., et al. (2017). DesignSafe: New Cyberinfrastructure for Natural Hazards Engineering. *Nat. Hazards Rev.* 18 (3), 06017001. doi:10.1061/(asce)nh.1527-6996.0000246

Razavi, A., and Sarkar, P. P. (2021). Effects of Roof Geometry on Tornado-Induced Structural Actions of a Low-Rise Building. *Eng. structures* 226, 111367. doi:10.1016/j.engstruct.2020.111367

Razavi, A., and Sarkar, P. P. (2018). Laboratory Study of Topographic Effects on the Near-Surface Tornado Flow Field. *Boundary-layer Meteorol.* 168 (2), 189–212. doi:10.1007/s10546-018-0347-5

Refan, M., and Hangan, H. (2016). Characterization of Tornado-like Flow fields in a New Model Scale Wind Testing Chamber. *J. Wind Eng. Ind. Aerodynamics* 151, 107–121. doi:10.1016/j.jweia.2016.02.002

Richman, M. B., and Leslie, L. M. (2012). Adaptive Machine Learning Approaches to Seasonal Prediction of Tropical Cyclones. *Proced. Comput. Sci.* 12, 276–281. doi:10.1016/j.procs.2012.09.069

Richman, M. B., Leslie, L. M., Ramsay, H. A., and Klotzbach, P. J. (2017). Reducing Tropical Cyclone Prediction Errors Using Machine Learning Approaches. *Proced. Comput. Sci.* 114, 314–323. doi:10.1016/j.procs.2017.09.048

Riedmiller, M., and Braun, H. "A Direct Adaptive Method for Faster Backpropagation Learning: The RPROP Algorithm," in Proceedings of the IEEE international conference on neural networks, San Francisco, CA, USA, March 1993 (Piscataway, New Jersey, United States: IEEE), 586–591.

Rizzo, F., and Caracoglia, L. (2020). Artificial Neural Network Model to Predict the Flutter Velocity of Suspension Bridges. *Comput. Structures* 233, 106236. doi:10.1016/j.compstruc.2020.106236

Robertson, B. W., Johnson, M., Murthy, D., Smith, W. R., and Stephens, K. K. (2019). Using a Combination of Human Insights and 'deep Learning' for Real-Time Disaster Communication. *Prog. Disaster Sci.* 2, 100030. doi:10.1016/j.pdisas.2019.100030

Romanic, D., LoTufo, J., and Hangan, H. (2019). Transient Behavior in Impinging Jets in Crossflow with Application to Downburst Flows. *J. Wind Eng. Ind. Aerodynamics* 184, 209–227. doi:10.1016/j.jweia.2018.11.020

Rosenblatt, F. (1957). *The Perceptron, a Perceiving and Recognizing Automaton Project Para*. Buffalo, New York, United States: Cornell Aeronautical Laboratory.

Rumelhart, D. E., Hinton, G. E., and Williams, R. J. (1986). Learning Representations by Back-Propagating Errors. *nature* 323 (6088), 533–536. doi:10.1038/323533a0

Russell, S., and Norvig, P. (2016). *Artificial Intelligence: A Modern Approach*. London, United Kingdom: Pearson Education Limited.

Rüttgers, M., Lee, S., Jeon, S., and You, D. (2019). Prediction of a Typhoon Track Using a Generative Adversarial Network and Satellite Images. *Sci. Rep.* 9 (1), 1–15. doi:10.1038/s41598-019-42339-y

Salehi, H., and Burgueño, R. (2018). Emerging Artificial Intelligence Methods in Structural Engineering. *Eng. structures* 171, 170–189. doi:10.1016/j.engstruct.2018.05.084

Santosa, B. (2007). Feature Selection with Support Vector Machines Applied on Tornado Detection. *IPTEK J. Technol. Sci.* 18 (1). doi:10.12962/j20882033.v18i1.178

Sarkar, P. P., Haan, F. L., Jr., Balaramudu, V., and Sengupta, A., "Laboratory Simulation of Tornado and Microburst to Assess Wind Loads on Buildings." in Proceedings of the Structures Congress 2006: Structural Engineering and Public Safety. St. Louis, Missouri, United States. May 2006. 1–10. doi:10.1061/40889(201)11

Saunders, J. W., and Melbourne, W. H. (1980). "Buffeting Effects of Upstream Buildings," in *Wind Engineering*. Editor J. W. Saunders (Pergamon: Pergamon Press), 593–606. doi:10.1016/b978-1-4832-8367-8.50059-0

Scholkopf, B., and Smola, A. J. (2018). *Learning with Kernels: Support Vector Machines, Regularization, Optimization, and beyond. Adaptive Computation and Machine Learning Series*. Cambridge, Massachusetts, United States: MIT Press.

Sfetsos, A. (2000). A Comparison of Various Forecasting Techniques Applied to Mean Hourly Wind Speed Time Series. *Renew. Energ.* 21 (1), 23–35. doi:10.1016/s0960-1481(99)00125-1

Sharma, R., Shikhola, T., and Kohli, J. K. (2020). Modified Fuzzy Q-Learning Based Wind Speed Prediction. *J. Wind Eng. Ind. Aerodynamics* 206, 104361. doi:10.1016/j.jweia.2020.104361

Silver, D., Schrittwieser, J., Simonyan, K., Antonoglou, I., Huang, A., Guez, A., et al. (2017). Mastering the Game of Go without Human Knowledge. *nature* 550 (7676), 354–359. doi:10.1038/nature24270

Simiu, E., and Scanlan, R. H. (1978). *Wind Effects on Structures*. Hoboken, New Jersey, United States: Wiley.

Smith, T. M., Elmore, K. L., and Dulin, S. A. (2004). A Damaging Downburst Prediction and Detection Algorithm for the WSR-88D. *Wea. Forecast.* 19 (2), 240–250. doi:10.1175/1520-0434(2004)019<0240:addpad>2.0.co;2

Snaiki, R., and Wu, T. (2017b). A Linear Height-Resolving Wind Field Model for Tropical Cyclone Boundary Layer. *J. Wind Eng. Ind. Aerodynamics* 171, 248–260. doi:10.1016/j.jweia.2017.10.008

Snaiki, R., and Wu, T. (2018). A Semi-empirical Model for Mean Wind Velocity Profile of Landfalling hurricane Boundary Layers. *J. Wind Eng. Ind. Aerodynamics* 180, 249–261. doi:10.1016/j.jweia.2018.08.004

Snaiki, R., and Wu, T. (2020c). An Analytical Model for Rapid Estimation of hurricane Supergradient Winds. *J. Wind Eng. Ind. Aerodynamics* 201, 104175. doi:10.1016/j.jweia.2020.104175

Snaiki, R., and Wu, T. (2020b). Hurricane hazard Assessment along the United States Northeastern Coast: Surface Wind and Rain fields under Changing Climate. *Front. Built Environ.* 6, 573054. doi:10.3389/fbuil.2020.573054

Snaiki, R., and Wu, T. (2019). Knowledge-enhanced Deep Learning for Simulation of Tropical Cyclone Boundary-Layer Winds. *J. Wind Eng. Ind. Aerodynamics* 194, 103983. doi:10.1016/j.jweia.2019.103983

Snaiki, R., and Wu, T. (2017a). Modeling Tropical Cyclone Boundary Layer: Height-Resolving Pressure and Wind fields. *J. Wind Eng. Ind. Aerodynamics* 170, 18–27. doi:10.1016/j.jweia.2017.08.005

Snaiki, R., and Wu, T. (2020a). Revisiting hurricane Track Model for Wind Risk Assessment. *Struct. Saf.* 87, 102003. doi:10.1016/j.strusafe.2020.102003

Solari, G., Burlando, M., De Gaetano, P., and Repetto, M. P. (2015). Characteristics of Thunderstorms Relevant to the Wind Loading of Structures. *Wind and Structures* 20 (6), 763–791. doi:10.12989/was.2015.20.6.763

Solari, G. (2020). Thunderstorm Downbursts and Wind Loading of Structures: Progress and prospect. *Front. Built Environ.* 6, 63. doi:10.3389/fbuil.2020.00063

Stiles, B. W., Danielson, R. E., Poulsen, W. L., Brennan, M. J., Hristova-Veleva, S., Tsae-Pyng Shen, T. P., et al. (2014). Optimized Tropical Cyclone Winds from QuikSCAT: A Neural Network Approach. *IEEE Trans. Geosci. Remote Sensing* 52 (11), 7418–7434. doi:10.1109/tgrs.2014.2312333

Subasri, R., Suresh, S., and Natarajan, A. M. (2014). Discrete Direct Adaptive ELM Controller for Active Vibration Control of Nonlinear Base Isolation Buildings. *Neurocomputing* 129, 246–256. doi:10.1016/j.neucom.2013.09.035

Subramanian, D., Salazar, J., Duenas-Osorio, L., and Stein, R. "Constructing and Validating Geographically Refined HAZUS-MH4 hurricane Wind Risk Models: A Machine Learning Approach," in Proceedings of the Advances in hurricane engineering: Learning from our past, Miami, Florida, United States, October 2013, 1056–1066. doi:10.1061/9780784412626.092

Sun, W., Bocchini, P., and Davison, B. D. (2020). Applications of Artificial Intelligence for Disaster Management. *Nat. Hazards* 103, 2631–2689. doi:10.1007/s11069-020-04124-3

Sun, Y., Yang, L., and Wu, Y. "Wind Load Prediction of Large-Span Dry Coal Sheds Based on GRNN and its Application," in Proceedings of International Structural Engineering and Construction, Valencia, Spain, July, 2017. doi:10.14455/isec.res.2017.189

Sutton, R. S., and Barto, A. G. (2018). *Reinforcement Learning: An Introduction*. Cambridge, Massachusetts, United States: MIT press.

Tagliaferri, F., Viola, I. M., and Flay, R. G. J. (2015). Wind Direction Forecasting with Artificial Neural Networks and Support Vector Machines. *Ocean Eng.* 97, 65–73. doi:10.1016/j.oceaneng.2014.12.026

Tang, Z., Feng, C., Wu, L., Zuo, D., and James, D. L. (2018). Characteristics of Tornado-like Vortices Simulated in a Large-Scale ward-type Simulator. *Boundary-layer Meteorol.* 166 (2), 327–350. doi:10.1007/s10546-017-0305-7

Taniike, Y., and Inaoka, H. (1988). "Aeroelastic Behavior of Tall Buildings in Wakes," in *Advances in Wind Engineering*. Editors C. Kramer and H. J. Gerhardt (Amsterdam, Netherlands: Elsevier), 317–327. doi:10.1016/b978-0-444-87156-5.50043-6

Tian, J., Gurley, K. R., Diaz, M. T., Fernández-Cabán, P. L., Masters, F. J., and Fang, R. (2020). Low-rise Gable Roof Buildings Pressure Prediction Using Deep Neural Networks. *J. Wind Eng. Ind. Aerodynamics* 196, 104026. doi:10.1016/j.jweia.2019.104026

Tian, W., Huang, W., Yi, L., Wu, L., and Wang, C. (2020). A CNN-Based Hybrid Model for Tropical Cyclone Intensity Estimation in Meteorological Industry. *IEEE Access* 8, 59158–59168. doi:10.1109/access.2020.2982772

Tian, Z., Ren, Y., and Wang, G. (2020). An Application of Backtracking Search Optimization-Based Least Squares Support Vector Machine for Prediction of Short-Term Wind Speed. *Wind Eng.* 44 (3), 266–281. doi:10.1177/0309524x19849843

Trafalis, T. B., Adrianto, I., Richman, M. B., and Lakshmivarahan, S. (2014). Machine-learning Classifiers for Imbalanced Tornado Data. *Comput. Manag. Sci.* 11 (4), 403–418. doi:10.1007/s10287-013-0174-6

Turkkan, N., and Srivastava, N. K. (1995). Prediction of Wind Load Distribution for Air-Supported Structures Using Neural Networks. *Can. J. Civ. Eng.* 22 (3), 453–461. doi:10.1139/l95-053

Twisdale, L. A., and Vickery, P. J. (1992). Research on Thunderstorm Wind Design Parameters. *J. Wind Eng. Ind. Aerodynamics* 41 (1-3), 545–556. doi:10.1016/0167-6105(92)90461-i

Uematsu, Y., and Tsuruishi, R. (2008). Wind Load Evaluation System for the Design of Roof Cladding of Spherical Domes. *J. wind Eng. Ind. aerodynamics* 96 (10-11), 2054–2066. doi:10.1016/j.jweia.2008.02.051

Ukkonen, P., Manzato, A., and Mäkelä, A. (2017). Evaluation of Thunderstorm Predictors for Finland Using Reanalyses and Neural Networks. *J. Appl. Meteorology Climatology* 56 (8), 2335–2352. doi:10.1175/jamc-d-16-0361.1

Varshney, K., and Poddar, K. (2012). Prediction of Wind Properties in Urban Environments Using Artificial Neural Network. *Theor. Appl. Climatology* 107 (3-4), 579–590. doi:10.1007/s00704-011-0506-9

Vickery, P. J., Skerlj, P. F., and Twisdale, L. A. (2000). Simulation of Hurricane Risk in the U.S. Using Empirical Track Model. *J. Struct. Eng.* 126 (10), 1222–1237. doi:10.1061/(asce)0733-9445(2000)126:10(1222)

Vickery, P. J., Wadhera, D., Twisdale, L. A., Jr., and Lavelle, F. M. (2009). U.S. Hurricane Wind Speed Risk and Uncertainty. *J. Struct. Eng.* 135 (3), 301–320. doi:10.1061/(asce)0733-9445(2009)135:3(301)

Vyavahare, A. Y., Godbole, P. N., and Nikose, T. (2012). Analysis of Tall Building for across Wind Response. *Int. J. Civil Struct. Eng.* 2 (3), 679–986.

Wang, H., and Wu, T. (2021). Fast Hilbert-Wavelet Simulation of Nonstationary Wind Field Using Noniterative Simultaneous Matrix Diagonalization. *J. Eng. Mech.* 147 (3), 04020153. doi:10.1061/(asce)em.1943-7889.0001897

Wang, H., and Wu, T. (2020). Knowledge-Enhanced Deep Learning for Wind-Induced Nonlinear Structural Dynamic Analysis. *J. Struct. Eng.* 146 (11), 04020235. doi:10.1061/(asce)st.1943-541x.0002802

Wang, H., Zhang, Y.-M., Mao, J.-X., and Wan, H.-P. (2020). A Probabilistic Approach for Short-Term Prediction of Wind Gust Speed Using Ensemble Learning. *J. Wind Eng. Ind. Aerodynamics* 202, 104198. doi:10.1016/j.jweia.2020.104198

Wang, J., and Cheng, C. M. "Aero-Data Based Wind Resistant Design of Rectangular Shaped Tall Buildings," in Proceedings of the International Conference on Innovations in Civil and Structural Engineering (ICICSE'15), Istanbul, Turkey, June 2015, 148–154.

Wang, J., Cheng, C. M., and Chen, C. H. "The Study of Wind Force Coefficient Predictions for Rectangular High-Rise Buildings," in Proceedings of The eighth Asia-Pacific conference on wind engineering, Chennai, India, December 2013, 10–14.

Wang, J., and Cheng, C. M. (2017). Formulation of Estimation Models for Wind Force Coefficients of Rectangular Shaped Buildings. *J. Appl. Sci. Eng.* 20 (1), 55–62. doi:10.6180/jase.2017.20.1.07

Wang, Y., Zhang, W., and Fu, W. "Back Propogation (BP)-neural Network for Tropical Cyclone Track Forecast," in Proceedings of the 2011 19th International Conference on Geoinformatics, Shanghai, China, June 2011 (Piscataway, New Jersey, United States: IEEE), 1–4.

Watkins, C. J. C. H. (1989). *Learning from Delayed Rewards*. Cambridge, UK: King's College.

Watkins, C. J., and Dayan, P. (1992). Q-learning. *Machine Learn.* 8 (3-4), 279–292. doi:10.1023/a:1022676722315

Wei, C.-C. (2015). Forecasting Surface Wind Speeds over Offshore Islands Near Taiwan during Tropical Cyclones: Comparisons of Data-Driven Algorithms and Parametric Wind Representations. *J. Geophys. Res. Atmos.* 120 (5), 1826–1847. doi:10.1002/2014jd022568

Wei, C.-C. (2019). Study on Wind Simulations Using Deep Learning Techniques during Typhoons: a Case Study of Northern Taiwan. *Atmosphere* 10 (11), 684. doi:10.3390/atmos10110684

Wen, Y.-K., and Chu, S.-L. (1973). Tornado Risks and Design Wind Speed. *J. Struct. Div.* 99 (12), 2409–2421. doi:10.1061/jsdeag.0003666

Wiederhold, G., McCarthy, J., and Feigenbaum, E. (1990). Arthur Samuel: pioneer in Machine Learning. *Commun. ACM* 33 (11), 137–139.

Wijnands, J. S., Qian, G., and Kuleshov, Y. (2016). Variable Selection for Tropical Cyclogenesis Predictive Modeling. *Monthly Weather Rev.* 144 (12), 4605–4619. doi:10.1175/mwr-d-16-0166.1

Wijnands, J. S., Shelton, K., and Kuleshov, Y. (2014). Improving the Operational Methodology of Tropical Cyclone Seasonal Prediction in the Australian and the South Pacific Ocean Regions. *Adv. Meteorology* 2014, 838746. doi:10.1155/2014/838746

Williams, R. J. (1992). Simple Statistical Gradient-Following Algorithms for Connectionist Reinforcement Learning. *Machine Learn.* 8 (3-4), 229–256. doi:10.1007/bf00992696

Wu, R.-T., and Jahanshahi, M. R. (2019). Deep Convolutional Neural Network for Structural Dynamic Response Estimation and System Identification. *J. Eng. Mech.* 145 (1), 04018125. doi:10.1061/(asce)em.1943-7889.0001556

Wu, T., and Kareem, A. (2013). Bridge Aerodynamics and Aeroelasticity: A Comparison of Modeling Schemes. *J. Fluids Structures* 43, 347–370. doi:10.1016/j.jfluidstructs.2013.09.015

Wu, T., and Kareem, A. (2011). Modeling Hysteretic Nonlinear Behavior of Bridge Aerodynamics via Cellular Automata Nested Neural Network. *J. Wind Eng. Ind. Aerodynamics* 99 (4), 378–388. doi:10.1016/j.jweia.2010.12.011

Wu, T., Li, S., and Sivaselvan, M. (2019). Real-time Aerodynamics Hybrid Simulation: a Novel Wind-Tunnel Model for Flexible Bridges. *J. Eng. Mech.* 145 (9), 04019061. doi:10.1061/(asce)em.1943-7889.0001649

Wu, T. (2013). "Nonlinear bluff-body Aerodynamics," (Indiana, USA: University of Notre Dame). Doctoral dissertation.

Wu, T., and Song, W. (2019). Real-time Aerodynamics Hybrid Simulation: Wind-Induced Effects on a Reduced-Scale Building Equipped with Full-Scale Dampers. *J. Wind Eng. Ind. Aerodynamics* 190, 1–9. doi:10.1016/j.jweia.2019.04.005

Wu, X., Ghaboussi, J., and Garrett, J. H., Jr. (1992). Use of Neural Networks in Detection of Structural Damage. *Comput. Structures* 42 (4), 649–659. doi:10.1016/0045-7949(92)90132-j

Yakut, O., and Alli, H. (2011). Neural Based Sliding-Mode Control with Moving Sliding Surface for the Seismic Isolation of Structures. *J. Vibration Control.* 17 (14), 2103–2116. doi:10.1177/1077546310395964

Yang, Q., Gao, R., Bai, F., Li, T., and Tamura, Y. (2018). Damage to Buildings and Structures Due to Recent Devastating Wind Hazards in East Asia. *Nat. Hazards* 92 (3), 1321–1353. doi:10.1007/s11069-018-3253-8

Yasen, M. Z. Y., Al-Jundi, R. A. S., and Al-Madi, N. S. A. "Optimized ANN-ABC for Thunderstorms Prediction," in Proceedings of the 2017 International Conference on New Trends in Computing Sciences (ICTCS), Amman, Jordan, October 2017 (Piscataway, New Jersey, United States: IEEE), 98–103.

Yu, C., Li, Y., Xiang, H., and Zhang, M. (2018). Data Mining-Assisted Short-Term Wind Speed Forecasting by Wavelet Packet Decomposition and Elman Neural Network. *J. Wind Eng. Ind. Aerodynamics* 175, 136–143. doi:10.1016/j.jweia.2018.01.020

Yu, M., Huang, Q., Qin, H., Scheele, C., and Yang, C. (2019). Deep Learning for Real-Time Social media Text Classification for Situation Awareness - Using Hurricanes Sandy, Harvey, and Irma as Case Studies. *Int. J. Digital Earth* 12 (11), 1230–1247. doi:10.1080/17538947.2019.1574316

Yu, Y., Yao, H., and Liu, Y. (2020). Structural Dynamics Simulation Using a Novel Physics-Guided Machine Learning Method. *Eng. Appl. Artif. Intelligence* 96, 103947. doi:10.1016/j.engappai.2020.103947

Zambrano, T. G., and Peterka, J. A. (1978). Wind Load Interaction on an Adjacent Building. *CER* 77, 78–26.

Zhang, A., and Zhang, L. (2004). RBF Neural Networks for the Prediction of Building Interference Effects. *Comput. Structures* 82 (27), 2333–2339. doi:10.1016/j.compstruc.2004.05.014

Zhang, C., Dai, L., Ma, L., Qian, J., and Yang, B. (2017). Objective Estimation of Tropical Cyclone Innercore Surface Wind Structure Using Infrared Satellite Images. *J. Appl. Remote Sensing* 11 (4), 046030. doi:10.1117/1.jrs.11.046030

Zhang, S., and Nishijima, K. "Statistics-based Investigation on Typhoon Transition Modeling," in Proceedingsof the Seventh International Colloquium on Bluff Body Aerodynamics and Application, Shanghai, China, September 2012, 364–373.

Zhang, T., Lin, W., Lin, Y., Zhang, M., Yu, H., Cao, K., et al. (2019). Prediction of Tropical Cyclone Genesis from Mesoscale Convective Systems Using Machine Learning. *Weather Forecast.* 34 (4), 1035–1049. doi:10.1175/waf-d-18-0201.1

Zhang, W., Fu, B., Peng, M. S., and Li, T. (2015). Discriminating Developing versus Nondeveloping Tropical Disturbances in the Western North Pacific through Decision Tree Analysis. *Weather Forecast.* 30 (2), 446–454. doi:10.1175/waf-d-14-00023.1

Zhang, Y., Chandra, R., and Gao, J. "Cyclone Track Prediction with Matrix Neural Networks," in Proceedings of the 2018 International Joint Conference on Neural Networks (IJCNN), Rio de Janeiro, Brazil, July 2018 (Piscataway, New Jersey, United States: IEEE), 1–8.

Zhao, M., Held, I. M., and Lin, S.-J. (2012). Some Counterintuitive Dependencies of Tropical Cyclone Frequency on Parameters in a GCM. *J. Atmos. Sci.* 69 (7), 2272–2283. doi:10.1175/jas-d-11-0238.1

Zhu, J., and Zhang, W. (2018). Probabilistic Fatigue Damage Assessment of Coastal Slender Bridges under Coupled Dynamic Loads. *Eng. Structures* 166, 274–285. doi:10.1016/j.engstruct.2018.03.073

Conflict of Interest: The authors declare that the research was conducted in the absence of any commercial or financial relationships that could be construed as a potential conflict of interest.

Publisher's Note: All claims expressed in this article are solely those of the authors and do not necessarily represent those of their affiliated organizations, or those of the publisher, the editors and the reviewers. Any product that may be evaluated in this article, or claim that may be made by its manufacturer, is not guaranteed or endorsed by the publisher.

APPENDIX A: LIST OF REVIEWED MACHINE LEARNING ALGORITHMS (NOTE: ACRONYMS WITH * REPRESENT THOSE REVIEWED IN THIS CONTRIBUTION).

A2C advantage actor critic
AdaBoost* adaptive boosting
AE* autoencoder
ALEN* adaptive linear element network
ANFIS* adaptive neuro-fuzzy inference system
ANN* artificial neural network
AWN* adaptive wavelet network
BNB* Bernoulli naive Bayes
BNN* Bayesian neural network
CGAN conditional GAN
CNN* convolutional neural network
CNN-AE* convolutional neural network-based autoencoder
ConvLSTM* convolutional Long Short-Term Memory
DCGAN deep convolutional GAN
DDPG* deep deterministic policy gradient
DDQN double deep Q-network
DNN* deep neural network
DQN deep Q-network
DRL* deep reinforcement learning
DRNN* diagonal recurrent neural networks
DT* decision tree
ENN* Elman neural network
ERBFN* radial basis function neural network
ERNN* Elman recurrent neural networks
FIS* fuzzy inference system
FNN* fuzzy neural network
GAN* generative adversarial network
GBRT* gradient boosted regression trees
GBTE* gradient-boosted tree ensembles
GMDH* group method of data handling
GNB* gaussian naïve Bayes
GPR* gaussian process regression
GRU* gated recurrent unit network
GRNN* generalized regression neural network
ICA independent component analysis
IIRANN* infinite impulse response artificial neural network
JRNN* Jordan recurrent neural networks
KEDL* knowledge-enhanced deep learning
KE-DRL* knowledge-enhanced deep reinforcement learning
KE-LSTM* knowledge enhanced long short-term memory
KM k-means
KNN* k-nearest neighbors
LAFMN* local activation feedback multilayer network
LDA* linear discriminant analysis
LNN* linear neural network
LR* logistic regression
LSSVM* least squares support vector machine
LSTM* long short-term memory
MC* multiple correlation
MFQL* modified fuzzy Q-learning
MLR* multiple linear regression
MNB* multinomial naive Bayes
MNN* matrix neural network
MSC mean-shift clustering
NB* naïve Bayes
NESN* nonlinear echo state networks
NLN* neural logic network
OLR* ordinary linear regression
PCA principal component analysis
PI* Physics-informed
PPO proximal policy optimization
QDA* quadratic discriminant analysis
QL* Q-learning
RBF* radial basis function
RBFNN* radial basis function neural network
RF* random forest
RL* reinforcement learning
RNN* recurrent neural networks
RR* ridge regression
SC spectral clustering
SD-AE* stacked denoising autoencoder
SLDA* supervised latent Dirichlet Allocation
SGD* stochastic gradient descent
SVM* support vector machines
SVR* support vector regression
TRPO trust region policy optimization
WGAN Wasserstein GAN
XGBoost* extreme gradient boosting

frontiers in Built Environment

REVIEW
published: 22 March 2022
doi: 10.3389/fbuil.2022.848698

Performance-Based Design of Tall Timber Buildings Under Earthquake and Wind Multi-Hazard Loads: Past, Present, and Future

S. Tesfamariam *

School of Engineering, The University of British Columbia, Kelowna, BC, Canada

The rapid growth of the urban population and associated environmental concerns are challenging city planners and developers to consider sustainable and cost-efficient building systems. Timber-based buildings, such as sustainable systems, are increasingly used. The timber buildings, however, being lighter and flexible, can be vulnerable to earthquakes and wind loads. This paper gives a state-of-the-art review on performance-based design (PBD) considerations and future direction for timber and timber-based hybrid buildings. The PBD review covered both earthquake and wind loads and multi-hazard design considerations. The review also provided 1) current practice and future direction in consideration of hazard, response, and loss assessment within the multi-hazard PBD, 2) damping and energy dissipation devices, 3) optimization under uncertainty, and 4) future of surrogate and multi-fidelity modeling in PBD.

Keywords: multi-hazard design, tall-timber building, damping, multi-fidelity models, energy dissipation devices, optimization

OPEN ACCESS

Edited by:
Gregory A. Kopp,
Western University, Canada

Reviewed by:
Teng Wu,
University at Buffalo, United States
Kohei Fujita,
Kyoto University, Japan

***Correspondence:**
S. Tesfamariam
Solomon.Tesfamariam@ubc.ca

Specialty section:
This article was submitted to Earthquake Engineering, a section of the journal Frontiers in Built Environment

Received: *05 January 2022*
Accepted: *17 February 2022*
Published: *22 March 2022*

Citation:
Tesfamariam S (2022) Performance-Based Design of Tall Timber Buildings Under Earthquake and Wind Multi-Hazard Loads: Past, Present, and Future. Front. Built Environ. 8:848698. doi: 10.3389/fbuil.2022.848698

INTRODUCTION

Evolution of Tall-Timber and Hybrid Buildings

The rapid growth of the urban population and associated environmental concerns challenged city planners to consider sustainable and cost-efficient building systems (Nygaard et al., 2019; Foster and Reynolds 2018; Smith and Frangi 2014). With the recent introduction of manufactured mass timber elements, such as cross-laminated timber (CLT), laminated veneer lumber, and glued laminated timber (glulam), sustainable tall-timber buildings have become a viable option (Tesfamariam et al., 2021a, 2019, 2015; Tesfamariam and Das 2021; van de Lindt et al., 2020; Ahmed and Arocho 2020; Ramage et al., 2017; Malo et al., 2016; Pei et al., 2015). What constitutes a "tall building" is relative to the time (Jennings 1970), and the definition of "tallness" in a mass-timber building is evolving (Foster et al., 2016). **Figure 1** depicts the evolution of constructed, under construction, and proposed tall-timber buildings.

Tall-timber buildings are lighter and more flexible (Foster and Reynolds 2018) and consequently are vulnerable to wind loads due to limited overturning moment resistance capacity and excessive vibration demand (Bezabeh et al., 2020a; Bezabeh et al., 2018a). Limited studies are published on wind performance of timber and timber-based hybrid

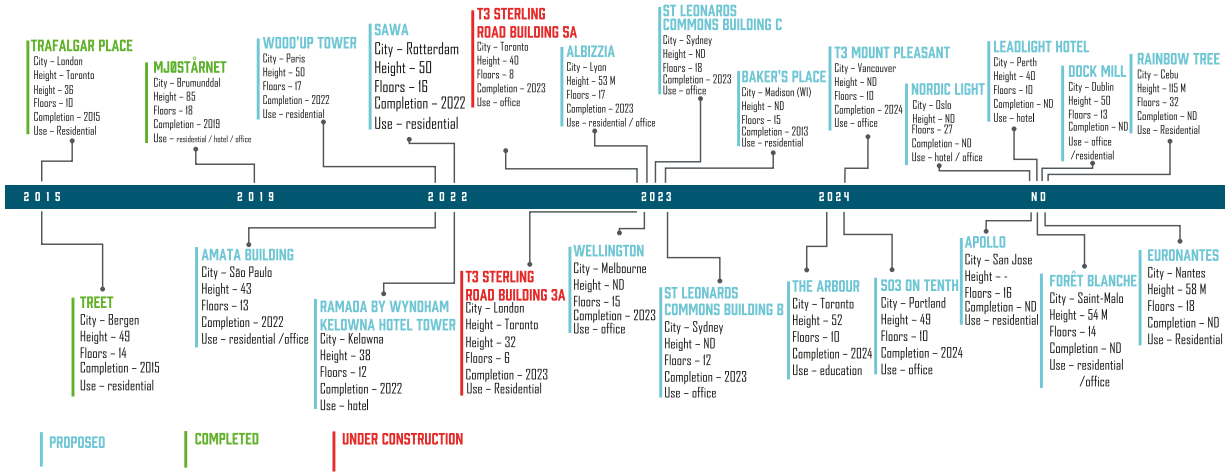

FIGURE 1 | Evolution of tall-timber design and construction (compiled from the Council on Tall Buildings and Urban Habitat database on January 1, 2022).

structure substantiated with wind tunnel tests (*e.g.*, Bezabeh et al., 2020b; Bezabeh et al., 2018a). Bezabeh et al. (2020a) carried out high-frequency pressure integration wind tunnel tests on tall-timber buildings (10, 15, 20, 30, and 40 stories). The dynamic response and serviceability-performance limits were assessed with respect to the 2015 National Building Code of Canada (NBC) (NRC 2015). With height beyond 10 stories, lateral drift and stiffness requirements can govern serviceability limit state and require stringent wind design consideration. Bezabeh et al. (2018c) experimentally and analytically assessed the performance of a 10-story mass-timber building under tornado-like laboratory simulations and atmospheric boundary layer flow at Western University, Canada. The results highlight that strong tornadoes pose significant damage to drift-sensitive nonstructural components.

Knowledge of damping in tall-timber buildings is limited and uncertain (Bezabeh et al., 2018b; Edskär and Lidelöw 2019; Reynolds et al., 2016; Kareem and Gurley 1996; Pagnini and Solari 1988). With emerging tall-timber building construction (*e.g.*, **Figure 1**), the importance of damping was noted, and practical solutions were provided. "Treet" (Malo et al., 2016), for example, a 14-story timber apartment building in Norway, is using the lateral-force resisting system that is diagonal glulam beams. The CLT was used for the elevator shaft and stairways, with additional concrete topped floor to improve the wind performance. "Scotia Place" (Moore 2000) is a 12-story steel-frame apartment building located in a high seismic zone in New Zealand. Using the wood floor, the overall weight was reduced with additional cost savings in material and floor finishing. However, the lighter structure showed vulnerability to wind and the need for supplemental damping. Considering different levels of uncertain damping values, Bezabeh et al. (2018a) showed the required damping values to satisfy the NBC criteria.

Motivation

Different national and international seismic design codes, *e.g.*, NBC (NRC 2015), International Building Code (ICC 2017), follow prescriptive (deterministic) and force-based design. The wind load design is mainly considering the first mode vibration and serviceability limit state (e.g., cladding failure, occupant comfort) (*e.g.*, Ouyang and Spence 2021; Bezabeh et al., 2018a; Bernardini et al., 2014). The seismic design principles are for first mode deformation response and collapse prevention limit state. This is not suitable for tall-timber buildings that have higher mode contributions (Ramage et al., 2017; Willford et al., 2008; Jennings 1970). In addition, under severe earthquakes, the building can sustain irreparable damage with post-earthquake occupancy and community recovery implications (Takagi and Wada 2019). For the tall-timber and hybrid buildings that are outside of the code-oriented practice, performance-based design (PBD) is a viable approach (Golesorkhi et al., 2017; Bezabeh et al., 2015; PEER 2017; Loss et al., 2018; LATBSDC 2020; Alinejad et al., 2021; Tesfamariam et al., 2021a). In wind engineering, there is a departure from prescriptive to PBD for wind as reflected in ASCE (2019) pre-standard.

The current building design codes use combination rules (*e.g.*, dead load and earthquake load) to achieve uniform reliability (Crosti et al., 2010; Duthinh and Simiu, 2010). In combination with other loads (dead load, live loads, snow loads, etc.), the design is governed by earthquake or wind loads (NBC 2015; ASCE 2017). The risk of exceeding a given limit state is implicitly assumed to be the same in the region where earthquake or wind is the dominant load (Kwag et al., 2021; Duthinh and Simiu 2010). In cities, such as Vancouver (high seismic zone) and Boston (low seismic zone), for example, the challenge for structural designers is an earthquake, and wind can be competing design loads (Wen and Kang 2001a; Mahmoud and Cheng 2017; Tesfamariam et al.,

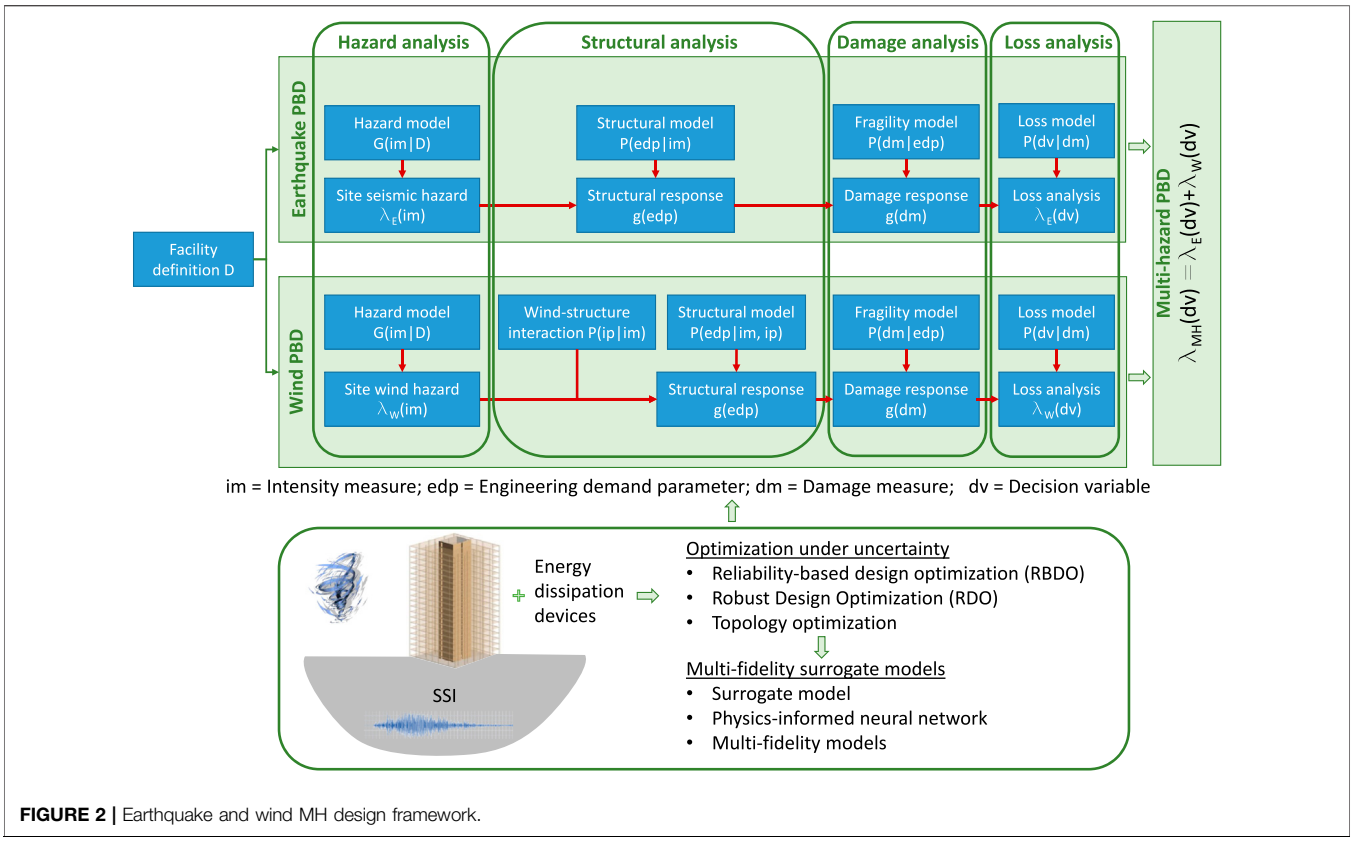

FIGURE 2 | Earthquake and wind MH design framework.

2019). The earthquake and wind loads multi-hazard (MH) design might not necessarily be governed by higher intensity single hazard but be dominated by the lower intensity and more frequent hazard (Wen and Kang 2001a; Wen 2001). Wen (1990) proposed a uniform reliability design rule of combination. With increasing building height, the need for MH design consideration of tall building design is apparent (*e.g.*, Suksuwan and Spence 2018).

With increasing demand in the design and construction of tall-timber buildings, MH PBD principles beyond the current design guideline are needed. The PBD framework for wind, earthquake, and MH tall-timber design is depicted in **Figure 2**. From the current literature review, for PBD of tall-timber building, issues related to modeling, consideration of site-specific soil–structure interaction (SSI), energy dissipation devices, efficient optimization algorithms, and damping are apparent (**Figure 2**). Thus, this paper is a state-of-the-art review of the MH design consideration and discussion on the emerging modeling consideration for tall-timber design and future implementation.

Objectives

In this paper, the first high-level review of the current PBD for seismic and wind loads is provided. In addition, the review is extended for the earthquake and wind MH framework. Within the PBD framework, emerging challenges for tall-timber buildings in quantifying site-specific hazard engineering demand parameters are discussed. The problem of PBD is faced with a plethora of information and computationally expensive models. This entails the use of machine learning techniques for surrogate models; emerging multi-fidelity models are discussed in more detail. The review provided in this paper is outlined below.

- Detailed review and evolution of PBD design for earthquake (*e.g.*, FEMA 2012; PEER 2017; LATBSDC 2020) and wind (Spence and Kareem 2014; Cui and Caracoglia 2018; Bezabeh et al., 2020b; Hou and Jafari 2020; Kareem 2020) are provided in the cited literature. Thus, the review provided here is brief to set the context for the MH design consideration and emerging modeling consideration.
- With limited tall-timber buildings designed, the damping value to use for design and analysis is an ongoing challenge. This paper provides a review of the source of damping and damping values obtained from *in situ* measurements.
- SSI is highlighted to be important in the damping quantification and review, and future direction is provided.
- The lighter and tall-timber buildings are vulnerable to wind, and this can be mitigated using damping technologies. The different damping technologies are briefly reviewed, and current applications are highlighted. Detailed reviews on different damping technologies and applications to tall buildings are discussed in the literature (*e.g.*, Soong and

TABLE 1 | PEER performance based design framework.

References	Equation
Cornell and Krawinkler (2000), PEER (2017)	$\lambda_E(dv) = \int_{dm}\int_{edp}\int_{im} G(dv\|dm)\|dG(dm\|edp)\|\|dG(edp\|im)\|\|d\lambda(im)\|$ $\lambda_E(dv)$ = mean annual rate of exceedance of earthquake impact; dv = decision variable corresponding to the performance metric (for example, repair cost, downtime); dm = damage measure; edp = engineering demand parameter; im = intensity measure for the ground motion; $\lambda(im)$ = mean annual rate that a certain level of im is exceeded, $G(x\|y)$ = complementary cumulative distribution function of x given y
Ciampoli et al. (2011)	$\lambda_W(dv) = \int_{dm}\int_{edp}\int_{ip}\int_{im} G(dv\|dm)\|dG(dm\|edp)\|\|dG(edp\|im, ip)\|\|dG(ip\|im)\|\|d\lambda(im)\|$ $\lambda_W(dv)$ = mean annual rate of exceedance of wind impact; dv = decision variable corresponding to the performance metric (for example, repair cost); dm = damage measure; edp = engineering demand parameter; ip = wind–structure interaction; im = intensity measure for the wind; $d\lambda(im)$ = mean annual rate that a certain level of im is exceeded, $G(x\|y,z)$ = complementary cumulative distribution function of x given y and z. The structural response (edp) is characterized conditional on the wind–structure interaction (ip) in addition to the wind effects (im)

Spencer Jr 2002; Christopoulos and Filiatrault 2006; Takewaki 2011; Lago et al., 2018).

- Finally, with evolving computational tools, the different optimization techniques and surrogate models are reviewed. With the computationally intensive design and optimization, the current application of the multi-fidelity models is reviewed.

This paper is intended to give a highlight and opportunity for current state-of-the-art and future research direction.

PERFORMANCE-BASED DESIGN FOR EARTHQUAKE LOADS

In the 1990s, PBD was introduced as a new structural design procedure to meet targeted building performance subject to ground shaking (SEAOC 1995; FEMA 1997). Although the first-generation PBD methods considered actual seismic demand and nonlinear building capacity, they were deterministic in nature. The second generation of performance-based earthquake engineering (PBEE) methodology was proposed to quantify the mean annual rate of exceedance of earthquake impact $\lambda_E(dv)$ by capturing the uncertainty in ground shaking, building behavior, and decision variables (Cornell and Krawinkler 2000; Porter 2003). The PBEE framework (summarized in **Table 1**) was put forward by the Pacific Earthquake Engineering Research Center (PEER) (Porter 2003).

The PEER framework has been applied in the seismic design and evaluation of buildings (*e.g.*, O'Reilly and Calvi 2019; Shome et al., 2015; Jayaram et al., 2012; Zareian and Krawinkler 2012; Liel et al., 2011; Goulet et al., 2007). The PEER's triple integral implicitly assumes that damage measure (dm) conditioned-on-engineering demand parameter (edp) is independent of intensity measure (im), and decision variable (dv) conditioned-on-dm is independent of im and edp. The seismic impact quantification is decomposed into subtasks that can be carried out by a different group of experts (Der Kiureghian 2005). This conditional independence of the PEER framework has enabled other researchers to extend it to PBD for fire (*e.g.*, Lange et al., 2014), hurricane (Barbato et al., 2013), tsunami (Attary et al., 2017; Goda et al., 2021), and wind (*e.g.*, Ciampoli et al., 2011; Petrini and Ciampoli, 2012).

Computing the mean annual rate of exceedance of dvs is computationally intensive, and different approximations are proposed. The triple integral in the PEER framework can be computed using computationally intensive Monte Carlo simulations (*e.g.*, Jayaram et al., 2012; Goulet et al., 2007). Different stochastic models, such as Poisson, Markov, semi-Markov, renewal, or trigger type, have been considered for earthquake modeling (Anagnos and Kiremidjian 1984). With Poisson's occurrence of the earthquake load assumption, Der Kiureghian (2005) formulated a closed-form solution of the PEER framework. The closed-form solution of the mean annual rate is identical to the PEER framework. However, when the PEER framework is extended beyond 1 year, it gives a conservative result (Der Kiureghian 2005). Similarly, with Poisson's earthquake arrival assumption, Wen and Kang (2001a) developed a closed-form solution for earthquake load formulated under life cycle cost (LCC) (**Table 2**). The LCC equation shown in **Table 2** is a generalized equation that can be used for earthquake, wind, and earthquake and wind MH. In addition, it accounts for the coincidence rate of earthquake and wind hazard in the calculation of the LCC. Takahashi et al. (2004) considered a renewal model of earthquake occurrences in the LCC analysis. The LCC approach has been used in buildings' seismic design applications (*e.g.*, Wen and Kang 2001b; Liu et al., 2003; Mitropoulou et al., 2011; Castaldo et al., 2016). Mahsuli and Haukaas (2013) proposed a reliability-based approach to solving the loss assessment.

PERFORMANCE-BASED DESIGN FOR WIND LOADS

The current wind load design follows the Davenport wind loading chain (Davenport 1967; Isyumov 2012). In the wind loading chain, the wind response of tall buildings is determined

TABLE 2 | LCC performance based design framework.

Reference	Equation
Wen and Kang 2001a; Wen and Kang 2001b	$E[C(t,\boldsymbol{X})] = C_o(\boldsymbol{X}) + C_F(\boldsymbol{X})\left(\frac{1-e^{-\lambda t}}{\lambda}\right) + \frac{C_m(\boldsymbol{X})}{\lambda}(1-e^{-\lambda t})$ $E(\cdot)$ = expected value, C_o = initial cost; $\mathbf{X}$ = design variable; $e^{-\lambda t}$ = discounted factor over time t, λ = constant discount rate per year; C_m = operation and maintenance cost per year; and $C_F(X)$ = total expected cost due to all (k) limit states; defined as $C_F(\boldsymbol{X}) = \sum_{i=1}^{k} C_i\left[\sum_{i=1}^{n} \upsilon_i P_l^i(\boldsymbol{X}) + \sum_{i=1}^{n-1}\sum_{j=i+1}^{n} \upsilon_{ij} P_l^{ij}(\boldsymbol{X}) + + \sum_{i}^{n-2}\sum_{j=1+1}^{n-1}\sum_{k=j+1}^{n} \upsilon_{ijk} P_l^{ijk}(\boldsymbol{X}) + \cdots\right]$ υ_i = mean occurrence rate of hazard i; $\upsilon_{ij} = \upsilon_i\upsilon_j(\mu_{d_i} + \mu_{d_j})$ = coincidence rate of hazards i and j; mean occurrence rate of hazard i;; $\upsilon_{ijk} = \upsilon_i\upsilon_j\upsilon_k(\mu_{d_i}\mu_{d_j} + \mu_{d_i}\mu_{d_k} + \mu_{d_i}\mu_{d_k})$ = coincidence rate of hazards i, j and k; mean occurrence rate of hazard i; P_l^i = probability of limit-state l given the coincidence of hazard i; P_l^{ij} = probability of limit-state l given the coincidence of hazard i and j; P_l^{ijk} = probability of limit-state l given the coincidence of hazard i, j and k; μ_{d_i} = mean duration of hazard i

by considering local wind climatology, local wind exposure and topography, structural aerodynamic characteristics (governed by building shape), and structural dynamic properties (Kareem et al., 2019; Bezabeh et al., 2020b; Solari 2020). The framework was developed for synoptic and stationary winds. Non-stationarity of the wind load, however, has been identified as an important factor to consider (Kareem and Wu 2013; Solari et al., 2015; Hong 2016). Kareem et al. (2019) generalized the Davenport wind loading chain to account for a non-stationary wind–force–response relationship. Unlike earthquake load, for wind load, the building's aerodynamic interactions are evolving with the change in the built environment (Davenport 1983; Elshaer et al., 2017). Thus, the design for wind loads should account for the evolution of the built environment.

Bezabeh et al. (2020b) have provided a state-of-the-art review on PBD for wind loads. The PEER framework was extended for "Performance-Based Wind Engineering" (PBWE, **Table 1**, Ciampoli et al., 2011). Different researchers have used the PBWE framework (*e.g.*, Augusti and Ciampoli 2008; Ciampoli et al., 2011; Ciampoli and Petrini 2012; Spence and Kareem 2014; Chuang and Spence 2017; Suksuwan and Spence 2019; Ouyang and Spence 2021). Similar to PBEE, the PBWE framework is computationally intensive and requires quantifying the probabilistic hazard to loss assessment. Wen and Kang (2001a) proposed an LCC-based closed-form solution of the probabilistic wind design framework (**Table 2**). The LCC framework has been applied for tall building wind load design (*e.g.*, Le and Caracoglia 2021; Micheli et al., 2019, 2021; Cui and Caracoglia 2018, Cui and Caracoglia 2020; Ierimonti et al., 2017; Ierimonti et al., 2018). Bezabeh et al. (2018a, 2018b) extended the Davenport wind loading chain to account for uncertainties and formulated it in a reliability framework.

The wind load design was mainly undertaken for a linear response that will consequently furnish over designed system (Alinejad and Kang, 2020). The consideration of nonlinear wind design is an emerging area (*e.g.*, Alinejad et al., 2020, 2021; Bezabeh et al., 2020b; Elezaby and El Damatty 2020; Huang and Chen 2022). To ameliorate this, the ASCE (2019) pre-standard has put forward a PBWD of buildings for wind load, where both linear elastic and nonlinear time history analysis (NLTHA) can be utilized. Chuang and Spence (2017) presented a wind PBD framework to account both for collapse and non-collapse limit states. Bezabeh et al. (2021a, 2021b) proposed a PBWD for a nonlinear wind design framework. Bezabeh et al. (2020b) proposed using self-centering systems to overcome the progressive unidirectional accumulation of plastic deformations.

MULTI-HAZARD DESIGN UNDER EARTHQUAKE AND WIND LOADS

For earthquake and wind MH design framework, fragility-based (Zheng et al., 2021; Li et al., 2021; Li et al., 2020), LCC-based (Kleingesinds and Lavan 2021; Kleingesinds et al., 2021; Venanzi et al., 2018; Mahmoud and Cheng 2017; Wen and Kang 2001a; Wen and Kang 2001b), and risk-based (Crosti et al., 2010; Duthinh and Simiu 2010; Suksuwan and Spence 2018; Wang M. et al., 2021; Kwag et al., 2021; Roy et al., 2021; Zheng et al., 2021) framework have been proposed to meet different performance objectives (*e.g.*, serviceability/comfort, life safety).

Wen and Kang (2001a) formulated a generalized LCC framework that considers both correlated and uncorrelated earthquake and wind loads (**Table 2**). The MH framework assumed that earthquake and wind hazards follow a Poisson model (Wen 1990). The MH PBD framework considers uncertainties in hazard, demand, capacity, and initial construction C_o and damage costs. The earthquake and wind loads vary over time; however, the co-occurrence of the maximum values for earthquake and wind loads is small, and this correlation can be ignored (Wen and Kang 2001a; Wen 2001). Suksuwan and Spence (2018) and Chulahwat and Mahmoud (2017), for example, integrated the PEER earthquake $\lambda_E(dv)$ and wind $\lambda_W(dv)$ PBD frameworks (**Table 1**) for earthquake and wind MH design, $\lambda_{MH}(DV)$, as:

$$\lambda_{MH}(dv) = \lambda_E(dv) + \lambda_W(dv) \tag{1}$$

With an increasing body of knowledge in the MH design framework, there is no reported study for tall-timber buildings. The MH framework for the tall-timber building is presented in **Figure 2**.

SITE-SPECIFIC HAZARD AND ENGINEERING DEMAND PARAMETERS

In 1910, the Seismology Society of America identified three emerging areas (McGuire 2004): 1) earthquake event, 2) associated ground motions, and 3) effect on structures. The three emerging areas are still valid today for innovative building systems to reliably quantify the *im* and *edp*s. In wind engineering, it has gone through similar evolution with the wind loading chain (*e.g.*, Kareem et al., 2019; Bezabeh et al., 2020b; Solari 2020).

The *edp*s in the PBD framework (**Table 1**) are structural responses, such as acceleration and inter-story drift ratio (*e.g.*, Tesfamariam and Goda 2015; Cui and Caracoglia 2020), obtained through NLTHA. The site-specific hazard can be undertaken using probabilistic seismic hazard analysis (McGuire 2004; Atkinson and Goda 2013; Bommer and Stafford 2020) framework, considering empirical equations (Shahi and Baker 2011; Stafford 2014) or physics-based (Atkinson and Silva 2000; Yamamoto and Baker 2013) ground motion characterization. Finally, different ground motion selection algorithms are used to carry out the NLTHA (e.g., Bradley et al., 2015; Goda, 2015).

Advances in computational resources have enabled researchers to develop high-resolution coupled physics-based ground motion sources to structural simulation models (Kenawy et al., 2021; McCallen et al., 2021). This eliminates the epistemic uncertainty in quantifying free field and foundation level shaking. This model, however, requires a detailed site-specific source model and is computationally intensive. The computationally intensive PBD simulations can be ameliorated with a cloud-enabled computational platform (Deierlein et al., 2020; Kareem 2020). This might not be suitable for preliminary design iterations and verifications; however, it can be used for final design validation.

Once the *im* at the site is obtained through the hazard analysis, the *im* and *edp* relation is established through fragility curves (e.g., Goda and Tesfamariam 2015; De Risi et al., 2019; Cui and Caracoglia 2020; Le and Caracoglia 2021; Silva et al., 2021). Other important areas that warrant investigation for tall-timber buildings are the effect of long-duration earthquakes (Jennings 1970; Tesfamariam and Goda 2017), mainshock and aftershock earthquake sequences (Goda 2015; Tesfamariam and Goda, 2017; Tesfamariam and Goda 2015), a dependency between *edp*s (Goda and Tesfamariam 2015; De Risi et al., 2019), and directionality of wind loads (*e.g.*, Cui and Caracoglia 2020).

LOSS ASSESSMENT

The accuracy of the loss assessment is influenced by the available data and the choices of relevant models and parameters (Hosseinpour et al., 2021; Cremen and Baker 2021; O'Reilly and Calvi 2019; Baker and Cornell 2008). In North America, the current seismic loss assessment has evolved from expert-driven (*e.g.*, ATC 13, ATC 1985) to detailed simulation-based models (HAZUS, FEMA–NIBS 2003; FEMA P58, FEMA 2000). In a case where historical data are scarce, simulation-based methods are viable options (Yang et al., 2009; Zareian and Krawinkler 2012). HAZUS (FEMA–NIBS 2003; Kircher et al., 2006) quantifies the loss assessment using the maximum inter-story drift ratio obtained through simulation. Response of tall buildings are subject to multimodal response, and the loss assessment is better captured using a nonuniform evaluation of loss distribution over the height (Shome and Luco 2010; Shome et al., 2015). FEMA P58 (FEMA 2012; ATC 2018) developed a fragility-based loss assessment tool named performance assessment calculation tool. The performance assessment calculation tool contains a large database consisting of the mean and dispersion values of different consequence functions (repair cost, repair time, casualty, and dollar loss). Aslani and Miranda (2005) proposed a story-based loss assessment by considering the damage, downtime due to business interruption, injuries, and loss of lives. Different authors have now developed simplified story-based loss assessments (e.g., Papadopoulos et al., 2019; Shahnazaryan et al., 2021). Similar trends are followed in the loss assessment under wind load (*e.g.*, Le and Caracoglia 2021; Micheli et al., 2019; Micheli et al., 2021; Cui and Caracoglia 2018, 2020; Ierimonti et al., 2017; Ierimonti et al., 2018).

The current state-of-the-art evaluation and design are moving from loss quantification to post-earthquake recovery, called resiliency (Cimellaro et al., 2010; Cimellaro 2013; McAllister 2016; Almufti and Willford 2021; Furley et al., 2021). A comprehensive resilience rating system, Resilience-Based Earthquake Design Initiative, was developed by Arup (Almufti and Willford 2021). Wilson et al. (2021) implemented loss assessment for CLT building using FEMA P58. Furley et al. (2021) implemented a stochastic model to quantify the resiliency of a two-story self-centering CLT building.

SOIL–STRUCTURE INTERACTION

SSI is influenced by the site conditions, foundation embedment, flexibility, and shape on foundation impedance (Stewart et al., 1999; Sotiriadis et al., 2020). This interaction is complex, and it can have both beneficial and detrimental effects on the response (Mylonakis and Gazetas 2000). Low-fidelity spring models (*e.g.*, Stewart et al., 1999; Sotiriadis et al., 2020) and high-fidelity finite element models (*e.g.*, Rahmani et al., 2014; Arboleda-Monsalve et al., 2020; McCallen et al., 2021) have been used for SSI. Low-fidelity, linear, and nonlinear spring models can be used at the foundation of the building structure (*e.g.*, Stewart et al., 1999; Sotiriadis et al., 2020). Lesgidis et al. (2018) proposed frequency- and intensity-dependent spring models for SSI.

The SSI is an important intrinsic source of damping for tall buildings (*e.g.*, Cruz and Miranda, 2017). The SSI will consequently impact the response of tall buildings under earthquake and wind loads. However, the SSI effect is not considered in the current tall-timber building design literature. Liu et al. (2008) showed that for a wind-induced response of tall buildings incorporating tuned mass damper (TMD), neglecting the SSI overestimated the response and underestimated the effectiveness of the TMD. Zhou et al. (2018), for eddy current

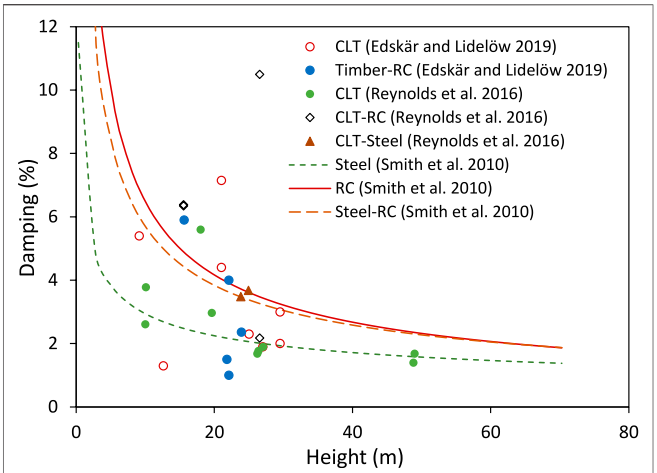

FIGURE 3 | Variation of damping with height.

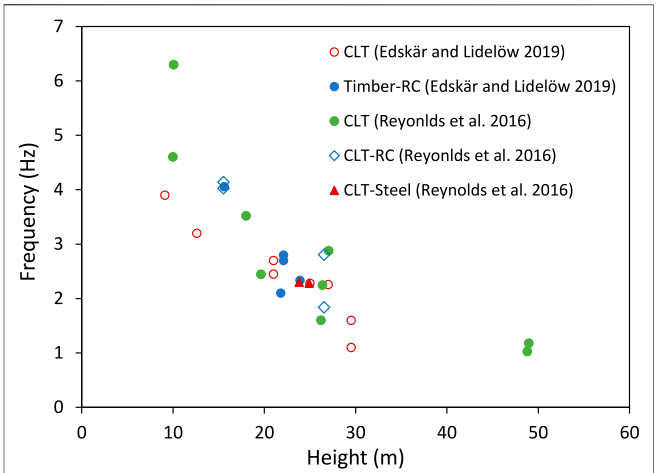

FIGURE 4 | Variation of frequency with height.

TMD and wind-load application on tall buildings, showed that, with consideration of SSI, the short return period acceleration response exceeded the human comfort limit states.

DAMPING

Damping mechanisms in tall buildings are associated with intrinsic/inherent (or structural), aerodynamic, hysteretic, and supplemental/additional (Smith et al., 2010; Lago et al., 2018). Factors that contribute to the damping are as follows (Yeh et al., 1971; Cruz and Miranda, 2016, 2017): material, friction between members and connections, structural system and joint types, foundation and soil types, interior partitions, exterior cladding, other nonstructural members, and vibration amplitude.

The damping associated with different mass timber building typologies and connections can be quantified from field measurement (*e.g.*, Smith et al., 2010; Kijewski-Correa and Pirnia, 2007). With *in situ* ambient vibration measurements, Edskär and Lidelöw (2019) and Reynolds et al. (2016) reported building height and damping relationship (**Figure 3**). From **Figure 3**, it is apparent that, as expected, with the increase in building height, the damping values are decreasing. The damping–height empirical equations for steel, concrete, and steel/concrete buildings reported in Smith et al. (2010) are plotted in **Figure 3**. Overall, both have a similar trend, and some of the timber-building damping values are bounded between the empirical equation for steel and RC damping values. The variability in the damping values for the timber building is high, and this warrants more investigation to understand the causal relation of different explanatory factors. The current analytical studies reported on mass timber building do not consider the SSI. Thus, the response obtained through the *in situ* measurements and analytical studies can be different (*e.g.*, Edskär and Lidelöw 2017, 2019). Thus, future analytical studies should incorporate the SSI in the damping calculations. The building height and frequency relationship is shown in **Figure 4**. One of the main explanatory factors for the reduction in damping and frequency can be intrinsic damping (*e.g.*, Tamura and Suganuma 1996; Smith et al., 2010).

ENERGY DISSIPATION DEVICES

Motions of a building, due to earthquake and wind loads, are traditionally controlled through mass and stiffness proportioning. Increasing the stiffness, however, can increase the acceleration demand. In addition, it can reduce the overall seismic energy dissipation capacity with consequent unintended failure of connections and capacity-protected elements (ASCE 2019). Using supplemental energy dissipators, the exceedance of serviceability limit state can be reduced. **Figure 5** depicts the high-level category of the different supplemental energy dissipation devices.

The supplemental energy dissipation devices can be categorized as passive, active, semiactive, and hybrid damping systems and seismic isolation systems (Soong and Spencer Jr 2002; Takewaki 2011; Lago et al., 2018; De Domenico et al., 2019; Jafari and Alipour 2021b; Takewaki and Akehashi 2021). Traditional passive control damping, such as TMD and tuned liquid damper, are tuned to the fundamental period of the structure and are not suitable for earthquake response mitigation (Willford et al., 2008; Lago et al., 2018). Under severe earthquake loads, the structural response will undergo yielding and consequent period elongation. On the other hand, metallic damper used for earthquake loads will not be suitable for wind loads, as the serviceability wind loads will not yield metallic dampers (Willford et al., 2008). Viscoelastic dampers (Christopoulos and Montgomery 2013) are attractive damping technology that can be used both for earthquake and wind loads. Under MH design consideration, finding the right damper and location by satisfying the MH performance limit states can be cast as an optimization problem (*e.g.*, Suksuwan and Spence 2018; Roy et al., 2021).

Different papers are published on the application of energy dissipation devices for tall buildings: earthquake (*e.g.*,

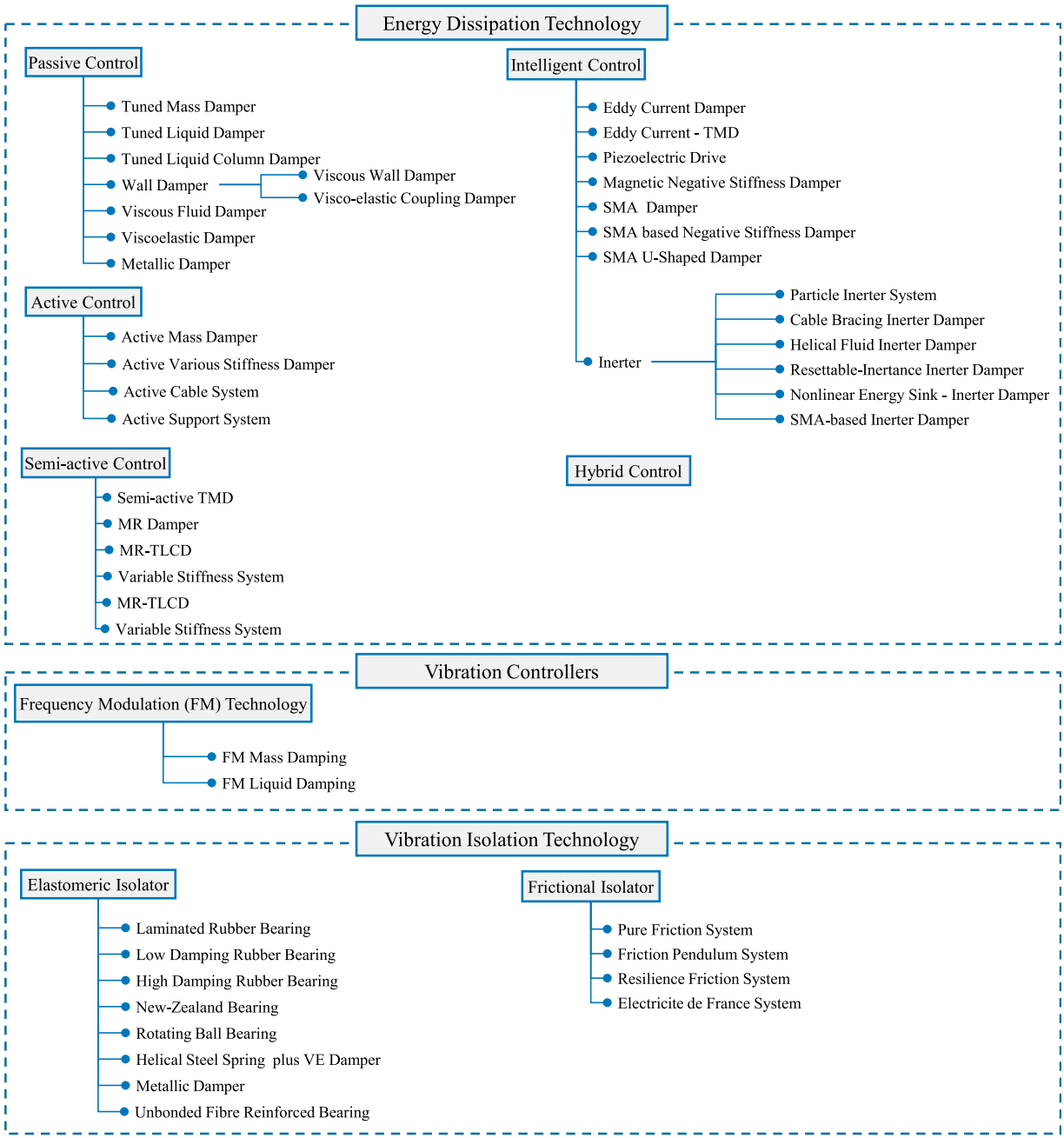

FIGURE 5 | General classification of supplemental energy dissipation devices.

Christopoulos and Montgomery 2013; Kasagi et al., 2016; Nakamura and Hanzawa 2017; Zhou et al., 2018; Hashizume and Takewaki 2020; Uemura et al., 2021), wind (*e.g.*, Liu et al., 2008; Giaralis and Petrini 2017), and MH (earthquake and wind) (*e.g.*, Roy and Matsagar 2019, 2020; Wang M. et al., 2021; Li et al., 2021) loads. Use of base isolations for tall buildings under earthquake (*e.g.*, Taniguchi et al., 2016; Makita et al., 2018), wind (*e.g.*, Chen and Ahmadi 1992; Vulcano 1998; Cheng et al., 2002), and MH (earthquake and wind) (*e.g.*, Roy et al., 2021) loads are also reported in the literature. Liu et al. (2008) and Zhou et al. (2018), respectively, considered the influence of SSI on TMD and eddy-current TMD on tall building response under wind loads. Façades of buildings often are considered nonstructural elements. Recent innovative connections, however, are paving the way for the potential use of the façades as distributed dampers (Jafari and Alipour 2021a,c).

The application of dampers in timber building is limited (*e.g.*, Huang and Chang 2018; Hashemi et al., 2020). The damping for the mass timber is mostly considered with

energy dissipating connectors (*e.g.*, Pu et al., 2016; Fitzgerald et al., 2020). More studies, however, in light timber structures are reported (Bolmsvik and Brandt 2013; Jayamon et al., 2018; Ugalde et al., 2019; Tesfamariam et al., 2021b; Nakamura and Fujii 2021).

OPTIMIZATION

The MH design optimization problems are subject to uncertainties both on the demand and capacity (*e.g.*, Rosenblueth 1986; Wen 2001; Franchin 2004; Der Kiureghian and Ditlevsen 2009; Spence and Kareem 2014; Kleingesinds et al., 2021). Different optimization under uncertainty algorithms is proposed. The design optimization, under uncertainty, can be cast under reliability-based design optimization (RBDO) (Aoues and Chateauneuf 2010; Valdebenito and Schuëller 2010; Song et al., 2021) and robust design optimization (RDO) (Chatterjee et al., 2019; Chakraborty et al., 2021; Das et al., 2021) frameworks. Subsequently, the problem is solved using gradient (*e.g.*, Franchin et al., 2018; Kleingesinds and Lavan 2021) or non-gradient (derivate-free) (*e.g.*, Hare et al., 2013; Afshari et al., 2019; Umeura et al., 2021) optimization algorithms. In addition, the design requirements to satisfy both earthquake and wind MH loads can be conflicting, and the problem can be formulated under a multi-objective optimization framework (*e.g.*, Afshari et al., 2019).

Reliability-Based Design Optimization

The RBDO technique has proven its utility for optimization under uncertainty (Song et al., 2021). In RBDO, although user-defined performance functions are optimized, probability failure criterion is added as a constraint. The solution for RBDO can be classified as formulated, among others, as two-level and decoupled methods (De et al., 2021). The two-level optimization, which is computationally intensive, entails the use of two nested loops, *i.e.*, the inner loop to solve the reliability analysis and the outer loop to carry out the design optimization. The decoupled method, which is less computationally intensive, entails carrying out deterministic RBDO by replacing the inner-loop reliability analysis (Madsen and Hansen 1992). Spence et al. (2016) proposed an efficient algorithm for the RBDO of a large-scale uncertain system. Chakraborty and Roy (2011) used RBDO for the optimal design of TMD under earthquake load. Altieri et al. (2018) investigated the optimal design of a nonlinear viscous damper using RBDO under earthquake load. Das et al. (2020) showed the effectiveness of the estimation of tuning parameters of nonlinear energy sink using RBDO. Ontiveros-Perez et al. (2019) used RBDO of passive friction damper for mitigation of earthquake-induced vibration. To enhance the seismic performance of the base-isolated structure, Peng et al. (2021) proposed a reliability-based optimization technique for an adaptive sliding base isolation system. Zou et al. (2010) studied the reliability-based optimization of the base-isolated concrete building considering the drift of the superstructure as a performance criterion.

Robust Design Optimization

A system is called robust when the system is insensitive to the effects of uncertainty. The RDO method propagates uncertainty by minimizing the mean and standard deviators of the structural responses. This problem is solved as a multi-objective optimization problem. Miguel et al. (2014) showed the optimal location and parameters of friction damper using RDO. Yu et al. (2013) carried out a reliability-based RDO of TMD to mitigate the earthquake-induced vibration of building structures. The effectiveness and robustness of TMD were studied by Greco et al. (2015) to mitigate the seismic-induced vibration for buildings. Lagaros and Fragiadakis (2007) proposed an LCC-based RDO for the design of steel moment-resisting frames. The RDO, for estimating the tuning parameters of nonlinear energy sink with negative stiffness, was investigated by Chakraborty et al. (2021) and Das et al. (2021).

Topology Optimization

With advances in finite element modeling, optimizing the shape and form of the tall-timber building can be undertaken under topology optimization. The topology optimization, for a prescribed structural domain, under a set of the objective function and design constraints, provides a rational approach to obtain optimal layout (Sigmund and Maute 2013). Beghini et al. (2014) presented a review of structural topology optimization and highlighted the means of finding the balance between engineering and architecture. This can be of particular interest in tall-timber buildings, as it can integrate aesthetics and structural factors in design. Martin and Deierlein (2020) proposed modal compliance-based topology optimization for the tall building subjected to dynamic seismic excitation. Suksuwan and Spence (2018) proposed a simulation-centered performance-based MH topology optimization framework for earthquake and wind loads. Goli et al. (2021) showed the parametric topology optimization of the lateral bracing systems for tall buildings subjected to wind and gravity loads using bidirectional evolutionary structural optimization. Gomez et al. (2020, 2021) showed the topology optimization of the building subjected to seismic and wind stochastic excitations, respectively. Bobby et al. (2016, 2017) proposed a data-driven and reliability-based topology optimization of uncertain wind-excited tall buildings, respectively. Bobby et al. (2014) proposed a performance-based topology optimization framework for wind-excited tall buildings.

MULTI-FIDELITY SURROGATE MODELS

High-fidelity and detailed three-dimensional building models can be used for the NLTHA of buildings (*e.g.*, Rinaldin and Fragiacomo 2016; Lu et al., 2018; Wang and Wu 2020; Tesfamariam et al., 2021a). For computationally intensive three-dimensional models or experimental data, however, the use of a physics-informed neural network, surrogate models, and multi-fidelity models can be the future direction (Peherstorfer et al., 2018; Swischuk et al., 2019; Deierlein et al., 2020; Chakraborty 2021; Karniadakis et al., 2021).

Surrogate Models

For computationally expensive design and optimization, a surrogate model (*e.g.*, artificial neural network, Lehký et al., 2018; response surface method, Foschi et al., 2002), constructed using few training samples, can replace the original limit state. In the surrogate model development, adaptive sampling techniques can be considered to enhance the reliability of the prediction. Such sampling techniques, for example, are Kriging (*e.g.*, Dubourg et al., 2011; Bernardini et al., 2014; Li et al., 2016; Zhang et al., 2017), adaptive Kriging (Das and Tesfamariam 2020; Kroetz et al., 2020; Zhang et al., 2022), adaptive Bayesian support vector regression (Wang J. et al., 2021), polynomial chaos-based Kriging (Das et al., 2020), spectral representation (Zhao et al., 2021), Kriging and adaptive wavelet network (Micheli et al., 2020a), and Bayesian deep learning (Luo and Kareem 2020). In uncertainty propagation, assemble of surrogate models can be used (*e.g.*, Wang et al., 2019; Das et al., 2021). Micheli et al. (2020b) used multiple-surrogate models for probabilistic performance assessment of wind-excited tall buildings.

Physics-Informed Neural Network

A physics-based (informed) neural network (Wu et al., 2018; Beucler et al., 2021; Haghighat and Juanes 2021) is an emerging and promising modeling technique. In a physics-based neural network, the physics of the problem (*e.g.*, structural model output) is coupled with machine learning (*e.g.*, neural network) to develop surrogate models. Lai et al. (2021) presented structural identification with physics-informed neural ordinary differential equations. Yucesan et al. (2021) proposed a framework using a physics-informed neural network for adjusting the outputs of torsional vibration dampers to experimental data. De (2021) applied a physics-based neural network model for base-isolated buildings and wind-excited tall structures. Wang and Wu (2020) implemented a physics-informed neural network for wind-induced nonlinear structural dynamic analysis.

Multi-Fidelity Models

A state-of-the-art review on multi-fidelity models is discussed in Peherstorfer et al. (2018). The multi-fidelity approach considers the integration of a high-fidelity (higher accuracy, higher computational cost) model with low fidelity (lower accuracy, lower computational cost). The integration in the multi-fidelity approach entails adaptation (*i.e.*, enhancing the low-fidelity model), fusion (*i.e.*, combining the low- and high-fidelity results), and filtering (*i.e.*, the high-fidelity model is invoked after filter using the low-fidelity results) (Peherstorfer et al., 2018).

The multi-fidelity approach is now applied to earthquake engineering problems. Zhang et al. (2022) developed adaptive multi-fidelity Gaussian process reliability analysis to solve reliability problems. Royset et al. (2019) presented a multi-fidelity analysis for risk-adaptive statistical learning method to predict structural response. Yang and Perdikaris (2019) presented conditional deep surrogate models for probabilistic data fusion and multi-fidelity modeling of stochastic systems. Patsialis and Taflanidis (2021) used a multi-fidelity Monte Carlo simulation for seismic risk assessment. Sevieri et al. (2021) presented a multi-fidelity Bayesian framework for robust seismic fragility analysis. Chatzidaki and Vamvatsikos (2021) used a multi-fidelity model for probabilistic seismic demand models for fragility assessment. Zhou and Tang (2021) used multi-fidelity data fusion for the efficient characterization of dynamic response variation. Li and Jia (2020) used a multi-fidelity Gaussian process model integrating low- and high-fidelity data considering censoring. Xu et al. (2016) proposed a computational framework for regional seismic simulation of buildings with multiple-fidelity models. This risk assessment is suitable for regional seismic and wind hazards loss assessment. Dey et al. (2021) used a multi-fidelity approach for uncertainty quantification of buried pipeline response undergoing fault rupture displacements. Lopez-Caballero (2021) utilized a multi-fidelity approach for probabilistic seismic analysis of liquefiable embankment.

Similar multi-fidelity approaches can be considered for computing the *edp*s under wind loads. To compute the *edp*s in the wind loading chain, high-frequency pressure integration wind tunnel tests (Bezabeh et al., 2021a) or computational fluid dynamics (CFD) (Kareem 2020) can be considered. Moni et al. (2020) implemented an aeroelastic hybrid simulation of a base-pivoting building model in a wind tunnel. The experimental testing is not readily available for preliminary design and iteration. Reducing our reliance on physical testing was one of the grand challenges put forward by Masters (2016). Kareem (2020) and Ding and Kareem (2018) implemented a multi-fidelity CFD modeling approach, where the results of low-fidelity (*e.g.*, Reynolds-averaged Navier–Stokes) and high-fidelity (*e.g.*, large eddy simulation) simulations can be combined. Lamberti and Gorlé (2021) implemented a multi-fidelity machine learning framework to predict wind loads on buildings. Karem and Kwon (2017) proposed cyber-based data-enabled wind load effects on civil infrastructures. Bobby et al. (2016) proposed a data-driven simulation-based framework for the effective topology optimization of uncertain and dynamic wind-excited tall buildings. Bernardini et al. (2014) proposed an aerodynamic shape optimization of civil structures using a CFD-enabled surrogate model.

CONCLUSION AND FUTURE DIRECTION

The rapid growth of the urban population and associated environmental concerns challenged city planners and developers to consider sustainable and cost-efficient building systems. Mass timbers, such as CLT panels and glulam members, have been used as viable, sustainable tall-timber buildings. The tall-timber buildings, however, are lighter and more flexible, which can make those buildings vulnerable to earthquakes and wind loads. With emerging computational tools and analytical models, carrying out PBD with high-fidelity models is apparent. With the current and future research direction in consideration, in this paper, we carried out a state-of-the-art review on PBD for earthquake, wind, and MH loads. The state-of-the-art review has highlighted the

challenge and future direction for tall-timber building, which is summarized below.

- With increasing complexity in the tall-timber buildings, the need for a high-fidelity model and validation through experimental work is apparent. Subsequently, multi-fidelity modeling can be developed for design and optimization.
- Damping is a critical factor that influences the response of the building under earthquake and wind loads. As more tall-timber buildings are constructed, quantifying the damping values for tall-timber buildings is vital. This will enhance the knowledge and confidence in designing the buildings under MH. With more data collected on tall-timber buildings, data-driven models (*e.g.*, Spence and Kareem 2013) are a viable alternative in the preliminary design phase. Frequency dependency of the intrinsic damping and different excitation levels, ameliorating the earthquake and wind MH design implementation, are challenging tasks.
- Current studies on tall-timber design and analysis do not take the SSI into consideration. The importance of the SSI was highlighted, and in this direction, future concerted efforts should be made. To reduce the computational cost, a multi-fidelity model of SSI, *e.g.*, finite element and spring models, can be implemented.
- For the MH design framework, component-based fragility curves and loss data for tall-timber buildings should be developed and ameliorated in the FEMA P58 database.
- The design of tall-timber buildings under MH loads is complex and subject to uncertainties. This paper has provided a review on design optimization under uncertainty, with consideration of RBDO, RDO, and topology optimization.

AUTHOR CONTRIBUTIONS

ST is the only contributor.

FUNDING

Funding for this research was provided by the Natural Science Engineering Research Council of Canada Discovery Grant (RGPIN-2019-05584) and the BC Forestry Innovation Investment's (FII) Wood First Program.

REFERENCES

Afshari, H., Hare, W., and Tesfamariam, S. (2019). Constrained Multi-Objective Optimization Algorithms: Review and Comparison with Application in Reinforced concrete Structures. *Appl. Soft Comput.* 83, 105631. doi:10.1016/j.asoc.2019.105631

Ahmed, S., and Arocho, I. (2020). Mass Timber Building Material in the U.S. Construction Industry: Determining the Existing Awareness Level, Construction-Related Challenges, and Recommendations to Increase its Current Acceptance Level. *Clean. Eng. Tech.* 1, 100007. doi:10.1016/j.clet.2020.100007

Alinejad, H., Jeong, S. Y., and Kang, T. H.-K. (2020). Performance-based Design of Tall Buildings for Wind Load and Application of Response Modification Factor. *Wind and Structures* 31 (2), 153–164.

Alinejad, H., and Kang, T. H. (2020). Engineering Review of ASCE 7-16 Wind-Load Provisions and Wind Effect on Tall concrete-frame Buildings. *J. Struct. Eng.* 146 (6), 04020100. doi:10.1061/(asce)st.1943-541x.0002622

Alinejad, H., Kang, T. H., and Jeong, S. Y. (2021). Performance-based Wind Design Framework Proposal for Tall Buildings. *Wind and Structures* 32 (4), 283–292.

Almufti, I., and Willford, M. REDi^{TM} Rating System. Arup. Available at:https://www.arup.com/-/media/arup/files/publications/r/redi_final-version_october-2013-arup-website.pdf (Accessed December 24, 2021).2013.

Altieri, D., Tubaldi, E., De Angelis, M., Patelli, E., and Dall'Asta, A. (2018). Reliability-based Optimal Design of Nonlinear Viscous Dampers for the Seismic protection of Structural Systems. *Bull. Earthquake Eng.* 16 (2), 963–982. doi:10.1007/s10518-017-0233-4

American Society of Civil Engineers (ASCE) (2019). Prestandard for Performance-Based Wind Design. *Am. Soc. Civil Eng. Reston, VA*.

American Society of Civil Engineers (2017). *Minimum Design Loads for Buildings and Other Structures. ASCE/SEI*. Reston, VA: Structural Engineering Institute, 7–16.

Anagnos, T., and Kiremidjian, A. S. (1984). Stochastic Time-Predictable Model for Earthquake Occurrences. *Bull. Seismological Soc. America* 74 (6), 2593–2611. doi:10.1785/bssa0740062593

Aoues, Y., and Chateauneuf, A. (2010). Benchmark Study of Numerical Methods for Reliability-Based Design Optimization. *Struct. Multidisc Optim* 41 (2), 277–294. doi:10.1007/s00158-009-0412-2

Applied Technology Council (ATC). 1985. Earthquake Damage Evaluation Data for California. Applied Technology Council.

Applied Technology Council (ATC) (2018). Washington, DC.*FEMA P-58-6, Guidelines For Performance-Based Seismic Design Of Buildings.* Federal Emergency Management Agency.

Arboleda-Monsalve, L. G., Mercado, J. A., Terzic, V., and Mackie, K. R. (2020). Soil–structure Interaction Effects on Seismic Performance and Earthquake-Induced Losses in Tall Buildings. *J. Geotechnical Geoenvironmental Eng.* 146 (5)–04020028.

Aslani, H., and Miranda, E. (2005). *Blume Earthquake Engineering Center*. Stanford: Stanford UniversityCA.Probabilistic Earthquake Loss Estimation and Loss Disaggregation in Buildings, Report No. 157, the John A.

Atkinson, G. M., and Goda, K. (2013). Chapter 1 in *Handbook Of Seismic Risk Analysis And Management Of Civil Infrastructure Systems*. Editors S. Tesfamariam and K. Goda (Cambridge: Woodhead Publishing), 23–28.*Probabilistic Seismic hazard Analysis of Civil Infrastructure*:

Atkinson, G. M., and Silva, W. (2000). Stochastic Modeling of California Ground Motions. *Bull. Seismological Soc. America* 90 (2), 255–274. doi:10.1785/0119990064

Attary, N., Unnikrishnan, V. U., van de Lindt, J. W., Cox, D. T., and Barbosa, A. R. (2017). Performance-based Tsunami Engineering Methodology for Risk Assessment of Structures. *Eng. Structures* 141, 676–686. doi:10.1016/j.engstruct.2017.03.071

Augusti, G., and Ciampoli, M. (2008). Performance-based Design in Risk Assessment and Reduction. *Probabilistic Eng. Mech.* 23 (4), 496–508. doi:10.1016/j.probengmech.2008.01.007

Baker, J. W., and Cornell, C. A. (2008). Uncertainty Propagation in Probabilistic Seismic Loss Estimation. *Struct. Saf.* 30 (3), 236–252. doi:10.1016/j.strusafe.2006.11.003

Barbato, M., Petrini, F., Unnikrishnan, V. U., and Ciampoli, M. (2013). Performance-based hurricane Engineering (PBHE) Framework. *Struct. Saf.* 45, 24–35. doi:10.1016/j.strusafe.2013.07.002

Beghini, L. L., Beghini, A., Katz, N., Baker, W. F., and Paulino, G. H. (2014). Connecting Architecture and Engineering through Structural Topology Optimization. *Eng. Structures* 59, 716–726. doi:10.1016/j.engstruct.2013.10.032

Bernardini, E., Spence, S. M., Kwon, D. K., and Kareem, A. (2014). Performance-based Design of High-Rise Buildings for Occupant comfort. *J. Struct. Eng.* 141 (10), 04014244.

Beucler, T., Pritchard, M., Rasp, S., Ott, J., Baldi, P., and Gentine, P. (2021). Enforcing Analytic Constraints in Neural Networks Emulating Physical Systems. *Phys. Rev. Lett.* 126 (9), 098302. doi:10.1103/physrevlett.126.098302

Bezabeh, M. A., Bitsuamlak, G. T., Popovski, M., and Tesfamariam, S. (2018a). Probabilistic Serviceability-Performance Assessment of Tall Mass-Timber Buildings Subjected to Stochastic Wind Loads: Part I - Structural Design and Wind Tunnel Testing. *J. Wind Eng. Ind. Aerodynamics* 181, 85–103. doi:10.1016/j.jweia.2018.08.012

Bezabeh, M. A., Bitsuamlak, G. T., Popovski, M., and Tesfamariam, S. (2018b). Probabilistic Serviceability-Performance Assessment of Tall Mass-Timber Buildings Subjected to Stochastic Wind Loads: Part II - Structural Reliability Analysis. *J. Wind Eng. Ind. Aerodynamics* 181, 112–125. doi:10.1016/j.jweia.2018.08.013

Bezabeh, M. A., Gairola, A., Bitsuamlak, G. T., Popovski, M., and Tesfamariam, S. (2018c). Structural Performance of Multi-story Mass-Timber Buildings under Tornado-like Wind Field. *Eng. Structures* 177, 519–539. doi:10.1016/j.engstruct.2018.07.079

Bezabeh, M., Bitsuamlak, G., Popovski, M., and Tesfamariam, S. (2020a). Dynamic Response of Tall Mass-Timber Buildings to Wind Excitation. *J. Struct. Eng.* 146 (10), 04020199. doi:10.1061/(asce)st.1943-541x.0002746

Bezabeh, M., Bitsuamlak, G., and Tesfamariam, S. (2021a). Nonlinear Dynamic Response of SDOF Systems Subjected to Along-Wind Loads. Part I: Parametric Study. *J. Struct. Eng.* (11), 14704021177.

Bezabeh, M., Bitsuamlak, G., and Tesfamariam, S. (2021b). Nonlinear Dynamic Response of SDOF Systems Subjected to Along-Wind Loads. Part II: Implications for Structural Reliability. *J. Struct. Eng.* 147 (11), 04021178.

Bezabeh, M., Bitsuamlak, G., and Tesfamariam, S. (2020b). Performance-based Wind Design of Tall Buildings: Concepts, Frameworks, and Opportunities. *Wind and Structures* 31 (2), 103–142.

Bobby, S., Spence, S. M. J., Bernardini, E., and Kareem, A. (2014). Performance-based Topology Optimization for Wind-Excited Tall Buildings: A Framework. *Eng. Structures* 74, 242–255. doi:10.1016/j.engstruct.2014.05.043

Bobby, S., Spence, S. M. J., and Kareem, A. (2016). Data-driven Performance-Based Topology Optimization of Uncertain Wind-Excited Tall Buildings. *Struct. Multidisc Optim* 54 (6), 1379–1402. doi:10.1007/s00158-016-1474-6

Bobby, S., Suksuwan, A., Spence, S. M. J., and Kareem, A. (2017). Reliability-based Topology Optimization of Uncertain Building Systems Subject to Stochastic Excitation. *Struct. Saf.* 66, 1–16. doi:10.1016/j.strusafe.2017.01.005

Bolmsvik, Å., and Brandt, A. (2013). Damping Assessment of Light Wooden Assembly with and without Damping Material. *Eng. Structures* 49, 434–447. doi:10.1016/j.engstruct.2012.11.026

Bommer, J. J., and Stafford, P. J. (2020). Selecting Ground-Motion Models for Site-specific PSHA: Adaptability versus Applicability. *Bull. Seismological Soc. America* 110 (6), 2801–2815. doi:10.1785/0120200171

Bradley, B. A., Burks, L. S., and Baker, J. W. (2015). Ground Motion Selection for Simulation-Based Seismic hazard and Structural Reliability Assessment. *Earthquake Engng Struct. Dyn.* 44 (13), 2321–2340. doi:10.1002/eqe.2588

Castaldo, P., Palazzo, B., and Della Vecchia, P. (2016). Life-cycle Cost and Seismic Reliability Analysis of 3D Systems Equipped with FPS for Different Isolation Degrees. *Eng. Structures* 125, 349–363. doi:10.1016/j.engstruct.2016.06.056

Chakraborty, S. (2021). Transfer Learning Based Multi-Fidelity Physics Informed Deep Neural Network. *J. Comput. Phys.* 426, 109942. doi:10.1016/j.jcp.2020.109942

Chakraborty, S., Das, S., and Tesfamariam, S. (2021). Robust Design Optimization of Nonlinear Energy Sink under Random System Parameters. *Probabilistic Eng. Mech.* 65, 103139. doi:10.1016/j.probengmech.2021.103139

Chakraborty, S., and Roy, B. K. (2011). Reliability Based Optimum Design of Tuned Mass Damper in Seismic Vibration Control of Structures with Bounded Uncertain Parameters. *Probabilistic Eng. Mech.* 26 (2), 215–221. doi:10.1016/j.probengmech.2010.07.007

Chatterjee, T., Chakraborty, S., and Chowdhury, R. (2019). A Critical Review of Surrogate Assisted Robust Design Optimization. *Arch. Computat Methods Eng.* 26 (1), 245–274. doi:10.1007/s11831-017-9240-5

Chatzidaki, A., and Vamvatsikos, D. (2021). Mixed Probabilistic Seismic Demand Models for Fragility Assessment. *Bull. Earthquake Eng.* 19, 6397–6421. doi:10.1007/s10518-021-01163-4

Chen, Y., and Ahmadi, G. (1992). Wind Effects on Base-Isolated Structures. *J. Eng. Mech.* 118 (8), 1708–1727. doi:10.1061/(asce)0733-9399(1992)118:8(1708)

Cheng, C. M., Lu, P. C., and Tsai, M. S. (2002). Acrosswind Aerodynamic Damping of Isolated Square-Shaped Buildings. *J. Wind Eng. Ind. Aerodynamics* 90 (12-15), 1743–1756. doi:10.1016/s0167-6105(02)00284-2

Christopoulos, C., and Filiatrault, A. (2006). *Principles of Passive Supplemental Damping and Seismic Isolation*. Milan, Italy: IUSS Press.

Christopoulos, C., and Montgomery, M. (2013). Viscoelastic Coupling Dampers (VCDs) for Enhanced Wind and Seismic Performance of High-Rise Buildings. *Earthquake Engng Struct. Dyn.* 42 (15), 2217–2233. doi:10.1002/eqe.2321

Chuang, W.-C., and Spence, S. M. J. (2017). A Performance-Based Design Framework for the Integrated Collapse and Non-collapse Assessment of Wind Excited Buildings. *Eng. Structures* 150, 746–758. doi:10.1016/j.engstruct.2017.07.030

Chulahwat, A., and Mahmoud, H. (2017). A Combinatorial Optimization Approach for Multi-hazard Design of Building Systems with Suspended Floor Slabs under Wind and Seismic Hazards. *Eng. Structures* 137, 268–284. doi:10.1016/j.engstruct.2017.01.074

Ciampoli, M., Petrini, F., and Augusti, G. (2011). Performance-based Wind Engineering: towards a General Procedure. *Struct. Saf.* 33, 367–378. doi:10.1016/j.strusafe.2011.07.001

Ciampoli, M., and Petrini, F. (2012). Performance-based Aeolian Risk Assessment and Reduction for Tall Buildings. *Probabilistic Eng. Mech.* 28, 75–84. doi:10.1016/j.probengmech.2011.08.013

Cimellaro, G. P., Reinhorn, A. M., and Bruneau, M. (2010). Framework for Analytical Quantification of Disaster Resilience. *Eng. Structures* 32 (11), 3639–3649. doi:10.1016/j.engstruct.2010.08.008

Cimellaro, G. P. (2013). "Resilience-based Design (RBD) Modelling of Civil Infrastructure to Assess Seismic Hazards," in *Handbook Of Seismic Risk Analysis And Management Of Civil Infrastructure Systems*. Editors S. Tesfamariam and K. Goda (Cambridge: Woodhead Publishing), 268–303. doi:10.1533/9780857098986.2.268:

Cornell, C. A., and Krawinkler, H. (2000). Progress and Challenges in Seismic Performance Assessment. *PEER Cent. News* 3 (2), 1–4.

Cremen, G., and Baker, J. W. (2021). Variance-based Sensitivity Analyses and Uncertainty Quantification for FEMA P-58 Consequence Predictions. *Earthquake Engng Struct. Dyn.* 50 (3), 811–830. doi:10.1002/eqe.3370

Crosti, C., Duthinh, D., and Simiu, E. (2010). Risk Consistency and Synergy in Multihazard Design. *J. Struct. Eng.* 137 (8), 844–849.

Cruz, C., and Miranda, E. (2016). Evaluation of Damping Ratios for the Seismic Analysis of Tall Buildings. *J. Struct. Eng.* 143 (1), 04016144.

Cruz, C., and Miranda, E. (2017). Evaluation of Soil-Structure Interaction Effects on the Damping Ratios of Buildings Subjected to Earthquakes. *Soil Dyn. Earthquake Eng.* 100, 183–195. doi:10.1016/j.soildyn.2017.05.034

Cui, W., and Caracoglia, L. (2020). Performance-based Wind Engineering of Tall Buildings Examining Life-Cycle Downtime and Multisource Wind Damage. *J. Struct. Eng.* 146 (1), 04019179. doi:10.1061/(asce)st.1943-541x.0002479

Cui, W., and Caracoglia, L. (2018). A Unified Framework for Performance-Based Wind Engineering of Tall Buildings in hurricane-prone Regions Based on Lifetime Intervention-Cost Estimation. *Struct. Saf.* 73, 75–86. doi:10.1016/j.strusafe.2018.02.003

Das, S., Chakraborty, S., Chen, Y., and Tesfamariam, S. (2021). Robust Design Optimization for SMA Based Nonlinear Energy Sink with Negative Stiffness and Friction. *Soil Dyn. Earthquake Eng.* 140, 106466. doi:10.1016/j.soildyn.2020.106466

Das, S., Tesfamariam, S., Chen, Y., Qian, Z., Tan, P., and Zhou, F. (2020). Reliability-based Optimization of Nonlinear Energy Sink with Negative Stiffness and Sliding Friction. *J. Sound Vibration* 485, 115560. doi:10.1016/j.jsv.2020.115560

Das, S., and Tesfamariam, S. (2020). Optimization of SMA Based Damped Outrigger Structure under Uncertainty. *Eng. Structures* 222, 111074. doi:10.1016/j.engstruct.2020.111074

Davenport, A. G. (1983). The Relationship of Reliability to Wind Loading. *J. Wind Eng. Ind. Aerodynamics* 13 (1-3), 3–27. doi:10.1016/0167-6105(83)90125-3

Davenport, A. G. (1967). Gust Loading Factors. *J. Struct. Div.* 93 (3), 11–34. doi:10.1061/jsdeag.0001692

De Domenico, D., Ricciardi, G., and Takewaki, I. (2019). Design Strategies of Viscous Dampers for Seismic protection of Building Structures: a Review. *Soil Dyn. Earthquake Eng.* 118, 144–165. doi:10.1016/j.soildyn.2018.12.024

De Risi, R., Goda, K., and Tesfamariam, S. (2019). Multi-dimensional Damage Measure for Seismic Reliability Analysis. *Struct. Saf.* 78, 1–11. doi:10.1016/j.strusafe.2018.12.002

De, S. (2021). Uncertainty Quantification of Locally Nonlinear Dynamical Systems Using Neural Networks. *J. Comput. Civil Eng.* (4), 3504021009. doi:10.1061/(asce)cp.1943-5487.0000965

De, S., Maute, K., and Doostan, A. (2021). Reliability-based Topology Optimization Using Stochastic Gradients. *Struct. Multidisc Optim* 64 (5), 3089–3108. doi:10.1007/s00158-021-03023-w

Deierlein, G. G., McKenna, F., Zsarnóczay, A., Kijewski-Correa, T., Kareem, A., Elhaddad, W., et al. (2020). A Cloud-Enabled Application Framework for Simulating Regional-Scale Impacts of Natural Hazards on the Built Environment. *Front. Built Environ.* 6, 558706. doi:10.3389/fbuil.2020.558706

Dey, S., Chakraborty, S., and Tesfamariam, S. (2021). Multi-fidelity Approach for Uncertainty Quantification of Buried Pipeline Response Undergoing Fault Rupture Displacements in Sand. *Comput. Geotechnics* 136, 104197. doi:10.1016/j.compgeo.2021.104197

Ding, F., and Kareem, A. (2018). A Multi-Fidelity Shape Optimization via Surrogate Modeling for Civil Structures. *J. Wind Eng. Ind. Aerodynamics* 178, 49–56. doi:10.1016/j.jweia.2018.04.022

Dubourg, V., Sudret, B., and Bourinet, J.-M. (2011). Reliability-based Design Optimization Using Kriging Surrogates and Subset Simulation. *Struct. Multidisc Optim* 44 (5), 673–690. doi:10.1007/s00158-011-0653-8

Duthinh, D., and Simiu, E. (2010). Safety of Structures in strong Winds and Earthquakes: Multihazard Considerations. *J. Struct. Eng.* 136 (3), 330–333. doi:10.1061/(asce)st.1943-541x.0000108

Edskär, I., and Lidelöw, H. (2019). Dynamic Properties of Cross-Laminated Timber and Timber Truss Building Systems. *Eng. Structures* 186, 525–535. doi:10.1016/j.engstruct.2019.01.136

Edskär, I., and Lidelöw, H. (2017). Wind-Induced Vibrations in Timber Buildings-Parameter Study of Cross-Laminated Timber Residential Structures. *Struct. Eng. Int.* 27 (2), 205–216. doi:10.2749/101686617x14881932435619

Elezaby, F., and El Damatty, A. (2020). Ductility-based Design Approach of Tall Buildings under Wind Loads. *Wind and Structures* 31 (2), 143–152.

Elshaer, A., Gairola, A., Adamek, K., and Bitsuamlak, G. (2017). Variations in Wind Load on Tall Buildings Due to Urban Development. *Sust. Cities Soc.* 34, 264–277. doi:10.1016/j.scs.2017.06.008

Federal Emergency Management Agency (FEMA) (1997). *FEMA 273, NEHRP Guidelines for the Seismic Rehabilitation of Buildings*. Washington, DC.

Federal Emergency Management Agency (FEMA) (2000). Washington, DC.FEMA 356, Prestandard and Commentary for the Seismic Rehabilitation of Buildings.

Federal Emergency Management Agency (FEMA) (2012). *FEMA P-58, Seismic Performance Assessment of Buildings, Volume 1 – Methodology, Volume 2 – Implementation Guide*. Washington, DC.

Fema–Nibs (2003). Washington, DC.Earthquake Loss Estimation Methodology – HAZUS Technical Manual. Federal Emergency Management Agency and National Institute of Building Sciences.

Fitzgerald, D., Miller, T. H., Sinha, A., and Nairn, J. A. (2020). Cross-laminated Timber Rocking walls with Slip-Friction Connections. *Eng. Structures* 220, 110973. doi:10.1016/j.engstruct.2020.110973

Foschi, R. O., Li, H., and Zhang, J. (2002). Reliability and Performance-Based Design: a Computational Approach and Applications. *Struct. Saf.* 24 (2-4), 205–218. doi:10.1016/s0167-4730(02)00025-5

Foster, R. M., and Reynolds, T. P. (2018). Lightweighting with Timber: An Opportunity for More Sustainable Urban Densification. *J. Architectural Eng.* 24 (1), 02518001.

Foster, R. M., Reynolds, T. P., and Ramage, M. H. (2016). Proposal for Defining a Tall Timber Building. *J. Struct. Eng.* 142 (12), 02516001. doi:10.1061/(asce)st.1943-541x.0001615

Franchin, P., Petrini, F., and Mollaioli, F. (2018). Improved Risk-Targeted Performance-Based Seismic Design of Reinforced concrete Frame Structures. *Earthquake Engng Struct. Dyn.* 47 (1), 49–67. doi:10.1002/eqe.2936

Franchin, P. (2004). Reliability of Uncertain Inelastic Structures under Earthquake Excitation. *J. Eng. Mech.* 130 (2), 180–191. doi:10.1061/(asce)0733-9399(2004)130:2(180)

Furley, J., van de Lindt, J. W., Pei, S., Wichman, S., Hasani, H., Berman, J. W., et al. (2021). Time-to-functionality Fragilities for Performance Assessment of Buildings. *J. Struct. Eng.* 147 (12), 04021217. doi:10.1061/(asce)st.1943-541x.0003195

Giaralis, A., and Petrini, F. (2017). Wind-induced Vibration Mitigation in Tall Buildings Using the Tuned Mass-Damper-Inerter. *J. Struct. Eng.* 143 (9), 04017127. doi:10.1061/(asce)st.1943-541x.0001863

Goda, K., De Risi, R., De Luca, F., Muhammad, A., Yasuda, T., and Mori, N. (2021). Multi-hazard Earthquake-Tsunami Loss Estimation of Kuroshio Town, Kochi Prefecture, Japan Considering the Nankai-Tonankai Megathrust Rupture Scenarios. *Int. J. Disaster Risk Reduction* 54, 102050. doi:10.1016/j.ijdrr.2021.102050

Goda, K. (2015). Record Selection for Aftershock Incremental Dynamic Analysis. *Earthquake Engng Struct. Dyn.* 44 (7), 1157–1162. doi:10.1002/eqe.2513

Goda, K., and Tesfamariam, S. (2015). Multi-variate Seismic Demand Modelling Using Copulas: Application to Non-ductile Reinforced concrete Frame in Victoria, Canada. *Struct. Saf.* 56, 39–51. doi:10.1016/j.strusafe.2015.05.004

Golesorkhi, R., Joseph, L., Klemencic, R., Shook, D., and Viise, J. (2017). *Performance-Based Seismic Design for Tall Buildings: An Output of the CTBUH Performance-Based Seismic Design Working Group*. Chicago, IL: Council on Tall Buildings and Urban Habitat.

Goli, A., Alaghmandan, M., and Barazandeh, F. (2021). Parametric Structural Topology Optimization of High-Rise Buildings Considering Wind and Gravity Loads. *J. Architectural Eng.* 274, 04021038. doi:10.1061/(asce)ae.1943-5568.0000511

Gomez, F., Spencer, B. F., Jr, and Carrion, J. (2020). Topology Optimization of Buildings Subjected to Stochastic Base Excitation. *Eng. Structures* 223, 111111. doi:10.1016/j.engstruct.2020.111111

Gomez, F., Spencer, B. F., Jr, and Carrion, J. (2021). Topology Optimization of Buildings Subjected to Stochastic Wind Loads. *Probabilistic Eng. Mech.* 64, 103127. doi:10.1016/j.probengmech.2021.103127

Goulet, C. A., Haselton, C. B., Mitrani-Reiser, J., Beck, J. L., Deierlein, G. G., Porter, K. A., et al. (2007). Evaluation of the Seismic Performance of a Code-Conforming Reinforced-concrete Frame Building-From Seismic hazard to Collapse Safety and Economic Losses. *Earthquake Engng Struct. Dyn.* 36, 1973–1997. doi:10.1002/eqe.694

Greco, R., Lucchini, A., and Marano, G. C. (2015). Robust Design of Tuned Mass Dampers Installed on Multi-Degree-Of-freedom Structures Subjected to Seismic Action. *Eng. Optimization* 47 (8), 1009–1030. doi:10.1080/0305215x.2014.941288

Haghighat, E., and Juanes, R. (2021). SciANN: A Keras/TensorFlow Wrapper for Scientific Computations and Physics-Informed Deep Learning Using Artificial Neural Networks. *Comp. Methods Appl. Mech. Eng.* 373, 113552. doi:10.1016/j.cma.2020.113552

Hare, W., Nutini, J., and Tesfamariam, S. (2013). A Survey of Non-gradient Optimization Methods in Structural Engineering. *Adv. Eng. Softw.* 59, 19–28. doi:10.1016/j.advengsoft.2013.03.001

Hashemi, A., Zarnani, P., and Quenneville, P. (2020). Seismic Assessment of Rocking Timber walls with Energy Dissipation Devices. *Eng. Structures* 221, 111053. doi:10.1016/j.engstruct.2020.111053

Hashizume, S., and Takewaki, I. (2020). Hysteretic-Viscous Hybrid Damper System for Long-Period Pulse-type Earthquake Ground Motions of Large Amplitude. *Front. Built Environ.* 6, 62. doi:10.3389/fbuil.2020.00062

Hong, H. P. (2016). Modeling of Nonstationary Winds and its Applications. *J. Eng. Mech.* 1424, 04016004. doi:10.1061/(asce)em.1943-7889.0001047

Hosseinpour, V., Saeidi, A., Nollet, M.-J., and Nastev, M. (2021). Seismic Loss Estimation Software: A Comprehensive Review of Risk Assessment Steps, Software Development and Limitations. *Eng. Structures* 232, 111866. doi:10.1016/j.engstruct.2021.111866

Hou, F., and Jafari, M. (2020). Investigation Approaches to Quantify Wind-Induced Load and Response of Tall Buildings: A Review. *Sust. Cities Soc.* 62, 102376. doi:10.1016/j.scs.2020.102376

Huang, H., and Chang, W.-S. (2018). Application of Pre-stressed SMA-Based Tuned Mass Damper to a Timber Floor System. *Eng. Structures* 167, 143–150. doi:10.1016/j.engstruct.2018.04.011

Huang, J., and Chen, X. (2022). Inelastic Performance of High-Rise Buildings to Simultaneous Actions of Alongwind and Crosswind Loads. *J. Struct. Eng.* 1482, 04021258. doi:10.1061/(asce)st.1943-541x.0003236

Ierimonti, L., Caracoglia, L., Venanzi, I., and Materazzi, A. L. (2017). Investigation on Life-Cycle Damage Cost of Wind-Excited Tall Buildings Considering Directionality Effects. *J. Wind Eng. Ind. Aerodynamics* 171, 207–218. doi:10.1016/j.jweia.2017.09.020

Ierimonti, L., Venanzi, I., and Caracoglia, L. (2018). Life-cycle Damage-Based Cost Analysis of Tall Buildings Equipped with Tuned Mass Dampers. *J. Wind Eng. Ind. Aerodynamics* 176, 54–64. doi:10.1016/j.jweia.2018.03.009

International Code Council (ICC) (2017). *International Building Code, 2018*. Country Club Hills, IL: International Code Council.

Isyumov, N. (2012). Alan G. Davenport's Mark on Wind Engineering. *J. Wind Eng. Ind. Aerodynamics* 104-106, 12–24. doi:10.1016/j.jweia.2012.02.007

Jafari, M., and Alipour, A. (2021a). Aerodynamic Shape Optimization of Rectangular and Elliptical Double-Skin Façades to Mitigate Wind-Induced Effects on Tall Buildings. *J. Wind Eng. Ind. Aerodynamics* 213, 104586. doi:10.1016/j.jweia.2021.104586

Jafari, M., and Alipour, A. (2021b). Methodologies to Mitigate Wind-Induced Vibration of Tall Buildings: A State-Of-The-Art Review. *J. Building Eng.* 33, 101582. doi:10.1016/j.jobe.2020.101582

Jafari, M., and Alipour, A. (2021c). Review of Approaches, Opportunities, and Future Directions for Improving Aerodynamics of Tall Buildings with Smart Facades. *Sust. Cities Soc.* 72, 102979. doi:10.1016/j.scs.2021.102979

Jayamon, J. R., Line, P., and Charney, F. A. (2018). State-of-the-art Review on Damping in wood-frame Shear wall Structures. *J. Struct. Eng.* 14412, 03118003. doi:10.1061/(asce)st.1943-541x.0002212

Jayaram, N., Shome, N., and Rahnama, M. (2012). Development of Earthquake Vulnerability Functions for Tall Buildings. *Earthquake Engng Struct. Dyn.* 41, 1495–1514. doi:10.1002/eqe.2231

Jennings, P. C. (1970). Earthquakes and Tall Buildings. *Bnzsee* 3 (2), 51–59. doi:10.5459/bnzsee.3.2.51-59

Kareem, A., and Gurley, K. (1996). Damping in Structures: Its Evaluation and Treatment of Uncertainty. *J. Wind Eng. Ind. Aerodynamics* 59 (2-3), 131–157. doi:10.1016/0167-6105(96)00004-9

Kareem, A. (2020). Emerging Frontiers in Wind Engineering: Computing, Stochastics, Machine Learning and beyond. *J. Wind Eng. Ind. Aerodynamics* 206, 104320. doi:10.1016/j.jweia.2020.104320

Kareem, A., Hu, L., Guo, Y., and Kwon, D. K. (2019). Generalized Wind Loading Chain: Time-Frequency Modeling Framework for Nonstationary Wind Effects on Structures. *J. Struct. Eng.* 14510, 04019092.

Kareem, A., and Kwon, D. K. (2017). A Cyber-Based Data-Enabled Virtual Organization for Wind Load Effects on Civil Infrastructures: VORTEX-Winds. *Front. Built Environ.* 3, 48. doi:10.3389/fbuil.2017.00048

Kareem, A., and Wu, T. (2013). Wind-induced Effects on bluff Bodies in Turbulent Flows: Nonstationary, Non-gaussian and Nonlinear Features. *J. Wind Eng. Ind. Aerodynamics* 122, 21–37. doi:10.1016/j.jweia.2013.06.002

Karniadakis, G. E., Kevrekidis, I. G., Lu, L., Perdikaris, P., Wang, S., and Yang, L. (2021). Physics-informed Machine Learning. *Nat. Rev. Phys.* 3 (6), 422–440. doi:10.1038/s42254-021-00314-5

Kasagi, M., Fujita, K., Tsuji, M., and Takewaki, I. (2016). Effect of Non-linearity of Connecting Dampers on Vibration Control of Connected Building Structures. *Front. Built Environ.* 1, 25. doi:10.3389/fbuil.2015.00025

Kenawy, M., McCallen, D., and Pitarka, A. (2021). Variability of Near-fault Seismic Risk to Reinforced concrete Buildings Based on High-resolution Physics-based Ground Motion Simulations. *Earthquake Engng Struct. Dyn.* 50 (6), 1713–1733. doi:10.1002/eqe.3413

Kijewski-Correa, T., and Pirnia, J. D. (2007). Dynamic Behavior of Tall Buildings under Wind: Insights from Full-Scale Monitoring. *Struct. Des. Tall Spec. Build.* 16 (4), 471–486. doi:10.1002/tal.415

Kircher, C. A., Whitman, R. V., and Holmes, W. T. (2006). HAZUS Earthquake Loss Estimation Methods. *Nat. Hazards Rev.* 7 (2), 45–59. doi:10.1061/(asce)1527-6988(2006)7:2(45)

Kiureghian, A. D., and Ditlevsen, O. (2009). Aleatory or Epistemic? Does it Matter? *Struct. Saf.* 31 (2), 105–112. doi:10.1016/j.strusafe.2008.06.020

Kiureghian, A. D. (2005). Non-ergodicity and PEER's Framework Formula. *Earthquake Engng Struct. Dyn.* 34 (13), 1643–1652. doi:10.1002/eqe.504

Kleingesinds, S., and Lavan, O. (2021). Gradient-based Multi-hazard Optimization of MTMDs for Tall Buildings. *Comput. Structures* 249, 106503. doi:10.1016/j.compstruc.2021.106503

Kleingesinds, S., Lavan, O., and Venanzi, I. (2021). Life-cycle Cost-Based Optimization of MTMDs for Tall Buildings under Multiple Hazards. *Struct. Infrastructure Eng.* 17 (7), 921–940. doi:10.1080/15732479.2020.1778741

Kroetz, H. M., Moustapha, M., Beck, A. T., and Sudret, B. (2020). A Two-Level Kriging-Based Approach with Active Learning for Solving Time-Variant Risk Optimization Problems. *Reliability Eng. Syst. Saf.* 203, 107033. doi:10.1016/j.ress.2020.107033

Kwag, S., Gupta, A., Baugh, J., and Kim, H.-S. (2021). Significance of Multi-hazard Risk in Design of Buildings under Earthquake and Wind Loads. *Eng. Structures* 243, 112623. doi:10.1016/j.engstruct.2021.112623

Lagaros, N. D., and Fragiadakis, M. (2007). Robust Performance-Based Design Optimization of Steel Moment Resisting Frames. *J. Earthquake Eng.* 11 (5), 752–772. doi:10.1080/13632460601087229

Lago, A., Trabucco, D., and Wood, A.2018. *Damping Technologies for Tall Buildings: Theory, Design Guidance and Case Studies*. 1st edition, Butterworth-Heinemann.

Lai, Z., Mylonas, C., Nagarajaiah, S., and Chatzi, E. (2021). Structural Identification with Physics-Informed Neural Ordinary Differential Equations. *J. Sound Vibration* 508, 116196. doi:10.1016/j.jsv.2021.116196

Lamberti, G., and Gorlé, C. (2021). A Multi-Fidelity Machine Learning Framework to Predict Wind Loads on Buildings. *J. Wind Eng. Ind. Aerodynamics* 214, 104647. doi:10.1016/j.jweia.2021.104647

Lange, D., Devaney, S., and Usmani, A. (2014). An Application of the PEER Performance Based Earthquake Engineering Framework to Structures in Fire. *Eng. Structures* 66, 100–115. doi:10.1016/j.engstruct.2014.01.052

Le, V., and Caracoglia, L. (2021). Life-cycle Cost Assessment of Vertical Structures under Nonstationary Winds: Downburst vs. Tornado Loads. *Eng. Structures* 243, 112515. doi:10.1016/j.engstruct.2021.112515

Lehký, D., Slowik, O., and Novák, D. (2018). Reliability-based Design: Artificial Neural Networks and Double-Loop Reliability-Based Optimization Approaches. *Adv. Eng. Softw.* 117, 123–135. doi:10.1016/j.advengsoft.2017.06.013

Lesgidis, N., Sextos, A., and Kwon, O.-S. (2018). A Frequency-dependent and Intensity-dependent Macroelement for Reduced Order Seismic Analysis of Soil-Structure Interacting Systems. *Earthquake Engng Struct. Dyn.* 47 (11), 2172–2194. doi:10.1002/eqe.3063

Li, C., Liu, Y., and Li, H.-N. (2021). Fragility Assessment and Optimum Design of a Steel-concrete Frame Structure with Hybrid Energy-Dissipated Devices under Multi-Hazards of Earthquake and Wind. *Eng. Structures* 245, 112878. doi:10.1016/j.engstruct.2021.112878

Li, H. N., Liu, Y., Li, C., and Zheng, X. W. (2020). Multihazard Fragility Assessment of Steel-concrete Composite Frame Structures with Buckling-Restrained Braces Subjected to Combined Earthquake and Wind. *The Struct. Des. Tall Spec. Buildings* 29 (11), e1746. doi:10.1002/tal.1746

Li, M., and Jia, G. (2020). Multifidelity Gaussian Process Model Integrating Low- And High-Fidelity Data Considering Censoring. *J. Struct. Eng.* 1463, 04019215. doi:10.1061/(asce)st.1943-541x.0002531

Li, X., Qiu, H., Chen, Z., Gao, L., and Shao, X. (2016). A Local Kriging Approximation Method Using MPP for Reliability-Based Design Optimization. *Comput. Structures* 162, 102–115. doi:10.1016/j.compstruc.2015.09.004

Liel, A. B., Haselton, C. B., and Deierlein, G. G. (2011). Seismic Collapse Safety of Reinforced concrete Buildings. II: Comparative Assessment of Nonductile and Ductile Moment Frames. *J. Struct. Eng.* 137 (4), 492–502. doi:10.1061/(asce)st.1943-541x.0000275

Liu, M., Burns, S. A., and Wen, Y. K. (2003). Optimal Seismic Design of Steel Frame Buildings Based on Life Cycle Cost Considerations. *Earthquake Engng. Struct. Dyn.* 32, 1313–1332. doi:10.1002/eqe.273

Liu, M. Y., Chiang, W. L., Hwang, J. H., and Chu, C. R. (2008). Wind-induced Vibration of High-Rise Building with Tuned Mass Damper Including Soil–Structure Interaction. *J. Wind Eng. Ind. Aerodynamics* 96 (6-7), 1092–1102. doi:10.1016/j.jweia.2007.06.034

Lopez-Caballero, F. (2021). Probabilistic Seismic Analysis for Liquefiable Embankment through Multi-Fidelity Codes Approach. *Soil Dyn. Earthquake Eng.* 149, 106849. doi:10.1016/j.soildyn.2021.106849

Los Angeles Tall Buildings Structural Design Council (LATBSDC) (2020). *An Alternative Procedure for Seismic Analysis and Design of Tall Buildings Located in the Los Angeles Region*. Los Angeles, CA, USA.

Loss, C., Tannert, T., and Tesfamariam, S. (2018). State-of-the-art Review of Displacement-Based Seismic Design of Timber Buildings. *Construction Building Mater.* 191, 481–497. doi:10.1016/j.conbuildmat.2018.09.205

Lu, X., Tian, Y., Cen, S., Guan, H., Xie, L., and Wang, L. (2018). A High-Performance Quadrilateral Flat Shell Element for Seismic Collapse Simulation of Tall Buildings and its Implementation in OpenSees. *J. Earthquake Eng.* 22 (9), 1662–1682. doi:10.1080/13632469.2017.1297269

Luo, X., and Kareem, A. (2020). Bayesian Deep Learning with Hierarchical Prior: Predictions from Limited and Noisy Data. *Struct. Saf.* 84, 101918. doi:10.1016/j.strusafe.2019.101918

Madsen, H. O., and Hansen, P. F. (1992). *A Comparison of Some Algorithms for Reliability Based Structural Optimization and Sensitivity Analysis. In Reliability and Optimization of Structural Systems' 91 (Pp. 443–451*. Berlin, Heidelberg: Springer.

Mahmoud, H., and Cheng, G. (2017). Framework for Lifecycle Cost Assessment of Steel Buildings under Seismic and Wind Hazards. *J. Struct. Eng.* 1433, 04016186. doi:10.1061/(asce)st.1943-541x.0001663

Mahsuli, M., and Haukaas, T. (2013). Seismic Risk Analysis with Reliability Methods, Part I: Models. *Struct. Saf.* 42, 54–62. doi:10.1016/j.strusafe.2013.01.003

Makita, K., Murase, M., Kondo, K., and Takewaki, I. (2018). Robustness Evaluation of Base-Isolation Building-Connection Hybrid Controlled Building Structures Considering Uncertainties in Deep Ground. *Front. Built Environ.* 4, 16. doi:10.3389/fbuil.2018.00016

Malo, K. A., Abrahamsen, R. B., and Bjertnæs, M. A. (2016). Some Structural Design Issues of the 14-storey Timber Framed Building "Treet" in Norway. *Eur. J. Wood Prod.* 74 (3), 407–424. doi:10.1007/s00107-016-1022-5

Martin, A., and Deierlein, G. G. G. G. (2020). Structural Topology Optimization of Tall Buildings for Dynamic Seismic Excitation Using Modal Decomposition. *Eng. Structures* 216, 110717. doi:10.1016/j.engstruct.2020.110717

Masters, F. J. (2016). Grand Challenges in Wind Engineering: Advancing Cyber-Physical Tools to Investigate Structural Performance of Buildings. *Front. Built Environ.* 2, 18. doi:10.3389/fbuil.2016.00018

McAllister, T. (2016). Research Needs for Developing a Risk-Informed Methodology for Community Resilience. *J. Struct. Eng.* 142 (8), C4015008. doi:10.1061/(asce)st.1943-541x.0001379

McCallen, D., Petersson, A., Rodgers, A., Pitarka, A., Miah, M., Petrone, F., et al. (2021). EQSIM-A Multidisciplinary Framework for Fault-To-Structure Earthquake Simulations on Exascale Computers Part I: Computational Models and Workflow. *Earthquake Spectra* 37 (2), 707–735. doi:10.1177/8755293020970982

McGuire, R. K. (2004). *CA*. Berkeley: Earthquake Engineering Research Institute.Seismic Hazard and Risk Analysis.

Micheli, L., Alipour, A., and Laflamme, S. (2021). Life-cycle Cost Optimization of Wind-Excited Tall Buildings Using Surrogate Models. *Struct. Des. Tall Spec. Buildings* 30 (6), e1840. doi:10.1002/tal.1840

Micheli, L., Alipour, A., and Laflamme, S. (2020b). Multiple-surrogate Models for Probabilistic Performance Assessment of Wind-Excited Tall Buildings under Uncertainties. *ASCE-ASME J. Risk Uncertainty Eng. Syst. A: Civil Eng.* 64, 04020042. doi:10.1061/ajrua6.0001091

Micheli, L., Alipour, A., Laflamme, S., and Sarkar, P. (2019). Performance-based Design with Life-Cycle Cost Assessment for Damping Systems Integrated in Wind Excited Tall Buildings. *Eng. Structures* 195, 438–451. doi:10.1016/j.engstruct.2019.04.009

Micheli, L., Hong, J., Laflamme, S., and Alipour, A. (2020a). Surrogate Models for High Performance Control Systems in Wind-Excited Tall Buildings. *Appl. Soft Comput.* 90, 106133. doi:10.1016/j.asoc.2020.106133

Miguel, L. F. F., Miguel, L. F. F., and Lopez, R. H. (2014). Robust Design Optimization of Friction Dampers for Structural Response Control. *Struct. Control. Health Monit.* 21 (9), 1240–1251. doi:10.1002/stc.1642

Mitropoulou, C. C., Lagaros, N. D., and Papadrakakis, M. (2011). Life-cycle Cost Assessment of Optimally Designed Reinforced concrete Buildings under Seismic Actions. *Reliability Eng. Syst. Saf.* 96 (10), 1311–1331. doi:10.1016/j.ress.2011.04.002

Moni, M., Hwang, Y., Kwon, O.-S., Kim, H.-K., and Jeong, U. Y. (2020). Real-time Aeroelastic Hybrid Simulation of a Base-Pivoting Building Model in a Wind Tunnel. *Front. Built Environ.* 6, 560672. doi:10.3389/fbuil.2020.560672

Moore, M. (2000). "Scotia Place – 12 story Apartment Building a Case Study of High-Rise Construction Using wood and Steel," in *WCTE 2000: World Conference on Timber Engineering* (British Columbia, Canada. July 31 – August 3, 2000.

Mylonakis, G., and Gazetas, G. (2000). Seismic Soil-Structure Interaction: Beneficial or Detrimental? *J. Earthquake Eng.* 4 (3), 277–301. doi:10.1080/13632460009350372

Nakamura, Y., and Fujii, H. (2021). Earthquake Damage Reduction in Timber Frame Houses Using Small-Size Fluid Damper. *Front. Built Environ.* 7, 767741. doi:10.3389/fbuil.2021.767741

Nakamura, Y., and Hanzawa, T. (2017). Performance-based Placement Design of Tuned Electromagnetic Inertial Mass Dampers. *Front. Built Environ.* 3, 26. doi:10.3389/fbuil.2017.00026

NRC (National Research Council Canada) (2015). *National Building Code of Canada (2015)*. Ottawa, Ontario: National Research Council of Canada.

Nygaard, M., Bashevkin, I. E. S., Groba, U., and Sunter, C. (2019). Increased Use of Timber in New Buildings in Oslo and Akershus: Potentials and GHG Emission Effects. *Front. Built Environ.* 5, 131. doi:10.3389/fbuil.2019.00131

O'Reilly, G. J., and Calvi, G. M. (2019). Conceptual Seismic Design in Performance-Based Earthquake Engineering. *Earthquake Engng Struct. Dyn.* 48 (4), 389–411. doi:10.1002/eqe.3141

Ontiveros-Pérez, S. P., Miguel, L. F. F., and Riera, J. D. (2019). Reliability-based Optimum Design of Passive Friction Dampers in Buildings in Seismic Regions. *Eng. Structures* 190, 276–284. doi:10.1016/j.engstruct.2019.04.021

Ouyang, Z., and Spence, S. M. J. (2021). Performance-based Wind-Induced Structural and Envelope Damage Assessment of Engineered Buildings through Nonlinear Dynamic Analysis. *J. Wind Eng. Ind. Aerodynamics* 208, 104452. doi:10.1016/j.jweia.2020.104452

Pacific Earthquake Engineering Research Center (PEER) (2017). *PEER Report 2017/06*. Berkeley, CA: University of California.Guidelines for Performance-Based Seismic Design of Tall Buildings.

Pagnini, L. C., and Solari, G. (1988). Serviceability Criteria for Wind-Acceleration and Damping Uncertainties. *J. Wind Eng. Ind. Aerodynamics* 74–76, 1067–1078.

Papadopoulos, A. N., Vamvatsikos, D., and Kazantzi, A. K. (2019). Development and Application of FEMA P-58 Compatible story Loss Functions. *Earthquake Spectra* 35 (1), 95–112. doi:10.1193/102417eqs222m

Patsialis, D., and Taflanidis, A. A. (2021). Multi-fidelity Monte Carlo for Seismic Risk Assessment Applications. *Struct. Saf.* 93, 102129. doi:10.1016/j.strusafe.2021.102129

Peherstorfer, B., Willcox, K., and Gunzburger, M. (2018). Survey of Multifidelity Methods in Uncertainty Propagation, Inference, and Optimization. *SIAM Rev.* 60 (3), 550–591. doi:10.1137/16m1082469

Pei, S., van de Lindt, J. W., Popovski, M., Berman, J. W., Dolan, J. D., Ricles, J. M., et al. (2015). Cross Laminated Timber for Seismic Regions: Progress and Challenges for Research and Implementation. *J. Struct. Eng.*, E2514001. doi:10.1061/(ASCE)ST.1943-541X.0001192

Peng, Y., Ma, Y., Huang, T., and De Domenico, D. (2021). Reliability-based Design Optimization of Adaptive Sliding Base Isolation System for Improving Seismic Performance of Structures. *Reliability Eng. Syst. Saf.* 205, 107167. doi:10.1016/j.ress.2020.107167

Petrini, F., and Ciampoli, M. (2012). Performance-based Wind Design of Tall Buildings. *Struct. Infrastructure Eng.* 8 (10), 954–966.

Porter, K. A. (2003). *An Overview of PEER's Performance-Based Earthquake Engineering Methodology. Proceedings of the 9th International Conference on Applications of Statistics and Probability in Civil Engineering*. San Francisco, California, USA, 1–8. July 6-9, 2003.

Pu, W., Liu, C., Zhang, H., and Kasai, K. (2016). Seismic Control Design for Slip Hysteretic Timber Structures Based on Tuning the Equivalent Stiffness. *Eng. Structures* 128, 199–214. doi:10.1016/j.engstruct.2016.09.041

Rahmani, A., Taiebat, M., and Liam Finn, W. D. (2014). Nonlinear Dynamic Analysis of Meloland Road Overpass Using Three-Dimensional Continuum Modeling Approach. *Soil Dyn. Earthquake Eng.* 57, 121–132. doi:10.1016/j.soildyn.2013.11.004

Ramage, M., Foster, R., Smith, S., Flanagan, K., and Bakker, R. (2017). Super Tall Timber: Design Research for the Next Generation of Natural Structure. *The J. Architecture* 22 (1), 104–122. doi:10.1080/13602365.2016.1276094

Reynolds, T., Feldmann, A., Ramage, M., Chang, W.-S., Harris, R., and Dietsch, P. (2016). Design Parameters for Lateral Vibration of Multi-Storey Timber Buildings. In International Network on Timber Engineering Research Meeting 49, Graz. *Austria*, 365–378.

Rinaldin, G., and Fragiacomo, M. (2016). Non-linear Simulation of Shaking-Table Tests on 3- and 7-storey X-Lam Timber Buildings. *Eng. Structures* 113, 133–148. doi:10.1016/j.engstruct.2016.01.055

Rosenblueth, E. (1986). Optimum Reliabilities and Optimum Design. *Struct. Saf.* 3, 69–83. doi:10.1016/0167-4730(86)90009-3

Roy, T., and Matsagar, V. (2019). Effectiveness of Passive Response Control Devices in Buildings under Earthquake and Wind during Design Life. *Struct. Infrastructure Eng.* 15 (2), 252–268. doi:10.1080/15732479.2018.1547768

Roy, T., and Matsagar, V. (2020). Probabilistic Assessment of Steel Buildings Installed with Passive Control Devices under Multi-hazard Scenario of Earthquake and Wind. *Struct. Saf.* 85, 101955. doi:10.1016/j.strusafe.2020.101955

Roy, T., Saito, T., and Matsagar, V. (2021). Multihazard Framework for Investigating High-rise Base-isolated Buildings under Earthquakes and Long-duration Winds. *Earthquake Engng Struct. Dyn.* 50 (5), 1334–1357. doi:10.1002/eqe.3401

Royset, J. O., Günay, S., and Mosalam, K. M. (2019). "Risk-adaptive Learning of Seismic Response Using Multi-Fidelity Analysis," in *13th International Conference on Applications of Statistics and Probability in Civil Engineering, ICASP13* (Seoul: South Korea), 26–30.

Sevieri, G., Gentile, R., and Galasso, C. (2021). A Multi-fidelity Bayesian Framework for Robust Seismic Fragility Analysis. *Earthquake Engng Struct. Dyn.* 50 (15), 4199–4219. doi:10.1002/eqe.3552

Shahi, S. K., and Baker, J. W. (2011). An Empirically Calibrated Framework for Including the Effects of Near-Fault Directivity in Probabilistic Seismic hazard Analysis. *Bull. Seismological Soc. America* 101 (2), 742–755. doi:10.1785/0120100090

Shahnazaryan, D., O'Reilly, G. J., and Monteiro, R. (2021). Story Loss Functions for Seismic Design and Assessment: Development of Tools and Application. *Earthquake Spectra*, 87552930211023523. doi:10.1177/87552930211023523

Shome, N., Jayaram, N., Krawinkler, H., and Rahnama, M. (2015). Loss Estimation of Tall Buildings Designed for the PEER Tall Building Initiative Project. *Earthquake Spectra* 31 (3), 1309–1336. doi:10.1193/121912eqs352m

Shome, N., and Luco, N., 2010. Loss Estimation of Multi-Mode Dominated Structures for a Scenario of Earthquake Event. In *9th US National and 10th Canadian Conference on Earthquake Engineering*, 25-29 July 2010, Toronto, Ontario, Canada, Paper No 388, 1–10.

Sigmund, O., and Maute, K. (2013). Topology Optimization Approaches. *Struct. Multidisc Optim* 48 (6), 1031–1055. doi:10.1007/s00158-013-0978-6

Silva, V., Bazzurro, P., and Vamvatsikos, D. (2021). Preface to the Special Issue: The Evolution of Fragility and Vulnerability. The Origin story of a Preface. *Bull. Earthquake Eng.* 19, 6269–6270. doi:10.1007/s10518-021-01261-3

Smith, I., and Frangi, A. (2014). Use of Timber in Tall Multi-Storey Buildings. *Struct. Eng. Documents 13, Int. Assoc. Bridge Struct. Eng.* doi:10.2749/sed013

Smith, R., Merello, R., and Willford, M. (2010). Intrinsic and Supplementary Damping in Tall Buildings. *Proc. Inst. Civil Eng. - Structures Buildings* 163 (2), 111–118. doi:10.1680/stbu.2010.163.2.111

Solari, G., De Gaetano, P., and Repetto, M. P. (2015). Thunderstorm Response Spectrum: Fundamentals and Case Study. *J. Wind Eng. Ind. Aerodynamics* 143, 62–77. doi:10.1016/j.jweia.2015.04.009

Solari, G. (2020). Thunderstorm Downbursts and Wind Loading of Structures: Progress and prospect. *Front. Built Environ.* 6, 63. doi:10.3389/fbuil.2020.00063

Song, J., Kang, W. H., Lee, Y. J., and Chun, J. (2021). Structural System Reliability: Overview of Theories and Applications to Optimization. *ASCE-ASME J. Risk Uncertainty Eng. Syst. Part A: Civil Eng.* 7 (2), 03121001. doi:10.1061/ajrua6.0001122

Soong, T. T., and Spencer, B. F., Jr (2002). Supplemental Energy Dissipation: State-Of-The-Art and State-Of-The-Practice. *Eng. Structures* 24 (3), 243–259. doi:10.1016/s0141-0296(01)00092-x

Sotiriadis, D., Klimis, N., Margaris, B., and Sextos, A. (2020). Analytical Expressions Relating Free-Field and Foundation Ground Motions in Buildings with Basement, Considering Soil-Structure Interaction. *Eng. Structures* 216, 110757. doi:10.1016/j.engstruct.2020.110757

Spence, S. M. J., Gioffrè, M., and Kareem, A. (2016). An Efficient Framework for the Reliability-Based Design Optimization of Large-Scale Uncertain and Stochastic Linear Systems. *Probabilistic Eng. Mech.* 44, 174–182. doi:10.1016/j.probengmech.2015.09.014

Spence, S. M. J., and Kareem, A. (2013). Tall Buildings and Damping: A Concept-Based Data-Driven Model. *J. Struct. Eng.* 1405, 04014005.

Spence, S. M. J., and Kareem, A. (2014). Performance-based Design and Optimization of Uncertain Wind-Excited Dynamic Building Systems. *Eng. Structures* 78, 133–144. doi:10.1016/j.engstruct.2014.07.026

Stafford, P. J. (2014). Crossed and Nested Mixed-Effects Approaches for Enhanced Model Development and Removal of the Ergodic assumption in Empirical Ground-Motion Models. *Bull. Seismological Soc. America* 104 (2), 702–719. doi:10.1785/0120130145

Stewart, J. P., Fenves, G. L., and Seed, R. B. (1999). Seismic Soil-Structure Interaction in Buildings. I: Analytical Methods. *J. Geotechnical Geoenvironmental Eng.* 125 (1), 26–37. doi:10.1061/(asce)1090-0241(1999)125:1(26)

Structural Engineers Association of California (SEAOC) (1995). *Vision 2000, Conceptual Framework for Performance-Based Seismic Design*. Sacramento, CA: Structural Engineers Association of California.

Suksuwan, A., and Spence, S. M. J. (2019). Performance-based Bi-objective Design Optimization of Wind-Excited Building Systems. *J. Wind Eng. Ind. Aerodynamics* 190, 40–52. doi:10.1016/j.jweia.2019.03.028

Suksuwan, A., and Spence, S. M. J. (2018). Performance-based Multi-hazard Topology Optimization of Wind and Seismically Excited Structural Systems. *Eng. Structures* 172, 573–588. doi:10.1016/j.engstruct.2018.06.039

Swischuk, R., Mainini, L., Peherstorfer, B., and Willcox, K. (2019). Projection-based Model Reduction: Formulations for Physics-Based Machine Learning. *Comput. Fluids* 179, 704–717. doi:10.1016/j.compfluid.2018.07.021

Takagi, J., and Wada, A. (2019). Recent Earthquakes and the Need for a New Philosophy for Earthquake-Resistant Design. *Soil Dyn. Earthquake Eng.* 119, 499–507. doi:10.1016/j.soildyn.2017.11.024

Takahashi, Y., Kiureghian, A. D., and Ang, A. H.-S. (2004). Life-cycle Cost Analysis Based on a Renewal Model of Earthquake Occurrences. *Earthquake Engng. Struct. Dyn.* 33 (7), 859–880. doi:10.1002/eqe.383

Takewaki, I. (2011). *Building Control with Passive Dampers: Optimal Performance-Based Design for Earthquakes*. John Wiley & Sons.

Takewaki, I., and Akehashi, H. (2021). Comprehensive Review of Optimal and Smart Design of Nonlinear Building Structures with and without Passive Dampers Subjected to Earthquake Loading. *Front. Built Environ.* 7, 631114. doi:10.3389/fbuil.2021.631114

Tamura, Y., and Suganuma, S.-y. (1996). Evaluation of Amplitude-dependent Damping and Natural Frequency of Buildings during strong Winds. *J. Wind Eng. Ind. Aerodynamics* 59, 115–130. doi:10.1016/0167-6105(96)00003-7

Taniguchi, M., Fujita, K., Tsuji, M., and Takewaki, I. (2016). Hybrid Control System for Greater Resilience Using Multiple Isolation and Building Connection. *Front. Built Environ.* 2, 26. doi:10.3389/fbuil.2016.00026

Tesfamariam, S., Bezabeh, M., Skandalos, K., Martinez, E., Dires, S., Bitsuamlak, G., et al. (2019). Wind and Earthquake Design Framework for Tall Wood-Concrete Hybrid System. UBC Faculty Research and Publications. doi:10.14288/1.0380777

Tesfamariam, S., and Das, S. (2021). Resilient Tall Timber Building Design: Damped-Outrigger System. UBC Faculty Research and Publications. doi:10.14288/1.0403816

Tesfamariam, S., and Goda, K. (2017). Energy-Based Seismic Risk Evaluation of Tall Reinforced Concrete Building in Vancouver, BC, Canada, under Mw9 Megathrust Subduction Earthquakes and Aftershocks. *Front. Built Environ.* 3, 29. doi:10.3389/fbuil.2017.00029

Tesfamariam, S., and Goda, K. (2015). Loss Estimation for Non-ductile Reinforced concrete Building in Victoria, British Columbia, Canada: Effects of Mega-thrustMw9-Class Subduction Earthquakes and Aftershocks. *Earthquake Engng Struct. Dyn.* 44 (13), 2303–2320. doi:10.1002/eqe.2585

Tesfamariam, S., Madheswaran, J., and Goda, K. (2019). Displacement-based Design of Hybrid RC–Timber Structure: Seismic Risk Assessment. *J. Struct. Eng.* 145 (11), 04019125.

Tesfamariam, S., Skandalos, K., Goda, K., Bezabeh, M. A., Bitsuamlak, G., and Popovski, M. (2021b). Quantifying the Ductility-Related Force Modification Factor for 10-storey Timber-RC Hybrid Building Using FEMA P695 Procedure and Considering the 2015 NBC Seismic hazard. *J. Struct. Eng.* 147 (5), 3007. doi:10.1061/(asce)st.1943-541x.0003007

Tesfamariam, S., Skandalos, K., and Teweldebrhan, B. T. 2021a. *Design Of Tall-Coupled-Wall Timber Building: Energy Dissipating Coupling Beams*. UBC Faculty Research and Publications. doi:10.14288/1.0403817

Tesfamariam, S., Stiemer, S. F., Bezabeh, M., Goertz, C., Popovski, M., and Goda, K. 2015. Force Based Design Guideline for Timber-Steel Hybrid Structures: Steel Moment Resisting Frames with CLT Infill Walls. UBC Faculty Research and Publications. doi:10.14288/1.0223405

Tesfamariam, S., Wakashima, Y., and Skandalos, K. (2021b). Damped Timber Shear wall: Shake-Table Tests and Analytical Models. *J. Struct. Eng.* 147 (6), 04021064.

Uemura, R., Akehashi, H., Fujita, K., and Takewaki, I. (2021). Global Simultaneous Optimization of Oil, Hysteretic and Inertial Dampers Using Real-Valued Genetic Algorithm and Local Search. *Front. Built Environ.* 7, 795577. doi:10.3389/fbuil.2021.795577

Ugalde, D., Almazán, J. L., Santa María, H., and Guindos, P. (2019). Seismic protection Technologies for Timber Structures: A Review. *Eur. J. Wood Prod.* 77 (2), 173–194. doi:10.1007/s00107-019-01389-9

Valdebenito, M. A., and Schuëller, G. I. (2010). A Survey on Approaches for Reliability-Based Optimization. *Struct. Multidisc Optim* 42, 645–663. doi:10.1007/s00158-010-0518-6

van de Lindt, J. W., Amini, M. O., Rammer, D., Line, P., Pei, S., and Popovski, M. (2020). Seismic Performance Factors for Cross-Laminated Timber Shear wall Systems in the United States. *J. Struct. Eng.* 146 (9), 04020172. doi:10.1061/(asce)st.1943-541x.0002718

Venanzi, I., Lavan, O., Ierimonti, L., and Fabrizi, S. (2018). Multi-hazard Loss Analysis of Tall Buildings under Wind and Seismic Loads. *Struct. Infrastructure Eng.* 14 (10), 1295–1311. doi:10.1080/15732479.2018.1442482

Vulcano, A. (1998). Comparative Study of the Earthquake and Wind Dynamic Responses of Base-Isolated Buildings. *J. Wind Eng. Ind. Aerodynamics* 74-76, 751–764. doi:10.1016/s0167-6105(98)00068-3

Wang, F., Xiong, F., Chen, S., and Song, J. (2019). Multi-fidelity Uncertainty Propagation Using Polynomial Chaos and Gaussian Process Modeling. *Struct. Multidisc Optim* 60 (4), 1583–1604. doi:10.1007/s00158-019-02287-7

Wang, H., and Wu, T. (2020). Knowledge-enhanced Deep Learning for Wind-Induced Nonlinear Structural Dynamic Analysis. *J. Struct. Eng.* 146 (11), 04020235. doi:10.1061/(asce)st.1943-541x.0002802

Wang, J., Li, C., Xu, G., Li, Y., and Kareem, A. (2021a). Efficient Structural Reliability Analysis Based on Adaptive Bayesian Support Vector Regression. *Comp. Methods Appl. Mech. Eng.* 387, 114172. doi:10.1016/j.cma.2021.114172

Wang, M., Nagarajaiah, S., and Sun, F.-F. (2021b). Optimal Design of Supplemental Negative Stiffness Damped Outrigger System for High-Rise Buildings Resisting Multi-hazard of Winds and Earthquakes. *J. Wind Eng. Ind. Aerodynamics* 218, 104761. doi:10.1016/j.jweia.2021.104761

Wen, Y. K. (1990). *Structural Load Modelling and Combination for Performance and Safety Evaluation*. Amsterdam, Netherlands: Elsevier.

Wen, Y. K., and Kang, Y. J. (2001a). Minimum Building Life-Cycle Cost Design Criteria. I: Methodology. *J. Struct. Eng.* 127 (3), 330–337. doi:10.1061/(asce)0733-9445(2001)127:3(330)

Wen, Y. K., and Kang, Y. J. (2001b). Minimum Building Life-Cycle Cost Design Criteria. II: Applications. *J. Struct. Eng.* 127 (3), 338–346. doi:10.1061/(asce)0733-9445(2001)127:3(338)

Wen, Y. K. (2001). Minimum Lifecycle Cost Design under Multiple Hazards. *Reliability Eng. Syst. Saf.* 73 (3), 223–231. doi:10.1016/s0951-8320(01)00047-3

Willford, M., Whittaker, A., and Klemencic, R. (2008). Recommendations for the Seismic Design of High-Rise BuildingsCouncil on Tall Buildings and Urban Habitat. *A Consensus Document – CTBUH Seismic Working Group*.

Wilson, A. W., Phillips, A. R., Motter, C. J., Lee, J. Y., and Dolan, J. D. (2021). Seismic Loss Analysis of Buildings with post-tensioned Cross-Laminated Timber walls. *Earthquake Spectra* 37 (1), 324–345. doi:10.1177/8755293020944188

Wu, J. L., Xiao, H., and Paterson, E. (2018). Physics-informed Machine Learning Approach for Augmenting Turbulence Models: A Comprehensive Framework. *Phys. Rev. Fluids* 3 (7), 074602. doi:10.1103/physrevfluids.3.074602

Xu, Z., Lu, X., and Law, K. H. (2016). A Computational Framework for Regional Seismic Simulation of Buildings with Multiple Fidelity Models. *Adv. Eng. Softw.* 99, 100–110. doi:10.1016/j.advengsoft.2016.05.014

Yamamoto, Y., and Baker, J. W. (2013). Stochastic Model for Earthquake Ground Motion Using Wavelet Packets. *Bull. Seismological Soc. America* 103 (6), 3044–3056. doi:10.1785/0120120312

Yang, T. Y., Moehle, J., Stojadinovic, B., and Der Kiureghian, A. (2009). Seismic Performance Evaluation of Facilities: Methodology and Implementation. *J. Struct. Eng.* 135 (10), 1146–1154. doi:10.1061/(asce)0733-9445(2009)135:10(1146)

Yang, Y., and Perdikaris, P. (2019). Conditional Deep Surrogate Models for Stochastic, High-Dimensional, and Multi-Fidelity Systems. *Comput. Mech.* 64 (2), 417–434. doi:10.1007/s00466-019-01718-y

Yeh, C.-T., Hartz, B. J., and Brown, C. B. (1971). Damping Sources in wood Structures. *J. Sound Vibration* 19 (4), 411–419. doi:10.1016/0022-460x(71)90612-2

Yu, H., Gillot, F., and Ichchou, M. (2013). Reliability Based Robust Design Optimization for Tuned Mass Damper in Passive Vibration Control of Deterministic/uncertain Structures. *J. Sound Vibration* 332 (9), 2222–2238. doi:10.1016/j.jsv.2012.12.014

Yucesan, Y. A., Viana, F. A. C., Manin, L., and Mahfoud, J. (2021). Adjusting a Torsional Vibration Damper Model with Physics-Informed Neural Networks. *Mech. Syst. Signal Process.* 154, 107552. doi:10.1016/j.ymssp.2020.107552

Zareian, F., and Krawinkler, H. (2012). Conceptual Performance-Based Seismic Design Using Building-Level and story-level Decision Support System. *Earthquake Engng Struct. Dyn.* 41, 1439–1453. doi:10.1002/eqe.2218

Zhang, C., Song, C., and Shafieezadeh, A. (2022). Adaptive Reliability Analysis for Multi-Fidelity Models Using a Collective Learning Strategy. *Struct. Saf.* 94, 102141. doi:10.1016/j.strusafe.2021.102141

Zhang, J., Taflanidis, A. A., and Medina, J. C. (2017). Sequential Approximate Optimization for Design under Uncertainty Problems Utilizing Kriging Metamodeling in Augmented Input Space. *Comp. Methods Appl. Mech. Eng.* 315, 369–395. doi:10.1016/j.cma.2016.10.042

Zhao, N., Huang, G., Kareem, A., Li, Y., and Peng, L. (2021). Simulation of Ergodic Multivariate Stochastic Processes: An Enhanced Spectral Representation Method. *Mech. Syst. Signal Process.* 161, 107949. doi:10.1016/j.ymssp.2021.107949

Zheng, X.-W., Li, H.-N., and Gardoni, P. (2021). Reliability-based Design Approach for High-Rise Buildings Subject to Earthquakes and strong Winds. *Eng. Structures* 244, 112771. doi:10.1016/j.engstruct.2021.112771

Zhou, K., and Tang, J. (2021). Efficient Characterization of Dynamic Response Variation Using Multi-Fidelity Data Fusion through Composite Neural Network. *Eng. Structures* 232, 111878. doi:10.1016/j.engstruct.2021.111878

Zhou, Z., Wei, X., Lu, Z., and Jeremic, B. (2018). Influence of Soil-Structure Interaction on Performance of a Super Tall Building Using a New Eddy-Current Tuned Mass Damper. *Struct. Des. Tall Spec. Buildings*. doi:10.1002/tal.1501

Zou, X.-K., Wang, Q., Li, G., and Chan, C.-M. (2010). Integrated Reliability-Based Seismic Drift Design Optimization of Base-Isolated concrete Buildings. *J. Struct. Eng.* 136 (10), 1282–1295. doi:10.1061/(asce)st.1943-541x.0000216

Conflict of Interest: The authors declare that the research was conducted in the absence of any commercial or financial relationships that could be construed as a potential conflict of interest.

frontiers in Built Environment

REVIEW
published: 29 March 2022
doi: 10.3389/fbuil.2022.840303

Blockchain in Civil Engineering, Architecture and Construction Industry: State of the Art, Evolution, Challenges and Opportunities

Vagelis Plevris[1]*, *Nikos D. Lagaros*[2] *and Ahmet Zeytinci*[3]

[1]Department of Civil and Architectural Engineering, College of Engineering, Qatar University, Doha, Qatar, [2]Institute of Structural Analysis and Antiseismic Research, School of Civil Engineering, National Technical University of Athens, Athens, Greece, [3]School of Engineering and Applied Sciences, University of the District of Columbia, Washington, DC, United States

Blockchain is a technology that allows the recording of information in a way that it is difficult or practically impossible to alter, hack, or cheat. It is a new, promising technology, considered by many as a general-purpose technology (GPT). GPTs are technologies that have the potential to affect an entire economy, impacting economic growth and transforming both everyday life and the ways in which we conduct business. We present a bibliometric analysis of the relevant literature, followed by a discussion about monetary mediums and the evolution of bitcoin, as the first digital medium managing to solve the "double-spending" problem and the first successful implementation of blockchain technology. The computational operations involved in blockchain are presented, together with the cryptographic technologies associated with it, its unique characteristics, and the advantages it offers as a technology. A comprehensive literature review is provided, of the current state of the art in blockchain in the fields of civil engineering, architecture and the construction industry. Six important application areas are identified, and the relevant literature is investigated. Namely, building information modelling and computer aided design, contract management and smart contracts, construction project management, smart buildings and smart cities, construction supply chain management, and real estate. Finally, we discuss the future applications, the challenges and the opportunities that blockchain technology brings to these fields.

Keywords: blockchain, general purpose technology (GPT), distributed ledger, civil engineering, architecture, construction, engineering

OPEN ACCESS

Edited by:
Georgios Eleftherios Stavroulakis, Technical University of Crete, Greece

Reviewed by:
Ibrahim Yitmen, Jönköping University, Sweden
Sameh Samir F Mehanny, Cairo University, Egypt

***Correspondence:**
Vagelis Plevris
vplevris@qu.edu.qa

Specialty section:
This article was submitted to Computational Methods in Structural Engineering, a section of the journal Frontiers in Built Environment

Received: *21 December 2021*
Accepted: *10 March 2022*
Published: *29 March 2022*

Citation:
Plevris V, Lagaros ND and Zeytinci A (2022) Blockchain in Civil Engineering, Architecture and Construction Industry: State of the Art, Evolution, Challenges and Opportunities. Front. Built Environ. 8:840303. doi: 10.3389/fbuil.2022.840303

1 INTRODUCTION

Construction is arguably one of the largest industries in the world, creating infrastructure which is the backbone of productivity and economic growth. The Architecture, Engineering, and Construction (AEC) industry has entered a period of major disruption caused by a host of new and more mature digital technologies, such as Artificial Intelligence (AI), the Internet of Things (IoT), Virtual Reality (VR), Geographic Information Systems (GIS), digital photogrammetry, Building Information Modelling (BIM), 3D printing, laser scanning, global positioning systems (GPS), radio frequency identification devices (RFID), augmented reality (AR), sensors, robotics, big data management, and others (Wang et al., 2020). These technologies have been proven helpful due

to the numerous benefits they offer to project stakeholders, such as increased productivity, reduction in building waste, sustainable performance, enhanced visualization, safety improvement and improved data sharing.

Lately, another innovative digital technology, blockchain, has appeared, promising to change the way people do transactions, keep records, validate data and much more. For many, blockchain is a new general-purpose technology that can transform both our everyday lives and the ways we do business. Bitcoin was the first successful application of this technology and its first description as an algorithmic idea can be found in the work by (Nakamoto 2008). Blockchain was the technology which allowed Bitcoin to transfer value in a decentralized network, for the very first time in history. Many desirable characteristics of blockchain already exist in Bitcoin, even though Bitcoin was only the first application of the technology and further developments and improvements have been made since. For this reason, the present study will start with discussing monetary mediums, problems related to transferring value using digital currency and how blockchain technology managed to solve the well-known "double spending" problem in digital currency, opening horizons for other important applications of the technology.

Although blockchain is still at its early stages today, it probably has the potential to play a significant role in construction industry in the future, or even reshape it drastically to the better (Shojaei 2019). explored the applications of blockchain in improving information management systems in the construction industry. The author concludes that blockchain has the potential of addressing common problems of the construction industry, while it can be adaptable to the construction industry structure and the way it is practiced (Nawari and Ravindran 2019b). reviewed blockchain and how it is related to the built environment. They explored potential applications in the AEC industry, focusing mainly on Building Information Modeling (BIM) and highlighting its potential and its limitations.

(Tezel et al., 2022) examined blockchain opportunities and related issues in the Built Environment, with particular emphasis on its potential influence on trust, transparency and cybersecurity. The authors also provide directions for future research, contributing to the cyber-physical convergence in Construction 4.0 (Li et al., 2019). identified recent challenges in the construction industry and explored blockchain as a potential solution to some of these challenges. They performed a review of blockchain uses in the built environment and identified seven distinct areas of applications, namely 1) Smart Cities and the Sharing Economy, 2) Smart Energy, 3) Smart Homes, 4) Smart Government, 5) Intelligent Transport, 6) BIM and Construction Management, and 7) Business Models and Organizational Structures.

(Cheng et al., 2021) reviewed the present status and investigated the benefits, challenges, and future research opportunities of blockchain meeting the AEC industry. Their results show that relevant research on blockchain remains new and fragmented. Nevertheless, they managed to identify five relevant areas of benefit, namely 1) supply chain management, 2) information management, 3) contract management, 4) integration management, and 5) stakeholder management (Shojaei et al., 2021). investigated blockchain as a promising technology for the facilitation of a circular economy (CE) in the built environment. They presented and tested a blockchain model through a synthetic case study to provide a proof of concept as to the feasibility of blockchain as an enabler of a CE in the built environment. They conclude that blockchain is shown to be a feasible and novel approach for employing CE concepts in the built environment domain as it can provide full material and energy traceability, enabling the user to make predictions for the recycling and reuse of materials and goods used in the built environment.

The aim of this study is to formulate a picture of the current state and practice of the use of blockchain technology in fields related to the built environment such as civil engineering, architecture and construction industry areas, to identify the current state of the art and to examine the challenges and opportunities ahead. The study also summarizes and highlights specific application areas related to the AEC industry, where blockchain has the potential to provide new solutions, and how these solutions can be adopted to improve performance, sustainability, and safety in the future. The structure of the paper is as follows: **Section 1** is the introduction, followed by the bibliometric analysis of **Section 2**. **Section 3** presents the idea of monetary mediums, from bartering to digital money, the double spending problem and how it was first solved using blockchain technology. **Section 4** focuses on technical details of the technology, while **Section 5** discusses the applications of blockchain in the civil, architectural and construction industry, where six application areas as identified and discussed in detail. The conclusions and a relevant discussion are provided in **Section 6**.

2 BIBLIOMETRIC ANALYSIS

2.1 Papers Published in the Field

A simple look at the most recent scientific literature can reveal how important blockchain has become for the scientific community lately. The word "blockchain" returns 28,600 document results in Scopus when searching within "Article title, Abstract and Keywords" (Query string: "TITLE-ABS-KEY (blockchain)"). 28,355 of these results (99.14%) have a publication year of 2017 or later (i.e. last 5 years), as only 245 papers were published in the topic between 1990–2016. Even more interestingly, 85.77% of the results (24,531 documents) have a publication year of 2019 or later, i.e. published in the last 3 years. The same search, limited within the "Engineering" field only (Query string: "TITLE-ABS-KEY (blockchain) AND (LIMIT-TO (SUBJAREA,"ENGI"))") returns 11,969 document results. These queries were made on 6 March 2022. **Figure 1** shows these search results, per year, for the years from 2013 to 2021. Year 2022 was excluded from the plot as it is still a year in progress. It has to be noted that even for year 2021 the process of indexing and adding papers is still a work in progress in Scopus. The exponential growth in the production of scientific papers is clearly visible, showing the latest impact of blockchain in all scientific fields, engineering included.

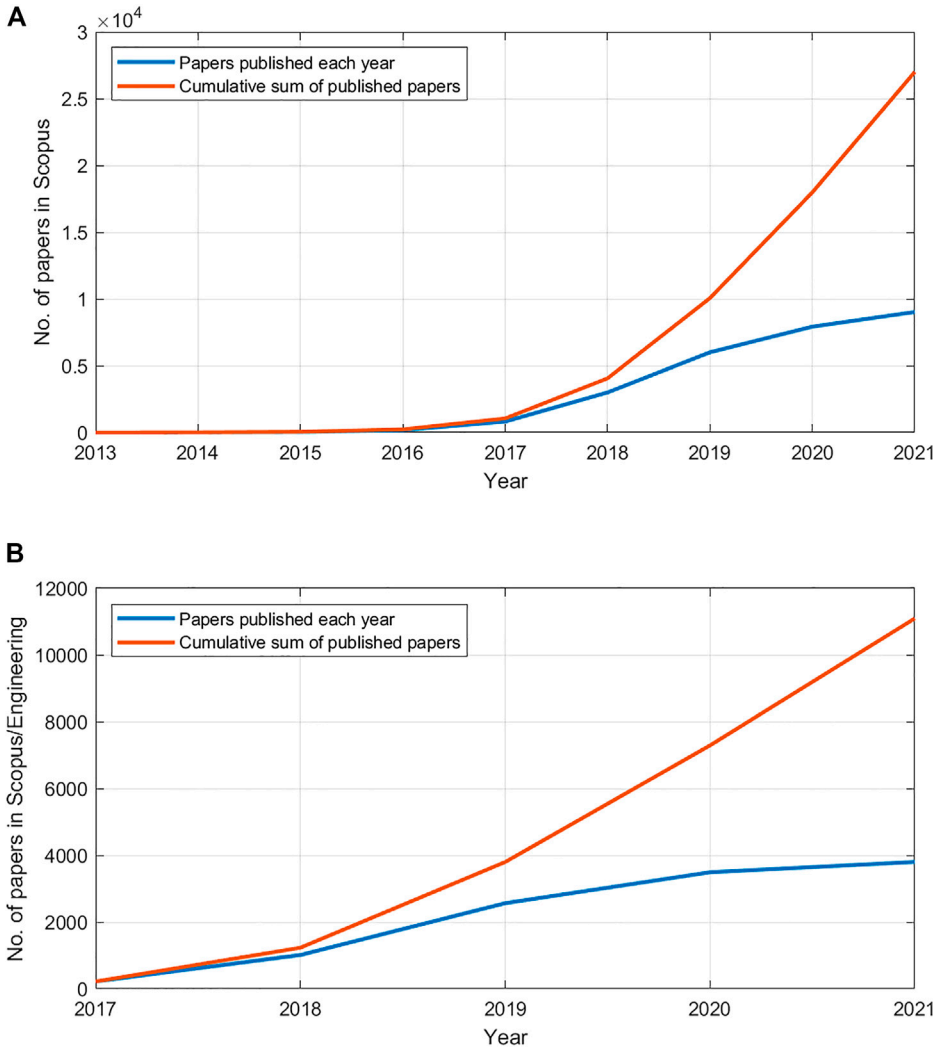

FIGURE 1 | Papers in "blockchain" in Scopus database, per year: **(A)** General search (all fields), **(B)** Search limited within the "Engineering" field.

2.2 Top Keywords

We performed a co-occurrence analysis of the top keywords, including author keywords and index keywords from the Scopus database. For this, we search Scopus with the word "blockchain" within "Article title, Abstract and Keywords" and we limit the search to the "Engineering" field and also to the years 2017–2022 (6 years in total). The full query string, performed on 7 March 2022, is therefore "*TITLE-ABS-KEY(blockchain) AND (LIMIT-TO (SUBJAREA,"ENGI")) AND (LIMIT-TO (PUBYEAR, 2022) OR LIMIT-TO (PUBYEAR, 2021) OR LIMIT-TO (PUBYEAR, 2020) OR LIMIT-TO (PUBYEAR, 2019) OR LIMIT-TO (PUBYEAR, 2018) OR LIMIT-TO (PUBYEAR, 2017))*". The query returned 11,926 documents. Within this result, we found the top-30 keywords of the papers. Similar keywords needed to be merged manually, as follows: blockchain (blockchain, blockchains, blockchain technology), internet of things (iot, internet of things (iot), internet of thing (iot)), smart contract (smart contracts), supply chain (supply chains, supply chain management), building information model (bim, building information model - bim, building information modeling, building information modelling), where the word in bold is the main keyword and the words in parentheses are the different variations that have been merged within the main keyword. The network visualization of the co-occurrence of the top-30 keywords is presented in **Figure 2**, generated using the VOSviewer software (van Eck and Waltman 2007), with 5 clusters presented with different colors, and minimum strength equal to 60.

In this map, the links (lines) between keywords express the frequency of co-occurrence of the keywords in the documents, while the size of each bubble (keyword) expresses the number of occurrences of a specific keyword. As expected, the keyword "blockchain" appears in the center of the network as the strongest keyword (10,135 occurrences), followed by "internet of things" (2072), "smart contract" (1873), "network security" (1,168), "digital storage" (1,058) and "security" (928). Interestingly, the

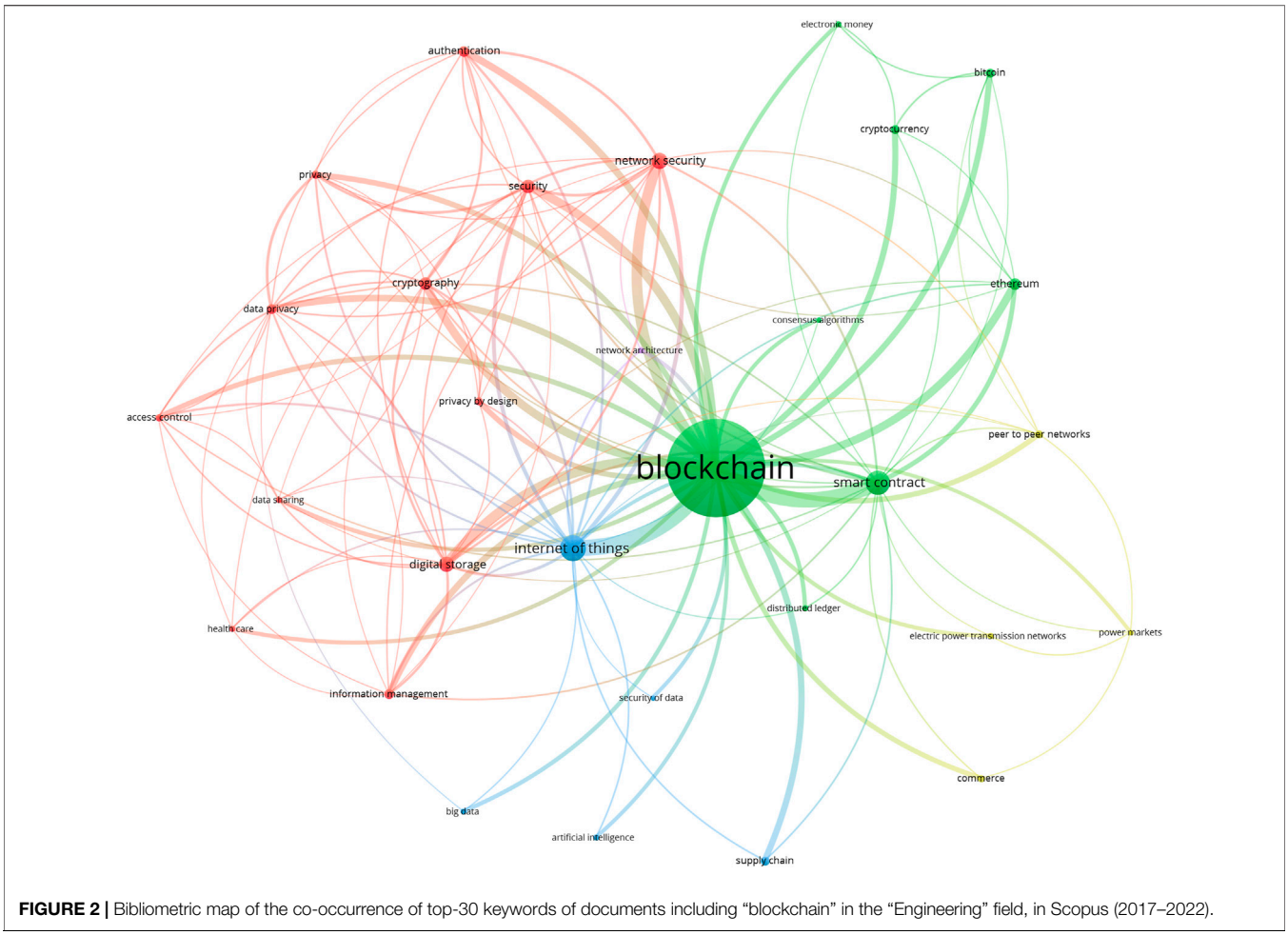

FIGURE 2 | Bibliometric map of the co-occurrence of top-30 keywords of documents including "blockchain" in the "Engineering" field, in Scopus (2017–2022).

keyword "bitcoin" appears as a small bubble on the top-right, which shows that despite it being the first application of blockchain, it is now somehow isolated as simply one of the numerous applications of the broader technology.

A clear cluster related to engineering applications is the yellow one, having to do with power markets and electric power transmission networks. Interestingly, keywords related to the civil engineering and the construction industry are not present in this network visualization, although the search has been limited to the "engineering" field. This shows that blockchain applications in these areas are still at a very premature state. It also confirms that the fact that the construction industry has been traditionally slow in adapting new digital technologies.

Next, we limit the search to areas related to civil engineering and the construction industry. For this, we search within the "Article title, Abstract and Keywords" with the query "*blockchain AND ("construction industry" OR "civil engineering" OR "construction management" OR "building information modelling" OR "smart buildings" OR "real estate")*", which returns 365 document results. We apply the same technique for merging similar keywords as we did before. Setting a minimum strength of connections equal to 10, and 5 clusters, we obtain the bibliometric map of **Figure 3**.

Again, the keyword "blockchain" is in the center of the network as the strongest keyword (280 occurrences), followed by "smart contract" (91), "construction industry" (76), "building information model" (56), "architectural design" (50), "internet of things" (49), "supply chain" (45) and "project management" (28). This map reveals some trends and the most important application areas of the technology in the civil engineering and the construction industry fields. It also shows the connections of different applications, for example the construction industry (as a central node) with BIM, architectural design, smart contract, information management and others.

2.3 Top Countries

Figure 4 is based on the same data from Scopus as **Figure 3**, but now the focus is on the co-authorship of the top countries in the field. Setting the minimum documents for a country to 2, the largest set of connected countries is found to be 27. The map is presented in **Figure 4** with the minimum connection strength set equal to zero.

In this map, the links (lines) between countries represent the frequency of co-authorship between the countries, while the size of each bubble (country) expresses the number of publications in the field by a specific country. In terms of the number of

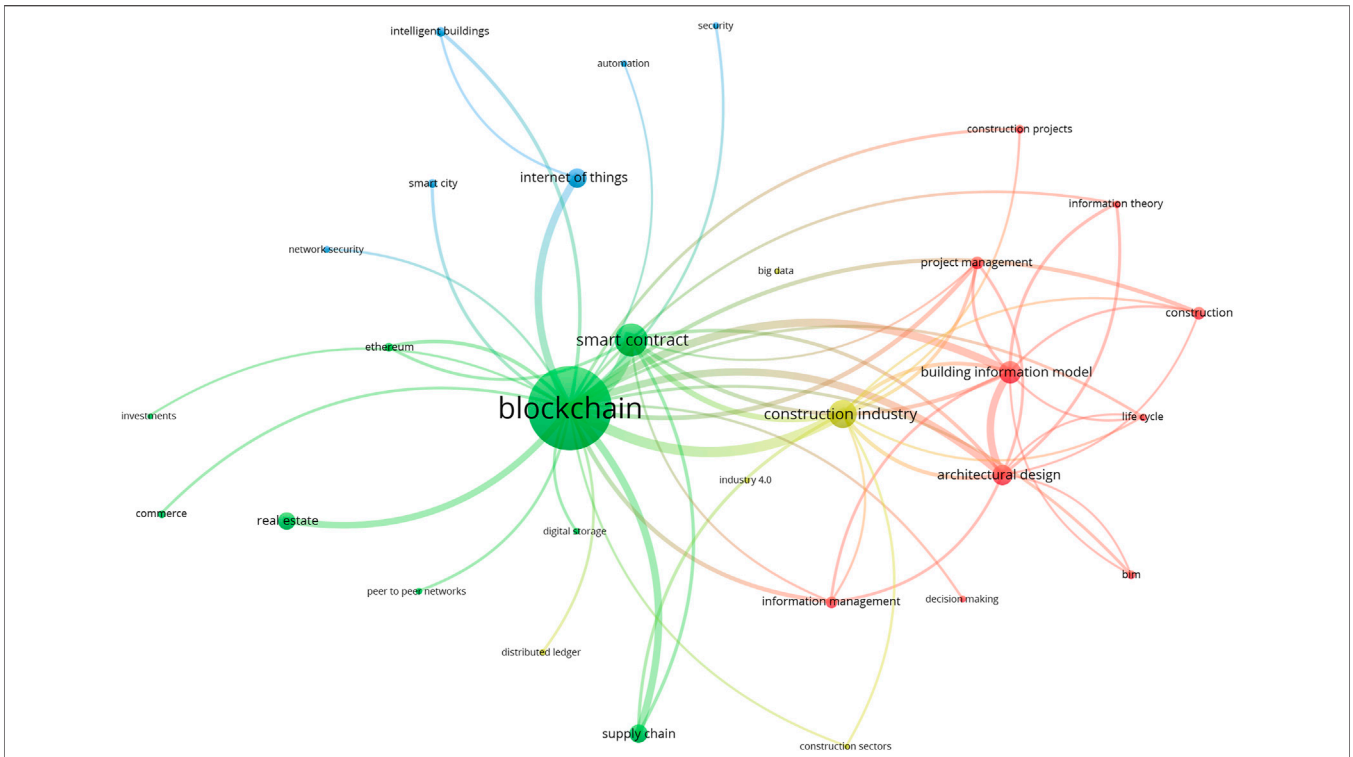

FIGURE 3 | Bibliometric map of the co-occurrence of the top-30 keywords of documents including blockchain in the civil engineering and the construction industry, in Scopus.

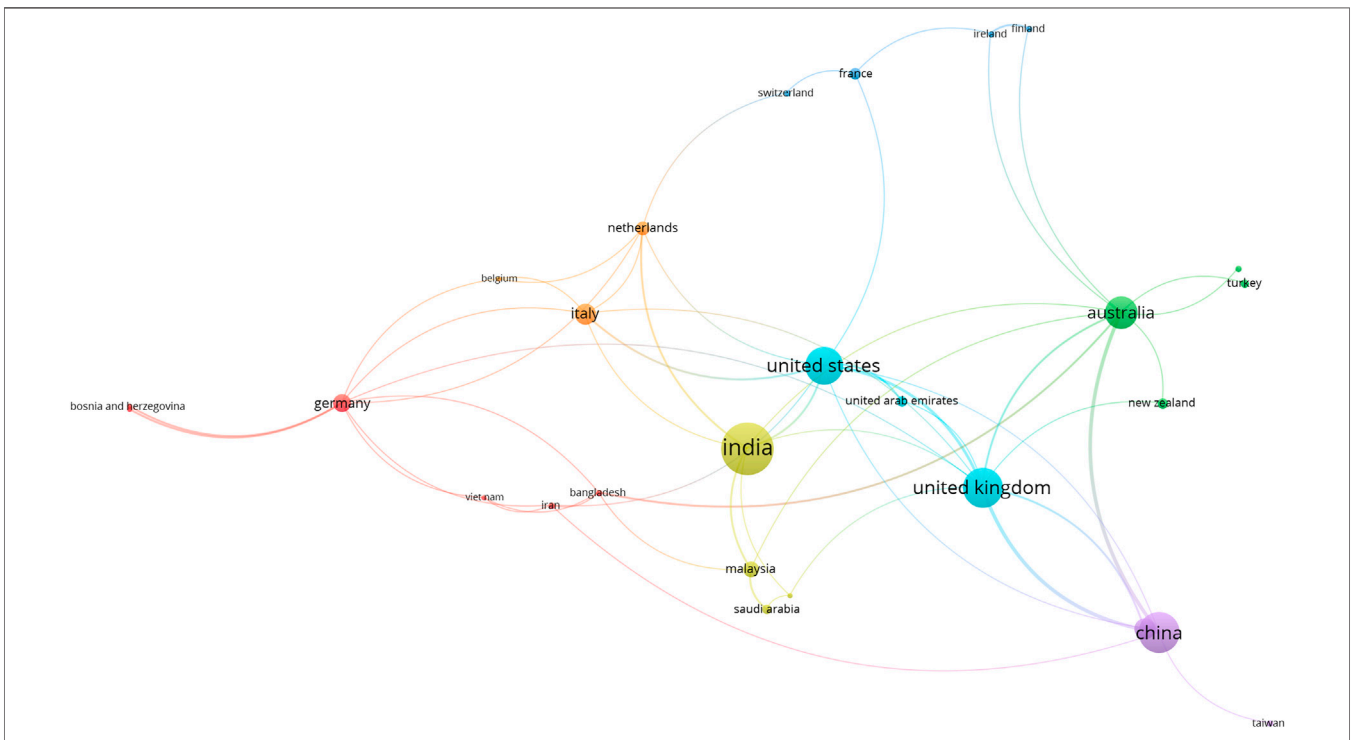

FIGURE 4 | Bibliometric map of the co-authorship of the top countries with documents including blockchain in the civil engineering and the construction industry, in Scopus.

documents published in the field, the most active country is India with 47 documents and 157 citations, followed by China (35, 446), the United Kingdom (34, 388), the US (32, 505), Australia (26, 440), Hong Kong (16, 135) and Italy (16, 44). It is not surprising that India leads this map, as in India IT is a vast industry comprising information technology services, consulting, and outsourcing, accounting for 8% of India's GDP in 2020.

3 MONETARY MEDIUMS: FROM BARTERING TO DIGITAL MONEY

In the long past, there were no monetary mediums. People in primitive societies would simply exchange goods using a fair barter arrangement. Bartering has to do with the exchange of services and goods between two people or parties without the use of money. It is based on equivalent estimates of the value of services and goods. This approach has significant limitations, one of the most important ones being not being able to store wealth in the long term.

Then came money, a monetary medium in the form of a metal coin, a piece of paper or even a shell or other object, that people could use as a medium of exchange, a unit for measuring value and a means to store wealth. The value of money depends mostly on the importance that the people place on it. The invention of money had an important role in the evolution and development of human societies as it allowed people to trade services and goods indirectly, providing also a very effective and direct way to store wealth. Historians believe that objects made of metal were first used as money as early as 5,000 BC. Around the second half of the 7^{th} century B.C., the Lydians were the first western civilization to make coins. The Lydian stater was the first coin officially issued by a state in the world history and was the model for virtually all subsequent coinage (Kroll 2012). Later on, other civilizations began to mint their own coins, having specific properties and values. Around 700 B.C., the Chinese moved to paper money. In Europe, the first banknotes were issued in 1,666 by the Bank of Stockholm while in the US, the Massachusetts Bay Colony was said to have issued the first paper money in 1,690.

3.1 Digital Money and the Need for a Trusted Third Party

The 21st century and the evolution of computers and digital technology gave rise to a new form of currency, digital money, allowing digital, mobile payments between different parties. Mobile payments can be used to buy a service or product through the use of a portable electronic device, such as a smartphone, tablet, laptop or desktop computer, to name a few. Money nowadays needs not have a physical form. It can merely sit in bank accounts, waiting to be used online for whatever necessary. Mobile payments offer the advantage that the parties involved in a transaction do not have to be in the same physical location for a successful transaction to take place. Unlike hand-to-hand physical payments by cash, digital payments can be made remotely, through an institution (usually a bank). The bank acts as an intermediary or a "trusted third party". When Alice pays Bob the amount of $100 remotely, she makes the relevant request at a bank online. The bank needs to verify and process the transaction. First, it checks if Alice has $100 at her disposal, in her account. If yes, it proceeds with the payment to Bob. For the bank this is simply a couple of records in the transactions' ledger. The bank will debit Alice's account with the amount of $100 and simultaneously credit Bob' account with the same amount. Everything happens at the level of the bank ledger which is a "book" in which account transactions are recorded. In such bookkeeping system with double entries, credits and debits are simply entries that are made in the account ledgers to record changes in value, as a result of transactions.

As mentioned, such online payments need a trusted third party to act as an intermediary. Unlike cash transactions, that are truly "peer-to-peer" from one party to the other, traditional online payments need to go through a bank. This causes problems and difficulties in certain cases. First of all, the bank needs to be online, it needs to be working during the transaction and it needs to be there to validate the payment. Although these may seem to be small problems in the real world, there are other more significant problems and difficulties arising from the fact that an intermediary is always necessary. For example, banks may delay or even censor transactions, while in some cases transaction fees may be too high. This is the case with international payments between two banks in different, distant countries and especially when a third world country is involved. In addition, one needs to open a bank account to send or receive such payments. All banks have specific regulations. There are certain requirements for opening an account and rules on who can pay or who can get paid. According to the 2019 National Survey of Household Use of Banking and Financial Services by FDIC (Federal Deposit Insurance Corporation 2020), 5.4% of households in the US had no access to a checking or savings account at a bank or credit union. This represents approximately 7 million U.S. households or a total of approximately 14 million American adults who are literally unbanked. Interestingly, nearly half of them reported that they did not have a bank account due to lack of enough money to meet minimum requirements, while approximately 1/3 of unbanked households reported that they did not have an account because they do not trust banks (Federal Deposit Insurance Corporation 2020). Privacy is a major concern as a lot of personal information is revealed in every transaction and the bank or a bank employee have access to this sensitive information.

3.2 The "Beauty" of Cash, Digital Cash and the "Double-Spending Problem"

Cash payments do not have these issues. The "beauty" of cash lies in its simplicity and on the fact that it is truly "peer-to-peer", without the need of any intermediaries. But cash has other problems: For example, when Alice gives Bob a bank note, the two parties need to be in the same place at the same time for the physical object (the bank note) to be handed from one person to the other. In addition, cash is bulky and therefore it cannot be easily used for big transactions. At this point the question arises: Could we have online, digital payments that are just like cash, i.e.

peer-to-peer, with no need for intermediaries, no banks, no delays, no censorship and no privacy issues? Is there a way to have digital money that would behave just like cash?

Many researchers had tried to deal with this issue, but they faced the so called "double-spending problem." Unlike physical currencies that cannot be easily replicated, digital currencies can be easily reproduced digitally. Double spending has to do with the problem of a digital currency or token being spent twice, which should not be allowed in a fair system. In other words, if somebody tries to use a digital token for a second time, after it has been already spent, the system should be able to detect it and reject the second transaction.

3.3 The Solution to the Double-Spending Problem

In 2008, Satoshi Nakamoto introduced Bitcoin to the world. In his novel work (Nakamoto 2008) the brilliant idea of a system for electronic transactions which does not rely on a "trusted third party" is explained. This system was the first successful application managing to solve the double-spending problem and the first implementation of blockchain technology. It is a peer-to-peer electronic cash system which uses cryptography and the concept of "proof-of-work" (PoW) to record the history of transactions. The real identity of Satoshi Nakamoto remains a matter of dispute until today.

The code of Bitcoin was released in 2009, after the original paper was published in 2008. In Bitcoin, there is no bank, no central system, no single institution in the middle playing a special role. That's why it is called a "decentralized network". All parties in this network are equal and there is no central authority or special player. The technology that enabled Bitcoin to make this breakthrough, is called blockchain. Bitcoin and other cryptocurrencies, all based on blockchain technology, offer peer-to-peer transactions with privacy for any amount of money, just like cash.

The system uses a decentralized approach which is based on the creation of blocks which are linked together, forming a chain of blocks, the so-called "block chain". This is what we nowadays call blockchain technology. In the blockchain, every transaction and every block have a timestamp and blocks are linked together with their hash values and "proof-of-work". The record of a transaction is distributed among many nodes in the system which makes it practically impossible for a bad actor to gain control of the system and manipulate the ledger to their advantage. Using proof of work, the amount of computational power needed to reverse or change a transaction is enormous. This technology allows bitcoin to transfer value in a decentralized way without the need for any intermediary, or a trusted third party such as a bank. In addition, the system uses public-key cryptography which allows users to transact anonymously or more accurately, pseudonymously.

Bitcoin has a market capitalization of more than $700 billion (as of 6 March 2022) and it is the largest application of blockchain technology until today. Despite its widespread fame and its high value, Bitcoin itself remains a controversy. For many, it is the ultimate democratic tool and the currency of the future. They highlight its advantages, such as payment freedom, availability, total control of one's money, security, transparency and low fees. On the other hand, some economists and other experts have characterized Bitcoin as a speculative bubble or even an advanced Ponzi scheme. They criticize Bitcoin for its use in illegal transactions, large carbon footprint, price volatility, scalability problems and low speed.

4 BLOCKCHAIN

4.1 Technical Details

4.1.1 Asymmetric Cryptography

Asymmetric cryptography, also known as public-key cryptography uses a pair of keys, a Public and a Private key to encrypt and decrypt a message. Each user has a pair of keys. The two keys are mathematically related. The private key cannot be shared with others and works similarly to a password, while the public key can be shared with and is visible to everyone. Both keys are needed to perform an operation. A message which is encrypted with the private key can only be decrypted with the public key, and vice-versa: a message or data encrypted with the public key can only be decrypted with the private key. Based on which key is used first, there are two main uses of asymmetric cryptography, as shown schematically in **Figure 5**.

In the first case depicted in **Figure 5**, called Digital signature or Sender authentication, data is encrypted with the private key of the sender and can be decrypted with the corresponding public key. This ensures that the message came from the stated sender. Example: Alice sends a message to Bob and she encrypts it with her private key. Bob receives the message. He decrypts it using the public key of Alice and that guarantees that the message came indeed from Alice.

In the second case, called Digital envelope or Receiver authentication, data is encrypted with the public key of the recipient and can be decrypted with the corresponding private key. This ensures that the message can only be read by the intended recipient. Example: Alice sends a message to Bob and she encrypts it using the public key of Bob. Then Bob is the only one who can decrypt and read the message as only he has access to the pairing private key. This ensures confidentiality of a message.

Together, the two keys help ensure the security of the exchanged data. Asymmetric encryption has many applications such as in key exchange, email security and web security. In Bitcoin and other blockchain applications, asymmetric encryption is used to ensure the integrity of transactions. Bitcoin uses the ECDSA algorithm (Elliptic Curve Digital Signature Algorithm) and in particular the Secp256k1 elliptic curve and the double-SHA hash to implement its public key cryptography.

When a person creates a crypto wallet, the system generates a pair of keys. The private key can generate the public key, but the public key cannot be converted back into the private key. The public key itself is not a bitcoin address. The address of a wallet, which is similar to a bank account number (where one can receive payments) is derived from the public key by putting the public key into a hash function (see next subsection). Bitcoin addresses

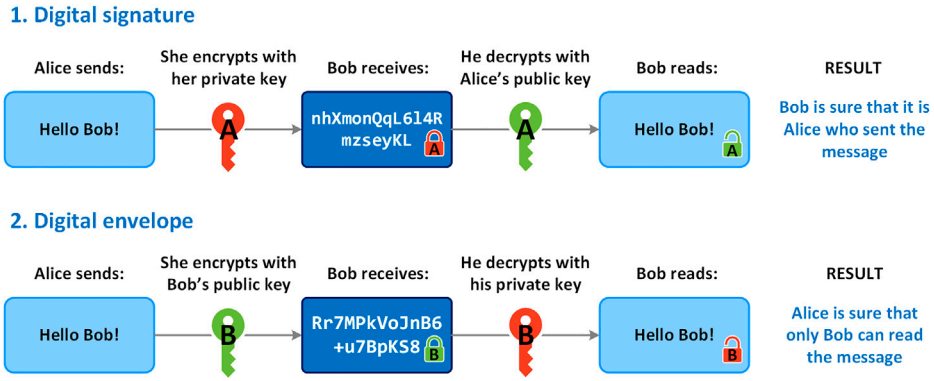

FIGURE 5 | Uses of asymmetric cryptography in message sending.

are 34-digit alphanumeric. An example Bitcoin address is "1J7mdg5rbQyUHENYdx39WVWK7fsLpEoXZy". Such an address appears most commonly as the recipient of funds. Note that several of the characters in an address are used as a checksum. This way typographical errors can be automatically found and rejected by the system.

On the other hand, the private key is used for the digital signature of the transactions, and it provides access to the funds in the wallet. In other words, it is equivalent to a password or PIN code that provides control over a bank account. Mathematically speaking, a signature is generated from a hash of something to be signed, plus a private key. When Alice sends Bob an amount of Bitcoin, she presents her public key and a signature (transaction fingerprint). The signature, which is different each time, is created with her private key and can only be produced by someone who has access to Alice's private key. However, anyone in the network can verify the signature if they have access to the public key and the transaction fingerprint. In other words, it is ensured that only Alice, having the private key, can spend the bitcoin she has in her account, but anyone in the network, having her public key, can easily verify that it is Alice who made the payment.

4.1.2 Cryptographic Hash Functions

A hash function is a one-way function that maps data of an arbitrary size to fix-sized values (Estébanez et al., 2014). The return of a hash function is called the hash value, digest, hash code, or simply hash. A hash function is deterministic, meaning that for a given input value it should always generate the same output. Hash functions are designed to be irreversible, a property which is usually referred to as pre-image resistance, which means that it is not possible to generate the input from the hash, and therefore a hash function is essentially a one-way function.

A cryptographic hash function has additionally some desired special properties:

- *Quick computation*: The hash value is computationally inexpensive to compute, for a given message.
- It is practically impossible to generate a message that will give a given hash
- *Collision resistance*: Practically, it is impossible to find two messages giving the same hash value.
- *Avalanche effect*: A slight change in a message will result to a drastic change in the hash value, so that the new hash appears to be completely different and uncorrelated to the old one.

Bitcoin uses the SHA-256 hashing algorithm, which belongs to the SHA-2 set of cryptographic hash functions designed by the US NSA (National Security Agency). The algorithm was first published in 2001 (Penard and van Werkhoven 2008). Irrespective of the size of the message, the hash values of SHA-256 will always be 256 bits and they are represented by 64 hexadecimal "digits" (each one taken from the set "0123456789abcdef" containing 16 such "digits").

The value set of SHA-256 contains $2^{256} = 16^{64} \approx 10^{77}$ different message digests, an unfathomably large number considering that, for example, it is estimated that there are between 10^{78} to 10^{82} atoms in the known, observable Universe. Examples of SHA-256 hash values can be found in **Table 1**. One can see that the hash value of the message "This is a message" is completely different than the one of "This is a message." with an added dot in the end, which shows the avalanche effect. Also, it is seen that the hash value remains always the same length (64 digits), even for longer messages.

Other than Bitcoin, the SHA algorithm is used in many applications, such as Digital Signature Verification, Secure Sockets Layer (SSL) Handshake, Integrity Checks, Password Hashing and others. For example, using password hashing, the password of a user need not to be stored in a website's database. Instead, the hash value of the password is stored. This is enough to validate a given password when a user tries to log in. On the other hand, if a hacker gets access to the database, all they will find is the hashes of the passwords and not the passwords themselves, which increases security.

4.1.3 Blockchain Definition, Characteristics and Structure

Distributed Ledger Technology (DLT) or simply blockchain is a technology able to simplify and secure transactions among

TABLE 1 | Examples of hash values generated by the SHA-256 hash algorithm.

Message	Hash Value
Empty string SHA256("")	e3b0c44298fc1c149afbf4c8996fb92427ae41e4649b934ca495991b7852b855
This is a message	a826c7e389ec9f379cafdc544d7e9a4395ff7bfb58917bbebee51b3d0b1c996a
This is a message.	a39648909123660008dee9864a4dfddf88446f354b989e340f826e21b2e83bd9c
This is a longer message. But the hash length remains always the same!	4a7af8b298b8988523ab80bf572960aca294e0fd47ae860ee9c0f80f0b233645

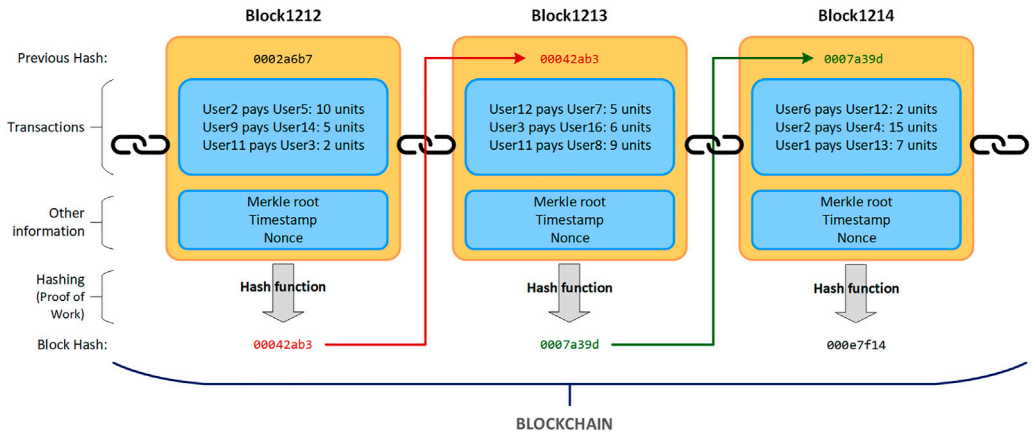

FIGURE 6 | An example of a simple blockchain.

parties and record keeping in general. It has to do with a growing number of blocks containing records. These records are usually transaction data and timestamps, but it can be virtually anything that can be recorded. The blocks are linked together using hash values created with a cryptographic hash function. The innovation lies in the connection of each new block of data with the previous one, using the cryptographic hash. In particular, the hash value of a given block is part of the information stored in the next block. Any small change in a block would lead to a new hash value for the block, which would automatically invalidate all subsequent blocks. In addition, the ledger is not stored in a central location, but it is distributed in thousands of copies among the nodes of the network, which are also asked to validate the blocks containing the transactions. Blockchain technology uses a decentralized architecture based on distributed computing, crypto-chain block structures to store data, node consensus algorithms to verify data and smart contracts to program data (Xu et al., 2021).

The structure of a blockchain is depicted in a simplistic way in **Figure 6**. Note that in this example, for illustration purposes, we use simple hash values with 8 digits instead of real SHA-256 hashes with 64 digits. After several transactions have taken place within a predefined time interval, a miner node will pack the transaction data into a new block, together with some additional information, with a timestamp and a signature. As shown, each block contains the hash value of the previous block, making a chain of blocks. The miner node will send the package to all the other nodes of the network. After the block is validated by the other nodes, it is added to the main chain and all the nodes of the network are synchronized with the latest main chain. Each block has its unique hash value, which is not included in the block itself (it can be easily calculated anytime), but it is added to the next block in the chain.

In Bitcoin and similar systems relying on blockchain to transfer value, the steps needed for a transaction to get into the blockchain are the following:

- A peer-to-peer transaction is requested by a user.
- Each user has a private key and a public key. A transaction is signed with the private key of the user, for authentication purposes.
- The transaction is sent first to the closest node of the network, and it is verified and propagated to other nodes.
- The transaction waits until a miner picks it up to include it in the next block to be mined
- The transaction, together with a number of other transactions are packed together in a block by a miner. Other miners may try to create other blocks using probably different combinations of transactions.
- The first miner achieving to solve the "Proof of Work" cryptographic puzzle adds the block to the main chain and receives a reward in cryptocurrency
- The update in the blockchain is distributed across the network
- Other nodes verify the result and propagate the block
- The transaction is complete.

TABLE 2 | Details of Block 712,650 of the Bitcoin blockchain.

Property	Value
Hash	**0000000000000000000**1a4110f39e05a871b04fdc43ccdb5d1fbe45e14a97249
Timestamp	2021-12-05 07:45
Height	712,650
Number of Transactions	129
Difficulty	22,335,659,268,936.39
Merkle root	9ef36627c62611d1cfa6fd2ce4e29b4c8c709fbe45325de542dd65666f4a00a0
Size	1,861,938 bytes
Nonce	3,134,706,325
Transaction Volume	739.76,687,155 BTC
Block Reward	6.25 BTC
Fee Reward	0.20322136 BTC

If a bad actor goes back in time and tries to change a transaction record in a given old block, this will cause a change in the hash of the block and the block will be no longer connected to the next block in the chain. Such an attempt will be easily spotted and be denied by the decent nodes of the blockchain network.

4.1.4 Proof of Work

As mentioned, calculating the hash function of a block would be a computationally easy operation as SHA-256 hashes are easy to calculate on any modern computer. In other words, generating any hash for a given set of transactions is trivial. The bitcoin protocol and other similar blockchain networks make this harder by introducing a level of difficulty in the hashing operation. In particular, a miner has to add some special info into the header of the block, an integer number known as a nonce ("number used once"), to achieve a hash that has a value which is lower than a predefined threshold value, or in other words it has a number of leading zeros. Since hash values cannot be predicted and the outcome is completely "random" (although deterministic), a miner node has to try many times with different nonces until it finds the right nonce that will give the hash with the desired properties.

In Bitcoin, this mechanism aims to add a new block to the blockchain every 10 min, on average. To do so, it adjusts the difficulty of the cryptographic puzzle depending on how quickly miner nodes are adding blocks. If miners have high computational power and add blocks too quickly, the difficulty increases, and hash computations become harder. In contrast, if blocks are added too slowly, hash computations become easier. This concept, called "Proof of work" (PoW) is a consensus mechanism requiring members in a decentralized network to do some computational work in order to prevent bad actors from gaming the system.

In the simple example of **Figure 6**, we see that the hash values of the blocks, all have 3 leading zeros, which means that some "work" was needed for finding the proper nonce that would provide the hash for each block. As a practical example and a case study, **Table 2** shows some properties of Block 712,650 of the Bitcoin blockchain, mined on 05 December 2021 at 7:45 AM (GMT+3). We see that the block has a hash value with 19 leading zeros. To achieve this number of leading zeros, one would need to try on average approximately $16^{19} \approx 7.55579 \cdot 10^{22}$ hashes with different nonces. A more accurate estimation for the needed number of tries is in fact given by formula $D \cdot 2^{32}$, where D is the difficulty of the block, shown in **Table 2** for Block 712,650. In our case, this formula will result to $22335659268936.39 * 2^{32} = 9.59309 \cdot 10^{22}$ hashes. Since a block is created every 10 min (600 s) on average. In **Table 2**, we see that the hash value of the block has 19 leading zeros (in bold), as a result of mining and the relevant difficulty. The computational power of the bitcoin network for the time period related to the generation of block 712,650 can be calculated as $9.59309 \cdot 10^{22}$ hashes/600 s $\approx$ 160 million TH/s (tera hash per second) = 160 EH/s (exa hash per second). This shows how computationally demanding Bitcoin mining has become lately. It also has a huge effect on the carbon footprint of Bitcoin.

Miners race and compete to solve the cryptographic puzzle first, i.e. to find the nonce that produces a target hash that is below the threshold set by the block difficulty. The winning miner receives two kinds of reward: 1) in the form of newly mined crypto coins (currently 6.25 BTC per block), and 2) transaction fees. In the example of Block 712,650, the miner will receive 6.25 + 0.20322136 = 6.45322136 BTC as the total reward.

The first reward is set by the bitcoin protocol. The rate at which new Bitcoins are generated (mined) is reduced over time, as rewards are halved every approximately 4 years. Today, there have been three halving events. When bitcoin started in 2008, the reward was 50 BTC which was halved to 25 BTC in 2012, 12.5 BTC in 2016 and lately 6.25 BTC in 2020. Bitcoin last halved on 11 May 2020, around 3 p.m. EST, resulting in a block reward of 12.5/2 = 6.25 BTC. Halving occurs after every 210,000 blocks are mined. Given that a block is produced every 10 min on average, 210,000 blocks require 2,100,000 min which is 1,458.33 days or 3.99 years (considering each year equal to 365.25 days). The maximum supply of BTC coins will be 21 million coins, after all bitcoins have been "mined".

Eventually, after all bitcoins have been generated, miners will keep receiving only the second reward, in the form of transaction fees. Transaction fees are therefore used to 1) avoid spam transactions in the bitcoin network, and 2) give incentive to the miners to keep mining even after the generation of new bitcoin has come to end. Transaction fees also reflect the speed with which one would like their

transaction to be validated in the system. Transactions with higher fees are more likely to be processed first, as miners have the incentive to include them in their blocks, in order to get a higher cumulative mining reward.

PoW is an efficient mechanism which protects the network against malicious and fraudulent actors. In a hypothetic scenario concerning Block 712,650, we suppose that after 30 min another 3 blocks have been added to the chain (i.e. blocks 712,651, 712,652, 712,653) and at that time everybody is working on making the next block, i.e. block 712,654. Bill, a bad actor, instead of building the next block wants to alter a transaction in block 712,650 to his favor. If Bill does that, then the hash of the block will be changed and the link of the blockchain will be broken. The community will simply reject the copy of the blockchain presented to them, unless Bill manages to properly "redo" the next blocks, i.e. 712651, 712,652, 712,653 before the other nodes manage to generate block 712,654. This is the only way that Bill can cheat the network and alter an existing transaction in the blockchain. To do so, Bill must be fast enough, which means he needs to have at least 51% of the computational power of the whole network, which is very difficult to achieve. If 51% or more of the computational power remains in good hands, then this assures that the network will work in a decent way, rejecting such fraudulent attempts.

4.1.5 Proof of Stake: An Alternative to PoW

Validators in a blockchain network have to carry out the task of appending a block of transactions to the blockchain. In most cases, they will receive a reward for doing so. For security purposes, the blockchain protocol must have a mechanism to prevent a bad actor from taking over the majority of validation. PoW systems use validation based on computational power to verify transactions, which incentivizes consuming huge quantities of energy. Although PoW offers some advantages, such as a decentralized way of verifying transactions, high security level, and allowing miners to earn rewards, it also has disadvantages and limitations. Its main drawbacks are high energy usage, slow transaction speeds, and scalability problems. PoW has mathematical limitations on scalability, as the block size and the block creation frequency need to be within certain bounds, to maintain security. For Bitcoin, these bounds set a limit of a few transactions per second (TPS), far below requirements for worldwide adaption and practical applications at a global scale. At this time, Bitcoin executes around 5 TPS, compared, for example, to VISA's 24,000 TPS. To make things even worse, the energy needed for a single Bitcoin transaction is equivalent to the one needed for several hundreds of thousands of VISA transactions.

Another promising approach is Proof of Stake (PoS), which extends the voting power to the stakeholders of the system. In PoS, participants owning crypto coins can stake them, which will give them the right to check new blocks, validate them and add them to the blockchain. The first functioning implementation of a PoS cryptocurrency was Peercoin, introduced in 2012. PoS is tremendously more energy-efficient than PoW (Bach et al., 2018). did a comparative analysis of typical consensus mechanisms and some of their contemporaries that are in use in modern blockchains. The analysis focused on the algorithms, scalability issues, reward mechanisms and security risks.

In PoS, when a block is ready, the system chooses a node to act as its reviewer and validator. The validator will check if the transactions are accurate. In this case, they will add the block to the blockchain and they will receive a reward. The probability of being selected to act as a validator is proportional to the number of staked coins one has. The more coins one has staked, the more probable it is to be selected as validator. In case a validator validates a block which has inaccurate information in it, there will be a penalty and the validator will lose part of their staked coins. In such a system, the mining power is proportional to the number of staked coins one has. Unlike PoW, which uses a difficult computational puzzle, requiring tremendous amounts of computing power and electricity with a huge carbon footprint, PoS is simpler, faster and more eco-friendly.

Consensus mechanisms, such as PoW and PoS, usually deal with the trilemma of decentralization, scalability and security. Both PoW and pure PoS have a decentralized nature where all participants have the right to participate in validation. An alternative approach is the so-called "Delegated PoS", which is a more centralized system where only a limited number of people with known identities have the power to validate transactions and generate blocks.

4.1.6 Merkle Tree

A Merkle tree is an inverse tree structure where every leaf node has a label which is the cryptographic hash of a transaction (or any other data) and every non-leaf node has a label which is the hash of the labels of its child nodes. A simple Merkle tree is depicted in **Figure 7**.

This structure allows for an efficient and secure validation of records of large data structures. The validation that a leaf node is part of the tree requires the computation of a number of hashes which is proportional to the logarithm of the number of the leaf nodes in the tree. Merkle trees are used in Bitcoin and other crypto networks. An average Bitcoin block contains over 1,000 transactions, so the Merkle tree is in fact much larger than the one presented in **Figure 7**. A full ("thick") node of the network has full, complete blocks. On the other hand, a "thin" node has only headers but still needs to be able to verify transactions. In thin nodes, the Merkle tree is used to verify a specific transaction without the need to download the whole blockchain. For example, in **Figure 7**, to verify that Transaction B is included in the Block, we have to query the network about HA and HCD, only. Given HB and HA, we calculate HAB. Then, given HAB and HCD, we calculate HABCD and we compare it with the Merkle root of the tree, which is part of the header. The transaction is proved to be valid, unaltered and part of the block if the final hash is equal to the Merkle root of the tree, on top of it. In a Merkle tree with 1,000 transactions, one would need to have only about 10 hash outputs to validate a given transaction.

4.2 General Purpose Technologies

General Purpose Technologies (GPTs) can affect an entire economy. They can impact economic growth and transform both our everyday lives and the ways we do business. Such

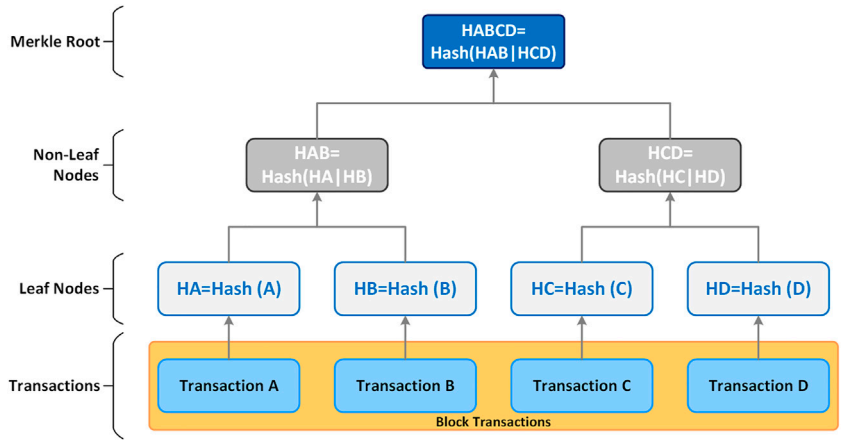

FIGURE 7 | A simple Merkle tree.

technologies have the inherent potential for technical improvements, and innovational complementarities, giving rise to increasing returns-to-scale (Bresnahan and Trajtenberg 1995). Thus, they can drastically alter societies and foster generalized productivity gains through their impact on pre-existing economic and social structures. Examples of GPTs include electricity, the electric motor, the steam engine, the computer and the internet. These technologies fundamentally impacted how we live, expanded our lives (physically and emotionally), helped build our cities and changed how people interact with the world.

4.3 Blockchain as GPT

Given its unique characteristics, such as immutability, transparency, and distribution (Sandner and Schulden 2019), blockchain is recognized by many as a new form of GPT. Naturally, it takes time for a GPT to diffuse through the economy. Although blockchain is still at the infrastructure building stage, it is expected to unleash several applications across different verticals within the next 5–15 years. Like the internet in its first years, blockchain is difficult to predict or even understand well, but in the future, it could become ubiquitous in the exchange of physical and digital goods, record keeping, information, and online platforms. According to an article by Harvard Business Review, "Blockchain is the first native digital medium for value, just as the internet was the first native digital medium for information."

4.4 The Properties of Distributed Ledger Technology

A distributed ledger has some specific properties. In particular, it is:

- Programmable. For example, it can be programmed to run specific smart contracts
- Secure. All the records are encrypted
- Immutable. The validated records cannot be deleted or changed as they are irreversible.
- Anonymous. The identity of participants can be either fully anonymous or pseudonymous.
- Unanimous. The participants agree to the validity of the records.
- Distributed. Copies of the ledger are distributed to all participants, for complete transparency.
- Time-stamped. Every block and every transaction have a timestamp.

4.5 Decentralized and Centralized Ledgers

In a fully decentralized blockchain, e.g. Bitcoin, anyone can participate and transact on the ledger. There are no "privileged" users, and a distributed consensus protocol is used. As a result of this system design, there should be mechanisms in place to combat the vulnerabilities arising from it. These mechanisms prevent people from corrupting the system and ensure that transactions are correct. Bitcoin uses Proof-of-Work (PoW) and "mining" for this.

In a centralized blockchain, not anyone can transact on the ledger. There are a few trusted centralized authorities that have the right to validate transactions and modify the ledger. In this case the blockchain can still be distributed, meaning that many parties can again hold copies of the ledger. Yet, the validity of the system comes from the fact that only some credible and reputable participants can modify the ledger. And because participants' identities are known, their transactions can therefore be audited.

Centralization can undermine the technology's purpose as a shared ledger. Too much power can be placed in the control of a single entity or a few special "players". The past has shown that when a single entity takes too much power then it may no longer operate for the benefit of the society. Fully decentralized distributed systems can mitigate risk and prevent attacks while centralized systems are more prone to them. A centralized ledger would essentially act like a third-party and thus the concept of peer-to-peer, fully distributed network without intermediaries would no longer be valid.

TABLE 3 | Key areas of the civil, architectural and construction industry where blockchain can be applied.

Application Area	References
1. Building information modelling and Computer Aided Design	Pradeep et al., (2020) Nawari and Ravindran (2019c) Das et al. (2021) Lemeš and Lemeš (2020) Dounas et al. (2021) Lee et al. (2021) Zheng et al. (2019) Nawari and Ravindran (2019a) Androulaki et al. (2018)
2. Contract management and smart contracts	Vigliotti. (2021) McNamara and Sepasgozar. (2021) Hamledari and Fischer (2021b) Ahmadisheykhsarmast and Sonmez (2020) Nanayakkara et al. (2021) Xu et al. (2021)
3. Construction project management	Perera et al., (2020) Udokwu et al., (2021) Hargaden et al., (2019) Hewavitharana et al. (2019) Turk and Klinc. (2017) Li et al. (2021)
4. Smart buildings and smart cities	Berglund et al. (2020) Lam et al., (2018) Valtanen. (2021) Liu et al., (2021) Tiwari and Batra. (2021) Bindra et al. (2021)
5. Construction supply chain management	Qian and Papadonikolaki. (2021) Tezel et al., (2020) Tezel et al. (2021) Hamledari and Fischer. (2021a) Yoon and Pishdad-Bozorgi (2022)
6. Real estate	Mehendale et al. (2019) Perera et al. (2021) Mishra et al. (2021) Wouda and Opdenakker (2019) Nasarre-Aznar (2018)

5 BLOCKCHAIN IN THE CIVIL, ARCHITECTURAL AND CONSTRUCTION INDUSTRY

In this section we identify several key areas of the civil, architectural and construction industry where blockchain can be applied, and we investigate the current state of the art, the benefits that blockchain technology can offer and the challenges and opportunities ahead. The summarized results are presented in **Table 3**, while the following sub-sections provide further details and a relevant discussion for each application area.

5.1 Building Information Modelling and Computer Aided Design

Blockchain can be used to provide live and trustworthy information for BIM, by information sharing among present and future information owners. Furthermore, it can help enhance the benefits of BIM by allowing architects and engineers to design on the same BIM model with clear ownership, while design and construction decisions can be recorded on the blockchain for future analysis and liability.

Information exchange in BIM is critical yet complex due to the multi-party collaboration nature of a construction project. Bimchain, funded in 2017, is a blockchain technology software aiming at accelerating the BIM revolution in the Building Industry by integrating the BIM software and processes to create a binding traceability of data exchanges. As paper-based solutions are often insufficient, (Pradeep et al., 2020), investigated the use of blockchain technology and in particular the commercial software Bimchain for improving Trust in BIM Data Exchange. Their work showed that Bimchain manages to accomplish most of its objectives, such as improving data reliability, limiting the scope of liability, and clarifying stakeholder responsibilities, among others. However, the legal validity of the tool's proofs is still untested and therefore it is still not able to establish a global acceptance for real-world applications.

(Nawari and Ravindran 2019c) proposed the use of blockchain in a BIM workflow environment. They presented an overview of the blockchain and discussed its integration with the Building information process, focusing on how blockchain can help in improving the BIM working environment by providing reliable data storage and management of permissions, reinforcing network security, and ensuring data ownership and change tracing (Das et al., 2021). presented a comprehensive study on the requirements of BIM security, claiming that although the technologies to support BIM security are available in research and on the market, they are not customized in existing collaborative BIM platforms to support security. They proposed a conceptual encryption strategy for securing BIM data distribution and a distributed blockchain-based framework for BIM change recording.

(Lemeš and Lemeš 2020) presented a work on using blockchain technology in Distributed and collaborative CAD (Computer Aided Design) environments, such as BIM and Geographical Information Systems (GIS). They argue that blockchain can provide answers to key issues such as data integrity and confidence in information stored in information systems (Dounas et al., 2021). introduced a framework for decentralized architectural design BIM and blockchain integration in the context of the 4^{th} industrial revolution. The authors examined the constraints of BIM regarding collaboration and trust. Then they introduced a blockchain solution for creating new operational and business models for architectural design, through scaling collaboration, project governance, and shifting trust to the infrastructure. They focused on the design process and validated the framework with a prototype of BIM design optimization integrated with blockchain.

(Lee et al., 2021) proposed an integrated digital twin and blockchain solution to support accountable information sharing in construction projects. In this implementation, the digital twin updates the BIM in nearly real-time using sensors and internet of things, while the blockchain has the role of authentication and adding confidence to the transaction data. The framework was tested with a case study where virtual positioning data from a prefabricated brick was transmitted to a digital twin in real-time and recorded on the blockchain using time stamps (Zheng et al., 2019). presented a novel BIM system called bcBIM to facilitate BIM data audit for historical modifications by blockchain in mobile cloud with big data sharing. The authors proposed a method of BIM data organization based on private or public blockchains. Using blockchain, the system can trace, authenticate and prevent tampering of historical data related to BIM (Nawari N. and Ravindran S. 2019). proposed a new framework with the integration of BIM and blockchain to improve the efficiency of building permit processes in post-disaster events, with the application of smart contracts and Hyperledger Fabric (HLF) (Androulaki et al., 2018).

5.2 Contract Management and Smart Contracts

A *Smart Contract* is a computer program that works based on an "if/then" principle. Smart contracts can identify accountabilities and trigger payments based on milestones (Vigliotti 2021). They are executed automatically reducing the necessity of intermediaries and as a result time and money can be saved. They can be used to automate agreements, thus revolutionizing construction contracts and payments which usually rely on traditional methods.

(McNamara and Sepasgozar 2021) discussed and investigated the use of blockchain and intelligent contracts (iContracts) for the digitalization of the construction industry. The authors identified 9 influencing factors based on 46 studies and presented a conceptual three-dimensional model for iContract system adoption. The study aims to identify key considerations for such contracts, develop a theoretical adoption model and offer an agenda of 6 research directions for the future (Hamledari and Fischer 2021b). investigated the role of smart contracts in the automation of construction progress payments. Current computerized payment applications cannot support reliable automation of progress payments due to the fact that they rely on centralized control mechanisms and no guaranteed execution. The authors argue that decentralized smart contracts based on blockchain can address these limitations in an effective way. They explore the conceptual underpinning for the design of an automated payment system and investigate the role of smart contracts in enabling reliable and autonomous conditioning of cash flow on product flow status. They also use a test case for payments based on progress and smart contracts in the context of unmanned aerial vehicle-based progress monitoring.

(Ahmadisheykhsarmast and Sonmez 2020) proposed the use of smart contracts for securing the payments in construction contracts. This can guarantee payments while eliminating administrative costs and burdens related to trusted intermediaries, by employing an automated protocol running on a decentralized blockchain. On the other hand (Nanayakkara et al., 2021), investigated the suitability of blockchain and smart contracts for dealing with payment issues in the construction industry. They concluded that solutions based on blockchain and smart contracts can mitigate the payment and the related financial issues in the construction industry, including non-payments, partial payments, long payment cycle, cost of finance, retention, security of payments, among others.

In the structural engineering field, very powerful capabilities are available today for the simulation and analysis of structures, given the development of computational methods, numerical analysis software and hardware during the last decades (Plevris and Tsiatas 2018). In this area (Xu et al., 2021), presented a work on the application of a blockchain network and smart contracts in structural health monitoring (SHM). Their results showed that such a system can provide several advantages, such as monitoring authority verification, generation of abnormal alerts, data immutability, resistance to attacks, and traceability query.

5.3 Construction Project Management

Construction project management (CPM) can potentially benefit from an agile and more decentralized approach based on blockchain, with high transparency, and the parties being compensated for outcomes and for work performed. Given

that the construction industry has been historically reported as one of the slowest sectors in the adaptation of information technology, the question of whether blockchain as a technology is hype or real in the construction industry was addressed by (Perera et al., 2020). Their work aimed at analyzing the potential of blockchain applications in construction through case analyses and a comprehensive literature review. According to the study, blockchain has indeed a credible potential in the construction industry, due to its exponential general use, the investments involved, and a number of start-up businesses contributing to Industry 4.0.

In the work of (Udokwu et al., 2021), a blockchain-based CPM platform implementing smart contract technologies was presented for facilitating the peer-to-peer collaboration between parties in the construction industry, leading to improved information flow, cost and time reduction, and improvement in the quality of the services. The system relies on diligent up-front requirement studies with a coherent system architecture and the use of cooperation protocols (Hargaden et al., 2019). examined the role of blockchain technologies in CPM, providing insights into the performance of blockchain in construction and investigating the feasibility of its potential adoption with case studies. The authors claim that blockchain can increase the efficiency of processes within the construction industry and eliminate current issues related to trust, verification and transparency (Hewavitharana et al., 2019). examined how blockchain can address the project management perspectives in the construction industry regarding the guidelines mentioned in the Project Management Body of Knowledge (PMBOK). Five criteria were selected for the analysis using the relevant guidelines, namely 1) contract management, 2) purchase management, 3) finance management, 4) asset and inventory management, and 5) subcontractor management. It was identified that blockchain can indeed assist in all these areas.

(Turk and Klinc 2017) presented an investigation on the potential of blockchain for construction management. The authors highlighted that blockchain can improve the trustworthiness and reliability of logbooks in construction, while it can also help secure storing of sensitive data. They concluded that blockchain can offer solutions to various problems in construction information management while decentralizing the construction processes (Li et al., 2021). proposed the use of a 2-layer adaptive supervision model based on blockchain for off-site modular housing production, where the 1st layer includes the adaptive private sidechains of participants and the 2nd is the main blockchain for trading and communication among all participants. The blockchain-based methodology has the benefit of avoiding tampering of the operation records, while driving the participants to promptly publish their operation records, without any privacy risks.

5.4 Smart Buildings and Smart Cities

As urbanization is increasing rapidly, offering improved livability and a higher standard of living, the concept of "smart cities" are one of the main focus areas of many governments across the globe. Many countries attempt to establish special strategies for transforming their cities into smart cities, utilizing the potential opportunities and limiting any relevant threats arising from urbanization. Smart cities enable operational efficiency, maximize environmental sustainability efforts and create new citizen services. Blockchain innovation can be utilized to make smarter cities. Blockchain-based solutions can be utilized to enhance our cities and provide for better economic development and livability, by offering enhanced security, immutability, resilience and transparency.

(Berglund et al., 2020) investigated the role of civil engineering in smart cities and smart infrastructures. They examined a number of smart technologies that can be used for infrastructure management, such as crowdsourcing and citizen science, sensors, data transmission, actuators, big data analytics, data visualization, Internet of Things, and blockchain. They identified the gaps in the application of such technologies for infrastructure systems and they highlighted how civil engineering can adopt new roles toward the development of applications related to smart cities (Lam et al., 2018). investigated the use of a blockchain system in smart cities, claiming that malpractices related to civil engineering can be avoided if there are transparent, timely, and unalterable records of the relevant activities, based on a blockchain (Valtanen 2021). identified several design challenges regarding the development of blockchain-enabled capabilities of a smart home. They analyzed and classified these challenges and did an organized literature review to identify the best practices and find possible solutions (Liu et al., 2021). explored the impact of integrating BIM and blockchain into a smart city environment, on making more sustainable buildings. They investigated the relationships between BIM, blockchain, and sustainable building throughout the life cycle of a construction project.

(Tiwari and Batra 2021) examined the application of blockchain-based solutions for the reparations in smart buildings, proposing a prototype simulating the system architecture and discussing how blockchain can further expedite security, automation, and transparency in smart buildings. The work focused on the use of smart contracts in smart buildings, for repairs and service. On the other hand (Bindra et al., 2021), investigated the use of blockchain technology and smart contracts for the flexible, decentralized access control of smart buildings. According to the study, visitor and occupant access to equipment and spaces within the buildings continue to be managed in a conservative, old-fashioned, and inflexible way, through inefficient, unsystematic, and human-intensive processes. Their work describes a methodology relying on blockchain and smart contracts that can securely and flexibly manage building access privileges for both short-term visitors and long-term occupants, taking into consideration the risk associated with accessing a space in the building, in an efficient, decentralized way.

5.5 Construction Supply Chain Management

The construction industry is characterized by fragmentation in processes, operations and services. One of its major problems is the disconnect between construction and design, due to the lack of trustworthy and open information across the supply chain. Blockchain has the potential to adverse these issues using open and transparent transactions. It can be used to trace physical

objects from the origin to the destination. It can also improve payment settlements, compliance management and material planning, while smart contracts can be implemented to automatically purchase, track, and verify items in the supply chain, in real-time.

According to the study of (Qian and Papadonikolaki 2021), supply chain management (SCM) has long been committed to the reduction of cost and increase of efficiency, while trying to reduce fragmentation and optimize resources. Since trust has always been a significant factor in managing SCM relationships, the study aimed at examining how trust can be affected by introducing blockchain technology in the construction SCM. Based on semi-structured interviews and information from experts, the study suggests that blockchain can help enhance trust in SCM and provide supply chain partners with proper protection mechanisms to avoid the risks and costs associated with opportunistic behaviour in collaboration. This can shift trust from relational to system-based and cognition-based. However, the authors highlight that the extent to which blockchain can develop and spread will ultimately depend on the readiness of the social capital to accept decentralised governance schemes.

(Tezel et al., 2020) examined the potential and future directions of blockchain applied to construction supply chains. For this, the authors collected empirical data through semi-structured interviews with seventeen experts in the field. They used SWOT analysis to present the strengths, weaknesses, opportunities and threats involved and they also exhibited the requirements for and steps toward a construction supply structure facilitated by blockchain technology. The same group (Tezel et al., 2021) later investigated the implementation of blockchain in construction, presenting discussions on SCM applications of blockchain for construction by collecting feedback for 3 models based on blockchain: reverse auction-based tendering for bidding, project bank accounts for payment purposes, and asset tokenization for the financing of projects. A set of general and model-specific challenges and opportunities were identified for the implementation of blockchain in construction.

(Hamledari and Fischer 2021a) presented the implementation of crypto assets based on blockchain for the integration of the physical and financial supply chains in the construction industry. The paper demonstrated how blockchain-based crypto assets used for payments made conditionally on the flow of products can address the limitations of physical and financial supply chains due to high fragmentation and relying on financial institutions. The study also highlights the problem of price volatility and examines potential solutions (Yoon and Pishdad-Bozorgi 2022). aimed to explore the applications of blockchain in addressing issues related to CSC. They identified the main problems in CSC as related to collaboration, information sharing and sustainability. Although these issues have been dealt with individually in the past, they are essentially coupled and interconnected. Blockchain technology can provide a holistic system view approach to address all of them together, i.e., enhance sustainability, promote collaboration, and facilitate information sharing, all at once.

5.6 Real Estate: Property Ownership, Land Titles, Asset Management and Maintenance

Real estate is known as one of the most important sectors of the economy, playing a crucial role in the lives of people across the world. The size of the global real estate assets managed professionally was estimated at $8.5 trillion in 2017. Real estate investments provide better returns than the stock market without as much volatility, providing also tax benefits in many cases. Although real estate is so important and despite the technological advancements that have affected other sectors, it has not changed much during the last decades. It is still a "pen and pencil" business, relying on archaic methods for keeping records and doing transactions. The industry suffers from various problems, such as limited participation due to barriers to enter, slow and costly verification procedures involving a lot of intermediaries and very limited foreign investments, to name only a few.

Figure 8 presents the real estate ecosystem today and depicts the number of different parties involved and the relevant interactions. This traditional model has several drawbacks and limitations:

- There are a lot of intermediaries, that increase the cost and reduce the transactions' speed.
- The current approach requires significant time and effort for due diligence and financial verification.
- Foreign investments are difficult, expensive, and slow. International bank accounts, accreditation, financing, credit score, cash requirements, access to sponsors, fund managers, even citizenship, might be needed for investing in real estate in a foreign country. As a result, the real estate business remains very "local", in geographical terms.
- Real estate transactions are done via wire transfers and require costly and slow verification processes with increased likelihood or error.
- Real estate investment can be very expensive and as a result there is limited participation. Although everybody is interested in housing, real estate is the investment choice of the rich and not open to all. People with small amounts of money are not allowed to invest in expensive real estate assets as the current system does not support fractional ownership. One needs to either buy a whole building/ apartment or nothing.
- Low liquidity. Real estate assets are traditionally difficult to trade or convert to cash because of their high value and the cost of the intermediaries, each time a transaction is made.

Real estate is entering the blockchain era and it can benefit from the numerous advantages that the technology can offer. Traditionally, real estate transaction records are housed in central servers controlled by a single administration point. With Blockchain, all real estate ownership and transaction records can be stored securely as tamper-proof digital records on the blockchain, in a decentralized way. Such records are fully accurate, safe, and immutable. Blockchain immutability proves ownership and facilitates transactions. In addition, with the use of blockchain, verification becomes an easy task which does not

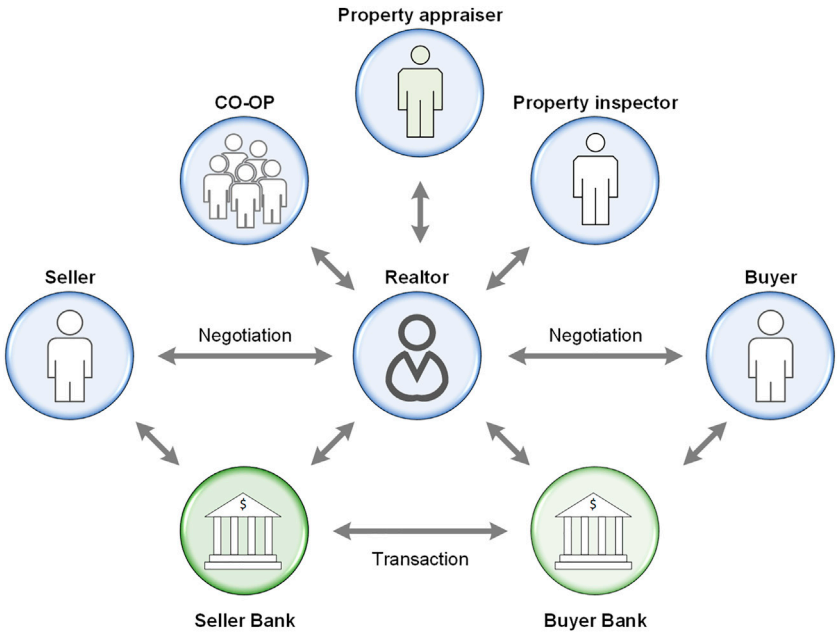

FIGURE 8 | The Real Estate ecosystem today.

require lengthy procedures, high cost and intermediaries (Mehendale et al., 2019). discussed how blockchain can revolutionize the real estate industry, by reducing the paperwork and the time needed for property assessment, document collection, the preparation of contracts, and others (Perera et al., 2021). highlighted the potential of blockchain in real estate, with respect to property transactions, where businesses depend on the reliability of transaction records and blockchain can be user to enhance trust and ensure ownership. Their paper demonstrates a methodology for developing a blockchain system starting from problem analysis, selection of blockchain platform, system modelling, prototype development, and evaluation. Their findings provide the foundation for developing proofs of concept for other potential applications of blockchain in the built environment.

Information and data related to the building or structure need to be tracked at every stage of its life cycle. Blockchain can provide a living ledger that records everything happening with the asset. Blockchain can allow tracking and access to all the necessary information and data through the life cycle of the asset. In case of any refurbishments or other improvements to a building, these changes can be documented and recorded, and the whole repository can be transferred to new owners when the property is sold. In the future, each property will come with a universally shared data set, which will include background information such as past sales, repairs and amenities. This digital history of transactions will help every stakeholder prove their ownership, increase transparency and eliminate fraud attempts. This alone will have tremendous consequences in countries where one cannot rely on public authorities because of corruption. The transactions can be made easy, safe, and inexpensive due to the use of blockchain technology which offers quick and costless verification (Mishra et al., 2021). discussed the digitalization of land records using blockchain technology. According to the authors, the immutable, auditable and traceable features of blockchain entice governments around the world to implement decentralized technology within the process of land registration.

In addition, real estate assets can be fully tokenized in the blockchain system, allowing participation to people having limited amounts of savings. Real estate tokenization is the process of creating a digital asset that represents a property on the blockchain. The tokenization process addresses various challenges in capital formation and liquidity, although it requires a legal wrapper around the property, to securitize and create an investment vehicle. The use of intermediaries can be minimized, while the system can facilitate foreign real estate investments and liquidity as anyone will be able to buy or sell even tiny shares of real estate assets (Wouda and Opdenakker 2019). investigate the application of a blockchain solution for improving the transaction process of an office building in the Netherlands. The authors highlight the problems of the current system, such as lack of market transparency, slow speed and inefficiency (Nasarre-Aznar 2018). investigate the relationship between collaborative housing and blockchain. The authors conclude that the technology has the potential to facilitate access to housing through the reduction of cost and time and minimizing the role of intermediaries.

6 CONCLUSION AND DISCUSSION

We are moving to a digital economy where financial and physical assets will increasingly have digital representations. According to

the World Economic Forum, by 2025, blockchains will store around 10% of the world's GPD. Countries are trying to make the necessary legislative and regulatory changes to adapt to the new environment and make this change a reality. New opportunities arise. Looking towards the future, it appears that blockchain is something that we will be hearing a lot more of. Although nobody can predict the degree to which it will affect the economy, our lives and every single sector particularly in the long run, most experts agree that it has the potential to play a significant role in the future, in a wide range of fields across different verticals. This is evidenced by the fast-growing occurrence of blockchain-related articles in the scientific literature during the very recent years, in several scientific areas, including engineering.

The present study briefly examined the technical details, main concepts and aspects of blockchain technology and aimed at formulating a picture of the current state and practice of its use in fields related to civil, architectural and construction engineering. The study also summarized and highlighted specific application areas related to the Architecture, Engineering, and Construction (AEC) industry where blockchain has the potential to provide new solutions, and how they can be adopted to improve performance, sustainability, and safety in the future. We identified six important application areas and examined the relevant challenges and opportunities ahead, namely in: 1) Building information modelling (BIM) and Computer Aided Design (CAD); 2) Contract management and smart contracts; 3) Construction project management; 4) Smart buildings and smart cities; 5) Construction supply chain management; and 6) Property ownership, land titles, asset management and maintenance in real estate. The conclusion of the study is that although blockchain technology is new and there are certainly several early challenges to tackle, it has great potential to become an extremely positive force of change in the construction industry. As engineers, it is our inherent responsibility to facilitate the digital transformation of the AEC industry and to make it ready for the challenges and opportunities of the future, and blockchain is bound to play a pivotal role in this transformation.

AUTHOR CONTRIBUTIONS

All authors listed have made a substantial, direct, and intellectual contribution to the work and approved it for publication.

REFERENCES

Ahmadisheykhsarmast, S., and Sonmez, R. (2020). A Smart Contract System for Security of Payment of Construction Contracts. *Automation in Construction* 120, 103401. doi:10.1016/j.autcon.2020.103401

Androulaki, E., Barger, A., Bortnikov, V., Muralidharan, S., Cachin, C., Christidis, K., et al. (2018). "Hyperledger Fabric: A Distributed Operating System for Permissioned Blockchains," in Proceedings of the 13th EuroSys Conference (Porto, Portugal: ACM). doi:10.1145/3190508.3190538

Bach, L. M., Mihaljevic, B., and Zagar, M. (20182). "Comparative Analysis of Blockchain Consensus Algorithms," in *41st International Convention on Information and Communication Technology, Electronics and Microelectronics (MIPRO)21-25 May 2018*, 1545–1550. doi:10.23919/MIPRO.2018.8400278

Berglund, E. Z., Monroe, J. G., Ahmed, I., Noghabaei, M., Do, J., Pesantez, J. E., et al. (2020). Smart Infrastructure: A Vision for the Role of the Civil Engineering Profession in Smart Cities. *J. Infrastruct. Syst.* 26 (2), 03120001. doi:10.1061/(asce)is.1943-555x.0000549

Bindra, L., Eng, K., Ardakanian, O., and Stroulia, E. (2021). Flexible, Decentralised Access Control for Smart Buildings with Smart Contracts. *Cyber-Physical Syst.*, 1–35. doi:10.1080/23335777.2021.1922502

Bresnahan, T. F., and Trajtenberg, M. (1995). General Purpose Technologies 'Engines of Growth'? *J. Econom.* 65 (1), 83–108. doi:10.1016/0304-4076(94)01598-T

Cheng, M., Liu, G., Xu, Y., and Chi, M. (2021). When Blockchain Meets the AEC Industry: Present Status, Benefits, Challenges, and Future Research Opportunities. *Buildings* 11 (8), 340. doi:10.3390/buildings11080340

Das, M., Tao, X., and Cheng, J. C. P. (2021). BIM Security: A Critical Review and Recommendations Using Encryption Strategy and Blockchain. *Automation in Construction* 126, 103682. doi:10.1016/j.autcon.2021.103682

Dounas, T., Lombardi, D., and Jabi, W. (2021). Framework for Decentralised Architectural Design BIM and Blockchain Integration. *Int. J. Architectural Comput.* 19 (2), 157–173. doi:10.1177/1478077120963376

Estébanez, C., Saez, Y., Recio, G., and Isasi, P. (2014). Performance of the Most Common Non-cryptographic Hash Functions. *Softw. Pract. Exper.* 44 (6), 681–698. doi:10.1002/spe.2179

Federal Deposit Insurance Corporation. (2020). "*How America Banks: Household Use of Banking and Financial Services, 2019 FDIC Survey*."

Hamledari, H., and Fischer, M. (2021b). Role of Blockchain-Enabled Smart Contracts in Automating Construction Progress Payments. *J. Leg. Aff. Dispute Resolut. Eng. Constr.* 13 (1), 04520038. doi:10.1061/(ASCE)LA.1943-4170.0000442

Hamledari, H., and Fischer, M. (2021a). The Application of Blockchain-Based Crypto Assets for Integrating the Physical and Financial Supply Chains in the Construction & Engineering Industry. *Automation in Construction* 127, 103711. doi:10.1016/j.autcon.2021.103711

Hargaden, V., Papakostas, N., Newell, A., Khavia, A., and Scanlon, A. (2019). "The Role of Blockchain Technologies in Construction Engineering Project Management," in IEEE International Conference on Engineering, Technology and Innovation (ICE/ITMC), Valbonne Sophia-Antipolis, France, June 17-19, 2019 (IEEE), 1–6. doi:10.1109/ICE.2019.8792582

Hewavitharana, T., Nanayakkara, S., Nanayakkara, S., and Perera, S. (2019). Blockchain as a Project Management Platform. *World Construction Symp.*, 137–146. doi:10.31705/WCS.2019.14

Kroll, J. H. (2012). "The Monetary Background of Early Coinage," in *The Oxford Handbook of Greek and Roman Coinage*. Editor W. E. Metcalf (Oxford University Press). doi:10.1093/oxfordhb/9780195305746.013.0003

Lam, R. C. Y., Junus, A., Mak, J. Y. W., Lam, L. C. H., and Lee, P. K. K. (2018). "Blockchain for Civil Engineering Practices in Smart Cities," in *2018 IEEE International Conference on Internet of Things (iThings) and IEEE Green Computing and Communications (GreenCom) and IEEE Cyber, Physical and Social Computing (CPSCom) and IEEE Smart Data (SmartData)*, 1294–1300. doi:10.1109/Cybermatics_2018.2018.00225

Lee, D., Lee, S. H., Masoud, N., Krishnan, M. S., and Li, V. C. (2021). Integrated Digital Twin and Blockchain Framework to Support Accountable Information Sharing in Construction Projects. *Automation in Construction* 127, 103688. doi:10.1016/j.autcon.2021.103688

Lemeš, S., and Lemeš, L. (2020). Blockchain in Distributed CAD Environments. *Lecture Notes Networks Syst.* 76, 25–32. doi:10.1007/978-3-030-18072-0_3

Li, J., Greenwood, D., and Kassem, M. (2019). Blockchain in the Built Environment and Construction Industry: A Systematic Review, Conceptual Models and Practical Use Cases. *Automation in Construction* 102, 288–307. doi:10.1016/j.autcon.2019.02.005

Li, X., Wu, L., Zhao, R., Lu, W., and Xue, F. (2021). Two-layer Adaptive Blockchain-Based Supervision Model for Off-Site Modular Housing Production. *Comput. Industry* 128, 103437. doi:10.1016/j.compind.2021.103437

Liu, Z., Chi, Z., Osmani, M., and Demian, P. (2021). Blockchain and Building Information Management (BIM) for Sustainable Building Development within the Context of Smart Cities. *Sustainability* 13 (4), 2090. doi:10.3390/su13042090

McNamara, A. J., and Sepasgozar, S. M. E. (2021). Intelligent Contract Adoption in the Construction Industry: Concept Development. *Automation in Construction* 122, 103452. doi:10.1016/j.autcon.2020.103452

Mehendale, D. K., Masurekar, R. S., and Patil, H. V. (2019). Implications of Block Chain in Real Estate Industry. *Int. J. Recent Techn. Eng.* 8 (1), 500–503. https://www.ijrte.org/wp-content/uploads/papers/v8i1/A5388058119.pdf.

Mishra, I., SupriyaSahoo, A., Sahoo, A., and Vivek Anand, M. (2021). "Digitalization of Land Records Using Blockchain Technology," in International Conference on Advance Computing and Innovative Technologies in Engineering, Greater Noida, India, March 4-5, 2021 (IEEE), 2021, 769–772. doi:10.1109/ICACITE51222.2021.9404678

Nakamoto, S. (2008). "*Bitcoin: A Peer-To-Peer Electronic Cash System*."

Nanayakkara, S., Perera, S., Senaratne, S., Weerasuriya, G. T., and Bandara, H. M. N. D. (2021). Blockchain and Smart Contracts: A Solution for Payment Issues in Construction Supply Chains. *Informatics* 8 (2), 36. doi:10.3390/informatics8020036

Nasarre-Aznar, S. (2018). Collaborative Housing and Blockchain. *Administration* 66 (2), 59–82. doi:10.2478/admin-2018-0018

Nawari, N. O., and Ravindran, S. (2019b). Blockchain and the Built Environment: Potentials and Limitations. *J. Building Eng.* 25, 100832. doi:10.1016/j.jobe.2019.100832

Nawari, N. O., and Ravindran, S. (2019c). Blockchain Technologies in BIM Workflow Environment. *Comput. Civil Eng.* 2019, 343–352. doi:10.1061/9780784482421.044

Nawari, N., and Ravindran, S. (2019a). Blockchain and Building Information Modeling (BIM): Review and Applications in Post-Disaster Recovery. *Buildings* 9 (6), 149. doi:10.3390/buildings9060149

Penard, W., and van Werkhoven, T. (2008). "On the Secure Hash Algorithm Family," in *Cryptography in Context*. Editor G. Tel (Utrecht, 1–18.

Perera, S., Hijazi, A. A., Weerasuriya, G. T., Nanayakkara, S., and Rodrigo, M. N. N. (2021). Blockchain-Based Trusted Property Transactions in the Built Environment: Development of an Incubation-Ready Prototype. *Buildings* 11 (11), 560. doi:10.3390/buildings11110560

Perera, S., Nanayakkara, S., Rodrigo, M. N. N., Senaratne, S., and Weinand, R. (2020). Blockchain Technology: Is it Hype or Real in the Construction Industry? *J. Ind. Inf. Integration* 17, 100125. doi:10.1016/j.jii.2020.100125

Plevris, V., and Tsiatas, G. C. (2018). Computational Structural Engineering: Past Achievements and Future Challenges. *Front. Built Environ.* 4 (21), 1–5. doi:10.3389/fbuil.2018.00021

Pradeep, A. S. E., Amor, R., and Yiu, T. W. (2020). "Blockchain Improving Trust in BIM Data Exchange: A Case Study on BIMCHAIN. *Construction Res. Congress* 2020, 1174–1183. doi:10.1061/9780784482865.124

Qian, X., and Papadonikolaki, E. (2020). Shifting Trust in Construction Supply Chains through Blockchain Technology. *Ecam* 28 (2), 584–602. doi:10.1108/ECAM-12-2019-0676

Sandner, P., and Schulden, P. M. (2019). Speciality Grand Challenges: Blockchain. *Front. Blockchain* 2 (1). doi:10.3389/fbloc.2019.00001

Shojaei, A. (2019). "Exploring Applications of Blockchain Technology in the Construction Industry," in ISEC 2019 - 10th International Structural Engineering and Construction Conference. doi:10.14455/isec.res.2019.786

Shojaei, A., Ketabi, R., Razkenari, M., Hakim, H., and Wang, J. (2021). Enabling a Circular Economy in the Built Environment Sector through Blockchain Technology. *J. Clean. Prod.* 294, 126352. doi:10.1016/j.jclepro.2021.126352

Tezel, A., Febrero, P., Papadonikolaki, E., and Yitmen, I. (2021). Insights into Blockchain Implementation in Construction: Models for Supply Chain Management. *J. Manag. Eng.* 37 (4), 04021038. doi:10.1061/(ASCE)ME.1943-5479.0000939

Tezel, A., Papadonikolaki, E., Yitmen, I., and Bolpagni, M. (2022). "Blockchain Opportunities and Issues in the Built Environment: Perspectives on Trust, Transparency and Cybersecurity," in *Industry 4.0 for the Built Environment: Methodologies, Technologies and Skills*. Editors M. Bolpagni, R. Gavina, and D. Ribeiro (Cham: Springer International Publishing), 569–588. doi:10.1007/978-3-030-82430-3_24

Tezel, A., Papadonikolaki, E., Yitmen, I., and Hilletofth, P. (2020). Preparing Construction Supply Chains for Blockchain Technology: An Investigation of its Potential and Future Directions. *Front. Eng. Manag.* 7 (4), 547–563. doi:10.1007/s42524-020-0110-8

Tiwari, A., and Batra, U. (2021). Blockchain Enabled Reparations in Smart Buildings Cyber Physical System. *Def. Sc. J.* 71 (4), 491–498. doi:10.14429/DSJ.71.16454

Turk, Ž., and Klinc, R. (2017). Potentials of Blockchain Technology for Construction Management. *Proced. Eng.* 196, 638–645. doi:10.1016/j.proeng.2017.08.052

Udokwu, C., Norta, A., and Wenna, C. (2021). "Designing a Collaborative Construction-Project Platform on Blockchain Technology for Transparency, Traceability, and Information Symmetry," in ASSE '21: 2021 2nd Asia Service Sciences and Software Engineering Conference, Macau, February 24 - 26, 2021 (ACM), 1–9. doi:10.1145/3456126.3456134

Valtanen, K. (2021). "Design Challenges of Developing a Blockchain-Enabled Smart home," in 2021 Conference on Information Communications Technology and Society, Durban, South Africa, March 10-11, 2021 (IEEE), 34–39. doi:10.1109/ICTAS50802.2021.9395016

van Eck, N. J., and Waltman, L. (2007). *VOS: A New Method for Visualizing Similarities between Objects*. Berlin, Heidelberg, 299–306. doi:10.1007/978-3-540-70981-7_34

Vigliotti, M. G. (2021). What Do We Mean by Smart Contracts? Open Challenges in Smart Contracts. *Front. Blockchain* 3 (45), 55371. doi:10.3389/fbloc.2020.553671

Wang, M., Wang, C. C., Sepasgozar, S., and Zlatanova, S. (2020). A Systematic Review of Digital Technology Adoption in Off-Site Construction: Current Status and Future Direction towards Industry 4.0. *Buildings* 10 (11), 204. doi:10.3390/buildings10110204

Wouda, H. P., and Opdenakker, R. (2019). Blockchain Technology in Commercial Real Estate Transactions. *Jpif* 37 (6), 570–579. doi:10.1108/JPIF-06-2019-0085

Xu, J., Liu, H., and Han, Q. (2021). Blockchain Technology and Smart Contract for Civil Structural Health Monitoring System. *Computer-Aided Civil Infrastructure Eng.* 36 (10), 1288–1305. doi:10.1111/mice.12666

Yoon, J. H., and Pishdad-Bozorgi, P. (2022). State-of-the-Art Review of Blockchain-Enabled Construction Supply Chain. *J. Construction Eng. Manag.* 148 (2), 03121008. doi:10.1061/(asce)co.1943-7862.0002235

Zheng, R., Jiang, J., Hao, X., Ren, W., Xiong, F., and Ren, Y. (2019). bcBIM: A Blockchain-Based Big Data Model for BIM Modification Audit and Provenance in Mobile Cloud. *Math. Probl. Eng.* 2019, 1–13. doi:10.1155/2019/5349538

Conflict of Interest: The authors declare that the research was conducted in the absence of any commercial or financial relationships that could be construed as a potential conflict of interest.

Publisher's Note: All claims expressed in this article are solely those of the authors and do not necessarily represent those of their affiliated organizations, or those of the publisher, the editors and the reviewers. Any product that may be evaluated in this article, or claim that may be made by its manufacturer, is not guaranteed or endorsed by the publisher.

frontiers | Frontiers in Built Environment

ORIGINAL RESEARCH
published: 14 April 2022
doi: 10.3389/fbuil.2022.856380

Optimized Strengthening Based on Concrete Jacketing for Minimum Eccentricity

Chara Ch. Mitropoulou[1], *Iordanis A. Naziris*[1,2], *Nikos Ath. Kallioras*[1] *and Nikos D. Lagaros*[1]*

[1]*Institute of Structural Analysis and Antiseismic Research, School of Civil Engineering, National Technical University of Athens, Athens, Greece,* [2]*Special Service of European Union Structural Funds for the Ministry of Maritime Affairs and Insular Policy, Piraeus, Greece*

The coupled lateral-torsional response is observed in building structures subjected to dynamic excitation due to lack of symmetry in terms of mass/stiffness in any of the stories' plan views; such structural systems are called eccentric. Much damage and even collapse are concerned with building structures with asymmetric plan views. Combined torsional-translational vibration of their structural system results in higher ductility demands, especially to vertical structural elements located at the perimeter of the plan view. This study examines the minimization problem of the torsional response of an eccentric, multi-story reinforced concrete (RC) building by strengthening its vertical structural elements with RC jackets. The problem of minimizing the eccentricity between mass and rigidity centers for all story layouts and the corresponding minimization problem of the eccentricity between mass and strength centers for all stories are considered two separate formulations for the reduction of the torsional response optimization problem. Based on recent studies, the center of strength is preferable for assessing the torsional response of buildings in case of inelastic response. The imperialist competitive algorithm (ICA), a member of the family of evolutionary search algorithms, is used to solve the two optimization problems. The optimization problems are formulated for the case study building considered after assessing its structural behavior and capacity through nonlinear static analyses before and after strengthening. The later process was implemented to meet code requirements and examine the improvements achieved through optimization.

Keywords: strength eccentricity, stiffness eccentricity, metaheuristics, column strengthening, concrete jacketing, optimization

OPEN ACCESS

Edited by:
Vagelis Plevris,
Qatar University, Qatar

Reviewed by:
Michele Palermo,
University of Bologna, Italy
Rajai Zuheir Al Rousan,
Jordan University of Science and Technology, Jordan
Sameh Samir F. Mehanny,
Cairo University, Egypt

***Correspondence:**
Nikos D. Lagaros
nlagaros@central.ntua.gr

Specialty section:
This article was submitted to Computational Methods in Structural Engineering, a section of the journal Frontiers in Built Environment

Received: *17 January 2022*
Accepted: *09 March 2022*
Published: *14 April 2022*

Citation:
Mitropoulou CC, Naziris IA, Kallioras NA and Lagaros ND (2022) Optimized Strengthening Based on Concrete Jacketing for Minimum Eccentricity. Front. Built Environ. 8:856380. doi: 10.3389/fbuil.2022.856380

1 INTRODUCTION

During the structural design phase, which remains the subject of research for engineers and scientists, the goal is to develop a structural system that can reliably and predictably withstand dynamic excitation (i.e., due to extreme actions such as blast loading or seismic excitation). Coupling translational with torsional response can be observed due to either variance between actual and considered mass distribution and stiffness or dynamic excitations that introduce a torsional component on the structural response. This component is developed due to eccentricity between the centers of mass (CM) and rigidity (CR) of the structural system. Such a structural system is called eccentric or torsionally unbalanced. When this kind of structural system is subject to horizontal dynamic excitations, the inertia forces developed can be represented by point loads passing through

the mass center, while the forces modeling the resisting extreme action can be represented as point loads passing through the stiffness center. This pair of opposing point loads generates the torsional component of the response on the structural system coupled with the translational one.

It is worth mentioning that the foundations of modern research on the dynamic behavior of single and multi-story asymmetric structures were set by a series of studies that identified some of the key parameters influencing the performance of such systems. For instance, Goel and Chopra (1990) and Kan and Chopra (1977) identified and assessed the distribution of stiffness and strength and the torsional coupling, respectively. Further influential studies regarding the response of one-story structures are included in the works of Peruš and Fajfar (2005), Palermo et al. (2013), Palermo et al. (2017), and Trombetti and Conte (2005). Additionally, Fajfar (2000) and Fischinger (Fajfar and Fischinger, 1988; Fajfar and Gašperšič, 1996; Marušić and Fajfar, 2005) analyzed the nonlinear response of multi-story buildings under seismic loads. Bosco et al. (2012), Bosco et al. (2013), Bosco et al. (2015) also approached the behavior of multi-story asymmetric buildings, while De Stefano and Pintucchi (2008) presented a useful overview of the research advancements about the seismic response of both the plan and vertically irregular structures.

As proved by Kan and Chopra (1977) and presented in more detail by Reem and Chopra (1987), accurate and reliable prediction and assessment of the response of eccentric multi-story buildings in the elastic stage cannot be determined because, in multi-story buildings, except in a special case, the center of rigidity is not defined unambiguously but depends on seismic loading. Eurocode 8 (1994) and its Greek national annex provided the definition of a fictitious axis of rotation (optimum torsion axis) from which static eccentricity is measured. Regarding the post-elastic structural response stage, things are even vaguer. For example, Stathopoulos and Anagnostopoulos (2005) questioned the adoption of a single coefficient of behavior q provided by modern earthquake design provisions. However, during the past 30 years, research efforts were performed in this direction (estimating and predicting the response of eccentric buildings), and various design criteria/estimation of torsional action have been proposed (Stathi et al., 2015).

In buildings designed with older regulations (before 1995 and especially before 1985), significant non-uniformities are observed during the formation of the static system. On the contrary, new buildings are characterized by greater regularity, thanks to the provisions of modern earthquake design codes (Anastassiadis et al., 1998; Makarios and Anastassiadis, 1998; Xenidis et al., 2006). Modern earthquake design codes try to provide general directions (simple as possible structural systems, arrangement of strong stiffness elements in the perimeter, etc.), aiming to derive as rigid as possible buildings but also with limitations in terms of geometry and distribution of stiffness and mass along the height and floor plans. However, in relevant provisions based on simplified shear-beam, one-story models, the "flexible" side frames exhibit higher ductility demands than the "stiff" side ones (Stathopoulos and Anagnostopoulos, 2005). The advancements of computational techniques and algorithms have allowed scientists in several fields to approach multiple complex problems in new and efficient ways. Particularly in engineering, such techniques have significantly contributed to the shift from traditional trial-and-error practices to fully automated ones, incorporating search algorithms. There are many examples from the past where researchers have explored the potential of implementing optimization approaches to structural engineering challenges. Furthermore, the behavior of asymmetric structures subjected to horizontal loads, such as earthquakes, especially regarding their torsional response, is addressed in numerous research studies, which in some cases also incorporate optimization approaches to solve the arising problems.

Specifically, Terzi and Athanatopoulou (2021) proposed a measure to define the optimum torsion axis through the twist axis. This measure demands the sum of story translational displacements of the axis to be minimal. Dang et al. (2021) developed a two-stage optimization approach for designing isolated buildings incorporating genetic algorithms to identify the optimal parameters of the isolated layer. Almazán and de la Llera (2009) showed that the optimal damper location depends on the static eccentricity and frequency ratio of the bare structure, the total amount of supplemental damping considered, and the frequency content of the excitation. Li and Han (2003) optimized the positioning of multiple tuned mass dampers (MTMD) for asymmetric structures, while Ismail (2015) aimed at forcing the isolated asymmetric structures to behave as symmetric structures, eliminating torsional responses. Similarly, Georgoussis (2015) suggested a way to minimize the torsional response of inelastic multi-story buildings with simple eccentricity, and Yiu et al. (2014) introduced a practical method for evaluating lateral-torsional coupling in the elastic earthquake response of asymmetric multi-story buildings. In order to minimize the torsional effects in asymmetric tall buildings, Şahin (2012) proposed a new algorithm in MATLAB. Lagaros et al., in two studies (2006 and 2009), developed optimum design approaches for improving the seismic performance of 3D RC buildings, including the minimization of the rigidity eccentricity. In the same context, Duan and Chandler (1997) developed an optimized procedure for designing torsionally unbalanced structures subjected to earthquake loading, considering both the serviceability and the ultimate limit states. Three studies (Li et al., 2008a; Li et al., 2008b; Li et al., 2008c) extensively dealt with the properties of soil-asymmetric building-active multiple tuned mass dampers (AMTMD) interaction system, suggesting guidelines for the design and implementation in earthquake reduction of asymmetric structures built on soft soil foundation. Guo and Li (2009) established a model of primary-secondary systems concerning lateral-torsion coupling and interaction between primary and secondary systems and used a complex mode theory and pattern research method for the secondary system's optimal position. They also analyzed the influencing factors of optimal position, such as eccentricity of the primary system, direction of earthquake input, site of different classification, mass, frequency, and damping ratio of the secondary system. Chandler et al. (1995) examined the

influence of accidental eccentricity on inelastic seismic torsional effects in buildings reaching some useful conclusions regarding the effectiveness of code accidental torsional provisions and the ductility demand for the flexible-edge element in torsionally unbalanced structures. Finally, Etedali and Kareshk (2022) proposed a procedure for the optimal design of isolators in the base story of asymmetric base-isolated structures to mitigate torsional responses. In this work, the minimum eccentricity optimization problem is formulated for the case of multi-story reinforced concrete (RC) building structures associated with the problem of selecting the characteristics of their vertical structural elements strengthening strategy. In order to offer the designer/practitioner a tool to understand the procedures described in the study, an open-access web application is provided, where optimization-based strengthening is provided, among others (LINK).

2 ECCENTRICITY IN MULTI-STORY BUILDING STRUCTURES

2.1 Equations of Motion

Contrary to what is observed for the case of single-story building structures, in the case of multi-story ones, the centers of mass, rigidity, and strength do not lie over a vertical axis. Another difference observed in the case of multi-story buildings is that the locations of the centers of stiffness, twist, and shear depend on the stiffness of the system and the torsional or lateral loads exerted. However, a special type of multi-story buildings can be designed where, in each story, these centers coincide, laying over a common, vertical axis independent of lateral loading. The typical centers that can be defined for each story of the multi-story building are the following: stiffness center (also called rigidity center) is the location on each floor where any set of static horizontal forces of arbitrary magnitude and direction is applied to cause no rotation or twisting on any of the stories (Hejal and Chopra, 1989). Another definition of the stiffness center of a building is that it corresponds to the location on each floor where if a static horizontal force is applied, it develops translational deformation without rotation or twisting. However, the rest of the floors may rotate or twist (Humar, 1984). The principal axes of a floor are two orthogonal axes passing through its center of rigidity. If a set of static horizontal loads is applied along one of the two principal axes of each floor, then the floor is deformed along the direction of the applied loads, without a twist. The mass center is the location on the diaphragm where the component of the inertial forces of the floor passes. If the masses of the vertical elements are negligible compared to those of the floor and the mass distribution on the floors of the building is uniform, then the center of mass coincides with the geometric center of the floor. The static eccentricity of the ith story refers to the distance between mass and stiffness centers.

The equations of motion of a multi-story building, considering linear behavior, where damping is ignored for simplicity in the description, for the case of a dynamic action along the x- and y-axis, developing accelerations $a_{gx}(t)$ and $a_{gy}(t)$, respectively, are formulated as follows for various reference points. With reference to a randomly selected reference point O,

$$\begin{bmatrix} m & 0 & -my_{CM} \\ 0 & m & mx_{CM} \\ -my_{CM} & mx_{CM} & J_0 \end{bmatrix} \begin{Bmatrix} \ddot{u}_x \\ \ddot{u}_y \\ \ddot{u}_\theta \end{Bmatrix} + \begin{bmatrix} K_x & K_{xy} & K_{x\theta} \\ K_{yx} & K_y & K_{y\theta} \\ K_{\theta x} & K_{\theta y} & K_\theta \end{bmatrix} \begin{Bmatrix} u_x \\ u_y \\ u_\theta \end{Bmatrix} = -\begin{Bmatrix} mIa_{gx}(t) \\ mIa_{gy}(t) \\ -y_{CM}mIa_{gx}(t) + x_{CM}mIa_{gy}(t) \end{Bmatrix}, \tag{1}$$

with reference to the center of mass CM,

$$\begin{bmatrix} m & 0 & 0 \\ 0 & m & 0 \\ 0 & 0 & J_M \end{bmatrix} \begin{Bmatrix} \ddot{u}_x \\ \ddot{u}_y \\ \ddot{u}_\theta \end{Bmatrix} + \begin{bmatrix} K_x & K_{xy} & K_{x\theta} \\ K_{yx} & K_y & K_{y\theta} \\ K_{\theta x} & K_{\theta y} & K_\theta \end{bmatrix} \begin{Bmatrix} u_x \\ u_y \\ u_\theta \end{Bmatrix} = -\begin{Bmatrix} mIa_{gx}(t) \\ mIa_{gy}(t) \\ 0 \end{Bmatrix}, \tag{2}$$

with reference to the rigidity center CR,

$$\begin{bmatrix} m & 0 & -me_y \\ 0 & m & me_x \\ -me_y & me_x & J_R \end{bmatrix} \begin{Bmatrix} \ddot{\tilde{u}}_x \\ \ddot{\tilde{u}}_y \\ \ddot{u}_\theta \end{Bmatrix} + \begin{bmatrix} \tilde{K}_x & \tilde{K}_{xy} & 0 \\ \tilde{K}_{yx} & \tilde{K}_y & 0 \\ 0 & 0 & \tilde{K}_\theta \end{bmatrix} \begin{Bmatrix} \tilde{u}_x \\ \tilde{u}_y \\ u_\theta \end{Bmatrix} = -\begin{Bmatrix} mIa_{gx}(t) \\ m1a_{gy}(t) \\ -e_y m1a_{gx}(t) + e_x m1a_{gy}(t) \end{Bmatrix}, \tag{3}$$

where I denotes a vector of ones of dimension N; $\ddot{u}_x$, $\ddot{u}_y$, and $\ddot{u}_\theta$ denote vectors of dimension N; J_0 is the diagonal matrix of dimension N (number of stories in a multi-story building structure) and its elements $J_{0,j}$ denote the polar moment of inertia of the j^{th} story with respect to point O_j; r is the radius of rotation; x_{CM} and y_{CM} are diagonal matrices of dimension N and their elements $x_{CM,j}$ and $y_{CM,j}$ denote the coordinates of the mass center (CM) of the j^{th} story with respect to the reference system $X_jO_jY_j$; J_M is the diagonal matrix of dimension N where its elements $J_{M,j} = m_j r_j^2$ represent the polar moment of inertia of the j^{th} story with reference to its mass center; J_R denotes the diagonal matrix of dimension N and its elements $J_{R,j} = m_j(e_j^2 + r_j^2)$ denote the polar moment of inertia of the j^{th} story with respect to the center of stiffness; and e_x and e_y are diagonal matrices of dimension N and their elements are defined as follows:

$$e_{xj} = x_{CMj} - x_{CRj}, \tag{4a}$$

$$e_{yj} = y_{CMj} - y_{CRj}, \tag{4b}$$

where scalars e_{xj} and e_{yj} are the components of the static eccentricity of the j^{th} story along the x- and y-axis and x_{CRj} and y_{CRj} are coordinates of the stiffness center of the j^{th} story with respect to the reference system $X_jO_jY_j$.

2.2 Location of Stiffness or Rigidity Center

To calculate the coordinates of the stiffness center (also called rigidity center) for the case of a multi-story building structure, let us consider the stiffness matrix of **Eq. 1**, which is defined

according to degrees of freedom (DOF) u at a randomly selected reference point O. Hence, for calculating the coordinates, the following transformation of u (corresponding to reference point O) to $\tilde{u}$ (corresponding to reference point CR) is considered:

$$u = \begin{Bmatrix} u_x \\ u_y \\ u_\theta \end{Bmatrix} = \begin{bmatrix} I & 0 & y_{CR} \\ 0 & I & -x_{CR} \\ 0 & 0 & I \end{bmatrix} \begin{Bmatrix} \tilde{u} \\ \tilde{u} \\ u_\theta \end{Bmatrix} = \tilde{a}\tilde{u}. \tag{5}$$

Thus,

$$\tilde{\mathrm{K}} = \tilde{a}^T K \tilde{a} \Leftrightarrow \tilde{\mathrm{K}} = \begin{bmatrix} K_x & K_{xy} & K_x y_{CR} - K_{xy} x_{CR} + K_{x\theta} \\ K_{yx} & K_y & K_{yx} y_{CR} - K_y x_{CR} + K_{y\theta} \\ K_{\theta x} + y_{CR} K_x - x_{CR} K_{yx} & K_{\theta y} + y_{CR} K_{xy} - x_{CR} K_y & \tilde{K}_\theta \end{bmatrix}, \tag{6}$$

where $\tilde{K}_\theta = K_\theta + 2K_{\theta x} y_{CR} - 2K_{\theta y x_{CR}} + K_x y_{CR}^2 - 2K_{xy} x_{CR} y_{CR} + K_y x_{CR}^2$, given that **Eq. 6** refers to the stiffness matrix with reference to CR, and as denoted in **Eq. 3**, the off-diagonal coefficients of the stiffness matrix that correspond to the coupling of translational with rotational DOF are equal to zero:

$$K_{\theta x} + y_{CR} K_x - x_{CR} K_{yx} = 0, \tag{7a}$$

$$K_{\theta y} + y_{CR} K_{xy} - x_{CR} K_y = 0, \tag{7b}$$

Thus, solving the system of **Eq. 7a**, **Eq. 7b**, with respect to the unknowns x_{CR} and y_{CR} that denote diagonal matrices containing the coordinates of the rigidity centers along the stories of the building structure and their coefficients ($K_{\theta x}$, K_x, etc.,) referring to square matrices, the following expressions are derived:

$$x_{CR} = \frac{K_{y\theta} - K_{yx} K_x^{-1} K_{x\theta}}{K_y - K_{yx} K_x^{-1} K_{xy}}, \tag{8a}$$

$$y_{CR} = -\frac{K_{x\theta} - K_{xy} K_y^{-1} K_{y\theta}}{K_x - K_{xy} K_y^{-1} K_{yx}}. \tag{8b}$$

However, **Eq. 8a**, **Eq. 8b** do not always lead to diagonal matrices, thus unique definition of the centers of stiffness. Unique locations of stiffness centers do not always exist. They depend on loading; that is, different load distributions lead to different locations of the stiffness centers. In such a case, the coordinates of the stiffness centers can be derived through the following procedure:

$$\tilde{P} = \tilde{K}\tilde{u} \Leftrightarrow \begin{Bmatrix} \widetilde{P_x} \\ \widetilde{P_y} \\ 0 \end{Bmatrix} = \begin{bmatrix} K_x & K_{xy} & K_x y_{CR} - K_{xy} x_{CR} + K_{x\theta} \\ K_{yx} & K_y & K_{yx} y_{CR} - K_y x_{CR} + K_{y\theta} \\ K_{\theta x} + y_{CR} K_x - x_{CR} K_{yx} & K_{\theta y} + y_{CR} K_{xy} - x_{CR} K_y & \tilde{K}_\theta \end{bmatrix} \begin{Bmatrix} \tilde{u}_x \\ \tilde{u}_y \\ u_\theta \end{Bmatrix}, \tag{9}$$

where static lateral loads are introduced along the height of the building structure, leading to the following expressions:

$$x_{CR} = \left[\widetilde{P_y}\right]^{-1} \frac{K_{\theta y} - K_{\theta x} K_x^{-1} K_{xy}}{K_y - K_{yx} K_x^{-1} K_{xy}} \widetilde{P_y}, \tag{10a}$$

$$y_{CR} = -\left[\widetilde{P_x}\right]^{-1} \frac{K_{\theta x} - K_{\theta y} K_y^{-1} K_{yx}}{K_x - K_{xy} K_y^{-1} K_{yx}} \widetilde{P_x}, \tag{10b}$$

where $\widetilde{P_x}$ and $\widetilde{P_y}$ are diagonal matrices. Therefore, the location of the stiffness centers is unique and dependent on the applied load. It is possible to identify unique stiffness centers along the floors of multi-story building structures, regardless of the horizontal loads, for a special type of multi-story buildings that allows the identification of unique centers and has the following properties: 1) the mass centers of all floors lie along a vertical axis and 2) the vertical structural elements are arranged in such a way that their local axes form an orthogonal grid in the floor plan view and are connected to each floor by a rigid diaphragm. The result of the last two characteristics is that the stiffness centers of all floors are on the same vertical axis. The static eccentricities of the floors are also the same (Lagaros et al., 2006; Lagaros et al., 2009).

2.3 Location of Strength Center

As mentioned earlier, the regulations are based on an elastic response; the simulation of the torsional effect, however, needs to consider the inelastic state of the body (determination of the torsional axis in the inelastic phase, ability to receive the shear forces of torsion from the structural elements) that will determine the collapse mechanisms of the building and thus give the ability to the engineer to estimate the required ductility of the components and compare it with the available one. There are many relevant ones in the literature (e.g., Stathopoulos and Anagnostopoulos, 2005). It has been proposed to replace the rigidity center (CR) with that of the strength center (CV). The center of strength (CV) is the position of the diaphragm through which the recommended strength of all vertical elements passes. Strictly unrestrained is a building whose mass and stiffness centers are not identical (eccentric) (Paulay, 1998; Penelis and Penelis, 2019). According to the above, the CV endurance center is determined as follows:

$$x_{CV} = \frac{\Sigma_i V_{yi} \cdot x_i}{\Sigma_i V_{yi}}, \tag{11a}$$

$$y_{CV} = \frac{\sum_i V_{xi} \cdot y}{\sum_i V_{xi}}, \tag{11b}$$

where x_i and y_i are the coordinates of the vertical elements' center of mass of the ith story with respect to the typical reference system on the specific story, V_{xi} and V_{yi} denote the horizontal (shear) nominal resistance (strength) of the vertical elements along the directions x and y, respectively, which are calculated in case of a fragile element:

$$V_y = min\left\{\frac{M_x}{L_{s,k}}; V_{Ry}\right\}, \tag{12a}$$

$$V_x = min\left\{\frac{M_y}{L_{s,k}}; V_{Rx}\right\}, \tag{12b}$$

with $L_{s,k}$ denoting the distance of the extreme cross section $k = 1$, 2 of the specific element from the position of zero moments (shear length), where the shear strength of the element along the

two directions (V_{Ry} and V_{Rx}) is calculated based on appendix 7Γ of Kanepe (2017).

3 STRENGTHENING OF RC BUILDING STRUCTURES

Several options are available for intervention aiming to retrofit structures (Costa et al., 2017; Ganguly, 2020). 1) Repair–reinforcement of critical areas on existing structural elements: jacketing is the most popular method of this category, contributing to strengthening and retrofitting structural elements. It is adopted to upgrade bearing load capacity based on improvements on the structural design or restore its integrity due to failures on the structural elements (steel jacketing, reinforced concrete jacketing, glass fiber reinforced polymer jacketing, fiber-reinforced polymer (FRP) jacketing, hybrid jacketing and shape memory alloy (SMA) wire jacketing, near-surface mounted (NSM) fiber-reinforced polymer (FRP) jacketing, etc.). 2) Add new load-bearing elements (new structural system, shear walls, steel frame, etc.): filling shear walls of the load-bearing frame structural system, expansion (reinforcement of existing brickwork, demolition of brickwork and addition of RC shear walls, steel stiffeners/dampers). 3) Addition of dampers: seismic isolation systems. All the above-mentioned options are part of a structural intervention strategy.

3.1 Structural Intervention Aiming to Remove Irregularities in the Floor Plan

In order to choose how and where to intervene in the building aiming to improve its structural performance is to increase stiffness and flexural strength of some structural elements selectively, for example, for the case of columns aiming to modify the location of the centers of elastic stiffness and strength and possibly minimize the corresponding eccentricities. According to Tassios (1982), a selective increase in stiffness takes place 1) after low-intensity random actions (e.g., low-intensity explosions and small earthquakes), 2) when the building is very flexible, and 3) when it is necessary to correct irregularities in the distribution of stiffness in height or extent. Selective increase of flexural strength occurs due to 1) irregularity of strengths in height or plan (i.e., torsion might be observed during yield of some elements) and 2) insufficiency of flexural strength locally or damage of a structural element. Such problems require a selective increase in stiffness and flexural strength of the columns. The most suitable strengthening method is the use of reinforced concrete jacketing (Kanepe, 2017).

3.2 Column Jacketing

The construction of jackets on RC columns is a repair and reinforcement method successfully applied in numerous cases. The method is used to repair or strengthen the element (local or total jacketing). In addition to improving the three basic features of the column, jacketing also does not affect the architectural characteristics of the strengthened section, reduces slenderness of the strengthened element, improves the structural performance of the columns due to confinement, and increases the level of fire protection. Based on the type of concrete, jacketing is classified into two different categories. Jacketing made of cast concrete is used in jackets where the thickness exceeds 8 cm ($t \geq 8$ cm), while their construction requires formwork. Casting is implemented by means of low pressure, and the size of the aggregates should not be large. The use of fluids and admixtures that prevent drying shrinkage is recommended. The disadvantages of this technique are the difficulty of concreting, especially at the top of the column. In cases where the total thickness is less than 10 cm ($t \leq 10$ cm), Jacketing made of sprayed/shot concrete is used, while no formwork is required for pouring or placing into them. Particular attention should be paid to ensuring the vertical surface of the jackets *via* guides usage. The drying shrinkage in this type of concrete jackets is greater. Thus, proper maintenance is required.

The construction provisions of RC jackets are the result of research and experience from the application of the method in practice: For sprayed/shot concrete jacketing, the minimum thickness must be 5 cm; for cast concrete jacketing with one row of reinforcements, the thickness must be 8–12 cm; and for cast concrete jacketing with two rows of reinforcement, the minimum thickness must be 12 cm. In the case where the thickness of the jacketing is small (i.e., less than 7.50 cm), the provisions of the concrete regulations related to the coatings of the reinforcement bars are not satisfied together with those related to the form of hooks at the ends of the stirrups. Thus, in case of a small thickness of the jacket, the ends of the stirrups need to be welded.

4 THE MINIMUM ECCENTRICITY PROBLEM COMBINED WITH COLUMNS STRENGTHENING FOR RC BUILDING STRUCTURES

4.1 Problem Formulation

The main objective of this study is to formulate optimization problems that will lead to the redesign of existing RC structures, which may have been reinforced to meet the required safety conditions of the applicable Regulations, in order to create designs with the minimal torsional response and therefore improved behavior. The wording used in this work is based on the problem of minimizing the e_{CM-CV} eccentricity of centers of mass (CM) and strength (CV) for each story. Design variables (in the case of existing buildings) are the thickness and the longitudinal reinforcement of the RC jackets. Restrictions refer to the value ranges in which these variables move due to construction and regulatory requirements. The problem refers to a mixed optimization problem mathematically expressed as follows:

$$\min_{[t]} e_{CM-CR}([t]) = \sqrt{\left(x^j_{CM}([t]) - x^j_{CR}([t])\right)^2 + \left(y^j_{CM}([t]) - y^j_{CR}([t])\right)^2},\ j = 1\,2,\ \cdots, n_{storeys}, \tag{13a}$$

$$\min_{[t,p]} e_{CM-CV}([t,p]) = \sqrt{\left(x^j_{CM}([t,p]) - x^j_{CV}([t,p])\right)^2 + \left(y^j_{CM}([t,p]) - y^j_{CV}([t,p])\right)^2},\ j = 1\,2,\ \cdots, n_{storeys}, \tag{13b}$$

where $[x^j_{CM}, y^j_{CM}]$, $[x^j_{CR}, y^j_{CR}]$, and $[x^j_{CV}, y^j_{CV}]$ are the positions of the mass, rigidity, and strength centers of the j^{th} story, $n_{storeys}$ is the total number of floors of the building, $t = [t_{NS}, t_S]$ are the RC jackets' thicknesses of the non-strengthened and strengthened (based on safety criteria) columns, respectively, $n_{columns,NS}$ and $n_{columns,S}$ denote the total number of non-strengthened and strengthened columns of the story, respectively, p denote the percentage of longitudinal reinforcement of the RC jackets, and $n_{columns} = n_{columns,NS} + n_{columns,S}$ is the total number of columns of the story.

The notations marked in **Figure 1** are the following: $t_{tot} = t_0 + t_{new}$ is the total thickness of the RC jacket resulting from the strength requirements plus the one needed to minimize eccentricity, $A_{s,ini,y}$ is the initial longitudinal reinforcement of the cross section, perpendicular to the y direction, and $A_{s,ini,x}$ is the initial longitudinal reinforcement of the cross section, perpendicular to X direction. Accordingly, $A_{s,tot} = A_{s,0} + A_{s,new}$ is the total reinforcement of the RC jacket resulting from the strength requirements plus the one needed to minimize eccentricity. In order to calculate the strength moment and the corresponding shear forces, the cross section is discretized into layers of number:

$$l_x = round\left[\frac{h + 2t_{tot}}{h_l}\right], // \ with\ direction\ x\,, \tag{14a}$$

$$l_y = round\left[\frac{b + 2t_{tot}}{h_l}\right], // \ with\ direction\ y, \tag{14b}$$

where h_l is the thickness of the layer, after trial-and-error tests, to achieve a compromise between convergence to acceptable results and velocity $h_l = 1.0\,cm$.

The following assumptions are considered for the implementation of the algorithm. First assumption: a common RC jacket is constructed with thickness $t_{tot} = t_0 + t_{new}$ and reinforcement lying on the same level as shown in **Figure 1**. Second assumption: in order to calculate the bending moment resistance, only the longitudinal reinforcement distributed along the edge of the cross section perpendicular to the specific direction is used because the contribution of the rest is rather limited. Third assumption: uniform distribution of the stresses over the layer thickness is considered equal to its upper limit. Fourth assumption: 3 cm reinforcement coating is considered for the initial cross section and RC jacket.

4.1.1 Calculation of the Objective Functions

The steps of the algorithm for calculating the rigidity eccentricity e_{CM-CR} for each floor are as follows, for each column and in each direction:

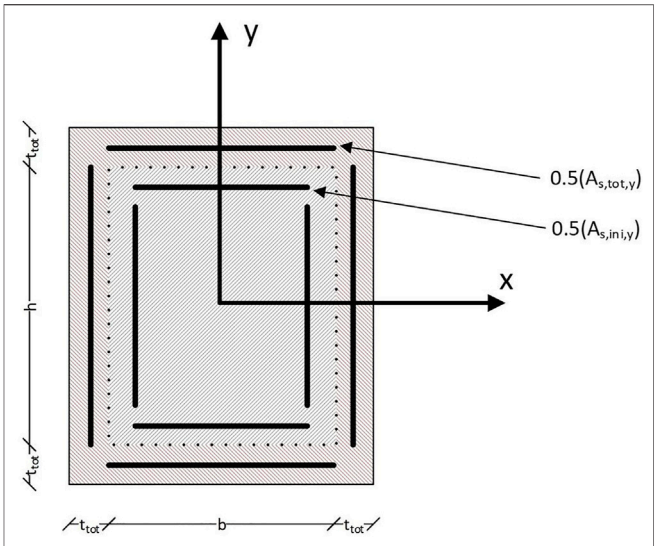

FIGURE 1 | Strengthening of RC cross section to calculate its resistance to axial bending with axial force.

Step 1: calculation of the moment of inertia along the directions of local axes x and y for each column by the method of the equivalent cross section.
Step 2: calculation of the cracked stiffness of the cross section for each column.
Step 3: calculation of CR stiffness center coordinates (for the pure frame or wall system).
Step 4: calculation of the objective function according to **Eq.13a**.

Accordingly, the steps of the algorithm for calculating the strength eccentricity e_{CM-CV} for each floor are as follows, for each column and in each direction:

Step 1: discretization of the cross section according to **Eq. 14b**, **Eq. 14a**.
Step 2: calculation of bending moment resistance for combined loading of bending and axial loading. Given that the element is considered monolithic, its strength was reduced by coefficient $k_r = 0.90$ according to KANEPE (Code of Structural Interventions).
Step 3: calculation of shear strength considering a bending failure according to **Eq. 12a**, **Eq. 12b**.

Then, given that the shear strength of the columns is available along the two principal axes, the following steps are performed:

Step 4: calculation of the coordinates of the center of resistance.
Step 5: calculation of the objective function according to **Eq.13b**.

4.1.2 Data Entry

In order to introduce the information required by the problem formulation, a common matrix of the input data is used [data (N,14)], where $N = n_{columns}$ is the number of columns in each story. The 14 columns of the matrix correspond to (c1) column dimension parallel to the x-axis [b (m)], (c2) column dimension

parallel to the y-axis [h (m)], (c3) initial mechanical percentage of reinforcement (p), (c4) abscissa of the column's section mass center [x (m)], (c5) ordinate of the column's section mass center [y (m)], (c6) stiffness reduction coefficient due to cracking, (c7) initial reinforcement thickness (element strength requirements), (m), (c8) mechanical reinforcement rate of initial reinforcement, (c9) additional reinforcement thickness resulting from minimizing construction eccentricity [t_{new} (m)], (c10) mechanical percentage of additional reinforcement (ρ_{new}), (c11) modulus of elasticity of concrete [E_c (kPa)], (c12) modulus of elasticity of steel reinforcement [E_s (kPa)], (c13) column length [L (m)], and (c14) axial compressive strength of concrete for the combination G + 0.3Q (with positive sign), [N (kN)].

4.2 Solving the Optimization Problem

Search algorithms represent an iterative procedure that requires an initial guess of the problem solution. Then, a sequence of improved designs are generated until the optimal or the best compromise solution is achieved. The type of strategy that the algorithm relies on for generating the new designs categorizes the optimization procedure. The search algorithm is characterized by robustness, in which the algorithm needs to be able to handle a variety of problems efficiently; efficiency, in which the algorithm should not require too much computing power to converge; and accuracy in which the algorithm needs to be able to recognize an acceptable solution accurately, without being sensitive to arithmetic errors.

A fast algorithm may require too much storage to deal with problems with many design variables. On the contrary, a highly robust algorithm may require many iterations, thus increasing computational time to reach the optimal design. Some algorithms preserve part of the information from the previous designs, while others only use information from the current design. As far as the type of information, the algorithms are classified into zero-, first-, or second-order algorithms. Zero-order algorithms use the information obtained through objective function value only during the search process. First-order algorithms, in addition to the objective function value, make use of the information obtained through the first-order derivative of the objective function. In contrast, second-order algorithms, in addition to the objective function value and its first derivative, use the information obtained through the second-order derivative of the objective function.

Zero-order algorithms are divided into deterministic or mathematical and stochastic algorithms, depending on how the new designs are generated. In general, deterministic ones approach the optimal design very quickly. Their main disadvantage is that they are easily trapped in local minima. Stochastic algorithms search for the optimal solution through random processes, generating better designs based on the existing ones. They are not as easily trapped into local minima as deterministic algorithms. They require much more computing power to converge. For many years, deterministic algorithms were the exclusive tool for solving structural design optimization problems. However, stochastic algorithms have been explored since the 1960s. During the last 2 decades, stochastic algorithms have been extensively applied in the field of structural design optimization at the research level and have managed to provide solutions to particularly demanding and complex problems. Search algorithms are also classified into algorithms that, in each iteration, deal with one design only and those that deal with a population of designs. All deterministic algorithms deal with one design in each iteration. Concerning the stochastic algorithms, simulated annealing is the most popular search algorithm that also deals with one design in each iteration.

A large and very popular category of stochastic search algorithms that deal with a population of designs in each iteration are the well-known evolutionary or Darwinian algorithms. They usually model a natural, social, or biological process. Evolutionary algorithms are characterized by robustness and the ability to identify the area of the global optimum design due to the random search process. However, they require a large number of function evaluations. Genetic algorithms and evolution strategies are the best-known evolutionary algorithms. For dealing with the optimization problems addressed in the framework of the IMSFARE project, the imperialist competitive algorithm (ICA) was employed, which is briefly described in the next section.

4.3 Imperial Competitive Algorithm

ICA (Atashpaz-Gargari and Lucas, 2007) is an evolutionary search algorithm inspired by imperialist competition. So far, it has been used successfully in different optimization problems of numerous areas of engineering and science. The independent populations are called countries and are of two types, colonies and imperialists, all of which together form empires. The colonial/imperialistic competition between empires is the basis of the algorithm. During this competition, the weak empires collapse while the strong ones take over the colonies of the weak empires. This competition successfully converges to the stage where there is only one empire after the collapse of all the rest, whose colonies are positioned in the same location with the imperialist, having the same cost (i.e., the same objective function value). From one point of view, ICA can be considered the social equivalent of genetic algorithms. ICA is the mathematical model and computational simulation of human social evolution, while genetic algorithms are based on the biological evolution of species. Subsequently, the steps of the algorithm and how the imperialist competition between empires is modeled is provided in more detail.

Step 1 (creation of initial empires): like any other evolutionary algorithm, ICA starts with a random initial population (countries in the world). Some of the countries are chosen to be the colonialists/imperialists and the rest form the colonies of these imperialists. These original colonies are divided among the imperialists according to their power, proportional to their cost. It should be mentioned that the cost of a country (design) refers to the objective function value. Let $p_1, p_2, \cdots p_n$ denote the design variables required to model the optimization problem at hand. Thus, a country is defined with the vector $country = [p_1, p_2, \cdots p_n]$. The design variables take various values randomly chosen over the design space, and thus the

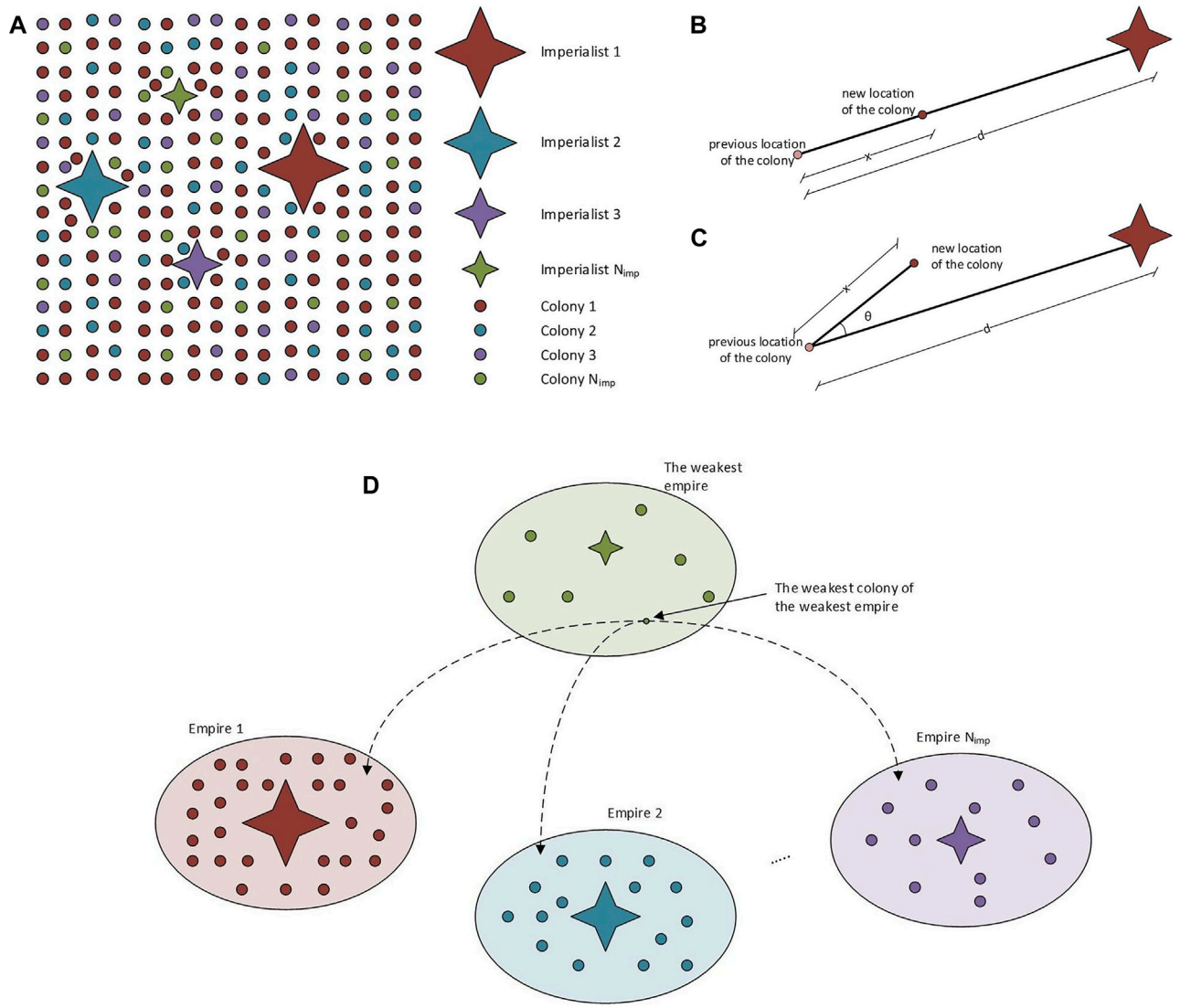

FIGURE 2 | The imperial competitive algorithm. **(A)** Formation of the initial empires. **(B)** Movement of colonies toward their associated colonialist. **(C)** Moving colonies to their associated colonialist with a possible deviant address. **(D)** Imperialist competition. The stronger an empire, the more likely it is to take possession of the weakest colony of the weakest empire.

initial population of size N_{pop} is formed (in the framework of this study and the applications of the IMSFARE project, an initial population of 200 countries was used). The cost of each country is calculated by means of the objective function F of the problem in the variables $(p_1, p_2, \cdots p_n)$. Thus, $cost = F(countr\,y) = F([p_1, p_2, \cdots p_N])$.

Depending on the initial cost of the countries, they are divided into N_{imp} (for the needs of this study and the IMSFARE project N_{imp} was considered equal to 8) where the most powerful ones define the first imperialists and the remaining countries N_{col} represent the initial colonies $(N_{imp} + N_{col} = N_{pop})$. Depending on the cost of the imperialists, the colonies are divided among the imperialists in order to form the initial empires. For this purpose, the normalized cost of each imperialist is defined as $C_n = c_n - max\{c_1, c_2, \cdots c_{N_{imp}}\}$, where c_n is the cost of nth imperialist and C_n is its normalized cost value. Based on the normalized cost value, the power, p_n, of each colonialist can be calculated as follows:

$$p_n = \left| \frac{C_n}{\sum_{i=1}^{N_{imp}} C_i} \right|. \tag{15}$$

Thus, the original colonies pass into the possession of each colonialist and form the first empires, depending on the power of each colonialist according to the relation $NC_n = round(p_n \cdot N_{col})$, which denotes the initial number of colonies in the nth empire. NC_n are randomly selected and assigned to the nth empire. **Figure 2A** shows the initial population of each empire. The strongest empires own the largest number of colonies while the weakest ones possess the smallest.

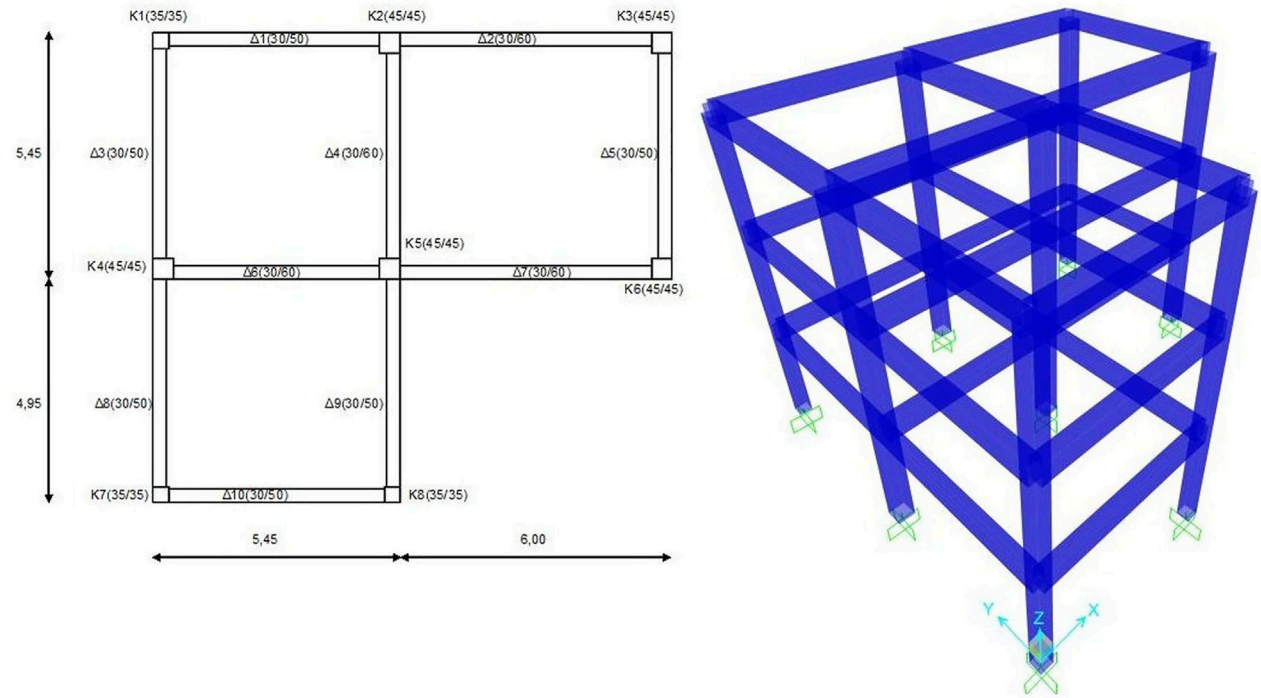

FIGURE 3 | Typical floor plan of the case study building structure and its simulation.

Step 2 (movement of colonies of an empire to the imperialist): once the colonies are divided into empires, they start moving toward their imperialist. In this way, the imperialists improve their colonies by moving the whole population of countries toward positions of lower cost. This movement takes place along the vector joining the colony to the imperialist, as shown in **Figure 2B**. The colony travels a distance of x units in the direction of this vector, which is considered a random variable with uniform distribution $x \approx U(0, \beta \cdot d)$, where β is a number greater than 1 and d is the Euclidean distance between a colony and its imperialist. In most applications, the value $\beta = 2$ gives rapid convergence of countries to the global best. Aiming to enable the search process for the colony in different places around its imperialist, a random deviation in the direction of the movement is provided. This is implemented with the random deviation angle θ (**Figure 2C**), which is a random number with a uniform distribution $\theta \approx U(-\gamma, \gamma)$. In most applications, the value $\gamma = \pi/4$ gives rapid convergence of countries to the global best.

Step 3 (change of position between the colonialist and a colony): if a colony moving toward the colonialist identifies a better position of lower cost than the colonialist, then they change their positions. In other words, this colony becomes the new colonialist of the empire. The algorithm continues with the new colonialist, and the colonies of the empire (including the former colonialist) move toward the new colonialist.

Step 4 (total power of the empire): The total cost of the nth empire is calculated as follows:

$$c_{n,total} = c_n + \xi \cdot average\left(F\left(country_i\right)\right), i = 1, 2, \cdots, NC_n, \quad (16)$$

where the value $\xi = 0.1$ is used in most applications.

Step 5 (imperialist competition): imperialist rivalry gradually leads to loss of power for the weakest empires and strengthening the strongest ones, while all empires try to take possession of colonies of other empires. This is modeled in the algorithm by selecting some of the weakest colonies of the weakest empires and making competition between the other empires over who will acquire these colonies (**Figure 2D**). The empires with the greatest power are most likely to dominate this competition. The normalized cost of the empire is given by $C_{n,total} = c_{n,total} - max\{c_{1,total}, c_{2,total}, \cdots c_{N_{imp},total}\}$, and its power

$$p_{pn} = \left| \frac{C_{n,total}}{\sum_{i=1}^{Nimp} C_{i,total}} \right|. \quad (17)$$

Vector D is defined as $D = P - R = [d_1, d_2, \cdots, d_{N_{imp}}] = [p_{p1} - r_1, p_{p2} - r_2, \cdots, p_{pN_{imp}} - r_{N_{imp}}]$, where P represents the power vector of the empires and R is a vector with random numbers uniformly distributed in the space (0, 1). With reference to vector D, the referenced colonies will be brought to the empire whose element in vector D is the maximum.

Step 6 (exclusion of powerless empires): empires left without colonies are considered collapsing and excluded from the competition.

Step 7 (convergence): in the end, only one empire will remain (the most powerful) after the collapse of the rest, and all colonies

TABLE 1 | Calculation of moment-chord rotation angles θ_y, θ_{um}, and $\theta_{u,pl}$, for the structural elements.

Element	b/h (cm)	d_b (m)	L_{net} (m)	L_s (m)	$(1/R)_y$	$(1/R)_u$	M_y(kNm)	M_u(kNm)	θ_y	θ_{um}	$\theta_{u,pl}$
Beams											
Δ1	30/50	0.016	4.63	2.31	0.0057	0.0579	176.38	194.37	0.0078	0.0566	0.0488
Δ2	30/60	0.020	5.60	2.80	0.0045	0.0579	206.17	242.40	0.0076	0.0568	0.0493
Δ3	30/50	0.016	4.65	2.33	0.0057	0.0579	176.38	194.37	0.0078	0.0568	0.0489
Δ4	30/60	0.020	4.60	2.30	0.0045	0.0579	206.17	242.40	0.0069	0.0530	0.0461
Δ5	30/50	0.016	4.60	2.30	0.0057	0.0579	176.38	194.37	0.0078	0.0565	0.0487
Δ6	30/60	0.020	4.63	2.31	0.0045	0.0579	206.17	242.40	0.0069	0.0531	0.0462
Δ7	30/60	0.020	5.60	2.80	0.0045	0.0579	206.17	242.40	0.0076	0.0568	0.0493
Δ8	30/50	0.016	4.65	2.33	0.0057	0.0579	176.38	194.37	0.0078	0.0568	0.0489
Δ9	30/50	0.016	4.63	2.31	0.0057	0.0579	176.38	194.37	0.0078	0.0566	0.0488
Δ10	30/50	0.016	4.65	2.33	0.0057	0.0579	176.38	194.37	0.0078	0.0568	0.0489
Columns											
K11	35/35	0.02	3.00	1.5	−258.15	0.0091	0.0526	98.37	124.69	0.0090	0.0610
K12	45/45	0.02	3.00	1.5	−698.90	0.0066	0.0439	187.81	253.48	0.0073	0.0595
K13	45/45	0.02	3.00	1.5	−364.74	0.0066	0.0439	187.81	253.48	0.0073	0.0550
K14	45/45	0.02	3.00	1.5	−605.59	0.0066	0.0439	187.81	253.48	0.0073	0.0582
K15	45/45	0.02	3.00	1.5	−1,012.96	0.0066	0.0439	187.81	253.48	0.0073	0.0640
K16	45/45	0.02	3.00	1.5	−327.93	0.0066	0.0439	187.81	253.48	0.0073	0.0546
K17	35/35	0.02	3.00	1.5	−276.97	0.0091	0.0526	98.37	124.69	0.0090	0.0614
K18	35/35	0.02	3.00	1.5	−265.58	0.0091	0.0526	98.37	124.69	0.0090	0.0612
K21	35/35	0.02	3.00	1.5	−172.53	0.0091	0.0526	98.37	124.69	0.0090	0.0590
K22	45/45	0.02	3.00	1.5	−465.53	0.0066	0.0439	187.81	253.48	0.0073	0.0564
K23	45/45	0.02	3.00	1.5	−243.19	0.0066	0.0439	187.81	253.48	0.0073	0.0535
K24	45/45	0.02	3.00	1.5	−403.56	0.0066	0.0439	187.81	253.48	0.0073	0.0556
K25	45/45	0.02	3.00	1.5	−675.45	0.0066	0.0439	187.81	253.48	0.0073	0.0592
K26	45/45	0.02	3.00	1.5	−218.41	0.0066	0.0439	187.81	253.48	0.0073	0.0532
K27	35/35	0.02	3.00	1.5	−184.53	0.0091	0.0526	98.37	124.69	0.0090	0.0593
K28	35/35	0.02	3.00	1.5	−177.96	0.0091	0.0526	98.37	124.69	0.0090	0.0591
K31	35/35	0.02	3.00	1.5	−83.29	0.0091	0.0526	98.37	124.69	0.0090	0.0570
K32	45/45	0.02	3.00	1.5	−233.54	0.0066	0.0439	187.81	253.48	0.0073	0.0534
K33	45/45	0.02	3.00	1.5	−120.23	0.0066	0.0439	187.81	253.48	0.0073	0.0520
K34	45/45	0.02	3.00	1.5	−201.29	0.0066	0.0439	187.81	253.48	0.0073	0.0530
K35	45/45	0.02	3.00	1.5	−347.56	0.0066	0.0439	187.81	253.48	0.0073	0.0548
K36	45/45	0.02	3.00	1.5	−106.91	0.0066	0.0439	187.81	253.48	0.0073	0.0518
K37	35/35	0.02	3.00	1.5	−90.86	0.0091	0.0526	98.37	124.69	0.0090	0.0572
K38	35/35	0.02	3.00	1.5	−86.50	0.0091	0.0526	98.37	124.69	0.0090	0.0571

will be under its occupation. At this point, all colonies are in the same place and have the same cost to each other as to the colonial. In this ideal world, there is no difference between colonies and the colonialist.

5 NUMERICAL TESTS

This section provides the numerical tests for describing the implementation of the proposed design framework to achieve the optimized strengthening of the vertical structural elements of an RC building structure. Aiming to assess and then minimize the torsional response, a three-story RC building structure is considered. The plan view, common for all stories, is gamma-shaped (**Figure 3**) with an area of 89 m^2, and the storys' height is equal to 3 m. It corresponds to a residential building and is located in the Municipality of Zografou (hazard zone Z1, according to the Greek hazard map for the city of Athens (Papazachos et al., 1993).

The building is analyzed as a space frame structural system, where the contribution of infill walls on the structural response against the horizontal loads of the random action (e.g., explosion and earthquake) is neglected. Therefore, it is assumed that these loads are received from the other structural elements, namely, beams, columns, and shear walls, the first two of which are simulated with frame elements having 6-DOF. The slabs are not inserted in the model, but the diaphragm function of the floors is ensured by coupling the story's model nodes, while the ground supports are considered to be fully fixed.

Some characteristics of the construction materials were used. Concrete: the original structural system was considered to use concrete of quality C20/25 with a modulus of elasticity E_{cm} = 29 Gpa. Given that the case study refers to an existing structure that will be assessed by means of inelastic analyses, the average strength is considered, $f_c = \frac{f_{ck}+8}{\gamma_m} = \frac{(20+8)}{1.10} = 25.454\,MPa$. Steel: regarding reinforcing steel quality, S400 was considered, with a modulus of elasticity of Es = 200 Gpa. It was also considered post-yield hardening of 1.10; that is, the failure stress is equal to

Capacity curve, uniform X+03Y		
Step	D (m)	V (KN)
3	-0.0494	1121.98
4	**-0.0711**	**1218.44**
PP	**-0.0810**	**1242.32**
5	**-0.0887**	**1261.43**
6	-0.1206	1311.10

Capacity curve, uniform -X-03Y		
Step	D (m)	V (KN)
4	0.0534	1147.39
5	**0.0747**	**1228.96**
PP	**0.0800**	**1241.47**
6	**0.0876**	**1262.43**
7	0.1082	1294.30

Capacity curve, uniform Y+0.3X		
Step	D (m)	V (KN)
5	-0.0127	1126.46
6	**-0.0159**	**1222.84**
PP	**-0.0170**	**1245.32**
7	**-0.0185**	**1277.45**
8	-0.0220	1323.28

Capacity curve, uniform -Y-0.3X		
Step	D (m)	V (KN)
5	0.0121	1098.54
6	**0.0156**	**1209.40**
PP	**0.0170**	**1241.52**
7	**0.0190**	**1283.93**
8	0.0221	1325.93

Capacity curve, eigenmode based X-0.3Y		
Step	D (m)	V (KN)
4	-0.0603	1029.09
5	**-0.0822**	**1088.46**
PP	**-0.0930**	**1105.41**
6	**-0.1134**	**1138.67**
7	-0.1334	1168.37

Capacity curve, eigenmode based -X+0.3Y		
Step	D (m)	V (KN)
4	0.0482	967.23
5	**0.0715**	**1065.27**
PP	**0.093**	**1106.05**
6	**0.1012**	**1121.53**
7	0.1283	1159.93

Capacity curve, eigenmode based Y-0.3X		
Step	D (m)	V (KN)
5	0.0101	988.06
6	**0.0122**	**1046.97**
PP	**0.013**	**1065.75**
7	**0.0144**	**1096.85**
8	0.0182	1156.52

Capacity curve, eigenmode based -Y+0.3X		
Step	D (m)	V (KN)
5	-0.0085	930.48
6	**-0.0111**	**1019.58**
PP	**-0.013**	**1065.47**
7	**-0.0140**	**1087.01**
8	-0.0174	1140.84

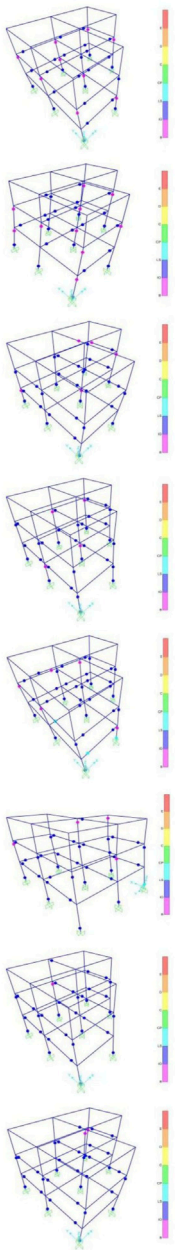

FIGURE 4 | Deformation view of the structural system at the performance point for the different distributions of the horizontal loads.

$f_{tk} = 440\,MP$ and the yield stress is calculated as follows: $f_{sy} = \frac{f_{yk}}{\gamma_m} = \frac{400}{1.10} = 363.636\,MPa$. Beams and columns were grouped according to their dimensions and reinforcement. The longitudinal reinforcement of the original design was 8Ø20 for beams labelled as Δ2, Δ4, Δ6, and Δ7; 10Ø16 for beams Δ1, Δ3, Δ5, Δ8, Δ9, and Δ10; 8Ø20 for columns K1, K7, and K8; and 12Ø20 for columns K2, K3, K4, K5, and K6. The active stiffness of the structural elements is less than the geometric one due to cracking. The reduction of the stiffness was implemented according to the regulation (Earthquake Planning and Protection Organization, 2017). In order to consider the stiffness reduction in analysis/design software, the $\frac{K_{eff}}{K_{el}}$ coefficient is introduced on the modifiers of each section at the moment of inertia.

The vertical loads considered for assessing the building comply with Eurocode 1 (1995). Permanent loading: self-weight of slabs (considering the thickness of 18 cm) is equal to 4.5 kN/m^2, roof covering 1.5 kN/m^2, and infill walls 1.7 kN/m. Live loading: rooms 2.0 kN/m^2. The elastic design spectrum used to evaluate the building in implementing the ATC-40 (Applied Technology Council, 1996) methodology was defined based on EC8. In the specific building, the parameters are Z1 ($a_{gR} = 0.16$), significance II ($\gamma_I = 1.00$), and ground B ($T_B = 0.15$, $T_C = 0.50$, $T_D = 2.50$, $S = 1.20$). Initially, a maximum number of 12 eigenmodes is selected. As already mentioned, the vibrating mass is set for the combination of G + 0.3Q.

It is observed that the first eigenmode is the fundamental one for the Y direction with a mass participation rate of around 83%, while the second eigenmode is the fundamental one for the X direction with a participation rate of around 81%. The primary step in introducing the non-linearity of the members is to define the non-linear properties of the materials. For concrete failure, deformation in compression and bending was considered equal to 2‰ and 3.5‰, respectively, while for steel, the failure deformation was considered equal to 20‰. The ETABS for the extraction of the baring capacity curve during the static inelastic analysis is based on the step-by-step method, that is, the formation of concentrated plastic hinges on the elements until the establishment of the baring collapse mechanism implementing a force-control approach. The next step is the definition of the location of plastic hinges in the structural elements and the definition of their inelastic behavior, that is, the formation of their behavior curve in terms of the moment-chord rotation angle. Given the values of φ_y and φ_u, the value of chord rotation angle for yield and failure, and θ_y and θ_{um}, respectively, for the structural elements, the required quantities are calculated according to KANEPE (Earthquake Planning and Protection Organization, 2017). Note here that $\rho_s = \rho_d = 0$ was considered.

For the calculations in the case of columns, it is necessary to determine the axial forces for the load combination G + 0.3Q (**Table 1**) for beams and columns. In **Table 1**, the first index for the column elements denotes the story and the second one its location in the plan view; that is, K34 is K4 (as denoted in **Figure 4**) at the third story. In **Table 1**, b and h refer to the dimensions of the rectangular cross section; d_b denotes the mean diameter of the longitudinal steel reinforcement; L_{net} and L_s denote the net length of the element and the distance of extreme cross section from the location of zero bending moment, respectively; $(1/R)_y$ and $(1/R)_u$ represent the yield and ultimate capacity values of the curvature; and M_y and M_u symbolize the yield and ultimate bending capacity of the element. A plastic failure mode is selected, and then, depending on the element for which the plastic hinge is defined, the critical failure mode is selected (bending based for the beams and interaction of bending and axial one for the columns). The performance levels of the element are also defined on the curve. Note here that all elements were considered primary, and the positions of the plastic hinge formation are defined at the ends of the beams and columns.

TABLE 2 | Status of plastic hinge in the various steps of pushover analysis.

Step	D (m)	V (kN)	AtoB	BtoIO	IOtoLS	LStoCP	CPtoC	CtoD	DtoE	>E	Total
Uniform X + 03Y											
3	−0.0494	1,121.98	89	2	17	0	0	0	0	0	108
4	−0.0711	1,218.44	81	4	23	0	0	0	0	0	108
5	−0.0887	1,261.43	72	9	27	0	0	0	0	0	108
6	−0.1206	1,311.10	71	3	23	11	0	0	0	0	108
Uniform −X−03Y											
4	0.0534	1,147.39	87	1	20	0	0	0	0	0	108
5	0.0747	1,228.96	79	6	23	0	0	0	0	0	108
6	0.0876	1,262.43	73	10	25	0	0	0	0	0	108
7	0.1082	1,294.30	70	5	25	8	0	0	0	0	108
Uniform Y + 0.3X											
5	−0.0127	1,126.46	90	2	16	0	0	0	0	0	108
6	−0.0159	1,222.84	80	4	24	0	0	0	0	0	108
7	−0.0185	1,277.45	72	5	31	0	0	0	0	0	108
8	−0.0220	1,323.28	70	4	27	7	0	0	0	0	108
Uniform −Y−0.3X											
5	0.0121	1,098.54	93	1	14	0	0	0	0	0	108
6	0.0156	1,209.40	81	1	26	0	0	0	0	0	108
7	0.0190	1,283.93	72	4	32	0	0	0	0	0	108
8	0.0221	1,325.93	70	4	29	5	0	0	0	0	108
Eigenmode-based X−0.3Y											
4	−0.0603	1,029.09	83	5	20	0	0	0	0	0	108
5	−0.0822	1,088.46	74	6	28	0	0	0	0	0	108
6	−0.1134	1,138.67	67	5	33	3	0	0	0	0	108
7	−0.1334	1,168.37	66	3	28	11	0	0	0	0	108
Eigenmode-based −X + 0.3Y											
4	0.0482	967.23	89	7	12	0	0	0	0	0	108
5	0.0715	1,065.27	76	7	25	0	0	0	0	0	108
6	0.1012	1,121.53	69	4	34	1	0	0	0	0	108
7	0.1283	1,159.93	66	3	30	8	0	0	1	0	108
Eigenmode-based Y−0.3X											
5	0.0101	988.06	86	2	20	0	0	0	0	0	108
6	0.0122	1,046.97	78	2	28	0	0	0	0	0	108
7	0.0144	1,096.85	73	1	34	0	0	0	0	0	108
8	0.0182	1,156.52	68	1	32	7	0	0	0	0	108
Eigenmode-based −Y + 0.3X											
5	−0.0085	930.48	93	4	11	0	0	0	0	0	108
6	−0.0111	1,019.58	81	3	24	0	0	0	0	0	108
7	−0.0140	1,087.01	71	2	35	0	0	0	0	0	108
8	−0.0174	1,140.84	68	2	34	4	0	0	0	0	108

5.1 Assessment of the Original RC Building Structural System

5.1.1 Distributions of Horizontal Loads

According to KANEPE, for the needs of the nonlinear static analyses, the application of at least two different load distributions in height is required. Thus, the "uniform" and the "eigenmode-based" distributions are used. The eigenmode-based distribution is in line with the shape of the fundamental eigenmode along the direction examined. As observed through the eigenmode analysis, the fundamental eigenmode along the X direction is the second one, while for the Y direction, it is the first. For spatial superposing of the random actions, the structure according to KANEPE is analyzed for loads in two directions, where the base shear relative contribution 10:3 and 3:10, "positive" and "negative" sign, is also considered and assessment takes place for the most unfavorable stress/strain

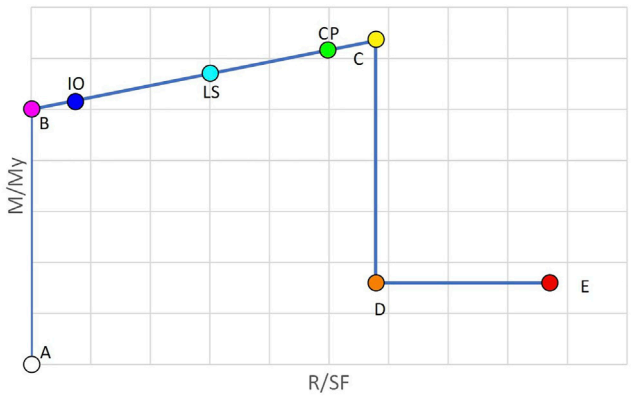

FIGURE 5 | A typical moment rotation curve (M: moment, My: yield moment, R: rotation, SF: safety factor).

quantities observed for each structural element. In particular for both uniform and eigenmode-based distribution + X + 0.3Y and + X−0.3Y (positive direction X); X + 0.3Y and −X−0.3Y (negative direction X), accordingly for Y direction, the application of loads is performed in two phases. Initially, the vertical loads (combination G + 0.3Q) are applied, followed by sixteen nonlinear static analyses for the combination of horizontal loads.

5.1.2 Results of the Assessment

Figure 4 depicts the performance point (PP) along with the previous and next steps of the base shear-deformation (V-D) resistance curve together with the view of the deformed structural system with the location of the formation of the plastic hinges for the eight most unfavorable combinations of horizontal loads. The definition of PP is carried out according to Procedure A described in ATC-40 report [Applied Technology Council (ATC), 1996], and the target displacement is calculated through an iterative procedure using the elastic demand diagram for equivalent damping ratio updated during the iterations. According to Procedure A, the capacity of a structure to resist lateral forces is compared to the demand given by a response spectrum. The response spectrum represents the demand, while the pushover curve (or the "capacity curve") represents the available capacity. The steps of the method are briefly summarized. 1) Perform pushover analysis and determine the capacity curve in base shear (V_b) versus roof displacement of the building (D). This diagram is then converted to acceleration–displacement terms (AD) using an equivalent single degree of system (ESDOF). The conversion is performed using the first mode participation factor C_0 ($D^* = D/C_0$) and the modal mass ($A = V_b/M$). 2) Plot the capacity diagram on the same graph with the 5%-damped elastic response spectrum that is also in AD format. 3) Select a trial peak deformation demand d_t^* and determine the corresponding pseudo-acceleration A from the capacity diagram, initially assuming $\zeta = 5\%$. 4) Compute ductility $\mu = D^*/u_y$ and calculate the hysteretic damping ζ_h as $\zeta_h = 2(\mu - 1)/\pi\mu$. The equivalent damping ratio is evaluated from a relationship of the form $\zeta_{eq} = \zeta_{eq} + \kappa\zeta_h$, where κ is a damping modification factor that depends on the hysteretic behavior of the system. Update the estimate of d_t^* using the elastic demand diagram for ζ_{eq}. 5) Check for convergence of the displacement d_t^*. When convergence has been achieved, the target displacement of the MDOF system is equal to $d_t = C_0 d_t^*$.

In particular, for the uniform distribution by + X (the most unfavorable combination is X + 0.3Y), the analysis based on the uniform X + 0.3Y distribution of the horizontal loading was performed in seven steps. The performance point (V, D) = (1,242.32, −0.0810) was observed between steps 4 and 5. In **Table 2**, it is observed that plastic hinges have been formed in 9 + 27 = 36 edges of structural elements (denoted in pink (BtoIO) and blue (IOtoLS) columns). However, the limit of the chord rotation angle for the "life safety" performance level (blue) has not been exceeded for any of them. The building is therefore considered safe for this distribution of horizontal loads.

For the uniform distribution by −X (worst combination o −X−0.3Y), the analysis based on the uniform −X−0.3Y distribution of the horizontal loading was performed in eight steps. The performance point (V,D) = (1,241.47, 0.080) was observed between steps 5 and 6. In **Table 2**, it is observed that plastic hinges have been formed in 10 + 25 = 35 edges of structural elements (denoted in pink (BtoIO) and blue (IOtoLS) columns). However, the limit of the chord rotation angle for the "life safety" performance level (blue) has been exceeded for any of them. The building is therefore considered safe for this distribution of horizontal loads. For the uniform distribution by + Y (the most unfavorable combination is Y + 0.3X), the analysis based on the uniform Y + 0.3X distribution of the horizontal loading was performed in eleven steps. The performance point (V, D) = (1,245.32, −0.0170) was observed between steps 6 and 7. In **Table 2**, it is observed that plastic hinges have been formed in 5 + 31 = 36 edges of structural elements (denoted in pink (BtoIO) and blue (IOtoLS) columns). However, the limit of the chord rotation angle for the "life safety" performance level (blue) has been exceeded for any of them. The building is therefore considered safe for this distribution of horizontal loads. For the uniform distribution by −Y (worst combination −Y−0.3X), the analysis based on the uniform −Y−0.3X distribution of the horizontal loading was performed in eleven steps. The performance point (V, D) = (1,241.52, 0.017) was observed between steps 6 and 7. In **Table 2**, it is observed that plastic hinges have been formed in 4 + 32 = 36 edges of structural elements (denoted in pink (BtoIO) and blue (IOtoLS) columns). However, the limit of the chord rotation angle for the "life safety" performance level (blue) has been exceeded for any of them. The building is therefore considered safe for this distribution of horizontal loads.

Accordingly, for the eigenmode-based distribution by + X (the most unfavorable combination is X−0.3Y), the analysis based on the eigenmode-based X−0.3Y distribution of the horizontal loading was performed in eight steps. The performance point (V, D) = (1,105.41, −0.093) was observed between steps 5 and 6. In **Table 2**, it is observed that plastic hinges have been formed in 5 + 33 + 3 = 41 edges of structural elements [denoted in pink (BtoIO), blue (IOtoLS), and light blue (LStoCP) columns)]. In three of them, the limit of the chord rotation angle was exceeded for the "life safety" performance level (blue). These elements

TABLE 3 | Status of plastic hinges in the various steps of pushover analysis.

Step	D (m)	V (kN)	AtoB	BtoIO	IOtoLS	LStoCP	CPtoC	CtoD	DtoE	>E	Total
Uniform X + 03Y											
PP init	−0.0810	1,242.32	—	—	—	—	—	—	—	—	—
5	−0.0887	1,261.43	72	9	27	0	0	0	0	0	108
PP streng	−0.0770	1,356.83	—	—	—	—	—	—	—	—	—
5	−0.0772	1,359.61	78	5	25	0	0	0	0	0	108
Uniform −X−03Y											
PP init	0.0800	1,241.47	—	—	—	—	—	—	—	—	—
6	0.0876	1,262.43	73	10	25	0	0	0	0	0	108
PP streng	0.0770	1,347.15	—	—	—	—	—	—	—	—	—
5	0.0935	1,402.22	72	6	30	0	0	0	0	0	108
Uniform Y + 0.3X											
PP init	−0.0170	1,245.32	—	—	—	—	—	—	—	—	—
7	−0.0185	1,277.45	72	5	31	0	0	0	0	0	108
PP streng	−0.0170	1,369.07	—	—	—	—	—	—	—	—	—
4	−0.0194	1,439.69	68	6	34	0	0	0	0	0	108
Uniform −Y−0.3X											
PP init	0.0170	1,241.52	—	—	—	—	—	—	—	—	—
7	0.0190	1,283.93	72	4	32	0	0	0	0	0	108
PP streng	0.0170	1,354.49	—	—	—	—	—	—	—	—	—
6	0.0177	1,373.64	77	2	29	0	0	0	0	0	108
Eigenmode-based X−0.3Y											
PP init	−0.0930	1,105.41	—	—	—	—	—	—	—	—	—
6	−0.1134	1,138.67	67	5	33	3	0	0	0	0	108
PP streng	−0.0880	1,195.85	—	—	—	—	—	—	—	—	—
6	−0.1026	1,224.96	65	7	36	0	0	0	0	0	108
Eigenmode-based −X + 0.3Y											
PP init	0.0930	1,106.05	—	—	—	—	—	—	—	—	—
6	0.1012	1,121.53	69	4	34	1	0	0	0	0	108
PP streng	0.0890	1,200.39	—	—	—	—	—	—	—	—	—
6	0.0924	1,208.42	68	7	33	0	0	0	0	0	108
Eigenmode-based Y−0.3X											
PP init	0.0130	1,065.75	—	—	—	—	—	—	—	—	—
7	0.0144	1,096.85	73	1	34	0	0	0	0	0	108
PP streng	0.0130	1,136.45	—	—	—	—	—	—	—	—	—
6	0.0135	1,141.22	76	2	30	0	0	0	0	0	108
Eigenmode-based −Y + 0.3X											
PP init	-−0.0130	1,065.47	—	—	—	—	—	—	—	—	—
7	−0.0140	1,087.01	71	2	35	0	0	0	0	0	108
PP streng	−0.0130	1,141.32	—	—	—	—	—	—	—	—	—
6	−0.0134	1,142.45	73	4	31	0	0	0	0	0	108

correspond to beams Δ4 and Δ10 of the ground floor and column K18. For the eigenmode-based distribution by −X (most unfavorable combination o −X + 0.3Y), the analysis based on the eigenmode-based −X + 0.3Y distribution of the horizontal loading was performed in seven steps. The performance point (V, D) = (1,106.05, 0.093) was observed between steps 5 and 6. In **Table 2**, it is observed that plastic hinges have been formed in 4 + 34 + 1 = 39 edges of structural elements [denoted in pink (BtoIO), blue (IOtoLS), and light blue (LStoCP) columns)]. In one of them, the limit of the chord rotation angle was exceeded for the "life safety" performance level (blue). This element corresponds to column K17. For the eigenmode-based distribution by + Y (the worst combination is Y−0.3X), the analysis based on the eigenmode-based Y−0.3X distribution of the horizontal loading was performed in ten steps. The performance point (V, D) = (1,065.75, 0.013) was observed between steps 6 and

TABLE 4 | Ground floor data register.

Elem	b (m)	h (m)	ρ	x (m)	y (m)	cc	t_o (m)	ρ_o	E_s(kPa)	E_{cm}(kPa)	l (m)	Ng (kN)	N1 (kN)	N2 (kN)
K1	0.35	0.35	0.0205	0.175	10.225	0.6	0	0	29.10^6	$30.5{\cdot}10^6$	3	239.01	159.10	76.6
K2	0.45	0.45	0.0186	5.225	10.175	0.6	0	0	29.10^6	$30.5{\cdot}10^6$	3	723.36	482.33	242.33
K3	0.45	0.45	0.0186	11.225	10.175	0.6	0	0	29.10^6	$30.5{\cdot}10^6$	3	365.24	243.71	120.41
K4	0.45	0.45	0.0186	0.225	5.175	0.6	0	0	29.10^6	$30.5{\cdot}10^6$	3	620.43	413.29	206.32
K5	0.45	0.45	0.0186	5.225	5.175	0.6	0	0	29.10^6	$30.5{\cdot}10^6$	3	995.15	663.24	340.53
K6	0.45	0.45	0.0186	11.225	5.175	0.6	0	0	29.10^6	$30.5{\cdot}10^6$	3	333.69	221.20	108.23
K7	0.35	0.35	0.0205	0.175	0.175	0.6	0.1	0.014	29.10^6	$30.5{\cdot}10^6$	3	321.73	214.91	107.3
K8	0.35	0.35	0.0205	5.275	0.175	0.6	0	0	29.10^6	$30.5{\cdot}10^6$	3	248.54	165.75	79.95

7. In **Table 2**, it is observed that plastic hinges have been formed in 1 + 34 = 35 edges of structural elements [denoted in pink (BtoIO) and blue (IOtoLS) columns]. However, none of them has exceeded the limit of the chord rotation angle for the "life safety" performance level (blue). The building is therefore considered safe for this distribution of horizontal loads. For the eigenmode-based distribution by −Y (worst combination o −Y + 0.3X), the analysis based on the eigenmode-based −Y + 0.3X distribution of the horizontal loading was performed in ten steps. The performance point (V, D) = (1,065.47, −0.013) was observed between steps 6 and 7. In **Table 2**, it is observed that plastic hinges have been formed in 2 + 35 = 37 edges of structural elements [denoted in pink (BtoIO) and blue (IOtoLS) columns]. However, none of them has exceeded the limit of the chord rotation angle for the "life safety" performance level (blue). The building is therefore considered safe for this distribution of horizontal loads. A typical moment rotation curve along with the notation of the PP and the coloring of **Table 2** and those that follow is provided in **Figure 5**.

Based on the most unfavorable responses of the structural system obtained for the random design action of EC8 (European Committee for standardization ENV 1998-1-1:1994) through the various distributions of horizontal loads, it is concluded that the structural system as a whole is not safe for the specific intensity of the random action because structural elements Δ6 and Δ10 of the ground floor, K17 and K18, develop deformations larger than the acceptable ones, those defined by the "life safety" performance level in terms of the chord rotation angle. The next step is to strengthen some of these elements to enter the safe region.

5.2 Strengthening Based on Design Provisions

Based on the investigation of the previous section during the assessment of the structural system presented, for some elements (Δ6 and Δ10 of the ground floor, K17, K18), the chord rotation angle exceeded the limit set for "life safety" performance level defined by Kanepe (2017); that is, these elements during the design earthquake develop damage greater than acceptable. Given that all the structural elements are considered primary, the specific structural system as a whole is not considered safe. For this reason, in this part of the investigation, strengthening interventions of these elements will be examined so that the redesigned structural system meets the design goal B1 of Kanepe (2017), that is, for the design earthquake (10% probability of exceeding within the conventional life time of 50 years), all structural elements of the construction to be located before the level corresponding to the "life safety" performance level. After various tests of interventions that did not always have positive results for the redesigned structural system, strengthening column K7 along its height with RC jacketing was selected. The process of strengthening and re-assessment of the redesigned structural system, during which this new design is considered safe (meeting the design objective), is described in this section.

A 10 cm RC jacketing with 8Ø20 reinforcement is used to strengthen column K7. The strengthened structural system is assessed by means of nonlinear static analyses based on the distributions of the horizontal loads. Note that for the strengthened structural system, the first eigenmode is the fundamental one along the Y direction while the second one is along the X direction. In **Table 3**, the performance points for the strengthened structural system are compared with those of the original one.

As observed from **Table 3**, the performance points of the strengthened structural system for the various loading combinations show a small increase of the base shear by 90–130 kN, of the order of about 8%. As far as the target displacements are concerned, they are significantly reduced for the distributions of the X direction while they practically remain unchanged for the distributions of the Y direction. This can be partially explained as follows: in the X direction, column K7 participates in the baring frame K7-Δ10-K8, where both columns K7 and K8 contribute with the less rigid orientation of their cross section. Thus, it becomes the weakest one among all baring frames of the structural system. Along the Y direction, strengthening did not contribute significantly because the Y-baring frames were originally more rigid. Due to the reduction of target displacements along the X direction, no structural element of the redesigned structural system develops any longer damage for the design earthquake larger than the acceptable ones, those defined by the "life safety" performance level. For the original structural system, distributions along the X direction developed structural elements exceeding this performance level. In addition, the number of edges entering the plastic zone was also reduced in most loading distributions. As a general conclusion, it can be said that the specific strengthening operation is considered successful because the redesigned structural system is now safe and shows better structural behavior for the design earthquake.

TABLE 5 | Stiffness and strength eccentricities for the two structural systems.

	Stiffness eccentricity		Strength eccentricity					
	Same for all stories		Ground story		1st story		2nd story	
	Original	Strengthened	Original	Strengthened	Original	Strengthened	Original	Strengthened
x_{CR} (m)	5.77	4.67	5.29	4.75	5.33	4.73	5.40	4.72
y_{CR} (m)	6.52	5.27	6.33	5.68	6.33	5.61	6.33	5.52
$e_{CM\text{-}CR}$ or $e_{CM\text{-}CV}$ (m)	1.03	0.86	0.52	0.44	0.55	0.50	0.63	0.60
Variation (%)	−17%		−15%		−9%		−5%	

TABLE 6 | Column reinforcement thickness to minimize the strength eccentricity of the second floor.

Column	2nd story (Problem A)		1st story (Problem B)		Ground story (Problem C)	
	RC jacket		RC jacket		RC jacket	
	Thickness (cm)	Reinforcement percentage	Thickness (cm)	Reinforcement percentage	Thickness (cm)	Reinforcement percentage
K1	20	0.0260	0	0.0	20	0.0290
K2	20	0.0167	20	0.0400	0	0
K3	16	0.0278	0	0.0	0	0
K4	0	0.0	16	0.0314	0	0
K5	20	0.0400	0	0.0	20	0.0216
K6	0	0.0	20	0.0100	15	0.0296
K7	10	0.0400	0	0.0	10	0.0100
K8	15	0.0400	20	0.0255	0	0

TABLE 7 | Minimized strength eccentricity values obtained for the tree problems.

Story	$e_{CM\text{-}CV}$ (m)		
	Problem A	Problem B	Problem C
Ground	0.0290	0.0094	0.0003
1st	0.0162	0.0018	0.0143
2nd	0.00063	0.0065	0.0260

5.3 Strengthening Based on Minimizing Torsional Response

In this part of the study, the process described previously for calculating the components of the problem formulations is integrated into the ICA algorithm, aiming to minimize the torsional response of the building. Previously, the structural system was strengthened to meet the design target B1 of Kanepe (2017); then, two cases are considered for strengthening the structural system based on improved torsional response: minimum stiffness and strength eccentricities. As a result, the following information is obtained through the solution of the two optimization problems: 1) thickness of RC jacketing to strengthen the columns, in case of minimizing stiffness eccentricity, and 2) thickness and reinforcement of RC jacketing to strengthen the columns, in case of minimizing the eccentricity of strengths. The designs obtained for the two cases are assessed by means of nonlinear static analyses in comparison with the original design (OD: original design) and the re-design based on strengthening by Kanepe (2017) (KSD: KANEPE based strengthened design). For the implementation of the ICA-based strengthening design framework, a set of data needs to be provided required by the formulation of the optimization problem. Based on these data and with reference to the problem formulation (rigidity or strength eccentricity) during the iterations of the ICA search procedure, new designs, defined with respect to the location, width, and reinforcement of the RC jacketing of each vertical structural element, are derived. For handling the discrete design variables, the procedure described by Lagaros et al. (2022) is followed, according to which they are treated as equivalent continuous variables, using the correction function of the following simple expression:

$$t_j = \frac{floor\left(t_j \times 10\right)}{10}, \; for\; discrete\; variables\; of\; 0.1\; step\; size. \tag{18}$$

5.3.1 Entry of Building Data Into Problem Formulation

According to the previous description, the data required for the two problem formulations are configured (**Table 4**) below.

The plan view is the same for all stories, and the only difference can be found in the last column corresponding to the axial forces of the columns. The axial forces of the columns are obtained by means of linear analyses of KBD for the combination G + 0.3Q. Regarding the minimization problem of strength eccentricity, three cases will be examined (one for each story). The solution corresponding to the best compromise solution will be adopted, where lower eccentricities for all three stories are derived. The data required (columns 2 to 13 of **Table 4**) for solving the minimization

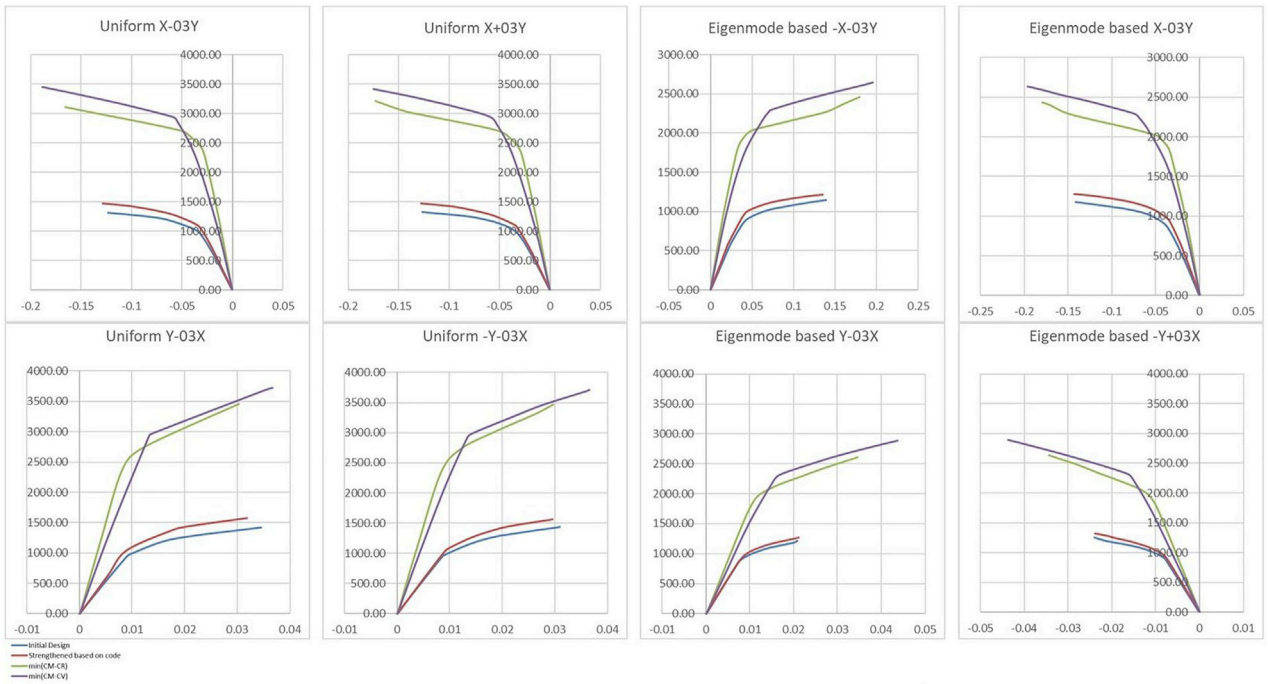

FIGURE 6 | Capacity curves.

problem of stiffness eccentricity are the same for all three stories. In particular, for each vertical structural element, ρ and ρ_o denote the percentage of longitudinal reinforcement and the one of existing RC jackets, respectively; t_o refers to the width of the RC jackets; x and y denote the coordinates of the center of mass; and cc is the cracking coefficient; that is, *Ng* stands for the axial force of the ground floor, *N1* of the first floor, and *N2* for the second one. For the RC jacketing, concrete quality C20/25 is considered, as well as steel reinforcement B500C. The mass centers of all floors coincide because the plan view is the same for all stories, thus creating a centripetal axis for the building. Uniform distribution of the vertical loads was considered on the floor slabs; thus, the mass center coincides with the geometric center of the floors.

5.3.2 Eccentricities of Initial and Strengthened by KANEPE Structural System

The eccentricities of the original structural system and those of the strengthened one are calculated first (**Table 5**), where variation stands for the reduction of the eccentricity values corresponding to the strengthened design compared to the ones of the original design. The axial forces used to calculate the strength eccentrics are derived from linear analyses performed for the two structural systems (OD and KBD) for the combination G + 0.3Q. For the case of KBD, they are identical to those of **Table 4**.

5.3.3 Minimize Stiffness Eccentricity

In this part of the study, the problem of the minimum rigidity eccentricity problem is solved and the results obtained are discussed. The specific problem is formulated once. Thus, a unique solution is derived for all three stories. Given that ICA is an evolutionary search algorithm, it operates based on a population of solutions. The convergence history records the best solution found so far and that of the average value among the population members. Although the convergence history of the optimization procedure takes place shortly before the 2000 iterations, ICA managed to significantly reduce the stiffness eccentricity (cost function) value in less than 500 iterations. When an empire is left, the average cost is equal to the minimum. The optimal solution is located in the position (imperialist position) (0.19, 0.20, 0, 0.20, 0.15, 0.20, 0, 0.19) and has a cost, that is, giving value to the objective function of the problem (imperialist cost) equal to e = 0.0074 m ≈ 7 mm. Each column will therefore be reinforced accordingly. The K7 column is already reinforced with a 10 cm RC jacket. Its final RC jacket will be 10 cm. The RC jackets, for the design of the new body with the minimized rigidity eccentricity, are introduced with the minimum mechanical reinforcement rate of 1%.

5.3.4 Minimize Strength Eccentricity

In this part of the study, the minimum strength eccentricity problem is solved and the results obtained are discussed. The iteration histories of the problems solved independently for the three stories are obtained. Similar to the problem of minimum rigidity, the convergence history is recorded for each of the three problems solved, with respect to the best solution found so far and the average objective function value. The strength eccentricity minimization problem is more time-consuming (1 min/iteration) in contrast to the stiffness eccentricity one, where 2,500 iterations

TABLE 8 | Status of plastic hinges in the various steps of pushover analysis.

Step	D (m)	V (kN)	AtoB	BtoIO	IOtoLs	LStoCP	CPtoC	CtoD	DtoE	>E	Total
Uniform X + 03Y											
PP IN	–0.0810	1,242.32	—	—	—	—	—	—	—	—	—
5	–0.0887	1,261.43	72	9	27	0	0	0	0	0	108
PP DC	–0.0770	1,356.83	—	—	—	—	—	—	—	—	—
5	–0.0772	1,359.61	78	5	25	0	0	0	0	0	108
PP CR	–0.0530	2,715.96	—	—	—	—	—	—	—	—	—
6	–0.0707	2,789.60	69	1	38	0	0	0	0	0	108
PP CV	–0.0610	2,947.67	—	—	—	—	—	—	—	—	—
4	–0.0610	2,954.88	73	9	26	0	0	0	0	0	108
Uniform –X–03Y											
PP IN	0.0800	1,241.47	—	—	—	—	—	—	—	—	—
6	0.0876	1,262.43	73	10	25	0	0	0	0	0	108
PP DC	0.0770	1,347.15	—	—	—	—	—	—	—	—	—
5	0.0935	1,402.22	72	6	30	0	0	0	0	0	108
PP CR	0.0540	2,714.78	—	—	—	—	—	—	—	—	—
6	0.0851	2,830.27	68	0	40	0	0	0	0	0	108
PP CV 5	0.0600	2,942.17	—	—	—	—	—	—	—	—	—
5	0.0614	2,960.08	70	11	27	0	0	0	0	0	108
Uniform Y + 0.3X											
PP IN	–0.0170	1,245.32	—	—	—	—	—	—	—	—	—
7	–0.0185	1,277.45	72	5	31	0	0	0	0	0	108
PP DC	-0.0170	1,369.07	—	—	—	—	—	—	—	—	—
4	–0.0194	1,439.69	68	6	34	0	0	0	0	0	108
PP CR	–0.0130	2,762.90	—	—	—	—	—	—	—	—	—
6	–0.0168	2,950.89	68	1	39	0	0	0	0	0	108
PP CV	–0.0140	2,987.62	—	—	—	—	—	—	—	—	—
3	–0.0139	2,984.51	74	7	27	0	0	0	0	0	108
Uniform –Y–0.3X											
PP IN	0.0170	1,241.52	—	—	—	—	—	—	—	—	—
7	0.0190	1,283.93	72	4	32	0	0	0	0	0	108
PP DC	0.0170	1,354.49	—	—	—	—	—	—	—	—	—
6	0.0177	1,373.64	77	2	29	0	0	0	0	0	108
PP CR	0.0130	2,769.07	—	—	—	—	—	—	—	—	—
4	0.0188	3,023.95	68	1	39	0	0	0	0	0	108
PP CV	0.0140	2,966.24	—	—	—	—	—	—	—	—	—
4	0.0141	2,974.64	73	5	30	0	0	0	0	0	108
Eigenmode-based X–0.3Y											
PP IN	–0.0930	1,105.41	—	—	—	—	—	—	—	—	—
6	–0.1134	1,138.67	67	5	33	3	0	0	0	0	108
PP DC	–0.0880	1,195.85	—	—	—	—	—	—	—	—	—
6	–0.1026	1,224.96	65	7	36	0	0	0	0	0	108
PP CR	–0.0640	2063.18	—	—	—	—	—	—	—	—	—
6	–0.0808	2,113.77	70	0	38	0	0	0	0	0	108
PP CV	–0.0690	2,241.80	—	—	—	—	—	—	—	—	—
5	–0.0745	2,289.60	68	9	31	0	0	0	0	0	108
Eigenmode-based –X + 0.3Y											
PP IN	0.0930	1,106.05	—	—	—	—	—	—	—	—	—
6	0.1012	1,121.53	69	4	34	1	0	0	0	0	108
PP DC	0.0890	1,200.39	—	—	—	—	—	—	—	—	—
6	0.0924	1,208.42	68	7	33	0	0	0	0	0	108
PP CR	0.0630	2059.63	—	—	—	—	—	—	—	—	—
6	0.0751	2093.18	68	3	37	0	0	0	0	0	108
PP CV	0.0690	2,240.31	—	—	—	—	—	—	—	—	—
5	0.0747	2,293.44	68	11	29	0	0	0	0	0	108

(Continued on following page)

TABLE 8 | (*Continued*) Status of plastic hinges in the various steps of pushover analysis.

Step	D (m)	V (kN)	AtoB	BtoIO	IOtoLs	LStoCP	CPtoC	CtoD	DtoE	>E	Total
Eigenmode-based Y–0.3X											
PP IN	0.0930	1,106.05	—	—	—	—	—	—	—	—	—
6	0.1012	1,121.53	69	4	34	1	0	0	0	0	108
PP DC	0.0890	1,200.39	—	—	—	—	—	—	—	—	—
6	0.0924	1,208.42	68	7	33	0	0	0	0	0	108
PP CR	0.0630	2059.63	—	—	—	—	—	—	—	—	—
6	0.0751	2093.18	68	3	37	0	0	0	0	0	108
PP CV	0.069	2,240.31	—	—	—	—	—	—	—	—	—
5	0.0747	2,293.44	68	11	29	0	0	0	0	0	108
Eigenmode-based –Y + 0.3X											
PP IN	–0.0130	1,065.47	—	—	—	—	—	—	—	—	—
7	–0.0140	1,087.01	71	2	35	0	0	0	0	0	108
PP DC	–0.0130	1,141.32	—	—	—	—	—	—	—	—	—
6	–0.0134	1,142.45	73	4	31	0	0	0	0	0	108
PP CR	–0.0160	2,138.10	—	—	—	—	—	—	—	—	—
6	–0.0188	2,221.73	67	1	40	0	0	0	0	0	108
PP CV	–0.0160	2,311.81	—	—	—	—	—	—	—	—	—
5	–0.0164	2,317.61	69	8	31	0	0	0	0	0	108

were performed in just a few minutes. Thus, fewer iterations were chosen to identify convergence (around 100). However, as shown in the above history diagrams, the strength eccentricity value is reduced quickly, reaching zero during the first 40 to 80 iterations. Specifically, the optimal solution is located in the position (imperialist position) reported for all three stories in **Table 6**.

The cost values obtained for the three problems A, B, and C along with the eccentricities of the other two stories are provided in **Table 7**. For Problem A, the imperialist cost value is equal to e = 0.00063 m < 1 mm. For Problem B, the imperialist cost value is equal to e = 0.0018 m ≈ 2 mm. For Problem C, the imperialist cost value is equal to e = 0.0003 m < 1 mm. For this solution, the strength eccentricities of the other floors of the building are as follows:

It can be noticed that the optimal floor solutions show a sensitivity because they differ quite a lot from floor to floor. Nevertheless, the optimal solution obtained for the first floor (Problem B) gives low values of eccentricity to the other floors (less than 1 cm). Therefore, it is neither realistic nor practical to use different RC jacketing for a given column along the stories of the building. The strengthening solution obtained through Problem B, according to **Table 7**, is used.

5.4 Assessment of the Strengthened Structural Systems

5.4.1 Eigenmode Analyses

The results of the eigenmode analyses performed for each of the two new structural systems derived through minimization of the eccentricities are presented below. Based on the eigenvalue analyses results, it seems that, for both structural systems, the first eigenmode is the fundamental one along the Y direction while the second eigenmode is the fundamental one along the X direction. It is also worth mentioning that the first three eigenperiod values were significantly reduced in relation to the ones of the original structural system, as expected because due to strengthening, the structural systems became significantly more rigid compared to the original one. Also, note that the mass participation rate of the third eigenmode, which is mainly torsional, was decreased.

5.4.2 Nonlinear Static Analyses

Nonlinear static analyses are performed for the two new structural systems. Their seismic behavior is compared with the corresponding one of the original and the strengthened ones designed to meet the B1 goal of Kanepe (2017). The 16 distributions of the horizontal loads mentioned earlier are also used to perform these analyses. The capacity curves derived are presented first (**Figure 6**), where an estimate of how the interventions affected the overall behavior of the structural systems can be obtained. For every horizontal load distribution, two groups of curves are obtained: those of the original and strengthened designs and those of the designs obtained through eccentricities minimization. These two groups of curves show similar stiffness and capacity. As observed in **Figure 6**, the ultimate load capacity and the initial stiffness of the designs obtained through eccentricity minimization were almost doubled, while the post-cracking stiffness was increased slightly.

Subsequently, the behavior of the structural systems measured for the design earthquake (target displacement, yield base shear demand) for the most unfavorable distributions per direction is presented. Finally, the tables containing the ductility demand of the columns also for the design earthquake are presented. The structural systems derived through the optimization process in comparison to the original and strengthened based on Kanepe (2017) depict a large increase in the stiffness and bearing capacity (almost doubled) and a significant increase in ductility due to the extensive use of RC jackets at the columns. In **Table 8** the following notations are used, performance points for the initial

TABLE 9 | Required ductility values of the columns for the distributions of the horizontal loads.

	Initial design			Strengthened by							
				Code			min (CM-CR)			min (CM-CV)	
	θ_y	$\theta_{pl,dem}$	μ_{dem}	θ_y	$\theta_{pl,dem}$	μ_{dem}	θ_y	$\theta_{pl,dem}$	μ_{dem}	θ_y	$\theta_{pl,dem}$	μ_{dem}
Ground floor columns—uniform distribution X + 0.3Y												
K11up	0.0090	0.0000	1.00	0.0090	0.0000	1.00	0.0081	0.0000	1.00	0.0090	0.0000	1.00
K11dn		0.0096	2.07		0.0072	1.80		0.0041	1.51		0.0000	1.00
K12up	0.0073	0.0000	1.00	0.0073	0.0000	1.00	0.0078	0.0000	1.00	0.0087	0.0000	1.00
K12dn		0.0107	2.47		0.0086	2.18		0.0046	1.59		0.0000	1.00
K13up	0.0073	0.0000	1.00	0.0073	0.0000	1.00	0.0073	0.0000	1.00	0.0073	0.0000	1.00
K13dn		0.0106	2.45		0.0086	2.17		0.0033	1.45		0.0009	1.12
K14up	0.0073	0.0000	1.00	0.0073	0.0000	1.00	0.0078	0.0000	1.00	0.0084	0.0000	1.00
K14dn		0.0094	2.29		0.0069	1.94		0.0045	1.58		0.0004	1.05
K15up	0.0073	0.0004	1.06	0.0073	0.0000	1.00	0.0085	0.0000	1.00	0.0073	0.0000	1.00
K15dn		0.0100	2.37		0.0074	2.01		0.0044	1.51		0.0004	1.06
K16up	0.0073	0.0000	1.00	0.0073	0.0000	1.00	0.0078	0.0000	1.00	0.0077	0.0000	1.00
K16dn		0.0103	2.41		0.0076	2.04		0.0046	1.59		0.0023	1.30
K17up	0.0090	0.0000	1.00	0.0094	0.0000	1.00	0.0098	0.0000	1.00	0.0098	0.0000	1.00
K17dn		0.0085	1.95		0.0072	1.76		0.0031	1.32		0.0009	1.09
K18up	0.0090	0.0003	1.04	0.0090	0.0000	1.00	0.0081	0.0000	1.00	0.0085	0.0000	1.00
K18dn		0.0100	2.11		0.0067	1.75		0.0042	1.52		0.0008	1.09
μ	—	—	1.64	—	—	1.48	—	—	1.26	—	—	1.04
σ	—	—	0.64	—	—	0.49	—	—	0.26	—	—	0.08
CoV	—	—	0.39	—	—	0.33	—	—	0.21	—	—	0.07
1st story columns—uniform distribution X + 0.3Y												
K21up	0.0090	0.0009	1.10	0.0090	0.0000	1.00	0.0081	0.0000	1.00	0.0090	0.0000	1.00
K21dn		0.0000	1.00		0.0000	1.00		0.0000	1.00		0.0000	1.00
K22up	0.0073	0.0024	1.33	0.0073	0.0013	1.18	0.0078	0.0000	1.00	0.0087	0.0000	1.00
K22dn		0.0000	1.00		0.0000	1.00		0.0000	1.00		0.0000	1.00
K23up	0.0073	0.0013	1.17	0.0073	0.0000	1.00	0.0073	0.0000	1.00	0.0073	0.0000	1.00
K23dn		0.0000	1.00		0.0000	1.00		0.0000	1.00		0.0000	1.00
K24up	0.0073	0.0000	1.00	0.0073	0.0000	1.00	0.0078	0.0000	1.00	0.0084	0.0000	1.00
K24dn		0.0000	1.00		0.0000	1.00		0.0000	1.00		0.0000	1.00
K25up	0.0073	0.0028	1.38	0.0073	0.0012	1.17	0.0085	0.0000	1.00	0.0073	0.0000	1.00
K25dn		0.0000	1.00		0.0000	1.00		0.0000	1.00		0.0000	1.00
K26up	0.0073	0.0013	1.18	0.0073	0.0000	1.00	0.0078	0.0000	1.00	0.0077	0.0000	1.00
K26dn		0.0000	1.00		0.0000	1.00		0.0000	1.00		0.0000	1.00
K27up	0.0090	0.0011	1.13	0.0094	0.0000	1.00	0.0098	0.0000	1.00	0.0098	0.0000	1.00
K27dn		0.0000	1.00		0.0000	1.00		0.0000	1.00		0.0000	1.00
K28up	0.0090	0.0026	1.29	0.0090	0.0008	1.09	0.0081	0.0000	1.00	0.0085	0.0000	1.00
K28dn		0.0000	1.00		0.0000	1.00		0.0000	1.00		0.0000	1.00
μ	—	—	1.10	—	—	1.03	—	—	1.00	—	—	1.00
σ	—	—	0.13	—	—	0.06	—	—	0.00	—	—	0.00
CoV	—	—	0.12	—	—	0.06	—	—	0.00	—	—	0.00
2nd story columns—uniform distribution X + 0.3Y												
K31up	0.0090	0.0000	1.00	0.0090	0.0000	1.00	0.0081	0.0000	1.00	0.0090	0.0014	1.16
K31dn		0.0000	1.00		0.0000	1.00		0.0000	1.00		0.0000	1.00
K32up	0.0073	0.0000	1.00	0.0073	0.0000	1.00	0.0078	0.0000	1.00	0.0087	0.0000	1.00
K32dn		0.0000	1.00		0.0000	1.00		0.0000	1.00		0.0000	1.00
K33up	0.0073	0.0000	1.00	0.0073	0.0000	1.00	0.0073	0.0000	1.00	0.0040	0.0000	1.00
K33dn		0.0000	1.00		0.0000	1.00		0.0000	1.00		0.0000	1.00
K34up	0.0073	0.0000	1.00	0.0073	0.0000	1.00	0.0078	0.0000	1.00	0.0084	0.0000	1.00
K34dn		0.0000	1.00		0.0000	1.00		0.0000	1.00		0.0000	1.00
K35up	0.0073	0.0000	1.00	0.0073	0.0000	1.00	0.0085	0.0000	1.00	0.0073	0.0019	1.26
K35dn		0.0000	1.00		0.0000	1.00		0.0000	1.00		0.0000	1.00
K36up	0.0073	0.0000	1.00	0.0073	0.0000	1.00	0.0078	0.0000	1.00	0.0077	0.0000	1.00
K36dn		0.0000	1.00		0.0000	1.00		0.0000	1.00		0.0000	1.00
K37up	0.0090	0.0000	1.00	0.0098	0.0000	1.00	0.0098	0.0000	1.00	0.0098	0.0000	1.00
K37dn		0.0000	1.00		0.0000	1.00		0.0000	1.00		0.0000	1.00
K38up	0.0090	0.0000	1.00	0.0090	0.0000	1.00	0.0081	0.0000	1.00	0.0085	0.0000	1.00
K38dn		0.0000	1.00		0.0000	1.00		0.0000	1.00		0.0000	1.00

(Continued on following page)

TABLE 9 | (*Continued*) Required ductility values of the columns for the distributions of the horizontal loads.

	Initial design				Strengthened by							
					Code			min (CM-CR)			min (CM-CV)	
	θ_y	$\theta_{pl,dem}$	μ_{dem}	θ_y	$\theta_{pl,dem}$	μ_{dem}	θ_y	$\theta_{pl,dem}$	μ_{dem}	θ_y	$\theta_{pl,dem}$	μ_{dem}
μ	—	—	1.00	—	—	1.00	—	—	1.00	—	—	1.03
σ	—	—	0.00	—	—	0.00	—	—	0.00	—	—	0.07
CoV	—	—	0.00	—	—	0.00	—	—	0.00	—	—	0.07
Ground floor columns—uniform distribution Y + 0.3X												
K11up	0.0090	0.0003	1.03	0.0090	0.0000	1.00	0.0081	0.0000	1.00	0.0090	0.0000	1.00
K11dn		0.0028	1.32		0.0022	1.25		0.0016	1.19		0.0000	1.00
K12up	0.0073	0.0000	1.00	0.0073	0.0000	1.00	0.0078	0.0000	1.00	0.0087	0.0000	1.00
K12dn		0.0034	1.46		0.0027	1.37		0.0016	1.21		0.0000	1.00
K13up	0.0073	0.0000	1.00	0.0073	0.0000	1.00	0.0073	0.0000	1.00	0.0073	0.0000	1.00
K13dn		0.0035	1.48		0.0027	1.37		0.0014	1.19		0.0004	1.05
K14up	0.0073	0.0000	1.00	0.0073	0.0000	1.00	0.0078	0.0000	1.00	0.0084	0.0000	1.00
K14dn		0.0030	1.40		0.0030	1.41		0.0016	1.20		0.0001	1.02
K15up	0.0073	0.0000	1.00	0.0073	0.0000	1.00	0.0085	0.0000	1.00	0.0073	0.0000	1.00
K15dn		0.0033	1.45		0.0035	1.48		0.0013	1.16		0.0002	1.03
K16up	0.0073	0.0000	1.00	0.0073	0.0000	1.00	0.0078	0.0000	1.00	0.0077	0.0000	1.00
K16dn		0.0024	1.33		0.0027	1.37		0.0016	1.21		0.0007	1.10
K17up	0.0090	0.0000	1.00	0.0094	0.0000	1.00	0.0098	0.0000	1.00	0.0098	0.0000	1.00
K17dn		0.0033	1.37		0.0035	1.37		0.0014	1.14		0.0003	1.03
K18up	0.0090	0.0000	1.00	0.0090	0.0000	1.00	0.0081	0.0000	1.00	0.0085	0.0000	1.00
K18dn		0.0024	1.26		0.0036	1.40		0.0017	1.21		0.0002	1.03
μ	—	—	1.19	—	—	1.19	—	—	1.09	—	—	1.02
σ	—	—	0.20	—	—	0.19	—	—	0.10	—	—	0.03
CoV	—	—	0.16	—	—	0.16	—	—	0.09	—	—	0.03
1st story columns—uniform distribution Y + 0.3X												
K21up	0.0090	0.0006	1.07	0.0090	0.0004	1.05	0.0081	0.0000	1.00	0.0090	0.0000	1.00
K21dn		0.0000	1.00		0.0000	1.00		0.0000	1.00		0.0000	1.00
K22up	0.0073	0.0006	1.08	0.0073	0.0003	1.04	0.0078	0.0000	1.00	0.0087	0.0000	1.00
K22dn		0.0000	1.00		0.0000	1.00		0.0000	1.00		0.0000	1.00
K23up	0.0073	0.0030	1.41	0.0073	0.0002	1.03	0.0073	0.0000	1.00	0.0073	0.0000	1.00
K23dn		0.0000	1.00		0.0000	1.00		0.0000	1.00		0.0000	1.00
K24up	0.0073	0.0007	1.10	0.0073	0.0005	1.06	0.0078	0.0000	1.00	0.0084	0.0000	1.00
K24dn		0.0000	1.00		0.0000	1.00		0.0000	1.00		0.0000	1.00
K25up	0.0073	0.0006	1.08	0.0073	0.0005	1.07	0.0085	0.0000	1.00	0.0073	0.0000	1.00
K25dn		0.0000	1.00		0.0000	1.00		0.0000	1.00		0.0000	1.00
K26up	0.0073	0.0000	1.00	0.0073	0.0000	1.00	0.0078	0.0000	1.00	0.0077	0.0000	1.00
K26dn		0.0000	1.00		0.0000	1.00		0.0000	1.00		0.0000	1.00
K27up	0.0090	0.0007	1.08	0.0094	0.0000	1.00	0.0098	0.0000	1.00	0.0098	0.0000	1.00
K27dn		0.0000	1.00		0.0000	1.00		0.0000	1.00		0.0000	1.00
K28up	0.0090	0.0005	1.06	0.0090	0.0038	1.42	0.0081	0.0000	1.00	0.0085	0.0000	1.00
K28dn		0.0000	1.00		0.0000	1.00		0.0000	1.00		0.0000	1.00
μ	—	—	1.05	—	—	1.04	—	—	1.00	—	—	1.00
σ	—	—	0.10	—	—	0.10	—	—	0.00	—	—	0.00
CoV	—	—	0.09	—	—	0.10	—	—	0.00	—	—	0.00
2nd story columns—uniform distribution Y + 0.3X												
K31up	0.0090	0.0000	1.00	0.0090	0.0000	1.00	0.0081	0.0000	1.00	0.0090	0.0002	1.03
K31dn		0.0000	1.00		0.0000	1.00		0.0000	1.00		0.0000	1.00
K32up	0.0073	0.0000	1.00	0.0073	0.0000	1.00	0.0078	0.0000	1.00	0.0087	0.0000	1.00
K32dn		0.0000	1.00		0.0000	1.00		0.0000	1.00		0.0000	1.00
K33up	0.0073	0.0000	1.00	0.0073	0.0000	1.00	0.0073	0.0000	1.00	0.0040	0.0000	1.00
K33dn		0.0000	1.00		0.0000	1.00		0.0000	1.00		0.0000	1.00
K34up	0.0073	0.0000	1.00	0.0073	0.0001	1.01	0.0078	0.0000	1.00	0.0084	0.0000	1.00
K34dn		0.0000	1.00		0.0000	1.00		0.0000	1.00		0.0000	1.00
K35up	0.0073	0.0000	1.00	0.0073	0.0001	1.01	0.0085	0.0000	1.00	0.0073	0.0006	1.08
K35dn		0.0000	1.00		0.0000	1.00		0.0000	1.00		0.0000	1.00
K36up	0.0073	0.0000	1.00	0.0073	0.0000	1.00	0.0078	0.0000	1.00	0.0077	0.0000	1.00
K36dn		0.0000	1.00		0.0000	1.00		0.0000	1.00		0.0000	1.00

(Continued on following page)

TABLE 9 | (*Continued*) Required ductility values of the columns for the distributions of the horizontal loads.

	Initial design			Strengthened by							
				Code			min (CM-CR)			min (CM-CV)	
	θ_y	$\theta_{pl,dem}$	μ_{dem}	θ_y	$\theta_{pl,dem}$	μ_{dem}	θ_y	$\theta_{pl,dem}$	μ_{dem}	θ_y	$\theta_{pl,dem}$	μ_{dem}
K37up	0.0090	0.0000	1.00	0.0098	0.0000	1.00	0.0098	0.0000	1.00	0.0098	0.0000	1.00
K37dn		0.0000	1.00		0.0000	1.00		0.0000	1.00		0.0000	1.00
K38up	0.0090	0.0000	1.00	0.0090	0.0000	1.00	0.0081	0.0000	1.00	0.0085	0.0000	1.00
K38dn		0.0000	1.00		0.0000	1.00		0.0000	1.00		0.0000	1.00
μ	—	—	1.00	—	—	1.00	—	—	1.00	—	—	1.01
σ	—	—	0.00	—	—	0.00	—	—	0.00	—	—	0.02
CoV	—	—	0.00	—	—	0.00	—	—	0.00	—	—	0.02

design (**PP IN**), strengthened based on the design code (**PP DC**), strengthened based on minimum rigidity eccentricity (**PP CR**), and strengthened based on minimum strength eccentricity (**PP CV**).

Comparing the performance points (PPs) of the structural systems derived through the optimization process with the original one and the strengthened one based on the design code (Kanepe, 2017), the following observations can be stated: 1) the base shear value for PP was almost doubled for both new structural systems. 2) The deformation for PP was significantly reduced for almost all horizontal load combinations examined (by 25%–30%). These results were more or less expected because, as observed previously, the rigidity and bearing capacity of the two new structural systems increased significantly compared to the original and strengthened ones. However, it is worth noting that 3) both new structural systems derived are considered safe because no end of structural element exceeds the "life safety" performance level. The number of ends of columns that enter the plastic zone is reduced (limited to the bottom ends of the ground floor columns). However, the total number of edges of the structural elements that enter the plastic zone does not change substantially. This is due to increase of base shear. Thus, beams without being strengthened further take over larger forces, resulting in plasticized ends. Even so, no beam exceeded the "life safety" performance level.

5.4.3 Ductility Demand of the Columns

The view of the structure where deformation due to torsion is added to the one due to translational motion is called the "flexible view," while the view on which deformation due to torsion is subtracted due to translational motion is called "rigid view." It was observed through nonlinear static analyses that increased inelastic deformation is observed for the flexible side and reduced for the rigid in comparison to the corresponding deformation of symmetrical structural systems. Therefore, the unbalanced distribution of the ductility demand to eccentric buildings can lead to failures due to unexpected excitations (Stathopoulos and Anagnostopoulos, 2005; Anagnostopoulos et al., 2015). In this section, the distribution of ductility demand for the design earthquake will be measured for the columns of each floor for all four structural systems. In order to control the distribution of ductility demand, the coefficient of variation (*CoV*) will be used, which is a measure of the relative variability and measures the spread of the data in relation to the mean value defined as

$$CoV = \frac{StDev}{Mean} \tag{19}$$

where *StDev* is the standard deviation and *Mean* is the mean value of data. The ductility of beams or columns is defined as follows:

$$\mu_\theta = 1 + \frac{\theta_{pl}}{\theta_y}, \tag{20}$$

where θ_{pl} is the plastic rotation angle at the edges of the structural elements and θ_y is the yield rotation angle, both calculated based on Kanepe (2017). In order to calculate the required ductility, the value of θ_{pl}, for each edge of the column structural element for the design earthquake of EC8, is calculated. Based on the values of θ_{pl} and θ_y of the ends of the columns and using **Eq. 19**, **Table 9** is formed. Based on the results presented in **Table 9**, it can be observed that the distribution of ductility in the columns for the two optimization-based strengthening designs is more balanced in relation to the original structural system and the one strengthened based on the design goal B1 of Kanepe (2017), resulting into more controllable structural performance.

The ground floor is a representative story to identify changes in ductility distribution over the columns where plastic hinges are formed at the edges of all columns in each structural system. On the ground floor, it is observed that *CoV* of ductility demand decreases for the designs resulting from the optimization process. Thus, unbalanced distribution of ductility demand over the columns is mitigated. For the first story, in the case of the structural systems derived through the solution of the minimum stiffness and strength eccentricity problems due to higher stiffness, no plastic hinge was created, while for the second story where, as expected, due to the lowest stress intensity developed, none plastic hinge was formed in any of the four structural systems.

6 CONCLUSION AND DISCUSSION

In the present study, the aim was to minimize the torsional response of a multi-story reinforced concrete (RC) building by strengthening its columns. The ultimate goal was to improve its structural behavior

through an automized procedure that could be easily utilized in relevant structural analysis and design software. In this direction, design optimization problems were formulated based on the torsional response criterion. Therefore, the problem was mathematically developed with two independent formulations: minimization of the eccentricity between mass and rigidity centers and minimization of the eccentricity between mass and strength centers. The first one was formulated as a discrete structural optimization problem, where the dimensions of the columns' cross sections were the unknowns. In contrast, the second was formulated as a mixed one, where, in addition to the dimensions, the percentage of the reinforcement was the unknowns. The two problems were solved using the evolutionary algorithm called the imperialist competitive algorithm (ICA).

In the first part of the investigation, the case study building was assessed based on nonlinear static analyses aiming to assess its behavior for the case of the design earthquake. The nonlinear static analyses revealed that larger deformations are observed along the X direction. Subsequently, strengthening interventions were to be decided on some of the structural elements aiming to meet the B1 design goal of Kanepe (2017), that is, for the design seismic action, the structural system should not exceed the "life safety" performance level. Given that all structural elements were considered primary ones, none of them should exceed the specified performance level. In order to meet these needs, it was decided to strengthen column K7 using RC jacketing, resulting in the reduction of target deformation demands along the X direction, and no structural element of the structural system developed damage larger than the acceptable one for the design earthquake.

The next step, in terms of strengthening, used the optimization framework developed to minimize stiffness and strength eccentricities. By means of nonlinear static analyses performed for the two new structural systems resulting by solving the two optimization problems, it was found that the bearing capacity and stiffness almost doubled compared to the original and the strengthened ones based on Kanepe (2017), while their ductility was significantly increased. The deformation corresponding to the performance point was significantly reduced for almost all horizontal load combinations examined by 25%–30%. Due to the large increase in the base shear at the performance point, the number of plastic hinges at the ends of the beams was increased since the cross sections of the columns were strengthened. Even so, none beam exceeded the "life safety" performance level. These results were expected due to extensive strengthening of the columns. The main conclusion that emerged is that the distribution of ductility in the columns is more balanced in relation to the original structural system and the one strengthened based on the design goal B1 of Kanepe (2017).

DATA AVAILABILITY STATEMENT

The original contributions presented in the study are included in the article/Supplementary Material, Further inquiries can be directed to the corresponding author.

AUTHOR CONTRIBUTIONS

All authors have made a substantial, direct, and intellectual contribution to the work and approved it for publication.

FUNDING

The research was funded by the Hellenic Foundation for Research and Innovation (H.F.R.I.) under the "Second Call for H.F.R.I. Research Projects to support Post-Doctoral Researchers," IMSFARE project: "Advanced Information Modelling for SAFER Structures against Manmade Hazards" (Project Number: 00356).

REFERENCES

Almazán, J. L., and de la Llera, J. C. (2009). Torsional Balance as New Design Criterion for Asymmetric Structures with Energy Dissipation Devices. *Earthquake Engng Struct. Dyn.* 38 (12), 1421–1440. doi:10.1002/eqe.909

Anagnostopoulos, S. A., Kyrkos, M. T., and Stathopoulos, K. G. (2015). Earthquake Induced Torsion in Buildings: Critical Review and State of the Art. *Earthquakes and Structures* 8 (2), 305–377. doi:10.12989/eas.2015.8.2.305

Anastassiadis, K., Athanatopoulou, A., and Makarios, T. (1998). Equivalent Static Eccentricities in the Simplified Methods of Seismic Analysis of Buildings. *Earthquake Spectra* 14 (1), 1–34. doi:10.1193/1.1585986

Applied Technology Council (ATC) (1996). *Methodology for Evaluation and Upgrade of Reinforced concrete Buildings, Report N. ATC-40*. Sacramento, California: California Seismic Safety Commission.

Atashpaz-Gargari, E., and Lucas, C. (2007). Imperialist Competitive Algorithm: An Algorithm for Optimization Inspired by Imperialistic Competition. *IEEE Congress Evol. Comput.*, 4661–4667. doi:10.1109/CEC.2007.4425083

Bosco, M., Ferrara, G. A. F., Ghersi, A., Marino, E. M., and Rossi, P. P. (2015). Predicting Displacement Demand of Multi-Storey Asymmetric Buildings by Nonlinear Static Analysis and Corrective Eccentricities. *Eng. Structures* 99, 373–387. doi:10.1016/j.engstruct.2015.05.006

Bosco, M., Ghersi, A., and Marino, E. M. (2012). Corrective Eccentricities for Assessment by the Nonlinear Static Method of 3D Structures Subjected to Bidirectional Ground Motions. *Earthquake Engng Struct. Dyn.* 41 (13), 1751–1773. doi:10.1002/eqe.2155

Bosco, M., Marino, E. M., and Rossi, P. P. (2013). An Analytical Method for the Evaluation of the In-Plan Irregularity of Non-regularly Asymmetric Buildings. *Bull. Earthquake Eng.* 11 (5), 1423–1445. doi:10.1007/s10518-013-9438-3

Chandler, A. M., Correnza, J. C., and Hutchinson, G. L. (1995). Influence of Accidental Eccentricity on Inelastic Seismic Torsional Effects in Buildings. *Eng. Structures* 17 (3), 167–178. doi:10.1016/0141-0296(94)00003-c

Costa, A., Arêde, A., and Varum, H. (2017). *Strengthening and Retrofitting of Existing Structures (Building Pathology and Rehabilitation Book 9) Part of: Building Pathology and Rehabilitation (21 Books)*. Singapore: Springer.

Dang, Y., Zhao, G., Tian, H., and Li, G. (2021). Two-Stage Optimization Method for the Bearing Layout of Isolated Structure. *Adv. Civil Eng.* 2021, 1–10. art. No. 4895176. doi:10.1155/2021/4895176

De Stefano, M., and Pintucchi, B. (2008). A Review of Research on Seismic Behaviour of Irregular Building Structures since 2002. *Bull. Earthquake Eng.* 6 (2), 285–308. doi:10.1007/s10518-007-9052-3

Duan, X. N., and Chandler, A. M. (1997). An Optimized Procedure for Seismic Design of Torsionally Unbalanced Structures. *Earthquake Engng. Struct. Dyn.* 26 (7), 737–757. doi:10.1002/(sici)1096-9845(199707)26:7<737::aid-eqe673>3.0.co;2-s

Etedali, S., and Kareshk, M. K. (2022). Mitigation of Torsional Responses in Asymmetric Base-Isolated Structures Using an Optimal Distribution of Isolators in Base story. *Structures* 35, 807–817. doi:10.1016/j.istruc.2021.11.053

Eurocode 8 (1994). *European Committee for Standardization ENV 1998-1-1:1994. Design of Structures for Earthquake Resistance – Part 1: General Rules, Seismic Actions and Rules for Buildings*. Brussels, Belgium.

Eurocode 1 (1995). *European Committee for Standardization ENV 1991-1-1:1995. Actions on Structures – Part 1-1: General Actions – Densities, Selfweight, Imposed Loads for Buildings*. Brussels, Belgium.

Fajfar, P. (2000). A Nonlinear Analysis Method for Performance-Based Seismic Design. *Earthquake Spectra* 16 (3), 573–592. doi:10.1193/1.1586128

Fajfar, P., and Fischinger, M. (1988). Discussion of " Evaluation of Building Code Formulas for Earthquake Forces " by Anil K. Chopra and Ernesto F. Cruz (August 1986, Vol. 112, No. 8). *J. Struct. Eng.* 114 (3), 735–737. doi:10.1061/(asce)0733-9445(1988)114:3(735)

Fajfar, P., and Gašperšič, P. (1996). The N2 Method for the Seismic Damage Analysis of RC Buildings. *Earthquake Engng. Struct. Dyn.* 25 (1), 31–46. doi:10.1002/(sici)1096-9845(199601)25:1<31::aid-eqe534>3.0.co;2-v

Ganguly, K. K. (2020). *Reinforced Concrete Design: Repair/Restoration, Strengthening of RC Structures and Concrete Technology*. India: Medtech.

Georgoussis, G. K. (2015). Minimizing the Torsional Response of Inelastic Multistory Buildings with Simple Eccentricity. *Can. J. Civ. Eng.* 42 (11), 966–969. doi:10.1139/cjce-2015-0091

Goel, R. K., and Chopra, A. K. (1990). Inelastic Seismic Response of One-Storey, Asymmetric-Plan Systems: Effects of Stiffness and Strength Distribution. *Earthquake Engng. Struct. Dyn.* 19 (7), 949–970. doi:10.1002/eqe.4290190703

Guo, W., and Li, H.-N. (2009). Secondary System's Optimal Position Analysis Concerning the Lateral-Torsion Coupling Effect. *Jisuan Lixue Xuebao/Chinese J. Comput. Mech.* 26 (6), 797–803+810. doi:10.1088/0256-307x/26/7/074218

Hejal, R., and Chopra, A. K. (1989). Earthquake Response of Torsionally Coupled, Frame Buildings. *J. Struct. Eng.* 115, 834. doi:10.1061/(asce)0733-9445(1989)115:4(834)

Humar, J. L. (1984). Design for Seismic Torsional Forces. *Can. J. Civ. Eng.* 11 (2), 150–163. doi:10.1139/l84-027

Ismail, M. (2015). Elimination of Torsion and Pounding of Isolated Asymmetric Structures under Near-Fault Ground Motions. *Struct. Control. Health Monit.* 22 (11), 1295–1324. doi:10.1002/stc.1746

Kan, C. L., and Chopra, A. K. (1977). Effects of Torsional Coupling on Earthquake Forces in Buildings. *J. Struct. Div.* 103 (4), 805–819. doi:10.1061/jsdeag.0004608

Kanepe (2017). *Earthquake Planning & Protection Organization (EPPO). Greek Code for Assessment and Retrofitting*. 2nd revision(in Greek). Athens, Greece.

Lagaros, N. D., Bakas, N., and Papadrakakis, M. (2009). Optimum Design Approaches for Improving the Seismic Performance of 3D RC Buildings. *J. Earthquake Eng.* 13 (3), 345–363. doi:10.1080/13632460802598594

Lagaros, N. D., Papadrakakis, M., and Bakas, N. (2006). Automatic Minimization of the Rigidity Eccentricity of 3D Reinforced concrete Buildings. *J. Earthquake Eng.* 10 (4), 533–564. doi:10.1080/13632460609350609

Lagaros, N. D., Plevris, V., and Kallioras, N. Ath. (2022). *The Mosaic of Metaheuristic Algorithms in Structural Optimization*. Archives of Computational Methods in Engineering. (to appear).

Li, C.-X., and Han, C.-F. (2003). Optimum Placements of Multiple Tuned Mass Dampers (MTMD) for Suppressing Torsional Vibration of Asymmetric Structures. *J. Earthquake Eng. Eng. Vibration* 23 (6), 149–155.

Li, C.-X., Qu, Y., Wang, C., and Li, J.-H. (2008a). Characteristics of a Soil-Asymmetric Building-Active Tuned Mass Damper Interaction System. *Zhendong yu Chongji/Journal of Vibration and Shock* 27 (9), 26–31.

Li, C.-X., Qu, Y., Wang, C., and Li, J.-H. (2008b). Optimum Properties of Soil-Asymmetric Building-Amtmd Interaction System. *Zhendong yu Chongji/Journal of Vibration and Shock* 27 (10), 10–14.

Li, C.-X., Xu, Z.-M., and Zhang, L.-Q. (2008c). Earthquake Reduction Behaviors of Active Tuned Mass Dampers for an Asymmetric Building. *Zhendong yu Chongji/Journal of Vibration and Shock* 27 (1), 76–83+88.

Makarios, T., and Anastassiadis, K. (1998). Real and Fictitious Elastic Axes of Multi-Storey Buildings: Theory. *Struct. Des. Tall Build.* 7 (1), 33–55. doi:10.1002/(sici)1099-1794(199803)7:1<33::aid-tal95>3.0.co;2-d

Maruić, D., and Fajfar, P. (2005). On the Inelastic Seismic Response of Asymmetric Buildings under Bi-axial Excitation. *Earthquake Engng Struct. Dyn.* 34 (8), 943–963. doi:10.1002/eqe.463

Palermo, M., Silvestri, S., Gasparini, G., and Trombetti, T. (2017). A Comprehensive Study on the Seismic Response of One-Storey Asymmetric Systems. *Bull. Earthquake Eng.* 15 (4), 1497–1517. doi:10.1007/s10518-016-0030-5

Palermo, M., Silvestri, S., Gasparini, G., and Trombetti, T. (2013). Physically-based Prediction of the Maximum Corner Displacement Magnification of One-Storey Eccentric Systems. *Bull. Earthquake Eng.* 11 (5), 1467–1491. doi:10.1007/s10518-013-9445-4

Papazachos, B. C., Papaioannou, C. A., Margaris, B. N., and Theodulidis, N. P. (1993). Regionalization of Seismic hazard in Greece Based on Seismic Sources. *Nat. Hazards* 8 (1), 1–18. doi:10.1007/bf00596232

Paulay, T. (1998). Torsional Mechanisms in Ductile Building Systems. *Earthquake Engng. Struct. Dyn.* 27, 1101–1121. doi:10.1002/(sici)1096-9845(199810)27:10<1101::aid-eqe773>3.0.co;2-9

Penelis, G., and Penelis, G. (2019). *Concrete Buildings in Seismic Regions*. United States: CRC Press.

Peruš, I., and Fajfar, P. (2005). On the Inelastic Torsional Response of Single-Storey Structures under Bi-axial Excitation. *Earthquake Engng Struct. Dyn.* 34 (8), 931–941. doi:10.1002/eqe.462

Reem, H., and Chopra, A. K. (1987). *Earthquake Response of Torsionally-Coupled Buildings, Earthquake Engineering Research Center*. Berkeley: College of Engineering: University of California at Berkeley.

Şahin, A. (2012). A New Algorithm for Geometrical Design of Asymmetric Tall Buildings against Seismic Torsional Behaviour. *Struct. Des. Tall Spec. Build.* 21 (9), 642–668. doi:10.1002/tal.634

Stathi, C. G., Bakas, N. P., Lagaros, N. D., and Papadrakakis, M. (2015). Ratio of Torsion (ROT): An index for Assessing the Global Induced Torsion in Plan Irregular Buildings. *Earthquakes and Structures* 9 (No. 1), 145–171. doi:10.12989/eas.2015.9.1.145

Stathopoulos, K. G., and Anagnostopoulos, S. A. (2005). Inelastic Torsion of Multistorey Buildings under Earthquake Excitations. *Earthquake Engng Struct. Dyn.* 34, 1449–1465. doi:10.1002/eqe.486

Tassios, T. P. (1982). *The Mechanics of Column Repair with a Reinforced concrete Jacket*. Athens, Greece: 7th European Conference on Earthquake Engineering ECEE.

Terzi, V. G., and Athanatopoulou, A. (2021). Optimum Torsion axis in Multistory Buildings under Earthquake Excitation: A New Criterion Based on axis of Twist. *Eng. Structures* 249, 113356. doi:10.1016/j.engstruct.2021.113356

Trombetti, T. L., and Conte, J. P. (2005). New Insight into and Simplified Approach to Seismic Analysis of Torsionally Coupled one-story, Elastic Systems. *J. Sound Vibration* 286 (1-2), 265–312. doi:10.1016/j.jsv.2004.10.021

Xenidis, H., Makarios, T., and Athanatopoulou, A. (2006). The Properties of the Optimum Torsion axis in Asymmetric Multi-Storey Buildings. *Technica Chronica, Sci. J. Tcg*, 99–112.

Yiu, C.-F., Chan, C.-M., Huang, M., and Li, G. (2014). Evaluation of Lateral-Torsional Coupling in Earthquake Response of Asymmetric Multistory Buildings. *Struct. Des. Tall Spec. Build.* 23 (13), 1007–1026. doi:10.1002/tal.1102

Author's Disclaimer: The content of this paper expresses the views of the authors and not the official position of the Ministry of Maritime Affairs and Insular Policy.

Conflict of Interest: The authors declare that the research was conducted in the absence of any commercial or financial relationships that could be construed as a potential conflict of interest.

Publisher's Note: All claims expressed in this article are solely those of the authors and do not necessarily represent those of their affiliated organizations or those of the publisher, the editors, and the reviewers. Any product that may be evaluated in this article, or claim that may be made by its manufacturer, is not guaranteed or endorsed by the publisher.

Advantages of publishing in Frontiers

OPEN ACCESS
Articles are free to read for greatest visibility and readership

FAST PUBLICATION
Around 90 days from submission to decision

HIGH QUALITY PEER-REVIEW
Rigorous, collaborative, and constructive peer-review

TRANSPARENT PEER-REVIEW
Editors and reviewers acknowledged by name on published articles

Frontiers
Avenue du Tribunal-Fédéral 34
1005 Lausanne | Switzerland

Visit us: www.frontiersin.org
Contact us: frontiersin.org/about/contact

REPRODUCIBILITY OF RESEARCH
Support open data and methods to enhance research reproducibility

DIGITAL PUBLISHING
Articles designed for optimal readership across devices

FOLLOW US
@frontiersin

IMPACT METRICS
Advanced article metrics track visibility across digital media

EXTENSIVE PROMOTION
Marketing and promotion of impactful research

LOOP RESEARCH NETWORK
Our network increases your article's readership